The effect of *in vitro* culture on the stability, expansion and neuronal differentiation of human pluripotent cell lines.

Margaret Gillett

University College London

Engineering Doctorate in Biochemical Engineering and Bioprocessing

To my parents

Elizabeth and James Gillett

DECLARATION

'I, Margaret Gillett confirm that the work presented in this thesis is my own. Where information has been derived from other sources, I confirm that this has been indicated in the thesis.'

ABSTRACT

Pluripotent cells are defined by their ability to both self-renew and to differentiation into any cell type within the human body. As such, pluripotent cell lines are of great interest as starting material for drug screening and cell therapies for regenerative treatment of diseased tissues. Pluripotent cell lines were originally derived from germ cell tumors (embryonal carcinoma cells; EC), but have since been isolated and expanded from the inner cell mass of an early embryo (human embryonic stem cells; hESCs).

This project set out to investigate the relative ability of the pluripotent NTERA2 (EC) cell line and hESC lines: Shef3, HUES7 and RH5, to differentiate into neurons, using mechanical and enzymatic culture methods. Focus was placed on monitoring differentiation efficiency and function between the different lines.

The tumour origin, in addition to the poor reproducibility, low yield and reduced functionality of NTERA2 derived neurons, compared to primary neurons, makes their incorporation into regenerative therapies unlikely. As such, an enhanced neuronal differentiation protocol was developed for use in hESCs. Cell populations were monitored for relative changes in gene and protein expression at selected time points throughout differentiation using standard RT-PCR, Q-PCR and immuno fluorescence analysis. End stage neurons were screened for functionality using patch clamping and calcium imaging techniques. Monitoring of cellular behavior through differentiation was aided by the concurrent development of a portable microscope incubator stage in collaboration with Linkam scientific Ltd.

These data demonstrate a variation in the ability to generate neurons from pluripotent cell lines, and suggests a predetermined, preferential cell fate within each line, even at the level of pluripotency. This study also characterises in detail neuronal differentiation from pluripotent cells, adding to the understanding which is essential for translation into therapies for neurodegenerative diseases such as Parkinson's, Alzheimer's, and Huntingdon's disease.

ABBREVIATIONS

aCGH	array comparative genomic hybridisation
AFP	alpha feto protein
ALS	amyotrophic lateral sclerosis
ANOVA	analysis of variance
AP	action potential
ATP	adenosine triphosphate
ATRA	all-*trans*-retinoic acid
BDNF	brain derived neurotrophic factor
BMP	bone morphogenetic protein
$CaCl_2$	calcium chloride
CNS	central nervous system
CRAPB2	cellular retinoic acid binding protein 2
DMEM	Dulbecco's modification of eagle's medium
DMSO	dimethyl sulfoxide
DNMT3B	DNA (cytosine-5-)-methyltransferase 3 beta
EB	embryoid body
EBAF	Endometrial bleeding associated factor
EC	embryonal carcinoma
ECM	extra cellular matrix
EDTA	ethylenediaminetetraacetic acid
EM	electron microscope
ES	embryonic stem
ESC	embryonic stem cell
FCS	foetal calf serum
FGF	fibroblast growth factor
FITC	fluorescein isothiocyanate
FLIPR	fluorescence imaging plate reader
GABA	gamma-aminobutyric acid

GAD	glutamate decarboxylase
GAPDH	glyceraldehyde-3-phosphate dehydrogenase
GDF3	growth differentiation factor 3
GDNF	glial cell derived neurotrophic factor
GE	ganglionic eminence
GFAP	glial fibrillary acidic protein
GFP	green fluorescent protein
GLP	good laboratory practice
GMP	good manufacturing practice
GOI	gene of interest
HBS	HEPES buffered saline
HCl	hydrochloric acid
hEC	human embryonal carcinoma
hES	human embryonic stem
hESC	human embryonic stem cell
HFEA	human fertilisation and embryology authority
HLXB9	homeobox gene HB9
HTA	human tissue authority
ICM	inner cell mass
Ig	immunoglobulin
iMEF	inactivated mouse embryonic fibroblast
ISL1	islet1
KCl	potassium chloride
KCL	Kings College London
LCI	live cell imaging
LDA	low density array
LN2	liquid nitrogen
MAP2	microtubule associated protein
MCB	master cell bank
MSC	Microbiological safety cabinet

MEF	mouse embryonic fibroblasts
$MgCl_2$	magnesium chloride
MNX1	motor neuron and pancreas homeobox 1,
MS	multiple sclerosis
NaCl	sodium chloride
Nanog	Nanog homeobox
NaOH	sodium hydroxide
NB	neurobasal
NI	neural induction
NIBSC	National Institute for Biological Standards and Control
OCT4	octamer binding protein 4
NMDA	N-methyl-D-aspartic acid
OLIG2	oligodendrocyte lineage transcription factor 2
PAX6	paired box 6
PBS	phosphate buffered saline
PCR	polymerase chain reaction
PD	Parkinson's disease
PNS	peripheral nervous system
PTEN	phosphatase and tensin homolog
PTF1A	pancreas specific transcription factor, 1a
QC	quality control
Q-PCR	quantitative PCR
RA	retinoic acid
REST	RE1-silencing transcription factor
RT	room temperature
RT-PCR	reverse transcription PCR
SCI	spinal cord injury
SEM	scanning electron microscope
SOP	standard operative procedure
SOX2	SRY (sex determining region Y)-box 2

SSEA	stage specific embryonic antigen
SYP	synaptophysin
T	brachyury
TGF-β	transforming growth factor beta
TDGF1	teratocarcinoma derived growth factor 1
TERT	telomerase reverse transcriptase
TH	tyrosine hydroxylase
Tra	trafalgar antigen
TUBB3	β-III-tubulin
UCL	University College London
UKSCB	UK Stem Cell Bank
UTF1	undifferentiated embryonic cell transcription factor 1
UV	ultra violet
VE	visceral endoderm

ACKNOWLEDGMENTS

I would like to thank my principle supervisors: Dr. Roland Fleck and Professor Chris Mason for their guidance and support during this project. I would also like to thank the following people for their continued assistance and advice throughout:

- Professor Glyn Stacey
- Dr. Lyn Healy
- Ludmilla Ruban
- Vince Kamp
- Arnold Kamp
- Peter Grocutt
- Rob Duncan
- Dr. Diana Hernandez
- Lesley Young

I would also like to thank the following people for dedicating their time and service to this project, helping to ensure that it was carried out to the best possible standard.

- Professor Steve Bolsover – patch clamping and calcium imaging
- Dr. Alan Heath – statistical analysis
- Dr. Ross Hawkins and Dr. Chris Burns – gene expression analysis
- Paula Timmons and Hayley Jones – hESC culture training
- Dr. Julia Sung – microbiological screening
- Megan Christie – aCGH analysis
- TDL Fingerprinting
- TDL Karyology
- UKSCB – cell supply
- Christine Piggot – NTERA2 cell supply
- Sam Ranasinghe – FLIPR
- Angela Iriajen – QC Co-ordinator, UKSCB and Cell Biology, NIBSC
- Sancha Osborn – karyology advice
- Dr. Brenda Williams and Dr. Sophie Finch – primary rat neurons
- Dr. Iolanda Vendrell and Dr. Jun Wheeler - proteomics
- Paul Mondragon-Teran - advice for live cell imaging systems
- Professor Nigel Titchener-Hooker
- Professor Mike Hoare
- Professor Peter Dunnill
- Martin Town

I would also like acknowledge the EPSRC and Linkam Scientific for funding this project, and additional funding by ESACT-UK and UCL Graduate School which enabled attendance to the 2009 annual International Society for Stem Cell Research.

Finally I would like to acknowledge and give thanks to the following people, who's continued support and encouragement have been key to the completion and success of this project and without whom, there would have been many even later nights ……

- Dr. Edward Byrne
- Dr. Jenny Boyle
- Dr. Carolina Machado
- Alexandra Hemsley
- Dr. Matthew Scutcher
- Jim Gillett
- Liz Gillett
- Vic Gillett
- Family Byrne

TABLE OF CONTENTS

TABLE OF FIGURES

LIST OF TABLES

1 Introduction

An estimated 35.5 million people worldwide are living with the debilitating effects of neurodegenerative diseases such as Alzheimer's disease, Parkinson's disease, Multiple Sclerosis and Amyotrophic Lateral Sclerosis (Parkinson's Disease Society, 2009; Alzheimers Research Trust, 2009; ALS Society of BC, 2009; Multiple Sclerosis Society, 2009). With modern advances in nutrition and health care, these figures are predicted to rise in future years amongst patients who may previously have died from unrelated conditions before reaching the age of onset. Current therapies for such diseases rely on pharmacological intervention to relieve symptoms and prolong normality of life; however, over time the efficacy of treatment is reduced and disease symptoms inevitably return (Lindvall and Kokaia, 2009). Cell therapies may provide the answer for long term alleviation of symptoms or curing disease, through transplantation of healthy cells which regenerate or replace the damaged tissue. For neurodegenerative diseases, cell therapies carry hope for recovery of motor control and cognition, and a subsequently improved quality of life (Lindvall and Kokaia, 2009; Martinez et al., 2009).

The concept of cell therapies for the treatment of debilitating and degenerative diseases has been around for many decades. Benefits were realised as early as 1894, when the first islet cell transplantation was carried out from a sheep pancreas into a 15-year old boy suffering diabetic ketoacidosis (Williams, 1894). Unsurprisingly, these early attempts at cell therapy were unsuccessful due to immune rejection; however, they paved the way for further research. Today, bone marrow transplantations containing adult stem cells are a realisation of the benefits associated with cell therapies and have been routinely and successfully preformed since 1957 (Thomas et al., 1957). However, donor stem cells for therapies such as bone marrow transplantation are in short supply and require immunosuppression to prevent rejection, which increases a patient's susceptibility to secondary infections. Alternative therapies from readily available cell stocks which do not require immunosuppression would therefore be desirable.

In recent decades, stem cells have been focused upon as potential sources of cells for therapy. A stem cell is defined by its ability to self renew and differentiate into any definitive cell type of the body (Thomson et al., 1995). The ability of a stem cell to continually self-renew is key to the success of cell therapies, providing ever increasing numbers of cells for transplantation.

Different classifications of stem cells exist throughout embryonic development into adulthood. An early cleavage stage embryo contains just a small number of cells, each of which is capable of developing into any of the cell types within the embryo, or the extra embryonic tissues of the placenta. These cells are termed 'totipotent' and may be considered the 'master' of all stem cells. As embryonic development progresses, the potency of individual cells; that is the number of possible cell types which can be generated, is subsequently reduced. When the embryo reaches the blastocyst stage approximately 4-5 days after fertilisation, two distinct groups of cells are identifiable: the outer trophectodermal cells which form the placental tissue and extra-embryonic ectoderm (Gardner et al., 1973; Rossant and Ofer, 1977), and an inner clump of cells known as the inner cell mass (ICM). Cells of the ICM go on to form the epiblast from which all of the different tissues of the foetus are descended in addition to a layer of visceral endoderm (VE; Figure 1.1) which surrounds the developing embryo; as such these cells are termed 'pluripotent'.

1.1 Embryonic development

The early tissue specification in the embryo is largely controlled by nodal and BMP signalling throughout the cells of the epiblast (Varlet et al., 1997). Gradients in nodal signalling are largely responsible for establishing the anterior-posterior axis of the embryo which arise from two localised signalling cascades (Waldrip et al., 1998; Brennan et al., 2001). The extra-embryonic ectoderm cells in the proximal portion of the embryo secrete a range of nodal pro-protein convertases (Furin and Pace4) which cleave the nodal protein into its active form, enhancing the downstream effect of nodal signalling in the nearby posterior region of the epiblast (Varlet et al., 1997; Beck et al., 2002; Schier, 2003). In concurrence with this, the anterior visceral endoderm (AVE) secretes nodal/BMP inhibitor molecules such as Cerberus-like and Lefty1 towards the anterior portion of the epiblast driving these cells into an ectodermal cells fate (Figure 1.1) (Schier, 2003). This is the first of three embryological germ lineages to develop and is considered to be the default pathway for differentiation due to its occurrence in the absence of inhibitory signals (Munoz-Sanjuan and Brivanlou, 2002). Cells from this region of the developing embryo will eventually go on to produce all the derivatives of the nervous system (Section 1.2) and epidermis (skin).

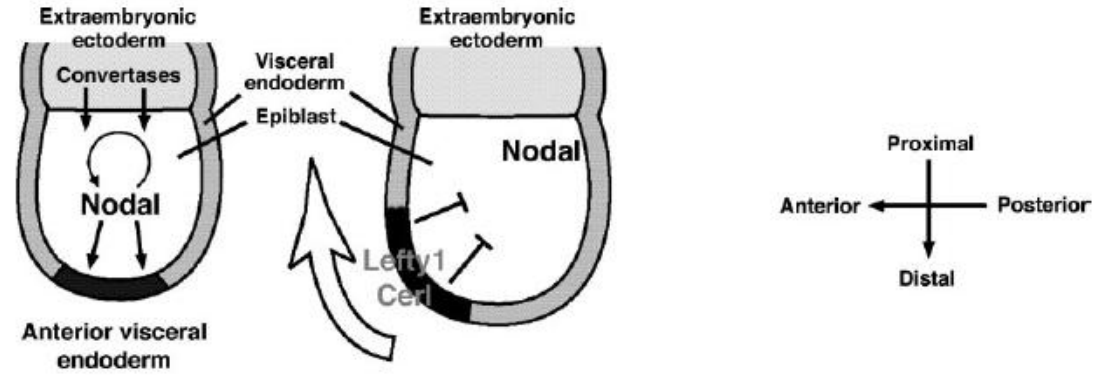

Figure 1.1. Tissue specification in the early embryo.

Representative image of early tissue specification in the developing mouse embryo (5.5-6.5dpc), highlighting the location of the extra-embryonic ectoderm in the proximal portion of the embryo, the epiblast and its surrounding visceral endodermal layer (VE). Nodal gradients are present throughout the epiblast as a result of convertase secretion by the extra-embryonic ectoderm, and nodal inhibitors (Lefty1 and Cerberus-like) secreted by the AVE. Image taken from Schier et al., 2003.

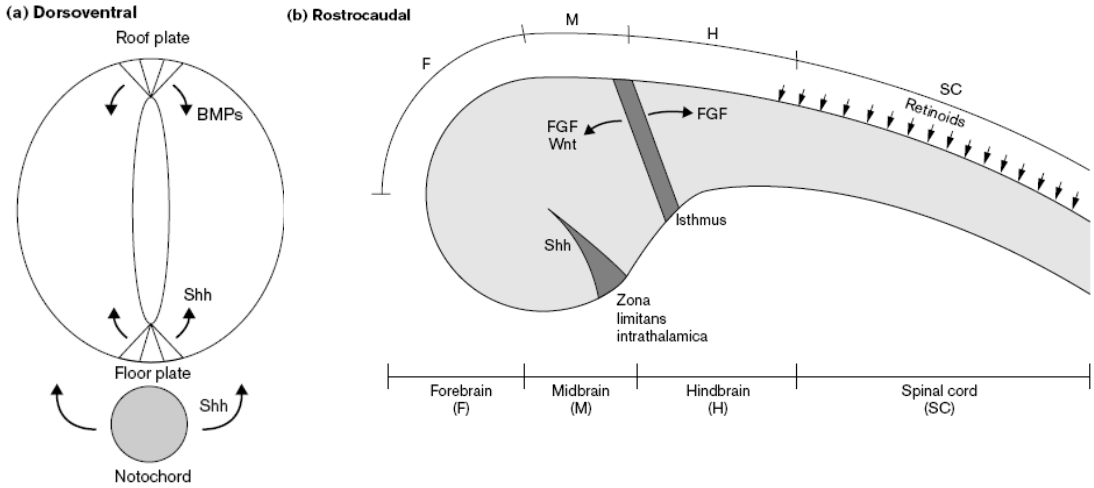

Figure 1.2. Axis formation in the neural tube.

SHH and BMP work in combination to initiate the dorso-ventral axis of the embryo (a). SHH from the notochord and floor plate ventralise the base of the neural tube. BMP signalling from the roof plate overlying the neural tube dorsalises neighbouring cells. The rostro-caudal axis of the neural tube is specified by a combination of SHH, FGF, Wnt and retinoid signalling (b). Concentration gradients of these molecules segregate the nervous system into four distinct regions: forebrain, midbrain, hindbrain and spinal cord. Image taken from Jessell and Sanes., 2000.

The high concentrations of nodal and BMP signalling at the posterior of the embryo is thought to play a key role in establishing formation of the primitive streak (Perea-Gomez et al., 2002; Schier, 2003) through which the mesendodermal cells of the epiblast migrate in a process known as gastrulation. Gastrulation results in the transformation of mesendodermal cells into the innermost endodermal cell layer to form the gut and its appendages (liver and lungs etc) and the mesodermal cells (sandwiched between the endo- and ecto-dermal germ layers) which will differentiate into the muscles and connective tissue of the embryo. By this developmental stage, embryonic cells are assigned along one of the three developmental pathways (ectodermal, mesodermal or endodermal) and are termed 'multipotent'. Throughout the remainder of development, cells progress through their germ lineage of choice becoming sequentially more committed into defined cell types (reviewed by Alberts et al., 2002b).

1.2 Neural induction

The nervous system derives from the outermost ectodermal cell layer of the embryo. The process of committing these ectodermal cells into neural precursors rather than epidermal precursors of the skin, is known as neural induction, and is considered to be the result of BMP inhibition since exposure to BMP signalling in the ventral ectoderm confers and epidermal cell fate amongst these cells (Wilson and Edlund, 2001). Inhibition of BMP signalling the in dorsal ectoderm by secreted molecules such as noggin, cerberus and follistatin specifies a neural cell fate amongst these cells. Once committed into the neural differentiation pathway these cells can be referred to as neural precursors which go on to generate the various components of the nervous system (Section 1.3).

Formation of the nervous system begins with the generation of the neural tube on the dorsal side of the embryo, in a process referred to as neuralation. Neuralation is initiated by signalling from the mesodermal cells underlying the neural plate which localise into a transient rigid rod-like structure (notochord) along the dorsal midline of the embryo during gastrulation (Reviewed by Wolpert et al., 2002; Alberts et al., 2002b). Signalling from the notochord by morphogens such as sonic hedgehog (SHH) induces thickening and inward rolling of the neural plate into the neural tube (Jessell and Sanes, 2000). In opposition to BMP signalling gradients from the overlying dorsal roof plate, SHH signalling later promotes ventralisation of the neural tissue, thus creating its dorsal-ventral axis. Subsequent development and regional specificity along the rostro-caudal axis of the neural tube is

driven by gradients in FGF, Wnt and retinoid signalling, which segregate the nervous system into forebrain, midbrain, hindbrain and the spinal cord regions (Figure 1.2; reviewed by Jessell and Sanes., 2000).

The neural tube comprises numerous cells of epithelial phenotype which detach to from the ectodermal sheet and subsequently differentiate into the many neurons and glia of the central nervous system (CNS; brain and spinal cord; Section 1.3) in a process known as neurogenesis (Section 1.4) (Alberts et al., 2002b). The cluster of cells located between the neural tube and developing epidermis are known as the neural crest. Closure of the neural tube, initiates the migration of these neural crest cells away from the spinal cord to radial locations. These cells mainly give rise to neurons (and glia) of the peripheral nervous system (PNS) (Baroffio et al., 1988; Artinger et al., 1999; Le Douarin and Dupin, 2003).

1.3 Cell types of the nervous system

The nervous system comprises two main groups of cells; neurons which generate electrical impulses to co-ordinate communication between cells throughout the body, and glial cells which are located throughout nervous system and collectively serve a supportive role for neurotransmission. These cells have been described in more detail below.

1.3.1 Glia

Developing glial cells retain this epithelial-like phenotype from the early neural tube and form the supporting structures down which neurons migrate and extend axonal and dendritic projections for communication (Gasser and Hatten, 1990; Koul and Seth, 2008). There are numerous classes of glial cells throughout the nervous system; oligodendrocytes and astrocytes are the most well characterised glial cell populations.

Oligodendrocytes are a form of glial cell within the CNS which wrap around neurons forming an insulating myelin sheath. These cells phagocytose damaged nerve cells. In the PNS, this function is carried out by Schwann cells (Keirstead et al., 2005; Nistor et al., 2005; Franklin and ffrench-Constant, 2008). Spinal cord injury or trauma often causes damage to nerves which release excess glutamate into surrounding tissue. Excess extracellular glutamate is toxic to glial cells (Park et al., 2004; Káradóttir and Attwell, 2007), resulting in a depletion of oligodendrocytes at the site of injury. The loss of oligodendrocytes prevents

nerve re-myelination and is thought to be one of the main contributors to continued degeneration following spinal cord injury (SCI) (Park et al., 2004). Regenerative cell therapies which transplant oligodendrocytes into the site of tissue damage have shown promising results for improvement of sensation and motor control following SCI (Keirstead et al., 2005; Nistor et al., 2005). Indeed, in January 2009, after promising results from early clinical trials, the first cell therapy using human embryonic stem cell (hESC; Section 1.9) derived oligodendrocytes for treatment of SCI was approved (Geron Corporation, California).

Astrocytes (astroglia) are so named after their 'star' shape. They serve to provide both physical and biochemical support for the endothelial cells of the blood brain barrier, transferring nutrients to the nerves as required (Abbott et al., 2006). Astrocytes promote survival and differentiation of neurons and influence neuronal migration (Denis-Donini and Estenoz, 1988; Guerri et al., 1989; Gasser and Hatten, 1990). They are also involved in scarring following trauma to the brain or spinal cord (Faulkner and Keirstead, 2005). Similarly to neurons, astrocytes are able to respond to stimulation by releasing neurotransmitters such as glutamate and adenosine triphosphate (ATP) in a calcium responsive manner to induce neuronal signalling (Carmignoto, 2000; Newman, 2003).

1.3.2 Neurons

A neuron is a nerve cell which sends and receives electrical impulses in response to a stimulus, in order to initiate an effect. Neurons are characterised by the extension of processes, typically a single long axon which transmits a signal towards a new cell, and a number of smaller dendrites which receive incoming signals from neighbouring cells. Neuronal projections can be identified by the expression of β-III-tubulin (TUBB3) and microtubule associated protein 2 (MAP2), which are commonly used as markers for neuronal phenotype.

Neurons function to control movement, sensation, speech and cognition. The plasma membrane of a mature neuron contains numerous ion channels, most of which fall into two main classes; ligand-gated (ionotropic) or voltage-gated ion channels, the presence and functionality of ligand-gated ion channels can be detected using calcium imaging analysis (Section 1.11.3.2). Voltage gated ion channels are activated by a sudden change in local voltage which alters their confirmation to allow influx/efflux of positive Na^{+} or Ca^{2+} ions

through the membrane. The movement of these positive ions alters the polarity of the cell, causing depolarisation and generation of an electrical impulse, or action potential (AP; Figure 1.3). The change in polarity results in the opening of membrane voltage gated K^+ channels, which allows K^+ ions to flow out of the cell and recover the polarisation. The presence of functional K^+ channels is essential for the generation of recurrent APs. The ability of a neuron to fire APs in response to stimulation can be tested using a technique known as patch clamping (Section 1.11.3.1).

Inside the terminus of a mature axon are numerous synaptic vesicles containing neurotransmitters. Release of these vesicles is regulated by cytosolic Ca^{2+}. A resting cell maintains a comparatively low free cytosolic Ca^{2+} concentration of 10^{-7} M, compared to the extracellular fluid of 10^{-3} M (Alberts et al., 2002a), creating a concentration gradient across the plasma membrane. When a ligand-gated channel is stimulated by binding of a neurotransmitter, Ca^{2+} channels in the plasma membrane open and Ca^{2+} ions flood into the cytosol, increasing the polarity of the cell. This triggers Ca^{2+} responsive proteins to induce synaptic secretion, releasing neurotransmitter into the synaptic cleft between two neurons. Released transmitters will then go on to stimulate a response in a neighbouring cell. In this way a signal is transmitted between cells at speeds of 120 $m.s^{-1}$ (Káradóttir and Attwell, 2007). Finally, the change in polarity of the stimulated cell, triggers Ca^{2+} transporters in the plasma membrane to pump free Ca^{2+} back out of the cell, (or sequester into internal cytoplasmic stores) returning the cell to its resting levels (Alberts et al., 2002a).

1.3.2.1 Neurotransmitters

There are two classes of neurotransmitters in the brain; excitatory and inhibitory. Excitatory neurotransmitters induce an inward flux of positive ions into the cells, usually Ca^{2+} ions, causing depolarisation and initiation of an excitatory electrical impulse. Inhibitory neurotransmitters regulate impulse transmission, usually by inducing an influx of Cl^- ions into the cell to induce repolarisation and inhibit further electrical impulses.

Glutamate: Glutamate is the main excitatory neurotransmitter in the nervous system; however, extreme doses of glutamate are toxic to neural cells, resulting in apoptosis and cell death. For this reason, glutamate is sequestered by surrounding glial cells, following release and broken down into glutamine, preventing neurotoxicity by over stimulation (Rothstein et al., 1996). Glutamate is also the precursor for the inhibitory neurotransmitter

GABA, which is generated from glutamate by the glutamate decarboxylase (GAD) enzyme (Buddhala et al., 2009).

NMDA: N-methyl-D-aspartic acid (NMDA) is an excitatory neurotransmitter which binds to the NMDA group of ionotropic glutamate receptors in the plasma membrane (Hardingham and Bading, 2003). This results in an influx of Ca^{2+} ions into the cell, generating an electrical impulse for cell-cell communication. NMDA is expressed largely in the hippocampal region of the brain and as such is mainly thought to function in learning and memory (Bliss and Collingridge, 1993). NMDA receptors have been located across alternative areas including: cerebral cortex, striatum, hippocampus, amygdala, and cerebellum (Hanaoka et al., 2003). The response to NMDA is considered to be potentiated by the presence of glycine as a co-agonist (Johnson and Ascher, 1987; Kleckner and Dingledine, 1988).

Glycine: Glycine is a non-essential amino acid with multiple functions in the body. In the nervous system glycine is an inhibitory neurotransmitter for the regulation of APs following excitatory stimulation. In addition, glycine serves as a co-agonist for stimulation of the excitatory NMDA receptor (Kleckner and Dingledine, 1988; Kemp and Leeson, 1993), perhaps functioning as a fine control over NMDA receptor activation.

Acetyl Choline: Acetyl choline is an excitatory neurotransmitter in both the CNS and PNS involved in learning, memory, stress, and sleep cycles (Reis et al., 2009). Acetyl choline is synthesised from acetyl CoA and choline by the enzyme choline acetyltransferase (Tucek, 1985), which also acts as a molecular marker of cholinergic neurons. Carbachol is a cholinergic agonist which binds to and activates the acetyl choline receptor (both muscarinic and nicotinic) on nerve cells. Due to the high cost of acetyl choline, carbachol can be used in functional studies to detect the presence and functionality of the acetyl choline receptors.

Gamma-aminobutyric acid: Gamma-aminobutyric acid (GABA) in another of the main inhibitory neurotransmitters of the CNS (Krnjevic and Schwartz, 1967), and is synthesised from glutamate by the enzyme glutamate decarboxylase (GAD) (Buddhala et al., 2009). GABA functions as a regulatory neurotransmitter; upon binding to its receptors GABA initiates an influx of Cl^- ions into the cells which reinstates the negative polarity of the cell (Thampy and Barnes, 1984). In this way, GABA inhibits the firing of Ca^{2+} induced action potentials caused by glutamate stimulation.

Serotonin: Serotonin is an alternative inhibitory neurotransmitter mainly involved in control of mood, pain, sleep patterns, muscle contraction and learning (Ressler and Nemerodd, 2000; Pakalnis et al., 2009). Serotonin also has many functional roles outside of the nervous system including bowel motility, bladder control and platelet aggregation (Berger et al., 2009). Serotonin receptors can found throughout the brain, emphasising the dynamic role played by serotonin signalling (Berger et al., 2009).

Dopamine: Dopamine is present throughout the body with a range of functions. In the brain, dopamine behaves as both an excitatory and inhibitor neurotransmitter where it controls movement, motivation and memory. A lack of dopamine can result in a loss of motor control (Parkinson's disease) and depression (Brown and Gershon, 1993; Obeso et al., 2004; Björklund and Dunnett, 2007). Elsewhere in the body it serves as a hormone controlling processes such as lactation and sexual arousal (Boullin et al., 1978; Hull et al., 1999). Dopamine synthesis occurs in several stages; L-tyrosine is first converted to L-3,4-dihydroxyphenylalanine (L-DOPA) by the enzyme tyrosine hydroxylase (TH) which is a distinguishing marker for dopaminergic neurons. L-DOPA is then converted to dopamine in the brain by the dopa decarboxylase enzyme. Loss of dopamine synthesis by dopaminergic neurons in the substantia nigra region of the brain causes Parkinson's disease, typified by the progressive loss of motor control. Epinephrine and norepinephrin are excitatory neurotransmitters derived from dopamine. These neurotransmitters are mainly involved in controlling anxiety, stress and mood.

The type of neurotransmitter released depends upon the neuronal phenotype of the cell, (e.g. GABAergic neurons release gamma-aminobutyric acid (GABA), glutamatergic neurons release glutamate and serotonergic neurons release serotonin), which is governed in part by the location of the neuron within the nervous system, and the environmental queues received during its development.

1.4 Neurogenesis

Neurogenesis is the formation of neurons from the neural precursors of the nervous system and occurs in two main waves during development, pre and post-natally (Hatten, 1999). The precise origin and sequence of signals which drive a neural precursor to become neuronal rather than glial remains to be fully characterised; however, it has been well documented that neurogenesis occurs first, and gliogenesis follows later in

development. Several signalling pathways have been implicated in these processes. Both *in vivo* and *in vitro* studies on neuronal differentiation from neural and embryonic stem cells have identified the BMP4 antagonist noggin, to play a crucial role in neurogenesis by inhibiting BMP signalling amongst neural fated tissues (Lamb et al., 1993; Lim et al., 2000; Pera et al., 2004; Itsykson et al., 2005; Stottman et al., 2006). Basic fibroblast growth factor (bFGF) signalling has also been shown to play a key role in neurogenesis, acting both to block BMP signalling, and independently to induce neuralisation (Hongo et al., 1999; Wilson et al., 2000; Pera et al., 2003; Bilican et al., 2008). However research has shown that, in addition to SHH, bFGF signalling is required for gliogenesis (Orentas et al., 1999; Chandran et al., 2003; Danesin et al., 2006; Bilican et al., 2008), suggesting that these signalling stimuli do not act alone in specifying a neuronal or glial cell fate, but rather that the time point, concentration and duration of a cells exposure must be critical to defining its terminal neuronal or glial cell fate. In support of this, it has been demonstrated that a neuro-glial switch occurs after the initial phase of neurogenesis in response to prolonged SHH exposure from the notochord and floor plate. This prolonged exposure induces the differentiation of neural precursors into the supporting glial cells, rather than continued neuronal generation (Kessaris et al., 2001; Danesin et al., 2006).

The terminal neuronal phenotype specified during differentiation is defined by the spatial arrangement of the cells during development and exposure to directive stimuli. Using knock-out animal models and gene expression analysis, numerous studies have been carried out to determine the various signalling cascades which specify the different neuronal phenotypes found throughout the nervous system. These studies have shown that a motor neuronal cell fate in the spinal cord is induced by retinoid exposure at the most caudal portion of the neural tube, this can be recapitulated *in vitro* using retinoic acid to induce motor neuronal phenotypes from both neural and embryonic stem cells (Li et al., 2005; Lee et al., 2007; Li et al., 2008). In contrast forebrain development at the most rostro-dorsal portion of the nervous system is induced as a results of reduced SHH concentration, in the absence of retinoid signalling. Forebrain neural precursors are identifiable by PAX6 expression which is inhibited in mid and caudal portions of the tube by increased SHH expression (Goulding et al., 1993; Ericson et al., 1997). Midbrain neuronal differentiation can be induced by enhancing the ventralising effects of SHH, in combination with FGF8 as is present in the mid-portion of the developing neural axis (Yan et al., 2005).

The possibility of generating the neuronal cell types lost during neurodegenerative disease, is fast becoming a reality thanks to the abundance of research into the processes of neural induction and neurogenesis. Following the derivation of the first hESC lines in 1998 (Thomson et al., 1998), researchers world-wide have picked away at these intricate processes of differentiation, working towards the overarching aim to produce functional neural cells for the replacement of disease/damaged nervous tissue, and to enhance the throughput and efficacy of pharmacological screening. Despite these advances, the reproducibility of differentiation to sufficiently generate the high cell yields required for therapy remains a challenge.

1.5 Neuronal differentiation *in vitro*

In order to generate neurons from pluripotent cells *in vitro* it is necessary to mimic the signalling events to which the cells would be exposed during embryonic development (Sections 1.1, 1.2, 1.4). Firstly, these cells must be committed into the ectodermal lineage, followed by further specification into neural stem cells (progenitor) and finally into a neuronal cell type. Commitment of pluripotent cells (Section 1.9) into the ectodermal lineage has been achieved using signalling molecules which mimic the signalling activities of the early epiblast (Section 1.1) incorporating nodal inhibitors such as SB431542, Lefty or follistatin (Schier, 2003; Vallier et al., 2005; Patani et al., 2009) to drive ectodermal commitment or BMP inhibitors such as noggin or chordin, which block the commitment of cells into mesodermal or endodermal lineages (Hemmati-Brivanlou et al., 1994; Piccolo et al., 1996; Gratsch and O'Shea, 2002; Itsykson et al., 2005; Iacovitti et al., 2007). Equally positive retinoic acid, FGF and SHH signalling, as well as inhibition of Wnt signalling have been shown to induce neuroectodermal differentiation in hESCs (Jones-Villeneuve et al., 1982; Roelink et al., 1995; Wilson et al., 2000; Wolpert et al., 2002; Baharvand et al., 2007; ten Berge et al., 2008).

Most neural differentiation protocols transfer adherent hESCs into suspension culture, thus mimicking the 3D nature of the embryo to drive differentiation. When cultured in suspension, pluripotent cells rapidly aggregate into clusters; signalling amongst these clusters has been shown to initiate differentiation in a pattern similar to that of early embryogenesis (Itskovitz-Eldor et al., 2000; Dang et al., 2002; Shin et al., 2005; Heeg-Truesdell and LaBonne, 2006; Li et al., 2007). These floating cell clusters are referred to as embryoid bodies (EBs).

1.5.1 Embryoid bodies

Embryoid bodies are three dimensional cell aggregates which can be generated from pluripotent cells by culture in suspension, methylcellulose, as hanging drops, or forced aggregation using centrifugation (Keller, 1995; Gassmann et al., 1996; Dang et al., 2004; Burridge et al., 2007). The size of an EB varies depending on the number of cells and process of formation, which in turn is thought to influence the terminal fate of the cells within. Signalling within the EB has been shown to initiate differentiation of the pluripotent cells into precursors from any of the three germ lineages, and on occasion recapitulate the developmental process of gastrulation (ten Berge et al., 2008).

Although EB formation and differentiation is a seemingly undirected, the size of the EB can be used to encourage differentiation into a specific germ lineage (Itskovitz-Eldor et al., 2000; Li et al., 2005; Ng et al., 2005; Burridge et al., 2007; Shim et al., 2007). The ectoderm germ lineage is thought to be the default pathway of differentiation in hESCs, as in the absence of the inhibitory signals (including BMP signalling events) cells of an ectodermal lineage develop (Munoz-Sanjuan and Brivanlou, 2002). Despite this, neuronal differentiation from hESCs remains suboptimal, indicating a commitment of cells into non-ectodermal fates during early stages of differentiation. In addition to the size of the EB, the media in which it is cultured can affect the direction of differentiation.

1.5.2 Directing neuronal differentiation using culture media

Pluripotent hESCs are most commonly expanded as an adherent monolayer culture in knock out-media (Section 1.9.3) for sustained pluripotency. Removal from adherent culture and transferral into suspension has been shown to effectively induce differentiation; however, the media requirements of a differentiating neural precursor and a neuron are vastly different to those of an ESC. The composition of the media in which these cells and EBs are cultured can be used to guide differentiation towards a specified neuronal cell fate. Over past years dedicated media formulations have been developed which provide a selective environment for neuronal differentiation.

1.5.2.1 DMEM:F12

The presence of serum was removed from early differentiation media to prevent attachment of EBs to the culture vessel, during their suspension culture phase. Barnes and

Sato combined first the high nutrient content DMEM with the relatively low nutrient content F12 in 1980 to create a media which was suitable for a range of cell types without the requirement for serum (Barnes and Sato, 1980). Ham's F12 does not contain serum and therefore is completely defined (Ham, 1965).

1.5.2.2 Neurobasal media

Neurobasal media specially was developed for selective differentiated culture of primary embryonic neurons (Brewer, 1995). Its recipe is based on standard DMEM but has a lower NaCl and $NaHCO_2$ concentrations, reducing the osmolarity which has been shown to be beneficial for neuronal cells in culture (Brewer et al., 1993; Brewer, 1995). In addition, neurobasal media contains a lower cysteine and glutamine concentration than DMEM which reduces glial cell proliferation (Brewer et al., 1993), and is supplemented with alanine, asparagine, proline and vitamin B12 which are absent from the standard DMEM formulation (Brewer et al., 1993). Neurobasal media does not contain ferrous sulphate (found in DMEM) because this has been shown to be toxic to neuronal cultures (Brewer et al., 1993). To enhance neuronal commitment and differentiation neurobasal base media can be further supplemented with N2 and B27 (Sections 1.5.2.3 and 1.5.2.4).

1.5.2.3 N2 supplement

N2 supplement is a chemically defined supplement based on Bottenstein's N-2 formulation (Bottenstein, 1985), recommended for the growth and survival of post-mitotic neurons in culture (Bottenstein, 1985). It contains a mixture of human transferrin, recombinant insulin, progesterone, putriscine, and selenium which protects the cells from peroxidises (McKeehan et al., 1976).

1.5.2.4 B27 supplement

B27 is a serum substitute, comprising insulin, transferrin, progesterone, putrescine, selenium, which is also supplemented with the thyroid hormone T3, fatty acids, vitamin E and other anti-oxidants (Brewer, 1995). Substitution of serum for B27 in neuronal cultures results in higher neuronal survival, reduced outgrowth by glial cells and increased number and extension of processes from neuronal cells (Brewer et al., 1993).

1.5.3 Gene expression analysis of neuronal differentiation

Differentiation is caused by a change in the molecular programming of the cell in response to stimuli. Changes in the genes being expressed is reflected in the altered array of proteins which bring about the morphological changes visible during differentiation. The gene expression profile of a neuron is different to that of a neural progenitor or other pluripotent cell. Analysis of a population of cells at the level of gene expression enables tracking through the process of differentiation and can be carried out using molecular techniques such as the polymerase chain reaction (PCR).

PCR can be used to amplify a specific DNA sequence within a sample. PCR requires the presence of forward and reverse DNA primers which are designed to bind to each end of a target nucleotide sequence. Activated DNA polymerase binds to the primers and moves along the target nucleotide sequence, generating a complimentary copy; the number of copies of a targeted DNA, double exponentially with each cycle of the PCR. Amplified products can be detected using agarose gel electrophoresis which separates DNA molecules by size. Incorporation of a DNA stain (e.g. SYBR Safe^{TM}) into the agarose can be used to visualise amplified PCR products under ultra violet (UV) light. The size of the PCR products can be determined using a DNA molecular marker ladder. These techniques are used for in genetic diagnostics or screening for disease genes, or identifying microbial contamination.

A variation of PCR can also be used to monitor changes in gene expression using RNA as a starting material. However, RNA must first be reverse transcribed into a DNA copy (cDNA) before PCR amplification can take place. This step is carried out by a reverse transcriptase enzyme such as Moloney Murine Leukemia Virus (MMLV), sourced from retroviruses which use these enzymes to integrate their RNA into a hosts DNA. For this reason, PCRs which monitor changes in gene expression (RNA products) are referred to as Reverse Transcription-PCR (RT-PCR). Prior to cDNA synthesis, it is necessary to isolate good quality RNA from the cell sample using RNA extraction methods.

1.5.3.1 RNA extraction

Early methods for RNA extraction were developed in the late 1960's using protein denaturants such as guanidinium thiocyanate and guanidinium chloride. In 1979, John Chirgwin discovered that RNA could be isolated from cells by homogenisation with guanidinium thiocyanate (a potent protein denaturant) followed by ethanol precipitation

or ultra centrifugation through a caesium chloride cushion (Chirgwin et al., 1979). However ultra-centrifugation took many hours and in 1987 the method was superseded by a single-step RNA isolation using acid Guanidinium Thiocyanate-Phenol-Chloroform (Chomczynski and Sacchi, 1987). During this procedure, total RNA remains in the upper aqueous phase, while most of DNA and proteins are held in the interphase or in the lower organic phase. Recovery of RNA from the aqueous phase is achieved by precipitation with isopropanol.

Despite its improvements on early extractions methods, the single-step RNA extraction method remains time consuming and in recent years high throughput spin column extraction kits were developed for clean RNA extraction in just 30 minutes from small amounts of starting material. The spin column uses glass fibres to bind nucleic acid within the column. Cells are lysed in a high concentration guanidinium salt solution (Chomczynski and Sacchi, 1987), followed by a dilution with ethanol (molecular grade), making the RNA competent for binding to the glass fibres. Once bound with RNA, glass fibres can then be washed, removing contaminants before eluting the RNA (Qiagen and Ambion Inc). It is essential that glass fibres are washed efficiently to avoid carry through of the protein denaturants used in extraction which would inhibit reverse transcriptase activity. In recent years, the use of on-column RNA extraction methods has increased due to their speed of process and quality of extraction (Christopher-Hennings et al., 2006; Mack et al., 2007).

Due to the similarity of DNA and RNA structure, small amounts of genomic DNA (gDNA) are frequently carried over in RNA preparations. Contamination by gDNA can interfere with downstream RT-PCR amplifications and skew data and must therefore be removed from the RNA preparation. DNA can be removed using DNase, which selectively targets and degrades DNA within a sample. This has proven to be highly effective in purifying RNA preparations; however, it must be carried out with caution. DNase is most commonly sourced from the bovine pancreas which also contains RNases (Moore and Stein, 1973). Whilst great care is taken during manufacture of DNase it is difficult to ensure complete removal of trace RNases. During RNA purification, insufficient DNase exposure will not remove all gDNA whilst prolonged exposure can also result in RNA degradation. Purification must therefore be rigorously controlled to ensure standardisation of DNase exposure across all samples.

1.5.3.2 RNA quantification

Following extraction the RNA concentration can be quantified using a spectrophotometer. Both RNA and DNA absorb UV light with an absorption peak at 260 nm wavelength. Highly concentrated RNA/DNA solutions absorb more light. A shorter path length on the Nanodrop ND-1000 spectrophotometer (Nanodrop®) compared with a standard spectrophotometer, means that the Nanodrop can quantify RNA that is 50 times more concentrated than a standard spectrophotometer. Just 0.5 µl RNA is required for quantification, thus reducing sample wastage. Spectrophotometer quantification does not take account of any other nucleic acid forms (gDNA, rRNA and tRNA etc) which will be part of the RNA fraction (Vandesompele et al., 2002). It must therefore be assumed that the quality and composition of RNA is consistent between preparations.

1.5.3.3 Primer design

A PCR uses gene specific primers to amplify a transcript (Saiki et al., 1988). It is essential to use primers which have been carefully designed to specifically target the correct gene of interest, and if necessary, a specific isoform of that gene. There are a number of genes which encode a range of different protein isoforms; including OCT4 (Section 1.9.1). In cases where different isoforms are expressed in different tissue, poor primer design can give misleading data on a population of cells.

One of the main complications for gene expression analysis using RT-PCR is the interference of contaminating genomic DNA (gDNA), when amplifying from cDNA. All hESCs from the same initial seed stock contain identical gDNA sequences; however expression of the mRNA will vary between cells, altering the protein content of the cell, depending on the developmental stage or external conditions.

Genomic DNA comprises coding and non-coding sequences. The coding regions are referred to as exons, which are separated by introns (regions of non-coding DNA). During transcription, the non-coding intron regions are spliced from the molecule, generating mRNA comprising entirely coding sequence, as reviewed by (Watson et al., 2008). Therefore gDNA can be distinguished from mRNA by PCR using primers located in alternate exons. In this case, the amplified gDNA product will encode both exons and introns, generating a larger product than the corresponding cDNA. Alternatively, if the nucleotide sequence is suitable, primers can be designed to sit across exon-exon junctions and will

only amplify from cDNA where the complementary sequence for primer binding has been brought together by transcription.

Primers should be designed with non-complementary 3' ends to prevent formation of primer-dimers or self annealing. They are usually 20 bp in length, which ensures specificity for the target sequence (Cha and Thilly, 1993). However, repeating sequences for many genes, especially those which are constitutively expressed such as GAPDH, are present throughout the genome (Zhang and Gerstein, 2003). Usually only a single copy encodes for mRNA, the others have usually inherited mutations which prevent their transcription, these are known as pseudogenes (Vanin, 1985). On occasion, pseudogenes share a high degree of nucleotide similarity to their true gene nucleotide sequence and may vary by only a single base pair. Pseudogenes most commonly retain the intronic sequence and so are easily excluded from analysis using cDNA sequence specific primers. However, in some cases the mRNA nucleotide sequence has been retrotransposed back into the gDNA without introns, generating a non-coding pseudogene with a nucleotide sequence which matches that of the mRNA. These types of pseudogene are referred to as processed pseudogenes and are highly conserved through evolution (Vanin, 1985). In genes with pseudogene copies, accurate BLAST and sequence alignments are especially important to ensure primer sequences are designed to incorporate any variations in sequence for cDNA specific amplification.

For a pseudogene to become established in a population, it must be inherited into the germ line (Pain et al., 2005). The likelihood of this happening is far higher in an embryonic cell prior to tissue specification, or in cells of the germ lineage, rather than in a somatic cell. Pluripotency genes are expressed by cells in the early blastocyst at very high levels and are therefore more likely to become established in a population following retrotransposition (Pain et al., 2005). It has therefore been suggested that the retrotransposition frequency of genes involved in pluripotency is greater than in non-pluripotency genes (Pain et al., 2005). There are 11 currently identified Nanog pseudogenes, which carry up to 97% nucleotide sequence similarity to the functional Nanog gene and 6 pseudogenes for OCT4 (Fairbanks and Maughan, 2006; Liedtke et al., 2007). In combination with their numerous isoform the presence of pluripotency pseudogenes creates additional confusion for gene expression analysis (Booth and Holland, 2004; Fairbanks and Maughan, 2006; Liedtke et al., 2007; Liedtke et al., 2008).

1.5.3.4 Quantitative-PCR

The use of RT-PCR is ideal for investigating which genes are actively transcribed but it is not able to quantify changes in expression relative to a reference sample. Throughout differentiation, genes are not only switched on and off but are also up and down regulated. Using quantitative PCR (Q-PCR) it is possible to determine how much of the gene is being expressed and gives an indication of the proportion of a population which are expressing the gene of interest (GOI). There are two methods for quantifying changes in gene expression: absolute or relative quantification. Absolute quantification gives a true value of the active copy number of an expressed gene, relative to a standard of known concentration. Relative quantification relates the signal of the target transcript in a treatment group to that of another sample such as an untreated control (Livak and Schmittgen, 2001).

Relative abundance can be calculated using the formula ($2^{-\Delta\Delta Ct}$) where the fold change in gene expression is calculated between a calibrator and the gene of interest (Livak and Schmittgen, 2001). During differentiation studies, gene expression levels at day zero are usually used as the calibrator.

A cycle threshold (Ct) value is the number of PCR cycles required for the fluorescence to reach an assigned threshold level for detection, this is usually when the log phase of amplification begins. This value can be inversely correlated to the amount of nucleic acid template in the reaction (Walker, 2002). A delta Ct (ΔCt) value is the difference in cycle number between the Ct value of the calibrator and the Ct value of the sample of interest. In order to account for variation in sample loading, a $\Delta\Delta$Ct value is calculated, which is the calculated difference between the ΔCt of the GOI and the ΔCt of the endogenous control gene.

For an untreated control sample the $\Delta\Delta$Ct value equals zero, and since 2^0 equals one, the fold change in gene expression relative to the untreated control is also one. For treated samples, calculation of $2^{-\Delta\Delta Ct}$ indicates the fold change in gene expression relative to the untreated control (Livak and Schmittgen, 2001).

Recent advances in gene expression analysis have seen the release of high throughput gene expression screening tools in the form of low density arrays. These arrays simultaneously analyse expression of a large number of genes. In 2003 the MRC set up an International Stem Cell Initiative (ISCI) to explore and compare the characteristics of different hESCs at a cellular and molecular level (Andrews et al., 2005; Adewumi et al., 2007). As part of this

study, the gene expression profile of 96 different genes across 59 hESC lines was carried out using a 'Human pluripotency panel' (Applied Biosystems™, California, USA). This array was designed to analyse six endogenous control genes for standardisation in addition to 90 different genes involved in pluripotency and differentiation from a single sample. Use of these cards enabled standardisation between laboratories and greatly reduced the volume of samples and time required for analysis. Alternative array cards have since been developed for gene expression analysis of definitive germ lineages by ABI and alternative suppliers (Anisimov et al., 2007).

Following on from the comparison of hESC lines at the level of gene and protein expression, the second phase of the ISCI (ISCI2) trials are expanding into analysis of the karyotypic stability of different hESC lines under the range of culture conditions adopted by laboratories worldwide. One of the main variables in hESC culture worldwide is the process by which hESCs are passaged. There are two typical methods which can be adopted for passaging hESCs; mechanical passaging, whereby the hESCs are placed under a dissection microscope and manually cut and replated onto a fresh culture surface, or enzymatic passaging which is commonly used in alternative adherent cell culture lines, cleaving the bonds between hESCs and the culture surface.

1.6 Neurodegenerative disease

Neurodegenerative diseases are caused by the progressive loss of function of cells within the nervous system, affecting motor control and/or cognition. Neurodegenerative disease can result from depletion of a small single neuronal population e.g. Parkinson's disease, or from wide spread loss of neural populations throughout the nervous system e.g. multiple sclerosis. In other cases such as Alzheimer's disease, the cause is less distinct and symptoms can occur as a result of multiple cell types at a range of locations. In each case, the causes and symptoms can vary, making a target therapy more challenging.

1.6.1 Alzheimer's disease

Alzheimer's disease is the most common form of dementia, occurring mainly in the elderly population affecting 1 in 14 people over the age of 65 (Alzheimer's Society, 2009). Incidence has increased significantly over recent years due to prolonged life expectancy and is predicted to continue over future years (Alzheimer's Society, 2009). There is no

single cause identified for Alzheimer's disease; however, progression is linked to the formation of plaques within the brain (Urbanc et al., 1999). Unlike the other common forms of neurodegenerative diseases, motor function remains intact in Alzheimer's patients who instead lose cognitive ability. A patient may live for many years suffering complete loss of memory and recognition, placing pressure on caregivers and the healthcare system to provide continued support. Subsequently Alzheimer's disease is thought to become one of the largest costs to the healthcare system from a single disease.

1.6.2 Huntingdon's disease

Huntingdon's disease (HD) is a genetic neurodegenerative disease caused by a mutation in the *huntingtin* gene resulting in a mutated form of the Huntingtin protein. This protein gradually damages areas within the brain and a HD patient loses motor control characterised by jerky movements and signs of dementia. Symptoms of HD do not usually appear until middle age but on occasion have presented in early childhood (Vargas et al., 2003). There is currently no cure for HD but future therapies are aimed towards improving symptoms and slowing disease progression. A HD patient will eventually die from suffocation, due to loss of control over the airways (Walker, 2007).

1.6.3 Amyotrophic lateral sclerosis

Amyotrophic lateral sclerosis (ALS) is a neurodegenerative disease which specifically targets motor neurons in the CNS. ALS is often referred to as Lou Gehrig's disease after the first diagnosed patient in 1939, which results in loss of motor control and as the disease progresses, muscle sparing and atrophy due to loss of innervations. The exact causes of ALS are unclear although in a number of patients, symptoms have been linked to a mutated form of the superoxide dismutase (SOD1) gene which plays a role in neuroprotection of motor neurons (Patel et al., 2002). In many patients, disease is sporadic with no current identifiable cause. In most cases, sensory neurons remain intact so a patient remains able to see, smell, taste, hear, feel and touch. The disease does not directly affect a patients mind; however, as the disease progresses patients frequently suffer depression from the distress of poor motor control. Symptoms can occur rapidly or gradually and most patients die as a result of loss of airway control.

1.6.4 Parkinson's disease

Parkinson's disease (PD) is primarily caused by the loss of A9 dopaminergic (DA) neurons from the substantia nigra region of the brain. Deterioration of this cell pool results in decreased dopamine synthesis and subsequent impairment or loss of motor function. Parkinson's disease affects over 4 million people worldwide (Anderson and Caldwell, 2007). Dopamine is unable to cross the blood-brain barrier so current PD therapies administer L-DOPA for conversion to dopamine *in situ*. Loss of therapeutic efficacy is in part caused by the inability to produce sufficient dopa decarboxylase for dopamine synthesis (Lloyd and Hornykiewicz, 1970). Transplantation of dopaminergic neurons back into the substantia nigra for synthesis of dopamine on demand is the focus of investigation for PD cell therapies. The relative simplicity in replacing just a single defective cell type means that cell transplantation is a realistic future approach for therapy.

1.7 Regenerative medicine

In a healthy being, tissue regeneration occurs continuously to repair damaged tissue after injury. 'Guardian type' cells are constantly surveying the body for damaged and diseased cells, maintaining healthy tissues. Even in the absence of injury, these cells ensure replacement of old worn out tissue; however as the body ages or during disease, the ability for regeneration becomes increasingly limited, resulting in tissue degeneration. The use of stem cell therapy for the treatment of disease is known as regenerative medicine which is an expanding area of scientific research.

Over the past 15 years, a range of regenerative therapies have come to market. 'Regenerative medicine' is an umbrella term for a range of treatments which induce or encourage regeneration of damaged or diseased tissue. Treatments might include growth factors, cell-based therapies or tissue engineering of a replacement tissue/organ.

Some of the first regenerative medicine products were growth factors: erythropoietin (EPO), granulocyte-colony stimulating factor (G-CSF) and keratinocyte growth factor 2 (Repifermin) which were applied to the damaged tissue to induce the body to self-repair (Petit-Zeman, 2001; Sebald, 2002). In 1995 the first cell therapy for repair of damaged cartilage using chondrocytes (Carticel®) was developed (Genzyme Inc, Massachusetts, USA) and in 1998 the first tissue engineered skin graft comprising dermal and epidermal tissue

(Apligraf®, Organogenesis Inc, Massachusetts, USA) was approved by the FDA for the treatment of patients with severe burns or persistent venous leg ulcers.

The major limitation for tissue engineering is the supply of nutrients, and removal of waste products from cells embedded within a solid matrix, without exposure to larger molecules such as immune complexes for tissue rejection (Langer and Vacanti, 1993). In April 2006 an expandable bladder-like replacement was artificially created as a major step forward in the field of tissue engineering of larger organs (Atala et al., 2006). In 2008, tissue engineering of a tracheal replacement for a damaged airway in a patient suffering bronchomalacia (Macchiarini et al., 2008), again emphasised the increasing success of regenerative medicines for treatment of disease and improved quality of life.

There is currently no routine cell therapy for the treatment of neurodegenerative diseases; however, early studies using transplantation of foetal derived brain tissue, containing neural precursors into the brain of a PD patient confirmed their proof of principal (Lindvall et al., 1988; Piccini et al., 2000). These studies demonstrated integration of graft cells into the host brain and partial recovery of motor control, following transplantation (Lindvall et al., 1988; Lindvall et al., 1989; Piccini et al., 1999). Despite this, supply of healthy foetal tissue is highly restricted and the yield of cells from a single donor is insufficient for a successful therapy, thereby requiring expansion of the neuronal population prior to transplantation. Unfortunately, neural precursors subsequently lose their ability to differentiate following *in vitro* expansion (Chung et al., 2006), demonstrating the need for an alternative source of neurons for therapy.

The ability of pluripotent stem cells to generate any cell type of the body makes them ideal targets for use in regenerative cell therapies, since a single source of cells could theoretically be infinitely expanded and committed into a vast arrange of cell types as and when required.

1.8 Commercialisation

In producing a cell therapy it is necessary to consider both the feasibility of production, the economic viability of manufacture and the overall requirement for therapy. For commercial success a therapy must produce consistently large numbers of cells in a reliable and reproducible process, within a time frame which is suitable for therapy.

Many of the limitations for regenerative medicine are in sourcing sufficient cells for treatment. Adult and foetal stem cells have limited capacity for expansion *in vitro* and subsequently require large volumes of donor tissue for a single therapy. When using progenitor cells for transplantation, it is essential to ensure that the phenotype of transplanted cells is consistent with no risk of uncontrollable proliferation or differentiation into an undesirable population (i.e. development of bone tissue in neural cell transplantation). For this reason, regenerative medicine is an interdisciplinary field, combining biological scientists with engineers to bring about scaled-up production of cells in a quality controlled manner for both small scale (autologous) and large scale (allogeneic) therapies.

Stem cells are not well adapted for scaled up culture. Human ESCs (Section 1.9) are most commonly passaged mechanically using manual cutting tools. However, mechanical passaging is a slow process which is undesirable for large scale production. Large stirrer vessels can be used for scaled up production of suspension cell cultures; however, hESCs grow as adherent monolayers. Addition of hESCs into stirred suspension culture vessels results in poor cell growth and high levels of cell agglomeration and differentiation (Section 1.5) (Dang et al., 2002).

The use of enzymatic passaging in hESC culture facilitates larger scale production in combination with a range of microcarriers are under investigation for increased culture surface for scaled-up monolayer culture. Equally, facilities for automated culture of hESCs have been developed for automated scaled-up production of hESCs (CompacT SelecT; the automation partnership) (Thomas et al., 2008). However, these facilities are yet to prove successful for therapeutic applications due to heterogeneous growth of hESCs on microcarriers and the inability to maintain prolonged passaging under controlled conditions. Despite this, the use of automated cell culture will undoubtedly be the future for standardised routine expansion or differentiation of hESCs for use in cell therapy once conditions have been optimised.

1.9 Embryonic stem cells

Embryonic stem cells (ESC) are pluripotent cells, which can generate all of the cell types within a developing embryo. These cells were first characterised following isolation of the ICM from a blastocyst stage mouse embryo in 1981, and were later shown to be capable to differentiating into a range of mature tissue types *in vitro* (Evans and Kaufman, 1981; Martin, 1981). The definitive criteria for a ESC line include: derivation from the pre-implantation embryo, prolonged undifferentiated proliferation, and stable developmental potential to form derivatives of all three embryonic germ layers even after prolonged culture (Thomson *et al.*, 1995). Some 18 years later, the first human ESCs (hESC) were derived, which demonstrated comparable capabilities for *in vitro* differentiation (Thomson *et al*, 1998). In the years following derivation, a range of signature characteristics of hESCs were compiled, including expression of typical markers found to be associated with pluripotency (Table 1.1).

1.9.1 Markers of pluripotency

Cellular markers can be either internal or surface proteins and are used to identify a population of cells. Transcription factors such as: NANOG, Octamer binding protein-4 (OCT4), and SRY-box 2 (SOX2) have been shown by various research groups to be essential for promoting self-renewal and pluripotency of ESCs (Nichols et al., 1998; Chambers et al., 2003; Mitsui et al., 2003; Avilion et al., 2003). Over or under expression of any one of these transcription factors results in differentiation (Niwa et al., 2000; Hyslop et al., 2005). These transcription factors interact directly with DNA targets for each other and for additional genes which are also highly expressed in pluripotent cell populations including: TDGF1, UTF1, FGF4, REST, DPPA4 and EBAF/LEFTY2 (Okuda et al., 1998; Ambrosetti et al., 2000; Boyer et al., 2005; Levine and Brivanlou, 2006; Babaie et al., 2007; Johnson et al., 2008). Co-occupancy of OCT4, SOX2 and Nanog at their target genes determines the activity of auto-regulatory feedback loops involved in retaining pluripotency (Boyer et al., 2005). As such these three genes are thought to be the master regulators of pluripotency.

The use of these transcription factors in characterising a pluripotent population must be undertaken following an understanding of their gene expression profile. In 2006, alternative splice variants of the OCT4 protein were identified in culture (OCT4A, OCT4B and OCT4B1), each with different expression patterns across different cell populations (Cauffman et al., 2006). Expression of the OCT4A isoform is detectable in hESC and EC

populations; however, OCT4B is located in the cytoplasm of non-pluripotent cells and is therefore likely to have an alternative role in cellular function (Atlasi et al., 2008). On further investigation, the OCT4B1 isoform was identified as nucleus specific, expressed only in pluripotent cells and has been shown to be down regulated following differentiation (Atlasi et al., 2008). Prior to identification of the various OCT4 isoforms, early pluripotency studies used antibodies raised towards all OCT4 splice variants, raising concerns over the validity of these results generated during historical differentiation studies. This example clearly highlights the need for further research in the field of pluripotency regulation, and a detailed understanding of different protein isoforms when used for population identification.

It is the complex interactions between OCT4, SOX2 and Nanog which retain a cells pluripotent state; however, SOX2 has also been shown to play a role in neurogenesis by regulating self renewal and differentiation of neural precursors (Graham et al., 2003; Episkopou, 2005)

Additional markers have been identified in pluripotent populations which are down regulated during differentiation (Table 1.1), these include a range of cell surface antigens: stage specific embryonic antigen-3 (SSEA3) and SSEA4, trafalgar-antigen-1-60 (Tra-1-60) and Tra-1-81, and enzymes: alkaline phosphatase and telomerase reverse transcriptase (TERT) (Thomson et al., 1998; Cowan et al., 2004; Adewumi et al., 2007).

Marker	Location	Description
SSEA3	Cell surface	Globoseries membrane bound glycolipid
SSEA4	Cell surface	Globoseries membrane bound glycolipid
Tra-1-60	Cell surface	Keratin sulphate associated antigen
Tra-1-81	Cell surface	Keratin sulphate associated antigen
OCT4	Nucleus	Transcription factor
SOX2	Nucleus	Transcription factor
Nanog	Nucleus	Transcription factor

Table 1.1. Human embryonic stem cell markers.
Expression of these markers were identified in the first hESC line derived and are used as signature markers for all pluripotent hESC lines.

The loss of pluripotency and the gain of neuron specific markers can be used to track a cells progress through differentiation. In this way, changes in marker expression can be used to

monitor the efficiency of differentiation and compare cell populations. Changes in the expression of these markers can be detected using immunocytochemistry, with fluorescently conjugated antibodies towards a specific epitope to identify the presence of the marker protein. Fluorescently labelled cells can be quantified using flow cytometry analysis or imaged using epi-fluorescence or confocal imaging, these tools help to build up the phenotypic profile of a population of cells. In addition to fluorescently conjugated antibodies, a number of hESC lines have been transfected with green fluorescent protein (GFP) conjugated to a promoter which is placed under the control of specific pluripotency genes (Singh Roy et al., 2005; Gerrard et al., 2005b; Wernig et al., 2007). By combining with bright field and epi-fluorescence imaging, the GFP expressing cell lines are proving to be excellent tools for observing changes in cellular behaviour *in situ*. Using this principal, changes in gene expression can be observed using long term live cell imaging, generating a wider picture of cellular behaviour and response to cell culture conditions. The additional benefits of live cell imaging have been described in detail in Chapter 6.

Whilst a number of key markers for pluripotency have been characterised, the factors which control their expression are less well understood. Under suboptimal culture conditions, hESCs lose expression of these markers and begin to differentiate. This would seem to be a logical process, since cells of ESC morphology are only transient in the developing embryo and quickly commit into a developmental pathway for embryogenesis. To retain the pluripotent state of these cells *in vitro*, it is necessary to block this natural progression to differentiate. Retention of pluripotency in hESCs is achieved using co-culture with a mouse fibroblast feeder cell layer.

1.9.2 Feeder layers

The co-culture of ESCs with feeder layers to retain pluripotency has been used since the derivation of the first mouse ESCs (Evans and Kaufman, 1981). The feeder layers for hESC culture, most commonly comprise mouse embryonic fibroblasts (MEFs), which secrete growth factors into the media and extracellular matrices onto the culture surface which work to sustain pluripotency amongst hESCs. Although not yet fully defined, many of these secreted factors have been identified, examples include: basic fibroblast growth factor (bFGF/FGF2), transforming growth factor-β2 (TGF-β2), extracellular matrix (ECM) proteins (type IV collagen, laminin and fibronectin), Wnts, BMP/TGF-β1, activin/Inhibin, and insulin-like growth factor-1 (IGF-1) (Alitalo et al., 1982; Moscatelli et al., 1986; Amit et al., 2004;

Wang et al., 2005a; Chen et al., 2006; Prowse et al., 2007; Villa-Diaz et al., 2009). To prevent the overgrowth of hESCs by the feeder layer, iMEFs are mitotically arrested by γ-irradiation or Mitomycin C which prevents MEF proliferation whilst retaining their metabolic activity (Roy et al., 2001; Conner, 2001).

Despite a loss of proliferative capacity and a subsequently reduced lifespan of the iMEFs, the use of cross species co-culture systems, raises concern over cross-species contamination of hESCs. These concerns were supported when murine sialic acids which had integrated into the membrane of hESCs were identified (Martin *et al.*, 2005). With this in mind, the likelihood of using hESC lines co-cultured with MEFs in therapeutic treatment is poor. However, their incorporation into hESC studies has generated considerable data covering behaviour and differentiation of hESCs and the affordability of using this co-culture system maintains their existence in hESC research.

With a view for therapeutic application, focus shifted towards the growth of hESCs in the absence of MEF layers. Initial studies using human dermal fibroblast feeders reported success in retaining pluripotency (Richards et al., 2002; Amit et al., 2003; Choo et al., 2004); however, even same species feeder layers do not negate all risk of human viral transmission creating additional problems for risk management and licensing in therapeutic applications.

Feeder-free hESC culture was subsequently achieved using MEF conditioned media supplemented with bFGF on a Matrigel™ coated surface (Ludwig et al., 2006a). Basic FGF is regularly supplemented into hESC culture media both in the presence and absence of iMEFs, to improve clonal efficiency and prolonged pluripotent cell culture by inhibiting BMP induced differentiation (Amit et al., 2000; Xu et al., 2005; Levenstein et al., 2006). However, Matrigel™ is a gelatinous protein matrix secreted by mouse tumour cells (Kleinman et al., 1982; Kleinman and Martin, 2005), and its use in combination with MEF conditioned media retains the exposure to animal derived products in hESC culture, thereby maintaining a risk of cross-species contamination.

The first hESC line which was entirely free from animal products was derived in 2006 (Ludwig et al., 2006a). These cells were cultured on a matrix of human derived collagen IV, fibronectin, vitronectin and laminin, in a synthetic media (TeSR1) containing a cocktail of recombinant growth factors known for their involvement in pluripotency; (Section 1.9.3.8) (Ludwig et al., 2006a).

1.9.3 Cell culture media

Different cell lines have different growth requirements which must be accounted for in the choice of media used for culture. In a differentiation study, whereby the cell population is changing, it is important to understand the different growth requirements for each transient cell type and identify the media components which can best provide support. In the case of directed differentiation, a change of media composition can be used to select for the survival of target cell populations.

During early cell culture the conditions required for cell expansion were poorly understood. The first *in vitro* cell cultures, used extracts of natural body fluids for survival and expansion (reviewed by Freshney, 2005). Extensive biochemical analysis of these fluids provided the formulations for artificial cell culture media (Freshney, 2005). In 1955, the formulation for the first defined cell culture media was produced – Eagle's Basal Medium, and subsequent decades saw the development and refinement of this media into a range of media for cell types of varied origin (Eagle, 1955; Freshney, 2005).

1.9.3.1 DMEM

Dulbecco's modification of Eagle's Medium (DMEM) was adapted from earlier media compositions for specific use in mouse fibroblast cultures but has since become a widely used medium for many different cell types (Freshney, 2005). DMEM is a highly nutritious media with twice the amino acid and four times the vitamin concentrations of basic MEM (Freshney, 2005). Most significantly, DMEM contains glucose, a carbon source for glycolysis. A CO_2 atmosphere is required to maintain a balanced pH in most for cell culture media. The presence of pyruvate in the media serves several purposes. Pyruvate is an energy source for rapidly dividing cells, and also enables increased oxidative decarboxylation of H_2O_2 resulting in the production of CO_2 and water; this reduces cellular exposure to reactive oxygen species whilst at the same time reducing the requirement for exogenous CO_2 (Freshney, 2005; Babich et al., 2009).

1.9.3.2 Serum

The continued reliance on natural serum for cell culture results from its as yet undefined composition. As time progresses the factors within serum which are essential for cellular survival and expansion are slowly being identified. In addition to uncharacterised growth

factors, serum contains a range of hormones including insulin which promotes the uptake of glucose and amino acids, which aids fatty acid and glycogen synthesis within the cells. Insulin has been shown to improve the plating efficiency of cells in the absence of serum, but must be supplemented at high concentrations due to its instability at 37 °C (Barnes and Sato, 1980; Freshney, 2005). The presence of fibronectin and fetuin improve cellular attachment and spreading of cells in media containing serum (Freshney, 2005).

Serum also contains iron binding proteins such as transferrin and albumin which carry lipids, minerals and globulins (Barnes and Sato, 1980; Freshney, 2005). These binding proteins stabilise and mop up toxic by-products of cell metabolism: oxygen radicals and peroxidase (Barnes and Sato, 1980). A range of protease inhibitors have also been identified in serum, which aid cell survival following passaging by scavenging proteases or hydrolases released by dead and dying cells (Barnes and Sato, 1980). It is therefore important to change serum-free media regularly and soon after passaging to remove cell debris and inhibitory enzymes from culture.

1.9.3.3 Glutamine/GlutaMAX™

Glutamine is utilised by most cells in culture as a carbon source for metabolism (Freshney, 2005). However glutamine stability at 37 °C is poor, and deamination produces ammonia which is toxic to the cells, limiting growth, requiring regular media changes. The use of synthetic glutamine substitutes such as GlutaMAX™, an alanyl-glutamine di-peptide, which have different break-down pathways has been shown to minimise ammonia accumulation and improve cell survival.

1.9.3.4 Knockout DMEM

The optimal osmolarity required by ESCs for successful culture is lower than that of the common fibroblast cell lines, as was determined from early studies on mESCs (Gonzalez et al., 2007). Knockout-DMEM (KO-DMEM) was developed with a lower osmolarity and bicarbonate content than standard DMEM to suit this ESC requirement. KO-DMEM is usually supplemented with 20 % Knockout™ serum replacement (KOSR) for optimal hESC growth and expansion.

1.9.3.5 KnockOut™ serum replacement

The use of KO-SR became standard in hESC culture following demonstration that the clonal efficiency of hESCs was improved when using KO-SR in place of serum (Amit et al., 2000). KO-SR is a defined product, with a proprietary mixture of reagents which support cell survival (Price Tilkins Goldsborough 1998 Embryonic stem cell serum replacement International patent application WO98/30679). The use of KO-SR reduces variation in hESC culture from the natural variation in foetal bovine serum; however, KO-SR retains transferrin, insulin, BSA and a mixture of other protein and non-protein components of animal origin which mean batch-batch variation is still a likely possibility. Batches of KO-SR must therefore be tested for optimum undifferentiated growth of hESCs before routine culture is carried out. The addition of BSA in this media means it is not animal component-free and therefore not likely to be approved for use in the culture of hESCs for therapy.

In addition to KO-SR supplementation of KO-DMEM, hESC media is supplemented with 2 mM GlutaMAX™ in place of L-glutamine for improved stability, 1 X NEAA, 10 µM β-mercaptoethanol and 4 $ng.ml^{-1}$ bFGF.

1.9.3.6 Non-essential amino acids

In 1955 an experiment was carried out to determine the amino acid requirement for *in vitro* culture of mammalian cells (Eagle, 1955). Mouse fibroblasts were used as the model line which identified 12 essential amino acids (arginine, cystein, histidine, isoleucine, leucine, lysine, methionine, phenylalanine, threonine, tryptophan, tyrosine and valine) and 7 non-essential amino acids (alanine, aspartic acid, glutamic acid, glycine, hydroxyproline, proline and serine (Eagle, 1955)). DMEM media contains all the essential amino acids in addition to serine and glycine (Freshney, 2005). Supplementation of KO-DMEM with non-essential amino acids improves protein synthesis and cellular growth and function.

1.9.3.7 Beta-mercaptoethanol

Beta-mercaptoethanol (β-ME) has been incorporated into embryonic stem cell culture since the first mESC lines were derived (Evans and Kaufman, 1981). It scavenges reactive oxygen species, protecting cells from oxidative stresses.

1.9.3.8 Feeder free media - TeSR1

A number of factors in addition to bFGF are involved in the support of pluripotency, including but not limited to: noggin, TGFβ1, lithium chloride (LiCl), γ-aminobutyric acid (GABA), neurotrophins (Wang et al., 2005a; Amit, 2006; Moore, 2006; Pyle et al., 2006; Ludwig et al., 2006a). In 2006 a defined serum- and animal-free medium was developed, comprising recombinant bFGF, TGF-β, LiCl, gamma-aminobutyric acid, pipecolic acid and human albumin in place of BSA. This media is referred to as TeSR1 (Ludwig et al., 2006a) and is used for hESC derivation and expansion in combination with cell culture surfaces pre-coated with fibronectin, human collagen and laminin for clinical grade lines (Ludwig et al., 2006a). A modified version of TeSR1 was later developed (mTeSR) using animal derived BSA and Matrigel™ to reduce the cost of the defined media, increasing its accessibility in smaller laboratories worldwide (Ludwig et al., 2006b). Although use of mTeSR enables hESC culture in the absence of MEFs, reducing variation and preparation times, the effect of long term culture on mTeSR media remains controversial with question over the karyotypic stability of hESCs after long term mTeSR culture.

1.9.4 Karyology

The existence of pluripotent cells in the developing embryo is only transient, before their programmed commitment into one of the three germ layers. The *in vitro* expansion of pluripotent populations therefore actively inhibits a cells natural progression into differentiation. Long term inhibition of the natural behaviour of a cell will inevitably impact upon internal programming, adapting for survival in what should be considered 'abnormal' conditions. Indeed, many laboratories have reported adaptations which enhance the survival and proliferation of hESCs in the form of karyotypic abnormalities, frequently resulting in additional copies of chromosomes 12, 14, 17, 20 and X (Cowan et al., 2004; Rosler et al., 2004; Draper et al., 2004a; Mitalipova et al., 2005; Catalina et al., 2008). Additional copies of these chromosomes, or the genes within them, have been associated with uncontrollable proliferation in tumours, especially trisomies for 17q (Petty et al., 1996; Plantaz et al., 1997; Glukhova et al., 1998; Katoh et al., 2005; Kasamatsu et al., 2005; Choi et al., 2006). The frequent occurrence of these reported instabilities is of high concern for the incorporation of hESCs into regenerative therapies, for fear of tumour formation following transplantation (Buzzard et al., 2004a). As such, karyotypic analysis of hESCs is rapidly becoming a routine part of hESC culture, and is frequently questioned in the event of unexpected behaviour.

The cause of karyotypic alterations is the subject of debate but are thought to be influenced by a range of factors including: the age of the hESCs, the choice of cell line or the adaptation to feeder-free culture (Buzzard et al., 2004a; Draper et al., 2004a; Catalina et al., 2008). In addition, the methods applied during routine passaging and expansion of hESC have also been targeted as a possible instigator of karyotypic instability (Buzzard et al., 2004a; Mitalipova et al., 2005). Following initial derivation of hESCs, mechanical passaging whereby cells are transferred to fresh culture in clusters, has proven to be efficient at retaining karyotypic stability (Buzzard et al., 2004a; Mitalipova et al., 2005); however, it is highly labour intensive and as such is not amenable to large scale hESC culture.

Enzymatic passaging was incorporated into hESC culture to facilitate hESC expansion; however, these reagents function by cleaving cell-cell bonds, frequently dissociating cell layers into single cell suspensions. The result of which is thought to reduce cross-talk amongst hESC populations, and induce the accumulation of mutations which facilitate survival under these conditions. Not all publications indicate gross karyotypic abnormalities following enzymatic passaging (Catalina et al., 2008; Thomson et al., 2008); however, it is possible that the reasons for this may be due poor detection of small abnormalities rather than an absence of their occurrence. More recently, small alterations in chromosome content amongst hESC lines previously reported as 'normal' have been identified using array Comparative Genomic Hybridisation (aCGH) (Thomson et al., 2008). Array CGH detects changes in copy numbers of small DNA nucleotide sequences. The use of this technique in hESC culture enables the detection of small gains or deletions in DNA to an accuracy of 100 kb, thus providing a more accurate report of a cell line's karyotype (Shinawi and Cheung, 2008). It should be noted that, aCGH does not detect chromosomal translocations, therefore serves as a supplement to G-banding analysis rather than a replacement. The effect of karyotypic instability on the behaviour of hESCs following differentiation is a largely unexplored area, and is investigated in more detail in later sections.

1.9.5 UK Stem Cell Bank (UKSCB)

In 2003 the Medical Research Council (MRC) and Biotechnology and Biological Sciences Research Council (BBSRC) funded the establishment of the UK Stem Cell Bank (UKSCB) at the National Institute for Biological Standards and Control (NIBSC; Potters Bar, UK); the

UKSCB holds master stocks of all stem cell lines (adult, foetal and embryonic) for use in stem cell research and therapeutic applications. Under HFEA and HTA regulations, every newly derived hESC line must be deposited with the UKSCB, for banking and characterisation under strict quality control (QC) procedures. In this way, a consistent source of stem cells is available for comparative research between laboratories (Healy et al., 2005).

Regulations by the human fertilisation and embryology authority (HFEA) and human tissue authority (HTA) stipulate that hESC lines may only be derived from embryos which are surplus to requirements following IVF treatment, which have been donated with parental consent and would otherwise be destroyed. However, the fact remains that the generation of hESC lines ultimately results in the destruction the embryo which has ethical implications. Advances in the hESC line derivation from single cells and the genetic reprogramming of somatic cells, to an induced pluripotent state (iPS cell) for subsequent directed differentiation, may reduce future reliance upon the embryo (Takahashi and Yamanaka, 2006; Takahashi et al., 2007). However, reprogramming currently relies upon retroviral transduction which has been shown to induce tumour formation in a murine model following incorporation into a developing blastocyst (Klimanskaya et al., 2006; Okita et al., 2007). Whilst this may be a promising avenue for generating large numbers of patient specific cells for therapy with limited ethical restriction, it is likely to be many years before reprogramming meets the safety regulations required for routine therapy.

1.10 Adult stem cells

An adult stem cell is an undifferentiated cell found in a differentiated tissue, capable of self-renewal and differentiation into specialised cell types. Adult stem cells have been discovered in a range of tissues in the body including bone marrow, cord blood, brain, intestinal tract, eye, liver, skin (Knudtzon, 1974; Potten and Loeffler, 1990; Weiss et al., 1996; Alonso and Fuchs, 2003; Limb et al., 2006) and there are likely to be many more yet to be discovered. Mesenchymal stem cells are probably the most well characterised adult stem cells, and can be used for the derivation of hematopoietic and non-hematopoietic cells, such as bone, cartilage, muscle and neural cells (Pittenger et al., 1999). Umbilical cord stem cells derived shortly after birth, can be used for bone marrow therapy in place of adult bone marrow. Adult stem cells have a defined expansion capacity and more limited

scope for differentiation when compared to pluripotent hESCs, limiting the number of applications for which a single sample can be applied.

1.11 Embryonal Carcinoma cells

Most of the current understanding of hESC culture derives from more than three decades of research on an alternative source of pluripotent cells, isolated from germ cell (GC) tumours which contain a haphazard array of differentiated cell types. These tumours are known as teratocarcinomas and occur most commonly in the testis and ovaries, although have been identified in alternative anatomical sites including the base of the spine (Andrews et al., 2001). In some cases these tumours are benign and can be removed without complication; however, if these tumours retain an uncommitted proliferating population of cells they often become malignant. The stem cells within these tumours were originally identified in 1964 and termed 'embryonal carcinoma' (EC) cells due to their apparent recapitulation of embryonic-like development within the tumour, generating an array of distinct cell types (Kleinsmith and Pierce, 1964).

Perhaps a symptom of the tumour origin of these cells, EC cells often gain and lose chromosomes over time in culture and are subsequently aneuploidy in nature. This may pose a problem when considering the use of hEC cells for therapy, for fear of tumour formation. Early trials from transplantation of hEC derived post mitotic neurons into the infracted site of the brain in stroke patients, showed cellular integration with no signs of tumour formation, in the 2 years following transplantation (Kleinsmith and Pierce, 1964; Nelson et al., 2002). Despite this result subsequent little investigation has been carried out into the incorporation of hEC derived cells into transplantation therapies, likely to be a result of fear from the unknown, and prevention of any possible deleterious side effects.

Many hEC cell lines maintain similar morphology to hESC lines, and are often easier and less expensive to culture, without ethical restrictions on their use. In alignment with their similarity to embryonic development, hEC cells are an excellent facility as a model for neurogenesis *in vitro*.

1.11.1 2102Ep

The 2102Ep cell line was derived from a testicular teratocarcinoma in 1980 (Andrews et al., 1980; Andrews et al., 1982). This cell line stably expresses the typical markers of pluripotency (Section 1.9.1) but responds poorly to differentiation stimuli (Matthaei et al., 1983). If consistently grown at low cell density, initial signs of differentiation can be observed (Andrews et al., 1982), although cultures can be readily recovered into a pluripotent state over time. The inability to successfully differentiate this line makes its incorporation into any cell therapy risky for fear of tumour formation. However, the likeness of hEC cells to hESCs in appearance and expression of pluripotency markers makes it a useful research tool as control line for studies into pluripotent hESC behaviour. Indeed the 2102EP hEC cell line was used as a control in a large scale comparative study of hESCs by the International stem cell initiative (Section 1.5.3.4; (Adewumi et al., 2007)).

1.11.2 NTERA2

NTERA2 is an alternative hEC cell line to 2102EP. The origin of NTERA2 dates back to 1975 when the predecessor cell line TERA2 was derived from a testicular germ cell tumour (Fogh and Trempe, 1975). In 1984 the TERA2 line was passaged through an athymic (nude) mouse, generating a tumour containing cell types from all three germ layers (Andrews et al., 1984). Subclones of the proliferating population of this tumour were later created in culture and to date the most common clone used in research is NTERA2.Cl.D1. Similarly to the 2102Ep cell line, undifferentiated NTERA2 can be continually expanded in culture and express common markers of pluripotency (Section 1.9.1), which are down regulated during differentiation (Andrews et al., 1996; Andrews et al., 2001).

The NTERA2 cell line presents a highly variable karyotype, which might be expected when reminded of its tumour origin. Early publications from the sourcing laboratory (Professor. P. Andrews, University of Sheffield) published a modal hyper-tetraploidy 63 XY karyotype including a translocation of the terminal arm of chromosome 1 (q23-qter) onto chromosome 9, in addition to the presence of a marker chromosome t(12;13)(q13;qter) in all cells (Andrews et al., 1984; Duran et al., 2001). In addition to the tumour origin, the many years of adaptation into *in vitro* culture across worldwide laboratories, is likely to have further contributed to additional karyotypic abnormalities.

Directed differentiation of the NTERA2.Cl.D1 subclone has shown that these cells readily differentiate into an array of different cell types, in response to hexamethylene bisacetamide (HMBA), bromodeoxyuridine (BUdR) and members of the BMP family of signalling molecules (Andrews et al., 1990; Andrews et al., 1994). However, since the discovery that all-*trans*-retinoic (ATRA) induces neuronal differentiation in EC cell lines (Jones-Villeneuve et al., 1982), NTERA2 has been used extensively in research towards understanding neurodegeneration and neurogenesis.

The NTERA2.Cl.D1 sub clone has been shown to lack many of the genes involved in the nodal signalling pathways (Schwartz et al., 2005) which are essential for the differentiation of mesodermal and endodermal derived cell types (Pfendler et al., 2005). This would suggest that the neuroectodermal lineage is the favourable option for NTERA2 differentiation and might explain why neurons are the predominant identifiable cell types within differentiated NTERA2 cells. For this reason the NTERA2 hEC cell line is an excellent starter line for understanding neuronal differentiation from pluripotent cell lines.

1.11.3 Screening for neuronal functionality

Neuronal functionality is not guaranteed by the ability to produce neurotransmitters, or by the presence of receptors for transmitters in the plasma membrane but rather by the behaviour of the neuron upon neurotransmitter binding. The functionality of neurons can be tested using techniques such as patch clamping and calcium imaging.

1.11.3.1 Patch clamping

The patch clamp technique was developed in 1976 by Bert Sakmann and Erwin Neher (Neher et al., 1978), revolutionising studies of cellular physiology by enabling the study of membrane bound ion channels. The method uses a fine glass capillary which is placed close to the membrane of the cell. Suction is usually applied to the capillary drawing the membrane and capillary into a seal, usually in the gigaohm (GΩ) range, referred to as a GΩ seal. For whole cell patching, where the behaviour of the entire cell rather than an individual ion channel is recorded, further suction may be applied to break the cell membrane. To prevent dialysis of the cell, the capillary tube is filled with a fluid roughly matching the composition of intracellular fluid. A fine electrode is located within the glass capillary and is able to transmit a current into the cell to alter its polarity. By controlling

the polarity of the cell, it is possible to monitor for the presence and activity of ion channels in the membrane. Patch clamping can be performed using either current clamp or voltage clamp modes.

Current clamping measures the voltage within a single cell, relative to the voltage outside. It is a method for recording the voltage of an excitable cell while keeping the electrical current constant. A low impedance microelectrode is attached to the cell through the patching capillary, and a background electrode in the fluid around the cell is connected to a differential voltage amplifier. The output from the amplifier is displayed on an oscilloscope for analysis.

In contrast, voltage clamping measures the flow of ions in and out of the cell whilst keeping the membrane voltage constant. Due to the sensitive nature of the currents under investigation, patching is usually carried within a Faraday cage to eliminate interference from external influences. (See Figure 1.3 for a typical recording from a neuronal action potential).

1.11.3.2 Calcium imaging

The fluorescence imaging plate reader-96 (FLIPR; Molecular Devices, California) is a high throughput screening device for real-time capture of receptor and ion channel activity across a population of cells. The FLIPR is primarily used in the pharmaceutical industry for drug screening to monitor dose dependent cellular responses to a neurotransmitter or novel drug. The UCL FLIPR is currently the only machine of its kind for use in an academic setting.

The system runs on a 96-well plate format enabling screening of up to 96 individual, or 32 triplicate samples in parallel. The FLIPR has precise control over temperature and humidity, minimising external influences on cell behaviour and is able to simultaneously deliver a drug to all 96 wells. As such, the FLIPR can be used to rapidly characterise the functional behaviour of large populations of neurons.

Calcium flux across a cell can be monitored by the coupling or decoupling of free Ca^{2+} to a pre-loaded calcium indicator dye: Fluo-4-AM. When bound by Ca^{2+}, the dye forms a complex which is excited by an argon laser at 488 nm. Emitted light (~550 nm) is captured by a charge coupled device (CCD) camera. Changes in fluorescence can be correlation to

levels of cytoplasmic Ca^{2+}. The ability of the camera to focus on a monolayer of cells, avoids detection of background fluorescence.

By measuring the fluorescence before, during and after stimulation, Ca^{2+} flux across the cell membrane can be observed. Fluorescence values are usually recorded every second for five minutes generating a detailed picture of the response to stimulation. The typical response of a cell can be divided into several phases (Figure 1.4; A-F). Recordings are usually captured for 30 seconds prior to addition of the stimulus to establish the background fluorescence from cytosolic Ca^{2+}(A). Addition of the neurotransmitter (B) dilutes the overall sample volume, therefore reducing background fluorescence (C). If a cell expresses functional receptors to the stimulant, membrane Ca^{2+} channels open and cytosolic Ca^{2+} levels increase, resulting in an overall increase in fluorescence (D-E). Increased cytosolic calcium levels alter a cells polarity, initiating the opening of ion pumps to pump free Ca^{2+} out of the cell (F), thus returning to basal levels.

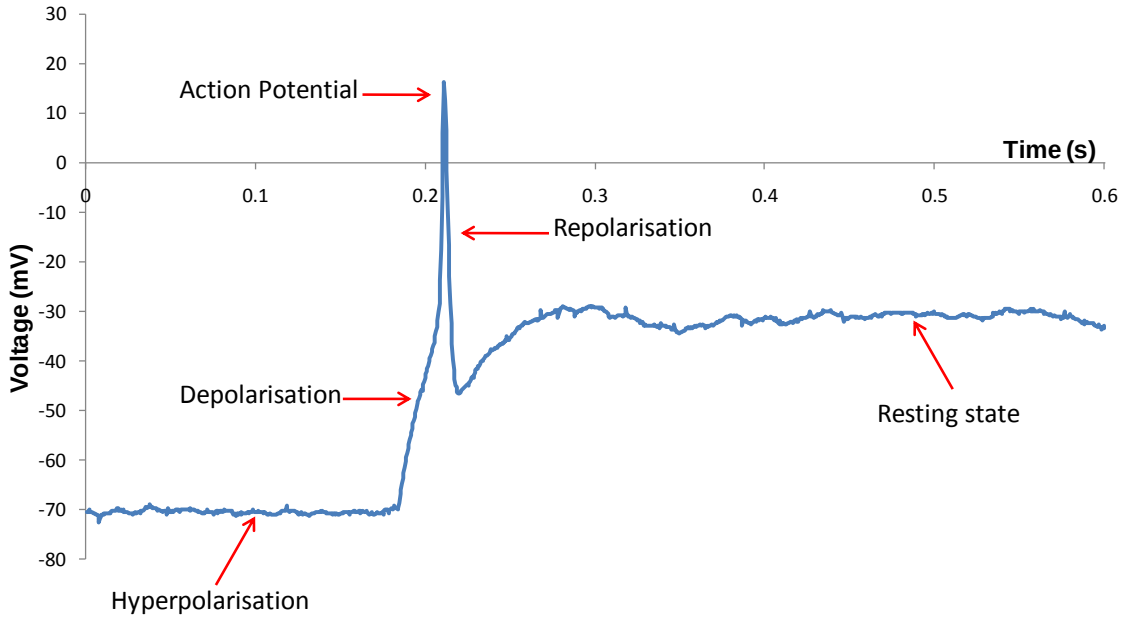

Figure 1.3. Description of a neuronal action potential.

During patch clamping a cell is commonly hyperpolarised to reduce the membrane voltage to -70 mV. Release of the hyperpolarising current causes voltage gated ion channels in the membrane to open and initiates an influx of Na^+ or Ca^{2+} ions into the cell. This causes rapid depolarisation, generating an electrical impulse (AP). The change in polarity causes membrane voltage gated K^+ channels to open and K^+ ions to flow out of the cell returning the polarity to its resting state.

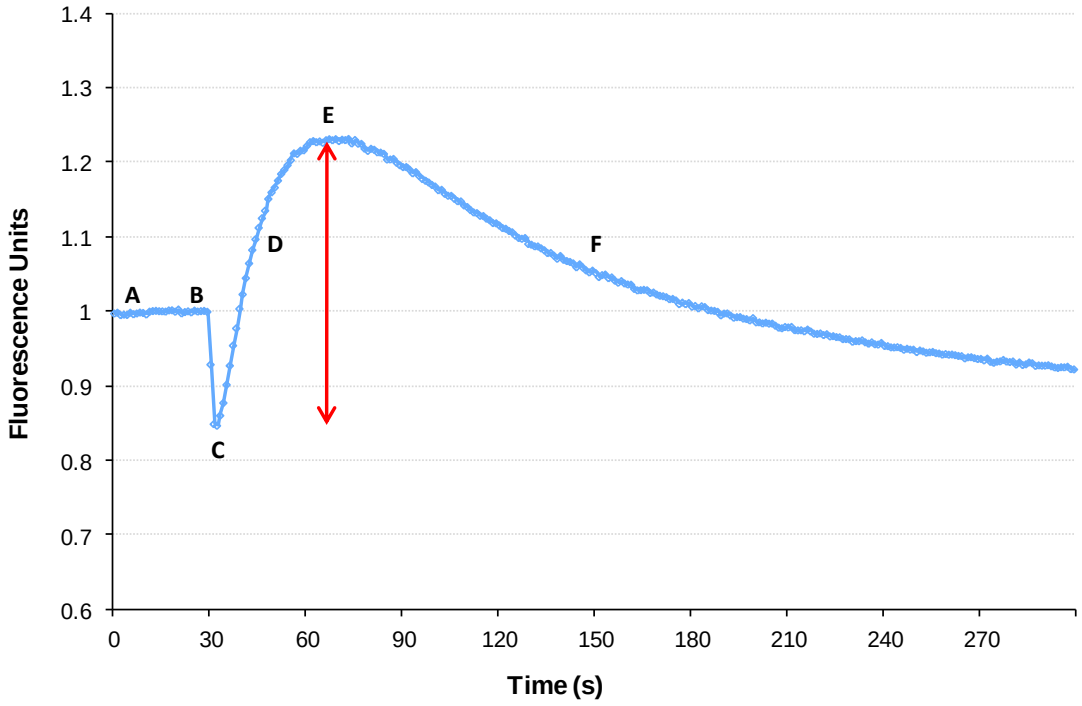

Figure 1.4. Typical cellular calcium response to stimulation on the FLIPR.

The 6 phases of a typical calcium response of a cell to neurotransmitters in the FLIPR. The response from each cell was standardised to ensure background fluorescence was equal to one. A - fluorescence from resting levels of cytosolic Ca^{2+}. B - addition of the neurotransmitter. C - baseline fluorescence, Ca^{2+} channels open. D - influx of calcium and binding to Fluor-4-AM resulting in increased fluorescence. E - maximum fluorescence. F - calcium pumped out of cell or sequestered to cytoplasmic stores. The overall calcium response can be determined by the difference between C and E. (i.e. the difference between the maximum and minimum fluorescence values after addition of the drug.)

1.12 The need for a reproducible source of neurons

The availability of human primary neurons is extremely limited. With the exception of olfactory neurons which are constantly renewing, mature mammalian neurons are not very mitotically active (Moulton, 1970). It is possible to commercially source neural stem cell lines such as Millipore's ReNcell® VM neural stem cell line (Millipore™, Massachusetts, USA) for expansion and differentiation; however, cells often lose their ability to differentiate into a range of terminal neurons following expansion which in itself is limited by the proliferative capacity of a neural progenitor cell (Elkabetz et al., 2008; Bajpai et al., 2009). It is possible to derive neurons from cell lines isolated from neuroblastomas such as the SH-SY-5Y (Encinas et al., 2000); however, expansion and maturation of these neurons *in vitro* and their response to stimulation is variable and in most instances is limited to a slow response.

Primary neurons for pharmacological screening are routinely sourced from animal models and are most commonly of mouse or rat origin. In such cases, animal derived neurons are usually sufficiently sensitive to stimulation for comparison to *in vivo* scenarios; however, sourcing these neurons requires regular animal sacrifice. There is therefore a requirement for a continual source of functional neurons to relieve the reliance on animal sacrifice and facilitate early drug screening. Ideally these would come from a continuous cell line which would enable expansion of neuronal populations as required.

Additionally, incorporation of primary animal source neurons into routine cell therapies is unlikely due to risks of transmission of cross-species infections. Production of a reliable supply of functional neurons *in vitro*, under GMP grade conditions, from a continual supply would enable routine applications for cell based regenerative therapies.

In order to generate a cell therapy which produces sufficiently large numbers of neurons it is essential to have a source of cells which are expandable, and a process of differentiation which generates reproducible yields of cells for transplantation. Incorporation of pluripotent cells into this process offers the opportunity for cellular expansion prior to neural commitment, enhancing the final neuronal yield for therapy. Many worldwide laboratories have researched neuronal differentiation from pluripotent cells with varied levels of success (Carpenter et al., 2001; Zhang et al., 2001; Baharvand et al., 2007; Iacovitti et al., 2007). In most cases, cells of neuronal morphology have been derived; however, comment is rarely made regarding the reproducibility of differentiation. Personal communications frequently report varying degrees of success.

In most pluripotent differentiation systems, comment over the purity of the definitive neuronal phenotype is largely avoided due to the mixed array of neurons (both inhibitory and excitatory) at the end stage of differentiation which would undoubtedly result in a varied response following stimulation. Equally, for a therapy to replace a definitive cell type (as would be the case for PD), the neuronal subclass would not only need to be of a dopaminergic phenotype but would also need to generate the specific A9 dopaminergic neurons lost during PD whilst expressing functional machinery for reliable dopamine synthesis on demand.

With this in mind, mechanisms of neuronal differentiation must be extensively characterised to yield sufficient numbers of neurons which may form just a small proportion of the final neuronal yield. In order to achieve this goal, it is first necessary to further our basic understanding of the starting cell pools for differentiation; that is the pluripotent cell populations.

The transient nature of hESCs in embryonic development would suggest that these cells are highly susceptible to differentiation stimuli. Indeed these cells will have already been exposed to differentiation cues prior to derivation to initiate their position within the ICM. Removal or addition of cells from the ICM results in a normal progression of embryonic development without the loss or gain of developmental features (Teramura et al., 2007), confirming that the cells of the ICM are uncommitted to differentiation into a specified tissue. However, when considering the speed to embryonic development, it might be suggested that the position of a cell within the ICM induces a preference rather than a commitment into a differential fate, which is overridden in the event of interruption.

The various methods of hESC derivation and expansion are likely to have varied affect on the communication and survival of hESCs during early stages of cell line establishment, inducing a selective advantage of hESC subpopulations for expansion. This might explain the variable behaviour observed between different hESC lines despite similar pluripotent morphology. Using this theory, it is possible that some pluripotent lines may be more suited to neuronal differentiation than others.

The characterisation of pluripotent cell lines in response to *in vitro* expansion has been subject to investigation throughout this project, focusing on the behaviour of different pluripotent cell lines in response to directed neuronal differentiation and their subsequent neuronal yield, phenotype and function. The results of this study are presented herein.

1.13 Aims and Objectives

This project aims to investigate the effect of *in vitro* culture on the comparative stability, expansion and neuronal differentiation of different pluripotent cell lines, with a view to testing the following hypotheses:

Hypotheses:

1. The method of culture (enzymatic or mechanical) does not affect the karyotypic stability of a pluripotent cell line in culture.
2. Pluripotent cells are equally directable into neuronal differentiation when cultured under standardised and controlled conditions.
3. The method of culture does not affect the ability of a pluripotent cell line to be differentiated into a functional neuron.

To our knowledge a comparative study into the effect of mechanical and enzymatic passaging on neuronal differentiation across a range of pluripotent cell lines has not been previously carried out.

2 Materials and Methods

2.1 Standard cell culture media

2.1.1 Glutamine culture media

Dulbecco's modified Eagle's medium (DMEM; Gibco, Rockville, MD, 21969-035), supplemented with 10 % (v/v) foetal bovine serum (FBS; Gibco, 10108-157) and 2 mM L-glutamine (Gibco, 25030-032).

2.1.2 GlutaMAX™ culture media

Dulbecco's modified Eagle's medium (Sigma, St Louis, D6546) supplemented with 10 % (v/v) FBS (Biosera, East Sussex, UK, S170G) and 2 mM GlutaMAX™ (Gibco, 31980-022).

2.1.3 Freeze media

Mix 10 % (v/v) dimethyl sulfoxide (DMSO; VWR international, 103232J) with 90 % (v/v) FBS.

2.2 Cryopreservation

Cells were detached from adherent culture using TrypLE™ Express (Gibco, 12604-013) and counted using a bright line haemocytometer (Section 2.3). Cells were washed in standard culture media, followed by centrifugation at 170 g for 3 minutes. Cells were resuspended at the desired density in standard freeze media (Section 2.1.3), and aliquoted into 1 ml cryovials (Corning, 430525). Vials of cells were placed in a Mr Frosty (Nalgene, 5100-0001) and transferred to -80 °C freezer for 24-48 hours to freeze at a slowed rate of -1 °C/minute. Finally cells were moved into Liquid Nitrogen (LN_2) for long term storage.

2.3 Cell counting

Cell viability and number counts throughout this project were calculated using a bright-line haemocytometer (Sigma, Z359629). Cells were resuspended in culture/wash solution and 100 µl sample removed for dilution 1:1 (v/v) with Trypan blue solution (Sigma, T8154). The haemocytometer and coverslip (Sigma, Z375357) were cleaned with 70 % ethanol and 10 µl of the cell suspension added to each side of the haemocytometer. Eight separate 4X4 grids

of the haemocytometer were counted per sample to obtain an idea of both cell number and viability. Viable cells are phase bright and dark cells which have taken up Trypan blue as a result of a permeable cell membrane were deemed to be non-viable. Live:dead cell counts were recorded and final numbers from all eight grids were averaged. Final cell counts were multiplied by the dilution factor then 10^4 giving total and viable cell count.ml^{-1}.

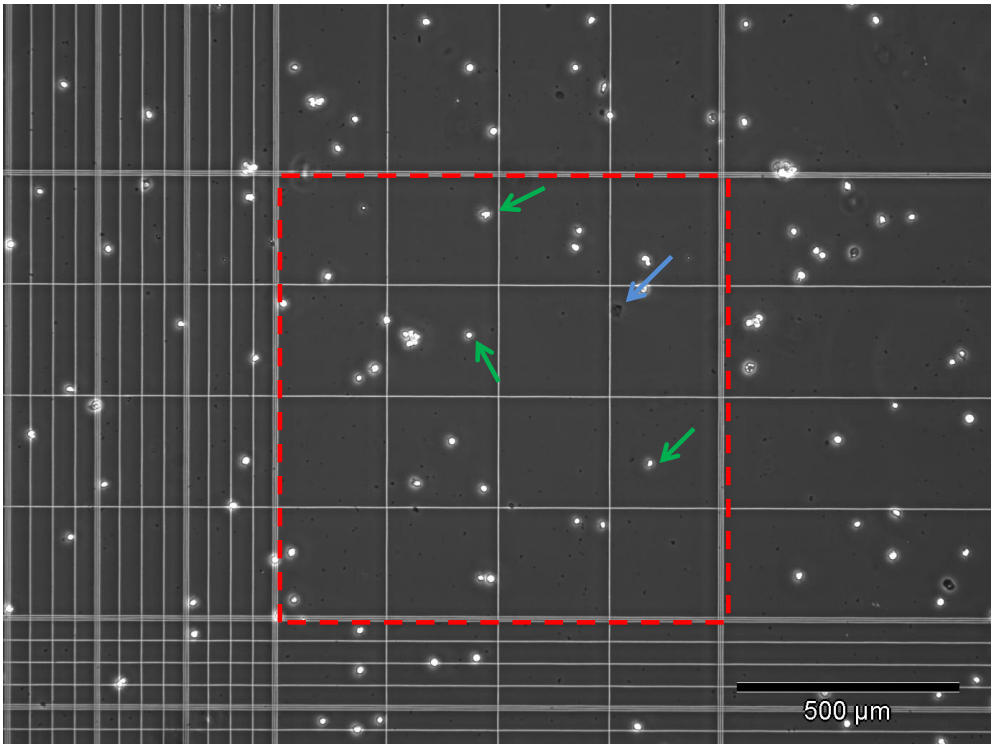

Figure 2.1. Bright-line Haemocytometer.

Cells were counted in eight 4x4 grids as highlighted by the red-dashed line. Cells on the top and right hand border of the 4x4 grid were counted. Outlying cells on the bottom and left hand border of the 4x4 grid were excluded from all counts. In the above NTERA2 cell sample 28 viable cells (green arrows), 1 non-viable cell was counted (blue arrow).

2.4 NTERA2

NTERA2.cl.D1 were sourced from Professor Peter Andrews (University of Sheffield) at passage 27 (p27) for use in this study. A master cell bank was prepared following standard protocols (Andrews., 1984). Cells were cultured in NTERA2 culture media (Section 2.4.1) in a humidified incubator at 37 ºC, 7 % (v/v) CO_2 using ventilated T75 tissue culture flasks (Nunc, TKT-130-210T). Cultures were grown to approximately 90 % confluence and passaged every 3-4 days (Section 2.4.2). Cultures were re-fed with complete media change, every other day.

2.4.1 NTERA2 culture media

High glucose DMEM with no sodium pyruvate (Gibco, 11960) supplemented with 2 mM GlutaMAX^{TM} and 10 % (v/v) FBS (Gibco).

2.4.2 NTERA2 passaging

Spent medium was removed, leaving approximately 5 ml in the flask. Sterile glass beads (Section 2.4.2.1) were added and rolled gently over the growth surface, removing the cells from the flask in clumps. Cells were aspirated up and down three times to break up large clumps of cells into small clusters. Cells were counted using a bright-line haemocytomer (Section 2.3) and resuspended in and 5 x 10^6 cells, seeded into a fresh T75 flasks 20 ml fresh culture media (this was approximately a 1:3 split ratio).

2.4.2.1 Glass bead preparation

Soda lime glass beads (3 mm; VWR, 1.04015.0500) were routinely used for passaging NTERA2 stocks. The beads were cleaned in 2 M hydrochloric acid (HCl) overnight, neutralised in an equal volume of 2 M sodium hydroxide (NaOH) and rinsed thoroughly in water. Beads were aliquoted: 20-30 beads/eppendorf tube (VWR, 211-0015) and autoclaved prior to use.

2.4.3 NTERA2 differentiation

Neuronal differentiation from NTERA2 was carried out as previously described by Pleasure et al., 1992. Cells were washed in PBS (without Ca^{2+} and Mg^{2+}: Gibco, 14190-094) and detached from adherent culture using 5 minute exposure to Trypsin/EDTA (Sigma, T4049) at 37 °C. Following detachment, cells were quenched in NTERA2 culture media, pipetted up and down to create a single cell suspension and centrifuged to pellet. Cells were seeded into a fresh culture vessel at 2.6 x 10^4/cm^2 flask 0.2 ml NTERA2 differentiation media/cm^2 (Section 2.4.4). Cells were left to grow for 4 weeks with twice weekly differentiation media feeds.

Four weeks after ATRA treatment, cells were detached from adherent culture and split 1:6 into fresh culture flasks. On the following two days, cells were exposed to a rapid 30 second Trypsin treatment and mechanically dislodged with a sharp knock of the flask

with the palm of the hand. Floating cells were washed with 5 ml NTERA2 culture medium and replated into a fresh culture vessel in NTERA2 culture medium supplemented with mitotic inhibitors: 1 µM cytosine arabinoside (Section 2.4.4.2), 10 µM fluorodeoxyuridine (Section 2.4.4.3) and 10 µM uridine (Section 2.4.4.4). Cytosine arabinoside has been found to kill post-mitotic neurons (Wallace and Johnson, 1989), in addition to fast replicating cells and was therefore supplemented into culture for just 1 week. Fluorodeoxyuridine and uridine were incubated for four weeks to prevent non-neuronal cell overgrowth with a media change every 3-4 days.

2.4.4 NTERA2 differentiation media

All-*trans*-retinoic acid (Section 2.4.4.1**)** was dissolved in NTERA2 culture media to 10^{-5} M final concentration.

2.4.4.1 All-trans-retinoic acid for NTERA2 differentiation

One hundred milligrams of all-trans-retinoic acid (ATRA) powder (Sigma, R2625) was dissolved in 33.3 ml DMSO producing a 10^{-2} M stock solution. The stock solution was aliquoted into 1 ml volumes and stored in the dark at -20 °C.

2.4.4.2 Cytosine arabinoside stock solution

One hundred milligrams cytosine-β-D-arabinofuranoside powder (Sigma, 30399) was dissolved in 411 ml water and passed through a 0.2 micron filter, producing a 10^{-3} M stock solution. This was stored in the dark at -20 °C for up to 12 months as per manufacturer's instructions.

2.4.4.3 Fluorodeoxyuridine stock solution

One hundred milligrams 5-fluoro-2-deoxyuridine powder (Sigma, F0503-100MG) was dissolved in 40.6 ml sterile water and passed through a 0.2 micron filter, producing a 10^{-2} M stock solution. This was stored in the dark at 4 °C as per manufacturer's recommendations.

2.4.4.4 Uridine stock solution

One hundred milligrams uridine powder (Sigma, U3003) was dissolved in 40.9 ml sterile water and passed through a 0.2 micron filter, producing 10^{-2} M stock solution for storage at 4 °C.

2.4.5 NTERA2 Cryopreservation

A master cell bank for NTERA2 was prepared at approximately 5 x 10^6 cells/vial in 1 ml as detailed in Section 2.2.

2.5 2102Ep – Human embryonal carcinoma

2.5.1 2102Ep cell culture

The 2102Ep embryonal carcinoma (EC) cell line was cultured in standard GlutaMAX™ culture media as previously described (Section 2.1.2). Cells were grown to approximately 90 % confluence, washed in PBS and exposed to TrypLE™ express at 37 °C for 3-4 minutes. The flask was knocked several times sharply against the palm of the hand to dislodge the cells from the growth surface. The TrypLE™ reaction was quenched in 5x volume growth media and the cells centrifuged to pellet at 170 g for three minutes before replating onto a fresh growth surface (~5 x 10^6 cells per T75 flask).

2.5.2 2102Ep cryopreservation

Cryopreservation of 2102Ep cells at approximately 5 x 10^6 cells/vial, was carried out as described in Section 2.2.

2.6 SH-SY-5Y - Human neuroblastoma

2.6.1 SH-SY-5Y cell culture

The SH-SY-5Y cell line was sourced at passage 7 from the Cell Supply group at NIBSC and cultured in MEM:F12 (Gibco, 21765-029: 21090-022) 1:1 (v/v), supplemented with 15 % (v/v) FBS, 2 mM L-glutamine and 1 % (v/v) Non-essential amino acids (NEAA; Gibco, 11140) in a standard humidified incubator at 37 °C, 7 % CO_2. Upon reaching confluence, cells were split 1:5 using 0.25 % (v/v) Trypsin/EDTA solution. Cultures were fed every 3-4 days.

2.6.2 SH-SY-5Y differentiation

Cells were grown to confluence as described in Section 2.6.1, before dissociation with 0.25 % (v/v) Trypsin/EDTA solution for 2 minutes at 37 °C. Samples were quenched with SH-SH-5Y culture media and centrifuged at 110 g for 5 minutes. Cells were resuspended in culture media supplemented with 10^{-5} M ATRA and incubated for eight days in a 37 °C, 7 % CO_2, humidified atmosphere.

2.6.3 SH-SY-5Y cryopreservation

Cryopreservation of SH-SY-5Y cells at approximately 5×10^6 cells/vial, was carried out as described in Section 2.2.

2.7 Primary neurons from an embryonic day 14 rat

Tissue sections were sourced from Sprague-Dawleys rats (UCL biological services), following procedures according to the National Institutes of Heath guidelines. Tissue sections were prepared by Ms. Sophie Finch (Centre for the Cellular Basis of Behaviour & MRC Centre for Neurodegeneration, Kings College London, UK).

2.7.1 Dissection of cortex and ganglionic eminence

The rat embryo (14 day) was removed from the mother and placed into a petri-dish containing HBS. A line was cut between each embryo using a sterile tool to allow the release of the embryonic sac. The sac was pierced at the abdomen end to remove the embryo. The head was separated from the rest of the body and placed in a fresh dish containing DMEM with streptomycin/penicillin (50 $\mu g.ml^{-1}$). Under a light microscope the skin and the skull was peeled back exposing the two hemispheres of the brain. The two hemispheres were removed and the rest of the brain discarded. The hemispheres were positioned with the cortex on the base of the petri-dish and the olfactory bulbs at the top. Using the olfactory bulb as a guide, an incision was made to open up the hemisphere. The ganglionic eminence (GE) and cortex were removed from each hemisphere. Sections were transferred into separate tubes containing either 10 ml DMEM wash media or warm Sato's media for transport (Section 2.7.1.1).

For patching and staining, tissue sections were prepared as follows. Media was removed and the tissue exposed to 1 ml Trypsin/EDTA (0.25 mg.ml^{-1}) containing 0.01 % (v/v) DNase for 10 minutes at 37 ^{o}C. After which, 1 ml Trypsin inhibitor containing 0.01 % (v/v) DNase, was added to the sample. Initial dissociation was carried out using a 21 g needle and pipetted up and down three times. This was repeated a further 3 times with a 23 g needle. Following dissociation, 10 ml Sato's media was added to the sample and cells left to settle for 20 minutes before transferring the liquid to a fresh tube, discarding large amounts of debris. Cells in suspension were counted and centrifuged at 180 g for 5 minutes. The supernatant was removed and cells resuspended in Sato's medium at the desired concentrations for plating. Cells were resuspended in Sato's medium such that a 50 µl drop was equivalent to 2 x 10^5 cells per 24-well for cortical cells and 3 x 10^5 cells per well for the GE. Cells were initially plated in droplets of small volumes into the centre of the well/cover slip and incubated for 1 hour so that cells adhered to the centre of the plate/slide (50 µl into the centre of each 24-well, 100 µl for 12-well or 300 µl for 6-well), after which media was increased to 0.5 ml per 24-well, 1 ml per 12-well and 2 ml per 6-well.

2.7.1.1 Sato's media

Dulbecco's modified Eagle's medium: F12 (Invitrogen, 31330-095) supplemented with 5.6 mg.ml^{-1} glucose (Sigma, G-6152), 100 µg.ml^{-1} BSA (Sigma, A-8806), 16 µg.ml^{-1} putrescine (Sigma, P-5780), 60 ng.ml^{-1}, progesterone (Sigma, P-8783), 400 ng.ml^{-1} L-thyroxine (Sigma, T-0397), 300 ng.ml^{-1} 3,3',5-triiodothyronine (Sigma, T-5516), 2 mM L-glutamine (Sigma, G-7513), 5 µg.ml^{-1} insulin (Sigma, I-1882), 5 µg.ml^{-1} transferrin, (SCIPAC, UK, T100-5) and 5 ng.ml^{-1} selenium (Sigma, S-5261).

2.8 Mouse embryonic fibroblast feeder cells (MEFs)

Mouse embryonic fibroblasts were derived from the MF1 mouse strain sourced from Harlan UK Ltd and supplied by the UKSCB at p0.

2.8.1 Mouse embryonic fibroblast culture

Mouse embryonic feeder cells (MEFs) were routinely cultured in standard GlutaMAX^{TM} culture media (Section 2.1.2). Cells were received from the UKSCB and typically cultured to

p3 before mitotically inactivating the cells with Mitocycin C (Section 2.8.1.1), for use as a supportive feeder layer in hESC culture.

2.8.1.1 Mitomycin C inactivation of MEFs

Feeder banks were grown up as described in Section 2.8.1 and typically mitotically inhibited when approximately 70 % confluent. Cells were mitotically inactivated using Mitomycin C inactivation media (Section 2.8.1.2) for 2 hours. Following inactivation, the monolayer of cells was washed twice in PBS before TrypLE^{TM} treating the cells to dislodge from adherent culture. Cells were centrifuged and washed once in standard GlutaMAX^{TM} culture media (Section 2.1.2) before finally centrifuging to pellet. Cells were resuspended in standard freeze media (Section 2.1.3) at 1-2 x 10^6 cells/cryovial. Vials were placed in a Mr Frosty for slow rate freezing overnight at -80 °C before transferral into racks for long term storage at -80 °C for use as required.

2.8.1.2 Inactivation media

Two milligrams Mitomycin C powder (Acros Organics, Belgium, 226940020) was dissolved in 200 ml DMEM (Sigma) creating a 10 µg.ml^{-1} solution which was filter sterilised and then supplemented with 10 % (v/v) FBS.

2.9 Human embryonic stem cells

2.9.1 Human embryonic stem cell culture

Human embryonic stem cells were routinely cultured in the presence of an inactivated MEF (iMEF) layer (Section 2.8). Cells lines were obtained from the UKSCB, with the appropriate permission from the Steering Committee. Cells were routinely cultured in 6-well plates pre-coated with 0.1 % gelatin to aid attachment. Cells were passaged using both mechanical and enzymatic techniques (Sections 2.9.1.1 and 2.9.1.2). Fresh stocks of cells were thawed approximately every six months in culture to retain young comparable hESCs for experimentation.

2.9.1.1 Mechanical passaging

Good quality hESC colonies were identified and located with an inverted dissection microscope under protection of a class II microbiological safety cabinet (MSC), using the criteria outlined in Section 4.2.1. Areas of pluripotent stem cells were mechanically dissected into grids (Figure 2.2) from the colony using a micro-tool 90° hook and handle (Agar, T5338 and T5344) and lifted away from the culture surface.

Fragments of cells ~400 µM across were transferred onto fresh feeders using a P20 Gilson pipette and distributed evenly across a fresh iMEFs layer for attachment (~10 colonies/IVF cell culture dish). Care was taken during passaging to avoid folding over of cut fragments which frequently resulted in stacking of cell layers and subsequent colony differentiation. In addition, areas of differentiation were also removed from culture using this method. Each time mechanical passaging was undertaken the passage number of the cells was increased by +1. Human ESCs colonies were mechanically passaged every 5-7 days.

2.9.1.2 Enzymatic passaging

Spent hESC media was removed from culture (Figure 2.3A). Cells were washed in sterile tissue culture grade PBS (without Ca^{2+} and Mg^{2+}) before exposure to TrypLE™ Express at 37 °C for 2 minutes. Care was taken to avoid over exposure of the cells to TrypLE™, preventing a single cell suspension following passaging. When cells began to detach (Figure 2.3), the TrypLE™ was gently aspirated away leaving the monolayer of detaching cells which were gently washed with fresh hESC media to remove residual TrypLE™. Fresh hESC media (Section 2.9.2) was triturated over the cells to break the culture into small fragments, roughly 10 cells per clump. The cell suspension was transferred onto a fresh iMEF layer with 3 ml fresh hESC media/well of a 6-well plate in a 1:6 split ratio (Figure 2.3C). *Note:* hESCs were not counted prior to passaging retaining cells in small clumps.

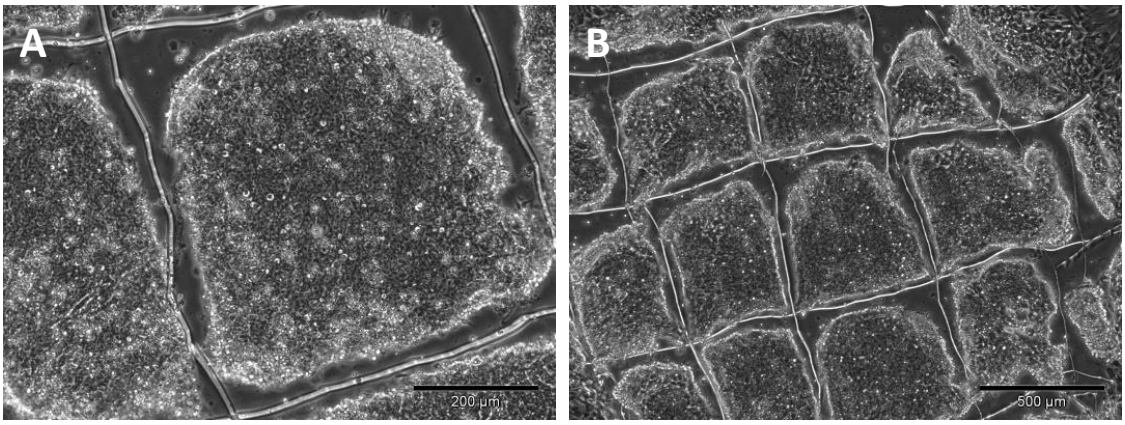

Figure 2.2. Mechanical passaging

Stem cell colonies were cut into fragments approximately 400 µM square (A; x10 magnification, B; x4 magnification). Fragments entirely comprised cells of hESC morphology (Section 4.2.1). Following dissection, fragments were lifted away from the culture surface from the corners and edges and transferred to fresh iMEFs.

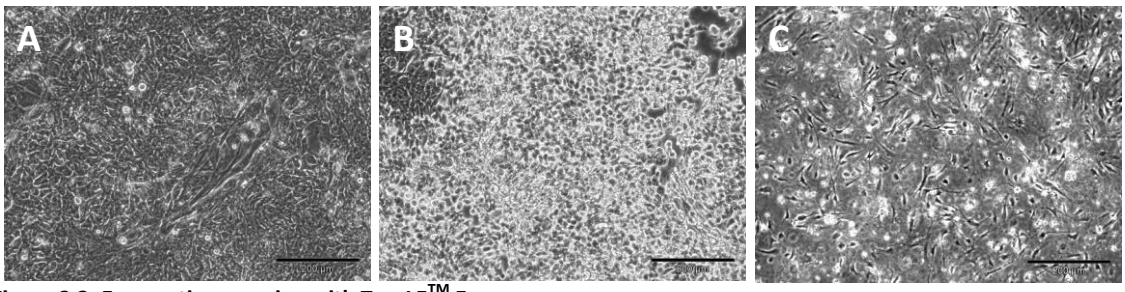

Figure 2.3. Enzymatic passaging with TrypLE™ Express.

Cell culture before (A), during (B), and after (C) TrypLE™ passaging (x10 magnification), cells were detached from monolayer into a suspension containing small clumps of cells for re-growth on a fresh iMEF layer.

2.9.2 Human embryonic stem cell culture (hESC) media

Knockout™ D-MEM (KO-DMEM; Gibco, 10829) was supplemented with 20 % (v/v) Knockout™ Serum Replacement (KO-SR; Gibco, 10828), 2 mM GlutaMAX™ (Gibco, 35050), 1x NEAA, 0.1 mM β-mercaptoethanol (Gibco, 31350-010) and 4 ng.ml^{-1} basic fibroblast growth factor (bFGF; Invitrogen, 13256-029).

2.9.2.1 Basic fibroblast growth factor

Basic fibroblast growth factor (bFGF) (Invitrogen, 13256-029) was prepared to 2 µg.ml^{-1} in PBS, supplemented with 0.1 % (v/v) BSA (Sigma, A1595) and 2 µg.ml^{-1} heparin.

2.9.2.2 Heparin stock solution

Twenty milligrams heparin (Sigma, H3149-2KKU) was dissolved in 10 ml DMEM (Sigma, D6546) to prepare a 2 $mg.ml^{-1}$ stock. The solution was filter sterilised through a 0.2 micron filter and stored at -80 °C

2.9.3 Vitrification

Vitrification solutions VS1 (Section 2.9.3.1) and VS2 (Section 2.9.3.3) were thawed and one 200 µl aliquot of VS1 solution and three 100 µl drops of VS2 solution were placed onto a sterile dish. Using a thumb prick, holes were pierced at the top and bottom ends of cryovials (Corning, 430663). Colonies were cut slightly larger than for routine passaging. A miniature vessel containing LN_2 was placed into the Class II Microbiological Safety Cabinet (MSC) and cryovials pre-cooled in the vessel. Using a Gilson P20 pipette 10-15 colonies were transferred in 20 µl hESC media (Section 2.9.2) into the first VS1 droplet for precisely 1 minute. The fragments were then transferred to the first VS2 droplet for 25 seconds followed by transferral into the second VS2 droplet for a non-critical time. Using a Gilson P20 pipette set at 4 µl, the stem cell fragments were collected and the small droplet dispensed onto the dish. A sterile vitrification straw (Minitüb Abfüll- und Labortechnik GmbH & Co, Germany, 19050/0150) was placed into the droplet and hESC fragments entered the straw. Finally VS2 solution was sucked from the final droplet to move the fragments away from the bottom of the straw. The straw end was placed into the cooled cryovial (2/3 straws into each vial). Cryovials were then transferred for long-term LN_2 storage.

2.9.3.1 Vitrification solution 1

A 10 % (v/v) vitrification solution (VS) 1 solution was prepared by supplementing HEPES media (Section 2.9.3.2) with 10 % (v/v) DMSO and 10 % (v/v) ethylene glycol (Sigma, E9129)

2.9.3.2 HEPES media

Knockout™ D-MEM was supplemented with 20 % (v/v) FBS and 1 M HEPES (Invitrogen, 15630-049).

2.9.3.3 Vitrification solution 2

A 20 % (v/v) VS2 solution was prepared by supplementing ES HEPES solution with 20 % (v/v) DMSO, 20 % (v/v) ethylene glycol and 30 % (v/v) 1 M sucrose solution (Section 2.9.3.4).

2.9.3.4 1 M sucrose solution

Sucrose powder (Sigma, S7903), 3.42 g, was dissolved in 8 ml DMEM supplemented with 2 ml FBS.

2.10 Human embryonic stem cell differentiation

2.10.1 Embryoid body directed neuronal differentiation

This method was adapted from an early dopaminergic neuronal differentiation protocol (Li et al., 2007) (Zhang et al., 2001; Yan et al., 2005). Prior to differentiation, stem cell colonies were grown to the density used for passaging. Spent culture media was removed, and pre-warmed dispase (Sigma, D4818; 1 $mg.ml^{-1}$ in DMEM/F12) was added to cells for incubation at 37 °C for 2-5 minutes until colonies began to curl up. Cells were dispersed in fresh hESC culture media (Section 2.9.2) and triturated 3-5 times to break up the colonies until they were twice the size of fragments for normal passaging. Fragments were washed in fresh hESC media to remove any remaining dispase before centrifuging at 200 g for 2 minutes. Fragments were resuspended in hESC media for suspension culture in non-attachment 6-well plates (Nunc, TKT220-006R). Suspension EBs were fed every day for four days before transferring into neural induction (NI) media (Section 2.10.1.1) supplemented with 20 $ng.ml^{-1}$ bFGF (Section 2.9.2.1) for a further two days before plating onto a laminin (20 $\mu g.ml^{-1}$, Section 2.10.1.4) or poly-L-ornithine (0.1 $mg.ml^{-1}$, Section 2.10.1.3) coated cover slips in NI media.

Fragments were expected to attach and spread after 1-2 days. On day ten, spent media was removed and fresh NI media supplemented with FGF8 (Section 2.10.1.5) 20 $ng.ml^{-1}$ and SHH (Section 2.10.1.6) 100 $ng.ml^{-1}$ added to each sample. Cultures were fed every other day with a half volume media change of fresh NI media containing FGF8 and SHH.

2.10.1.1 Neural induction media

DMEM/F12 (Gibco, 31330-038) was supplemented with 1x N2 (Gibco, 17502-048), 1x NEAA and 2 $\mu g.ml^{-1}$ heparin.

2.10.1.2 Neuronal differentiation media

Neurobasal media (Gibco, 21103-049) was supplemented with 1x N2 supplement and 0.1 mM MEM-NEAA.

2.10.1.3 Poly-L-ornithine

Poly-L-ornithine hydrobromide (Sigma, P3655-50 mg), 0.1 mg, was diluted in 1 ml sterile water for storage at 4 °C.

2.10.1.4 Human placental laminin

Human placental laminin (Sigma, L6274) was thawed in a Class II MSC hood on ice to avoid solidification and diluted in sterile water for a 250 $\mu g.ml^{-1}$ stock solution to be stored at -80 °C.

2.10.1.5 Fibroblast growth factor 8

One milligram of fibroblast growth factor 8 (FGF8; PeproTech, New Jersey, 100-25) was dissolved in 10 ml PBS with 0.1 % (v/v) BSA and 2 $\mu g.ml^{-1}$ heparin. Stock solution was prepared at 100 $\mu g.ml^{-1}$ and stored at -80 °C.

2.10.1.6 Sonic hedgehog

One milligram of Sonic Hedgehog (SHH; R+D systems, 1845-SH) was dissolved in 10 ml PBS with 0.1 % (v/v) BSA. Stock solution was prepared at 100 $\mu g.ml^{-1}$ and stored at -80 °C.

2.10.2 Adherent monolayer neuronal differentiation

This method was adapted from (Baharvand et al., 2007). Cells were cultured as described in Section 2.9.1. Colonies were left to proliferate for 4-5 days before exposure to 4 x 10^{-6} M

ATRA (Section 2.10.2.1) in hESC media without bFGF for six days at which point columnar cells organizing into rosettes were observed. Retinoic acid was removed from culture for a further six days to promote additional rosette formation. Cells were exposed to 25 $ng.ml^{-1}$ bFGF for a further six days, resulting in formation of neural tube-like structures which were mechanically dissected and plated on poly-ornithine (15 $\mu g.ml^{-1}$; Section 2.10.1.3) and laminin (5 $\mu g.ml^{-1}$; Section 2.10.1.4) coated tissue culture dishes in neurobasal medium (Gibco, 21103-049), supplemented with 1 % (v/v) N2 supplement (Gibco, 17502-048) and 2 % (v/v) B27 supplement (Gibco, 17504-044) for up to 30 days.

2.10.2.1 All-trans-retinoic acid for stem cell differentiation

Fifty milligrams ATRA (Sigma, R2625) was dissolved in 41.6 ml DMSO, producing a 4 x 10^{-3} M stock solution. The solution was stored at -20 °C in darkened conditions.

2.10.3 Semi-directed differentiation

Stem cell colonies were passaged, plated and fed as usual. Colonies beginning to differentiate neuronally in a spontaneous manner either due to long term culture or due to too high feeder density were identified by the presence of rosette-like structures in the colony. Rosettes were mechanically cut away and transferred into neurobasal differentiation (NBD) media (Section 2.10.3.1) onto poly-ornithine coated surface with half volume NBD media feed every other day.

2.10.3.1 Neurobasal media (NBD)

Neurobasal media supplemented with 2 mM glutaMAX™, 1 x N2 supplement (Gibco, 17502-048) and 1 x B27 supplement (Gibco, 17504-044).

2.10.4 Enhanced EB differentiation

Fragments were cut to roughly twice the size for normal passaging and cultured in suspension in 25-well bacteriological grade compartmentalised perti-dishes (Sterilin, PD/16630) in NI media (Section 2.10.1.1) supplemented with 20 $ng.ml^{-1}$ bFGF. Cell clusters were cultured in NI media for five days before transferring into NBD media (Section 2.10.3.1), removing bFGF from the culture for a further four days in suspension culture. On day nine fragments were transferred onto 0.1 $mg.ml^{-1}$ poly-ornithine and 1 $\mu g.ml^{-1}$ laminin

coated culture surface. Surfaces were coated and incubated overnight at 37 °C before plating. Floating cell clusters attached and collapsed over the following 1-3 days and were maintained in culture for up to ninety days and fed every other day with NBD media (Section 2.10.3.1).

2.11 Comparison of surface coatings for neuronal attachment and spreading

Eight-well chamber slides were coated with 75 µl/well of each of the following surface coatings,: poly-D-lysine (0.1 $mg.ml^{-1}$), gelatin (0.1 %, w/v), poly-L-ornithine hydrobromide (0.1 $mg.ml^{-1}$), human collagen IV (1 $\mu g.ml^{-1}$ BD Biosciences, 354245), laminin (20 $\mu g/ml^{-1}$) or fibronectin (200 $\mu g.ml^{-1}$, Sigma, F2006) and left to incubate for 3 hours at 4 °C, 1 hour at RT, 37 °C overnight, 1 hour at RT, 37 °C overnight and 30 minutes at RT, respectively. Rosette-like structures were mechanically dissected from Shef3 and RH5 cut hESC colonies grown at high feeder densities. A single fragment was transferred into each pre-coated well in NBD media (Section 2.10.3.1) and the attachment and spreading from each fragment monitored over a period of eight days.

2.12 Gene expression

2.12.1 RNA extraction

All RNA extractions were carried out using cooled reagents at 4 °C to minimise RNase activity.

2.12.1.1 Qiagen RNeasy

Cells were lysed and RNA harvested using Qiagen RNeasy (Qiagen, 74104) spin columns according to manufacturer's instructions. Briefly, cells were trypsinised from the culture surface and washed twice in PBS to remove all culture media from the sample. Cells were lysed in RLT buffer (for $\leq 5 \times 10^6$ cells 350 µl buffer RLT was used, for $5 \times 10^6 - 1 \times 10^7$ cells 700 µl RLT buffer was used). Samples were pipetted or vortexing to ensure complete cell lysis. The lysate was transferred into a QIA shredder column within a 2 ml collection tube and centrifuged at full speed for 2 minutes. One volume of 70 % (v/v) ethanol was added to the lysate and mixed well. The sample was transferred into an RNeasy spin column

within a fresh 2 ml collection tube, centrifuged for 15 seconds at ≥ 8,000 g and the flow through discarded.

RW1 buffer (350 µl), was added to the spin column and centrifuged for 15 seconds at ≥ 8,000 g to wash the membrane. Samples were DNase treated on the column using the Qiagen RNase-free DNase kit (Qiagen, 79254). Flow through was discarded from the RW1 buffer wash and a mixture of 10 µl DNase stock I solution and 70 µl RDD buffer was added to the spin column, before incubating at RT for 15 minutes. A further 350 µl RW1 buffer was added to the spin column and centrifuged at ≥ 8,000 g, and the flow through discarded. 700 µl buffer RW1 was then added to the column and centrifuged for 15 seconds at ≥ 8,000 g to wash and the flow through discarded. 500 µl RPE buffer was added to the spin column and centrifuged at ≥ 8,000 g for 15 seconds followed by a second 500 µl RPE wash step with a 2 minute centrifugation before removal of the flow through and returning the membrane for a final 2 minute centrifugation to dry. The membrane was then transferred into a fresh 1.5 ml collection tube and 30-50 µl RNase-free water added to the membrane. This was centrifuged for 1 minute at ≥ 8,000 g to elute the RNA. This elution step can be repeated if a high yield of RNA is expected. RNA samples were quantified using a Nanodrop spectrophotometer (Nanodrop Technologies Inc) before transferral to -80 °C for long term storage to inhibit endogenous RNase activity and prevent RNA degradation.

2.12.1.2 Ambion RNAqueous

RNA was extracted using Ambion's RNAqueous extraction kit (Ambion, AM1912) following manufacturer's instructions. Briefly, cells were Trypsinised from the culture surface, washed twice in PBS and centrifuged to pellet. Lysis/binding solution was added to the cell pellet in 200-700 µl volume depending on the cell number. Cell lysates were pipetted/vortexed to ensure complete lysis and a homogeneous solution. Equal volumes of 64 % ethanol were added to the lysate and mixed before applying the solution to a filter cartridge in a collection tube. The sample was then centrifuged at 10,000 g for 3 minutes and the flow through discarded. Wash solution #1, 700 µl, was added to the filter cartridge and centrifuged as before. Wash solution #2/3, 500 µl, was added to the cartridge and centrifuged, discarding the flow through. This step was repeated with an additional 500 µl wash solution #2/3. The supernatant was discarded and the filter cartridge centrifuged for 30 seconds to dry the membrane. The cartridge was placed into a fresh collection tube and

the membrane covered with 40 µl elution solution (pre-heated to 70 °C). The cartridge was centrifuged for 2 minutes to elute the RNA. Elution was repeated with an additional 10 µl elution solution. *Note*: the elution volume was increased for larger cell pellets. RNA samples were quantified using a Nanodrop spectrophotometer before transferral to -80 °C for long term storage.

2.12.2 DNase treatment

The Ambion RNAqueous extraction method required an additional DNase treatment step. This was carried out using TURBO DNA-free™ (Ambion, AM1907) in 28 µl volumes within RNase and DNase-free PCR tubes (Costar, 6547), according to manufacturer's instructions. Briefly, 2.5 µl 10x TURBO DNase Buffer and 1 µl TURBO DNase was added to the RNA, mixed gently and incubated at 37 °C for precisely 20 minutes. Samples were removed from 37 °C incubation and 2.5 µl DNase inactivation reagent was added to each tube for 2 minutes incubation at RT with occasional mixing to inhibit the DNase activity. In addition, the DNase inactivation reagent also removes divalent cations, such as magnesium and calcium, which can catalyze RNA degradation when RNA is heated in the RT-PCR reaction. Finally, samples were centrifuged at 10,000 g for 1.5 minutes and RNA supernatant transferred to a fresh tube for storage at -80 °C.

Note: TURBO DNase is less effective at RNA concentrations exceeding 200 $\mu g.ml^{-1}$. For highly concentrated samples (determined by Nanodrop quantification), RNA was diluted in nuclease free water to a concentration ~ 200 $\mu g.ml^{-1}$ before DNase treating.

2.12.3 Reverse transcription

Reverse transcription reactions converting RNA into cDNA were carried out using an Ambion RETROScript kit (Ambion, AM1710) following manufacturer's instructions in a pre-PCR laboratory. RNA was quantified using a NanoDrop Spectrophotometer (Nanodrop®). Total RNA, 1-2 µg, was combined with 2 µl Oligo (dT). The total volume was increased to 12 µl with nuclease free water and heated to 70 °C for 3 minutes using an Applied Biosystems 2720 Thermal cycler before placing on ice. 2 µl 10 X RT buffer, 4 µl dNTP mix, 1 µl RNase inhibitors and 1 µl MMLV-RT were added to each tube and mixed. The reverse transcription reaction was carried out at 44 °C for one hour before heating

samples to 92 °C for 10 minutes to inactivate the reverse transcriptase and transferring to -20 °C storage until use.

2.12.4 Custom primer design

To ensure that primers were specific for cDNA of mRNA transcripts only avoiding pseudogene amplification, primers were individually designed according to guidelines in Section 1.5.3.3. All sequences for primer design were taken from the reference assembly sequence in NCBI GENE. The genomic DNA sequence of each gene was identified using the NCBI genomic nucleotide reference assembly, in addition to the mRNA nucleotide sequence. Pseudogenes for genes of interest and their nucleotide sequences were also identified. All gDNA, RNA and pseudogene sequences were aligned using EMBL-EBI ClustalW2 alignment software (http://www.ebi.ac.uk/Tools/clustalw2/index.html). This software highlighted variations in sequences which were incorporated into RNA sequence specific primers (*sequence alignments available upon request*). Finally primer sequences were checked using the NCBI BLAST programme to ensure sequence specificity to the gene of interest (GOI). Due to the incorporation of an iMEF layer during hESC culture, where possible primers were also checked against the mouse genome sequence to ensure amplification was specific to the human GOI.

2.12.5 Polymerase Chain Reaction (PCR)

All RT-PCR reactions were loaded in a pre-PCR laboratory and transferred to a post-PCR laboratory to run. Each reaction used 250 ng cDNA (quantified at the RNA level using a Nanodrop spectrophotometer). All reagents were thawed and stored on ice during preparation. Reagents for reactions (Section 2.12.6) were mixed together with cDNA, gently vortexed and then loaded into an Applied Biosystems 2720 Thermal cycler machine. All samples were inactivated at 94 °C for four minutes, followed by 35 cycles of denaturation at 94 °C for 45 seconds, annealing at 55 °C for 45 seconds and elongation at 72 °C for 45 seconds. Final extension was 72 °C for 10 minutes before cooling to a 4 °C hold.

2.12.6 PCR reagents

2.12.6.1 Roche Faststart DNAtaq polymerase dNTPack

Roche Faststart DNAtaq polymerase dNTPack (Roche, 04738314001) reagents were mixed as follows: 5 µl PCR buffer (with $MgCl_2$), 1 µl nucleotide mix, 2 µl primer pair, 0.4 µl *FastStart* Taq polymerase and increased to 50 µl with nuclease-free water within a PCR tube.

2.12.6.2 Promega PCR master mix

The Promega PCR master mix (Promega, M7502) is a 2x pre-mixed PCR master mix including nuclease-free water, *Taq* DNA polymerase, dNTPs and $MgCl_2$ in optimal concentrations for PCR reactions. For 25 µl PCR reactions, 12.5 µl 2 X Promega PCR mix was added to a PCR tube and mixed with 1 µl forward primer (0.4 µM), 1 µl reverse primer (0.4 µM), 250 ng cDNA, and increased to 25 µl total volume with nuclease-free water.

2.12.7 Agarose gel electrophoresis

Agarose gels were prepared to the desired concentrations by dissolving agarose powder (Invitrogen, 10975-035) in 1X Tris-Borate EDTA (TBE) buffer (Sigma, T4415) 10X stock diluted to 1x in water. The gel was heated in a microwave to dissolve before adding 1X SYBR Safe™ (Invitrogen, S33102) and pouring into a cast to set for 30 minutes at RT, before loading into a gel electrophoresis tank and submerging in 1X TBE buffer. Each PCR sample was pre-loaded with three times loading buffer (Promega, G190A), mixed and dispensed into the wells of the agarose gel. A PCR ladder was added to each gel for identification of PCR products by size. DNA ladders were selected depending on the size of the PCR product.

2.12.8 Quantitative-PCR

2.12.8.1 Low density array cards

TaqMan Low density array Human stem cell pluripotency panel cards (Applied Biosystems (ABI), 4385225, Lot A3566) were used for screening 96 different genes throughout differentiation. Cells were cultured and differentiated as previously described. Cell samples were isolated at distinct time points through differentiation (day 0, 4, 10, 18 and 28), RNA was extracted and cDNA synthesised (Sections 2.12.1 and 2.12.3**)**. For each

sample 75 ng cDNA was resuspended in nuclease free water to a 50 µl volume (Ambion, AM9937) and combined with 50 µl TaqMan Gene expression master mix (ABI, 4369016) before loading into each lane on the LDA card. For all 96 genes screened, 2 x 100 µl samples were loaded. Once loaded the card was centrifuged to disperse the cDNA solution throughout the card which could then be sealed using the card sealer (ABI), and run on the ABI 7900HT Fast Real time PCR system. Data were collected and analysed using ABI Sequence detection systems (SDS) software version 2.3.

Triplicate samples were run for each differentiation time point using three different passages of each hESC line, allowing for internal variation within a cell line. Different passages of the same hESC line presented variation in gene expression. For this reason, changes in gene expression were standardised to the appropriate day 0 sample. Each LDA card analysed four samples simultaneously, therefore it was not possible to run all 5 differentiation time points on the same LDA card. It was therefore decided to run each of the three triplicate samples (same differentiation time point and cell line but different passage numbers) in addition to a day zero calibrator per card. All LDA cards were from the same manufactured batch and run on the same machine for analysis to minimise sample variation.

Relative changes in gene expression were determined using $2^{-\Delta\Delta Ct}$ to represent the fold change in expression for each gene. ΔCt values were calculated using the difference between Ct day X and Ct at day 0. $\Delta\Delta$Ct values were calculated by subtracting ΔCt for the endogenous control at day X, from ΔCt GOI at day X.

2.12.9 Fluorescence Imaging Plate Reader

Culture media was removed by gentle inversion of the plate, so as not to dislodge the cell layer. Each well was rinsed gently with 200 µl HEPES buffered saline (HBS; Section 2.12.9.2), prior to incubation with 70 µl of 2 µM Fluo-4 AM as a calcium indicator dye (Section 2.12.9.3) at room temperature (RT) for 45 minutes. Cells were washed twice in 200 µl HBS per well, and incubated in 150 µl HBS before loading into the FLIPR.

The drug plate, a transparent flat bottomed 96 well plate (Greiner Bio-One, 655180) was prepared in advance with 80 µl of the relevant drug under test [N-methyl-D-aspartic acid (NMDA; Sigma, 65831), glycine (Sigma, G8790), potassium chloride (KCl; Sigma, P−3911)], and loaded into the FLIPR. Each experiment was run for 5 minutes with fluorescence

sampling every second. The first 30 readings provided the baseline fluorescence data before addition of the drug to the cells. Following addition of the drug, fluorescence intensities of the cells was recorded for a further 270 sec. Finally data were exported for analysis.

2.12.9.1 Poly-D-lysine

Five milligrams poly-D-lysine powder (Sigma, P7405) was dissolved in 50 ml sterile tissue culture grade water producing a 0.1 $mg.ml^{-1}$ stock solution.

2.12.9.2 HEPES buffered saline

HEPES buffered saline solution, pH 7.2, was prepared fresh for each experiment. The following reagents were added to distilled water: 120 mM NaCl (Sigma, S5886), 4.5 mM glucose (Sigma, G7021), 5.5 mM KCl, 1.8 mM $CaCl_2$ (Sigma, C8106), 1 mM $MgCl_2$ (Sigma, M4880), 20 mM HEPES (Fluka, 54455).

2.12.9.3 Fluo-4 AM calcium indicator dye for FLIPR

The calcium indicator dye Fluo-4 AM (Invitrogen, F14201) was used in the FLIPR assay to monitor calcium flux across the cells. Fluo-4 AM was supplied as a 50 µg powder and mixed with 23 µl of 2.5 % (w/v) pluronic F-127 (Invitrogen, P6867) in DMSO (w/v). For use in the FLIPR, 1 µl of this stock solution was added/ml buffer.

2.12.10 Calcium imaging

Cells cultured on glass coverslips (40 mm X 22 mm) were transferred into a calcium imaging clamp and incubated in the dark under a CO_2 atmosphere with 1 ml culture media supplemented with 1 µl Fura-2 AM stock solution (Section 2.12.10.1) for 30 minutes. Cells were washed in HBS buffer for 1 minute before the addition of neurotransmitter drugs (High potassium (Section 2.12.10.2), glutamate (Sigma, G2834), NMDA and glycine) which were added to the sample at a constant flow rate of 0.6 $ml.minute^{-1}$. Cell images were captured every second using a Zeiss Axiovert 100 TV, fluorescence microscope fitted with an Oriel Arc lamp. Kinetic imaging, AQM Advance 6 software was used for image analysis.

Cells were washed in HBS following drug exposure to enable recovery of basal intracellular calcium levels.

2.12.10.1 Fura-2 AM - calcium indicator dye

Fura-2 AM (Invitrogen, F1221) stock solution was prepared to 2 mM in DMSO with 2.5 % (v/v) pluronic F-127.

2.12.10.2 High potassium solution

The following was prepared in water: 125.5 mM KCl, 1.8 mM $CaCl_2$, 1 mM $MgCl_2$ and 20 mM HEPES and the pH adjusted to 7.2 with NaOH.

2.12.11 Patch clamping

Patch clamping was performed using an Axopatch 200B (Axon instruments) patching rig and a Zeiss Axiovert 135 microscope under 40 X magnification. Data was collected using pCLAMP software (Molecular Devices, USA). Cells were plated onto 13 mm round glass cover glasses pre-coated with poly-D-lysine (10 $\mu g.ml^{-1}$) 24-72 hours prior to patching.

Fine glass pipettes were drawn out from capillary glass tubing, attached to the patching attachment arm of the micromanipulator (Burleigh PCS-500). The electrode was inserted down the pipette which was then filled with patch clamping fluid. A cell was selected with morphologically neuronal features (phase bright, rounded cell body and axon-like process). The pipette was gradually lowered onto the cell until a change in resistance was recorded at which point the cell membrane was sucked up to form a seal with the end of the pipette until a seal resistance exceeding 1 GΩ was recorded. The membrane of the cell was ruptured and the cell contents left to equilibrate with the fluid within the pipette. Each cell was current clamped (I-clamp) by hyperpolarisation to -70 mV, before releasing the current; after which electrophysiologically active cells fired action potentials. Following this a current-voltage curve (IV) for each cell was generated by firing a family of voltages though the cell. The changes in output current were recorded and plotted for each cell.

Cells were exposed to 1 µM Tetrodotoxin (TTX; Sigma, T8024) at a flow rate 0.6 $ml.minute^{-1}$ for 2 minutes before re-testing for the ability to fire an action potential.

2.13 Immuno-staining

2.13.1 Fixation

A 4 % (v/v) formaldehyde fixative solution was prepared from 16 % (v/v) formaldehyde stock (Polysciences Inc, 18814) diluted in PBS containing 0.1 % (v/v) BSA stored at 4 °C and pre-warmed to 37 °C before use. Following fixation, cells were gently washed in PBS and left in blocking solution (Section 2.13.1.1) ready for staining.

2.13.1.1 Blocking solution

Standard blocking solution was prepared with 0.1 % (v/v) BSA in PBS and stored at 4 °C.

2.13.2 Permeablisation

For staining internal cell markers, cells were fixed (Section 2.13.1) and permeablised using 0.1 % (v/v) Triton-X-100 (BDH, 30632 4N) in blocking solution (Section 2.13.1.1) for 20 minutes at 37 °C. After permeablising, cells were washed and left in blocking solution.

2.13.3 Staining

Cells were fixed as described in Section 2.13.1. All samples were blocked for a minimum 30 minutes in blocking solution (Section 2.13.1.1). Samples stored in blocking solution at 4 °C did not need to be blocked prior to staining unless intracellular proteins were targeted. For intracellular proteins the cell samples were permeablised prior to blocking (Section 2.13.2). Following blocking, cells were incubated with primary antibodies (Table 2.1) at 37 °C for 1 hour (antibodies towards intracellular targets were diluted in blocking solution containing 0.01 % (v/v) Triton-X-100). Samples were washed three times in PBS in quick succession (removing just 50 % volume for each successive wash so as not to detach cells from the culture surface) before washing twice for 15 minutes at RT on a bench-top shaker set to 30 rpm. Secondary antibodies (Table 2.2) were prepared in blocking solution (+/- 0.01 % (v/v) Triton-X-100) and incubated with cells at RT for 1 hour in the dark. Cells were washed as above, taking care to ensure minimal light exposure to the sample. If required, cells were incubated with Hoechst stain (Molecular probes, H-3570) for 30 seconds before washing the secondary antibody.

Stained samples were mounted using mounting media (DAKO, S3023) and sealed with clear nail varnish for imaging. Bright field and fluorescence images were captured using Olympus IX70 inverted epi-fluorescence microscope. Images were analysed using Olympus CellF/CellR software. Confocal images were captured using a Lecia DMRE microscope and a Leica TCS SP2 confocal scanner head.

2.13.4 Flow cytometry

Flow cytometry analysis was carried out using a Guava EasyCyte (Guava technologies). Cells (1×10^5) were cultured and differentiated as required before TrypLE™ treatment to create a single cell suspension. Cells were fixed in 4 % (v/v) formaldehyde (Section 2.13.1) and washed in PBS. For internal cell markers, cells were permeablised (Section 2.13.2**)** and incubated with blocking solution (Section 2.13.1.1). Primary antibodies (Table 2.1) were diluted and incubated with cells at 37 °C for at least 20 minutes. Samples were washed three times in PBS blocking solution and centrifuged at 240 g for five minutes. Secondary antibodies (Table 2.2) were diluted and incubated with the cells in the dark for at least 20 minutes. Cells were washed three times in PBS blocking solution and centrifuged at 170 g for five minutes before finally resuspending in 200 µl blocking solution and transferring into 96-well flat bottomed plate. Samples were run on the guava flow cytometer and data analysis was carried out using Guava Cytosoft software version 3.6.1.

2.13.4.1 Comparison of cell dissociation reagents

Embryoid bodies and neuronal clusters were washed twice in PBS without Ca^{+2} and Mg^{2+} before dissociation reagents: TrypLE™ Express (1 X), 0.25 % Trypsin-EDTA (Gibco, 25200-056), 1 $mg.ml^{-1}$ Collagenase IV (Gibco, 17104-019), Accutase™ (1 X, Chemicon, SR005) and 1 $mg.ml^{-1}$ Dispase (Stem Cell Technologies, 07923), were applied and incubated at 37 °C for 10 minutes. Samples were centrifuged to remove the dissociation reagents and resuspended in NBD media (Section 2.10.3.1). Each cell sample was triturated ten times to break up clusters before counting using a bright line haemocytometer to determine cell number and viability.

Primary antibodies						
Isotype	**Host**	**Target**	**Supplier**	**Product code**	**Concentration**	**working dilution**
IgY	Chicken	MAP2	Abcam	ab5392	19mg/ml	1:1000-5000
IgY	Chicken	TH	Millipore	AB9702	0.2mg/mL	1:200-1000
IgY	Chicken	Isotype control	Chemicon	PP25	1mg/ml	variable
IgG	Mouse	Isotype control	Chemicon	SCR060 Part PP54	1mg/ml	variable
IgG1	Mouse	Beta III tubulin	Chemicon	MAB1637	ascite	1:1000
IgG1	Mouse	70kD neurofilament	Abcam	ab7255	ascite	1:250-400
IgG1	Mouse	Nestin	Chemicon	SCR060 Part 2005895	1mg/ml	1:500
IgG1	Mouse	GFAP	Chemicon	MAB360	ascite	1:400-1:800
IgG2b	Mouse	OCT3/4	Santa Cruz	Sc5279	0.2mg/ml	1:75
IgG3	Mouse	SSEA4	Abcam	ab16287	1mg/ml	1:50
IgM	Mouse	Tra-1-60	abcam	ab16288	2mg/mL	1:70
IgM	Mouse	Tra-1-81	Chemicon	90233	1mg/ml	1:100
IgM	Mouse	Isotype control	Chemicon	PP50	0.74mg/ml	variable
IgM	Mouse	Isotype control	Chemicon	SCR060 Part 2003599	2mg/ml	variable
antiserum	Rabbit	GABA	Sigma	A2052	ascite	1:500
antiserum	Rabbit	Serotonin	Sigma	S5545	ascite	1:500
IgG	Rabbit	Synaptophysin	Abcam	ab52636	ascite	1:100
IgG	Rabbit	GFAP	Chemicon	SCR060 Part AB5804	ascite	1:200-250
IgG	Rabbit	Isotype control	Chemicon	PP64	1mg/ml	variable
IgG	Rabbit	Sox2	Abcam	ab59776	1.28mg/ml	1:400
IgG	Rabbit	Sox2	Chemicon	SCR060 Part 2003600	1mg/ml	1:1000

Table 2.1. Primary antibodies.

Antibodies listed were used throughout this project at the specified working dilution. Isotype controls were run for each sample at the same antibody concentration as the specific primary antibody. Ascite antibody concentrations were not specified by the supplier.

Secondaries labelled						
Host	**Target**	**Fluorochrome**	**Supplier**	**Product code**	**Concentration**	**Working dilution**
Chicken IgY	Donkey	FITC	Chemicon	AP194F	1mg/ mL	1:100
Mouse IgG	Goat	Alexa Fluor 488	Invitrogen	A31633	2mg/ml	1:100-500
Mouse IgG	Donkey	Cy3	Chemicon	AP192C	1mg/ml	1:500
Mouse IgG3	Goat	FITC	Caltag	M32601	-	1:500
Mouse IgM	Goat	FITC	Chemicon	AP500F	1mg/ml	1:100-200
Mouse IgM	Goat	FITC	Sigma	085K6118	-	1:500
Rabbit IgG	Donkey	Cy3	Chemicon	AP182C	1mg/ml	1:500
Rabbit IgG H+L	Goat	FITC	Abcam	ab6717	2mg/ml	1:500

Table 2.2. Secondary antibodies.

Secondary antibodies used throughout this project at the specified working dilution.

2.14 Karyology

Fresh methanol:acetic acid (3:1; BDH, 291926G; BDH, 10001CU) fixative was prepared and stored at -20 °C prior to use. Cells were harvested at 50 % confluence. Spent media was aspirate from cultures and transferred to a 15 ml centrifuge tube (Falcon). KaryoMAX® Colcemid® (Gibco, 15212-046) was added to each culture to a final concentration 0.04 $\mu g.ml^{-1}$ before incubation at 37 °C for 2-4 hours, to arrest cells in the metaphase stage of the cell cycle. Colcemid® media was carefully removed from cultures and cells washed in PBS. All spent and wash media was transferred to the 15 ml tube for centrifugation. Cells were dislodged using TrypLE™ Express before finally resuspending in original culture media from the morning. Cell samples were centrifuged at 240 g, for up to 5 minutes. Supernatant was removed leaving cells in 1.5 ml spent media to which 6 ml distilled water was added, creating a hypotonic solution. Cells were incubated to swell for 15 minutes at 37 °C before centrifugation at 240 g, 5 minutes. Supernatant was removed from the cell pellet and 2 ml pre-cooled fixative was added slowly to the cells. Cells were left to incubate at RT for ≥ 15 minutes. Cells were re-centrifuged and fixative supernatant replaced with 2 ml fresh fixative. Cell solutions were dropped onto ethanol cleaned glass slides at 60° angle and left to dry before staining with fresh Giemsa stain:water (1:3; Sigma, GS1L) for 20 minutes at RT. Slides were washed in distilled water and left to air dry for visualisation. *This protocol was sourced from the UKSCB.*

2.14.1 Modified karyotypic analysis

Cells were cultured as described in Section 2.9.1 and harvested at approximately 50 % confluence for enzymatically passaged lines or 5-6 days post-passaging for mechanically passaged lines. Healthy cells were treated with TrypLE™ Express, creating a single cell suspension, washed in PBS and resuspended in 1.5 ml media with 6 ml sterile tissue culture grade waster producing a hypotonic solution. Samples were incubated for 15 minutes at 37 °C. Following swelling, 1 ml methanol:acetic acid fixative, pre-cooled to -20 °C was added to the cells in hypotonic solution and centrifuged at 170 g for three minutes. The supernatant was poured off and 3 ml fix added per sample to resuspend the cells. Finally, three 20 µl volumes of cell suspension in fix were dropped onto a clean glass slide and left to dry. Slides were incubated with 2 ml Giemsa stain for 15 minutes at RT before rinsing thoroughly before imaging. Cell suspensions containing large numbers of metaphase spreads were sent to TDL Genetics (The Doctors laboratory; London, UK) for analysis.

3 Neuronal differentiation of the Embryonal Carcinoma cell line – NTERA2

3.1 Introduction to NTERA2

In order to generate a successful therapy for neurodegenerative diseases, it is necessary to understand neurogenesis in healthy tissue, and then determine at what point the system malfunctioned so that a suitable preventative or curative therapy can be identified. Studies on early embryonic development are excellent tools for understanding neurogenesis. Much of the work in this field has been carried out in animal models, mainly in the developing chick, mouse and rat. However, due to species variation, developmental cues are not always directly translatable to humans. Ethical constraints in researching human embryonic development mean that surrogate models must be applied to further our understanding in this area.

The derivation of the first hESC lines in 1998 created an alternative source of investigation, due to their ability to recapitulate embryonic development *in vitro* (Thomson et al., 1998). However, it was some time before these cells were widely accessible for research and difficulties with cell supply and sustained pluripotent culture limited their use in early years. Instead, research using alternative pluripotent cell lines such as hEC cells (Section 1.11) generated much of the underpinning for our knowledge of hESC culture and differentiation.

The hEC cell line: NTERA2 is a pluripotent cell line with a long published history of neuronal differentiation and serves as a model for characterising *in vitro* neuronal differentiation. NTERA2 derived neurons are sustainable in long term culture for up to 10 months with no sign of reversion to pluripotency (Pleasure et al., 1992). As such NTERA2 provides an alternative source of neurons for pharmacological screening including assay to test for the toxicity of Tetanus and Botulinum toxoids prior to batch release (Department of Bacteriology, NIBSC), reducing reliance on animals for primary neural tissue. However, neuronal yield and reproducibility of differentiation from NTERA2 was perceived to be poor. More significantly, the sensitivity of NTERA2 derived neurons to stimulation was considerably lower than that of primary tissue making them an unsuitable alternative cell source for routine screening (personal communication, Dr. C. Escargueil and Dr. T. Sesardic, Bacteriology, NIBSC). This highlights just one of the limitations in using neurons derived from pluripotent cell sources, for routine pharmacological screening. These assays in addition to many others, returned to using primary rat neurons with the required sensitivity, demonstrating the requirement for improvements in directed differentiation of

neuronal cell types, and identification of an optimal starting pool of cells for high neuronal yields. For any cell line to be a suitable source of neurons for use in cell based assays, like those described above, or to be incorporated into a cell based therapies, differentiation must be reliable, robust and reproducible, yielding a consistent supply of neurons with comparable functionality and sensitivity to that of a primary neuron.

All cells of the body are derived from the early pluripotent cells of the embryo, therefore under the correct stimuli; a pluripotent cell line should be capable of directed differentiation into highly functional neurons. With this in mind, this project placed early focus on characterisation the neuronal differentiation in NTERA2.

Whilst many groups have investigated neuronal differentiation in this hEC cell line, the overall objective for the work in this chapter was focused towards understanding the process of neuronal differentiation from pluripotent cell lines with a view to identifying the key parameters which affect the efficiency of differentiation. With the need for high reproducibility and enhanced functional response of cell line derived neurons in mind, the electrophysiological response of NTERA2 derived neurons was screened in comparison to primary neurons.

3.2 Results

3.2.1 Pluripotency in NTERA2

NTERA2 stocks were cultured and differentiated as detailed in Section 2.4. Pluripotent NTERA2 cells were identified by their compact cell body with large nucleus to cytoplasm ratio; prominent nucleoli and uniform morphology across the culture surface (Figure 3.1). NTERA2 cells grew most effectively when passaged every 3-4 days, seeding cells at relatively high density (6×10^4 cells/cm^2). Cultures often underwent spontaneous differentiation into an epithelial-like cell fate when seeded at lower low densities (Figure 3.2), losing the distinctive morphology which was not recoverable to a pluripotent state.

The reason behind the spontaneous differentiation at low cell density is yet to be confirmed; however, cell to cell contact is thought to play a key role in sustained pluripotency (Andrews et al., 2001). The NTERA2 cell line was therefore most successfully maintained using mechanical methods of passaging (i.e. sterile glass beads or cell scrapers) which retained cells in small clumps.

3.2.2 Neuronal differentiation in NTERA2

3.2.2.1 Neurons in culture

Neurons were identified by their large rounded, phase bright cell body forming long extensions (axons or dendrites) projected towards neighbouring cells (Figure 3.3). Neuronal projections differed in number and length between cells but were easily visible under bright field microscopy.

3.2.2.2 Directed differentiation in NTERA2

NTERA2 cells were differentiated towards a neuronal cell fate following an ATRA induced differentiation protocol detailed in Section 2.4.3 which was adapted from Pleasure et al., 1992. Images of cells differentiating along the six week process were captured using phase contrast imaging (Figure 3.5). In the early stages of ATRA-induced differentiation, a reduced rate of proliferation was evident during which, the NTERA2 cells flattened out and lost their defined cell edges. After 2 weeks in culture the cells formed a monolayer which remained tightly attached to the culture surface, amongst which small islands of tight cell clusters became visible. Between weeks 2-4 these clusters became larger and neuronal-like cells could be identified with rounded phase bright cell bodies, buried amongst them. At week 4 the entire cell layer was detached from the culture surface using Trypsin/EDTA cell dissociation reagent. Cells were dissociated into very small clusters/single cells and replated into fresh culture surfaces in a 1:6 ratio. Dissociation of the cell layer in this way enabled dispersal of the developing neurons from amongst the tight cell clusters.

The rounded neuronal cell body resulted in a minimal area for attachment to the fresh culture surface. Subsequently neurons were very weakly attached to the tissue culture surface. Neurons were most commonly seen to settle and attach on top of the non-neuronal cells in culture rather than directly onto the tissue culture surface (Figure 3.6). Weak attachment of neurons to the culture surface meant that these cells could be readily selected for purification. Neurons were usually the first cells to detach when mechanical or enzymatic detachment procedures were applied due to their rounded morphology meaning minimal contact with the culture surface.

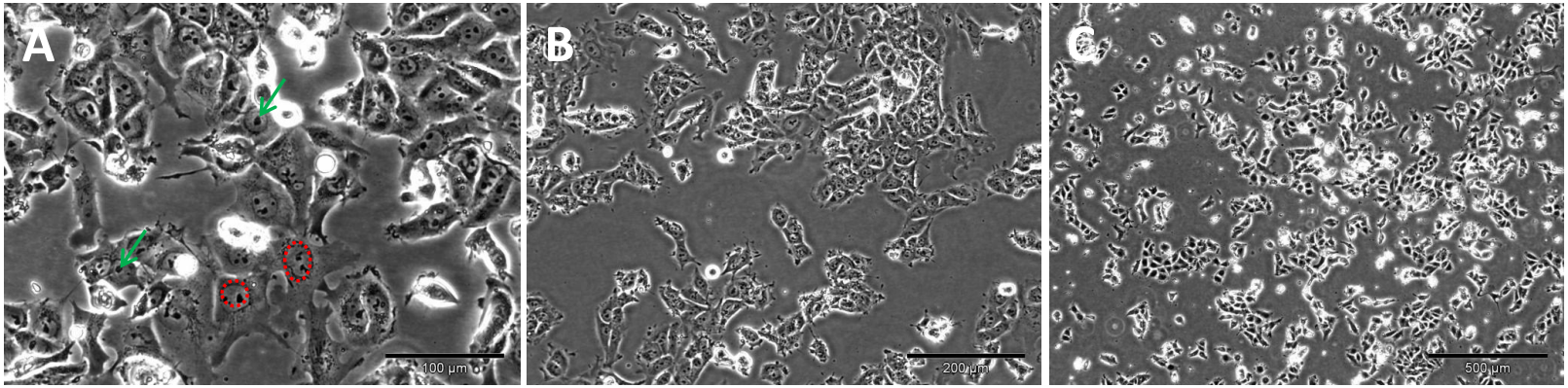

Figure 3.1. Identification of NTERA2.

Pluripotency in NTERA2 was identified by the high nucleus to cytoplasm ratio (red dotted lines) and prominent nucleoli (green arrows). A: x20, B: x10, C: x4 magnification.

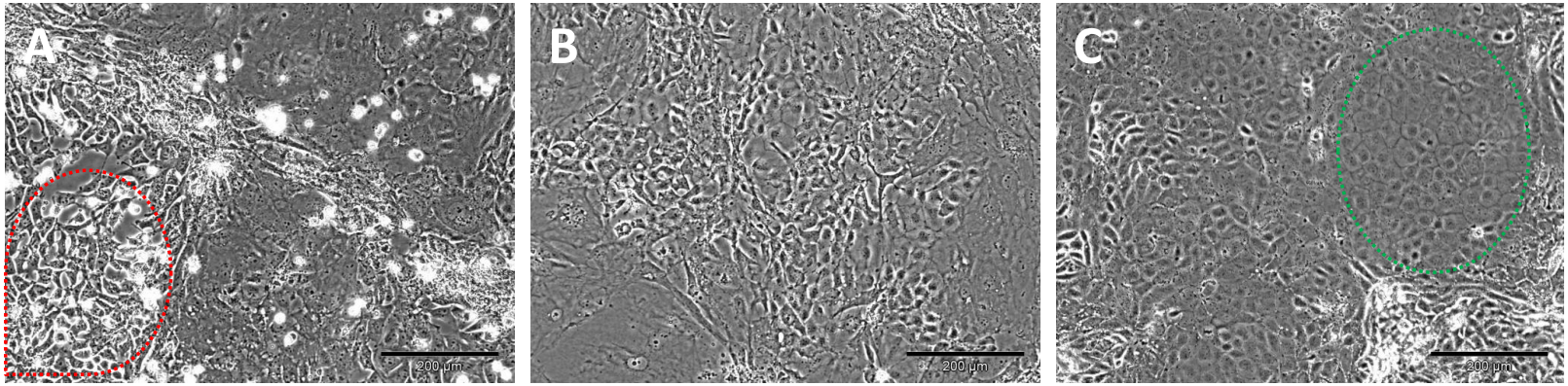

Figure 3.2. Spontaneous differentiation in NTERA2.

At low cell density (< 6 x 10^4 cells/cm^2) NTERA2 spontaneously differentiated, losing distinct features of pluripotency, forming a flattened epithelial-like morphology (green dash). Varying degrees of spontaneous differentiation occurred from small areas of patchy differentiation (A, B) to complete loss of pluripotent NTERA2 identity (C). A heterogeneous population was often evident across the culture surface with areas of pluripotent NTERA2 cells visible (A; red dash). Without intervention the culture completely differentiated (C) and it was necessary to recover fresh NTERA2 stocks LN2 storage.

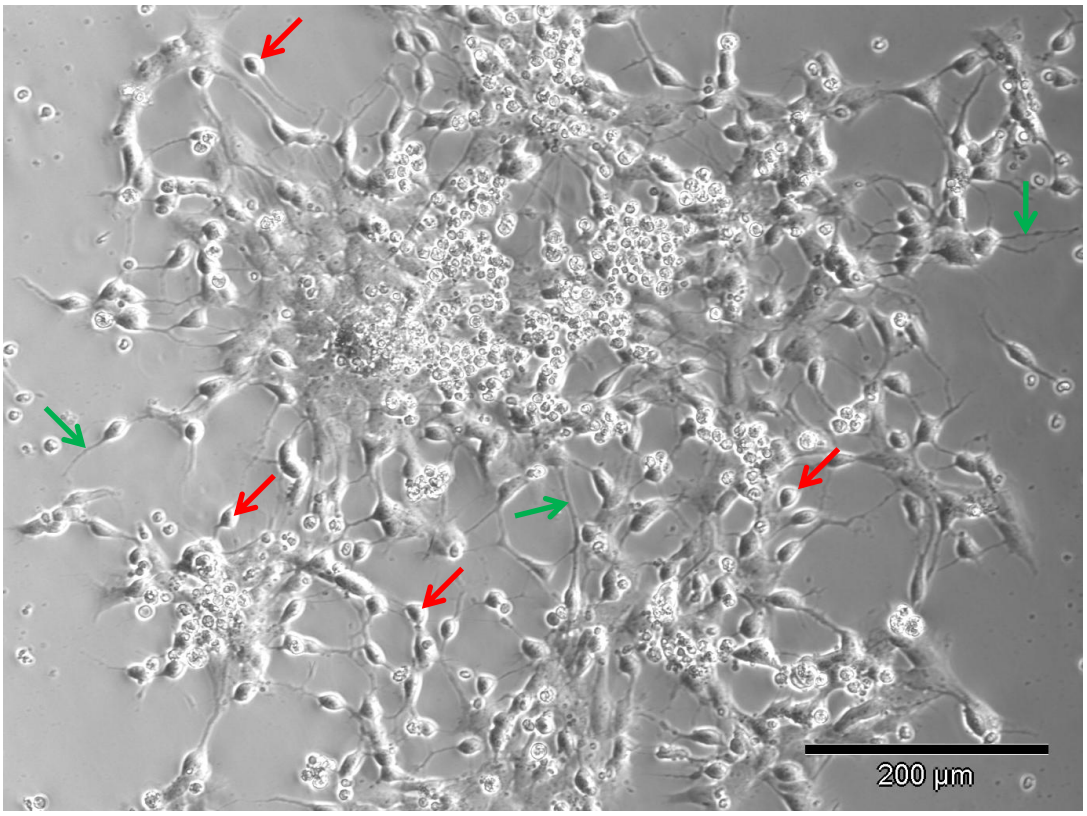

Figure 3.3. Typical neuronal morphology.

Typical neurons in culture with rounded, phase bright cell bodies (red arrows) and projecting axons and dendrites (green arrows). Image captured under phase contrast imaging at x10 magnification.

Following replating at week 4, cultures were incubated with mitotic inhibitors (cytosine arabinofuranoside, fluorodeoxyuridine and uridine) which block cell cycle progression. The activity of these inhibitors targeted proliferating epithelial-like cells, during the DNA synthesis phase of the cell cycle, initiating apoptosis (Figure 3.6). The loss of the epithelial cells also resulted in a depletion of neurons through their inability to attach directly to the culture surface.

To confirm that the neuronal differentiation of the NTERA2 pluripotent population was induced by ATRA rather than by seeding at low density, an untreated control sample of NTERA2 cells was prepared. In the presence of ATRA, NTERA2 cells proliferated at a slower rate than was seen in untreated samples (Figure 3.7; Day 3; (Encinas et al., 2000)). Upon reaching confluency, untreated cells began to detach from the culture surface and could not be rescued into pluripotent growth or differentiation (*data not shown*). After ten days in culture without ATRA the cell layer was completely detached (Figure 3.7).

Stock ATRA solution was prepared in DMSO (Section 2.4.4.1). DMSO is used in cryopreservation media and has been shown to induce differentiation in multipotent populations (lu et al., 2004). However, it have been previously shown that DMSO does not affect neuronal differentiation in NTERA2 either positively or negatively (Andrews et al., 1986; Bani-Yaghoub et al., 1999; Veal et al., 2000), therefore a DMSO control was not included in these experiments.

The differentiated NTERA2 population was largely heterogeneous containing cells of neuronal and non-neuronal morphology (Figure 3.5). The presence of contaminating non-neuronal cells in NTERA2 ATRA-induced differentiation has been previously described (Andrews, 1984; Pleasure et al., 1992; Encinas et al., 2000). The presence of non-neuronal cells will result in mixed signalling across the culture, which is likely to reduce the neuronal yield and possibly affect neuronal maturation. It was therefore clear that improvement in neuronal purity was necessary.

During experimental screening of NTERA2 derived neurons, cells were cultured in a range of different culture vessels. For routine differentiation, cells were differentiated in T75 tissue culture flasks. However, when larger numbers of neurons were required for study, differentiation was initiated in larger tissue culture vessels (T175). In running these protocols, variations in the yield of neurons achieved were observed. This led to a study to compare the effect of the size of culture vessel of the success of neuronal differentiation.

3.2.2.3 The effect of culture vessel size.

Differences in neuronal yield were observational using bright field microscopy. Cells were seeded into 24-well or 6-well plates, and tissue culture flasks T25, T75 and T150 at 2.6×10^4 cells/cm^2. The ratio of surface area to media volume was kept constant between samples. Initial studies suggested that smaller culture vessels generated larger proportion of neuronal cells. This was thought to have been a result less dispersion of the signalling molecules required for neuronal differentiation and retention close to the cell layer (*subjective data not included*). This would need to be repeated for confirmation and the numbers of neurons quantified following each culture vessel, ideally using flow cytometry to demonstrate whether this is a significant effect. The time required for handling and processing cells in smaller vessels is similar to that for handling larger vessels, although in smaller vessels the number of cells generated is markedly reduced. Therefore by means of a compromise between time for processing and optimal neuronal yield, NTERA2 were routinely cultured in T25 tissue culture flasks for neuronal differentiation rather than the T75 as is more standard for NTERA2 differentiation protocols (Pleasure et al., 1992).

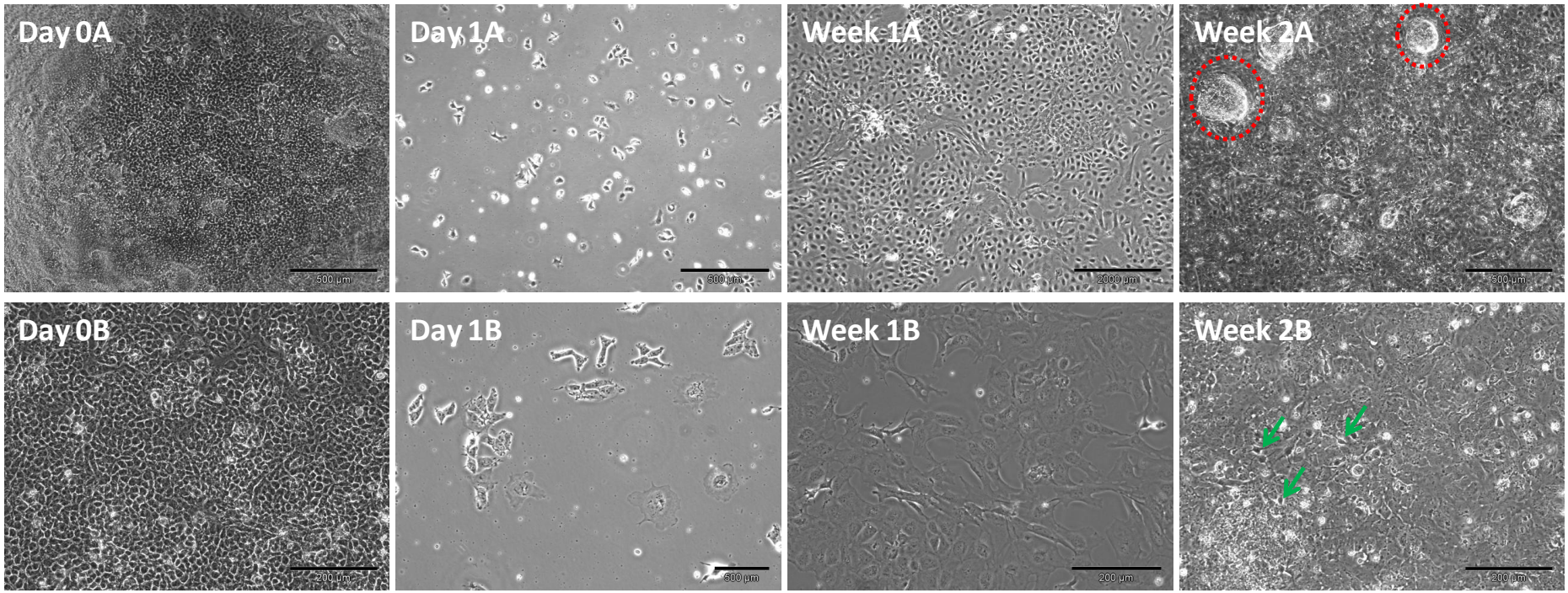

Figure 3.4. Differentiation of NTERA2 into neurons (part 1).

A: x4 magnification, B: x10 magnification. On day 0 a confluent layer of pluripotent NTERA2 cells were dissociated into small clusters/single cells and seeded into a fresh culture vessel at 1.3×10^4 cells/cm^2 in culture media containing 10^{-5} mM ATRA. After 24 hours in culture the cells were attached and proceeded to proliferate but lost their compacted cell structure. After 1 week in culture, the cells were mainly of a flattened morphology. On reaching confluency proliferation continued at a slower rate, until small compacted areas of cells were visible (week 2A – red dashed area) and cells with rounded phase bright cell bodies were visible (Week 2B – green arrow). S*ee part 2 for continued story*.

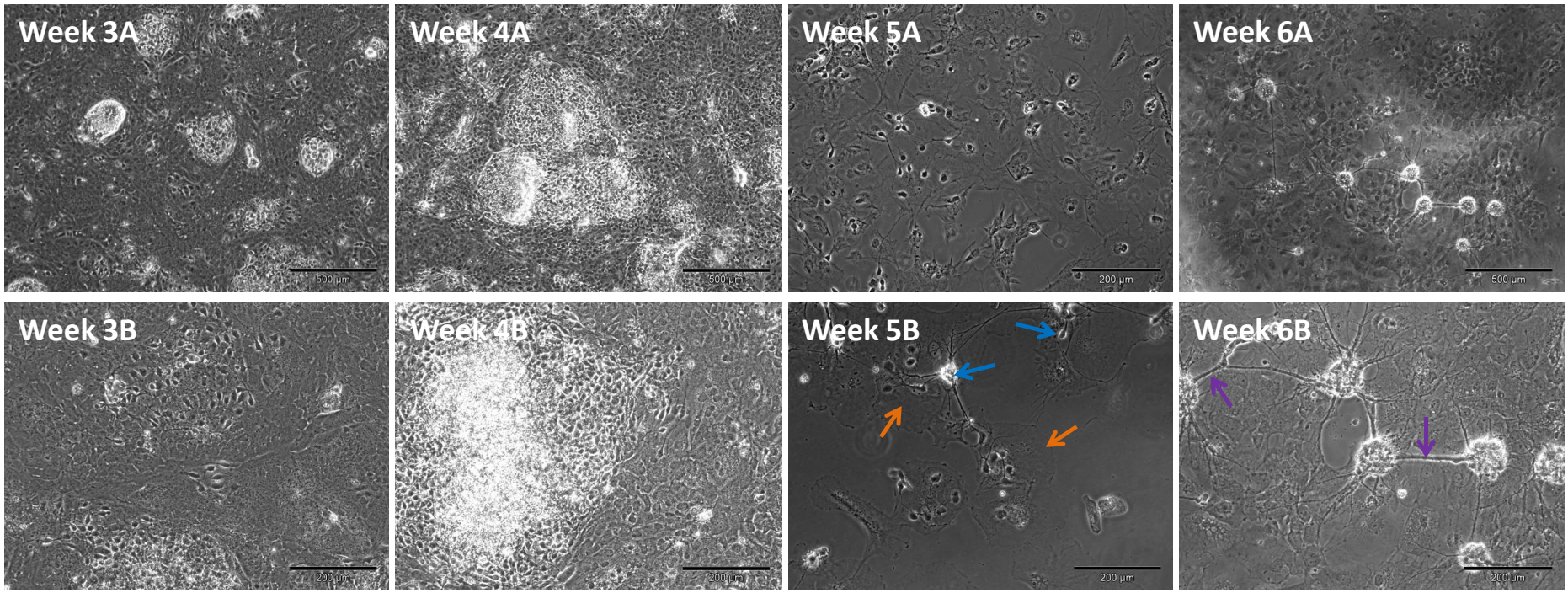

Figure 3.5. Differentiation of NTERA2 into neurons (part 2).

A: x4 magnification, B: x10 magnification. Between weeks 3 and 4 the number of compacted cell structures increased, in addition to the number of visible neuronal cells around the outside of these structures. After 4 weeks in ATRA, the cell layer was dissociated with Trypsin/EDTA and replated onto a fresh culture surface in a 1:6 split ratio. Cultures were incubated with mitotic inhibitors to remove non-neuronal cells from culture. At 5 weeks neurons (Week 5B - blue arrow) were clearly visible in culture, growing on the surface of flattened epithelial-like cells (Week 5B – orange arrow). By 6 weeks the overall number of neurons increased as clusters of neurons increased in size and fascicle of axons become obvious (Week 6B - purple arrow). However, the number of single neurons in culture was reduced. The differentiated population remained heterogeneous in cell type with non-neuronal cells forming a mostly confluent layer of cells on which the neurons attach.

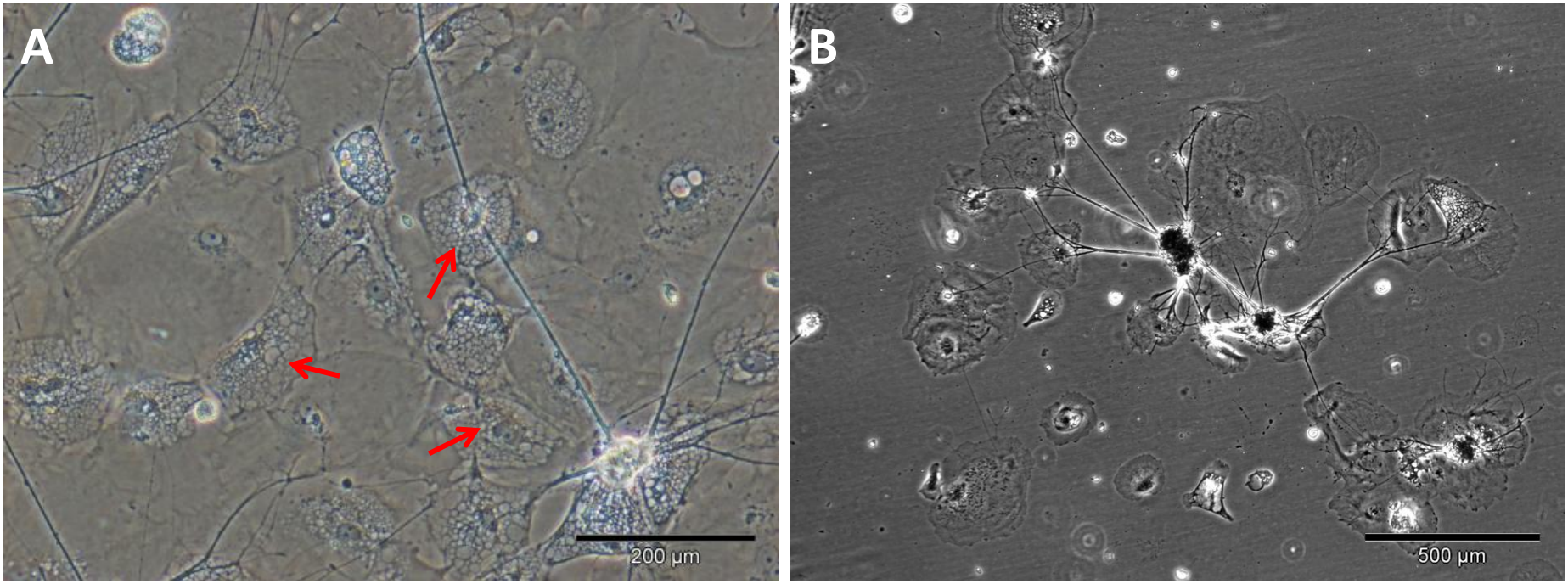

Figure 3.6. Purification of neurons using mitotic inhibitors.

Mitotic inhibitors selectively targeted the proliferating cells which were mostly of non-neuronal morphology and formed the largest fraction of the differentiated population (A; red arrows - apoptotic cells). Neurons attached to these cells in preference to the culture surface (B). Loss /death of these non-neuronal cells resulted in eventual depletion of neuronal population due to inability to adhere to the culture surface.

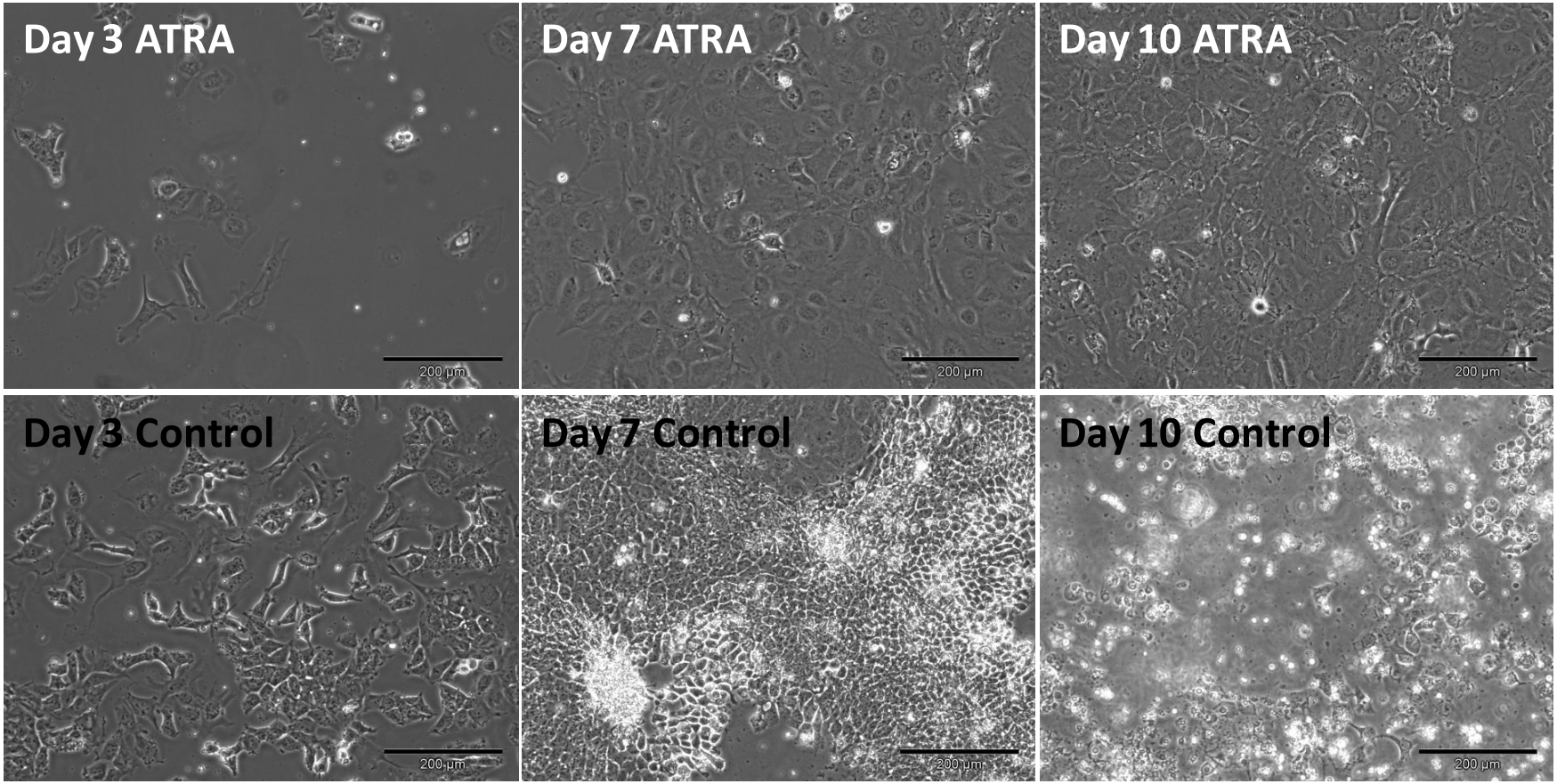

Figure 3.7. NTERA2 +/- ATRA.

NTERA2 cells were seeded at 1.3 x 10^4 cells/cm^2 in ATRA differentiation media and standard culture media (control). Cultured cells were fed twice weekly and left to grow. Images of cells were captured 3, 7 and 10 days after neuronal induction with ATRA. No obvious difference in cellular morphology was detected by day 3 although the overall number of cells was visibly higher in the untreated control than in the ATRA treated cells. By day 7 reduced rate of proliferation was very apparent in ATRA treated cultures. After 10 days ATRA induction cells in the untreated control samples had overgrown and were seen detaching from the culture surface, from which it was concluded that it was not the low seeding density which induced neuronal differentiation but a result of cellular exposure to ATRA in culture.

3.2.2.4 Improving neuronal purity

In an attempt to reduce the heterogeneity of the six week differentiated NTERA2 population, an experiment was carried out to identify the optimal conditions and exposure time for Trypsin detachment of the neurons from the non-neuronal cell layer. Heterogeneous neuronal populations were washed in fresh media or PBS, and exposed to Trypsin/EDTA for either: 30 seconds, 1 minute and 2 minutes followed by incubation at 37 °C. All experiments were carried out by a single operator to reduce additional variable factors. Samples without a PBS wash did not detach effectively due to the presence of serum which blocked the activity of the Trypsin. Exposure to Trypsin/EDTA for 1-2 minutes at 37 °C resulted in complete detachment of the cell layer, and therefore resulted in poor control over neuronal selection. Optimal separation of neurons from underlying epithelial-like cells was achieved following a rapid PBS wash and 30 seconds Trypsin/EDTA incubation at 37 °C. Cells were subsequently centrifuged to remove the Trypsin/EDTA and washed in differentiation media before replated into a fresh culture vessel.

3.2.3 Characterisation of differentiation using immunostaining

Throughout this study pluripotent NTERA2 and differentiated neurons were identified by morphology (Sections 3.2 and 3.2.2.1). To ensure that pluripotent cells expressed typical markers of pluripotency and that the morphology of the cells which appeared to be neuronal were truly neuronal, immunostaining analysis of populations was carried out.

NTERA2 cells at p37 were stained for a selection of markers to characterise the populations throughout differentiation according to the methods outlined in Section 2.13**.** Pluripotency markers: SSEA4, Tra-1-60, OCT4 and SOX2 (Section 1.9.1) and pan neuronal markers: TUBB3, MAP2 and synaptophysin (SYP; a glycoprotein found in the membrane of synaptic vesicles (De Camilli and Navone, 1987)) were used for identification of the differentiating populations. At the end of the 6 week differentiation procedure, cells were stained for the presence of neurotransmitters: Serotonin, TH and GABA in an attempt to identify the neuronal phenotype generated. Optimal antibody dilutions and immunostaining procedures were identified and Isotope controls run for each antibody at equivalent concentrations, confirming specificity of positive staining. Cellular morphology was found to be best preserved during fixation using pre-warmed reagents to 37 °C. A DNA stain was included in all preparations to confirm the localisation of positive staining.

Undifferentiated NTERA2 cells were positive for both SSEA4 (Figure 3.8) and Tra-1-60 (Figure 3.9), revealing variable levels of expression (high and low) across the population. Expression of SSEA4 was more consistent than Tra-1-60.

Expression of the pluripotency transcription factors OCT4 (Figure 3.11) and SOX2 (Figure 3.12) were positive in undifferentiated NTERA2. Some OCT4 and SOX2 negative cells were identified, suggesting a loss of pluripotency in parts of the population. OCT4/SOX2 negative cells were found as single cells or in small clumps on the outer edge of larger cell groups suggesting cell-to-cell contact aided retention of pluripotency.

Prior to induction of differentiation, NTERA2 cells did not express neuronal markers TUBB3 or MAP2 (*Images available on request*), confirming the absence of neurons in the starting cell pools; however, undifferentiated populations were positive for the neural stem cell marker Nestin (Figure 3.10). Expression of pluripotency and neuronal markers in differentiated NTERA2 cells were analysed after 6 weeks. Staining was carried out on the same day as for undifferentiated samples to eliminate variation in sample preparation during staining. Undifferentiated cells were fixed on day 0 and stored at 4 °C until 6 week differentiated samples were ready.

NTERA2-derived neurons stained positive for TUBB3 (Figure 3.13) and MAP2 (Figure 3.14), confirming the generation of neurons as a result of differentiation. Combined Hoechst and FITC images for these markers highlight the number of non-neuronal cells in culture after 6 weeks. Neuronal projections from large numbers of neurons align into fascicles and extended long distances to communicate with cells across the culture surface.

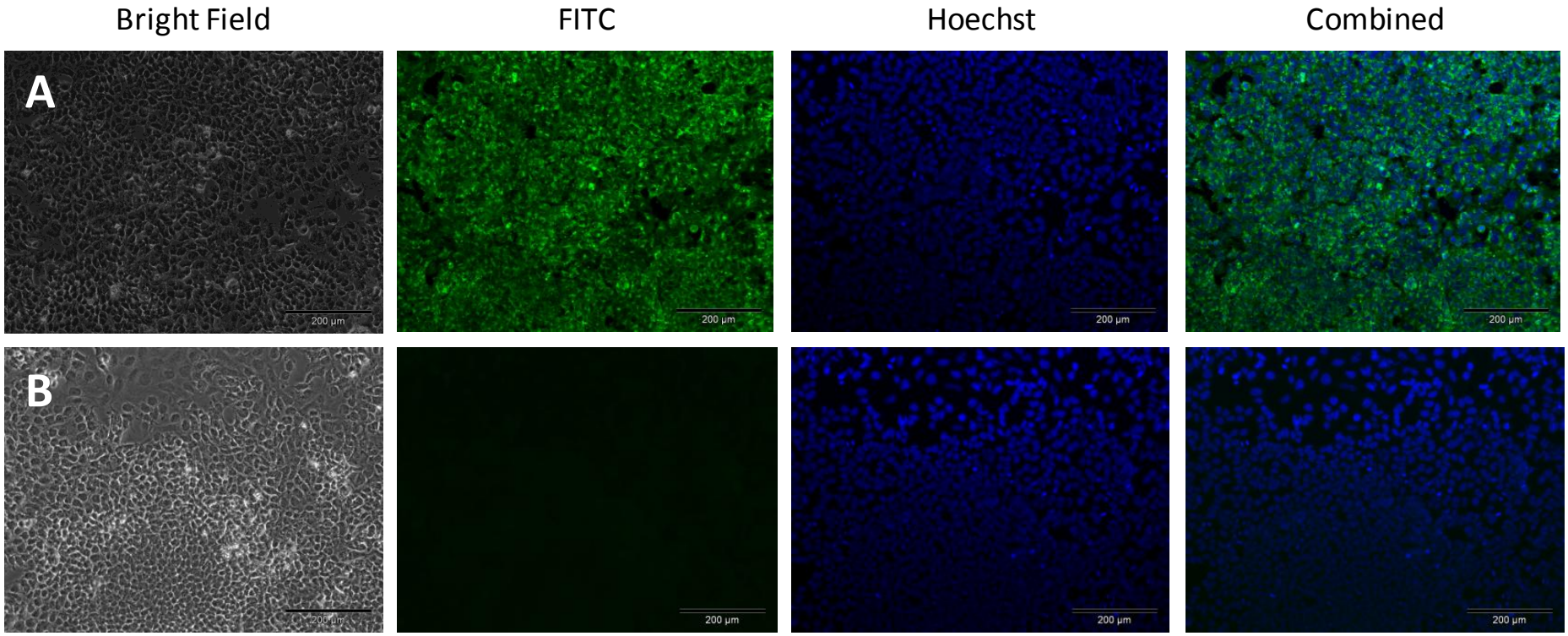

Figure 3.8. Immunostaining for SSEA4 in undifferentiated NTERA2

Expression of the surface pluripotency marker SSEA4 (A) was positve across the undifferentiated NTERA2 population (A: x10 magnification). Isotype controls were negtive (B: x10 magnification).

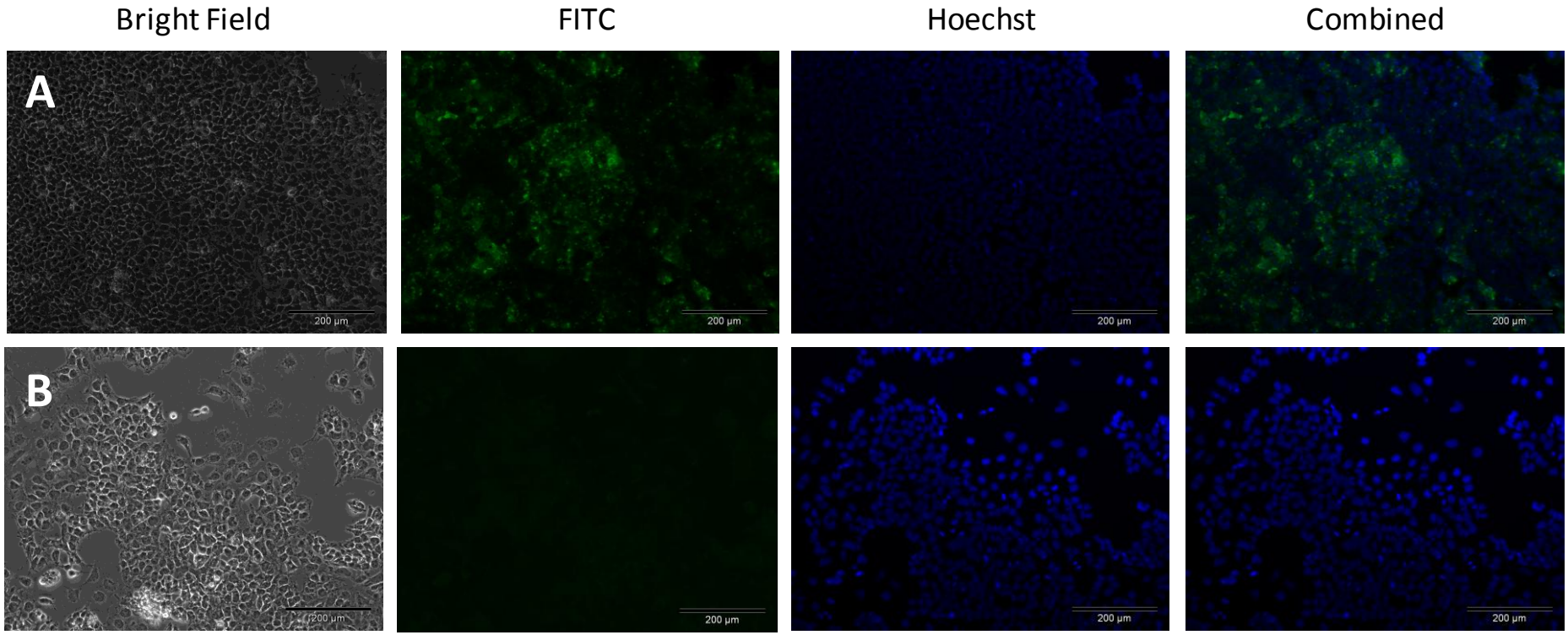

Figure 3.9. Immunostaining for Tra-1-60 in undifferentiated NTERA2.

Expression of the surface pluripotency marker Tra-1-60 was positve across the undifferentiated NTERA2 population (A: x10 magnification). Isotype controls were negtive (B: x10 magnification).

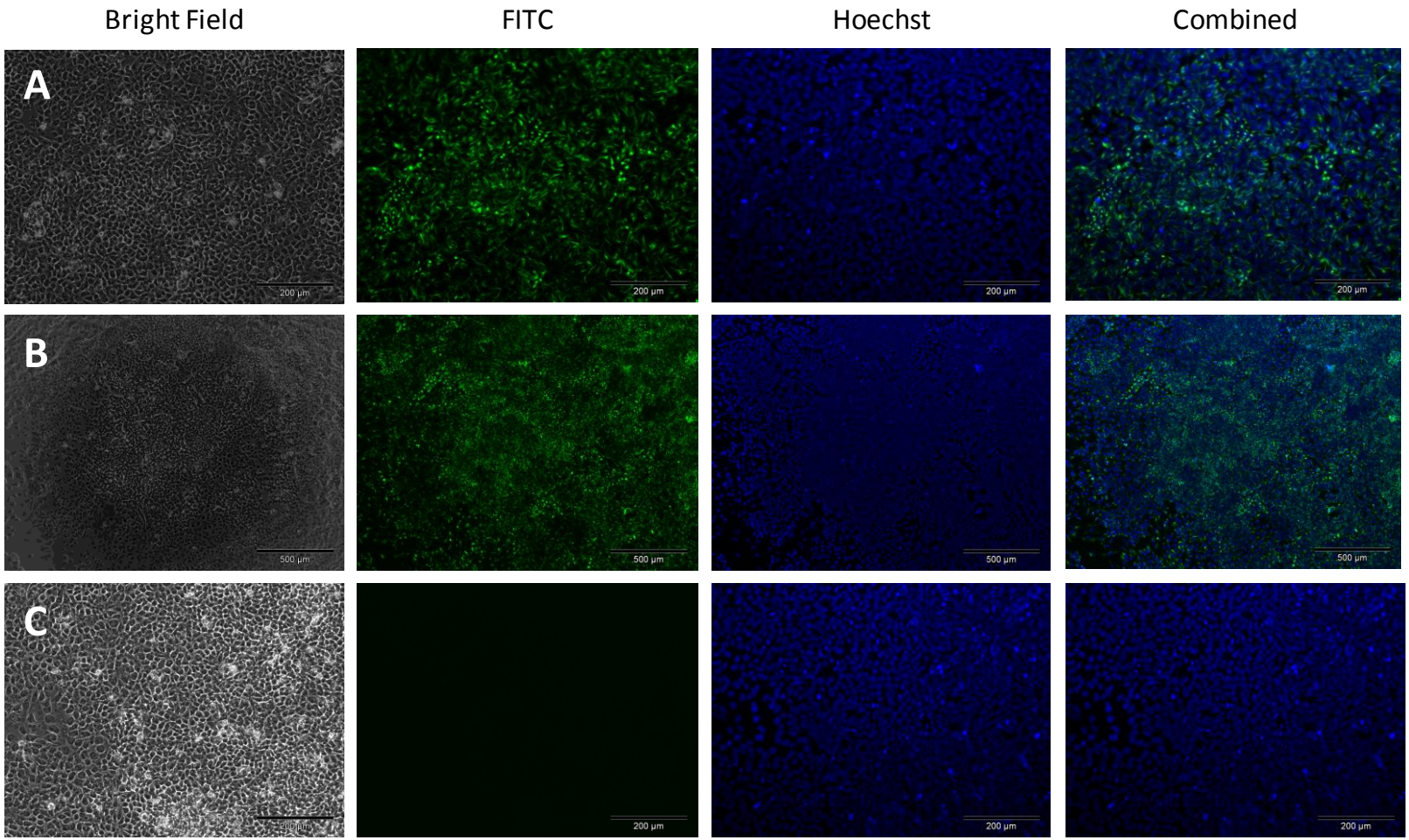

Figure 3.10. Immunostaining of Nestin in undifferentiated NTERA2.

Expression of the Type VI intermediate filament Nestin was positve across the undifferentiated NTERA2 population seen (A: x10 magnification, B: x4 magnificaiton). Isotype controls were negtive (C: x10 magnification).

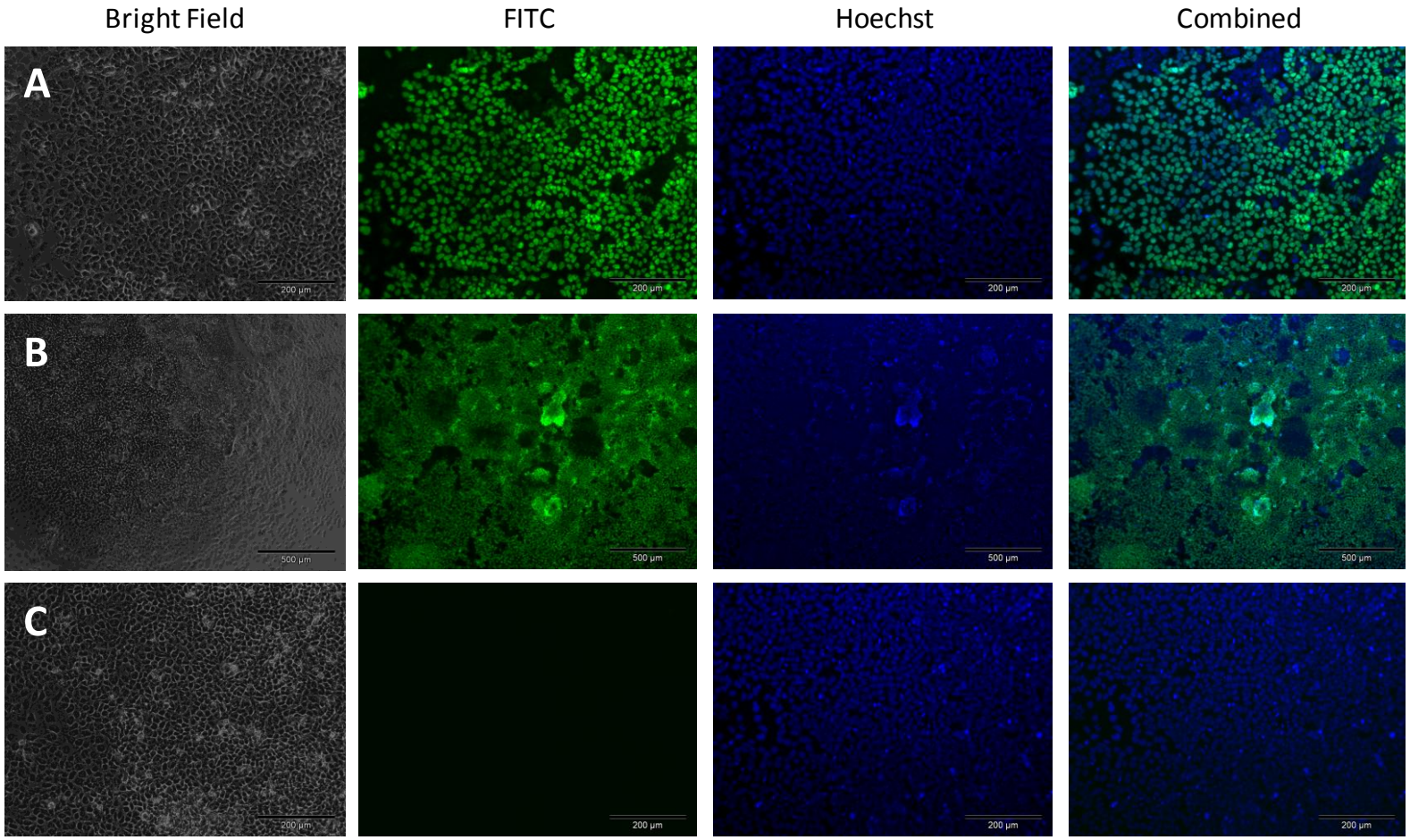

Figure 3.11. Immunostaining for OCT4 in undifferentiated NTERA2.

Expression of the OCT4 pluripotency transcription factor was positive across the undifferentiated cell population; however, OCT4 negative cells were present amongst the pluripotent population suggesting loss of pluripotency in some cells (A: x10 magnification). Variations in OCT4 protein levels were also evident across the population (B: x4 magnification). Isotype controls were negtive (C: x10 magnification).

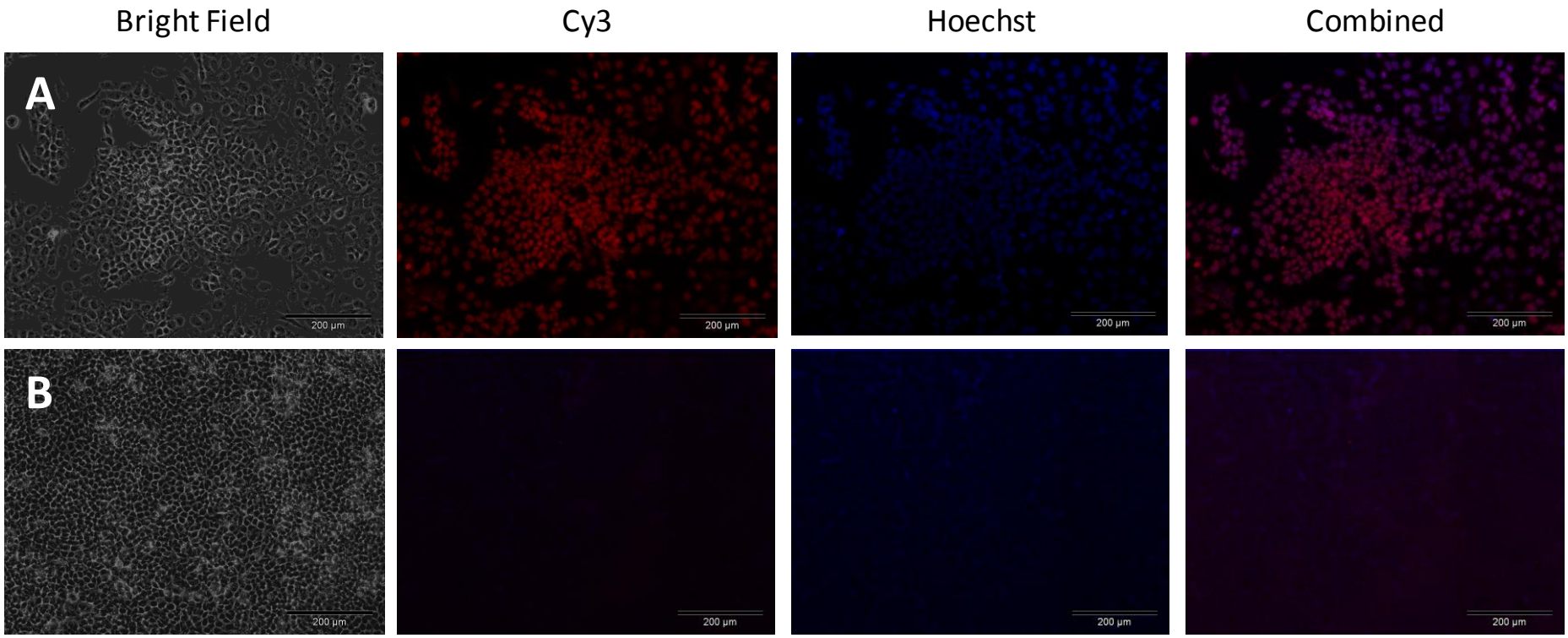

Figure 3.12. Immunostaining for SOX2 in undifferentiated NTERA2

Expression of the SOX2 pluripotency transcription factor was positive across the undifferentiated cell population. Expression of the protein was higher in the middle of the cell cluster than in individual cells outside the cluster suggesting that cell-cell contact aids the retention of pluripotency (A: x10 magnification). Isotype controls were negative (B: x10 magnification).

Positive Nestin staining was identified in the differentiated cells but staining was localised to mainly non-neuronal cells (Figure 3.17). Expression of the two surface markers of pluripotency (SSEA4 and Tra-1-60) and the OCT4 transcription factor was negative in 6 week ATRA treated cell populations (Figure 3.15). At first glance, SOX2 expression was also negative in the differentiated population (Figure 3.16). However, at high magnification it was possible to identify a few cells which retained some positive SOX2 expression (*data not shown due to inability to capture image*). Positive expression of SOX2 after 6 weeks might be an artefact of the staining process; however, it may also suggest retention of a small proportion of neural progenitor cells in the population after just 6 weeks induction, which might also explain retention of Nestin positive cells in this population.

The maturity of the NTERA2-derived neurons was investigated using an antibody towards synaptophysin. Synaptophysin is expressed in the membrane of synaptic vesicles in nerve terminals but have also been detected in dendrites (De Camilli and Navone, 1987). No positive staining for synaptophysin was observed (Figure 3.18). After 6 weeks in culture, NTERA2 derived neurons were stained for a range of markers to identify the class of neurons generated from this method. Due to limited resources, neurons were stained for only 3 subclasses of neuron: dopaminergic (tyrosine hydroxylase (TH) positive), serotonergic (serotonin (SERT) positive) and GABAergic (GABA positive) neurons. No positive stained was identified for SERT or TH (Figure 3.18). Staining for GABA resulted in a large amount of non-specific binding but staining of neuronal projections was considerably stronger than the background (Figure 3.19), suggesting that a proportion of neurons derived from ATRA induction of NTERA2 were of interneuron GABAergic morphology.

Differentiated cells were also stained for the glial cell marker GFAP but no positive staining was observed, suggesting that the epithelial-like cells supporting the neuronal attachment were not of a glial cell fate (*Image available upon request*). However, the reliability of this result is questionable as GFAP antibody sourced from different suppliers resulted in high and low levels of background with sporadic positive staining.

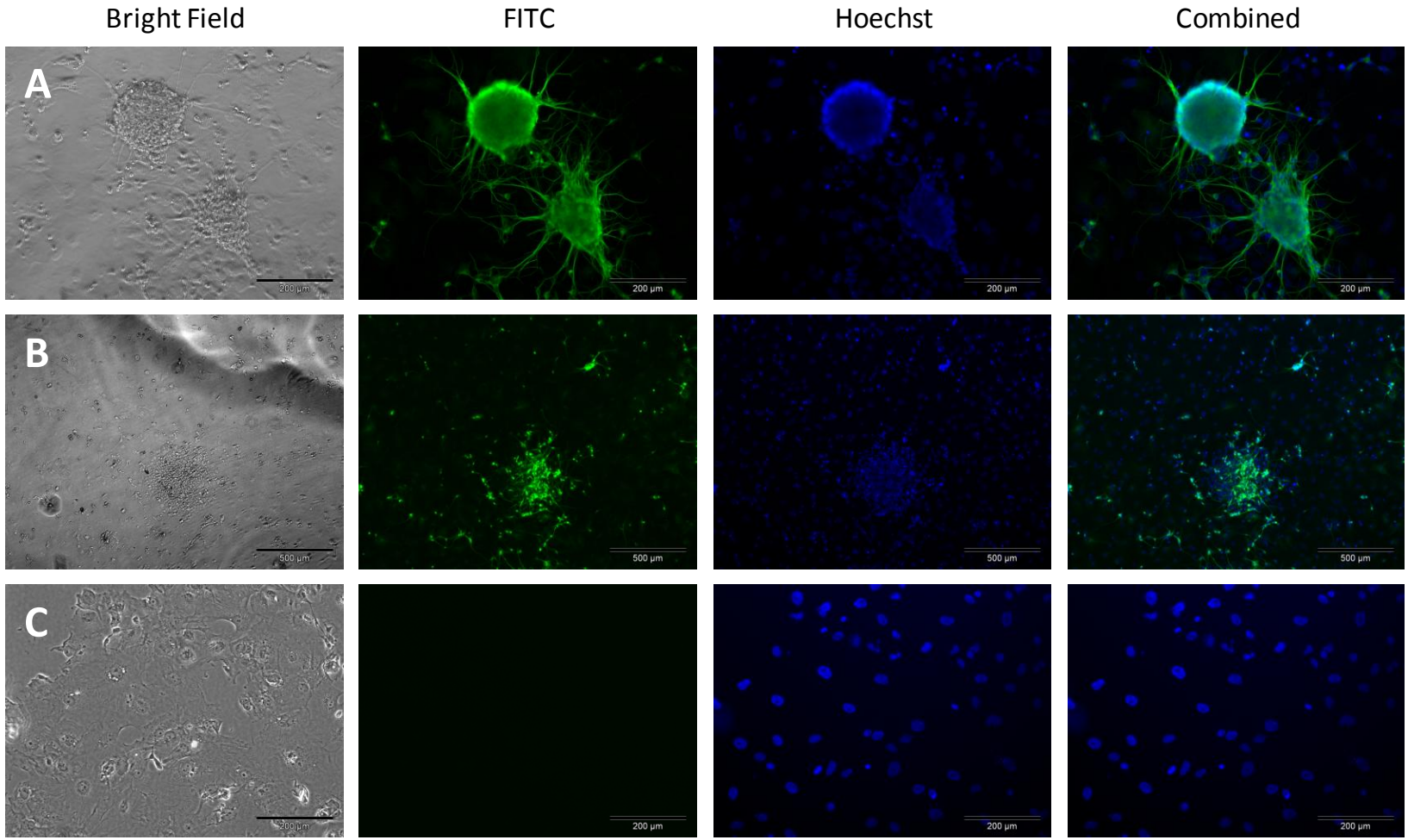

Figure 3.13. Immunostaining for neuronal marker TUBB3 in differentiated NTERA2.

NTERA2 derived neurons stained positive for TUBB3 along neuronal projections. Alignment of projections from numerous neurons were visible spreading from the cell cluster towards neighbouring cells (A: x10 magnification, B: x4 magnification). Isotype controls were negtive (C: x10 magnification).

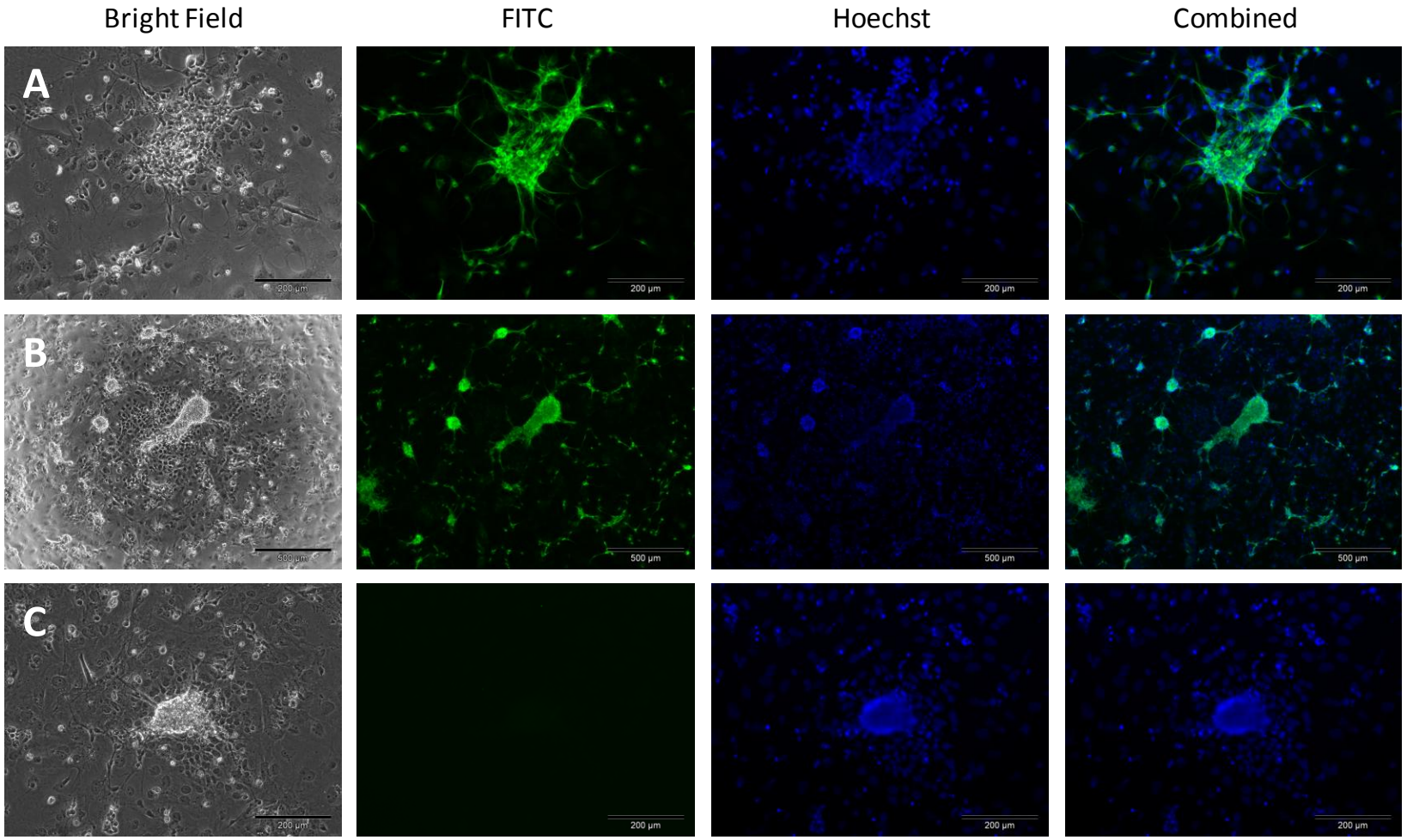

Figure 3.14. Immunostaining for neuronal marker MAP2 in differentiated NTERA2.

NTERA2 derived neurons stained positive for MAP2. FITC and Hoechst combined images highlighted the heterogeneity of the differentiated population (A: x10 magnification, B x4 magnification). Isotype controls were negtive (C: x10 magnification).

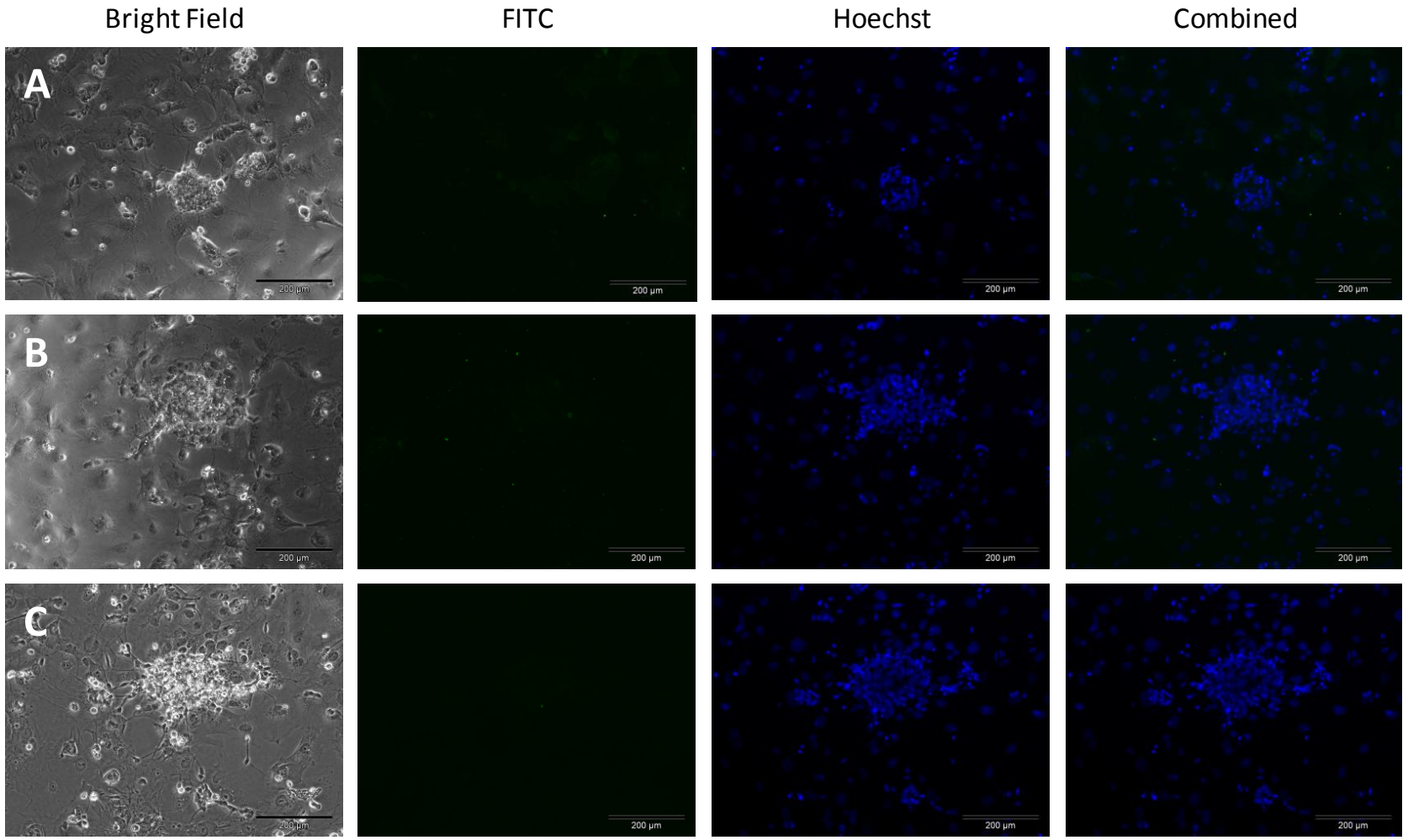

Figure 3.15. Immunostaining SSEA4, Tra-160 and OCT4 in differentiated NTERA2.

All cells were negative for SSEA4 (A), Tra-1-60 (B) and OCT4 (C) after 6 weeks ATRA induced differentiation x10 magnification). Isotype controls were negtive

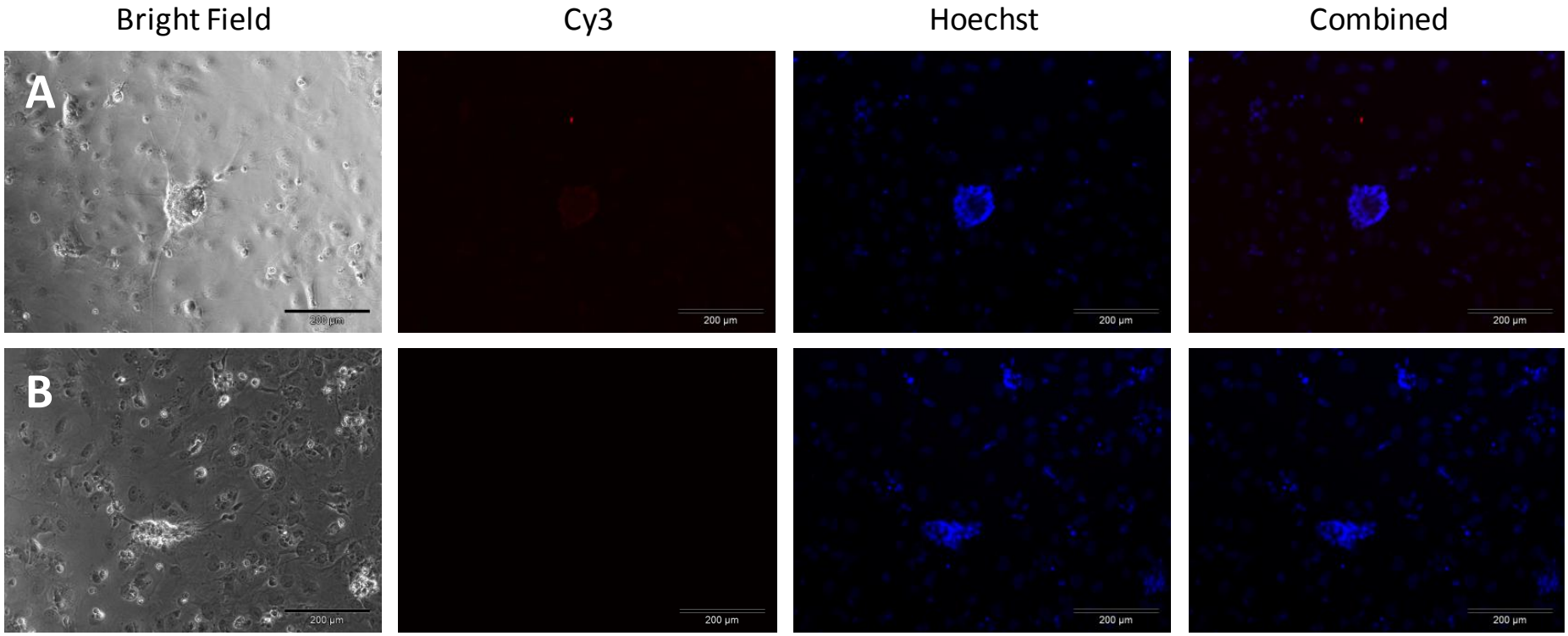

Figure 3.16. Immunostaining for pluripotency marker SOX2 in differentiated NTERA2.

SOX2 was mostly negative in the 6 week ATRA treated population (A: x10 magnification). At high magnification some remaining SOX2 expression was detected in sporadic cells but at a much reduced level to that of the undifferentiated cells (*data not shown*). Isotype controls were negtive (B: x10 magnification).

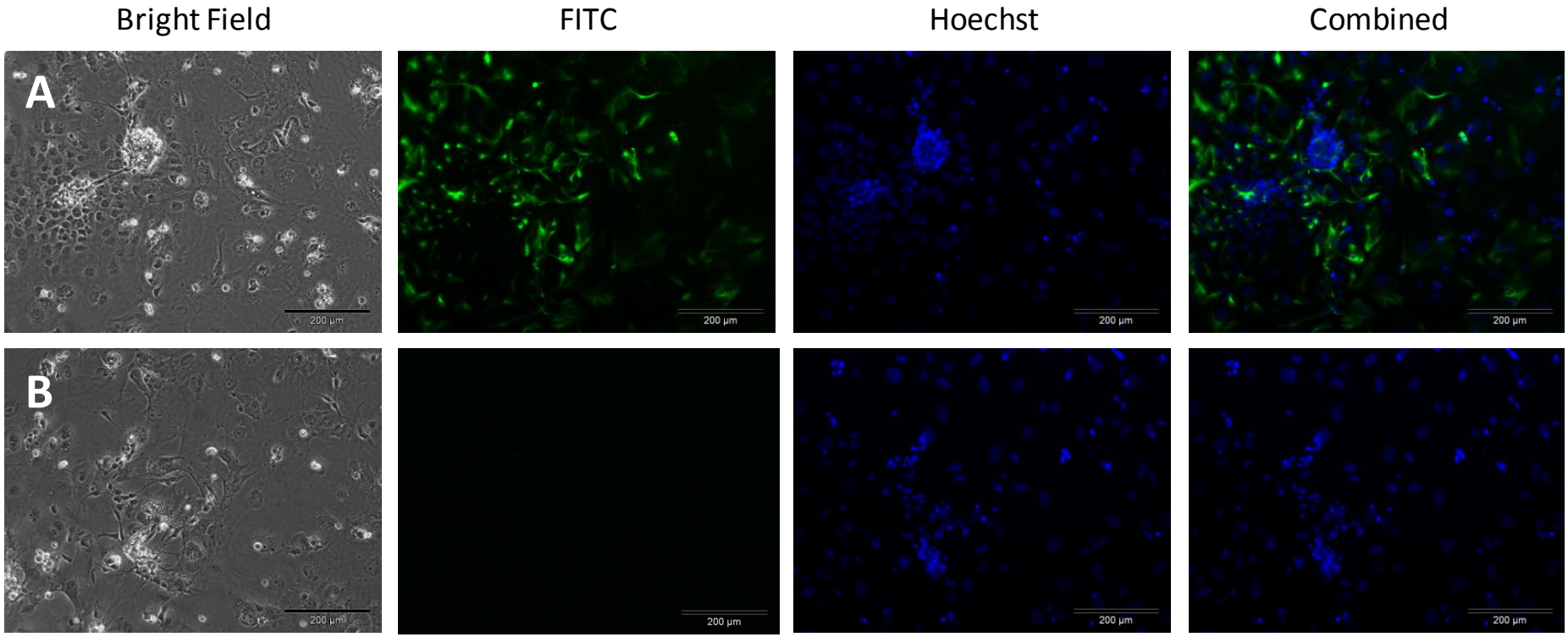

Figure 3.17. Immunostaining for Nestin in differentiated NTERA2.

Positive staining for Nestin was detected after 6 weeks differentiation. Expression was mainly located in non-neuronal cells (A: x10 magnification). Isotype controls were negtive (B: x10 magnification).

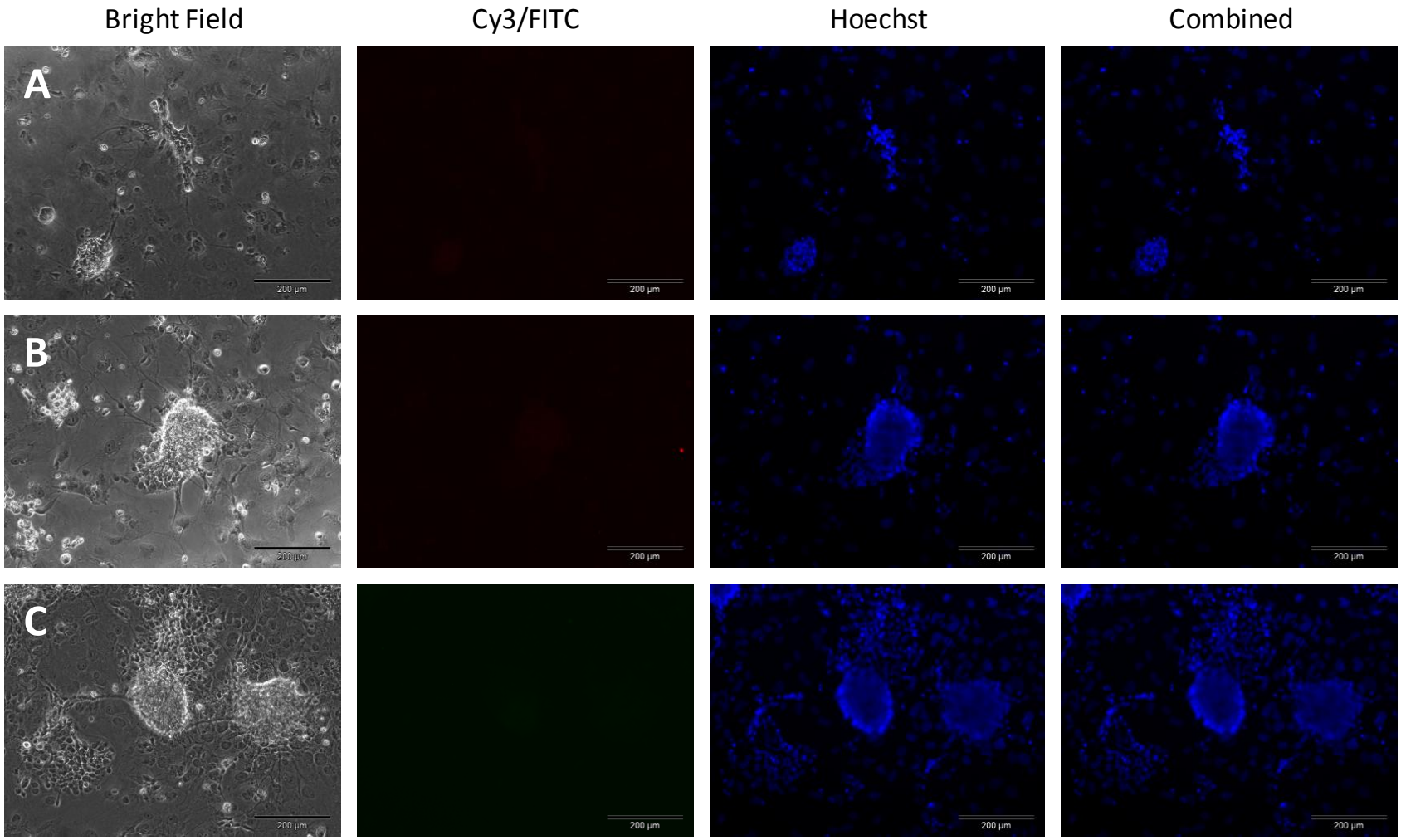

Figure 3.18. Immunostaining for SYP, SERT, TH in NTERA2 derived neurons.

No positive for SYP(A), SERT(B) or TH (C) was seen in NTERA2 derived neurons after 6 weeks (x10 magnification). Isotype controls were negtive.

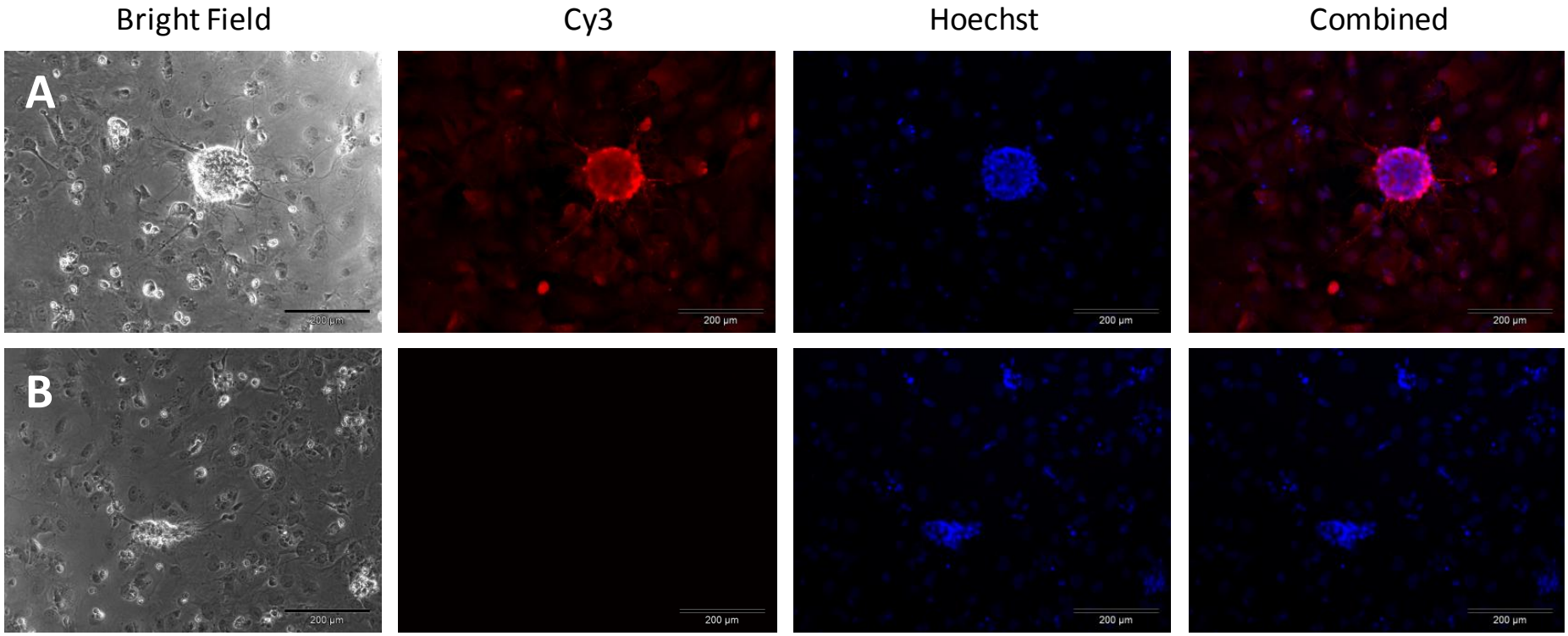

Figure 3.19. Immunostaining for GABA in differentiated NTERA2.

Neuronal axons stained positive for GABA. Background staining was high for the GABA antibody with staining visible in most cells; however, staining more intense in neuronal axons suggesting the presences of GABAergic neurons within the NTERA2 derived neurons after 6 weeks (A: x10 magnification). Isotype controls were negtive (B: x10 magnification).

To quantify the number and purity of neurons within the differentiated population following modifications to differentiation, cells were analysed using flow cytometry at day 0 and 6 weeks after ATRA induction for TUBB3 expression. The population was also analysed after 8 weeks to see whether the number of neurons continued to change. Samples were stained for TUBB3 following methods outlined in Section 2.13.4**,** before analysis on the Guava Easycyte flow cytometer (Guava Technologies, Millipore, Massachusetts). Isotype controls were run at the same antibody concentration as TUBB3 to determine the threshold above which staining could be assumed positive (Figure 3.20).

The purity of TUBB3 positive cells within the population increased from 1.3 % of cells in the undifferentiated population, to 61.4 % of cells after 6 weeks. After a further 2 weeks of purification, the proportion of TUBB3 positive cells further increased to 90.2 % due to the death of non-neuronal cells following exposure to mitotic inhibitors in culture. However, after 8 weeks the overall number of cells was considerably reduced due to the selection of neurons and death of non-neuronal cells in culture.

Flow cytometry analysis was also carried out for pluripotency markers at day 0 to correlate the level of expression throughout the population with the *in situ* immuno staining (Table 3.1). Positive Tra-1-81, SSEA4 and Nestin expression in the undifferentiated population were recorded at 84.6, 92.6 and 94.0 % respectively. Expression of OCT4 decreased from 79.4 % positive expression at day 0 to just 3.5 % after 6 weeks, confirming reduction in the pluripotent population.

As highlighted in previous sections, the morphology of a cell and its expression of neuronal genes is indicative of neuronal phenotype; however, a cell based therapy or assay relies on the functionality of the neuron. Previous sections also highlighted the requirement for functionality comparable to that of a primary neuron in order to be incorporated into a successful assay. NTERA2 derived neurons following the optimised differentiation protocol were screened for functionality in response to stimuli, including depolarisation and neurotransmitter activity. This was carried out using two basic approaches; patch clamping (the gold-standard for electrophysiology) which monitored a cell's ability to fire an action potential in response to depolarisation, and calcium imaging to monitor the activity of specific ion channels and cell surface receptors for specific neurotransmitters within the cell population.

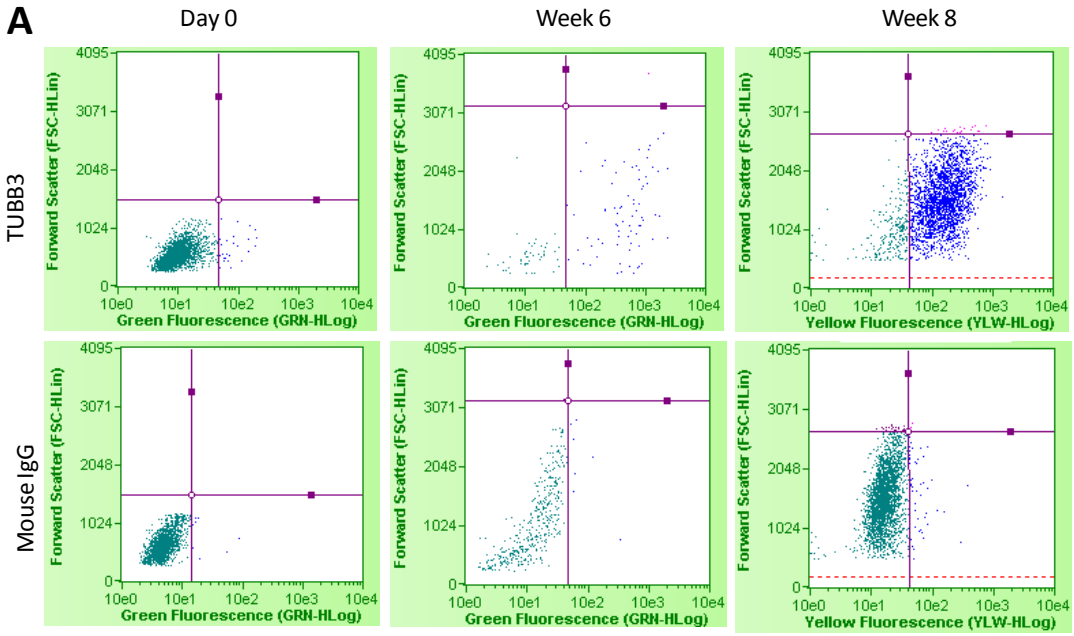

B

Day	Antibody	Cell count	% positive cells
0	TUBB3	2161	1.3
36	TUBB3	127	61.4
48	TUBB3	2692	90.2

Figure 3.20. Flow cytometry analysis of TUBB3 in differentiating NTERA2.

Dot plots (A) show the spread of differentiated cells and the gating applied to score positive staining according to the Mouse IgG Isotype control. The proportion of TUBB3 positive cells increased from 1.3 % to 90.2 % of differentiated cells after 8 weeks (B). The overall number of analysed cells in the 6 week sample was lower than at day 0 and 8 weeks due to a loss of cells in the staining process.

Day	Antibody	Cell count	% positive cells
0	Tra-1-81	4402	84.6
0	SSEA4	3469	92.6
0	Nestin	1981	94.0
0	OCT4	1193	79.4
36	OCT4	255	3.5

Table 3.1. Flow cytometry analysis of pluripotency markers in NTERA2.

84.6 and 92.6 % of undifferentiated NTERA2 cells stained positive for Tra-1-81 and SSEA4 respectively. 94 % of cells stained positive for Nestin and 79.4 % positive for OCT4.

3.2.4 Patch clamping NTERA2 derived neurons.

NTERA2 cells were cultured and differentiated as described in Section 2.4. After 4 weeks of ATRA induced differentiation, NTERA2 derived neurons were treated with Trypsin/EDTA and replated onto glass slides for patching. Cells were tested for their ability to fire both action potentials (AP) in response to a hyperpolarising current under current clamp mode.

To be confident of a functional response following stimulation, a neuronal control cell sample was required. Due to ethical limitations in sourcing primary human neural tissue, primary neurons were sourced from the ganglionic eminence (GE) region of an embryonic day 14 (e14) rat. The GE regions form part of the developing forebrain and are present transiently during embryonic development (Wai et al., 2008). Cells from the GE go on to develop into the basal ganglia comprising large numbers of GABAergic neurons. By e14 much of the neurogenesis in the rat has been completed and it is possible to isolate neural cells from the tissue. Immunostaining of differentiating NTERA2 neurons suggest a proportion of these cells were of GABAergic phenotype (Figure 3.19). Therefore primary cells from the GE were a logical positive control for electrophysiology studies. Primary neurons from the GE were isolated and kindly provided by Ms. S. Finch and Professor. B. Williams (Centre for the Cellular Basis of Behaviour & MRC Centre for Neurodegeneration, Kings College London).

NTERA2 cells were tested at weekly intervals of neuronal commitment, for their electrophysiological behaviour. The resting membrane voltage of each cell was recorded by setting the current to zero (Figure 3.21) before hyperpolarising at -70 mV. The flattened morphology of pluripotent and 1 week differentiated NTERA2 cells meant that it was not possible to reach a seal. No recordings were generated from pluripotent populations and only one of the seven cells attempted reached a seal after 1 week ATRA. For this reason, it was not possible to patch these cells or determine their resting membrane voltage. A typical mature neuron should present with a resting membrane voltage of -70 mV. Primary e14 rat GE neurons presented the lowest average membrane resting voltage of -56 mV (± 6.1) when compared to the NTERA2 derived neurons. However, ANOVA between all groups showed that there was no significant difference between the resting membrane voltage of differentiating NTERA2 derived neurons at week: 2, 3, 4, 5 and 6, or the primary e14 rat GE neurons ($p = 0.09$). The single resting voltage recording from 1 week ATRA treated cells meant that it was not possible to incorporate this sample into statistical analysis.

Prolonged exposure to ATRA did not appear to improve the neuronal resting membrane voltage but rather increased the overall number of excitable neurons. This was further supported by the increased success of patching following prolonged differentiation (Figure 3.22). A failure to patch was defined by the inability to generate a GΩ seal between the cell membrane and capillary to run a current and voltage clamp procedure.

After recording the resting membrane voltage of each cell, a hyperpolarising current was passed down the electrode to hold the membrane between -70 and -100 mV. Following release of the hyperpolarising current, electrically excitable cells fired electrical impulses. Examples of the APs generated from cells at each stage of differentiation are presented in (Figure 3.23). No recordings were taken from pluripotent or 1 week ATRA treated samples for reason described above. Action potentials were generated by NTERA2 derived neurons as early as 2 weeks following induction. However, the number of neurons which repeatedly fired APs in response to hyperpolarisation increased as the duration of differentiation increased. Despite a distinct AP fired from 1 of the 7 cells tested at 2 weeks (Figure 3.23C), none of the other 2 week cells responded to stimulation in this way. Equally, it was difficult to find a response from cells 3 weeks after induction and the response shown in Figure 3.23D did not cross the 0 mV threshold. The slower speed of these APs suggests that these were calcium responses rather than the normal fast sodium induce AP but its reverberating nature suggests this was a true response from an immature cell.

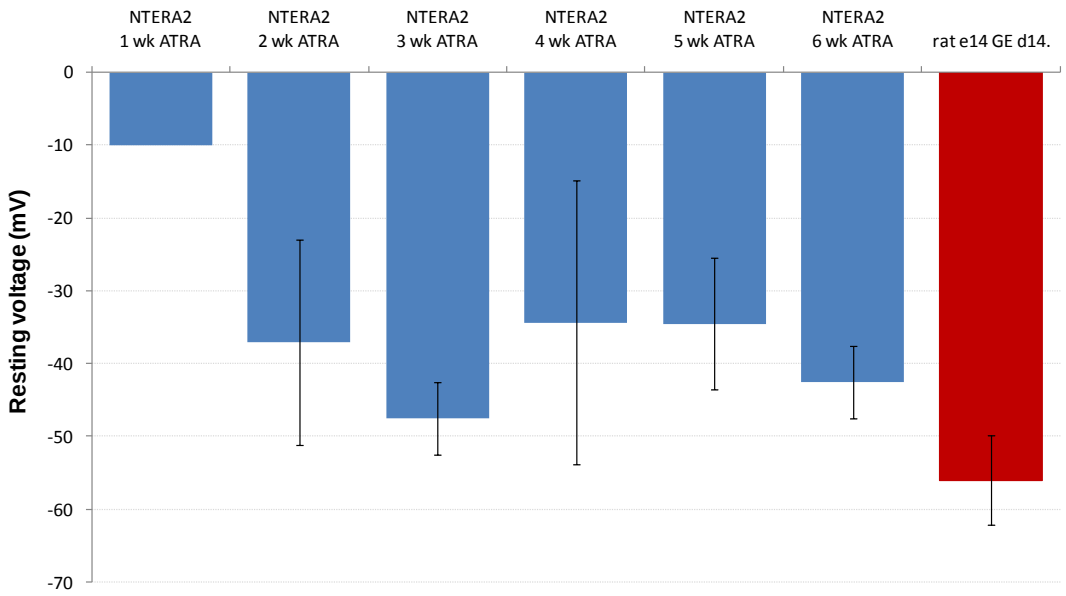

Figure 3.21. Average resting membrane voltage of patchable cells.

No correlation was determined between the resting membrane voltage of NTERA2 derived neurons between 1-6 weeks of ATRA treatment. Primary e14 rat GE neurons presented the lowest resting membrane voltage suggesting that these are more mature neurons than those derived from NTERA2; however, this was not significantly different from the resting membrane voltage of the NTERA2 cells throughout differentiation ($p = 0.09$). NTERA2 (blue) 1 week ATRA (n=1), 2 weeks ATRA (n=5), 3 weeks ATRA (n=2), 4 weeks ATRA (n=3), 5 weeks ATRA (n=4), 6 weeks ATRA (n=2), primary e14 rat GE neurons (red) 14 days post isolation (n=3). Error Bars represent ± 2SE.

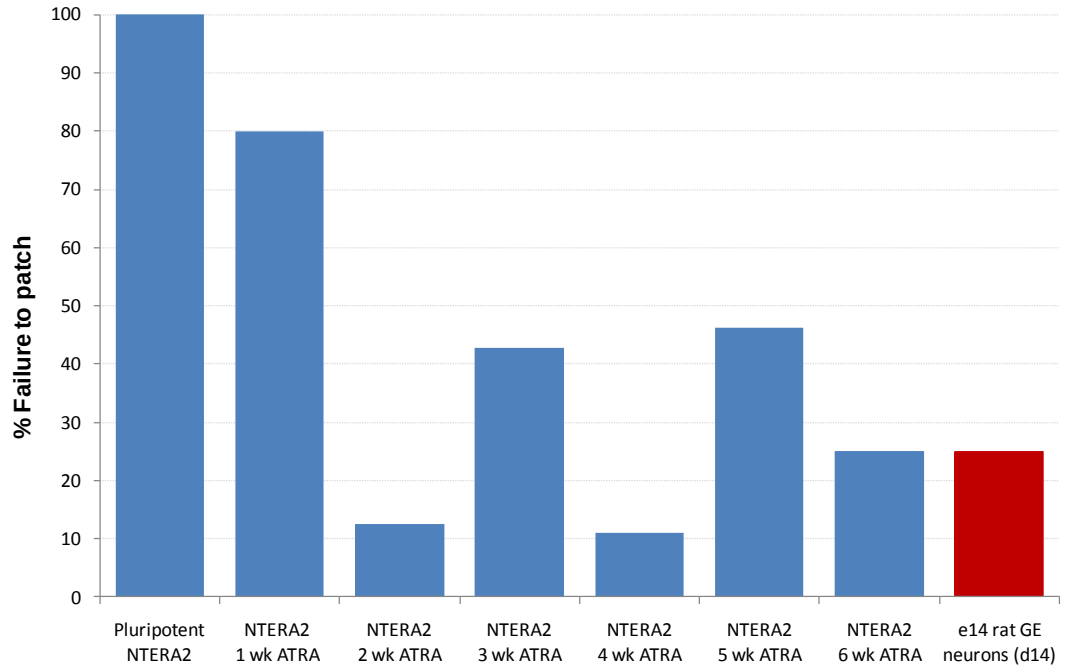

Figure 3.22. Failure rate of patching process.

Failure to patch these cells was defined by the inability to generate a GΩ seal with the patching capillary. The success rate of patching was vastly improved 2 weeks following induction of neuronal differentiation. The flattened morphology of undifferentiated and 1 week ATRA treated NTERA2 cells resulted in a high failure rate of seal generation and therefore an inability to patch. NTERA2 (blue) undifferentiated (n=3), 1 week ATRA (n=7), 2 weeks ATRA (n=8), 3 weeks ATRA (n=7), 4 weeks ATRA (n=9), 5 weeks ATRA (n=13), 6 weeks ATRA (n=4), primary e14 rat GE neurons (red) 14 days post isolation (n=4).

The overall number of cells which fired an AP in response to hyperpolarisation increased as the differentiation period increased (Figure 3.24). In the control primary rat e14 GE neuron sample, 100 % cells successfully fired APs confirming successful patching technique. In comparison, primary neurons also spontaneously fired APs without a hyperpolarising current, confirming the maturity of these cells (Figure 3.23A). When the primary neuron membrane was placed under a hyperpolarising current, the AP response increased, resulting in a reverberating burst of electrical impulses as would be seen *in vivo* (Figure 3.23B). The reduced ability to fire reverberating APs in NTERA2 derived neurons was therefore a true result rather than an inability to detect this response.

Neurons were voltage clamped and IV curves generated for each cell (*data available upon request*). Cells were depolarised through a range of voltages (-50, -30, -10, 10, 30, 50, 70, 90, 110, 130, 150, 170 mV) to test for the presence of voltage gated ion channels which would open in response to depolarisation resulting in an inward flux of Na^+ or Ca^{2+} ions. An example of the IV curve generated by an inward current in response to this stimulation is presented in Figure 3.25.

Calcium and sodium are the only ions with a large inward concentrations gradient in a neuronal cell. Inward currents observed were a result of the opening of these channels in a voltage dependent manner. The absence of inward current in response to voltage clamping from undifferentiated NTERA2 cells has previously been published (Rendt et al., 1989). In agreement with Rendt et al., these data have shown that NTERA2 derived neurons express functional Na^+ and/or Ca^{2+} gated channels which were detectable 2 weeks after induction of differentiation. The functionality of these membrane channels was variable between neurons within differentiation samples, and across the different time points of differentiation. No correlation between the length of differentiation and the ability to generate an inward current was identified (Figure 3.26); however, the size of the inward current increased with prolonged duration of differentiation.

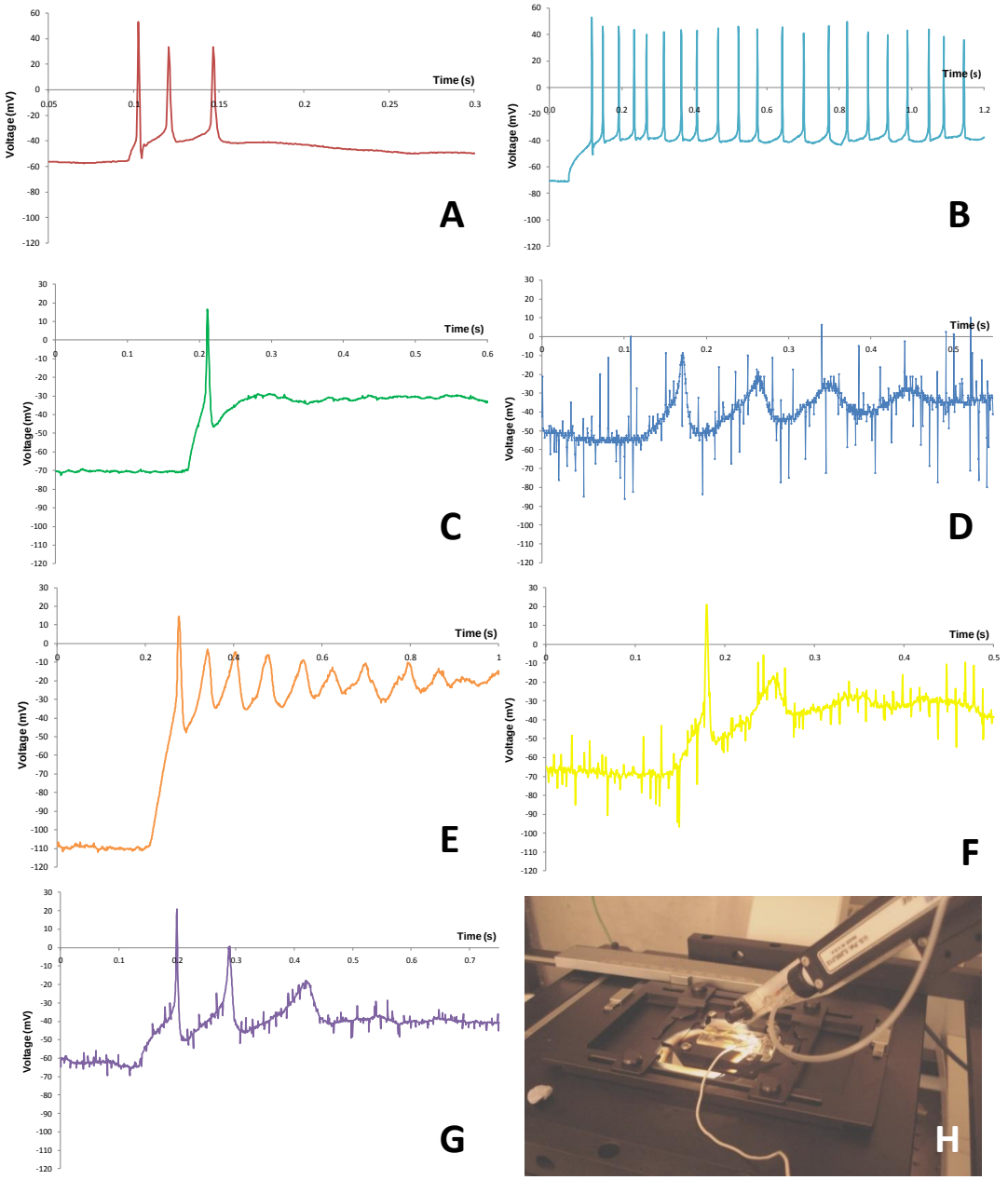

Figure 3.23. Action potential generation in NTERA2 derived neurons.

The resting membrane voltage of e14 rat GE neurons after 14 days of *in vitro* maturation was -58 mV. These cells sporadically fired Action Potentials (A). Following hyperpolarisation to -70 mV e14 primary rat neurons generated a series of reverberating action potentials typical of excitatory GABAergic neurons (B). A single cell from the 2 weeks ATRA induced population (n=7) fired an action potential in response to hyperpolrisation (C). The only 1 cell fired an AP after 3 weeks ATRA exposure (n=4), this AP did not cross the 0 mV line, suggesting that these neurons were still immature (D). Three cells fired APs after 4 weeks of differentiation (n=8; E). Three cells fired AP's after 5 weeks differentiation (n=7; F), the membrane of the representing cell at 5 weeks was very unstable under hyperpolarisation resulting in the notable fluctuations in membrane voltage throughout the trace. Two cells tested after 6 weeks of differentiation fired APs (n=3; G), these neurons were reliably firing reverberating APs as seen in primary neurons.

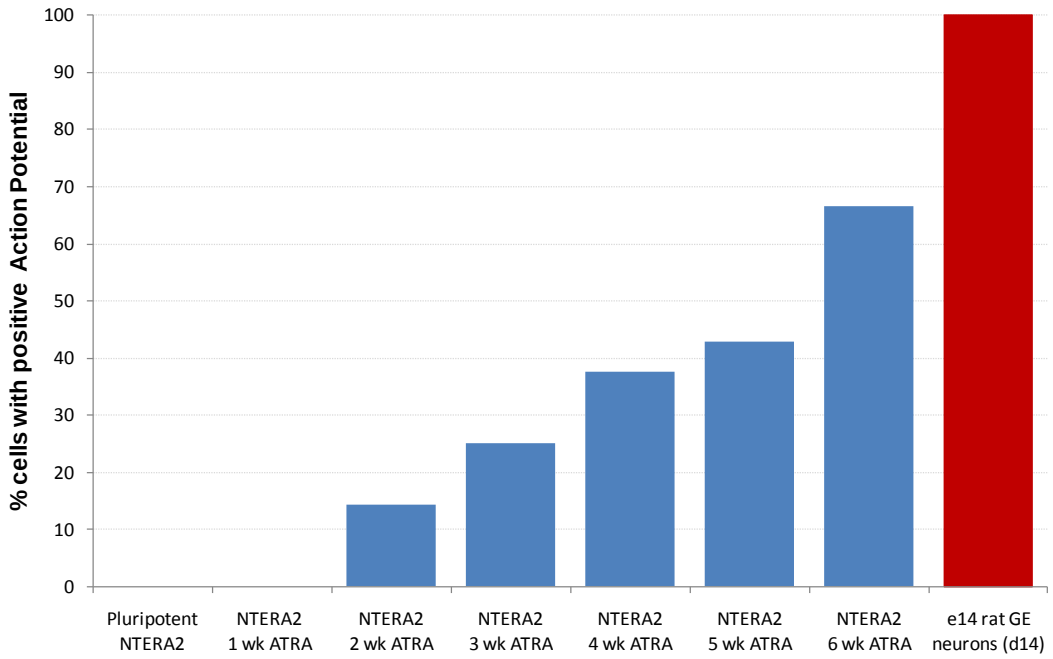

Figure 3.24. Action Potential generation in differentiated NTERA2 cells.

The proportion of neurons which fired APs increased with increasing duration of differentiation. NTERA2 (blue) undifferentiated (n=0), 1 week ATRA (n=1), 2 weeks ATRA (n=7), 3 weeks ATRA (n=4), 4 weeks ATRA (n=8), 5 weeks ATRA (n=7), 6 weeks ATRA (n=3), primary e14 rat GE neurons (red) 14 days post isolation (n=3).

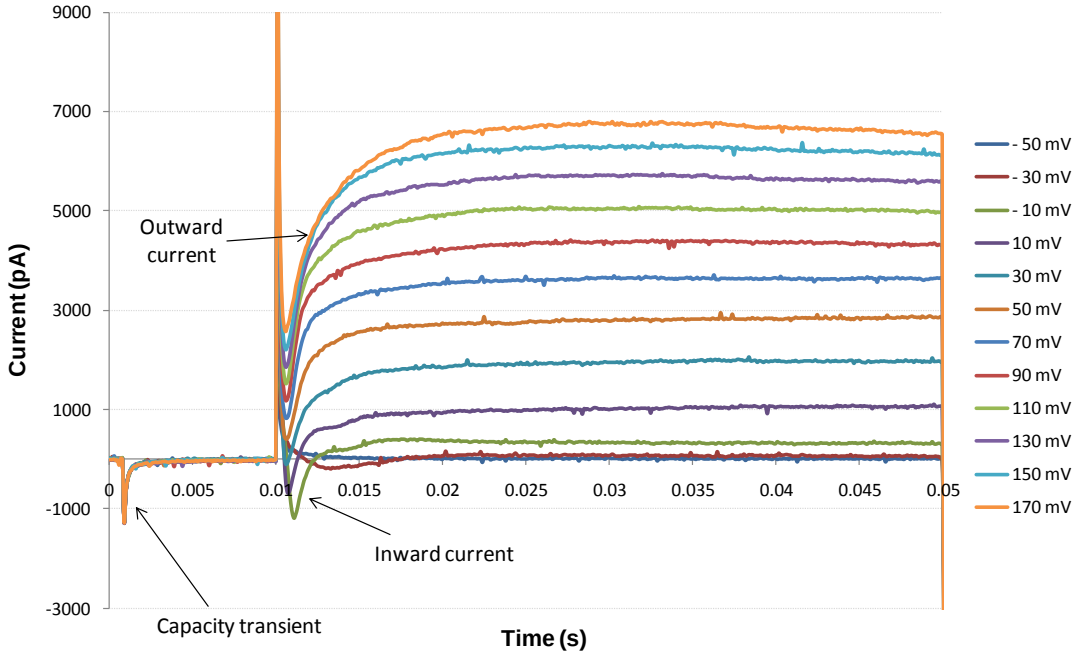

Figure 3.25. IV curve.

Inward current caused by the movement of Ca^{2+} and Na^{+} ions into the cell through ion gated channels, was visible by the current trace dropping below zero. Outward currents are caused by the flow of K^{+} ions out of the cell via K^{+} ion channels of the Na^{+}/K^{+} membrane pump, resulting in an increase in current recorded. The number of Ca^{2+}, Na^{+} and K^{+} membrane channels increased with neuronal maturity resulting in the detection of distinct inward currents followed by larger outward currents.

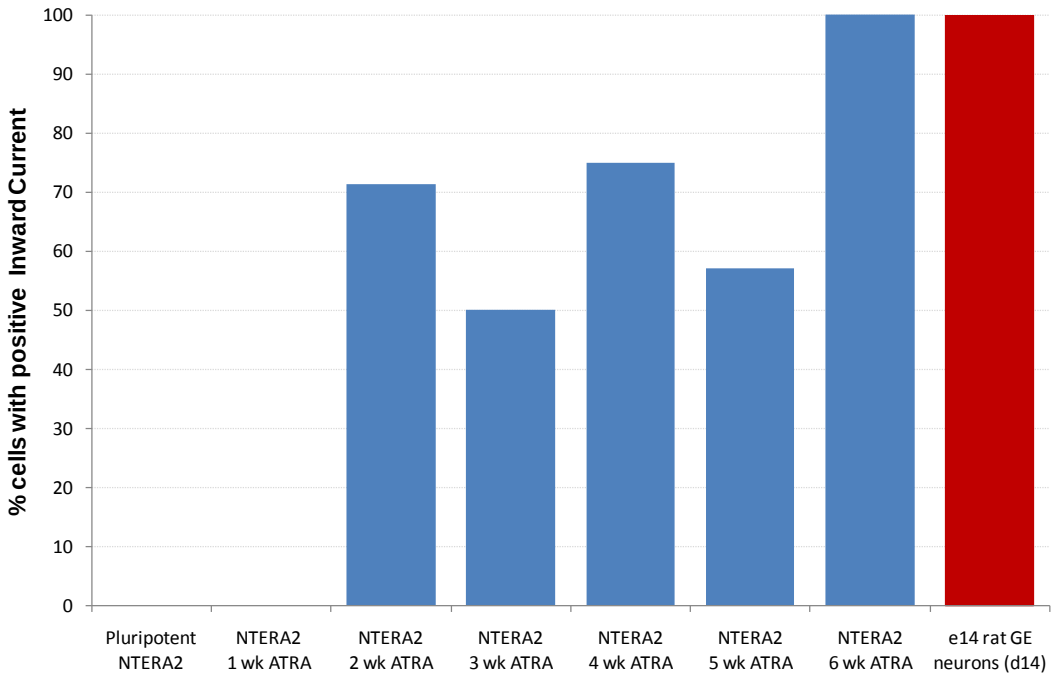

Figure 3.26. Inward currents in differentiating NTERA2 cells.

The efficiency of inward current generation was variable between neurons at different points of differentiation. By 6 weeks of differentiation 100 % of patched neurons generated an inward current in response to voltage clamping. NTERA2 (blue) undifferentiated (n=0), 1 week ATRA (n=1), 2 weeks ATRA (n=7), 3 weeks ATRA (n=4), 4 weeks ATRA (n=8), 5 weeks ATRA (n=7), 6 weeks ATRA (n=3). Primary e14 rat GE neurons (red) 14 days post isolation consistently generated a strong inward current (n=3).

Although the patch-clamping data demonstrates a correlation between neuronal morphology and electrophysiological activity, the neuronal population was heterogeneous in response to stimulation. However, the skill required and the labour intensity of the patch-clamping technique prevented the screening of the large numbers of cells required for a true representation of the population. To complement the data from patch clamping, a high throughout calcium imaging facility (FLIPR) was also incorporated into this study which was able to simultaneously screen large numbers of cells, capturing the behaviour the entire neuronal and non-neuronal population.

3.2.5 Fluorescence imaging plate reader

The FLIPR was incorporated into this study in an attempt to characterise the behaviour of NTERA2 derived neurons in response to stimulation. Cells were prepared as detailed in Section 2.12.9. Following a one hour incubation with the Fluor-4 AM calcium indicator samples were loaded into the FLIPR and background fluorescence levels recorded. Cells were stimulated with a range of neurotransmitters and images of changes in fluorescence captured every second for five minutes (Figure 3.27).

For the purpose of analysis, background fluorescence readings were standardised to one, and changes in fluorescence expressed relative to basal levels, enabling comparison between wells and samples. The overall calcium response was calculated from changes in fluorescence from the minimum to maximum recorded levels. An even monolayer of cells was required to ensure even excitation of the plate by the laser avoiding skewed results from auto fluorescence. Cellular responses were averaged across each well, providing the behaviour of the population rather than of individual cells.

Early trials highlighted the need for a pre-coating of the FLIPR plate with poly-D-lysine to aid cellular attachment and reduce loss during washing stages. Due to interference in fluorescence from cell culture media, it was not possible to run the FLIPR in standard culture media. Viability was maintained using pre-warmed HBS buffer, containing a glucose source for metabolism (Section 2.12.9.2) during all wash steps and incubations, in place of PBS.

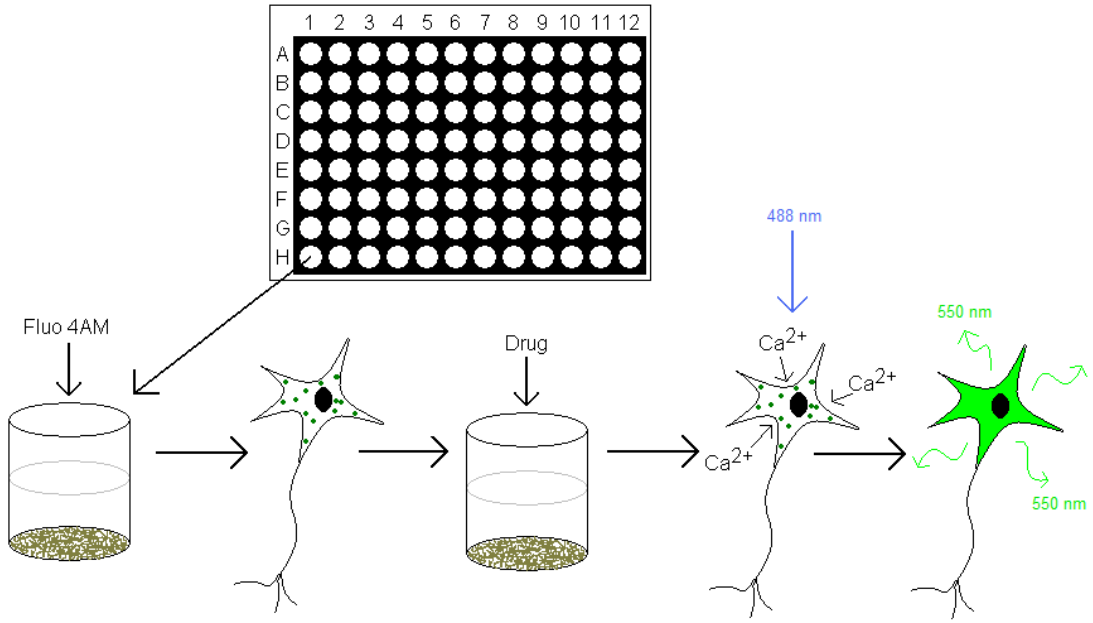

Figure 3.27. Schematic diagram of FLIPR stimulation

A confluent cell layer in a black bottomed 96-well plate was incubated for 1 hour with Fluo 4 AM (calcium indicator). Cells were washed to remove excess dye and loaded into the FLIPR. Addition of a drug stimulated calcium influx across the plasma membrane in responsive cells. Free cytosolic calcium binds to the Fluo-4 AM, which when excited by a 488 nm argon laser, emitted light in the 550 nm spectrum. Image capture of fluorescence emissions was correlated to the level of calcium influx.

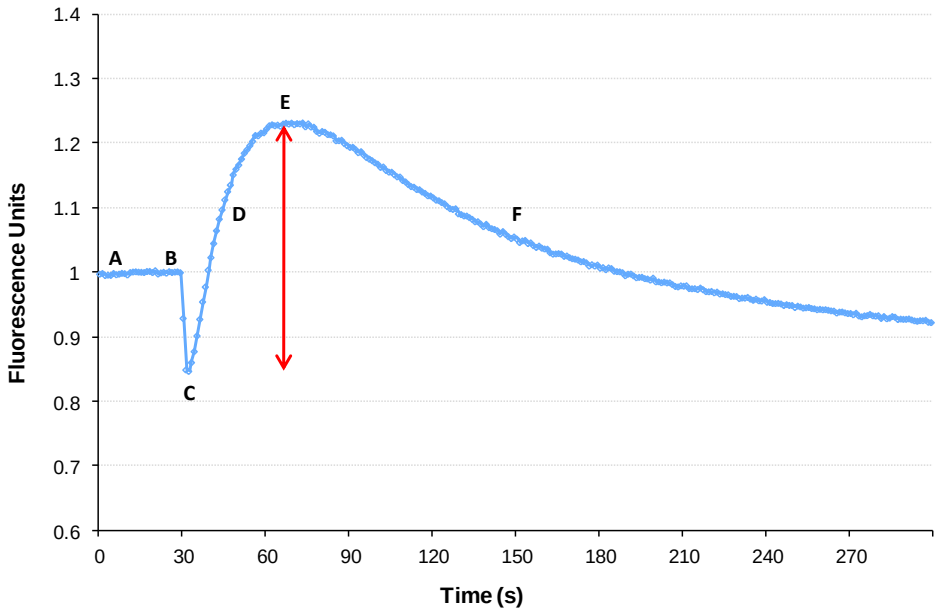

Figure 3.28. Typical cellular calcium response to stimulation.

The 6 phases of a classical response to neurotransmitters. The response from each cell is standardised to ensure background fluorescence is equal to 1. A; background fluorescence. B; drug stimulation. C; baseline fluorescence of cell, calcium channels open. D; influx of calcium and binding to Fluo-4-AM resulting in increased fluorescence. E; maximum fluorescence. F; calcium pumped out of cell or sequestered to cytoplasmic stores. The overall response is determined by the difference between C and E. (i.e. the difference between the maximum and minimum fluorescence values after addition of the drug.)

3.2.5.1 Calcium response to potassium chloride depolarisation.

To establish the FLIPR study, undifferentiated NTERA2 cells at p56 and p58 were seeded at 5×10^4 cells/well, in 200 µl standard GlutaMAX^{TM} media (Section 2.1.2) 24 hours before stimulation. Each sample was run in triplicate wells. The calcium response to KCl depolarisation was tested from high to low concentration (100 mM, 75 mM, 50 mM, 25 mM, 10 mM, 5 mM and 0 mM in PBS). The maximum cellular response was calculated relative to background fluorescence (Figure 3.29).

The large overlapping error bars and minimal response to KCl depolarisation suggested that there was no difference in Ca^{2+} response between the different KCl concentrations, this was confirmed by ANOVA ($p = 0.054$). The apparent response at 0 mM KCl suggests that these cells were responding to the addition of a volume of solution rather than to the KCl.

3.2.5.2 Comparative response of NTERA2 neurons to KCl depolarisation

The responses of undifferentiated NTERA2 cells and NTERA2 derived neurons to KCl were compared. Samples were run over a number of days and results combined for comparison. Results from undifferentiated NTERA2 at p58 (Figure 3.29) were used as the baseline response. Differentiating NTERA2 cells at 10 days, 3 weeks and 6 weeks post ATRA induction were not as actively proliferating as the undifferentiated cells (Figure 3.7) and so were seeded at a higher density 2×10^5 cells/well, ensuring even coverage across the base of the well. Cells were stimulated with 100 mM, 75 mM, 50 mM, 25 mM, 10 mM, 5 mM and 0 mM KCl in PBS. In order to determine whether the minimal response from undifferentiated cells in Figure 3.29 was a true response or an artefact due to addition of volume, an unexcitable human dermal fibroblast control cell line was included in analysis (p18, Karocell Tissue Engineering AB, Sweden).

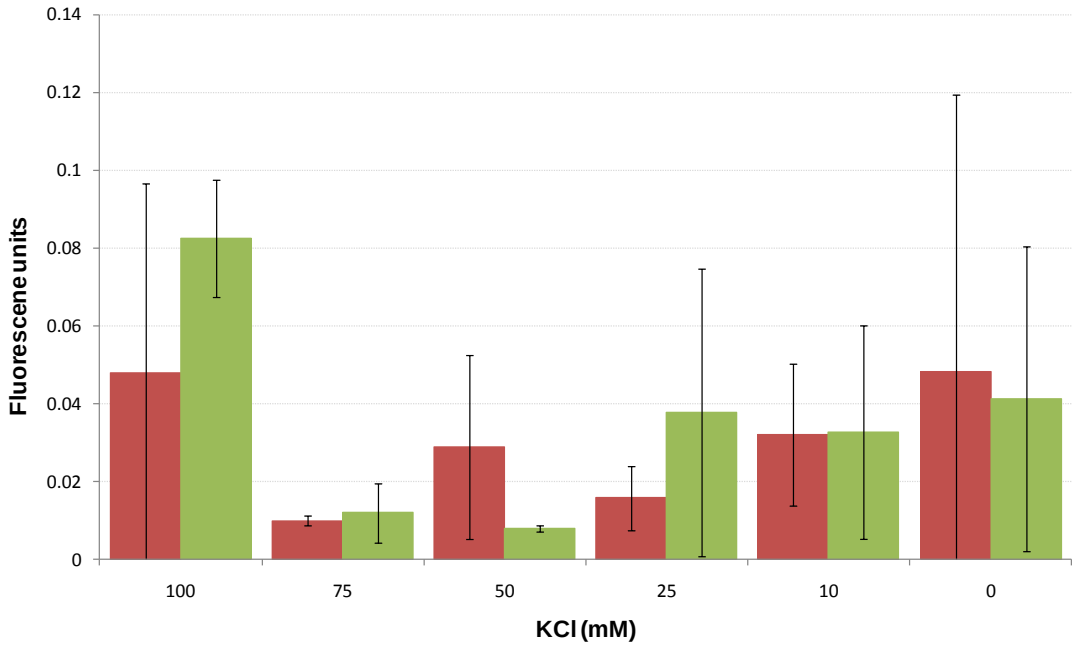

Figure 3.29. Calcium response by undifferentiated NTERA2 to KCl depolarisation

Pluripotent NTERA2 cells were seeded into a FLIPR plate and stimulated with KCl at concentrations ranging from 100 mM to 0 mM (X-axis). No true calcium response was detected from undifferentiated NTERA2 cells at p56 (red) or p58 (green) in response to KCl, suggesting the absence of voltage gated calcium channels in undifferentiated cells. Error bars represent ± 2SE.

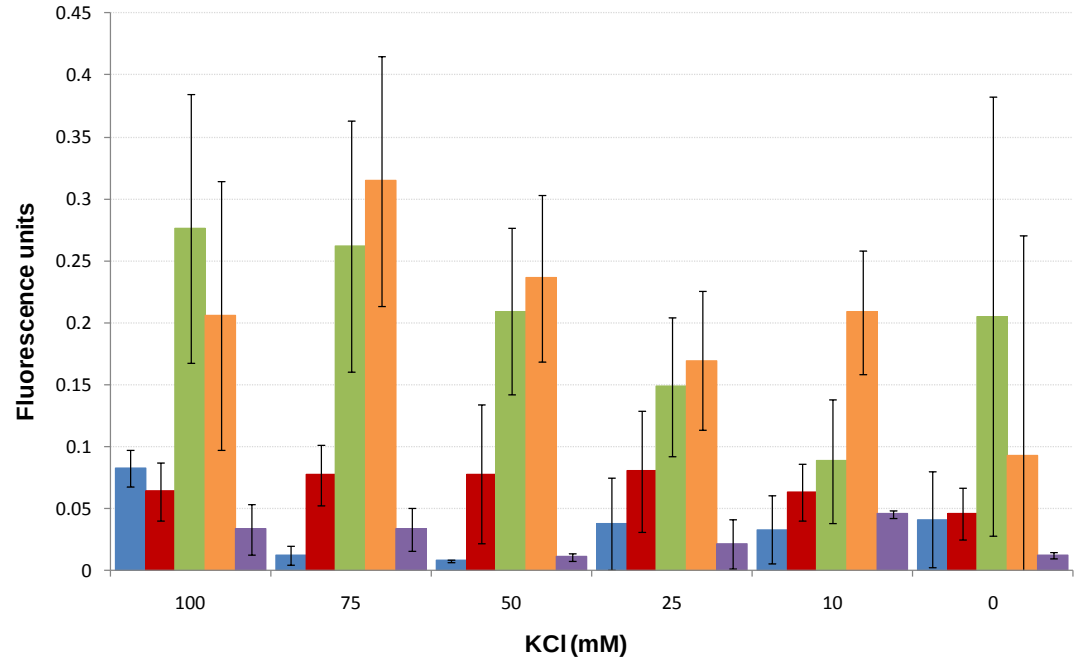

Figure 3.30. Comparison of Calcium response to KCl of differentiating NTERA.

Undifferentiated NTERA2 (blue), 10 days ATRA treated NTERA2 (red), 3 week ATRA treated NTERA2 (green), 6 week ATRA treated NTERA2 (orange), dermal fibroblasts (purple). Overlapping of error bars indicates that no difference in calcium response was detected following KCl stimulation between undifferentiated, 10 day ATRA treated and human dermal fibroblasts. A larger response to KCl was seen by cells which are 3 and 6 weeks differentiated compared to cells earlier in differentiation, although the concentration of KCl did not seem to affect the size of the calcium response, suggesting that the response was due to the addition of a drug volume rather than neuronal depolarisation. Error bars represent ± 2SE.

No difference was detected between the Ca^{2+} responses of undifferentiated NTERA2, 10 days differentiated NTERA2 and dermal fibroblasts, at KCl stimulation between 100 mM and 0 mM (Figure 3.30). The similarity of undifferentiated cells and the dermal fibroblasts confirmed the absence of a true response to KCl stimulation. This was not surprising when correlated to the morphology of the cells at each condition (Figure 3.5). Very few cells presented a neuronal morphology after 10 days of differentiation, and so would not be expected to express function voltage gated ion channels.

The response from NTERA2, 3 weeks and 6 weeks after ATRA induction was higher than that of the undifferentiated and 10 day ATRA treated cells (Figure 3.30) at ≥ 50 mM KCl, confirming the presence of voltage gated Ca^{2+} channels in the plasma membrane after this point. This correlates with data from the patch clamping experiments on these cells (Figure 3.23 and Figure 3.26). The relative indifference in response of cell between 3 and 6 weeks differentiation suggests that the number of voltage gated Ca^{2+} channels in the membrane does not increase with prolonged differentiation. However, the response of these cells to 0 mM KCl is suggestive of cellular reponse to the addition of a drug volume rather than specifically to KCl depolarisation.

3.2.5.3 Neurotransmitter stimulation

In an attempt to identify the neuronal phenotype within the differentiated population, cells were stimulated with a range of common neurotransmitters and monitored for a response. NTERA2 cells were screened throughout differentiation at 0, 10, 21 and 36 days post induction. Dermal fibroblasts were included as a baseline control for unresponsive cells.

Cells were stimulated with NMDA at a range of concentrations from 20 µM to 0 µM, 3-5 repeats were run for each cell type and stimulant. Due to the limited availability of fibroblasts when preparing this experiment, these cells were tested for a response to NMDA at just 20 µM, 10 µM and 0 µM.

No significant difference was detected in the response of undifferentiated NTERA2 cells or dermal fibroblasts to NMDA ($p = 0.61$, Figure 3.31) as would be expected for unexcitable cells. The response of the undifferentiated NTERA2 and the dermal fibroblasts to NMDA was of a similar level to that of KCl stimulation (Figure 3.30), suggesting that this was a normal baseline response by unstimulated cells in the FLIPR. The response of 3 and 6 week differentiated cells to NMDA was significantly higher than that of undifferentiated NTERA2

as determined by ANOVA ($p = 0.00002$ and 0.01 respectively), which would suggest that the expression of functional NMDA channels in neurons after 3 weeks ATRA induced differentiation. However, the response generated by cells at 0 µM NMDA, in combination with large error bars (2SE) suggests that the increased calcium flux detected may have been a consequence of cell number and coverage rather than overall cellular response, and that none of these populations were genuinely responding to NDMA stimulation.

To rule out the possibility the non-response was due to the absence of the NMDA co-agonist glycine, undifferentiated and 10 day differentiated cells were stimulated with NMDA (10 µM and 20 µM) in the presence of glycine at 10 µM and 20 µM concentrations. A glycine control for 10 day treated sample was also included to identify response to glycine alone. Results from the comparative response of undifferentiated NTERA2 cells with 10 day ATRA treated NTERA2 the NMDA ± glycine would suggest that no expression of NMDA receptors on cells up to 10 days of differentiation (Figure 3.31 and Figure 3.32). Cells did not respond to glycine stimulation. Variable cell coverage due to loss of sample during washing might explain the larger error bars within these samples.

3.2.5.4 The requirement for a neuronal control

The high variability in cellular response from undifferentiated and differentiating cells highlighted the need for a positive control. Limited availability to primary neurons, meant that it was not possible to source sufficient numbers of cells as a positive control for the FLIPR. Incorporation of the neuroblastoma-derived cell line SH-SY-5Y, was trialled as a positive control. There is extensive literature to demonstrate that these cells can be differentiated into post-mitotic neurons under the influence of ATRA and BDNF in just 8 days (Påhlman et al.;Encinas et al.). However, attempts to culture and differentiate these cells (Section 2.6) resulted in a population of cells which, despite being of neuronal morphology did not respond to KCl stimulation, instead these cells generated a response similar to undifferentiated NTERA2 ($p = 0.199$, Figure 3.33). From these data it was concluded that the SH-SY-5Y was an unsuitable cell line for use as a functional neuronal control, even with ATRA and BDNF differentiation.

3.2.5.5 6-week NTERA2 derived neurons

Following attempts to purify neurons using rapid trypsin exposure (Section 1.1.1.1), a comparative experiment was carried out to investigate the difference in response of the top layer of purified neurons and the remaining cells from 6 week ATRA treated NTERA2. Cells were seeded at 2 x 10^5/well, 72 hours before stimulation enabling the neurons to recover from damage caused by replating. Poor neuronal yield resulted in sufficient cells for only single well per stimulation. This meant that results were only representative and not conclusive for a comparison between these populations. Results demonstrated a consistently increased Ca^{2+} response of NTERA2-derived neurons to KCl stimulation in 6 week differentiated samples than in undifferentiated NTERA2 (Figure 3.34). Results also suggest a better response from the top layer of 6 week ATRA treated cells when compared to the underlying cells from which they were separated. This can be explained by a higher purity of neurons in the top layer of cells when compared to the remaining layer, generating a larger calcium flux across the well.

3.2.6 Calcium imaging

Due to the interference of non-neuronal cells in the output of the FLIPR, a higher magnification calcium imaging system was used to focus analysis on a selected population of neurons, distinguishable by morphology from that of the non-neuronal cells. Cells were cultured, differentiated and prepared for imaging as described in Section 2.12.10. Calcium indicator dye (Fura-2 AM) was incubated with the cells for 30 minutes before loading the cells into the system for stimulation. A continual feed and purge system was set up to deliver a constant flow of HBS (Section 2.12.9.2) or stimulus to the cells. At defined time points, a neurotransmitter of interest was added to the flow feed. The flow rate was set to 0.6 ml.min^{-1} to prevent disruption and detachment of the cell layer. Fluorescence images were captured in real time for the duration of the run and subtracted from background readings. Changes in fluorescence intensity were correlated to cytoplasmic Ca^{2+}.

The calcium imaging system was set to focus on a small group of neurons 6 weeks (Figure 3.35A) and 8 weeks (Figure 3.35B) post induction. Cells were stimulated with KCl (60 mM), NDMA (100 µM), glycine (20 µM), glutamate (100 µM) and carbachol (100 µM) and monitored for changes in Ca^{2+} response.

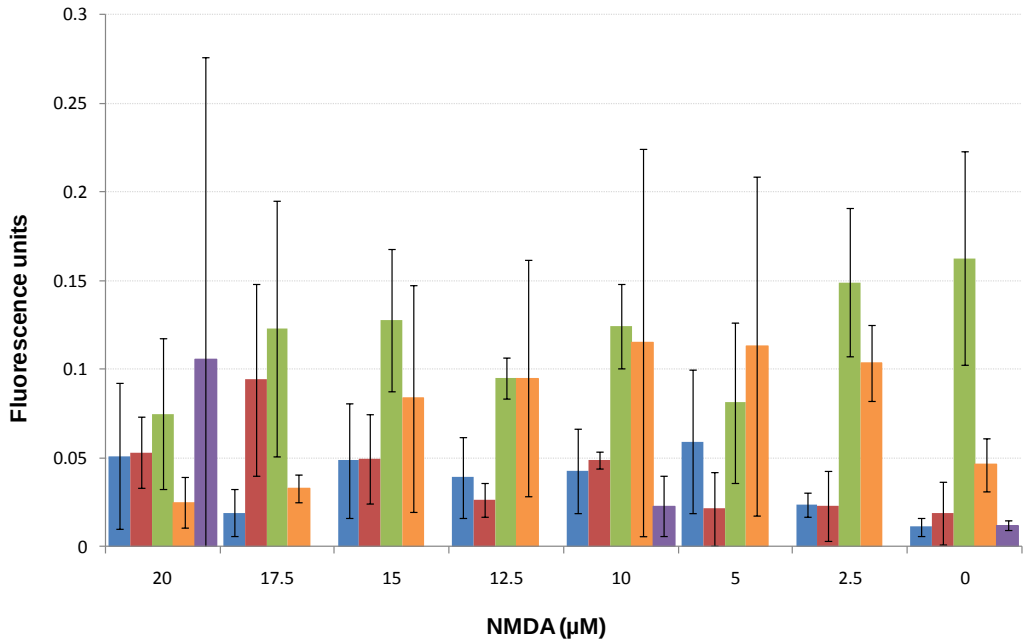

Figure 3.31. Calcium response of differentiating NTERA2 cells to NMDA stimulation.

Undifferentiated NTERA2 p58 (blue), 10 day ATRA treated NTERA2 p57 (red), 3 week ATRA treated NTERA2 (green), 6 week ATRA treated NTERA2 (orange), dermal fibroblasts p18 (purple) were stimulated with NMDA and subsequent calcium influx detected. No significant difference in the calcium influx of pluripotent NTERA2 and dermal fibroblasts was detected across all NMDA concentrations ($p = 0.61$). As with KCl stimulation, the response from 3 and 6 week differentiated NTERA2 was higher than that of undifferentiated and 10 day treated samples; however, this increased response was also observed at 0 µM NMDA and is therefore likely to be a result of difference in overall cell number rather than functionality. Error bars represent ± 2SE.

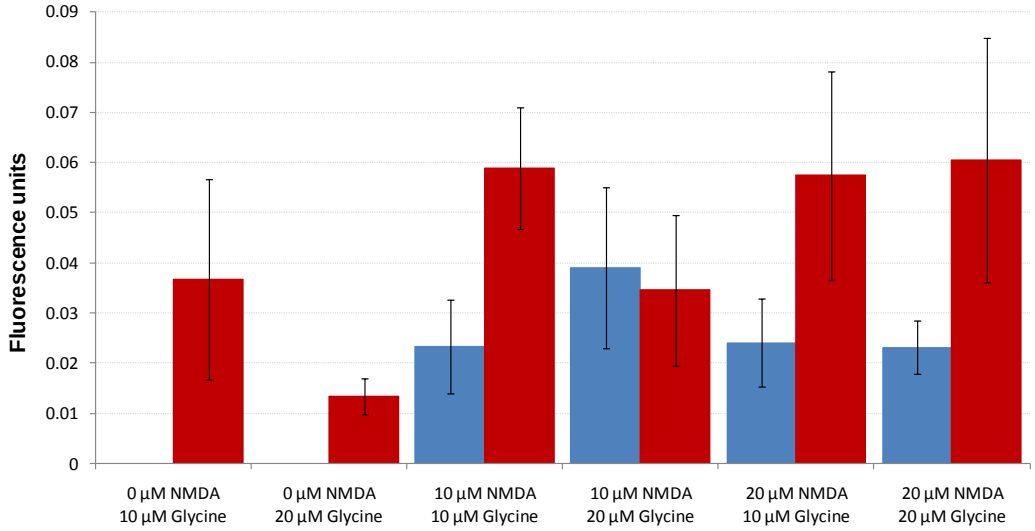

Figure 3.32. The affect of NMDA with Glycine on differentiating NTERA2 cells.

Undifferentiated (blue) and 10 day ATRA treated NTERA2 (red) were stimulated with NMDA (10 µM and 20 µM) in the presence of the co-agonist glycine at 10 µM and 20 µM. No difference was detected in the calcium response of undifferentiated NTERA2 at either concentration of NMDA with or without glycine, confirming that NDMA receptors are not expressed by these cells. The general response of 10 day ATRA treated cells to NMDA in the presence of glycine was higher than that of the undifferentiated cells but the concentration of NMDA and glycine did not affect the response, suggesting that the overall higher response may also be a factor of cell number not behaviour. Error bars represent ± 2SE.

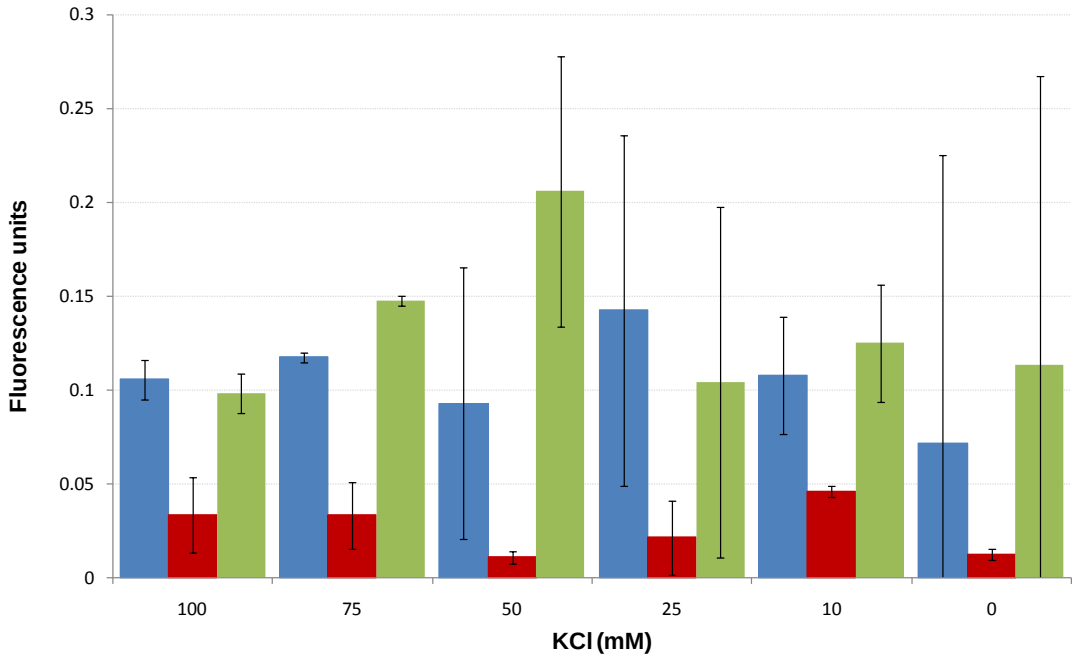

Figure 3.33. The use of SHSY5Y as a positive control.

SH-SY-5Y (green) cells were differentiated for 8 days with ATRA into a neuronal morphology, stimulated with KCl and the calcium response compared to that of undifferentiated NTERA2 (blue) and dermal fibroblasts (red). No significant difference between the calcium response of SY-SY-5Y derived neurons and undifferentiated NTERA2 cells was observed (p = 0.199). Error bars represent ± 2SE.

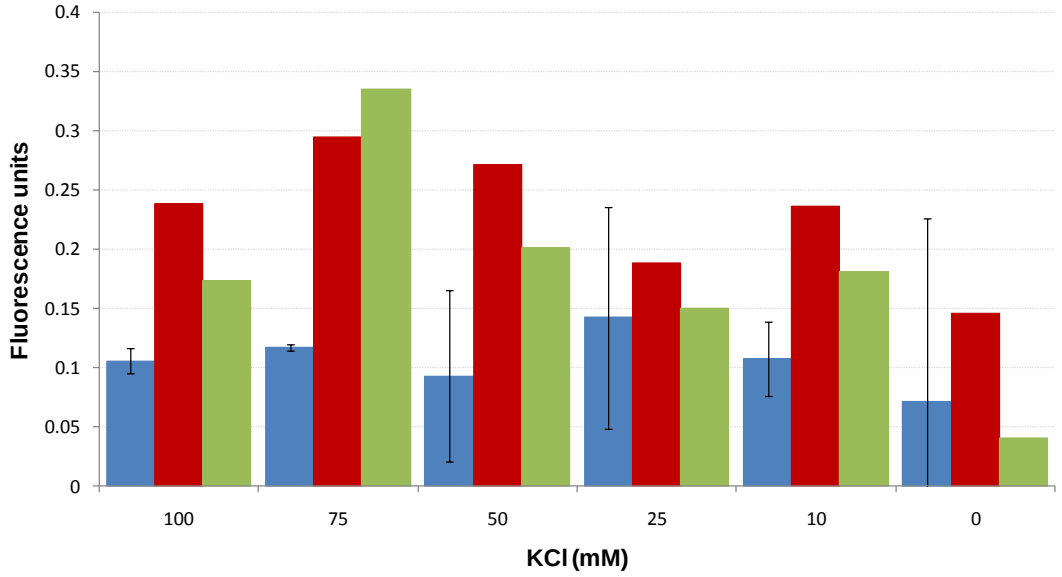

Figure 3.34. Calcium response of purified 6-week ATRA NTERA2 neurons.

Comparison of 6-week old NTERA2 derived neurons purified using rapid trypsin exposure. Both the top layer of purified neurons from a 6 weeks ATRA treated NTERA2 population (red) and the remaining cells from the ATRA treatment (green), generated a higher calcium influx than undifferentiated NTERA2 cells (blue). Error bars represent ± 2SE.

In combination with glycine, glutamate induced a delayed Ca^{2+} influx in 6 week ATRA neurons, demonstrating the presence of glutamate receptors in these cells. The response from cell 1 (200 nM cytosolic calcium) was greater than that of cell 2 (120 nM cytosolic calcium) which may be a result of more membrane glutamate channels, or a larger cell body. Both cells responded well to KCl confirming as with the patch clamping data, that these cells express function voltage gated ion channels. The response to KCl was comparable between cells (310 and 325 nM; Figure 3.36) and was higher than the response to glutamate but not significantly different ($p = 0.06$). The KCl response was also more instantaneous than the glutamate response due to the rapid opening of the voltage gated calcium channels in response to KCl depolarisation. It was not ideal to monitor the KCl response of the cells after stimulation with glutamate as the cells may have been exhausted by glutamate stimulation. However due to limited cell numbers, these neurons were left to recover to basal calcium levels in HBS buffer before re-stimulation with KCl.

In both examples the influx of Ca^{2+} came in two waves. A similar occurrence was seen in the patching data where recurrent bouts of depolarisation occurred following stimulation. This was a good sign for mature neuronal status.

After 8 weeks NTERA2 neurons were stimulated with NMDA with glycine (as run in the FLIPR), glutamate with glycine, KCl, and carbachol (Figure 3.37). None of the neurons elicited a Ca^{2+} response to NMDA stimulation, suggesting that the non-result on the FLIPR may have been a true result. Only one of the five cells monitored generated a Ca^{2+} influx in response to glutamate which was surprising when compared to the earlier results from 6 week ATRA neurons. Screening of such small neuronal samples was due to limited recovery following replating, but would not have generated a fair representation of the entire neuronal population at this age. No response was detected following carbachol stimulation suggesting an absence of acetyl choline receptors on these neurons. In contrast to early results from the FLIPR, all cells responded to KCl stimulation at 60 mM. It is likely that this response was not detected by the FLIPR due to the low purity of neurons in each well compared to the non-responsive non-neuronal cells.

The small sample size of neurons required for Ca^{2+} imaging meant it was possible to run a positive control with primary rat neurons, as for the patching, these neurons were isolated from the GE region of an e14 rat. Cells were prepared as for NTERA2 neurons and stimulated for a calcium response to NMDA (100 µM) with glycine (20 µM), KCl (60 mM), and carbachol (100 µM). The number of primary neurons on the slide was considerably

more than that of the NTERA2 derived neurons, suggesting a difference in the recovery of primary neurons to plating, or a survival benefit posed by the presence of larger numbers of neuronal cells. A background fluorescence image of these cells was captured (Figure 3.38) and each cell body highlighted (blue) for recording the fluorescence output. The response from a total of 38 cells was recorded (*video of the calcium response of these cells is available on request*).

The number primary neurons which responded to NMDA with glycine were considerably lower than the number of cell responding to glutamate stimulation (representative results from the first 20 cells presented in Figure 3.39). The cell which responded to NMDA, also responded to glutamate with a larger response than any other cell in culture. As was seen in the patching of these primary neurons, reverberating currents of Ca^{2+} flux were visible in these cells. It is likely that on each depolarisation, the neurons released a range of neurotransmitters which in turn stimulated a response in neighbouring cells, thereby creating waves of signalling across the plate. When the basal Ca^{2+} levels were restored after washing in HBS buffer, cells were stimulated with KCl (60 mM). Unsurprisingly the response by each cell was less than that seen in response to glutamate; this was likely to have been because these cells were exhausted from earlier stimulations.

The response of cells to carbachol was lower than that of NMDA, glutamate or KCl (Figure 3.40) but was a true response which generating a slowly oscillating Ca^{2+} influx in the cell. The response of the cell appeared to induce opening of ion channels in nearby cells generating Ca^{2+} waves across the dish. Carbachol stimulation was not toxic to the cells as a similar KCl response to the first run was seen in these cells after recovery of basal Ca^{2+} levels.

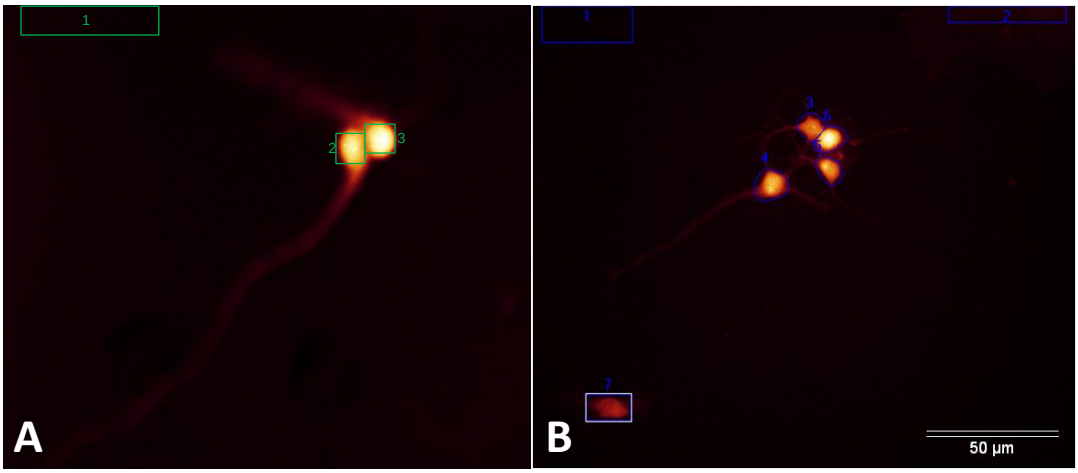

Figure 3.35. NTERA2 derived neurons for calcium imaging

NTERA2 derived neurons at 6 weeks (A) and 8 weeks (B) post induction. Areas monitored for changes in fluorescence highlighted in red (left) and blue (right).

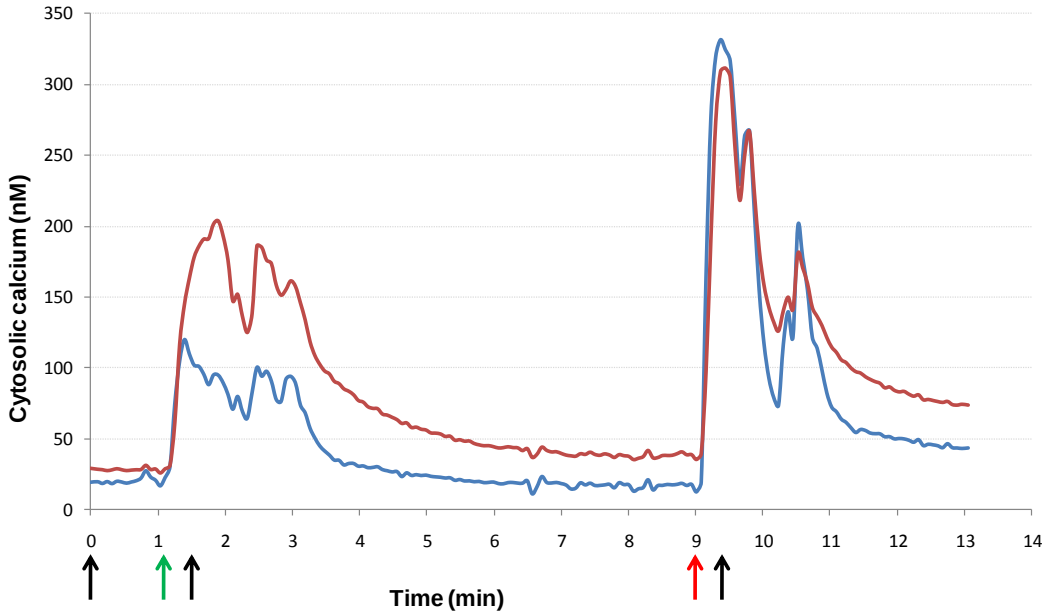

Figure 3.36. Calcium imaging of 6 week ATRA neurons.

Two neurons (cell 1 – red and cell 2 – blue) were imaged for calcium response to stimulation by glutamate with glycine (100 µM/20 µM; green arrow) and KCl (60 mM; red arrow). Changes in fluorescence were calculated relative to T_0. Background fluorescence readings were subtracted from all recordings. Cells were washed in HBS before and after stimulation until recovery of basal calcium levels returned. Start of the HBS washes as indicated by the black arrows. Both cells responded to glutamate/glycine and KCl stimulation. The response of cell 1 to glutamate and glycine was greater than that of cell 2. After recovery KCl stimulation resulted in a comparable response from both cells.

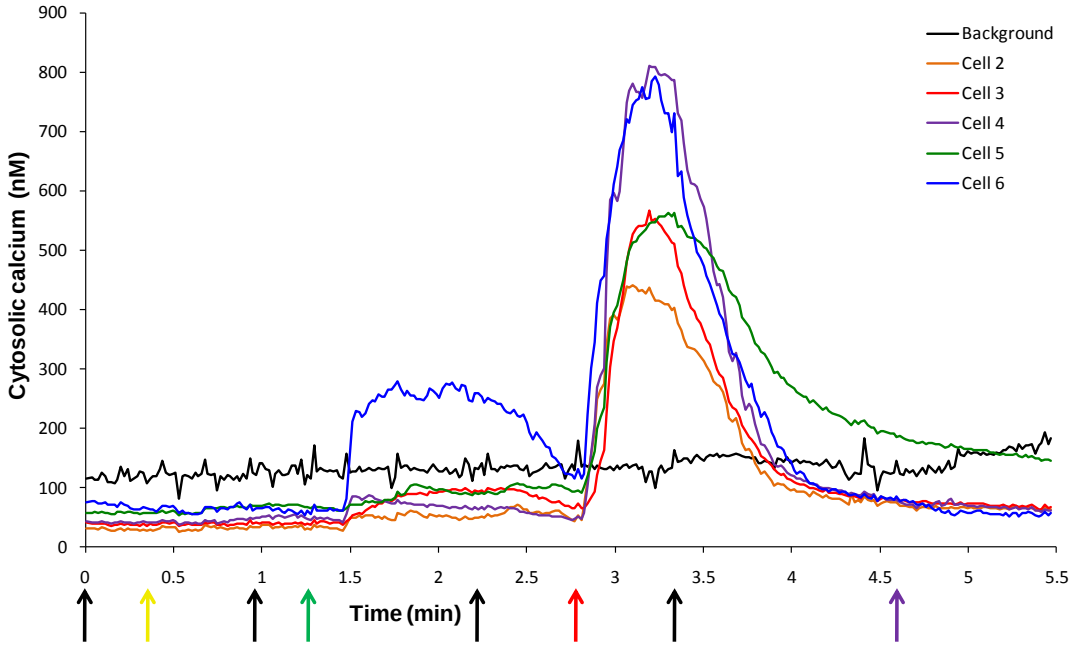

Figure 3.37. Calcium imaging from NT2-neurons,

None of the cells responded to NMDA and glycine stimulation (yellow arrow). Only one cell responded to glutamate and glycine stimulation (green arrow). A variable response was seen to high KCl stimulation (red arrow), suggesting the number of voltage gated channels on these cells may be inconsistent. No response to carbachol at 100 µM concentration (purple arrow). Between each stimulus cells were washed in HBS (black arrow).

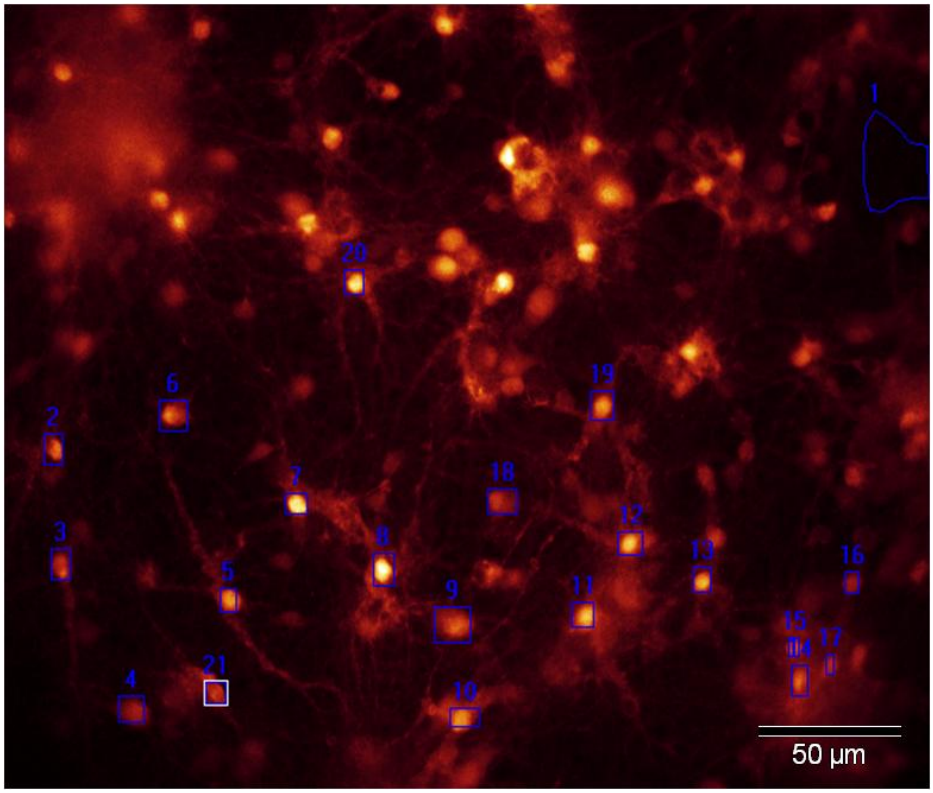

Figure 3.38. Rat e14 GE neurons for calcium imaging.

Cells were highlighted for recording fluorescence output in response to stimulation and labelled 2-20 (blue). Channel one recorded the background florescence which was subtracted from all readings.

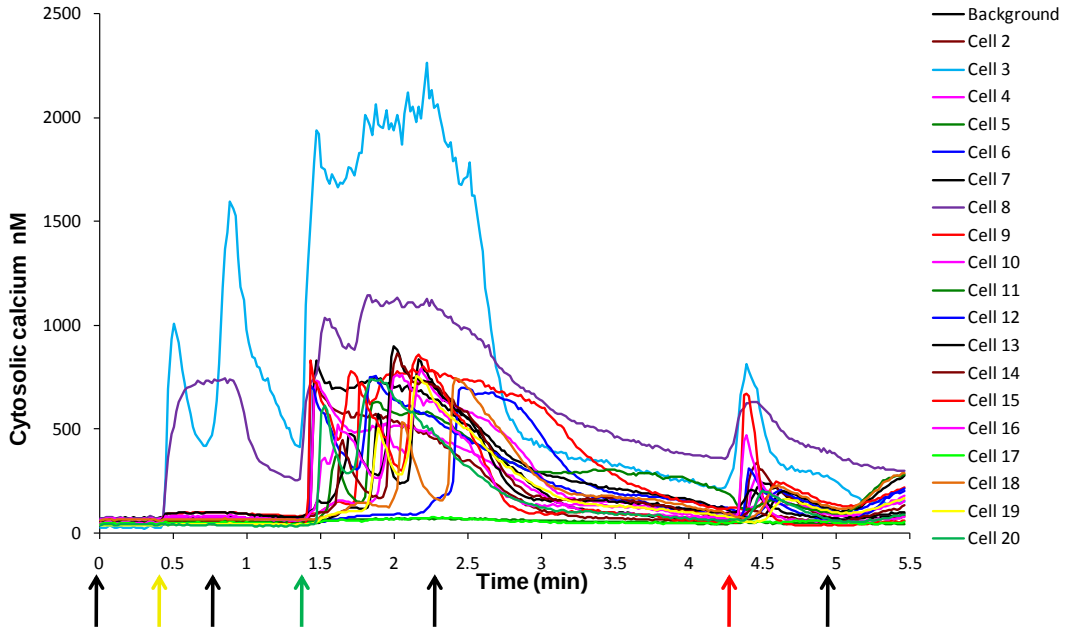

Figure 3.39. Calcium imaging from e14 rat neurons after 2 weeks maturation.

Two primary rat neurons generated a calcium flux in response to NMDA and glycine stimulation (yellow arrow). Between each stimulant the system was flushed with HBS (black arrow). Reverberating calcium waves were stimulated across the plate in response to glutamate and glycine stimulation (green arrow). KCl induced a simultaneous single calcium flux in primary neurons (red arrow).

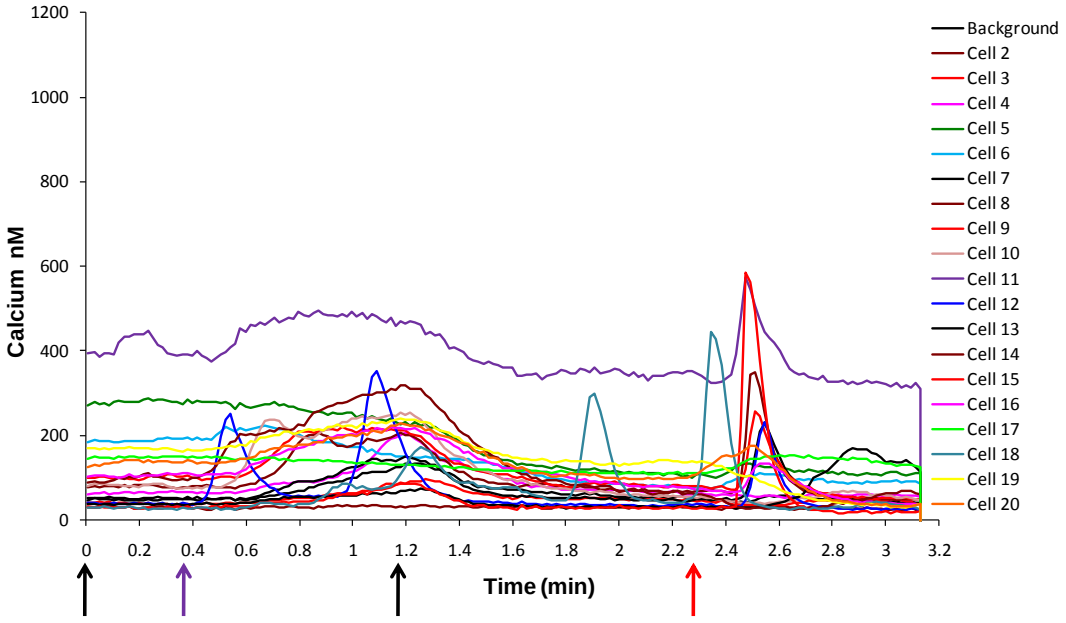

Figure 3.40. Calcium imaging from e14 rat neurons after 2 weeks maturation.

Few primary GE rat neurons responded to carbachol stimulation (purple arrow). A calcium flux was detected in response to KCl (red arrow). Between each stimulus, cells were flushed with HBS (black arrow).

3.3 Discussion

Culture of the pluripotent NTERA2 was highly variable during pluripotent expansion, with the population in apparent waves of sustained pluripotency versus spontaneous differentiation. Reagents for culture and trend systems of environmental conditions were consistently recorded for full traceability, yet no underlying cause for apparent loss of pluripotent self-renewal could be attributed to the culture conditions. Pluripotent expansion required culture at high cell density and close monitoring of confluency levels and routine passaging at ~90 % confluence (approximately every three days). When passaged too early, cells underwent spontaneous differentiation, suggesting close cell-cell contact was essential for pluripotent expansion. When left to culture beyond 100 % confluence, cells detached and were unrecoverable into adherent pluripotent culture.

Undifferentiated NTERA2 positively expressed the pluripotency markers OCT4 and SOX2. In addition, these cells also expressed the neural stem cell marker Nestin. Nestin is commonly used as an indicator of neural commitment following differentiation of pluripotent populations but has been shown to drop off in post-mitoitc neurons (Lendahl et al., 1990). In the absence of genes required for endodermal and mesodermal differentiation, the propensity for ectodermal differentiation in NTERA2 would be high, and might explain expression of early ectodermal markers such as Nestin in undifferentiated populations. Nestin was not detected in the 6-week neurons; however, it was observed in non-neuronal cells after 6-weeks ATRA induction. Nestin expression has been confirmed in the development of non-neural cell types including a range of epithelial cells (Frojdman et al., 1997; Lardon et al., 2002; Mokry et al., 2004; Bertelli et al., 2007; Cicero et al., 2009) which might explain its expression in the epithelial-like produce of ATRA induced differentiation.

NTERA2 cells were highly susceptible to spontaneous differentiation, demonstrating a preference for an epithelial-like cell fate (Damjanov and Andrews, 1983; Pleasure et al., 1992). During embryogenesis, neural cells in addition to a range of epithelial cells are derived from the ectodermal germ lineage. The discovery that NTERA2 cells lack many of the genes involved in mesodermal and endodermal differentiation (Schwartz et al., 2005), might explain the propensity for ectodermal derived epithelial cells during spontaneous differentiation and their frequent derivation during neuronal differentiation. In order to inhibit the formation of these cells it would be necessary to block epithelial differentiation following ectodermal commitment. Non-neural, ectodermal derived cell types, including epithelia have been induced from NTERA2 following exposure to BMP2 (Chadalavada et

al., 2005). Therefore inhibition of BMP2 signalling, using Noggin might shift ectodermal differentiation towards a neural fate in preference to epithelia. Incorporation of noggin would also aid ectodermal commitment by blocking BMP4 signalling required for mesodermal lineage commitment (Winnier et al., 1995; Marom et al., 1999).

The yield of neurons throughout the study remained variable. Successful differentiation was dependent upon a homogeneous pluripotent starting population, with fluctuations in pluripotency mirrored in the success of differentiation. On occasion, no neurons were visible in culture after 4 weeks of differentiation (*data available upon request*). Culture of cells in smaller vessels appeared to reduce spontaneous differentiation and increased neuronal yield (Section 3.2.2.3). Smaller vessels contained fewer cells, making it easier to select pure populations in which to initiate differentiation. This also enabled selective expansion of pluripotent populations.

Upon successful differentiation, neurons were derived as part of a heterogeneous population, containing different varieties of cells of non-neuronal phenotype. Mitotic inhibitors were incorporated into the latter stages of differentiation to prevent the over growth of post-mitotic neurons by non-neuronal cells. Mitotic inhibitors target fast replicating cells by integrating into the DNA to halt mitosis. However, in this study neurons demonstrated a preference for attachment to the non-neuronal cells layer (Figure 3.6) which supported their survival in culture. Loss of the epithelial-like cells consequently resulted in a depletion of the neuronal population. In addition, cytosine arabinofuranoside has been reported to have a cytotoxic affect on post mitotic neurons (Wallace and Johnson, 1989) which may also have contributed to the detachment and loss of neurons overtime. Some variations of ATRA induced neuronal differentiation only supplement cultures with mitotic inhibitors overnight (Park et al., 2007); however, this is unlikely to be sufficient long exposure to target all proliferating cells.

Alternative procedures remove serum from culture media which reduces the proliferation of glial cells in neuronal cultures (Brewer et al., 1993). Serum of bovine origin was incorporated into the media throughout this study which would explain the prevalence of non-neuronal cells. Instead, serum could be supplemented with alternative sources of neurotrophic factors such as N2 and B27 supplements (Sections 1.5.2.3 and 1.5.2.4) which selectively promote neuronal survival.

NTERA2 derived neurons displayed rounded phase bright cell bodies and extended projections which stained positively for TUBB3 and MAP2. Immunostaining of 6-week

neurons for the synaptic vesicle glycoprotein synaptophysin was unsuccessful; however, the absence of a positive neuronal control meant that it was not possible to confirm the absence of synaptophysin. In some cases during calcium imaging, an influx of Ca^{2+} within a population of neurons was visible in response to glutamate, followed by a secondary delayed Ca^{2+} wave in neighbouring cells. It is possible that dispersal of glutamate was not uniform; however, a more likely explanation for the secondary Ca^{2+} wave would be the release of neurotransmitters by the first cells in response to glutamate stimulation, which later stimulated Ca^{2+} influx in alternative cells, as would be seen during *in vivo* communication. This would suggest the presence of synaptic vesicles within a proportion of NTERA2 derived neurons, which would contain the synaptophysin. Communication of this nature has also been identified following formation of functional synapses by NTERA2 derived neurons (Hartley et al., 1999).

The lack of positive GFAP staining would suggest that there were no glial cells amongst the differentiated neurons populations. Although this may also have been a factor of poor antibody specificity, the absence of glia following NTERA2 differentiation is has also been observed by other laboratories (Marchal-Victorion et al., 2003; Podrygajlo et al., 2009). However, there are a number of groups who report the derivation of glia from NTERA2, suggesting that the method of culture is critical for glial cell derivation (Ozdener, 2007; Sanchez et al., 2009). When cultured in the presence of glial cells, the formation and functional activity of synapses is increased in both NTERA2 derived and primary neurons (Pfrieger and Barres, 1997; Hartley et al., 1999). The absence of glia derivation during differentiation may therefore reduce maturity of the neuronal population and subsequently reduce functional activity. This would suggest a requirement for co-culture of neurons and glia, during differentiation in accordance with *in vivo* neurogenesis, to improve neuronal functionality.

Immunostaining of 6-week neuronal populations confirmed an absence of both dopaminergic and serotonergic neurons. The presence of GABAergic neurons was confirmed by positive GABA staining. Indeed the presence of GABAergic neurons following differentiation has been confirmed by alternative research publications (Guillemain et al., 2000; Podrygajlo et al., 2009). In addition, alternative laboratories have also reported derivation of glutamatergic neurons from NTERA2 (Hartley et al., 1999; Podrygajlo et al., 2009). Due to limited resources, glutamatergic neuronal markers were not screened for in this study. However, glutamatergic and GABAergic neurons are two of the main classes of forebrain neuron. Development of the embryonic forebrain is regulated by retinoic acid

(Schneider et al., 2001; Ribes et al., 2006), as was used to induce neuronal differentiation in this study. It would therefore not be surprising to find glutamatergic neurons within the neuronal population.

The absence of a positive control for all the neuronal *in situ* immunostaining meant that these results are open to interpretation. During differentiation studies it is important to assign a suitable positive control to validate both positive and negative data. Limited access to primary human neurons restricted their incorporation into parts of this study. Attempts to use a neural cell line: SH-SY-5Y, derived from a bone marrow biopsy of a metastatic neuroblastoma site, and a record of neuronal functionality, failed due to the need for further differentiation of the control line (Biedler et al., 1973; Encinas et al., 2000). Many of the antibodies used in this study were specific to human isoforms, therefore non-human primary neurons would not have been suitable controls. Despite this positive controls should have been incorporated into this study and would be commercially sourced and included in any future immunostaining applications.

A control cell sample must be selected based upon the desired experimental outcome. For functionality studies where the control served to demonstrate function of the equipment rather than the cell, animal source primary neurons were sufficient. In addition, activity of the primary neurons during functional studies, enabled a comparison of activity and sensitivity between cell line derived and the currently used animal derived primary neurons for cell based functional assays. In order to reduce reliance on primary neurons in a cell-based assay, cell line derived neurons must at least as sensitive as the primary neurons currently used.

NTERA2 derived neurons were shown to generate electrical impulses as determined by patch-clamp analysis from just 2 weeks after ATRA induction. Patch-clamping is a highly skilled technique. The delicacy of the process meant that a negative result could have been a result of an unexcitable cell or poor technique. On the most efficient day, the behaviour of just 19 cells were screened. In addition, the high failure rate induced a subconscious selection of neurons for screening, which were accessible and displayed appropriate neuronal morphology. These cells were usually located towards the edge of neuronal clusters and so may have been exposed to different developmental stimuli, resulting in a different response to stimulation, compared to neurons in the centre of clusters. To this extent, patch-clamping generated a poor representation of the electrophysiological activity of the neuronal population.

Incorporation of the FLIPR for functional analysis meant that screening was reproducible across samples and analysis of the behaviour of an entire population could be carried out in minutes. However, neurons were highly susceptible to detachment during processing, leaving just a few neurons per well for screening. Resulting data was therefore derived mainly from the unexcitable non-neuronal population of cells.

In agreement with findings by (Rendt et al., 1989), undifferentiated cells were non-responsive to KCl depolarisation, confirming that EC cells do not express voltage gated Ca^{2+} channels in their pluripotent state. The Ca^{2+} response to KCl depolarisation was shown to increase with duration of differentiation, suggesting an increase in the number of voltage gated channels (Figure 3.30). However, it was not possible to determine whether the increased response was a results of an improve response by a few cells, or an increase in the overall number of cells responding. Data from the FLIPR was considered to be subjective due to low neuronal purity. In addition, the intervals between fluorescence detection (once/second) were considerably longer than the frequency of neurotransmission which has on occasion been shown to reach 100 Hz or faster (Dunant and Bloc, 2003). Data from immediate response of neurons to stimulation may therefore have been lost between sample intervals. Neuronal responses to stimulation by alternative neurotransmitters could not be confirmed by the FLIPR due to the low magnification of detection and overriding interference from unresponsive non-neuronal cells. A higher magnification calcium imaging facility was therefore incorporated into the study to more clearly identify the response attributable to NTERA2 derived neurons.

The presence and functionality of voltage gated channels in NTERA2 derived neurons was confirmed using higher magnification calcium imaging, in addition to the presence of functional glutamate receptors. These responses have been previously identified in NTERA2 (Squires et al., 1996).

Interestingly, NTERA2 derived neurons have been shown to respond to acetyl choline and NMDA stimulation (Squires et al., 1996), which was not detected in this study. Even in the presence of the co-agonist glycine, no Ca^{2+} response was initiated by NMDA stimulation. NMDA receptors are expressed by a subclass of neurons located amongst the cerebellum and cortex (Bliss and Collingridge, 1993) and which would not be expected to be present in such small numbers of ATRA induced neurons. As an inhibitory neurotransmitter which induces influx of Cl^- ions for repolarisation rather than Ca^{2+}, no visible response to glycine stimulation was expected or exhibited by NTERA2 derived neurons.

3.3.1 Summary

Data from this study revealed that neurons derived from the NTERA2 population following ATRA induction were of a morphological neuronal phenotype and expressed a range of functional membrane ion channels which initiated electrical impulses following stimulation. However, when compared to functional response of e14 GE primary neurons, NTERA2 derived neurons were consistently less sensitive and responsive to stimulation with no sign of the spontaneous activity which was consistently present throughout primary cultures. This suggests that immaturity in a large proportion of the derived neurons, which might be explained by the lack of supporting glial cells throughout the differentiating populations. Despite improvements to the efficiency of differentiation, these data confirm that hEC cell line derived neurons were not sufficiently responsive for reliable incorporation in cell based toxicity assays.

Successful directed differentiation requires an uncommitted starting cell pool. The originating cells of this line were germ cells which underwent a process of internal reprogramming to generate the pluripotent population. Despite expressing pluripotency markers, these cells may have retained memory from stimuli encountered during germ cell specification which would need to be over-ridden to allow efficient direction to a neuronal fate. Thus, a hEC line may not be the most effective starting cell source for efficiency in generating neurons, rather the use of a naïve pluripotent cell type such as a hESC line, with no somatic cell memory may be more amenable to a specified cell fate.

4 Stability and expansion of pluripotent hESCs in culture

4.1 Introduction - hESCs as a model for neuronal differentiation.

The need for an alternative source of neurons for cell therapies and pharmacological screening has been described in detail in the previous sections. Investigation into the use of a teratocarcinoma derived cell line NTERA2, demonstrated an inherent variability in the efficiency of neuronal differentiation and the reduced functional response when compared to primary neurons. Despite expression of pluripotent markers and a demonstrable ability to differentiate into cells from all three germ lineages (Andrews et al., 1984), both spontaneous and ATRA directed differentiation yielded large numbers of epithelial-like cells, suggesting a predetermined preference for differentiation, which limited neuronal yield.

It was hypothesised that the tumour origin of the NTERA2 cell line in addition to its aneuploidy karyotype (Andrews et al., 1984), was responsible for the poor efficiency in pluripotent expansion and directed neuronal differentiation. To investigate this hypothesis further, three pluripotent hESC lines (Shef3, HUES7 and RH5) with varying degrees of aneuploidy were compared for their stability in pluripotent expansion and their subsequent ability to generate functional neurons following directed differentiation.

4.1.1 Description of hESC lines

4.1.1.1 Shef3

The Shef3 hESC line was derived by Professor. H. Moore's group, (Centre for Reproductive Medicine and Fertility, Sheffield) in 2004 along with a range of other Shef hESC lines (Draper et al., 2004b). This line was sourced from the UKSCB at p33 for use in this study. The Shef3 line has a diploid XY karyotype, derived in standard knock-out hESC media (Section 2.9.2). Shef3 was routinely passaged mechanically onto iMEFs (UKSCB, cell line master file). At the start of this project there was no published literature using Shef3 and its ability to differentiate into a neuronal cell fate (or any other cell fate or germ lineage).

4.1.1.2 RH5

The RH5 (Roslin Human 5) stem cell line was derived in 2006 by The Roslin Institute, (Scotland, UK) and was aneuploidy with a 101 XX complement at the time of deposition to

the UKSCB (Fletcher et al., 2006). This line was sourced from the UKSCB at p36 for use in this study. This cell line was derived in MEF conditioned media supplemented with bovine serum replacement media, on mitoticaly inactivated neonatal human dermal fibroblasts. Following establishment, the RH5 cell line was routinely passaged enzymatically using collagenase (Fletcher et al., 2006). Very little research has been carried out using this line with regards to behaviour in culture and response to differentiation.

4.1.1.3 HUES7

The HUES7 cell line was derived in 2004 by the Harvard Stem Cell Institute, (Harvard University, USA), along with 16 other HUES lines freely available to the research community (Cowan et al., 2004). These hESC lines were derived and cultured on iMEFs. Cells were adapted to enzymatic passaging (using Trypsin) within five passages of derivation (Cowan et al., 2004). This line was sourced from the UKSCB at p20 for use in this project. Early karyotypic analysis of this line reported a normal 46 XY complement (Cowan et al., 2004). The HUES7 cell line has a small publication history for neuronal differentiation (Iacovitti et al., 2007; Kumar et al., 2008) and as such was known to differentiate neuronally. This line therefore served as a positive control of neuronal differentiation in hESCs and as a comparison for additional hESC lines.

4.2 Results

4.2.1 Defining hESCs in culture

During establishment of hESCs in culture, optimal conditions for maintenance of pluripotency were identified. Pluripotent hESCs were identifiable by their high ratio of nucleus to cytoplasm, prominent nucleoli (Figure 4.1A), and compact colony structure (Figure 4.1B); (Thomson et al., 1998; Cowan et al., 2004); to the untrained eye hESC colonies have an appearance similar to frog spawn. Healthy stem cell colonies presented clearly defined borders (Figure 4.1C-F) and appeared almost translucent under a dissection microscope (Figure 4.1D). These criteria were used for identification and scoring the quality of all hESCs throughout this project.

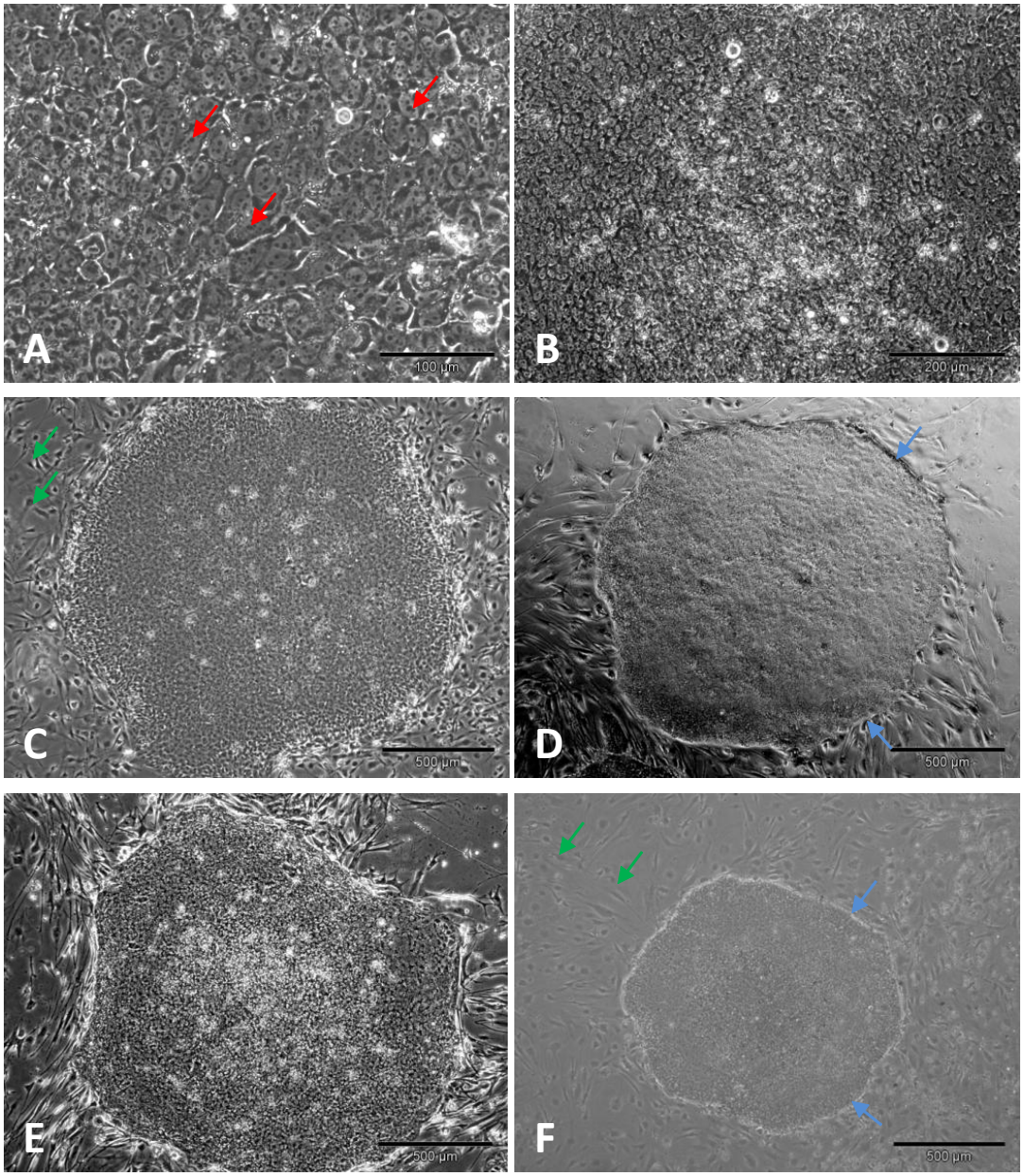

Figure 4.1. Human embryonic stem cell colonies.

Human embryonic stem cells were identified by their high nucleus to cytoplasm ratio, prominent nucleoli (A - red arrows, x20 magnification, B - x10 magnification), compact rounded colony structure with defined borders (blue arrow) against the iMEF feeder-layer (green arrows). C-F: x4 magnification.

4.2.2 Adaptation of hESCs to alternative culture

Human ESCs are largely reliant on their culture environment for retention of pluripotent characteristics (Section 4.2). The effect of different passaging techniques on the survival, expansion and subsequent neuronal differentiation of different hESC lines has been speculated but not fully investigated. Passaging of hESC can be broadly divided into two categories: mechanical and enzymatic (Sections 2.9.1.1 and 2.9.1.2). This project set out to investigate the differences which these techniques induce upon the pluripotent culture and expansion of different hESC lines (*herein*), and their subsequent effect on directed neuronal differentiation (Chapter 5).

To determine whether differences in behaviour were a consequence of cell line choice, or passaging technique, the RH5 cell line was adapted from enzymatic to mechanical passaging methods creating two different cell lines (RH5 cut and RH5 TrypLE). Attempts to adapt the Shef3 cell line into enzymatic passaging from mechanical passaging were unsuccessful. TrypLE treated Shef3 cells failed to proliferate following passage and rapidly differentiated losing all characteristics of pluripotent hESCs (*images available upon request*). This phenomenon has also been observed by alternative researchers during adaptation Shef3 into enzymatic culture (*Personal communications with Ms. A. Hemsley, Regenerative Medicine and Bioprocessing, UCL*).

Mechanically passaged hESC colonies retained a uniform rounded shape in culture, pushing iMEFs aside as colonies expanded, creating defined colony borders. Enzymatically passaged cells grew more efficiently as a monolayer, initiating outgrowth from smaller clusters of cells following passaging. Inactivated MEFs were identified with minimised spreading integrated amongst the hESC monolayer.

4.2.3 Confirmation of pluripotency using immunostaining

Immunostaining was carried out on each of the hESC lines to confirm pluripotency during culture. All hESC lines positively expressed the OCT4B1 isoform and SOX2, localised to the nucleus, conferring pluripotency (Figure 4.2); the Santa Cruz antibody for OCT4 was selected based upon its specificity to the pluripotent OCT4B1 isoform (Atlasi et al., 2008). During optimisation, staining for SSEA3 was weak compared with SSEA4 and difficult to detect under epi-fluorescence imaging. As such, SSEA4 was used in preference to SSEA3 as a marker of pluripotency (Figure 4.3). This phenomenon has been previously observed by

(Thomson et al., 1998). *Additional images of all immunostaining in all hESC lines available on request*. All four hESC lines also stained positively for SSEA4 and Tra-1-60. The iMEF feeder layer was clearly visible around the edge of mechanically passaged colonies and interspersed between TrypLE^{TM} passaged cells. iMEFs did not stain for OCT4, Tra-1-60 or SSEA4. Marginal staining in the iMEFs was visible for SOX2; however, this was detected throughout the nucleus and cytoplasm and was likely to be a result of non-specific staining (Figure 4.2).

4.2.4 Spontaneous differentiation in hESCs

Under suboptimal culture conditions, hESC underwent spontaneous differentiation. Examples of spontaneously differentiating colonies were captured and described, building a reference for healthy and unhealthy hESC colonies (Figure 4.4). During differentiation, the translucence of hESC colonies was lost, becoming opaque and yellow in appearance.

In the absence of sufficient support from iMEF layers, the hESCs failed to retain a compacted colony structure associated with pluripotency and individual cells aligned, collapsed and differentiated into a flattened cell layer (Figure 4.4A).

Spontaneous differentiation of hESCs did not always occur throughout the entire colony, more commonly partial differentiation was observed which occurred at the edge (B), in the middle (C), or at various sites within the colony (D). If hESC fragments were too large following mechanical passaging (> 600 µM diameter), colonies curled up before attaching to the culture surface, resulting in a multi layered fragment which underwent spontaneous differentiation (Figure 4.4D).

Following the removal of hESC fragments, remaining hESC's re-grew into the area from which fragments were removed. Resulting re-growth retained characteristics of hESCs (Section 4.2), but adopted a more flattened morphology, surrounded by differentiating cells at the edge of the pre-cut surface (Figure 4.4E).

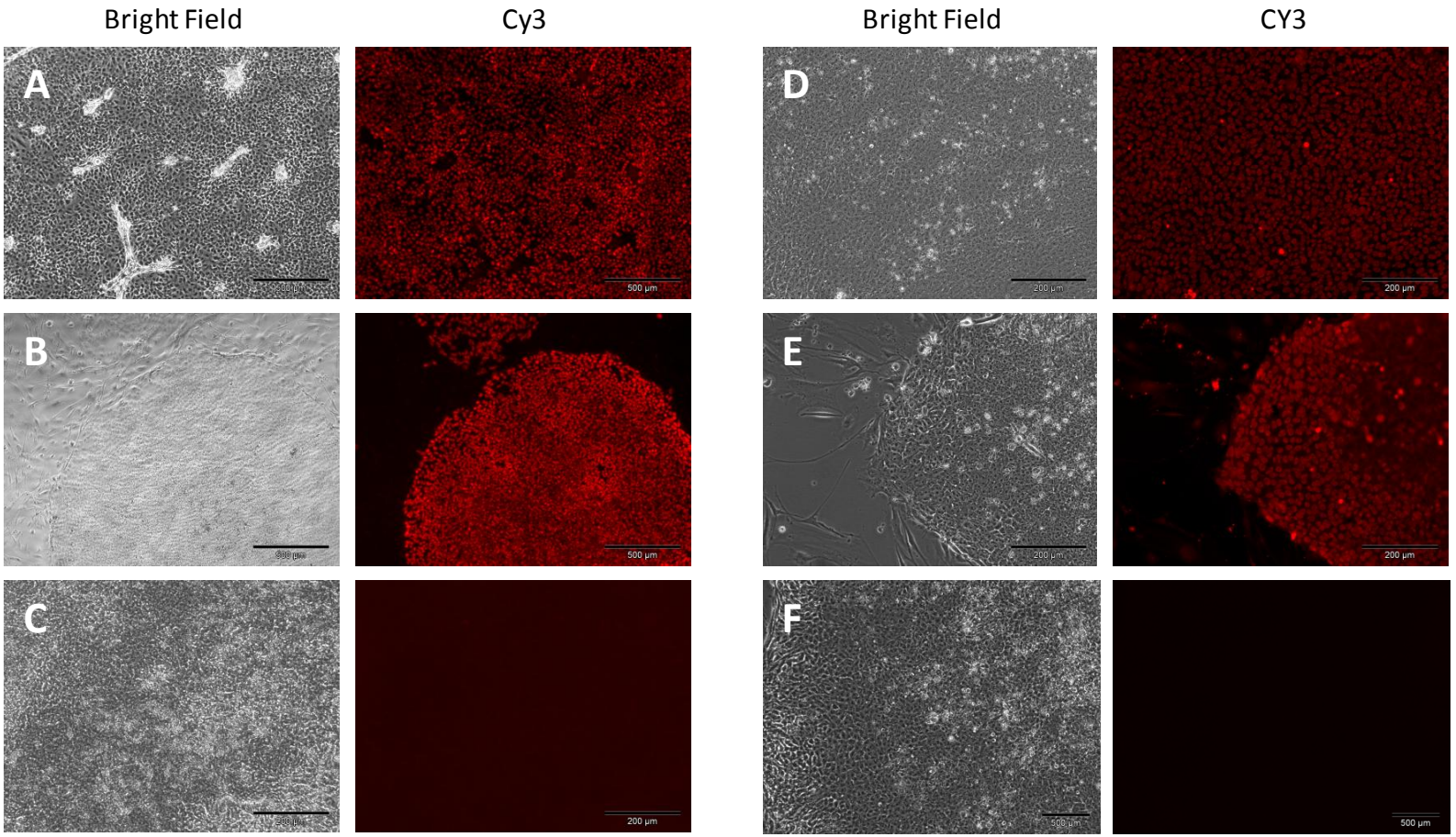

Figure 4.2. OCT4 and SOX2 immunostaining in undifferentiated hESCs.

Representative images for OCT4B1 isoform staining of enzymatically passaged cell line RH5 TrypLE (A; x4 magnification) and mechanically passaged line RH5 cut (B; x4 magnification). SOX2 staining for mechanically passaged cell line Shef3 (D; x10 magnification), and RH5 cut (E; x10 magnification). Staining was localised to the nucleus in all sample indicating specific staining for pluripotency genes. Mouse IgG (C) and Rabbit IgG (F) isotype controls were negative. Inactivated MEFs were negative for OCT4 but non-specific cytoplasmic staining was observed in iMEFs during SOX2 antibody.

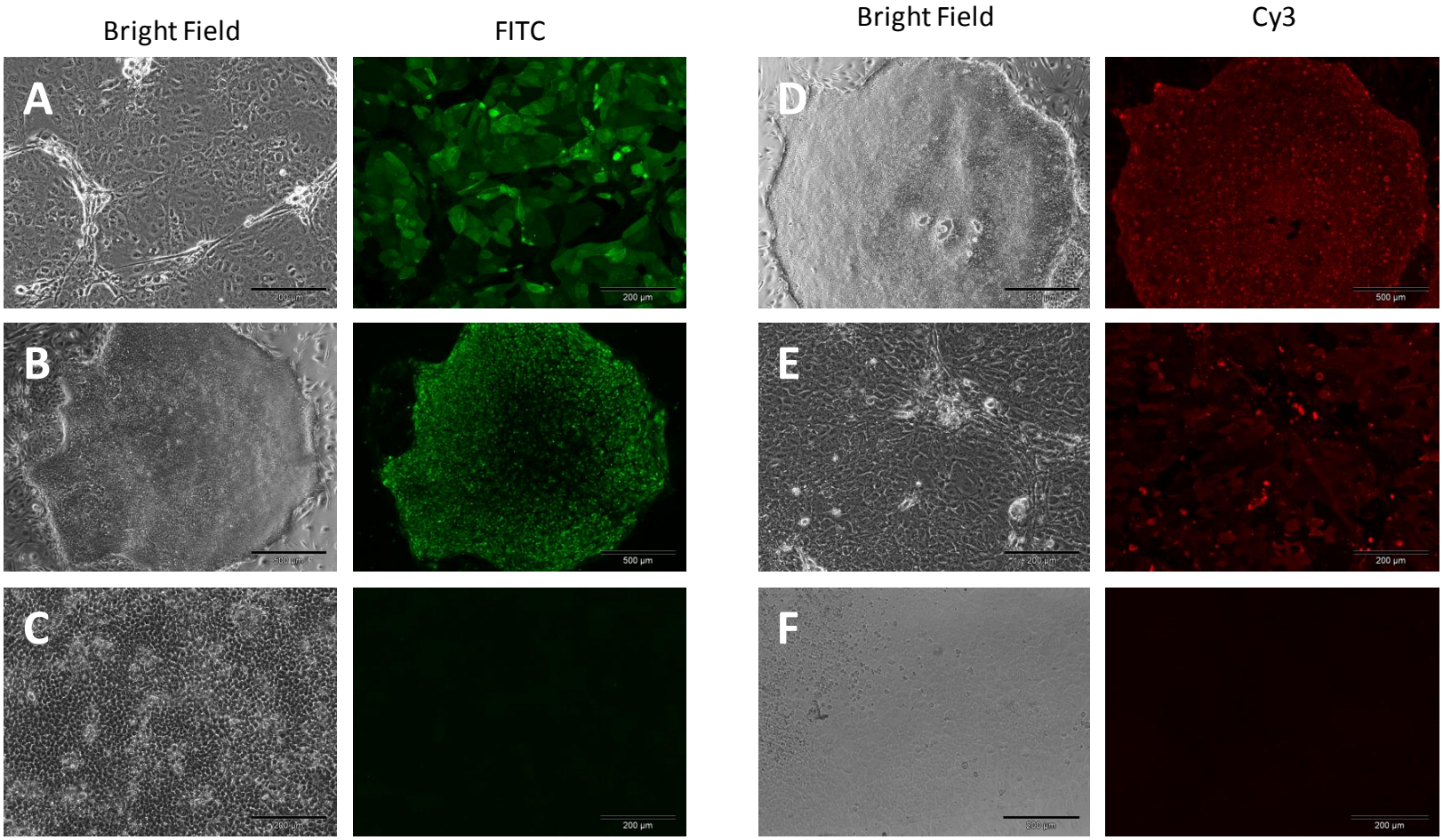

Figure 4.3. Tra-1-60 and SSEA4 immunostaining in undifferentiated hESCs.

Representative images of Tra-1-60 (green) staining in RH5 TrypLE (A; x10 magnification) and Shef3 (B; x4 magnification). All hESC cell lines RH5 cut (D; x4 magnification) and HUES7 (E; x10 magnification) stained positively for SSEA4 (red). Mouse IgM (C) and Mouse IgG (F) isotype controls were both negative confirming the absence of non-specific staining. Inactivated MEFs were negative for both Tra-1-60 and SSEA4.

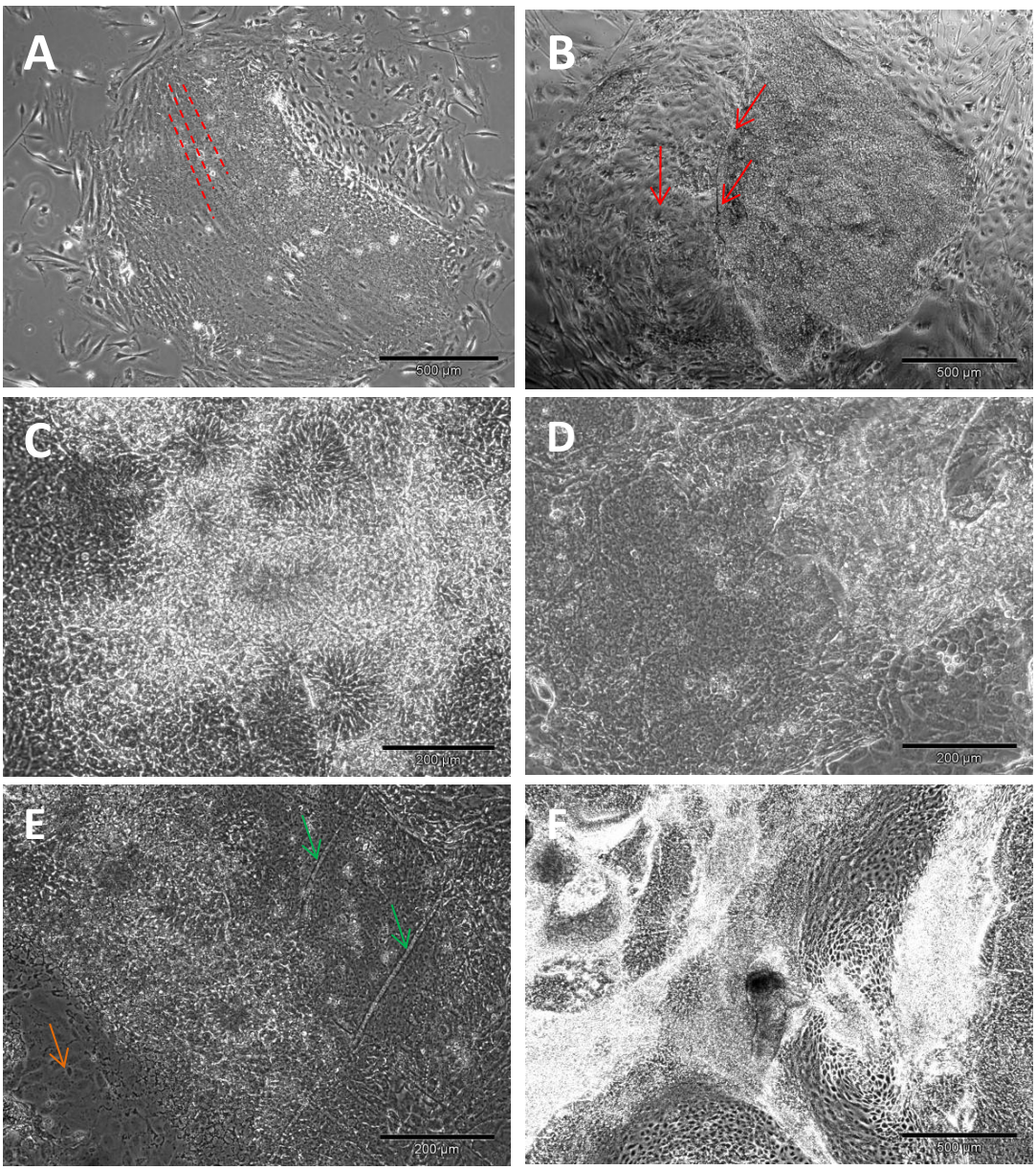

Figure 4.4. Spontaneous differentiation in human embryonic stem cell colonies.

Too low feeder cell density resulted in a flattened, collapsed hESCs morphology which were seen to align across the colony before eventually peeling from the plate (A). Spontaneous differentiation occurred at the edge (B; red arrows), in the middle (C) and at sporadic locations within the hESC colonies (D). Re-growth of hESCs into areas which have been mechanically removed showed a flattened collapsed morphology (E; orange arrow, green arrows – scratching on tissue culture vessel from mechanical passaging). Human ESCs colonies left in culture long term without passaging became spontaneously differentiated into a range of cell types (F) these colonies were opaque in nature and retained minimal pluripotent cells.

4.2.5 Mouse Embryonic Fibroblast feeder-layer

Human ESCs were routinely maintained in culture for 2-3 weeks; however prolonged culture eventually resulted in undirected differentiation. This was thought to be a result of failure by the iMEF layer to support pluripotent growth. To ensure a fair comparison between the behaviour of different hESC lines, it was necessary to identify the iMEF conditions which provided optimum support to their pluripotent expansion.

4.2.5.1 Feeder density

The primary origin of MEFs meant that different batches were inherently variable in behaviour and as such provided varying levels of support for hESC culture and expansion. The density of the feeder layer was found to be critical for sustained pluripotency in hESCs. For this reason, a feeder cell density experiment was carried out at the start of each new batch of feeders to determine the optimum seeding density for hESC support.

Human ESCs were most commonly cultured in 6-well plates, pre-coated with gelatin to aid cellular attachment. Inactivated MEFs were thawed from -80 °C and washed in standard GlutaMAX culture media (Section 2.1.2). Cells were counted using a bright-line haemocytometer (Section 2.3) and seeded onto well plates at the following cell densities 1.6×10^4, 2.1×10^4, 2.6×10^4, 3.1×10^4, 3.6×10^4, 4.2×10^4, 4.7×10^4, 5.2×10^4 cells/cm^2. Fibroblasts were plated in standard GlutaMAX culture media and left to attach overnight at 37 °C before changing the media for standard hESC culture media (Section 2.9.2). Cultures were left for a further 24 hours to condition the media, prior to hESC passaging. Optimum feeder density was determined by bright field observation of hESC colony morphology, scoring colonies according to the criteria outlined in Section 4.2. Images of typical colonies were captured from each of the iMEF seeding densities eight days after plating (Figure 4.5).

At low iMEF densities ($1.6 - 2.1 \times 10^4$ cell/cm^2), hESC fragments attached but rapidly lost their compact colony structure. Cells within the colony flattened out with an epithelial-like morphology (Figure 4.5A-B). At 2.6×10^4 cells/cm^2 colonies retained a high nucleus to cytoplasm ratio but the colony lost its compact structure with poorly defined borders (Figure 4.5C). Prolonged culture at low iMEF density resulted in elongation and alignment of individual hESC cells which eventually peeled away from the culture surface (Figure 4.5D). When the feeder density was $\geq 4.7 \times 10^4$ cells/cm^2, hESC colonies attached to the culture surface, but spreading was less noticeable; cells were seen piling up and colonies formed irregular shapes. Cells in the central region and very outer edge of these colonies

differentiated within a few days of plating (Figure 4.5G-H). Feeder cell densities at 3.6×10^4 - 4.2×10^4 cells/cm^2 maintained undifferentiated growth of hESC in uniform colonies with the classic hESC features outlined in Section 4.2.1. (Figure 4.5E-F) (*Note: seeding density correct for iMEF bank 3*).

4.2.5.2 The effect of MEF passage level

Upon reaching senescence, iMEFs lose their ability to support undifferentiated growth of hESCs (Stubban and Wesselschmidt, 2007). It was therefore critical to expanded and freeze each iMEF bank within an appropriate period to ensure support of pluripotency. Personal communication with Ms. L. Young, (UKSCB, NIBSC) suggested the optimum age for a iMEF bank was at p3. An iMEF bank at p3 generated approximately 4×10^7 ($\pm 9 \times 10^6$) cells (*calculated as an average of the nine iMEF banks created in this project*); however, with an additional expansion, a bank at p4 generated up to a four times higher yield (1.6×10^8 cells/bank), with the advantage of a longer working life for each bank, reducing the number of iMEF banks required. A comparison of hESC condition on iMEFs at p3 and p4 following Mitomycin C inactivation was subsequently carried out to determine the optimal expansion of iMEFs for sufficient hESC support. MEFs were sourced at p3 and p4 from the same feeder stock and inactivated as described in Section 2.8.1.1. Inactivated MEFs were seeded at a range of cell densities and hESC fragments (9-10 fragments/well) monitored after 72 hours, for attachment and morphology.

The age of the iMEF layer was crucial for fragment attachment (Table 4.1). At seeding densities 3.6×10^4 - 5.2×10^4 cells/cm^2, 100 % of hESC fragments attached on p3 iMEFs, compared with 60 % and 80 % fragment attachment at p4 respectively. At lower cell densities, 1.6×10^4 - 2.6×10^4 cells/cm^2, attachment of fragments at p3 dropped to 77.8 % in both cases, compared with 20 % and 45 % attachment at p4 respectively. Suggesting the p3 iMEF bank was most suitable for hESC fragment attachment.

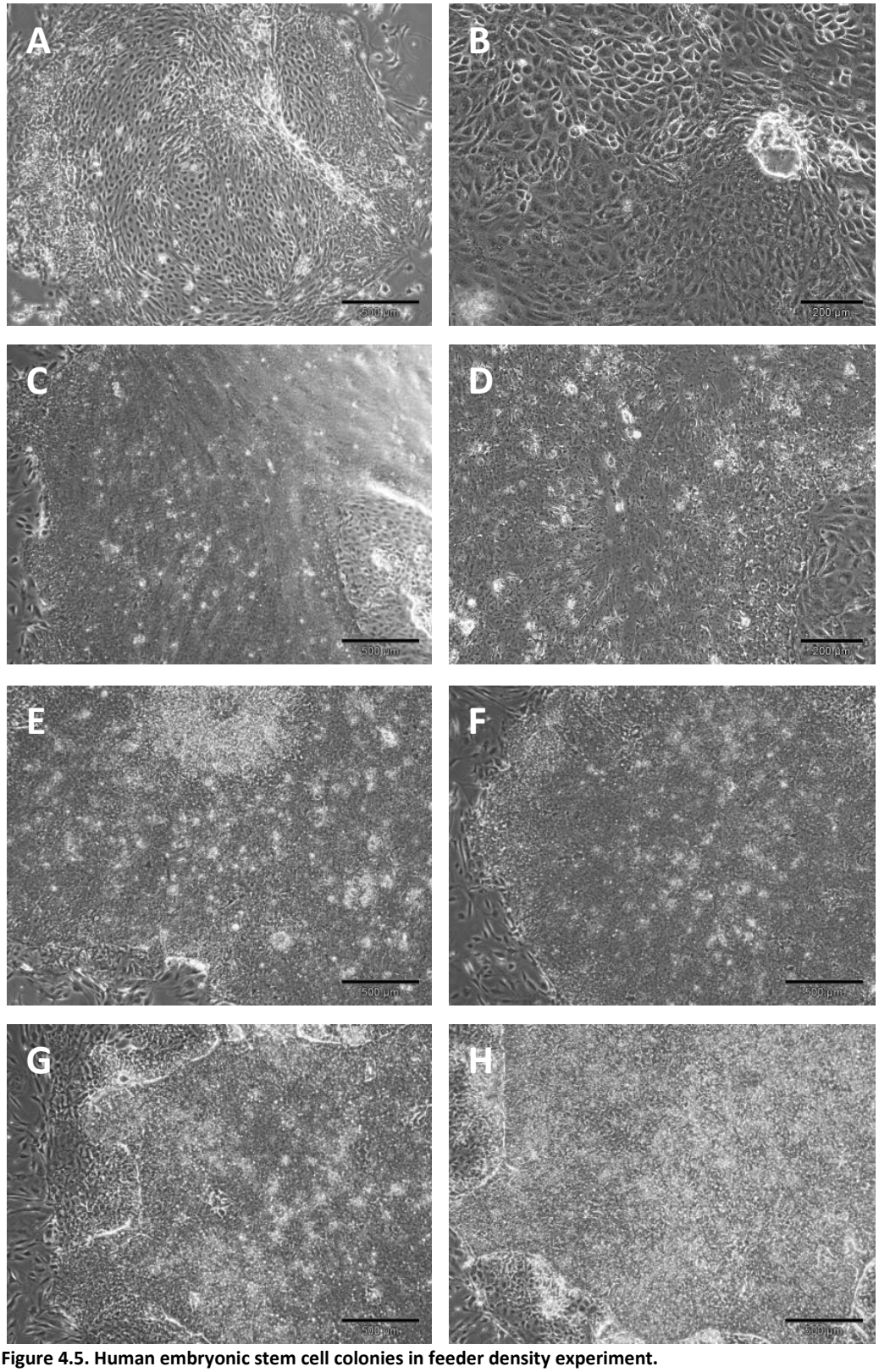

Figure 4.5. Human embryonic stem cell colonies in feeder density experiment.

Human ESCs were plated onto a range of iMEF cell densities and colony morphology observed for optimal retention of pluripotent characteristics. Images were captured eight days following passaging (x4 magnification). Low feeder cell density (1.6 x10^4 cells/cm^2) resulted entire differentiation of the hESC colonies into a flattened collapsed epithelial-like cell fate (A-B). With increased iMEF cell density increasing numbers of cells retained pluripotent characteristics (C-D - 2.6 x 10^4, E - 3.6 x 10^4). An optimal feeder cell density was determined for each bank where hESC colonies were maintained entirely undifferentiated (F - 4.2 x 10^4). Increased iMEF cell density beyond this point resulted in higher levels of spontaneous differentiation (G - 4.7 x 10^4, H - 5.2 x 10^4 cells/cm^2).

In addition to attachment, the support provided by the p3 and p4 iMEF layers was variable. Using p3 feeders, 88.9 % and 85.7 % undifferentiated colonies were supported at cell densities of 3.6×10^4 and 2.6×10^4 cells/cm^2 respectively (Table 4.1). Spontaneous differentiation was seen in all colonies on p3 feeder layers at a cell density 1.8×10^4 cells/cm^2 (100 %). Spontaneous differentiation was also seen in parts of 44.4 % of colonies on p3 fibroblasts at the higher density 5.2×10^4 cells/cm^2. Differentiation was mainly visible in the very centre or around the very edge of these colonies in agreement with data from Figure 4.5.

In contrast, all attached fragments on p4 feeder layers underwent spontaneous differentiation to some degree, varying from partial to complete differentiation. Wholly undifferentiated colonies were on p4 iMEFs at 2.6×10^4 cells/cm^2 but this was only seen in 33.3 % attached fragments (Table 4.1). Cells within undifferentiated colonies were not compact and over longer periods in culture flattened out into an epithelial-like appearance (*data not shown*). Therefore, in addition to the poor fragment attachment on p4 iMEFs, support of undifferentiated growth was also reduced. iMEFs were subsequently frozen at p3 for all hESC culture.

The optimal feeder density for support was determined for all new iMEF banks. It should be noted, that the iMEF passage level experiment was carried out on a different iMEF bank (iMEF bank 4) to the feeder density experiment (Section 4.2.5.1), highlighting the variability between iMEF banks and the need to routinely screen each fresh iMEF bank for the optimum feeder layer cell density to support undifferentiated growth of hESCs.

As an alternative approach MEFs could have been continually cultured and Mitomycin C inactivated prior to use rather than using frozen iMEF banks. (*Personal communications with Mrs. L. Ruban; Regenerative Medicine Group, Advanced Centre for Biochemical Engineering, UCL*). However, retaining MEFs in routine culture and inactivating for passaging hESCs as required (often twice weekly) is a more time consuming process than free-thaw retrieval of iMEF stocks. More significantly, the condition of fresh MEF banks would be difficult to standardise, creating variability in support of hESCs. For this reason, frozen iMEF banks were use throughout this study. Non-supportive (as determined by hESC morphology) iMEF banks were discarded.

4.2.6 Long term storage of iMEFs

Mouse embryonic fibroblast banks were bulked up in culture and mitotically inhibited using Mitomycin C as described in Section 2.8.1.1, and stored at -80 °C ready for use.

Unlike other cell types iMEFs were frozen and maintained at -80 °C for ready access. This is not ideal for long term storage of mammalian cells; however, fresh banks were prepared as required. Viability of feeder banks was monitored for the duration of the iMEF bank as an indicator to their healthy and support of pluripotent hESCs. A significant drop in viability may be indicative of a poor freeze/thaw process during which cells are exposed to DMSO. The function of DMSO within the freeze solution is to protect the cells from damage by ice crystal formation during freezing, by partially solubilising the cell membrane (Lovelock and Bishop, 1959). This solubilisation results in small holes in the membrane which prevent rupturing of the cells (Lovelock and Bishop, 1959). However, this solubilisation is toxic to the cells and upon thawing and must be rapidly washed away to minimise exposure. A delay in washing out, or an error in the rate of freezing will result in extended exposure of the cells to DMSO which may have been detrimental to survival and function.

A threshold in viability for usable iMEFs was set at 85 %. Following thawing and prior to seeding, viability counts were recorded using a bright-line haemocytometer (Figure 4.6). Inactivated MEFs cells retained high viability for their entire period of use. Inactivated MEF banks were used within a three month period from inactivation during which all MEFS retained viability above 88.9 %. Loss of cell viability was noted after storage at -80 °C for longer periods (79.2 % after 167 days).

In addition to seeding density and the age of the fibroblast cells before plating, other factors involved in the supportive ability of feeder layers include the length of time following plating before use as a feeder-layer (Villa-Diaz et al., 2009). Fibroblasts were seeded 24 hours prior to passaging hESCs, which provided the best support for pluripotent culture.

iMEFs	Number of wells	Density/cm^2	Fragments plated	Attached after 72 hours	Fragments attached (%)	Undifferentiated colonies (%)	Part differentiated colonies (%)	All differentiated colonies (%)
p3	1	5.2 x 10^4	9	9	100	55.6	44.4	0
p3	2	3.6 x 10^4	18	18	100	88.9	-	11.1
p3	1	2.6 x 10^4	9	7	77.8	85.7	-	14.3
p3	1	1.8 x 10^4	9	7	77.8	-	-	100
p4	2	5.2 x 10^4	20	16	80	0	12.5	87.5
p4	2	3.6 x 10^4	20	12	60	0	16.7	83.3
p4	2	2.6 x 10^4	20	9	45	33.3	-	66.7
p4	1	1.8 x 10^4	10	2	20	0	-	100

Table 4.1. Attachment and culture of hESCs on iMEFs.

At p3, iMEFs best supported undifferentiated hESC growth at 3.6 x10^4 cells/cm^2 with 88.9 % colonies wholly undifferentiated. Inactivated MEFs at p4 were unable to support high levels of undifferentiated hESC growth. At best, just 33.3 % colonies remained undifferentiated after 72 hours at 2.6 x 10^4 cells/cm^2, where 85.7 % colonies remained undifferentiated at the p3 feeder layer of the same cell density. Extreme levels of spontaneous differentiation were seen at all tested p4 feeder cell densities 5.2 - 1.8 x 10^4 cells/cm^2.

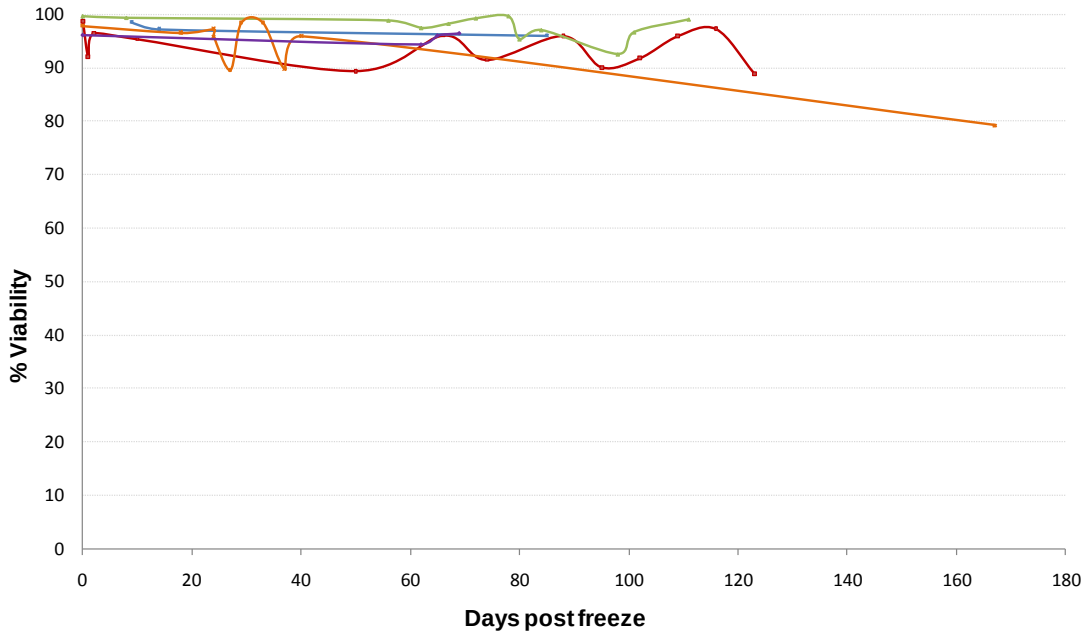

Figure 4.6. Viability of iMEF banks following storage at -80 °C.

Inactivated MEF bank A (red), B (blue), D (green), F (orange), H (purple). Some iMEF banks (C, E and G) were used within just a few weeks of production and are not presented here. Inactivated MEF banks were stored at -80 °C following Mitomycin C inactivation and thawed for use as required for up to 3 months, after which fresh iMEF banks were produced. Viability of all iMEFs remained high >88.9 % as determined by Trypan blue cell counting after three months storage. After 167 days at -80 °C viability of the iMEF bank F remained high at 79.2 %; however viability dropped below the 85 % threshold for use and were subsequently not used for hESC culture beyond this point.

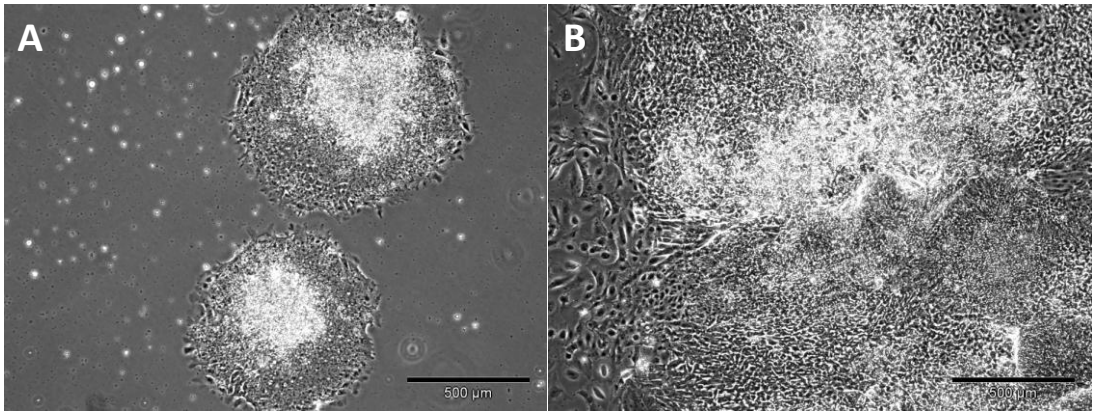

Figure 4.7. Human embryonic stem cell colony in conditioned media.

Shef3 colony on gelatin coated surface in the absence of iMEFS but in iMEF conditioned media 24 hours after plating (A) demonstrated outgrowth of cells with pluripotent characteristics. After five days hESCs cultured in iMEF conditioned media were entirely differentiated (B) demonstrating a need for the presence of iMEFs to support pluripotent growth.

4.2.6.1 Conditioned media

The requirement for iMEFs in co-culture with hESCs was investigated using iMEF conditioned media (CM). iMEFs were plated as for passaging, followed by 36 hours incubation with hESC media, creating iMEF CM. Culture surfaces were coated with gelatin before passaging hESC fragments in CM. All fragments attached within 24 hours of plating. Human ESCs were visible spreading around the edges of all colonies (Figure 4.7A); however, fragments failed to collapse in the centre, and showed initial signs of differentiation. On subsequent days, colonies lost all hESC morphology (according to guidelines set out in Section 4.2) and underwent complete differentiation within five days of plating (Figure 4.7B). It was therefore concluded that CM alone was insufficient to support pluripotent hESCs on a gelatin surface coating. An iMEF feeder layer was subsequently used for all hESC culture in this project.

4.2.7 Quality control

Quality control (QC) is an essential part of any bioprocess. It is especially critical in processes with pharmacological or therapeutic applications, ensuring full traceability from reagents to equipment and environmental parameters. In the event of a problem, traceability enables the user to identify potential areas of concern, whilst providing a record of progress for replication of any positive outcome. Work within this project was carried out according to good manufacturing practice (GMP) and good laboratory practice (GLP) guidelines. The main QC measures applied to this project included: laboratory records documenting suppliers and catalogue numbers for all reagents, servicing and calibration certificates for facilities and equipment, microbiological screening for contaminations, DNA fingerprinting to confirm identity of the cells in use, and karyotypic analysis to monitor stability of hESCs in culture.

4.2.7.1 Microbiological screening

Mycoplasma testing: Spent culture media was routinely collected from each cell line and screened for mycoplasma contamination using PCR amplification. All samples remained free from infection as compared to an in-house positive control (data *available upon request*).

Cell culture supernatant: In addition to routine mycoplasma screening, spent cell culture media was tested for microbial contamination using three common culture solutions: malt extract broth to test for mould and yeast, tryptone soya broth which indicates the presence of any microbial contamination, and thioglycollate medium to test for the presence of anaerobic, aerobic and microaerophilic contamination. All sterility broths were prepared in-house (NIBSC, Scientific Support Services) and incubated at 37 °C in a separate laboratory to cell culture for up to two weeks before discarding. Culture supernatants remained free from detectible microbial contamination for the duration of this project.

Viral testing: Human ESCs were screened for viral contamination as part of the UKSCB cell line release criteria. Cell lines were screened by The Doctors Laboratory (TDL; London) for viral contamination by Cytomegalovirus, Human T-lymphotropic virus Type I, Human immunodeficiency virus 1, Hepatitis C, Hepatitis B, Epstein Barr virus and Mycoplama genus/Ureaplasma. All hESC lines were negative for viral screens. Inactivated MEFs used for hESC feeder layers were sourced from virus-free certified mouse stocks (*personal communication, Ms. L. Young, UKSCB*,).

4.2.7.2 DNA fingerprinting

DNA fingerprinting was carried out on each cell line to ensure no cross contamination of lines occurred as a result of culturing multiple cell lines in parallel. Cell pellets were washed in PBS and shipped to TDL Genetics on dry ice for DNA profile analysis. Fingerprint traces were obtained and cross checked with records from the UKSCB. No cross contamination of cell lines occurred throughout this project. DNA profiles for each of the hESC lines and the two hEC lines used in this project are presented in Table 4.2.

Shef3	Genotype	
Marker	Allele 1	Allele 2
D8S1179	13	14
D21S11	28	30.2
D7S820	8	12
CSF1PO	12	13
D3S1358	16	18
TH01	7	9.3
D13S317	8	8
D16S539	12	12
D2S1338	24	24
D19S433	11	15
VWA	17	18
TPOX	8	8
D18S51	15.3	17
D5S818	11	13
FGA	21.2	23

HUES7	Genotype	
Marker	Allele 1	Allele 2
D8S1179	10	11
D21S11	27	32.2
D7S820	8	11
CSF1PO	12	12
D3S1358	15	18
TH01	6	9.3
D13S317	11	12
D16S539	11	12
D2S1338	16	17
D19S433	13	14
VWA	16	18
TPOX	8	8
D18S51	14	15
D5S818	11	13
FGA	25	25

RH5	Genotype	
Marker	**Allele 1**	**Allele 2**
D8S1179	11	15
D21S11	28	29
D7S820	10	11
CSF1PO	10	12
D3S1358	14	16
TH01	6	9
D13S317	11	12
D16S539	9	12
D2S1338	19	21
D19S433	14	14.2
VWA	16	18
TPOX	8	11
D18S51	15	18
D5S818	10	12
FGA	20	24

NTERA2	Genotype		
Marker	Allele 1	Allele 2	Allele 3
D8S1179	13	15	
D21S11	30	31	
D7S820	10	12	
CSF1PO	10	12	
D3S1358	16	16	
TH01	9.3	9.3	
D13S317	13	13	
D16S539	11	12	13
D2S1338	22	25	
D19S433	14	15.2	
VWA	-	-	
TPOX	8	8	
D18S51	14	14	
D5S818	9	12	
FGA	23	23	

2102Ep	Genotype		
Marker	**Allele 1**	**Allele 2**	**Allele 3**
D8S1179	14	15	
D21S11	28	29	
D7S820	7	13	
CSF1PO	11	12	
D3S1358	16	16	
TH01	9	9.3	
D13S317	8	8	
D16S539	11	12	
D2S1338	17	20	
D19S433	13	14	
VWA	16	17	18
TPOX	8	11	
D18S51	15	15	
D5S818	11	11	
FGA	22	22	

Table 4.2. DNA profiles for pluripotent cell lines.

DNA profiles for all pluripotent cell lines were carried out by TDL genetics: Shef3(orange), HUES7 (red) and RH5 (green) NTERA2 (purple), 2102Ep (blue), In agreement with the DNA profile for NTERA2 supplied by ATCC, a third allele was repeatedly detected at the D16S539 locus. An additional allele for locus VWA was consistently detected in the 2102Ep. Profiling for HUES7 was carried out at p22, p52 and p62. The RH5 cut line was originally DNA profiled at p33. Subsequent profiling was consistent at p50 and p96 (TrypLE passaged samples), and p80 (mechanically passaged samples). Shef3 was profiled at p48 and p61. No alterations in profile were identified throughout this project confirming no cross-contamination of cell lines had taken place in culture.

4.2.7.3 Karyology

The direct causes of karyotypic instability of hESCs are yet to be clarified; however, the passaging techniques used for hESCs expansion have been suggested to induce karyotypic alterations which enhance their proliferation and survival in culture. To detect for alterations in the karyotype caused by mechanical or enzymatic passaging, G-banding analysis was carried out on the hESC lines at the start and end of this project. Results were compared to the original starting populations from UKSCB cell line master files (*authorised by Mrs. A. Iriajen, QC coordinator, UKSCB*).

Metaphase spreads were prepared according to the UKSCB 'Karyological analysis of cell lines' SOP (Section 2.14). However, due to limited success in obtaining sufficient numbers of scorable metaphase spreads, a modified version of the protocol was developed (Section 2.14.1). The number of metaphase spreads were increased by incubating cells with KaryoMAX® Colcemid® (Gibco, 15212-046) 0.4 $\mu g.ml^{-1}$ in hESC media for just 30 minutes prior to harvesting. Colcemid® is an anti-mitotic reagent which depolymerises microtubules, limiting their formation, thus arresting cells in metaphase (Invitrogen, UK). Longer Colcemid® incubations were found to condense the chromosomes such that G-banding could not be analysed.

Using the modified protocol, sufficient metaphase spreads were usually visible for scoring by TDL (Figure 4.10); however, heterogeneity was visible across the spreads. This may have been partially due to processing artefacts in preparation, but it is also a likely indicator of heterogeneity of the karyology of the hESC population. Chromosome alignments and the number of metaphases scored for each cell line are presented in Figure 4.12 - Figure 4.11.

Despite publications of a normal 46 XY karyotype (Cowan et al., 2004), analysis by the UKSCB at the Master cell bank level reported this line to be triploidy for chromosomes 12 and 17 (48, XY,+12,+17; Figure 4.12, (UKSCB, cell line master file). After a further 46 passages throughout this project the HUES7 line had gained two additional chromosomes, resulting in the modal karyotype in the population 50 XXY, +12, +14, +17 (Figure 4.13).

Shef3 retained its normal 46 XY karyotype (Figure 4.15) throughout this project when compared to the original MCB (Figure 4.14). The RH5 cell line was originally published as an aneuploidy line with 101 chromosomes (Fletcher et al., 2006). At passage 99, 63 passages after sourcing from the UKSCB, the modal karyotype of RH5 cells was 73 XXX, +1, -4, +12, +13, -17, +(17q) +18, with an additional marker chromosome unidentifiable by TDL

(Figure 4.11). A metaphase spread was not available from the UKSCB Master Cell Bank (MCB) records.

Despite further optimisation of karyological preparations, the numbers of scorable metaphase spreads within the cell populations remained low. Personal communications with Ms. S. Osborn (Regional Cytogenetics Unit, St Marys Hospital Manchester) suggested the need to synchronise the cell population prior to karyotypic analysis in order to increase the number of cells in metaphase. This could have been achieved by incubation of cell cultures with thymidine for the duration of one cell cycle which may vary between 24-72 hours, depending on the cell lines (Cowan et al., 2004). Following thymidine incubation, cell cultures should then be left to progress through the remainder of the cell cycle into metaphase, for harvesting as previously described (Section 2.14.1). Optimisation of karyotypic analysis in this way would require an in depth understanding of the duration of each cell cycle phase in the different hESC lines; however, this would save significant time and reagents from unscorable metaphase cell preparations, and would therefore be a worthwhile investigation to undertake. However, with the common occurrence of karyotypic abnormalities which demonstrably alter cell cycle times, it may be necessary to fully understand the cell cycle duration for each cell line and treat accordingly to produce metaphase spreads for analysis, preventing a 'one for all' protocol for karyotypic analysis of hESCs.

Poor efficiency in metaphase spread preparation, meant that is was not possible to generate a record of the RH5 cut cell line for comparison of karyotypic stability with the RH5 TrypLE sample. In an attempt to determine differences between these samples, array Comparative Genomic Hybridisation (aCGH) analysis was carried out on the RH5 cut and RH5 TrypLE cell line, each compared to the UKSCB distribution cell bank (DCB).

4.2.7.4 Array Comparative Genomic Hybridisation

Array CGH was carried out to compare the karyotype of RH5 TrypLE and RH5 cut cell with the RH5 DCB from the UKSCB, monitoring for chromosomal aberrations which may have occurred between the two populations as a consequence of enzymatic versus mechanical passaging. Array CGH (Perkin Elmer, ProScanArray microarray scanner) was used to analyse alternations in copy number of 5000 human clones.

Results from aCGH analysis were preliminary and would need further in-depth analysis including sequencing of the chromosomal regions to confirm any findings. Each sample has been represented by red and blue spectral lines. In copy number match samples, the red lines were visible on the left of the central black line and the blue on the right. The two vertical blue lines on each side of the central black line define the 'limits' as set by the user, in this case limits were set as is used for standard genetic diagnostic analysis.

No complete chromosomal duplications or losses were identified amongst the RH5 cut and RH5 TrypLE populations which would have been identified by the spectral lines moved away from the centre for the entire length of the chromosome; however, losses of genomic content were identified by the movement of spectral lines at individual loci crossing over the central line to the opposite side (ie red to the right and blue to the left). Similarly duplications of genomic content were identified by mirrored extensions of the spectral lines beyond the detection limits.

When compared to the RH5 cut cell line, RH5 TrypLE demonstrated a gain of chromosome region 16p13.3 (Figure 4.8). Investigation into the behaviour of genes in this chromosomal region revealed that gains in this region, are used in diagnostics for a range of carcinomas including lung, liver and salivary gland (Katoh et al., 2005; Kasamatsu et al., 2005; Choi et al., 2006).

When compared to RH5 TrypLE, RH5 cut highlighted a gain of chromosomal region 17q25.2 (Figure 4.9A). Gains of chromosome 17 have been described in detail by many laboratories following *in vitro* culture of different hESC lines and have been associated with tumour formation *in vivo* (Skotheim et al., 2002; Westermann and Schwab, 2002; Draper et al., 2004a; Mitalipova et al., 2005; Catalina et al., 2008). However, alterations specifically in the 17q25.2 region have been attributed to breast cancers (Petty et al., 1996). Close inspection of this cell line suggest a possible gain of chromosomal region 2p25.2 (Figure 4.9B) which has been associated with autism, however this mutation is close to the limits set for analysis which are subjective, so would need to be repeated for confirmation.

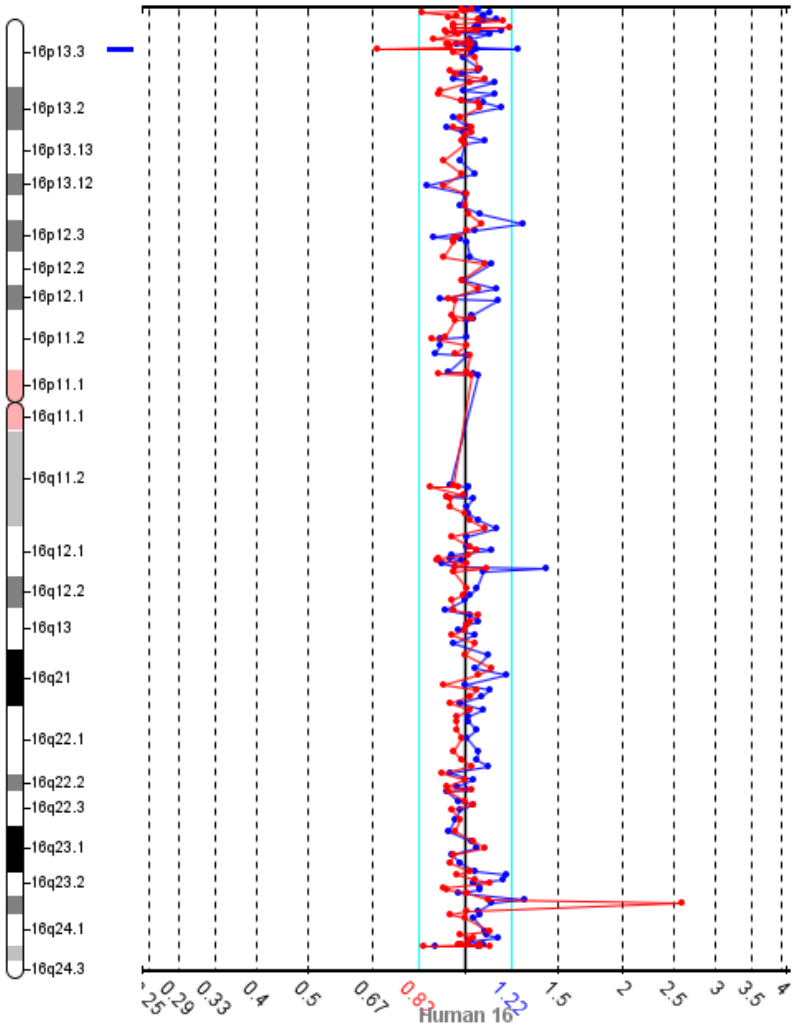

Figure 4.8. RH5 TrypLE aCGH idiogram.

The gain of chromosomal region 16p13.3 was identified by the movement of both the blue and the red lines away from the mid line, beyond the limits of detection on the aCGH idiogram output. Cross over of the spectral lines was also observed at various points on each chromosomal iodigram output but these cross-overs were not mirrored on each side and were therefore deemed to be due to sampling error or error in analysis.

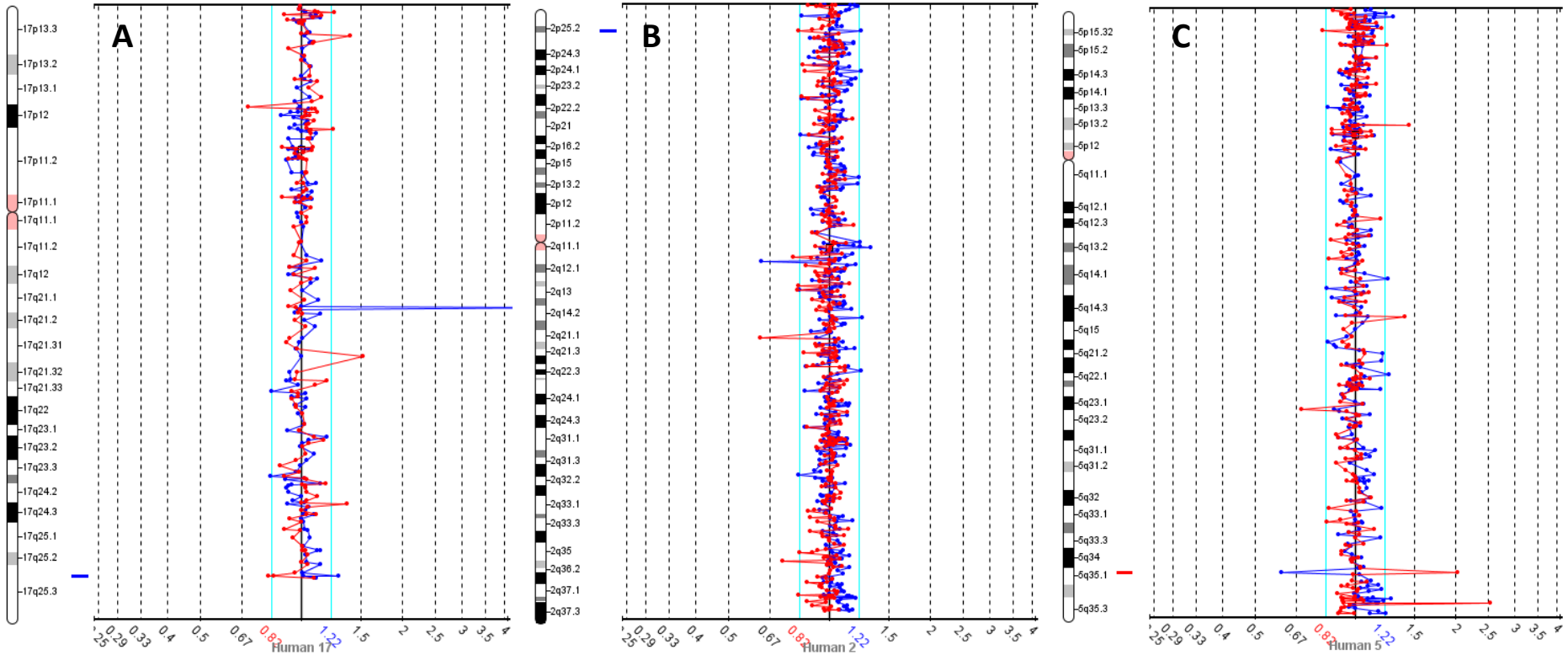

Figure 4.9. RH5 cut aCGH analysis idiogram.

The gain of chromosomal regions 17q25.2 (A) and 2p25.2 (B) was identified by the mirrored movement of both the blue and the red lines away from the mid line, beyond the limits of detection at these loci on the aCGH idiogram output. The loss of chromosomal region 5q35.1 (C) was identified by the mirrored cross-over of both the blue and the red lines onto the opposite side of the midline, beyond the limits of detection.

Perhaps most interestingly, a loss of the chromosomal region 5q35.1 was detected in the RH5 cut (Figure 4.9C). Using aCGH is was not possible to identify whether either of the RH5 cell lines expressed the normal two copies of this gene or whether both cell lines were abnormal. Instead it could only be concluded that the UKSCB RH5 DCB contained an additional copy of this gene, when compared with RH5 cut. This chromosomal region encodes the FBXW11 gene (NCBI, Entrez Gene) which is expressed at high levels during forebrain development in the foetus (Koolen et al., 2006). In addition, gains of this region have been associated with Holoprosencephaly (HPE), a developmental defect affecting the forebrain development in humans, also suggesting that this chromosomal region may be directly involved in brain development (Koolen et al., 2006). A mutation in this region might suggest a difference in directability of neuronal differentiation between the RH5 cut and RH5 TrypLE cell line but would also need to be repeated for confirmation.

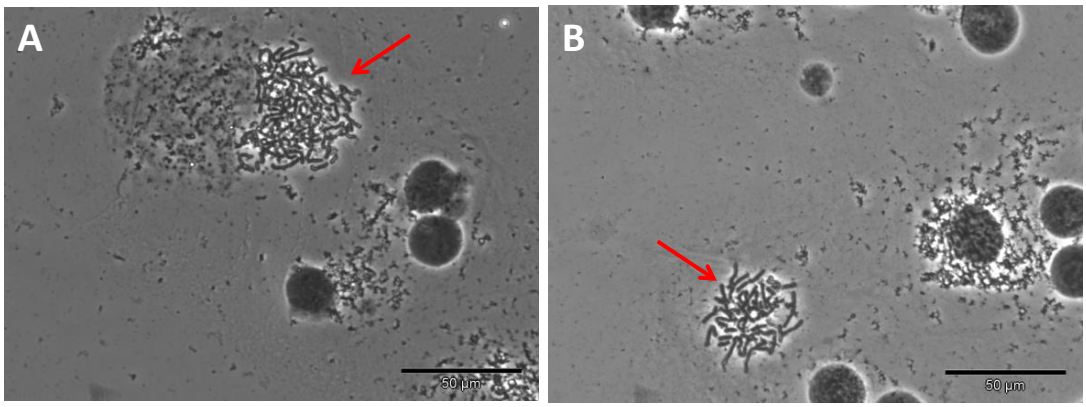

Figure 4.10. *In Situ* metaphase spreads from hESCs.

Considerably more chromosomes are visible in from the RH5 TrypLE sample, p99 (A) when compared to HUES7, p65 (B).

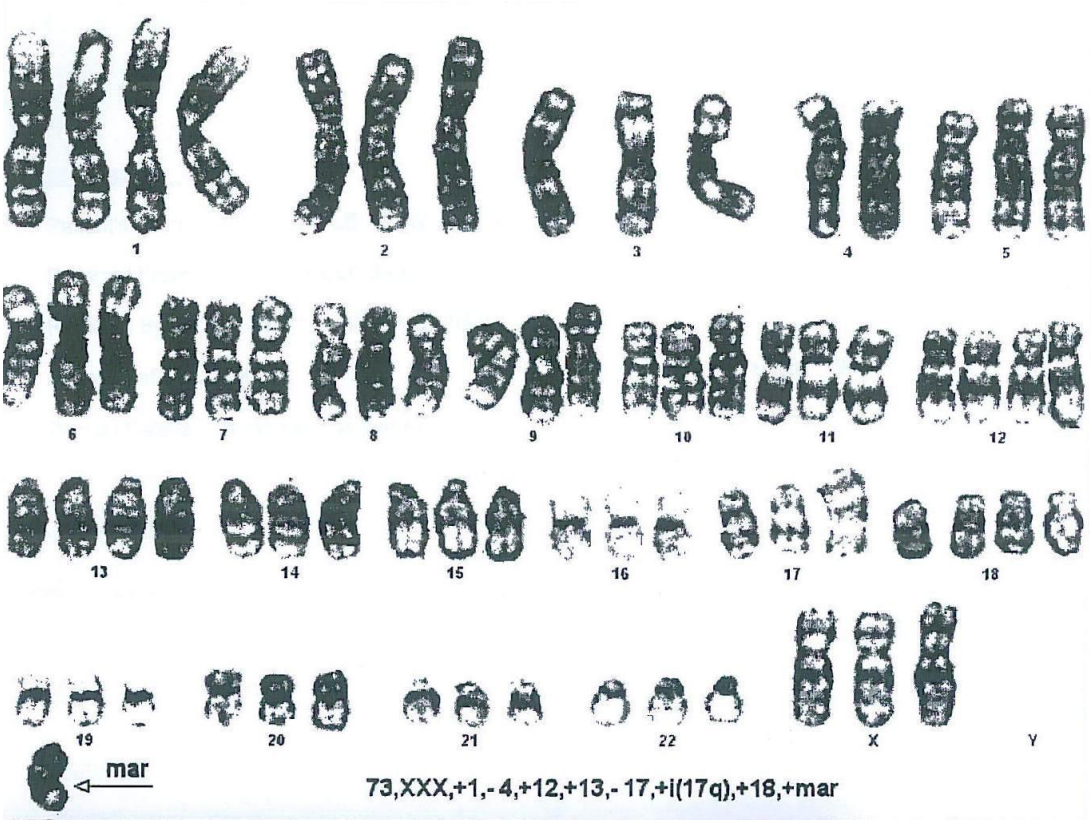

Figure 4.11. RH5 TrypLE p99.

Hypertriploid karyotype complement ranging from 72-78 chromosomes. Extra copies (4 or more) of chromosomes 1, 12 and 13 were seen in all cells examined as was a structurally abnormal isochromosome 17q and a structurally abnormal unidentified chromosome (above spread: 73XXX, +1, -4, +12, +13, -17, +(17q), +18, +mar). *Images supplied by TDL Genetics*.

Figure 4.12. HUES7 UKSCB Master Cell Bank.

HUES7 p19 Abnormal male karyotype with 48 chromosomes with trisomy 12 and 17 present (above spread: 48XY +12, +17). *Images supplied by TDL Genetics*.

Figure 4.13, HUES7 p65.

Abnormal male karyotype, with a complement of 50 chromosomes including two copies of the X chromosome and three copies of chromosomes 12, 14 and 17 seen in all analysable cells (above spread: 50, XXY +12, +14, +17). *Images supplied by TDL Genetics*.

Figure 4.14. Shef3 UKSCB Master Cell Bank.

The UKSCB master cell bank for Shef3 presented a diploid male chromosome complement (46 XY). *Images supplied by TDL Genetics*.

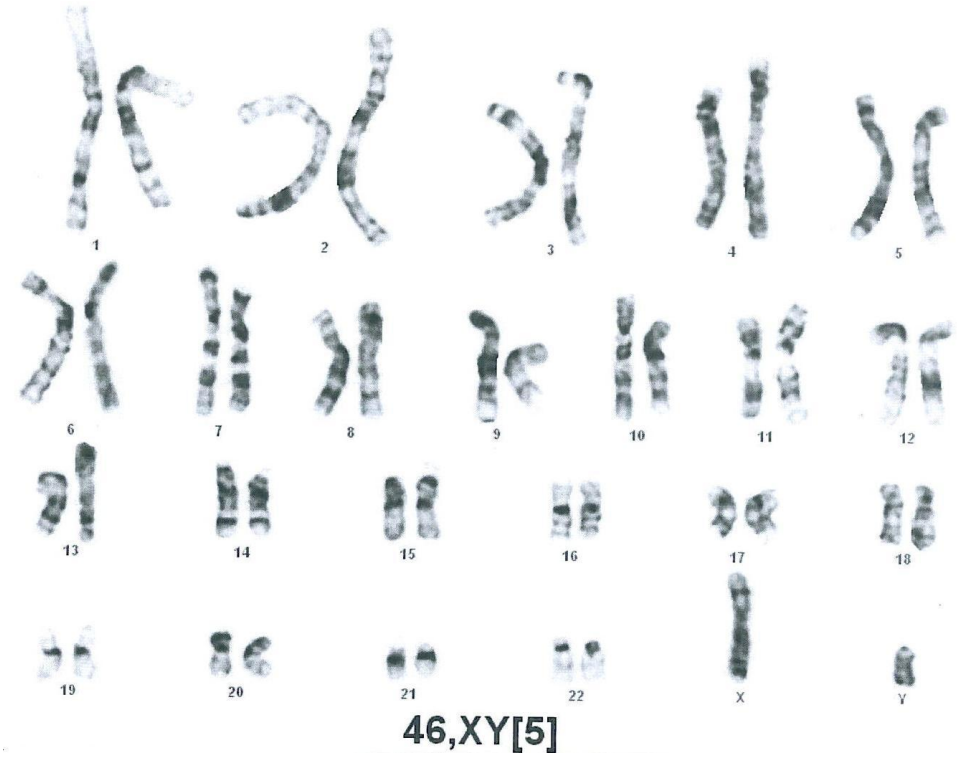

Figure 4.15. Shef3 p60 metaphase spread

Shef3 retained a normal diploid male chromosome complement (46 XY) throughout this project. Spread taken at p60, following 27 passages in culture. *Images supplied by TDL Genetics*.

4.3 Discussion

During establishment and expansion of the four hESC lines in culture (Shef3, HUES7, RH5 TrypLE and RH5 cut), it became apparent that there was no difference in appearance of hESCs in these lines. Mechanically passaged lines retained uniform colony shape, where enzymatically passaged cells grew as a monolayer but individual cells from all four lines retained the morphological features of pluripotent hESCs (Section 4.2) and expanded well under standard culture conditions. All hESC lines expressed typical markers of pluripotency (OCT4, SOX2, Tra-1-60 and Tra-1-81).

All hESCs were co-cultured with iMEFs which provided support for their pluripotent expansion. MEFs are primary cells, sourced from 13.5 day old embryos and as such have a finite expansion time in culture (Stubban and Wesselschmidt, 2007). Although there are commercial alternatives to the use of such feeder-layers (Xu et al., 2001; Rosler et al., 2004; Amit, 2006; Ludwig et al., 2006b), these systems are yet to be fully characterised for their ability to retain stable hESC culture over prolonged periods, whilst retaining the ability of hESCs to be directed into differentiation. Additionally, Matrigel^{TM} and mTeSR1 media systems are costly alternatives to iMEFs (Ludwig et al., 2006a). For this reason, hESCs were cultured on an iMEFs throughout this project. Inactivated MEF banks were prepared as required and stored at -80 °C prior to use. Stocks of iMEFs were stored for up to three months during which they retained high viability (> 85 %) and supportive capacity for hESC culture.

The density of the iMEF layer was crucial for sustained hESC pluripotency, and due to their primary origin was found to be variable between iMEF banks. Spontaneous differentiation was consistently observed in hESCs on iMEFs at the extremes of high (> 5.2 x $10^4/cm^2$) and low (< 1.8 x $10^4/cm^2$) seeding cell density (Section 4.2.4). The reasons for this have not been fully characterised; however, iMEFs are known to secrete soluble factors into the culture media including bFGF, TGF-β2, Wnts, BMP/TGF-β1, activin/Inhibin, and IGF-1 which work in combination to support pluripotency in hESCs (Alitalo et al., 1982; Moscatelli et al., 1986; Amit et al., 2004; Vallier et al., 2005; Wang et al., 2005a; Chen et al., 2006; Prowse et al., 2007; Saha et al., 2008; Villa-Diaz et al., 2009). However, throughout embryonic development chemical gradients of these growth factors are responsible for tissue specification. The concentration of secreted growth factors is therefore essential for determining either pluripotency of differentiation.

Insufficient support due to low feeder cell density or poor activity of individual fibroblasts (as seen in p4 versus p3 iMEFs) resulted in the differentiation of hESCs into a flattened epithelial-like morphology, which was likely to be a consequence of an imbalance in the secretion of soluble growth factors. This morphology has been previously identified in hESCs and has in part been attributed to insufficient bFGF signalling (Amit et al., 2000; Diecke et al., 2008) which was also supplemented into hESC media to improve pluripotent survival (Duran et al., 2001). When iMEFs were too dense, differentiation was also induced amongst hESCs. A high iMEF density would have increased the growth factor concentrations, again creating an imbalance in the signalling required for pluripotency. Alone, many of these growth factors are actively involved in tissue specification (Johansson and Wiles, 1995), thus, alterations to the concentrations of these factors are likely to have initiated spontaneous differentiation. In addition, high feeder cell density restricted the outgrowth of hESCs, resulted in piling up of cell layers which subsequently spontaneous differentiated. For this reason, the optimal iMEF density for pluripotent hESC support was determined for each fresh iMEF bank.

Inactivated iMEF conditioned media alone was insufficient for supporting pluripotent hESC expansion on gelatin coated surfaces as indicated by the rapid differentiation of hESC colonies (Section 4.2.6.1), despite supplementation with bFGF. This suggested that either the secreted factors were subject to rapid degradation, or that they were not the only form of support provided by iMEFs in the co-culture system. In feeder-free systems an extracellular matrix surface coating is used onto which hESCs can attach and proliferate. Interaction with ECM has been shown to be important in hESCs culture (Kleinman and Martin, 2005). Indeed, iMEFs secrete ECM (Villa-Diaz et al., 2009), which would explain why their presence was necessary for hESC pluripotency. Production of growth factors and ECM by iMEFs decreases with time, reducing their supportive capacity (Villa-Diaz et al., 2009). This would explain the propensity for spontaneous differentiation after prolonged culture.

Although no difference in hESC morphology was identified between the hESC lines, differences in their behaviour between the enzymatically and mechanically passaged lines were more apparent. Mechanically passaged hESCs were slower growing than enzymatically passaged lines which in combination with the more time consuming process of manual passaging, made production of large cell volumes more difficult, and a unfavourable approach for bioprocessing. However, both enzymatically passaged cell lines were identified to be karyotypically abnormal (Section 4.2.7.3). The RH5 TrypLE cell line

was abnormal from derivation, and the HUES7 cell line was aneuploidy for chromosomes 12 and 17 at the UKSCB MCB level. Extended enzymatic culture of HUES7 resulted in a further gain of chromosome X and 14, reaching a model karypotype of 50 XXY, +12, +14, +17. In accordance with observations from this study, karyotypic abnormalities have been correlated to a shortening in hESC doubling time (Cowan et al., 2004; Baharvand et al., 2006), suggesting a survival advantage following a gain of these chromosomes. This would also explain how the HUES7 line became abnormal in the short preparation time for a MCB. In contrast to these findings, publications by the depositors following derivation and alternative laboratories report a normal HUES7 karyotype (Cowan et al., 2004; Thomas et al., 2008); however, personal communication between the UKSCB and Professor D. Melton's laboratory (Harvard, USA) confirmed that similar abnormalities had been detected in the HUES3 and HUES4 cell lines (Cowan et al., 2004).

The common occurrence of genetic drift within hESCs under long term culture was first reported in 2004 (Draper et al., 2004a). The frequency at which hESC lines gain abnormalities in culture is of concern for their use in therapeutic application, seeding worries of tumour formation *in vivo*. In light of the fact that embryological development does not usually result in such abnormalities, their prevalence is likely to be a result of prolong exposure to suboptimal culture conditions. Most commonly accumulated abnormalities include a gain of chromosomes 12 and 17, but additional copies of chromosomes 14 and X have also been noted (Draper et al., 2004a; Mitalipova et al., 2005; Catalina et al., 2008), as was also seen in the HUES7 line throughout this project. It is likely, that additional abnormalities within the populations were also present but that alterations which did not confer a survival advantage died out before detection.

Karyotypic analysis of RH5 TrypLE revealed the presence of a marker chromosome which was unidentifiable by the cytogenetisist at TDL. The gain of this marker chromosome would be of serious concern for therapy but is a great indicator of the possible mutations which can arise from long term hESC culture. Whatever the cause, safety is of great concern for therapeutic application, and the possibility of tumourogensis following hESC cell therapy must be ruled out. For this reason, it is vitally important to understand the possible causes of genetic instabilities and to monitor cells both with and without theses instabilities for their behaviour in subsequent culture and differentiation.

Laboratories worldwide culture different hESC lines with various culture techniques, and report conflicting evidence for instabilities within different lines. Possible causes of

karyotypic instabilities include cell culture density, feeder-free culture or enzymatic passaging (Draper et al., 2004a; Buzzard et al., 2004b; Mitalipova et al., 2005; Catalina et al., 2008). It could also be argued that in addition to culture conditions, some hESC lines may simply be more susceptible to abnormalities than others. This would seem a reasonable, considering hESC lines are derived from embryos (surplus to requirement) following *In vitro* fertilisation (IVF) procedures. Couples undertake IVF for a variety of reasons, but in many cases this is due to genetic disease susceptibility. It is therefore not surprising that only 42 % of surplus IVF embryos were chromosomally normal at the blastocyst stage (Hardarson et al., 2003), and possible that hESC lines derived from 'normal' embryos would be less prone to instability than those from a family history pre-disposed to genetic disease.

Human ESC lines under enzymatic culture were more susceptible to karyotypic aberrations than mechanically passaged lines. The inability to adapt karyotypically normal hESC lines to enzymatic passaging, has also been observed in alternative laboratories, with persistence in enzymatic culture demonstrably resulting in the development of karyotypic abnormalities (Personal communications with Ms. A. Hemsley; Regenerative Medicine and Bioprocessing, UCL, and Dr. C. Machado; Cell Biology and Imaging, NIBSC). Thus supporting a link between enzymatic passaging and karyotypic instability.

Sadly the inability to adapt Shef3 to enzymatic culture did not enable comparison of pluripotent expansion and differentiation in this karyotypically normal hESC line under both mechanical and enzymatic conditions. However, the same originating starting pool of the RH5 cut and RH5 TrypLE cell lines did enabled a comparison of the effect of passaging on karyotypic stability and subsequent expansion and differentiation behaviour, since all other parameters of culture remained constant.

It was not possible to generate metaphase spreads from the RH5 cut line (thought to have been a result of lower cell numbers due to the nature of mechanical passage). Instead, comparison of these two lines was carried out in more detail using aCGH technology. Array CGH identifies discrepancies in the gDNA content between two samples to an accuracy of 100 kb, confirming the presence of duplications or deletions in whole genes or regions of a chromosome. Using aCGH analysis, laboratories claiming to have normal hESC karyotype under enzymatic passaging have later demonstrated small alterations in genomic content (Thomson et al., 2008), confirming the occurrence of chromosomal aberrations which are not detectable under standard G-banding analysis of metaphase spreads.

At the end of this project, both the RH5 cut and TrypLE cell lines were compared to the original gDNA content of the UKSCB RH5 DCB. Array CGH highlighted a number of differences between the two RH5 cell lines, included a gain of the chromosomal region 16p13.3 in RH5 TrypLE and 17q25.2 in RH5 cut, when compared to the UKSCB DCB. Both of these alterations have been associated with *in vivo* development of carcinomas, suggesting a link between the *in vitro* culture of these cell lines and a risk of tumour formation (Petty et al., 1996; Katoh et al., 2005; Kasamatsu et al., 2005; Choi et al., 2006). G-banding analysis of the RH5 TrypLE metaphase spread reported triplicate copies of both chromosomes 16 and 17; however, this does not indicate the duplications or deletions of individual genes which can go unnoticed under this form analysis. The inability to quantify copy number using aCGH technology meant that it was not possible to identify whether the UKSCB RH5 DCB contained normal copy number of these genes and *in vitro* culture induced duplication, or whether there were already numerous copies of these genes in the originating population, which already were subject to duplication.

Interestingly, the RH5 cut cell line also suffered a loss at chromosomal region 5q35.1, which encodes a number of genes including FBXW11 (NCBI, Entrez Gene). FBXW11 is expressed at high levels during foetal forebrain development and gains of this region have been associated with holoprosencephaly (HPE) (Koolen et al., 2006), a condition caused by a defect in foetal forebrain development. Clinical symptoms of HPE include a depletion of mature cortical interneurons neurons in the forebrain region of patients (Schell-Apacik et al., 2003; Fertuzinhos et al., 2009). Although these are only preliminary findings, mutations in this region might suggest a difference in directability of neuronal differentiation between the RH5 cut and RH5 TrypLE cell line, or a difference in their terminal neural cell fate.

The retention of a normal karyotype of Shef3 under mechanical passaging, and the additional alterations in enzymatically passaged cell lines from this study, indicate an affect of culture techniques on the karyotypic stability of hESCs which are not obvious upon morphological examination. However, when considering the incorporation of hESCs in pharmacological or therapeutic applications, the effects of karyotypic abnormalities are more important than their cause. A mutation inferring uncontrollable proliferation, would be unsuitable for incorporation into transplantation due to the high risk of tumour formation. Equally, a mutation which affects signalling involved in neuronal maturation are unlikely to be of use in cell lines required for the production of large numbers of post-mitotic functional neurons. To improve understand the effect of differences in

behaviour of enzymatic and mechanically passaged hESC lines, further investigation was carried out onto their subsequent directability into neuronal differentiation (Chapter 5).

5 Neuronal differentiation in pluripotent hESC lines

5.1 Introduction

Data from the previous chapter has compared the effect of *in vitro* culture and on the pluripotency and karyotypic stability of different hESC cell lines. Results from karyotypic analysis suggested a susceptibility of hESC lines under enzymatic passaging to chromosomal abnormalities. On occasion, abnormalities included just small alterations in genomic content; however, upon closer investigation copy numbers of genes associated with tumour formation (uncontrolled proliferation) and neuronal maturation were affected by the different culture techniques.

Despite this, any differences induced by passaging technique did not appear to affect the pluripotency of the cell lines as determined by expression of pluripotency markers OCT4, SOX2, Tra-1-60 and SSEA4. To determine whether the mode of passaging had implications on the directability of neuronal differentiation following pluripotent expansion, a study into the comparative efficiency of neuronal differentiation across the four hESC lines (Shef3, HUES7, RH5 cut and RH5 TrypLE) was carried out.

5.2 Results: Neuronal differentiation in hESCs

Neurons were first generated from hESCs in 2001 (Carpenter et al., 2001; Schuldiner et al., 2001; Zhang et al., 2001); however, on commencing this project there were only a limited number of protocols available for their neuronal differentiation and high neuronal yield and reproducibility remained a challenge. Initial phases of this study, required the development of a reliable and reproducible method of neuronal differentiation, to facilitate a comparison of different hESC lines.

5.2.1 Embryoid body directed mid/hind neuronal differentiation

Initial experiments into neuronal differentiation followed an established method using FGF8 and SHH to direct hESCs into a midbrain dopaminergic neuronal cell fate, based on the first neuronal differentiation protocols in hESCs (Zhang et al., 2001; Li et al., 2007). Due to limited availability of hESCs in the UK on commencing this project, early studies on neuronal differentiation were carried out on Shef3, a cell line with no prior history of neuronal differentiation. Human ESCs were differentiated according to the methods

outlined in Section 2.10.1; however attachment and spreading of the EBs following differentiation to the culture surface following plating was limited, making it difficult to identify individual differentiating cells and determine whether neuronal differentiation was successful, suggesting that identification of a suitable surface coating for optimised EB attachment was necessary.

5.2.1.1 Comparison of surface coating for neuronal attachment

To determine the optimal surface coating for EB attachment a comparison of six different coatings (laminin, poly-d-lysine, gelatin, poly-L-ornithine, fibronectin and collagen IV) was carried out. In an attempt to identify a surface coating which positively selected for EBs containing neuronal progenitors, this experiment was carried out using differentiating fragments containing known to contain neural progenitors in rosette-like structures. The methods for this experiment are detailed in Section 2.11. Results from eight wells per chamber slide for two cell lines (Shef3 and RH5 cut) were averaged for overall comparison. Images were captured of attached fragments on each of the surface coatings (Figure 5.1).

The highest level of fragment attachment after eight days in culture was seen on the poly-L-ornithine coated surface (93.8 % ± 4.4; Figure 5.2). High levels of attachment were also noted for fibronectin and collagen (87.5 % and 81.3 % respectively); however, the cells spreading from attached fragments were of predominantly non-neuronal morphology (Figure 5.1), suggesting that these coatings were not selective for neuronal selection and proliferation. Attachment on laminin coated surfaces was lower than other surface coatings with only 68.75 % fragments attached after eight days in culture; however, neuronal outgrowth from these attached fragments was higher than was seen for any other surface coating (37.5 % ± 22.1) as seen by the increased numbers of phase bright rounded neuronal cell bodies with outgrowing neurites, indicating a positive selection for attachment of fragments containing neurons.

The survival of Shef3 fragments for attachment after eight days was significantly lower than the RH5 cut fragments as determined by ANOVA ($p = 0.01$). When combining data from RH5 and Shef3, ANOVA revealed that there was no significant difference in the rate of fragment attachment ($p = 0.73$) or the level of neuronal outgrowth ($p = 0.94$) between all culture surfaces. However, based upon the average levels of attachment and neuronal outgrowth these data support findings that poly-L-ornithine and laminin are optimum surface coatings for improving attachment, differentiation and outgrowth of neuronal cell

types (Reynolds and Weiss, 1992; Lathia et al., 2007; Hall et al., 2008). A combination of poly-L-ornithine to aid attachment and laminin to promote survival of neural cells was subsequently used for all further studies.

Using this method of differentiation (Section 2.10.1), EBs were irregular in size and shape with very few containing visible rosette-like structures (Figure 5.3). Despite optimised conditions for attachment and spreading of EBs following FGF8 and SHH induced differentiation, the number of neurons which were visible spreading from these attached EBs was minimal and the majority of spreading cells were of a non-neuronal morphology. In a number of cases, EBs failed to collapse following attachment and retained a compacted cell cluster (Figure 5.4).

Under bright field microscopy it was not possible to detect cells of neuronal morphology due to the presence of large numbers of non-neuronal cells. To determine whether neurons were present amongst the differentiating EBs, samples were fixed with 4 % PFA (Section 2.13.1) and stained for a range of antibodies which confer neural identity. After ten days SOX2 was positively expressed in cells of rosette morphology (Figure 5.5) but predominantly negative in the surrounding non-neuronal cells. Expression of N-cadherin (an alternative marker for neuroepithelial cells) was detected throughout the attached EB (Figure 5.5), confirming the presence of cells with a neuroepithelial phenotype; however, further immunostaining for TUBB3 demonstrated that very few of these cells were of neuronal morphology (Figure 5.5). Continued culture and differentiation of these cells increased the numbers of TUBB3 positive cells.

By the presence of very few TUBB3 positive neurons within the EBs it was concluded that Shef3 hESCs were not responsive to EB directed neuronal differentiation using just FGF8 and SHH. Instead an alternative approach to differentiation was carried out using ATRA (as used for NTERA2 differentiation) whilst retaining the cells in an adherent monolayer, according to methods outlined in Section 2.10.2 (Baharvand et al., 2007).

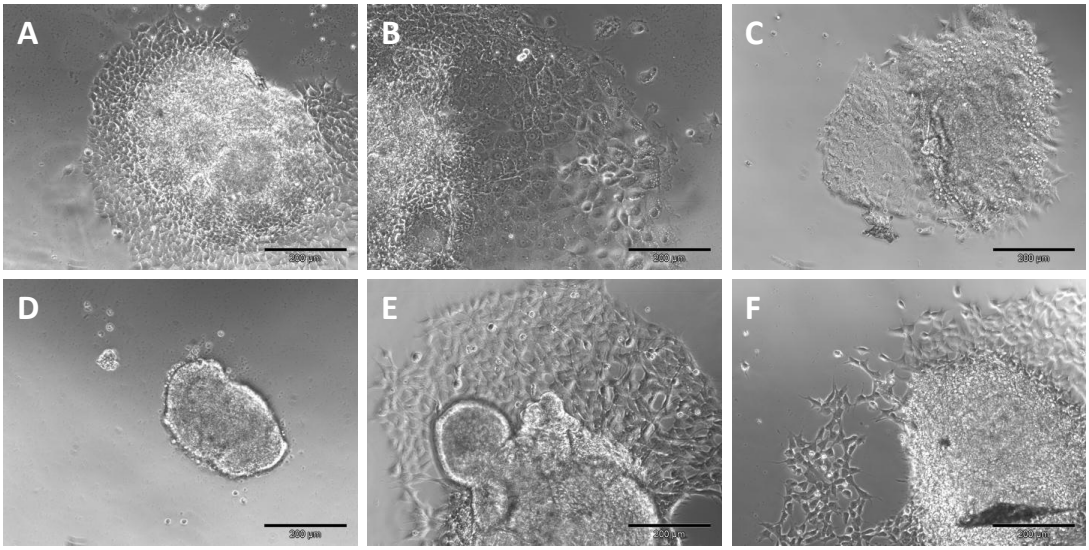

Figure 5.1. Comparison of six surface coatings for EB attachment.

Fragments containing neural rosettes were plated into 8-well chamber slides pre-coated with a range of factors which aided cellular attachment. Images of fragments following attachment were captured four days after seeding. Neural rosettes were clearly visible in fragments spreading on gelatin coated surface, but limited neuronal outgrowth was observed (A). Outgrowth from fragments on collagen IV (B) and fibronectin (C) comprised predominantly non-neuronal cells. Mixed behaviour was seen on poly-D-lysine from no cellular spreading (D) to outgrowth of neuronal and non-neuronal cell types. Neural progenitors were visible in large number spreading from fragments on poly-L-ornithine (E) and laminin (F) coated surface.

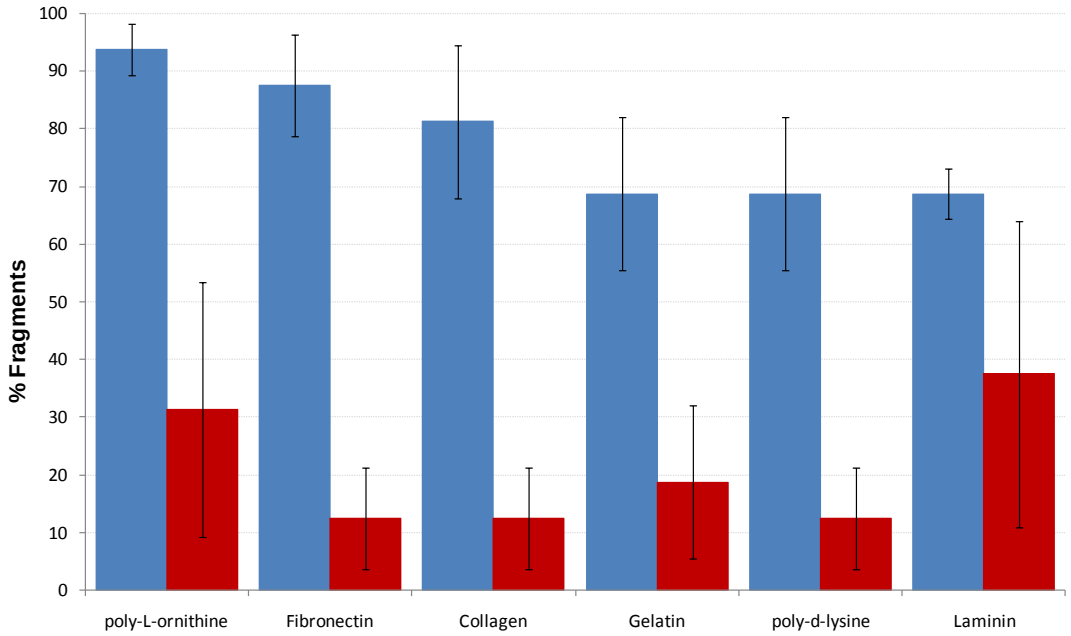

Figure 5.2. Surface coatings for optimal neuronal differentiation.

Six surface coatings were compared for attachment of cell fragments containing neural rosettes. Results from Shef3 and RH5 were combined. Optimal levels of fragment attachment (blue) were achieved using poly-L-ornithine when compared to alternative surface coatings. Optimal neuronal outgrowth from attached fragments (red) as determined by the numbers of rounded phase bright neuronal cell bodies with extended neurites, was achieved with a human laminin coated surface (37.5 % ± 22.1), with neuronal differentiation also seen in poly-L-ornithine (31.3 % ± 8.8). Error bars (2SE).

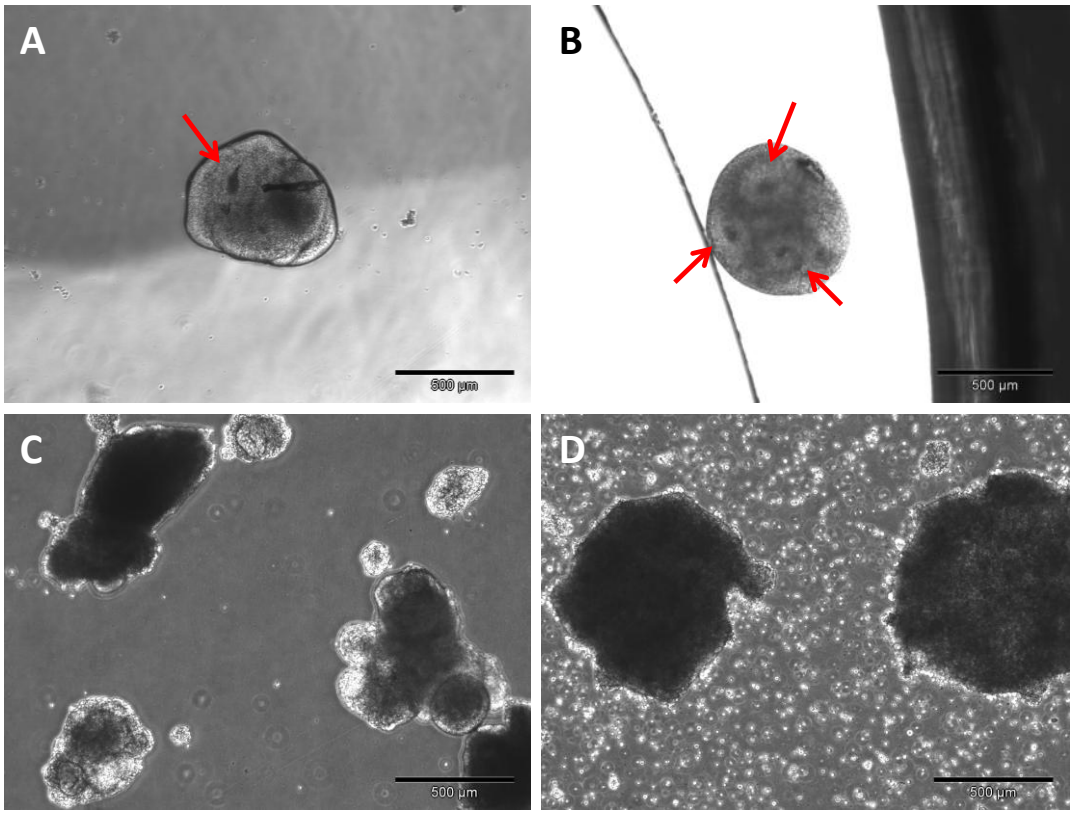

Figure 5.3. EBs displaying rosette-like structures following differentiation.

EBs displaying rosette-like structures (A-B) were present in very small numbers, and were irregular in size and shape (C-D) following differentiation according to methods outlined in Section 2.10.1.

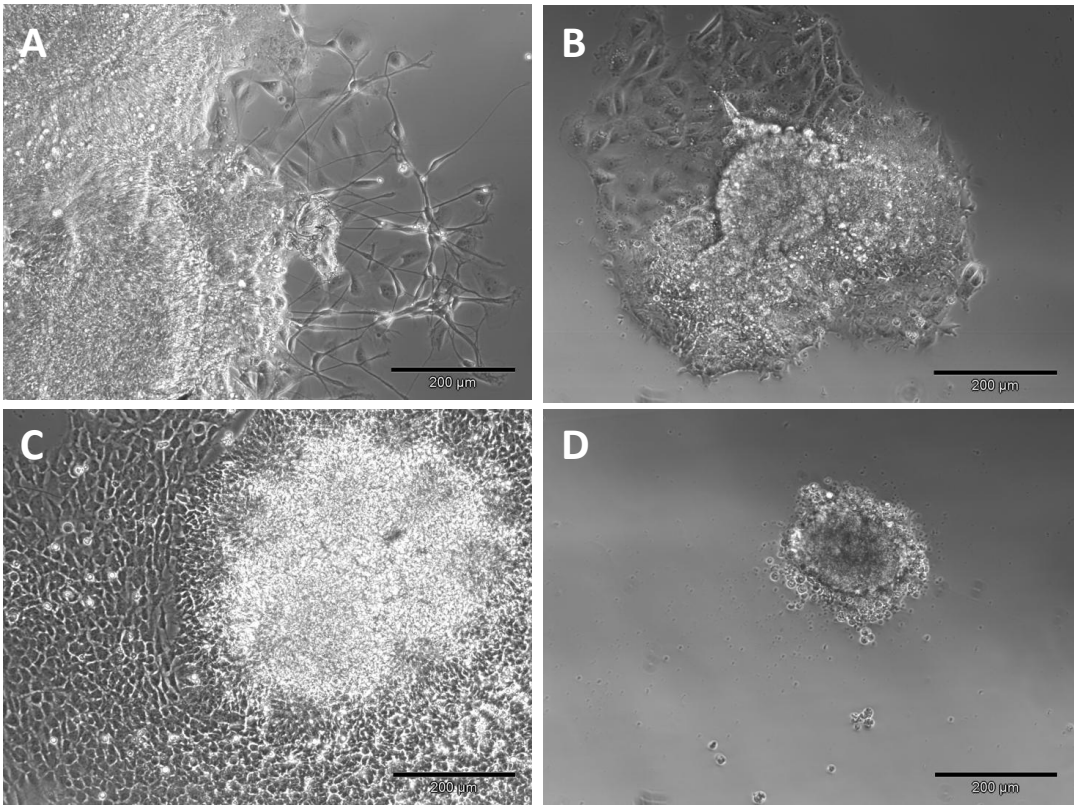

Figure 5.4. Non-neuronal outgrowth from FGF8 and SHH differentiated EBs.

Neuronal outgrowth was seen from a minority of differentiated EBs following differentiation (A). Outgrowth from the majority of attached EBs was of non-neuronal morphology (B-C). In a minority of cases, attached EBs failed to collapse and spread, retaining their compacted structure throughout differentiation D).

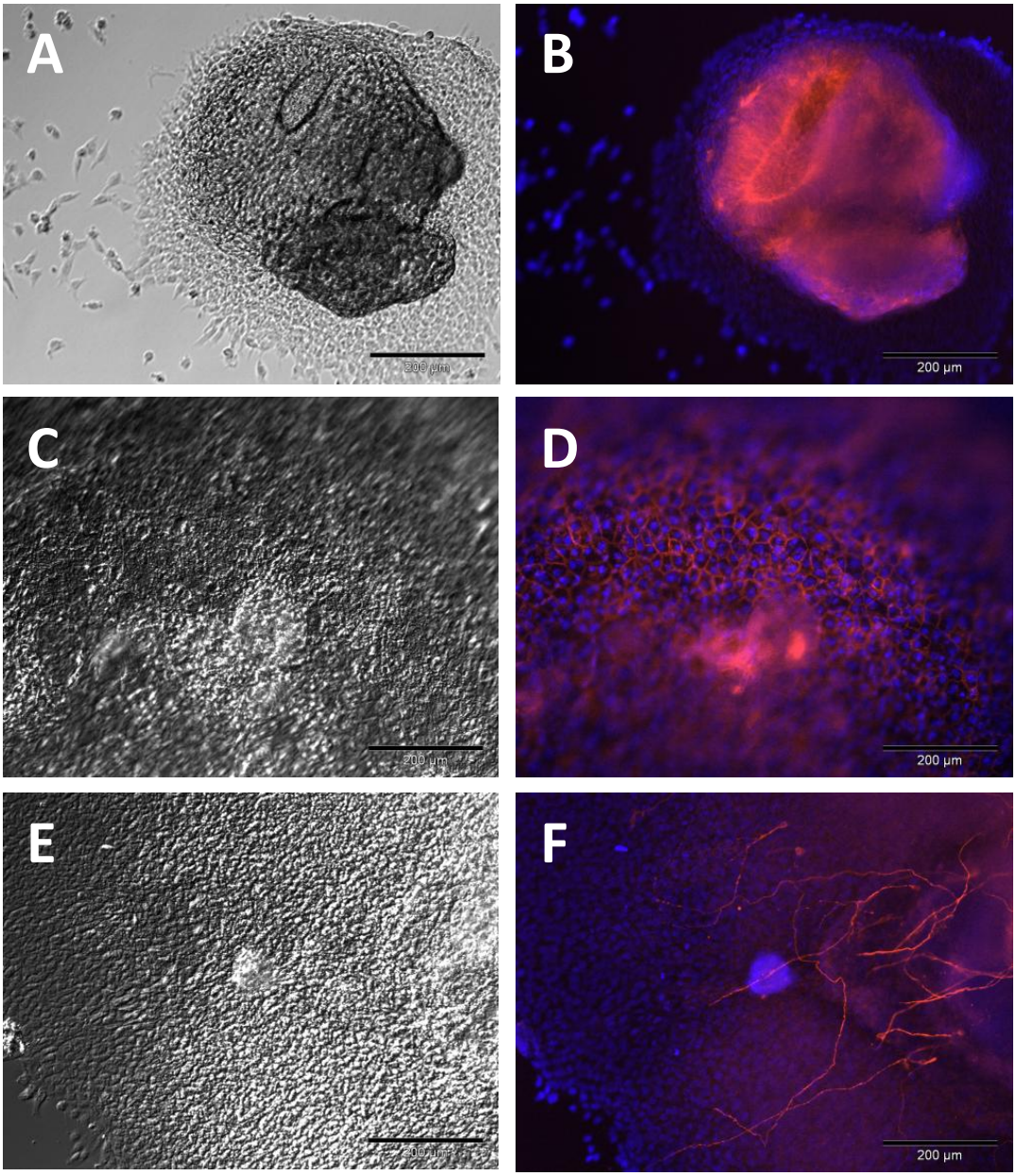

Figure 5.5. Immunostaining of neurons following EB directed differentiation.

Positive SOX2 staining was visible in neural rosettes within the attached EBs (A-B). Positive N-cadherin expression was detected throughout the attached EB (C-D). Very few cells within the attached cell mass were positive for TUBB3 (E-F), highlighting a poor efficiency of neuronal differentiation according to this method. TUBB3 positive neurons were deeply embedded within the cell mass, preventing isolation for functional analysis.

5.2.2 Adherent monolayer neuronal differentiation

Cells were differentiated according to the method outlined in Section 2.10.2. Following exposure to ATRA, large parts of the hESCs colonies collapsed and flattened out into epithelial like cells, which were apoptotic in appearance (Figure 5.6B). In areas of high density growth, some neural rosettes were visible (Figure 5.6C) which were mechanically dissected and transferred onto poly-ornithine/laminin coated IVF dishes in NBD media (4-6 fragments/dish). Following plating, 65.0 % ± 20.9 fragments attached, the remaining fragments either stayed in suspension or disintegrated. Small areas of neuronal outgrowth were visible from some attached fragments (Figure 5.6D; red arrows). However most fragments attached with no sign of neurons amongst outgrowing cells (Figure 5.6E). Non-ATRA treated controls retained features of hESCs (Section 4.2.1). After repeated attempts, Shef3 hESCs were also deemed unresponsive to ATRA induced differentiation when cultured on iMEFs.

5.2.3 Semi-directed differentiation

After many failed attempts to differentiate Shef3 neuronally, using two established protocol, (suspension EBs and monolayer), it was questioned whether the Shef3 line was capable of differentiating to cells of a mature neuronal phenotype. To investigate this further rosette-like structures from spontaneously differentiating Shef3 on high cell density iMEF layer, were mechanically dissected and transferred into NBD media (Figure 5.7A-B), for neuronal specification. For the purpose of this study, this process was referred to as semi-directed differentiation. As a comparison, cells from the RH5 TrypLE cell line were also treated in this way to control for cell line variation.

Twenty-four hours after attachment neuronal-like cells were visible spreading from rosettes in both cell lines, which continued to increase in number over time. Immunostaining of these cells confirmed the neuronal phenotype by positive TUBB3 expression (Figure 5.7C-D). Patch clamp analysis demonstrated the ability to fire electrical impulses in response to stimulation, thereby confirming true neuronal identity from cells of both RH5 TrypLE and Shef3 origin (*data available upon request*).

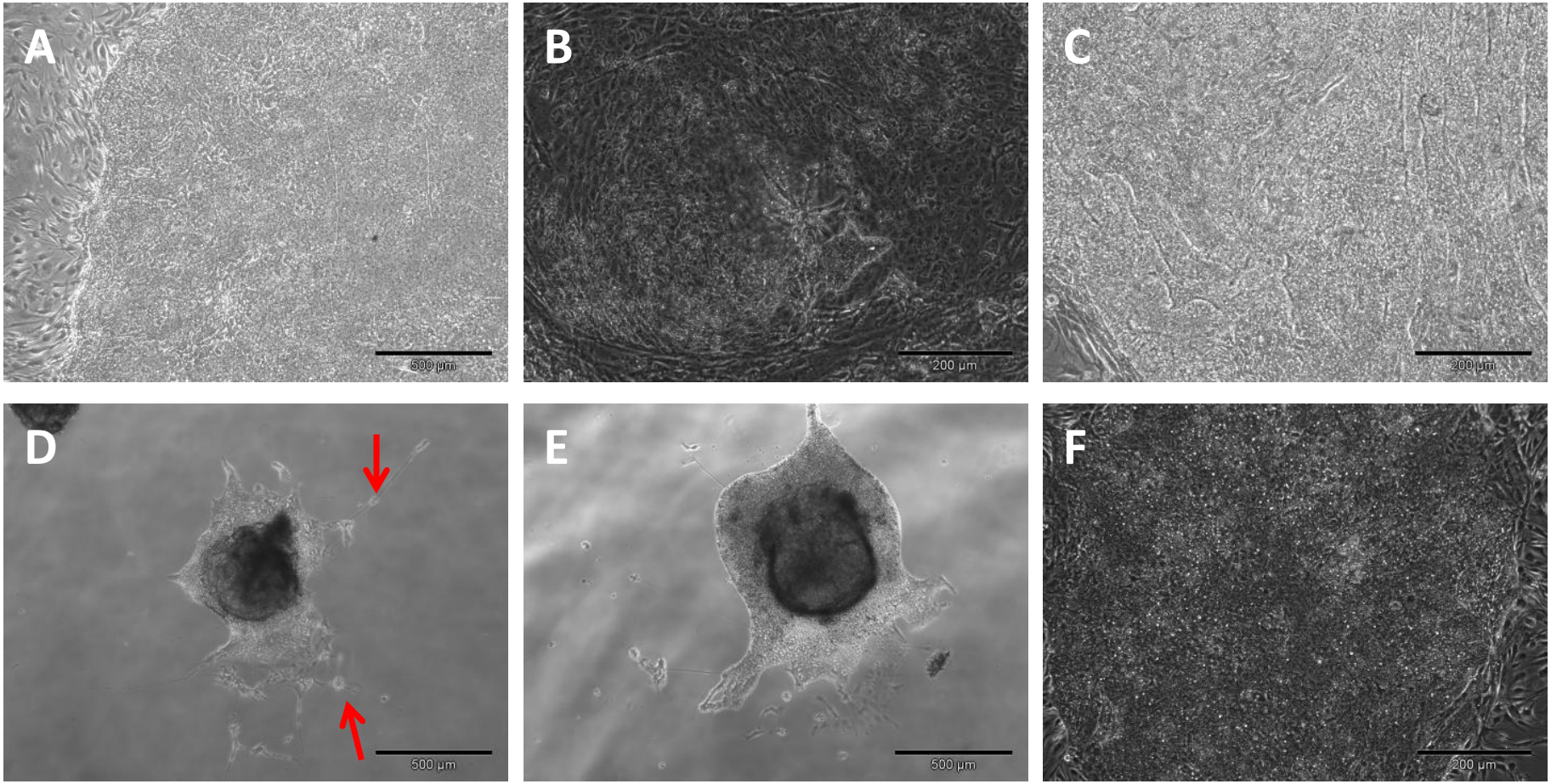

Figure 5.6. Adherent monolayer neuronal differentiation.

Pluripotent hESC colonies (A) were treated with ATRA. After five days in culture many of the colonies appeared collapsed and of an epithelial-like cell morphology (B). Some colonies developed high density rosette-like structures (C) which were mechanically dissected and transferred into NBD media for further differentiation. Neuronal outgrowth was visible from a minority of attached fragments (D). Outgrowth of non-neuronal cells (E) was most commonly observed indicating poor efficiency of neuronal differentiation. In non-ATRA treated controls, hESCs retained the morphology of pluripotent cells (F).

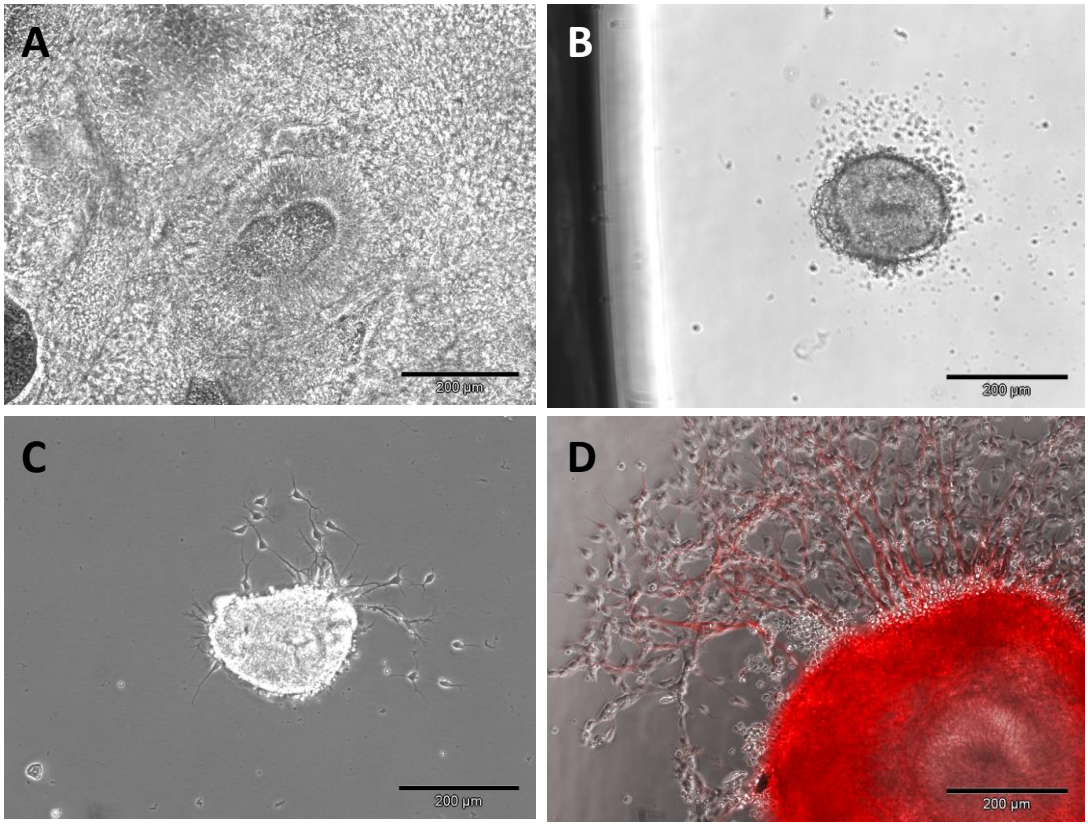

Figure 5.7. Neural rosettes following semi-directed neuronal differentiation.

When cultured on a high feeder density, hESC colonies underwent spontaneous differentiation. On occasion, this generated structures similar in appearance to neural rosettes A). Following mechanical dissection (B) these rosettes were transferred onto a poly-ornithine/laminin coated surface in NBD media (Section 2.10.3.1). After 24 hours neurons were seen spreading from the rosettes (C). After several days, the number of neuronal cells continued to increase and stained positively for TUBB3 (D-red, overlaid image)

The semi-directed method of differentiation demonstrated the ability of both the RH5 TrypLE and Shef3 to differentiate into functional neurons; however, the reproducibility of this process was limited by the rate of spontaneous differentiation, which was an adverse side-effect of poor hESC culture. A reproducible method for inducing the formation of neural rosettes in culture was therefore required to enable a reliable comparison of the neural differentiation capacity of different hESC lines. Using experience of differentiation from the above studies and additional literature an alternative 'enhanced' method of differentiation was established combining aspects of these different protocols.

5.2.4 Enhanced EB differentiation

The HUES7 cell line was incorporated into this part of the study as a comparative hESC line and a positive control for neuronal differentiation due to its history of neuronal differentiation. Human ESCs were cultured as described in Section 2.9.1**,** until TrypLE lines reached confluency (Figure 5.8A) and mechanically passaged colonies were sufficiently large for dissection. Prior to differentiation, all hESCs presented pluripotent characteristics (Section 4.2.1). Fragments approximately twice the size as for passaging (Figure 5.8B-C) were dissected and cultured in suspension as EBs. The cell signalling within an EB has been shown to recapitulate early embryonic development, inducing tissue specification into each of the three germ layers (Itskovitz-Eldor et al., 2000). In an attempt to reduce loss of cells into alternative germ lineages and increase the speed of specification into a neuronal cell fate, EBs were cultured directly into a neural Induction medium (NI; Section 2.10.1.1), rather than incubating the first four days in standard hESC as detailed in alternative protocols (Li et al., 2007).

The efficacy of this adaptation was demonstrated using flow cytometry to compare expression of OCT4 and Nestin (a neural stem cell marker) within these populations. Embryoid bodies were dissociated into single cells after four days in their respective medium. After four days in NI media the expression of OCT4 had dropped to 20.97 % when compared to 82.34 % positive expression on the day 0. The levels of OCT4 positive cells in the hESC treated EBs was also reduced after four days, but a higher proportion of cells retained OCT4 30.95 %, confirming that NI media induced more rapid down regulation of pluripotency than hESC media.

To determine whether the NI media was specifically directing differentiation neuronally, expression levels of Nestin were compared in NI and hESC media treated EBs after four days. EBs were imaged using confocal microscopy, confirming a consistent reduction in the number of OCT4 positive cells within the NI treated EBs when compared to EBs cultured directly in hESC media (Figure 5.9). Remaining OCT4 positive cells within the EB were located in clusters, rather than spread throughout the EB.

Neural induction media increased the yield of Nestin positive cells from 22.3 % on day zero to 63.68 % on day four, compared to just 40.14 % in hESC media. Direct culture in NI media also increased the final neuronal yield, as determined by increased outgrowth of cells with neuronal morphology after 28 days.

In light of published data and evidence from neuronal differentiation in NTERA2, demonstrating the effect of serum on the outgrowth of non-neuronal cells (Brewer et al., 1993; Brewer, 1995), serum-free media was used throughout differentiation. After four days differentiating in culture, neural progenitors were transferred into a NBD media (Section 2.10.3.1) for further differentiation which contained a range of neurotrophic factors to promote neuronal differentiation and survival (Section 1.5.2).

The cost and volume of differentiation media was also reduced by differentiating EBs in 25-well bacteriological grade perti-dishes, using 2 ml NI media per well, compared to the minimum 10 ml media required for 60 mm round petri-dishes as were used in earlier publications. Additional advantages of the square compartmentalised cultured dishes include stability in transit, reducing spillages and therefore reduced risk of contamination. Two wells of the compartmentalised dish were used to culture EBs from one confluent well of a 6-well plate.

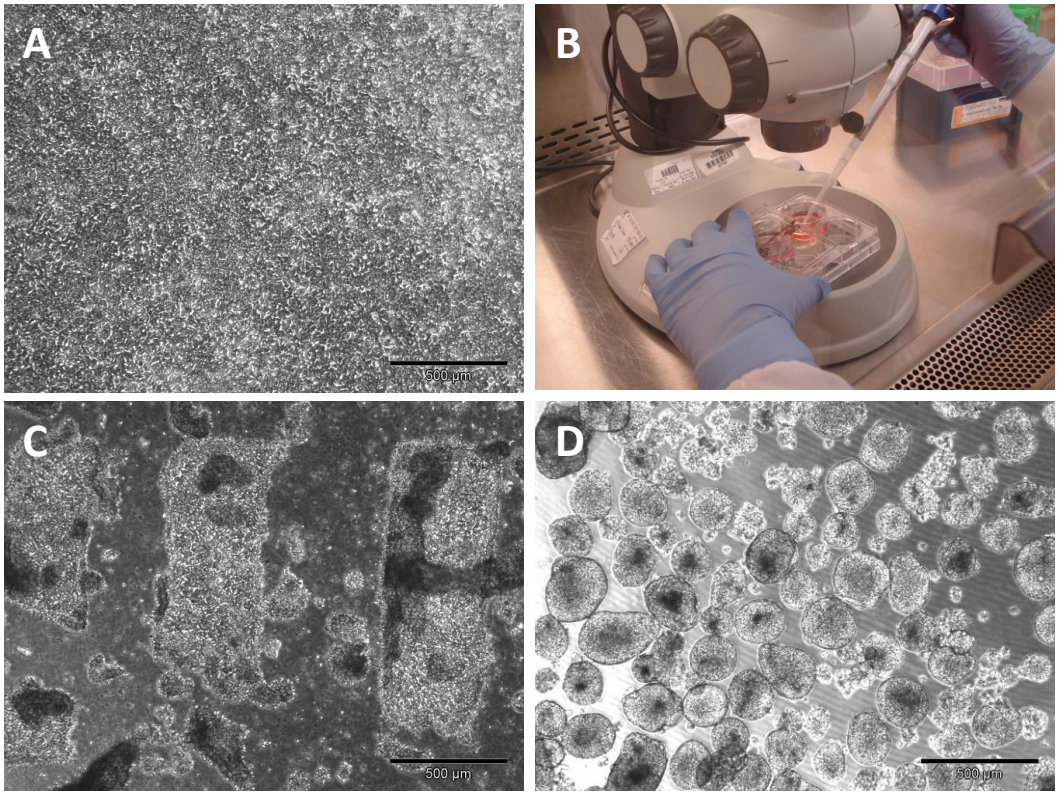

Figure 5.8. Generating embryoid bodies for neural induction.

Confluent hESCs (A) were washed in NI media and dissected from the culture surface under a dissection microscope using a sterile 1 ml pipette tip (B) using a scraping motion at perpendicular angles across the dish (C). Resulting EBs were relatively uniform in size and shape after 24hours in culture (D).

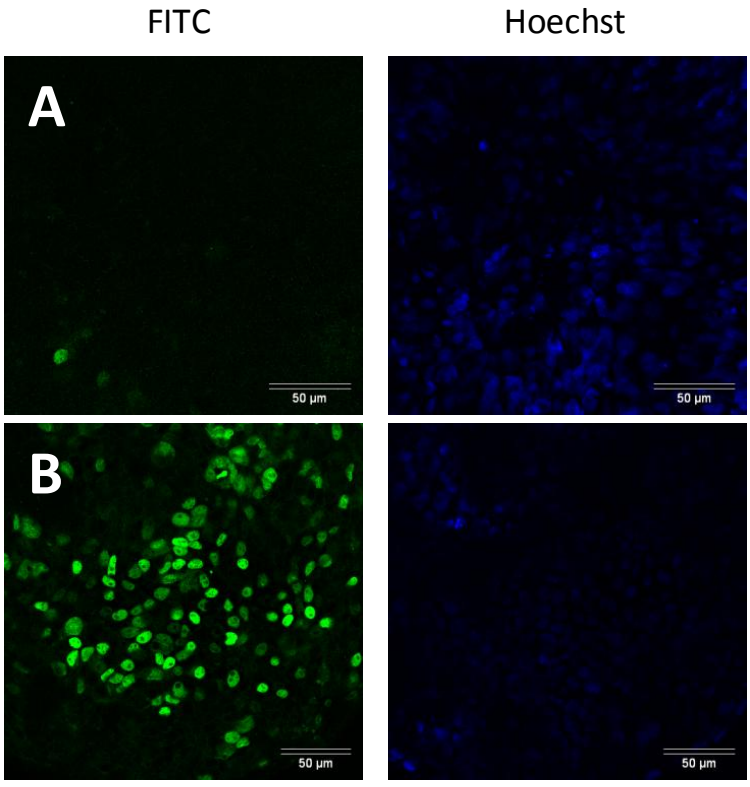

Figure 5.9. OCT4 after four days in neural induction media.

After four days in NI media, OCT4 expression was almost completely lost from the EBs (A). OCT4 positive cells were located in clusters rather than evenly dispersed through the EB (B). Images were captured using Leica DMRE confocal microscope on the RH5 cell line.

5.2.4.1 The effect of bFGF on neuronal differentiation

The effect of basic fibroblast growth factor (bFGF) on hESC culture and differentiation has been the subject for numerous studies. bFGF is a mitogen known to be required for maintaining pluripotent expansion of hESCs (Friesel and Maciag, 1995; Amit et al., 2000). It has also been shown to stimulate proliferation (Tienari et al., 1995). A proliferating cell will usually exit the cell cycle prior to differentiation (Walsh and Perlman, 1997; Maione and Amati, 1997; Brown et al., 2003). For this reason, removal of bFGF from differentiation media has been previously described, with reported increases in neural progenitors and outgrowth of mature neurons (Lee et al., 2000; Shin et al., 2005; Schwindt et al., 2009). As such, bFGF was removed from media following the first four days of neural induction in an attempt to improve commitment into neuronal differentiation. To identify the effect of bFGF removal on neuronal differentiation, a comparative study was carried out in the presence and absence of bFGF in NBD media.

Cellular outgrowth from EBs following attachment was greatly increased in NBD media containing bFGF (Figure 5.10); however cells were mainly of a non-neuronal morphology. Neurons were identifiable in samples cultured in both the presence and absence of bFGF, but neuronal purity was considerably higher in NBD media without bFGF. Non-neuronal cells continued to proliferate in bFGF containing media and eventually overgrew neurons in culture. The higher neuronal purity from samples grown in the absence of bFGF was confirmed using immunostaining where TUBB3 positive neurons were identified in both samples with a higher proportion of non-neuronal cells in NBD media containing bFGF (Figure 5.11). It was therefore decided to remove bFGF from NBD differentiation media.

To determine whether the removal of bFGF affected the function of hESC derived neurons, cells were screened using the patch-clamp. Neurons produced in both the presence and absence of bFGF generated APs in response to stimulation (Figure 5.12), which were reversibly inhibited by Tetrodotoxin (TTX; a sodium channel blocker), confirming genuine sodium APs. On several occasions neurons from samples differentiated in the absence of bFGF fired a series of APs which were not detected in neurons derived in bFGF containing media (Figure 5.12), indicating the presence of functional voltage gated K^+ channels. This suggests that the absence of bFGF improved neuronal maturation. Following confirmation of functional neuronal differentiation using the 'enhance' method of differentiation, hESC from all four hESC lines were directed into differentiation for comparison of efficiency and functionality between cell lines.

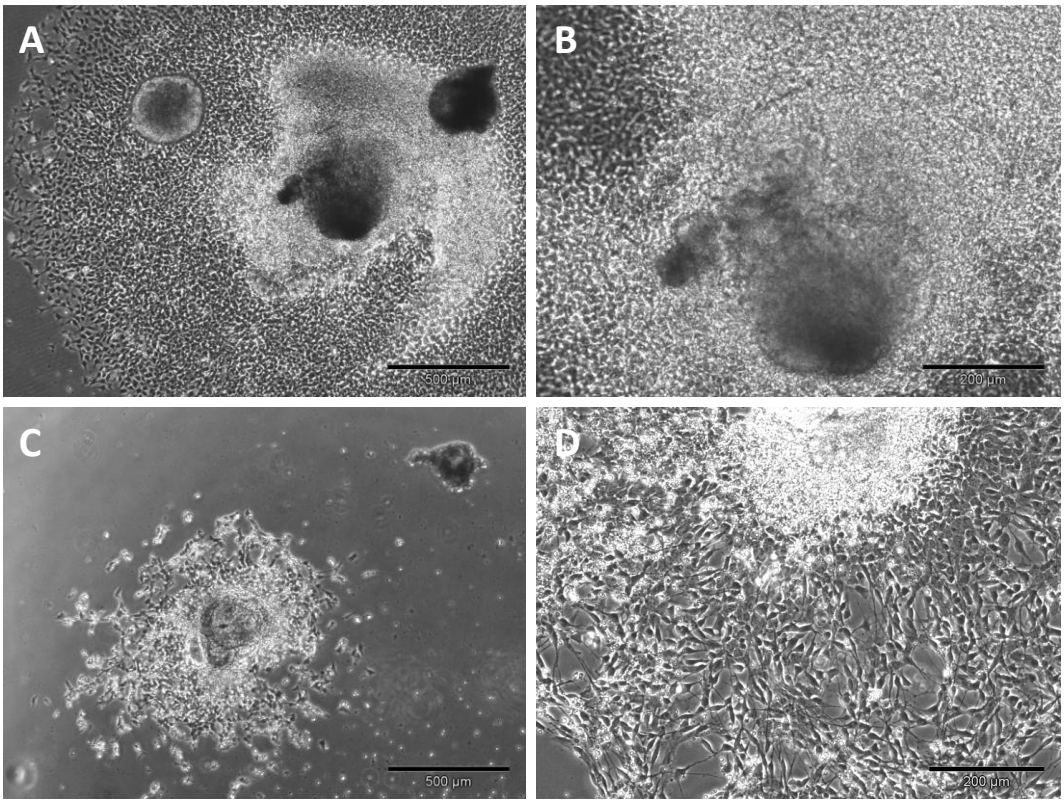

Figure 5.10. Cell proliferation with and without bFGF.

Following EB attachment, outgrowth from fragments was greater in bFGF containing NBD media (A-B, x4, x10 magnification) compared to media without bFGF (C-D, x4, x10 magnification). In the presence of bFGF neuronal outgrowth was accompanied by non-neuronal cells thus reducing the neuronal purity.

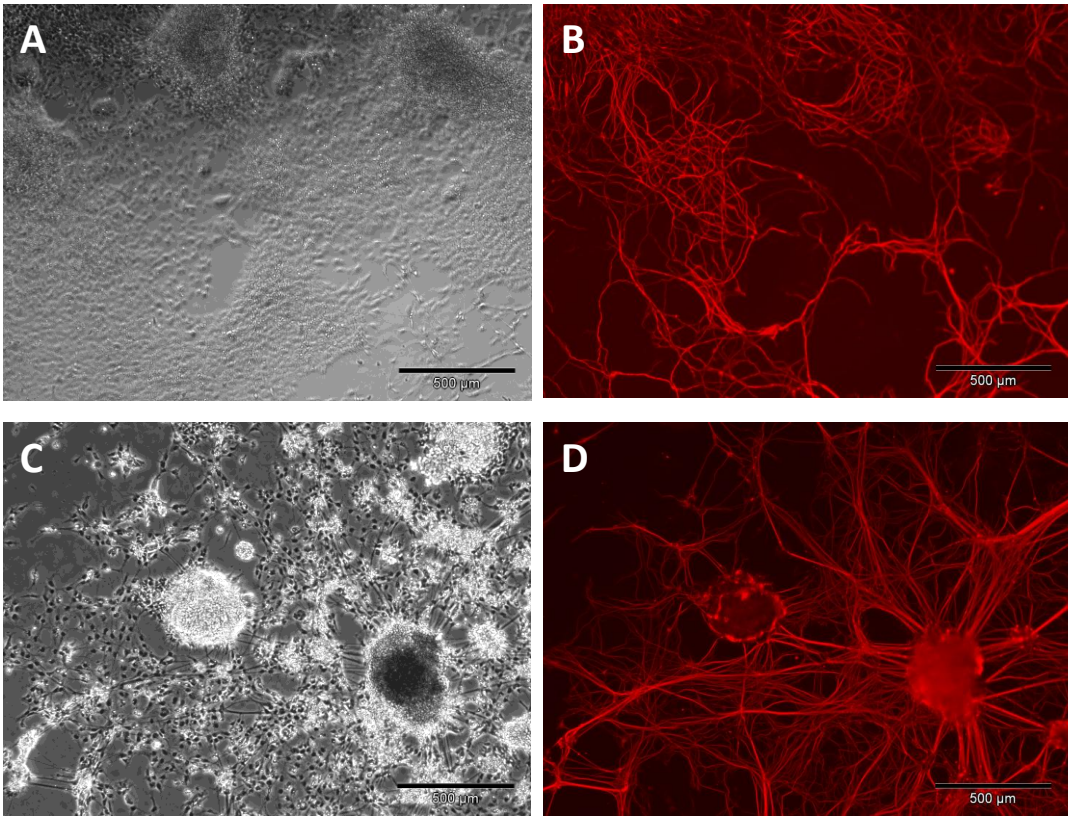

Figure 5.11. TUBB3 staining in neurons derived with and without bFGF.

TUBB3 (red) positive neurons were generated following differentiation protocols with bFGF (A-B) and without bFGF (C-D), x4 magnification.

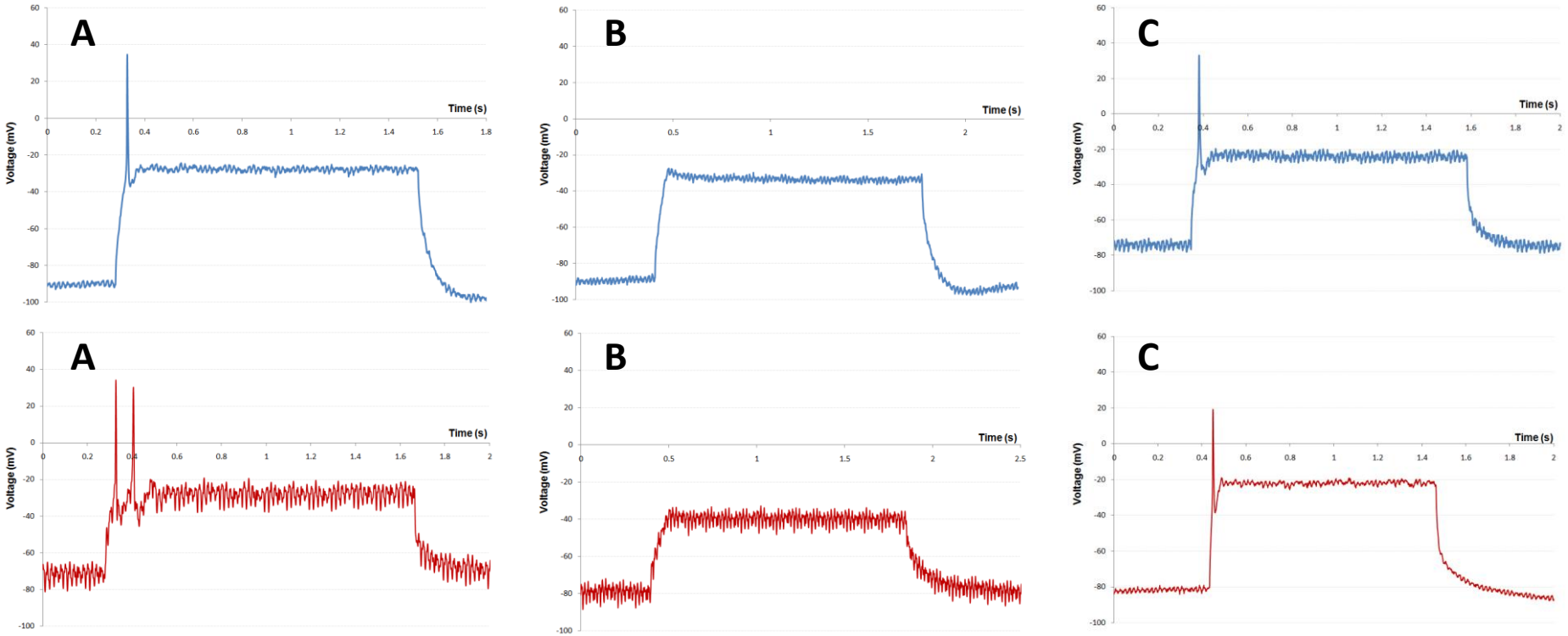

Figure 5.12. Action potentials from neurons derived +/- bFGF.

Positive action potentials were generated by neurons derived both in the presence of bFGF (blue) and in the absence of bFGF (red). Only single APs were fired by neurons derived in the presence of bFGF (A –blue) where in the absence of bFGF neurons were able to fire a series of AP's (A – red). Action potentials were inhibited by TTX (B) and recoverable following washing (C), confirming genuine sodium action potentials. Upon recovery only single APs were fired by neurons which previously fired multiple APs suggesting incomplete clearance of the membrane bound sodium channels following washing (C – red).

5.2.5 Determining neuronal yield

Flow cytometry analysis was carried out on undifferentiated and differentiating hESCs to quantify the efficiency of neuronal differentiation based on the expression of neuronal proteins. Before this was possible, it was first necessary to break up neuronal populations into single cells for analysis. Neurons were difficult to disrupt into small cell clusters, without damaging the delicate neurite projections. This frequently resulted in high levels of cell death and debris, making it difficult to quantify the true efficiency of differentiation. A comparison of cell dissociation reagents was carried out to determine the optimal method for dissociating EBs and neuronal cultures to retain cellular integrity and viability.

5.2.5.1 EB dissociation

There are a wide range of reagents available for cell dissociation based on different dissociation chemistries. Five different cell dissociation reagents were compared for their ability to dissociate clusters into single cells, whilst retaining high viability; TrypLE™ Express, Trypsin-EDTA, Collagenase IV, Accutase™ and Dispase. Each of these reagents have different modes of activity. Type IV collagenase is isolated from *Clostridium histolyticum* and is commonly used for enzymatic passaging of hESCs because it has low tryptic activity, retaining cellar integrity (Gonzalez et al., 2007). Accutase™ is an animal/bacterial free product comprising a mixture of proteolytic and collagenolytic enzymes in EDTA (Gonzalez et al., 2007). Trypsin is a porcine derived proteolytic enzyme which is produced by the pancreas to digest large proteins. Trypsin is one of the principle enzymes in the body for protein digestion and has a long history of use in tissue culture for cell dissociation. TrypLE™ Express is an animal product free, alternative to Trypsin. It is derived from microbial fermentation (Invitrogen) which is gentler on cellular dissociation.

Eight day differentiated EBs were treated as detailed in Section 2.13.4.1. Following incubation, EBs were triturated ten times to enhance dissociation, before determining cell number and viability (Figure 5.13). Due to variation in the size and shape of EBs, 20 EBs were used for each sample reducing error in dissociation which may arise from EBs of different sizes. Observations of cellular appearance and behaviour were noted for each of the reagents (Table 5.1).

Dissociation of EBs using was most efficient using Accutase™, TrypLE Express and Trypsin-EDTA, resulting in cells with 95.4, 95.8 and 98.5 % viability respectively (Figure 5.13). The overall number of single cells achieved was considerably higher using

Accutase™ (9.3×10^5 cells/ml) when compared to the other dissociation reagents. Collagenase and Dispase both retained cells in small clusters following incubation which were unable to be counted using the haemocytometer and would not be sufficiently dissociated for quantification using the flow cytometer; however, this was as expected since these enzymes are commonly used for hESC passaging due to their ability to retain cells in small clumps (Freshney, 2005) rather than single cells.

Reagent	Single cell suspension	Observation
Trypsin EDTA	No	Large amount of cell lysis. Stringy, sticky cell suspension. Clumps of cells visible after 10 triturations.
TrypLE™ Express	Yes	Dissociated into single cells in 10 triturations
Accutase™	Yes	Cells dissociated into single cells/ very small clusters. Minimal cell debris following trituration.
Dispase	No	Large cell clumps remain. Lots of debris following trituration.
Collagenase	No	Large cell clumps remain. Lots of debris following trituration.

Table 5.1. Enzymatic cell dissociation observations.

Each of the enzymes used for cell dissociation had different modes of action and consequently different end results for dissociation.

This experiment was repeated on monolayer samples of 18 day differentiating neurons which were visibly extending large numbers of intermingling axons and dendrites. Single wells of a 6-well plate of differentiating cells from the same starting pool were prepared as for suspension EBs (Section 2.13.4.1). In monolayer culture, Accutase™ also recovered the largest number of viable single cells 93.1 %, 1.8×10^6 cells/well).

Based on the number and viability of single cells generated, this data suggests that Accutase™ or TrypLE™ were the best reagents for single cell dissociation of EBs. This study would need to be repeated with up to three different cell samples for full validation; however, this trend supported finding by alternative research groups which use Accutase™ for dissociating neural cell cultures (*Personal communication: Dr. M. Caldwell*). Accutase™ or TrypLE Express were subsequently used for dissociating all samples for flow cytometry analysis.

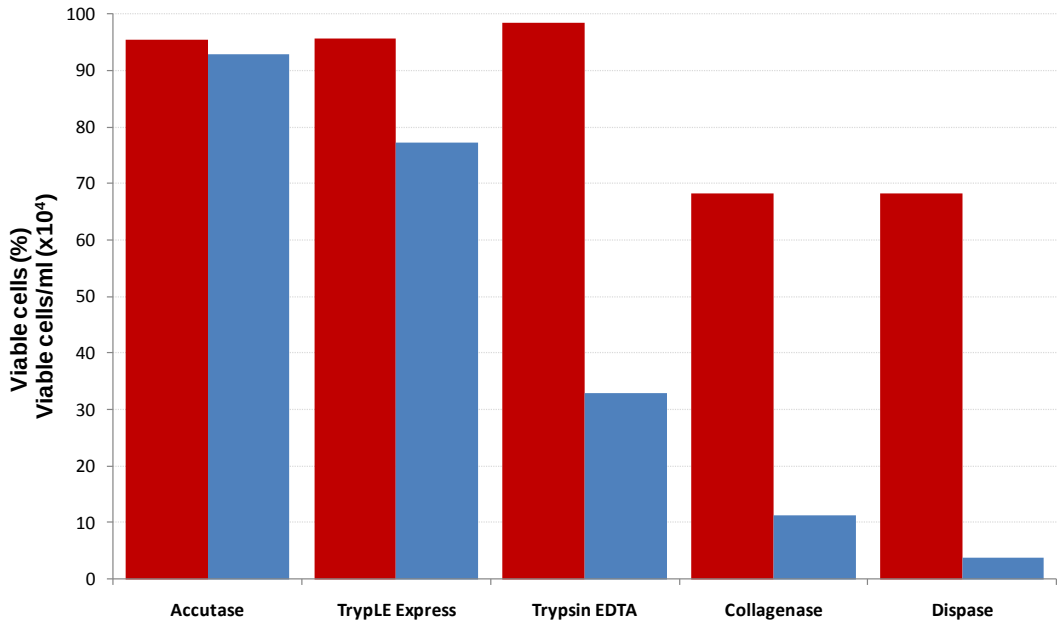

Figure 5.13. Comparison of cell dissociation regents.

Differentiating hESCs retained a high viability (red) following dissociation with all reagent; however, the total cell count x 10^4 (blue) following EB dissociation was variable between reagents. This was largely due to an inability of Collagenase and Dispase to separate EBs into single cell, retaining clumps of cells which were uncountable using the haemocytometer. Most efficient dissociation was achieved using Accutase™ and TrypLE express retaining 95.4 % and 95.8 % viability respectively and yielding 9.3 x 10^5 and 7.7 x 10^5 single cells/ml.

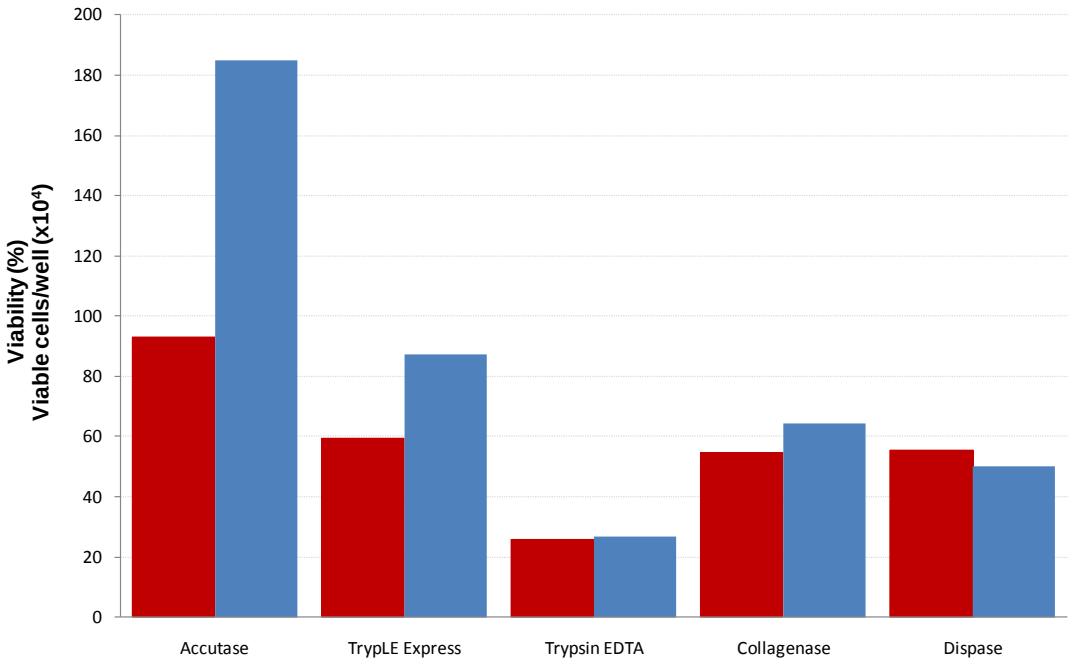

Figure 5.14. The efficiency of dissociation on 18 day neurons.

Cell viability (red) and count/well (x 10^4; blue) following dissociation of day 18 RH5 TrypLE derived neurons. The viability of cell following dissociation was relatively comparable between different dissociation reagents. However, the overall number of single cells was considerably higher following Accutase dissociation than from any of the alternative dissociation reagents (TrypLE, Trypsin, Collagenase and Dispase), due to higher efficiency of dissociating EBs into single cells. In alternative reagents, cells remained in clusters of varying sizes, resulting in a lower overall single cell count.

5.2.5.2 Flow cytometry analysis

Flow cytometry analysis was carried out on the RH5 TrypLE differentiating cells to identify neuronal yield following the newly developed method. The differentiating population were dissociated into single cells using Accutase™ and analysed at day 0, 4, 18 and 28 for changes in expression levels of OCT4, Nestin and TUBB3. Expression levels of OCT4 were significantly reduced from 82.3 % ± 7.4 at day 0 to 2.9 % ± 3.9 positive cells at day 28 ($p = 0.0001$) as determined by ANOVA. Nestin expression increased from 22.3 % ± 27.6 at day 0 to 62.7 % ± 23.5 at day 4, after which expression levels did not significantly change ($p = 0.14$). Neuronal yield reached 42.2 % ± 16.0, according to positive TUBB3 expression. However, this was contradictory to data from bright field and *In situ* immunostaining images which indicated a considerably higher neuronal purity. Attempts as analysing the expression of GABA within the neuronal population using flow cytometry were unsuccessful due to poor antibody detection.

Whist flow cytometry analysis was helpful for screening neuronal cell populations, damage to matured neurons during dissociation, might explain the lower neuronal yields than expected. This was also confirmed by the presence of debris amongst the flow cytometry analysed samples. With this in mind, despite optimising the dissociation reagents, the flow cytometer was not considered to be a suitable method for reliably comparing the efficiency of neuronal differentiation between the different hESC lines. *In situ* immuno fluorescence images were considered to be a better mode of comparison for differences in neuronal yield across hESC lines.

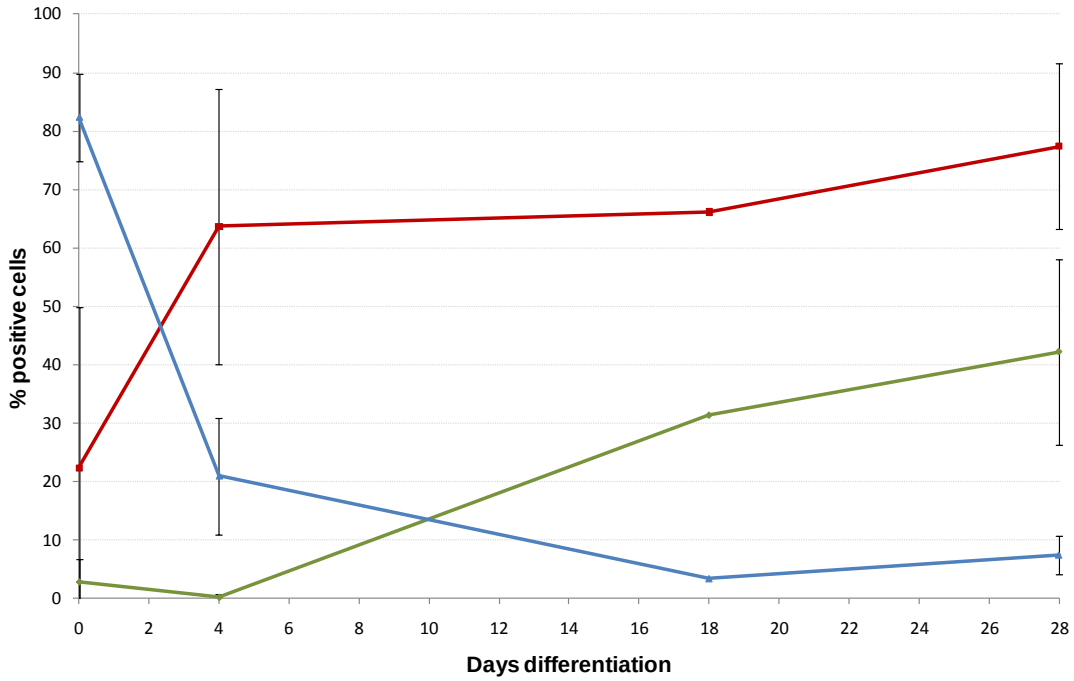

Figure 5.15. Flow cytometry analysis of in-house neuronal differentiation.

RH5 TrypLE cells were differentiated according to methods outlined in Section 2.10.4. Samples were taken at day 0, 4, 18 and 28. Only single samples were recorded at day 18. Cells were analysed for OCT4 (blue), Nestin (red) and TUBB3 (green). After 28 days, 42.2 % ± 16.0 cells were neuronal, as determined by positive TUBB3 expression. OCT4 expression decreased from 82.3 % ± 7.4 positive expression at day 0 to just 2.9 **%** ± 3.9 positive cells at day 28. Nestin expression reached 62.7 % ± 23.5 at day 4 from 22.3 % ± 27.6 at day 0, after which expression levels did not significantly increase ($p = 0.14$) as determined by ANOVA. Error bars represent 2SE.

5.2.6 Comparison of hESC lines for neuronal differentiation

After developing a successful method of neuronal differentiation, all four hESCs lines were differentiated as outlined in Section 2.10.4. The efficiency of differentiation, neuronal yield and subsequent neuronal functionality between each of the lines were compared to determine whether there was an inherent difference in their response to differentiation, despite all presenting morphological features of pluripotent cell lines.

Differentiation relies on a sequential chain of events to regulate the expression of genes in response to environmental stimuli. Up or down regulation of gene expression is used to regulate the level of RNA which is transcribed and thus control the protein content within a cell. Alterations to the gene and protein expression induce the necessary changes in behaviour and function required for differentiation. Analysis of the changes in gene and protein expression between the four hESC lines was used to compare their responses to neuronal differentiation. Changes in the expression of markers for pluripotency, neural progenitors and mature neuronal markers were monitored, in addition to the comparative functional responses of neurons from each cell line using patch-clamp analysis.

5.2.6.1 In situ immunocytochemistry of neuronal status

Cells undergoing differentiation according to the enhanced EB method were divided into five groups: day 0 – pluripotency, day 4 – after incubation in NI media, day 10 - following attachment in NBD media, day 18 and day 28 – neuronal populations. Undifferentiated day 0 samples positively expressed OCT4, SOX2, TRA-1-60 and SSEA4 (Section 4.2.3) confirming pluripotency. All immunostaining isotype controls were negative.

Similarly to NTERA2, all undifferentiated (day 0) samples stained positively for the neural stem cell marker Nestin (Figure 5.16) but were consistently negative for neuronal markers MAP2, TUBB3 and 70 kDa neurofilament (Figure 5.16), confirming that any increase in these markers was a result of differentiation. Inactivated MEF feeder layers were negative for antibodies used within these samples (*images available upon request*).

Embryoid bodies were plated onto a poly-L-ornithine and laminin coated surface, nine days after induction. By day ten, early signs of neuronal outgrowth were visible. Outgrowing populations stained positively for Nestin, TUBB3 and MAP2 (Figure 5.17).

After 18 days differentiation, all cell lines presented neurons which stained positively for Nestin, TUBB3, MAP2 and Neurofilament (Figure 5.18, Figure 5.19 and Figure 5.20). A

higher proportion of neuronal projections stained positively for TUBB3 and the 70 kDa neurofilament than was seen for MAP2. To confirm that the TUBB3 antibody was neuron specific, samples were co-stained for TUBB3 and the neuron specific 70 kDa Neurofilament, which demonstrated co-expression in all neural projections (Figure 5.19). Neurons were visible in the highest purity from the RH5 TrypLE cell line when compared to the additional three hESC lines. Synaptophysin was sporadically detected amongst day 18 neurons but in the absence of a positive control, it was not possible to determine whether fluctuations in synaptophysin were a true result or whether they were due to poor antibody specificity.

Day 28 differentiated neurons also retained positive expression for TUBB3, MAP2, and Neuroflament (Figure 5.21 and Figure 5.22). Synaptophysin expression remained sporadic amongst the neuronal populations (Figure 5.22). Positive Nestin expression was also detected amongst the day 28 neuronal samples (Figure 5.22), which was unexpected due to the apparent loss of Nestin in post-mitotic neurons (Lendahl et al., 1990)

The neuronal identity of differentiated populations at day 28 was screened according to Tyrosine hydroxylase (TH; for dopaminergic neurons), Serotonin (SERT; serotonergic neurons) and GABA (GABAergic neurons). A proportion of day 28 neurons stained positively for GABA in all cell lines except Shef3, where no staining for mature neuronal phenotypes was identified. Neurons from all hESCs were negative for TH and SERT (Figure 5.23). GABA was detected in day 18 samples but not in day 10 (Figure 5.17), suggesting that neurons were immature at this stage of differentiation. Day 28 neurons in all hESCs lines were negative for OCT4 (*images available upon request*).

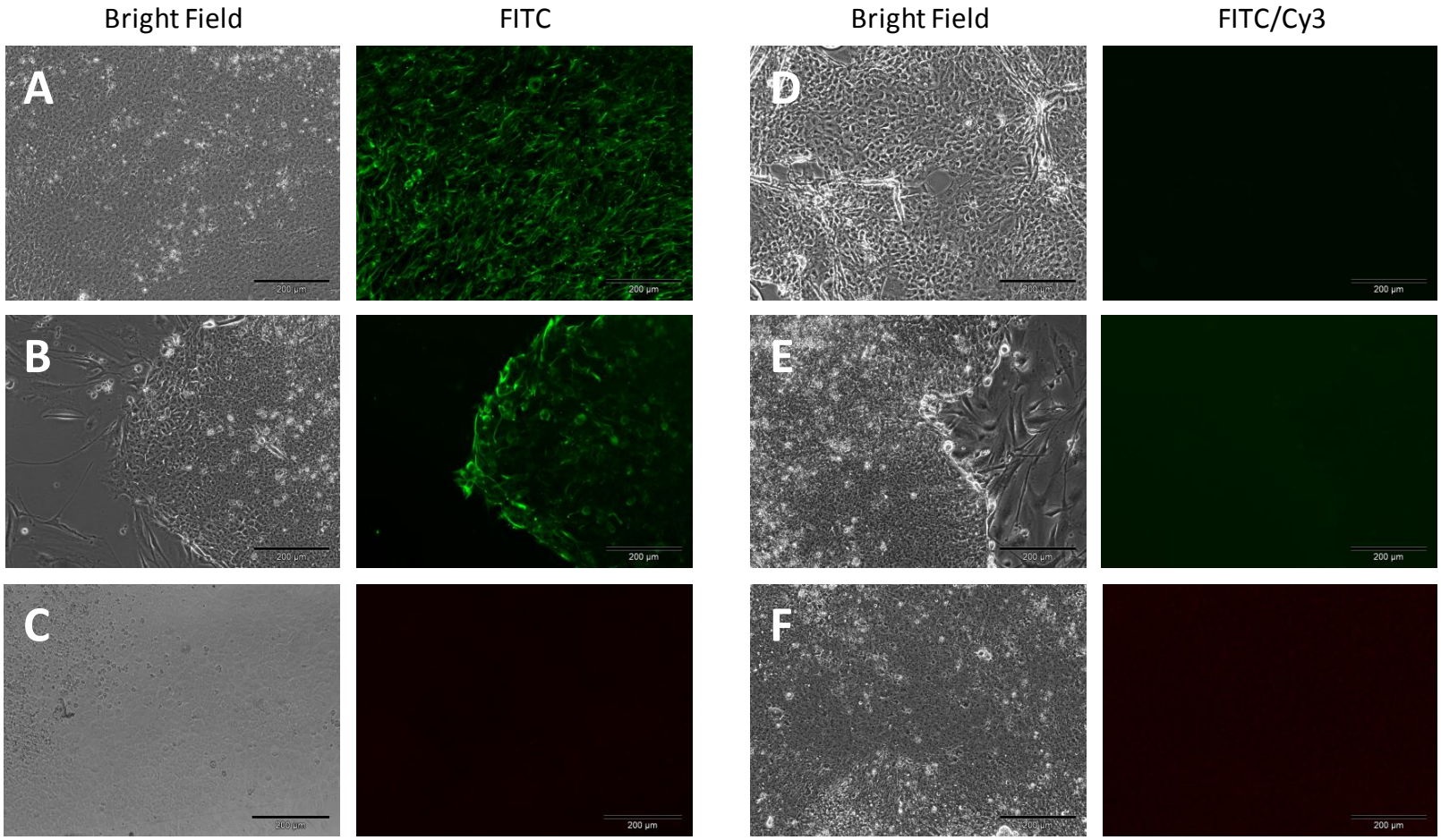

Figure 5.16. Immunostaining for Nestin in pluripotent hESCs

Representative images of hESC staining for Nestin (green) which was positive in all hESC lines; Shef3 (A; x10 magnification) and RH5 cut (B; x10 magnification). Staining for TUBB3 (D; HUES7, x10 magnification), MAP2 (E; RH5 cut, x10 magnification) and 70 kDa Neurofilament (F; Shef3, x10 magnification) were negative in all undifferentiated cells. Mouse IgG (C) isotype controls were negative. Mouse embryonic feeder layer were also negative for the above antibodies.

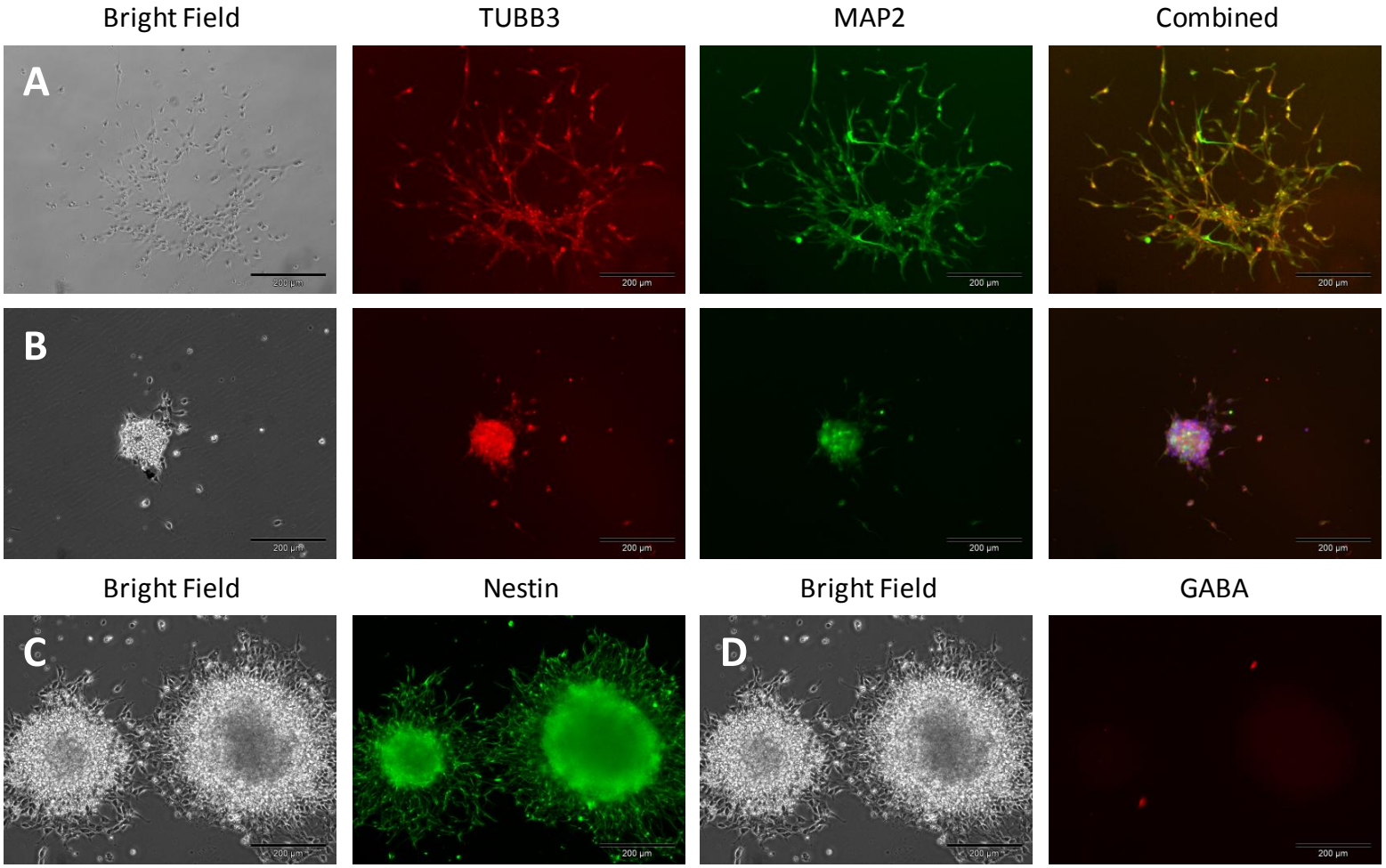

Figure 5.17. Attached embryoid bodies with neuronal outgrowth at day 10.

Cells from attached and spreading EBs staining positively for neuronal markers; TUBB3 and MAP2 (A - Shef3, and B – HUES7), and neural stem cell marker; Nestin (C – RH5 cut). No positive staining for GABA (D) was detected in cells after 10 days neural induction. Images were captured under x10 magnification. Isotype controls were negative.

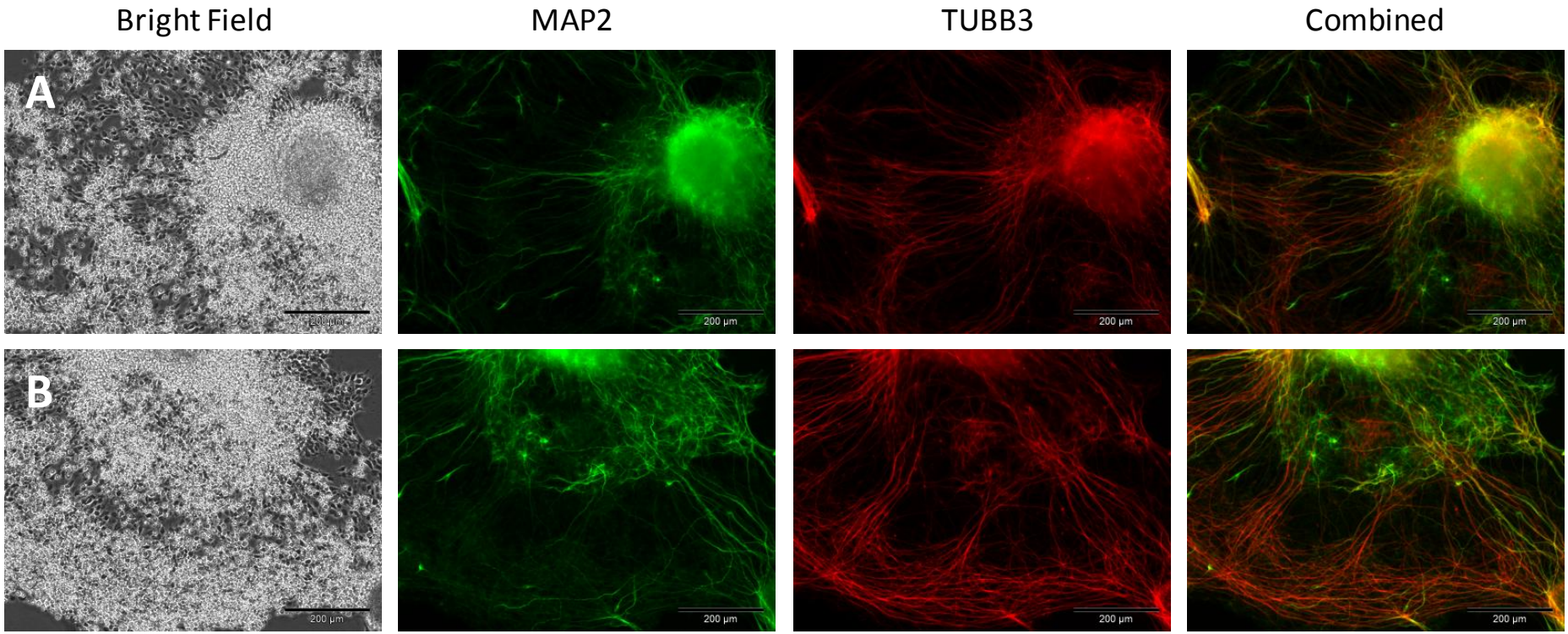

Figure 5.18. Immunostaining of hESCs on day 18; MAP2 and TUBB3.

Representative images for all for cell lines (A-B = Shef3). Images captured under x10 magnification. A larger proportion of the cells expressed neuronal marker TUBB3 than MAP2. Dual staining was visible in some cells as highlighted yellow in combined images. Isotype controls were negative.

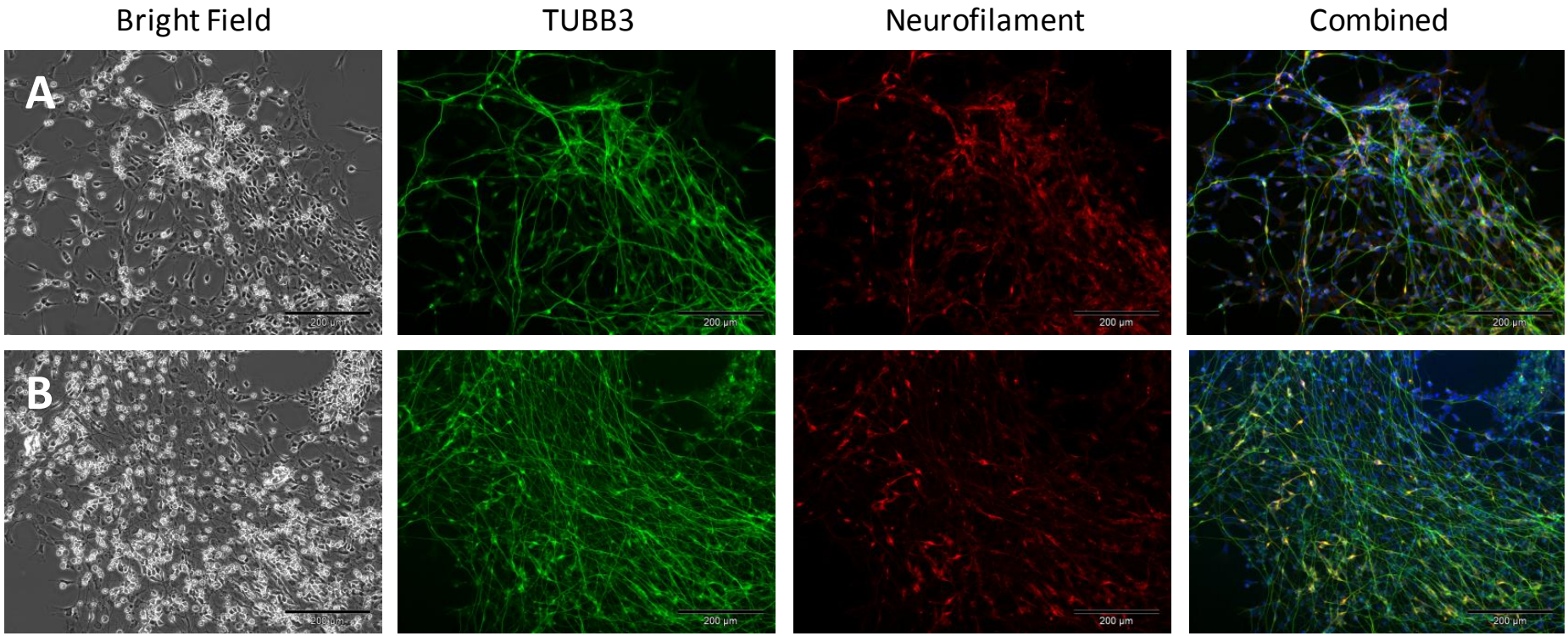

Figure 5.19. TUBB3 and Neurofilament in day 18 hESC derived neurons.

RH5 TrypLE (A-B). Combined images include Hoechst staining, demonstrating the high neuronal yield and purity in the RH5 TrypLE cell line, following 18 days neuronal differentiation and co-expression of TUBB3 and Neurofilament in neural projections. Isotype controls were negative. Images captured under x10 magnification.

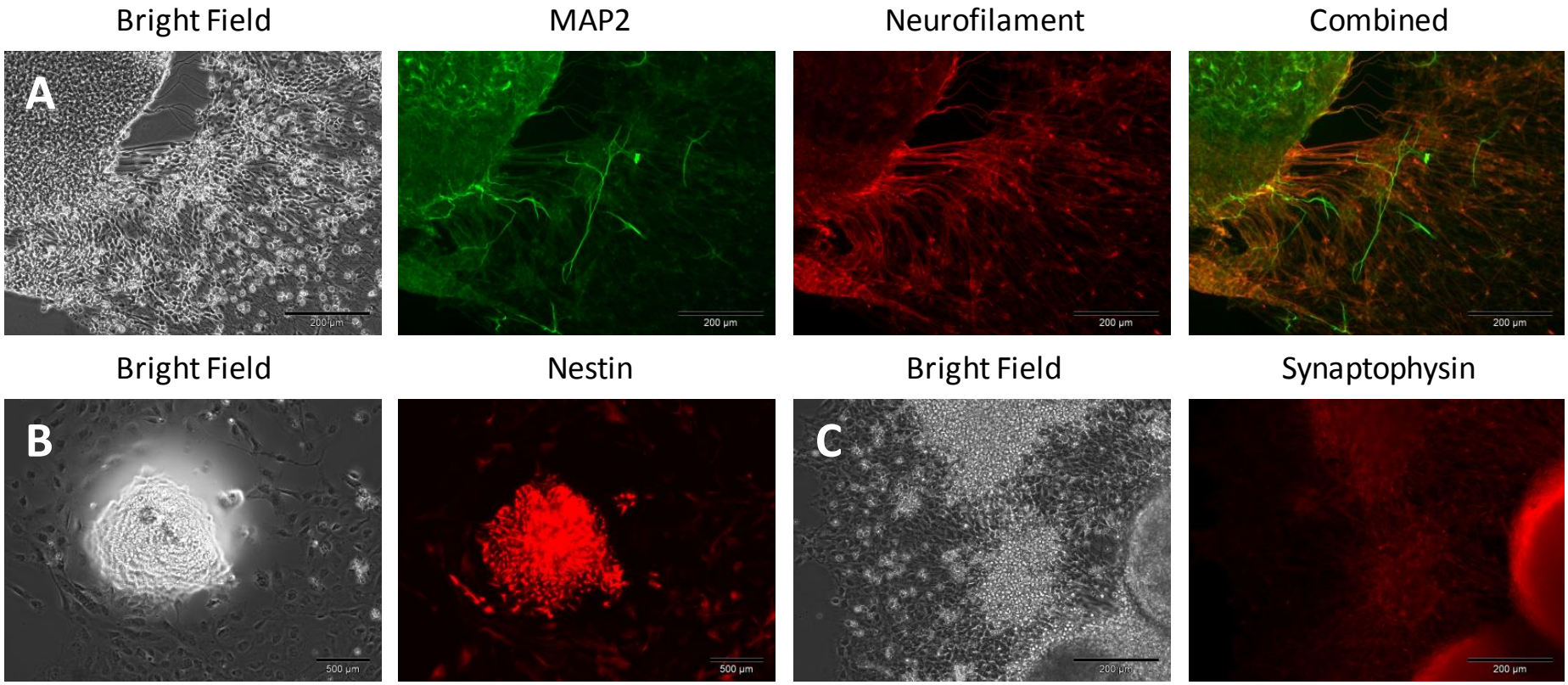

Figure 5.20. Synaptophysin, MAP2, Nestin and Neurofilament in day 18 neurons.

Representative images for all four hESC lines. Neural projections stained positively for Neurofilament (red) and MAP2 (green; A - RH5 cut). Higher Neurofilament expression was detected than MAP2. Neurons remained positive for Nestin (B - HUES7). Synaptophysin was sporadically detected in samples at day 18 (C - RH5 cut), although this followed trouble with the primary synaptophsyin antibody dilutions, which would need to be repeated for confirmation of expression levels. Isotype controls were negative. Images captured under x10 magnification.

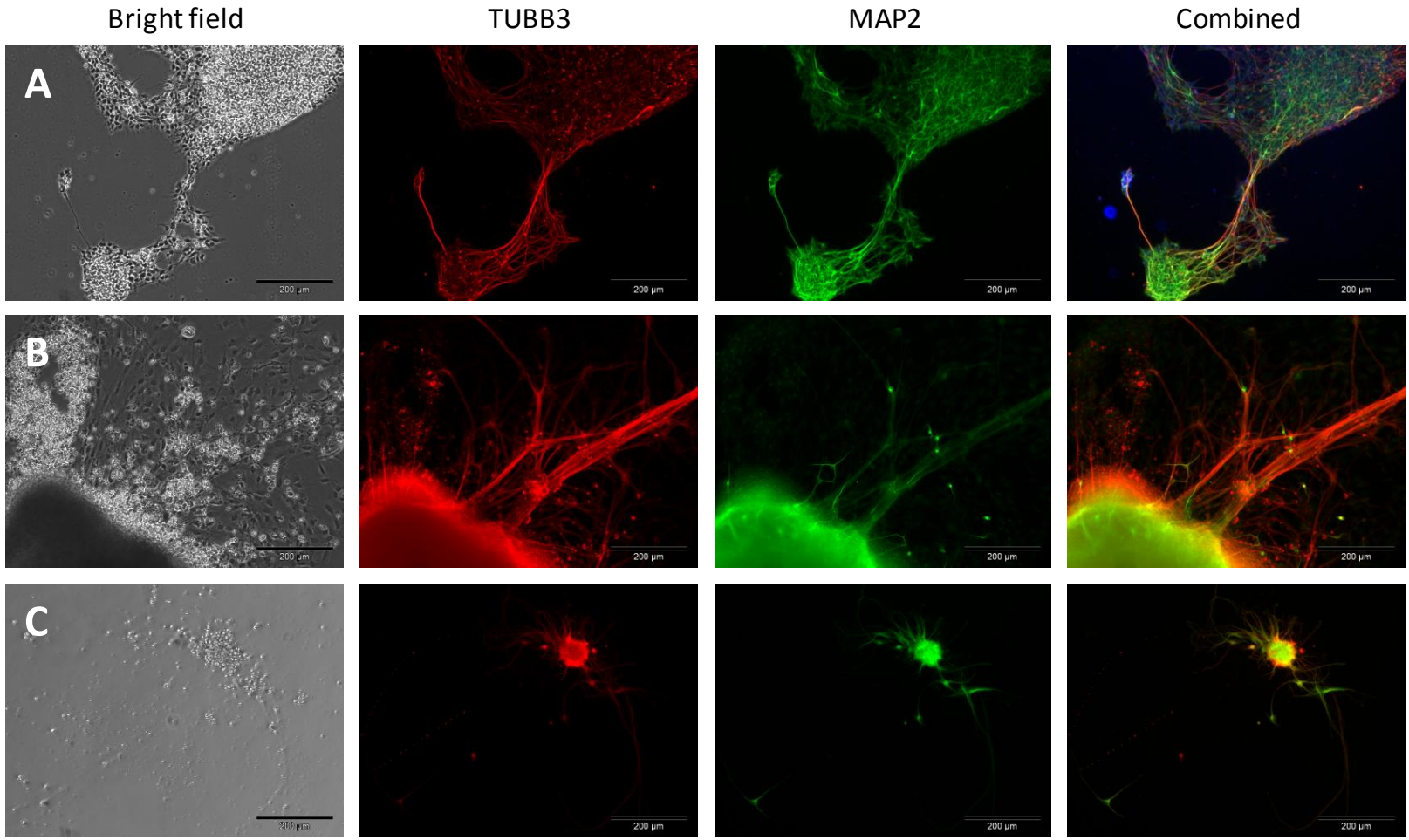

Figure 5.21. Immunostaining of hESCs on day 28; TUBB3 and MAP2.

A – HUES7, B – Shef3, C – RH5 cut. Neruons were identified which stainiend positive for TUBB3 and/or MAP2 after 28 days neuronal differentiation. Higher expression of TUBB3 was detected than MAP2 throughout all populations. Representative images for 4 cell lines, Isotype controls were negative. Images captured under x10 magnification.

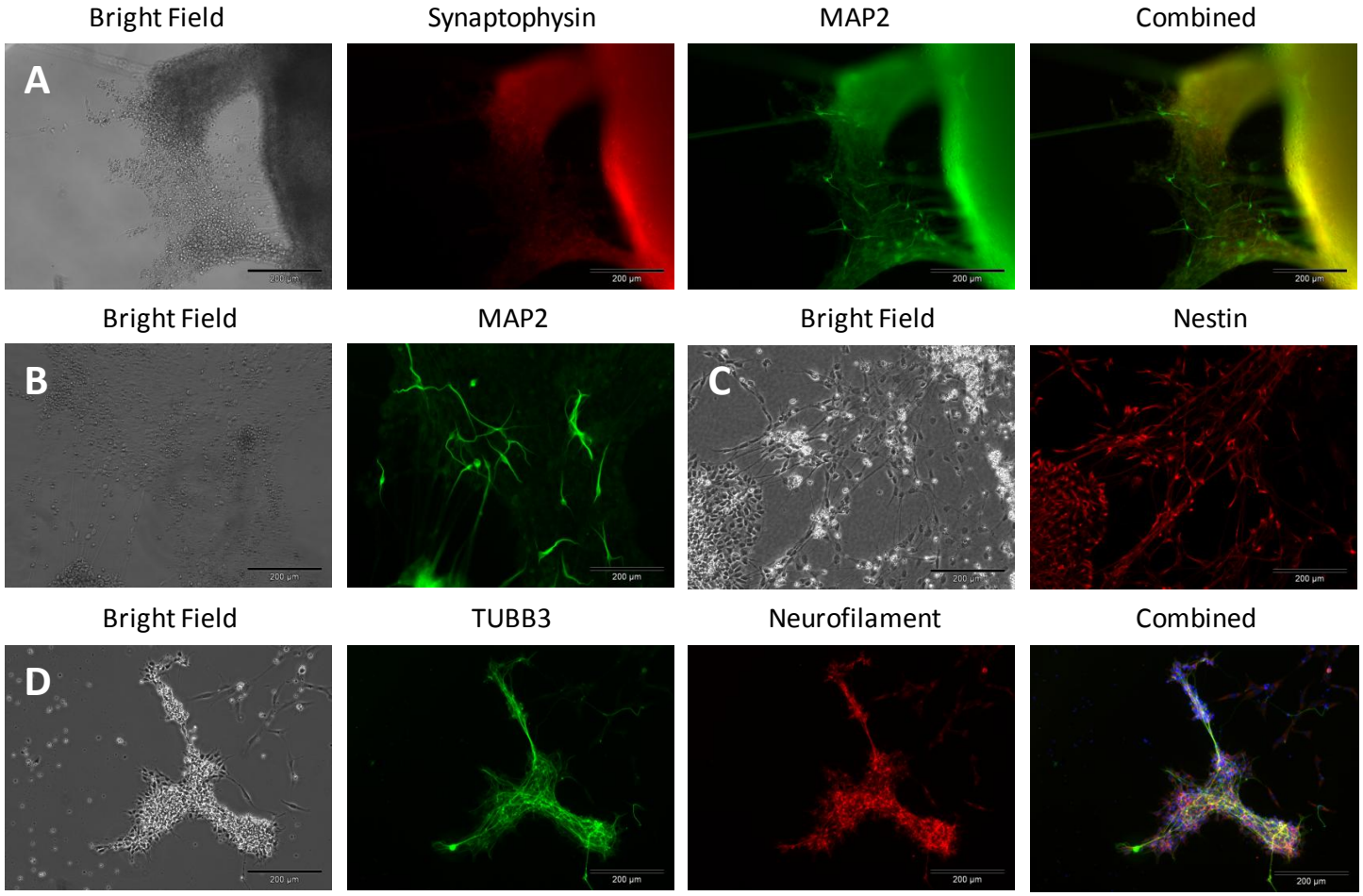

Figure 5.22. Synaptophysin, MAP2, Nestin and TUBB3 in day 28 neurons.

A – Shef3, B – RH5 TrypLE, C – RH5 TrypLE, D – HUES7. Images captured under x10 magnification. Positive staining for Nestin, MAP2 and TUBB3 was detected throughout neuronal populations. Synaptophysin expression was weakly detected in day 28 samples, although positive staining was not detected in all day 28 repeated samples. Representative images for all 4 cell lines. Isotype controls were negative.

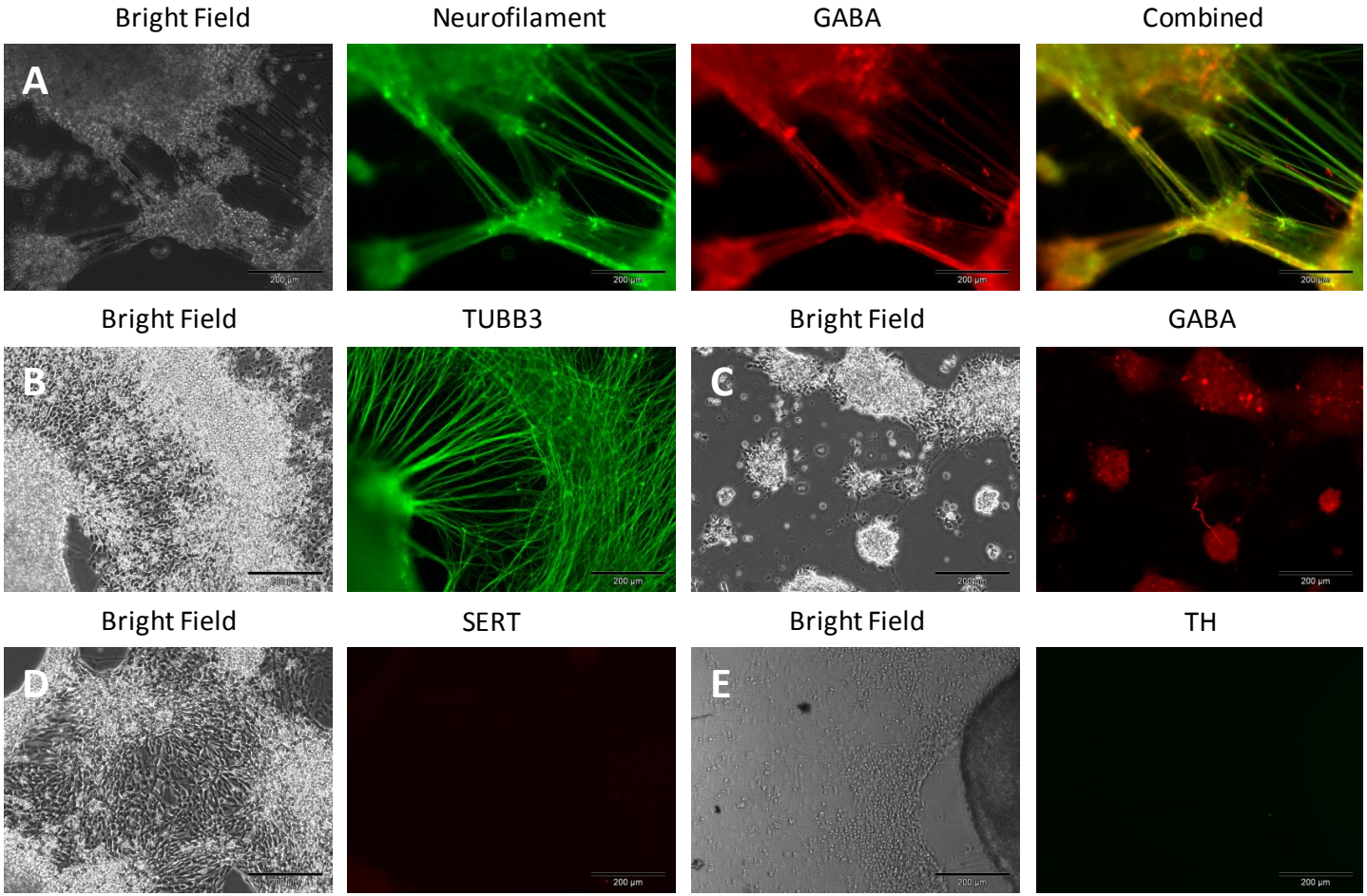

Figure 5.23. Neurofilament, GABA, TUBB3, Serotonin and TH in day 28 neurons.

A – RH5 cut, B – RH5 TrypLE, C – HUES7, D – RH5 TrypLE, E – RH5 TrypLE. Positive staining for Neurofilament was detected in all neuronal projections. GABA was detected in a proportion of neurons but all neurons were negative for TH and SERT at day 28. Representative images for all 4 cell lines. Isotype controls were negative. Images captured under x10 magnification.

5.2.7 Functionality of hESC derived neurons

It was clear from the immunostaining that all four hESC lines were capable of generating neurons as characterised by morphology according to Figure 3.3. To determine whether there was any difference in the functional behaviour of the four cell lines, cells were analysed using a patch-clamp.

Neurons derived from all four cell lines reproducibly fired APs following stimulation which were and reversibly inhibited by TTX. Due to time constraints on the equipment, it was not possible to test for recovery of HUES7 derived neurons to TTX inhibition. In the absence of these data, inhibition of APs due to cell death by TTX toxicity, rather than blockage of Na^+ channels cannot ruled out. However, neurons from all other lines recovered functional activity which would suggest TTX was not toxic to these neurons in culture, and that the HUES7 neurons would also have recovered with sufficient time. Preliminary calcium imaging data on Shef3 derived neurons confirmed the presence of voltage-gated ion channels.

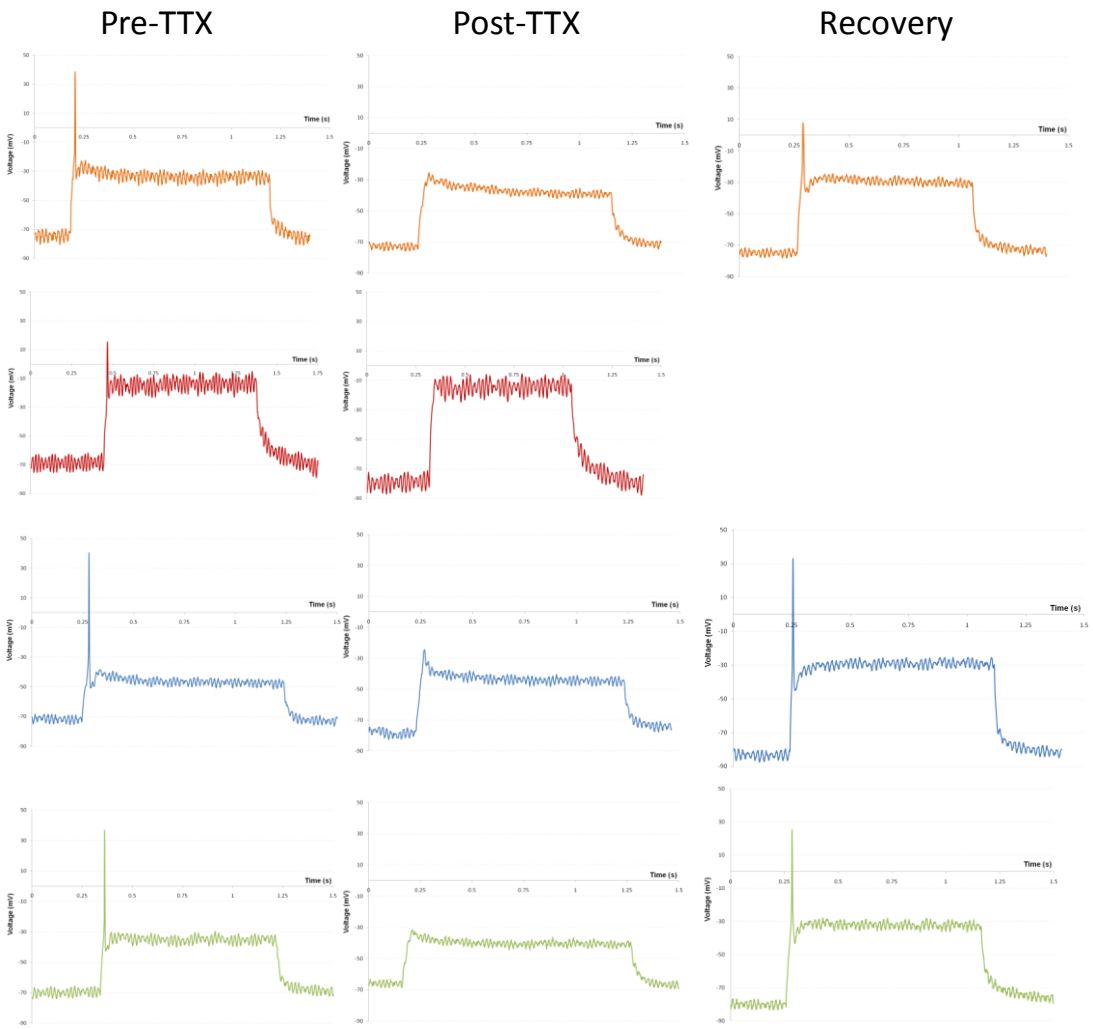

Figure 5.24. Patch clamping hESCs.

Neurons derived from all four hESC lines Shef3 (orange), HUES7 (red), RH5 cut (blue) and RH5 TrypLE (green), successfully fired sodium action potentials following manual depolarisation which were inhibited by TTX. Recovery of APs was observed following a five minute wash step with HBS buffer. *Example graphs presented for each cell line, recovery data for HUES7 was not available*.

5.2.8 Gene expression

No real difference was observed between the morphology of the neurons derived from each of the four hESC lines. However, there were clear differences in the response of each of these lines to neuronal differentiation which impacted up on the final neuronal yield. In an attempt to understand the different responses by these four hESC lines, a comparative study of the changes in gene expression in response to differentiation was carried out. Gene expression analysis monitors fluctuations in the levels of mRNA within a sample; therefore analysis was carried out using RT-PCR (Section 1.5.3).

5.2.8.1 RNA extraction

Total RNA was extracted as described in Section 2.12.1, using a column based method. The quality of RNA extracted was of key importance to ensuring a true representation of gene expression within a population of cells, therefore all RNA extractions and RT-PCRs were carried out in a clean pre-PCR laboratory using United Kingdom Accreditation Service (UKAS) calibrated equipment assigned for RNA work only. This reduced the risk of PCR-product contamination within the RNA preparations.

Two different spin column RNA extraction kits Qiagen RNeasy and Ambion RNAqueous were compared to identify the most suitable kit for obtaining RNA preparations with highest possible yield and purity. In each case, RNA was extracted following manufacturer's instructions (Sections 2.12.1.1 and 2.12.1.2). Extractions procedures were comparable in time with the exception of the DNase step, where the Qiagen kit included an on-column treatment prior to RNA elution and the Ambion kit required a separate DNase treatment following elution, extending the procedure by an additional 30 minutes.

On-column extraction kits were designed to remove gross gDNA contamination from the RNA elute; however, it is notoriously difficult to remove all traces of gDNA carryover. Less than 1 % contamination of gDNA in an RNA sample is considered to be sufficient for false positive data on gene expression (Dilworth and McCarrey, 1992). Therefore efficiency of gDNA removal in each of the extraction kits was tested using a PCR on from RNA prior to reverse transcription. DNA polymerase is only able to amplify from DNA, therefore any amplified product from the RNA elute would have originated from contaminating gDNA. To further test the efficiency of gDNA removal using DNase, half of each RNA sample was treated with DNase and a PCR run using two different primer pairs, encoding GAPDH and Nestin.

The presence of amplified product in both the Qiagen and Ambion RNA extractions in the absence of a DNase treatment (Figure 5.25) demonstrated the carryover of gDNA following RNA extraction. In DNase treated samples, these bands were absent highlighting the efficacy and requirement of a DNase incubation step prior to reverse transcription. Amplification of more than the single PCR product by both the Nestin and the GAPDH primers, demonstrated that the primers were not specific to the true RNA sequences. Non-specific amplification resulted in a range of products from gDNA amplification, as indicated by the Nestin primers. However, amplification of a product of the expected RNA size was indicative of retrotransposed pseudogene amplification (Section 1.5.3.3), which would confuse quantification of gene expression if gDNA amplification was not avoided.

The relative indifference in RNA extraction between the Qiagen and Ambion kits was further investigated using a minus reverse transcriptase (-RT) control during cDNA synthesis. Two parallel PCR reactions were run with and without reverse transcriptase using Nestin and GAPDH primers. The presence of amplified products in –RT samples was the result of DNA contamination.

All control cDNA samples without DNase treatment or reverse transcriptase, amplified multiple products confirming DNA contamination (Figure 5.26; A: lanes 7 and 11, B: lanes 8 and 12). The presence of reverse transcriptase in each reaction amplified product of the size expected for RNA, demonstrating the efficacy of both the primers and the MMLV-RT. In agreement with result from Figure 5.25, DNase was essential for removing contaminating DNA. No difference between amplification of the Nestin product using the two kits was identified. However, during GAPDH amplification (Figure 5.26; B) the Ambion kit with a separate DNase step removed more of the contaminating DNA than the Qiagen kit, indicated by the absence of a band at ~170 bp in lanes 11 and 13 when compared with lanes 7 and 9 (red arrow). The Ambion RNAqueous kit was therefore considered to be most appropriate and was used for all further RNA isolations. TURBO DNase was used throughout DNase preparations due to its higher affinity for DNA, thus reducing exposure to RNA (RNAqueous user manual, Ambion). DNase treatment was rigorously controlled to ensure consistent exposure across samples for comparison.

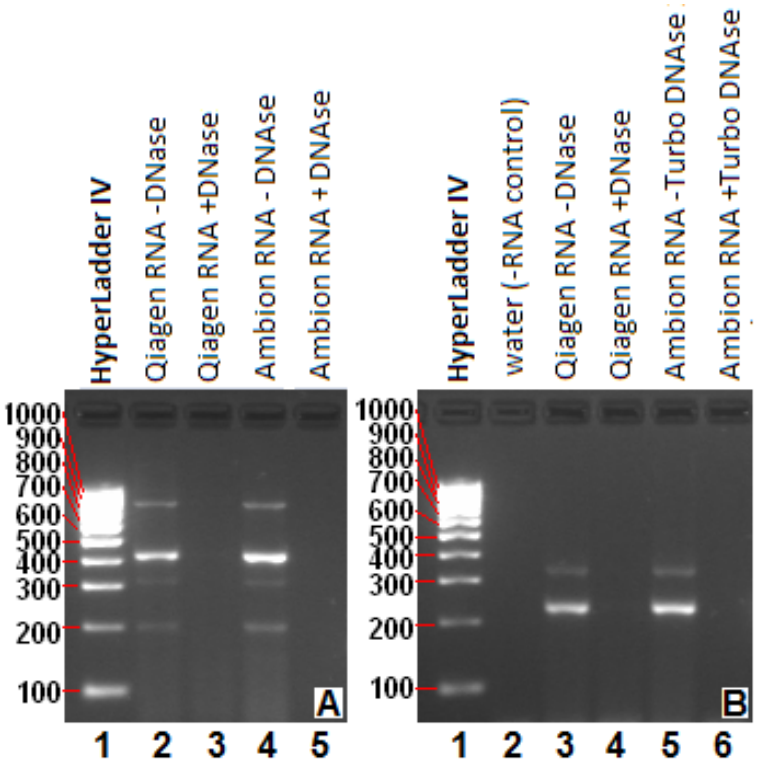

Figure 5.25. PCR amplification from RNA.

Genomic DNA products were amplified by both the Ambion and Qiagen RNA extraction kits, for Nestin (A; RNA - 160 bp, gDNA - 408 bp) and GAPDH (B; RNA – 224 bp, gDNA - 328 bp). Genomic DNA contamination was removed following exposure of RNA to DNase, confirming the requirement for DNase treatment of the RNA sample. Amplification of more than the single product in both Nestin and GAPDH suggests a cross reactivity of primers to alternative gDNA sequences in addition to the true Nestin and GAPDH genes.

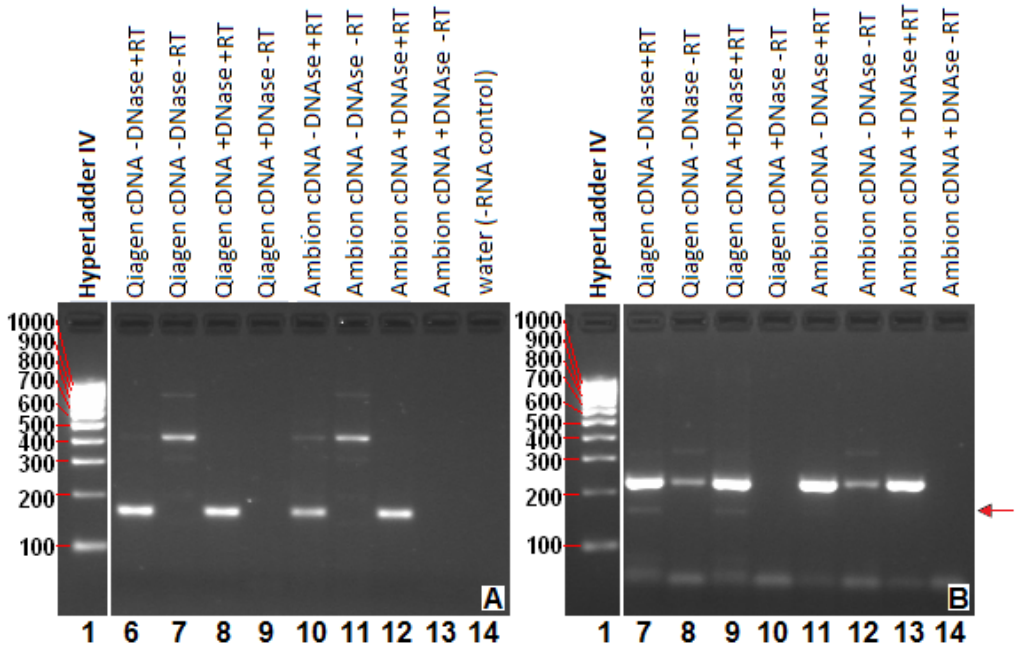

Figure 5.26. The effect of reverse transcriptase.

Nestin (A; RNA - 160 bp, gDNA - 408 bp) and GAPDH (B; RNA – 224 bp, gDNA - 328 bp). In the absence of DNase or reverse transcriptase (RT) gDNA contamination was amplified in all samples (A: lanes 7 and 11, B: lanes 8 and 12). In the presence of RT, expected RNA products were amplified. No difference between Nestin amplification (A) was identified from the Ambion and Qiagen extraction kits. During GAPDH amplification (B), the Ambion kit with separate DNase removed more gDNA than the Qiagen, indicated by the absence of a band at ~170 bp in lanes 11 and 13 when compared with lanes 7 and 9 (red arrow).

5.2.9 Reverse transcription-PCR

Reverse transcription PCRs were carried out on pluripotent and differentiating samples from all hESC lines to compare changes in gene expression throughout differentiation across the four hESC lines.

Primers were designed according to Section 2.12.4 to amplify the pluripotency genes; OCT4, Nanog, SOX2, and neural genes; Nestin, TUBB3, MAP2, PAX6, SOX1, and synaptophysin (Table 5.2). Where possible, primers were designed to span exon-exon junctions, avoiding amplification from contaminating DNA. However. the SOX family of genes are encoded by a single exon, therefore it was not possible to design primers which were specific to the cDNA of the mRNA transcript. In addition, there is a large repeated sequence which is present in a large proportion of the SOX genes, meaning that accurate sequence alignments and BLAST searches was essential for these genes to ensure amplification of the correct GOI.

Primer	RNA product (bp)	gDNA product (bp)
GAPDH	240	not amplified
OCT4	43	not amplified
Nanog	147	not amplified
Sox2	71	71
Sox1	71	71
Nestin	203	not amplified
Pax6	88	not amplified
MAP2	137	not amplified
TUBB3	132	not amplified
Synaptophysin	145	not amplified

Table 5.2. Expected product size for designed primers.

Where possible primers were designed to be RNA specific, crossing exon-exon junctions to prevent gDNA amplification. This was not possible for SOX genes which contain just a single exon.

5.2.9.1 Optimising PCR conditions

Each new primer pair was checked for amplified product size and the optimum annealing temperature using a gradient PCR ranging from 50 °C to 65 °C, according to methods outlined in Section 2.12.5. PCR products were subjected to agarose gel electrophoresis (Section 2.12.7) and the bands analysed with the aid of a DNA size marker. MAP2 and

TUBB3 primer pairs amplified the cDNA product of the expected product size: 137 bp and 132 bp respectively (Figure 5.27). The annealing temperature did not appear to affect amplification for MAP2. However, primer dimers were formed at all temperatures, visible by the consistent small band at the base of the agarose gel (Figure 5.27A). Primer dimers form when the forward and reverse primers, each 20 bp in length bind together. Formation of these dimers can interfere with amplification of the GOI, making these primers unsuitable for other applications such as Q-PCR reactions due to fluorescence interference, these MAP2 primers were subsequently re-designed.

The TUBB3 primer pair amplified products of the expected size across the temperature gradient (Figure 5.27B). Amplification was optimal at annealing temperatures below 62.7 °C, where brighter bands were visible (indicating more product amplification). Minimal primer dimer formations were detected using annealing temperatures above 62.7 °C. These primers were used for further PCR analysis.

During amplification of the SOX1 and SOX2 genes control samples without reverse transcriptase were included in the temperature gradient study to ensure amplification was cDNA specific (Figure 5.28). Both SOX1 and SOX2 primers amplified products of the expected 71 bp size. Amplification of the SOX1 product (Figure 5.28A) was most affected by annealing temperature, amplifying well at low temperature (50 - 52.5 °C) but failed to amplify at temperatures any higher. An additional band was amplified across all samples (including control samples without RNA or cDNA, suggesting contamination of the PCR reagents. Fresh reagents were ordered for future reactions. SOX2 primers amplified the correct product size but primer dimers formed throughout the temperature gradients (Figure 5.28B), suggesting that primer sequence optimisation was required. The absence of amplified product at 71 bp in the first three lanes for each reaction confirmed removal of DNA contamination from the samples.

In addition to designing primers, the primer sequence for GAPDH was taken from an earlier publication (Anisimov et al., 2007). These primers amplified the expected 240 bp product (Figure 5.29A); however, an additional an unexpected product was also amplified around 75 bp in size. This product was later identified to correlate with one of the many GAPDH pseudogenes, highlighting the importance of checking a primer sequence before use, and the requirement for specificity in design.

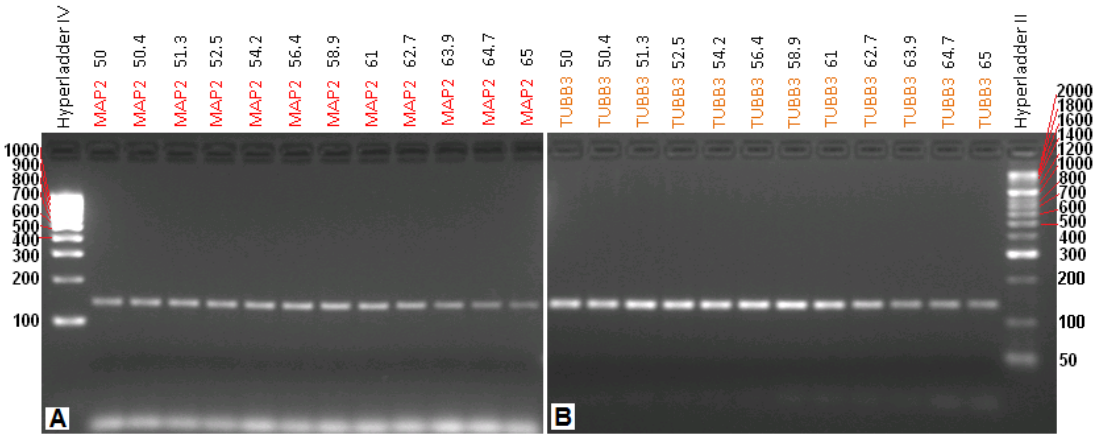

Figure 5.27. Optimising PCR conditions for MAP2 and TUBB3 primers

Both MAP2 (left) and TUBB3 (right) primers amplified product of the expected size for RNA. Primer dimer formation across the temperature gradient for MAP2 rendered these primers unsuitable for further PCR analysis. Clean amplification of TUBB3 with no additional products below 62.7 °C confirmed suitability of these primers for both RT-PCR and Q-PCR analysis.

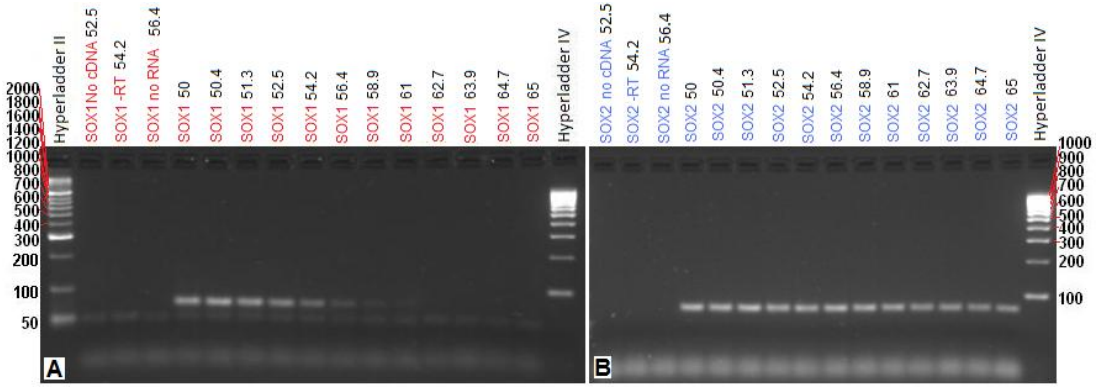

Figure 5.28. Optimising PCR for SOX1 and SOX2 primers.

SOX1 (left) and SOX2 (right) primers amplified the expected 71 bp RNA products. Amplification of SOX1 was achieved at lower annealing temperature (50 - 52.5 °C). An additional band was amplified across all samples (including control), indicating contamination of the PCR reagents. SOX2 primers also amplified the expected 71 bp product size but primer dimers formed throughout. Water and -RT controls confirmed the absence of contaminating DNA.

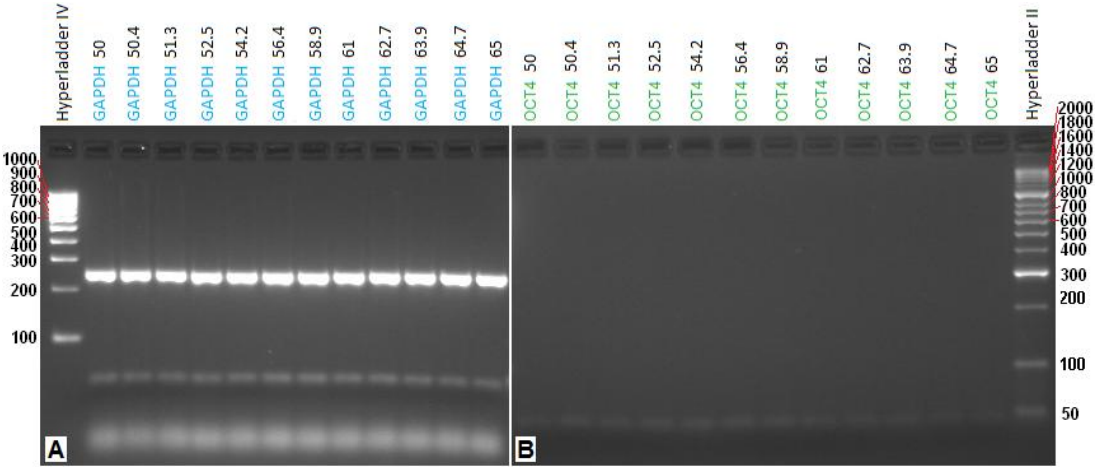

Figure 5.29. Optimising PCR conditions for GAPDH and OCT4 primers.

Both GAPDH (left) and OCT4 (right) amplified product of the expected size for RNA. In GAPDH amplification was not specific for the RNA product resulting in amplification of an additional product around 75 bp in size. Primer dimers were also visible at all annealing temperatures rendering these primers unsuitable for further PCR analysis. Amplification of the expected 43 bp OCT4 RNA product was considerably less than expected suggesting inefficient annealing of the primers across the investigated annealing temperature range.

The OCT4 primers were used in a PCR amplification cDNA from pluripotent hESCs (according to guidelines set out in Section 4.2.1). Amplification resulted in a product at 43 bp corresponding to the expected mRNA nucleotide sequence (Figure 5.29B); however, this band was considerably less intense than all other samples. The OCT4 primers was designed to span exon junctions and specifically bind only the true pluripotency mRNA nucleotide sequence, excluding amplification from alternative OCT4 splice variants and pseudogenes. It may have been that OCT4 expression was lower than expected; however, a more likely explanation it that the primers did not work and that the detected product was a result of primer dimer formation. Unsuccessful amplification of the OCT4 product, rendered them unsuitable for analysis of pluripotency and alternative OCT4 primers were subsequently designed.

5.2.10 Gene expression analysis by semi-quantitative

Following optimisation of each of the primer pairs (including re-design where necessary) RT-PCR reactions were carried out on cDNA from differentiated samples to identify when pluripotency genes (OCT4 and Nanog) were down regulated and neural stem cell genes (SOX1 and Nestin) and neuron specific genes (TUBB3, SYP and MAP2) were up regulated through differentiation. Total RNA was extracted at day 0, 4, 10 and 18 (Section 2.12.1.2), reverse transcribed (Section 2.12.3) and RT-PCR carried out (Section 2.12.5). Control samples without cDNA and in the absence of reverse transcriptase were run for each reaction. The RT-PCR amplified products were size separated by agarose gel electrophoresis (Figure 5.30; OCT4, Nanog, SOX1, TUBB3 and SYP).

Despite a clear loss of pluripotent morphology and a gain in neuronal identity, the band intensity of pluripotency genes Nanog and OCT4 was only slightly reduced in day 18 samples compared to day 0, 4 and 10 (Figure 5.30A-B). Expression of OCT4 and Nanog was expected to decrease following induction of differentiation, to undetectable levels by day 18 in correlation with immunostaining data (Section 5.2.6.1). It was also unexpected to detect high expression levels of the neuron specific genes TUBB3 and SYP in day 0 and 4 samples (Figure 5.30D-E), due to their absence in pluripotent populations.

SOX1 is involved in early neuroectodermal commitment (Pevny et al., 1998), yet its expression was consistently detected throughout differentiation using RT-PCR (Figure 5.30C). This could be explained if the pluripotent population were in very early stages of

lineage commitment or if the primers were poorly designed with cross reactivity between the range of SOX genes, due their similarity of mRNA nucleotide sequence. Synaptophysin was expressed in all samples but was up regulated in the day 18 samples, correlating with neuronal maturation; this was the only gene which presented a clear change in expression throughout differentiation using RT-PCR amplification (Figure 5.30E).

Consistent detection of these genes across all differentiation samples was considered to be a result of the RT-PCR process. With each successive PCR cycle, the amount of amplified product increased exponentially. After a certain number of cycles, amplification was limited by PCR reagents/polymerase enzyme and plateaux out to a constant level. Therefore, with excess PCR cycles a single cDNA would be detected as the same intensity as a highly expressed transcript. For SYP which is present only in the membrane of mature synaptic vesicles, gene expression would have been extremely low (undetectable) in pluripotent populations and would have increased throughout differentiation according to neuronal maturation. Using RT-PCR, it was not possible to quantify these expression changes and to address this, efforts were transferred to quantitative-PCR (Q-PCR) analysis.

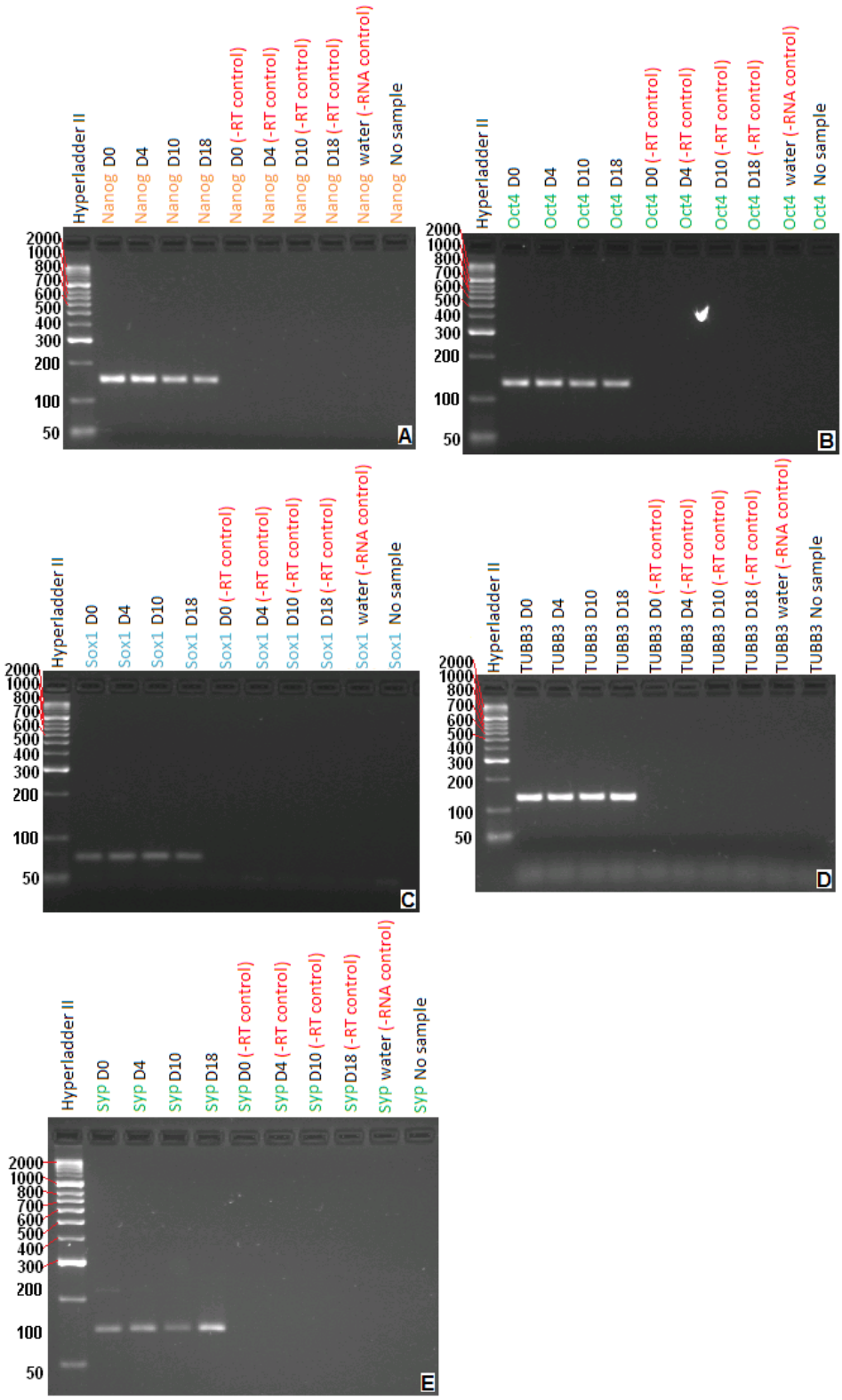

Figure 5.30. RT-PCR for OCT4, Nanog, SOX1, TUBB3 and SYP in differentiating hESCs.

RT-PCR for OCT4, Nanog, SOX1, TUBB3 and SYP each generated product of the expect band size (130, 147, 71 and 132 bp respectively). All controls samples were negative proving amplification from cDNA only. However, despite a slight drop in intensity of OCT4 and Nanog amplification by the day 18 sample, no real change in the levels of expression of these genes was detected throughout differentiation using RT-PCR. Expression of the neural gene SOX1 and the neuronal gene TUBB3 was detected in all differentiating samples, including day 0 samples were no cells of neural morphology were visible. Amplification of differentiating hESCs using primers for SYP showed an increase in SYP expression of the expected 145 bp product, during the latter stages of differentiation, corresponding to neuronal maturation. All control samples were negative.

5.2.11 Q-PCR - low density array cards

Q-PCR analysis was carried out using a low density array cards. The human pluripotency gene low density array cards were designed by Applied Biosystems (ABI; California, USA) and incorporated into the first ISCI study in 2007 for comparison of gene expression profiles across 59 hESC lines (Adewumi et al., 2007). Throughout this study, these LDA cards were used to quantify changes in expression of genes involved in pluripotency, and neural commitment throughout the five major differentiation time points (day 0, 4, 10, 18 and 28). Analysis was carried out using just 50 ng cDNA per sample, thus greatly reducing the sample size required for screening when compared to standard Q-PCR analysis.

5.2.11.1 Confirming reproducibility across LDA cards

To ensure differences in the samples were a result of differentiation rather than variability between cards, a single pluripotent hESC cDNA preparation was repeated across three lanes of an LDA card, and compared to cDNA from 2102Ep as a positive control. Across all the genes screened for pluripotency and differentiation, the average variability in Ct values was 0.53 ± 0.12, less than one amplification cycle, confirming reproducibility across the cards. Due to the high cost of the LDA cards, analysis of triplicate samples across cards was not carried out but reassurance of reproducibility between LDA cards was taken from the QC procedures during manufacture which demonstrated high reproducibility (*personal communication and data supplied by Ms. K. Warrington, ABI*).

5.2.11.2 Identifying a suitable endogenous control gene

Changes in gene expression were calculated using the $2^{-\Delta\Delta Ct}$ method (Section 1.5.3.4). The fold change in expression of the GOI was normalised to an endogenous control gene, relative to expression at day 0. LDA cards were processed for all samples before assigning an endogenous control. The endogenous control gene was calculated as the gene with minimum variation in Ct value throughout differentiation in all of the cell lines. The median Ct values were calculated for each gene and cell line, throughout differentiation and biological replicates, and aligned from lowest to highest.

A Ct value of 40 was assumed to be unexpressed (MYF5 and GCM1). Expression of 18S, GADPH and ACTB were the three highest expressed genes across the four hESC lines. Genes with low expression (Ct ≥ 30) were excluded from the endogenous control selection,

due to high error margins in the expression of these genes. This identified 30 genes which were expressed at suitable levels for further analysis of variability in Ct (Max Ct – Min Ct; Table 5.3). These values were determined separately for each hESC line. Genes with minimum variation in Ct value throughout differentiation and biological replicates (< 3 Ct) in all hESC lines were identified as GAPDH, ACTB and RAF1 (Table 5.3; red). The remaining genes were considerably more variable and were subsequently excluded from further analysis. Although ACTB and RAF1 occasionally showed lower variation in Ct values for individual cell line repeats, GAPDH was minimally variable for all cell lines, with the lowest maximum variation of 2.37 Ct values. GAPDH was therefore assigned as the most suitable gene for use as the endogenous control, remembering that ΔCt values ≤ 2.37 for Shef3, ≤ 2.12 for RH5 TrypLE, ≤ 1.98 for HUES7 TrypLE and ≤ 1.77 for RH5 cut, could not be assumed true changes in gene expression due to internal variation in the endogenous control.

Data for changes in gene expression of three commonly used Q-PCR endogenous control genes; 18S, ACTB, GAPDH in addition to RAF1 (identified in these samples as stably expressed) were combined for the four cell lines to demonstrate stability in expression throughout differentiation. Expression levels were not significantly variable throughout differentiation as determined by AVOVA ($p = 0.512$, 0.762, 0.314 and 0.960, for 18S, ACTB, GAPDH and RAF1 respectively; Figure 5.31).

Line	gene	Max Ct – Min Ct across differentiation and repeats
HUES7 tryple	18S	2.371019
RH5 cut	18S	3.818019
RH5 tryple	18S	6.237662
Shef3 cut	18S	5.037742
HUES7 tryple	ACTB	2.382473
RH5 cut	ACTB	2.870308
RH5 tryple	ACTB	2.31509
Shef3 cut	ACTB	1.575149
HUES7 tryple	AFP	7.360128
RH5 cut	AFP	6.47186
RH5 tryple	AFP	13.298605
Shef3 cut	AFP	11.288266
HUES7 tryple	BRIX	2.532546
RH5 cut	BRIX	3.740488
RH5 tryple	BRIX	1.718741
Shef3 cut	BRIX	1.800275
HUES7 tryple	CD9	5.178489
RH5 cut	CD9	3.504261
RH5 tryple	CD9	5.263254
Shef3 cut	CD9	3.010959
HUES7 tryple	COL1A1	4.173062
RH5 cut	COL1A1	3.533123
RH5 tryple	COL1A1	10.548433
Shef3 cut	COL1A1	5.857698
HUES7 tryple	COLA2A1	5.280939
RH5 cut	COLA2A1	4.586706
RH5 tryple	COLA2A1	10.101187
Shef3 cut	COLA2A1	6.635119
HUES7 tryple	CRABP2	3.100614
RH5 cut	CRABP2	2.010749
RH5 tryple	CRABP2	3.217194
Shef3 cut	CRABP2	1.888994
HUES7 tryple	CTNNB1	3.091623
RH5 cut	CTNNB1	1.848331
RH5 tryple	CTNNB1	2.920311
Shef3 cut	CTNNB1	1.946844
HUES7 tryple	DNMT3B	5.561177
RH5 cut	DNMT3B	6.232057
RH5 tryple	DNMT3B	6.746884
Shef3 cut	DNMT3B	6.896215

Line	gene	Max Ct – Min Ct across differentiation and repeats
HUES7 tryple	FN1	4.429905
RH5 cut	FN1	2.758682
RH5 tryple	FN1	5.737585
Shef3 cut	FN1	3.265968
HUES7 tryple	FOXD3	4.874696
RH5 cut	FOXD3	5.525645
RH5 tryple	FOXD3	3.098529
Shef3 cut	FOXD3	4.588144
HUES7 tryple	GABRB3	4.223007
RH5 cut	GABRB3	3.709299
RH5 tryple	GABRB3	3.886524
Shef3 cut	GABRB3	4.687573
HUES7 tryple	GAL	11.364713
RH5 cut	GAL	8.621433
RH5 tryple	GAL	10.680534
Shef3 cut	GAL	8.002324
HUES7 tryple	GAPDH	1.984163
RH5 cut	GAPDH	1.774199
RH5 tryple	GAPDH	2.124784
Shef3 cut	GAPDH	2.37153
HUES7 tryple	IFITM1	6.606448
RH5 cut	IFITM1	3.384272
RH5 tryple	IFITM1	5.614742
Shef3 cut	IFITM1	4.034235
HUES7 tryple	IFITM2	3.394109
RH5 cut	IFITM2	3.299866
RH5 tryple	IFITM2	2.501106
Shef3 cut	IFITM2	1.313399
HUES7 tryple	IMP2	3.532192
RH5 cut	IMP2	5.980346
RH5 tryple	IMP2	1.898939
Shef3 cut	IMP2	2.120135
HUES7 tryple	LAMB1	4.611481
RH5 cut	LAMB1	4.033489
RH5 tryple	LAMB1	2.43306
Shef3 cut	LAMB1	2.218597
HUES7 tryple	LAMC1	3.236291
RH5 cut	LAMC1	3.527588
RH5 tryple	LAMC1	5.21939
Shef3 cut	LAMC1	3.153822

Line	gene	Max Ct – Min Ct across differentiation and repeats
HUES7 tryple	LIN28	6.417068
RH5 cut	LIN28	4.595346
RH5 tryple	LIN28	4.19513
Shef3 cut	LIN28	6.866551
HUES7 tryple	NES	1.779337
RH5 cut	NES	3.123269
RH5 tryple	NES	3.139637
Shef3 cut	NES	2.450606
HUES7 tryple	NOG	2.636833
RH5 cut	NOG	3.601334
RH5 tryple	NOG	6.463183
Shef3 cut	NOG	4.322112
HUES7 tryple	PAX6	9.144992
RH5 cut	PAX6	4.63686
RH5 tryple	PAX6	10.461065
Shef3 cut	PAX6	7.584847
HUES7 tryple	PODXL	6.032442
RH5 cut	PODXL	6.475205
RH5 tryple	PODXL	7.893104
Shef3 cut	PODXL	5.021003
HUES7 tryple	PTEN	2.723984
RH5 cut	PTEN	3.880289
RH5 tryple	PTEN	3.109432
Shef3 cut	PTEN	2.029785
HUES7 tryple	RAF1	2.314371
RH5 cut	RAF1	2.707816
RH5 tryple	RAF1	2.179492
Shef3 cut	RAF1	1.958437
HUES7 tryple	SEMA3A	3.711927
RH5 cut	SEMA3A	2.843435
RH5 tryple	SEMA3A	4.484783
Shef3 cut	SEMA3A	2.613439
HUES7 tryple	SFRP2	3.472256
RH5 cut	SFRP2	1.746332
RH5 tryple	SFRP2	2.487529
Shef3 cut	SFRP2	2.630481
HUES7 tryple	SOX2	3.888494
RH5 cut	SOX2	3.89032
RH5 tryple	SOX2	3.112678
Shef3 cut	SOX2	3.337796

Table 5.3. Determining the endogenous control gene.

Variation in Ct value for each gene and cell lines were calculated. RAF1, GAPDH and ACTB were the least variable in expression throughout differentiation and biological replicates across the four hESC lines screened.

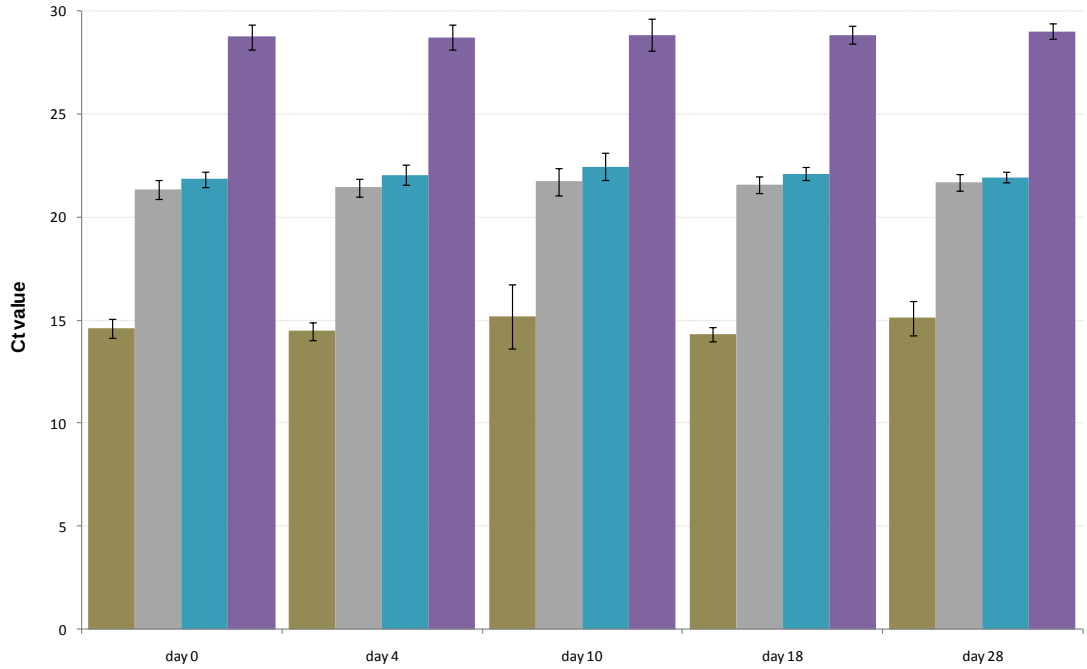

Figure 5.31. Gene expression for 18S, ACTB, GAPDH and RAF1.

Expression of the four house-keeping genes 18S (brown), ACTB (grey), GAPDH (turquoise), and RAF1 (purple) was consistent throughout differentiation when all four hESC lines were combined. Error bars representing 2SE, show the largest variation in 18S expression and minimal variation in GAPDH.

Gene	Lineage	Location	Gene	Lineage	Location
18S	house keeping	22p12	NOG	marker of stemness	17q21-q22
ACTB	house keeping	7p15-p12	OCT4	pluripotency	6p21.31
AFP	endoderm	4q11-q13	OLIG2	ectoderm	21q22.11
CRABP2	ectoderm	1q21.3	PAX6	ectoderm	11p13
DNMT3B	marker of stemness	20q11.2	PTEN	marker of stemness	10q23.3
EBAF	marker of stemness	1q42.1	PTF1A	endoderm	10p12.2
FGF4	marker of stemness	11q13.3	RAF1	house keeping	3p25
GAPDH	house keeping	12p13	REST	marker of stemness	4q12
GDF3	marker of stemness	12p31.1	SOX2	pluripotency	3q26.3-q27
GFAP	ectoderm	17q21	SYP	ectodermal	Xp11.23-p11.22
HLXB9	ectoderm/mesoderm	7q36	TDGF1	marker of stemness	3p21.31
ISL1	ectoderm	5q11.2	TERT	marker of stemness	5p15.33
NANOG	pluripotency	12p13.31	TH	ectoderm	11p15.5
NES	ectoderm	1q23.1	T	mesoendoderm	6q27
NODAL	mesoendoderm	10q22.1	UTF1	marker of stemness	10q26

Table 5.4. Genes analysed for changes in expression using LDA cards.

Thirty genes from the 96 included on the LDA card were analysed for changes in genes expression according to their roles in pluripotency and neural differentiation, or commitment to alternative germ lineages.

Technical replicates were not carried out due to high reproducibility of the LDA cards, and the prohibitive cost of running each sample three times. Standard errors (SE) for three replicates of each differentiation time point were calculated and plotted for the average ΔΔCt. One SE represented the spread of the average ΔΔCt values, two SE's would have presented the 95% confidence intervals of the mean; however, average values were calculated from only three biological replicates and as such 2SE was considered to be an inaccurate representation for the spread of the data *(Personal communication with Dr. A. Heath, Biostatistics, NIBSC)*.

Thirty genes from the 96 included on the LDA cards were selected for further investigation in this study, based on their role in pluripotency or ectodermal differentiation, or their key representation of alternative germ lineage (Table 5.4).

5.2.11.3 Expression of pluripotency genes

The average expression of both Nanog and OCT4 decreased throughout differentiation in all four of the cell lines (Figure 5.32). The largest variation in gene expression, as determined by the length of the error bars, was seen at day 4 for all samples. Immunostaining of EBs at day four also reported variable expression of OCT4. This may have been because larger EBs required longer for inner cells to commit to differentiation. After day 10 the error in OCT4 and Nanog expression was reduced suggesting by day 10 most cells had committed to differentiate.

The average expression of Nanog increased in day 28 samples, when compared to day 18, in both of the enzymatically treated cell lines (HUES7 and RH5 TrypLE), suggesting proliferation of a background pluripotent population in the late stages of differentiation (Figure 5.32A), ANOVA showed that these increases were not significant ($p = 0.460$ and 0.379, in RH5 TrypLE and HUES7 respectively). In addition, to Nanog, the RH5 TrypLE line also showed an increase in average OCT4 expression in the day 28 sample of differentiation (Figure 5.32B), ANOVA revealed that this difference was not statistically significant ($p = 0.213$) from day 18. Expression of SOX2 did not change significantly throughout differentiation in the RH5 cut, RH5 TrypLE or HUES7 cell lines ($p = 0.479$, 0.118 and 0.950 respectively). However, in the Shef3 cell line average expression of SOX2 consistently decreased, with a significant 0.33-fold change in expression on day 28 from levels at day 0 ($p = 0.007$).

5.2.11.4 Markers of stemness

In addition to OCT4, Nanog and SOX2 there are numerous other genes which are expressed in pluripotent or progenitor populations which play a key role in the commitment of cells into specified germ lineages; a range of these genes were analysed for their involvement in differentiation. These genes were referred to as markers of stemness because they are most commonly expressed in pluripotent or progenitor cell populations but do not appear to actively regulate pluripotency.

DNA (cytosine-5-)-methyltransferase 3 beta (DNMT3B) is involved in DNA methylation and has been associated with early stages of embryonic development and pluripotent embryonic stem cells (Watanabe et al., 2002; Adewumi et al., 2007). The DNMT3B mRNA was expressed in day 0 samples and decreased throughout differentiation. Fibroblast growth factor 4 (FGF4) expression is regulated by SOX2 and OCT4 and as such is expressed amongst pluripotent populations (Yuan et al., 1995; Ambrosetti et al., 2000; Avilion et al., 2003; Mayshar et al., 2008). The FGF4 mRNA was detected in day 0 pluripotent populations and decreased as differentiation progressed (*data available upon request*).

Endometrial bleeding associated factor (EBAF; also known as LEFTY2) and growth differentiation factor 3 (GDF3) are both members of the TGF-β family of signalling molecules involved in maintaining pluripotency (Levine and Brivanlou, 2006). Expression of these genes decreased throughout differentiation in all four cell lines, in accordance with a loss of pluripotency (*data available upon request*). Expression of telomerase reverse transcriptase (TERT), an enzyme required for active maintenance of telomere length in pluripotent cells (Yang et al., 2008), was also detected in all pluripotent populations and decreased throughout differentiation. No increase in TERT expression was detected in the latter stages of differentiation (*data available upon request*).

In the mechanically passaged hESCs lines, average expression of Noggin (BMP inhibitor) increased to a peak on day 10 (11.7-fold and 4.6-fold in Shef3 and RH5 cut respectively), followed by a decrease in expression until day 28 (Figure 5.33B). In the HUES7 cell line, Noggin expression increased by 4.4-fold between day 0 and day 4. Levels of Noggin expression in HUES7 plateaux out after day 4 at approximately 2.5-fold increase from expression at day 0. The RH5 TrypLE cell line presented considerably higher Noggin expression than the other three lines, between 24.5-fold and 35.5–fold increased expression from day 10 onwards, when compared to day 0.

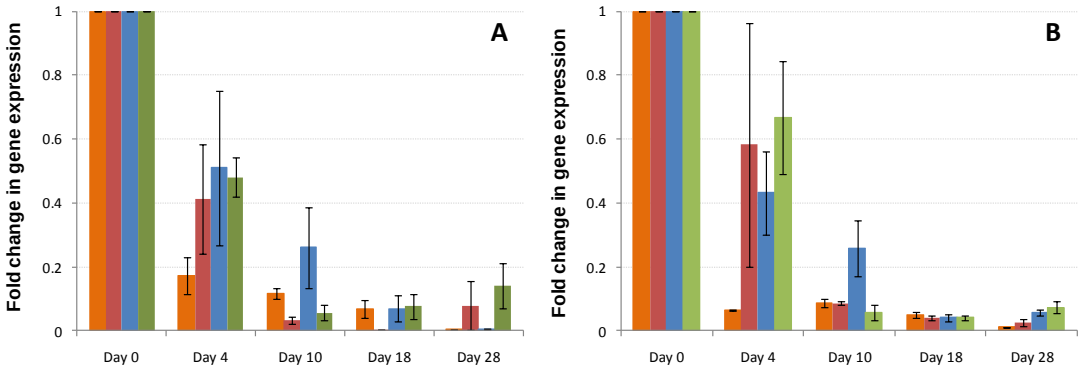

Figure 5.32. Gene expression analysis for Nanog and OCT4.
Average gene expression for Nanog (A) and OCT4 (B) decreased throughout differentiation, with the largest drop in expression in the first 4 days of induction. The average expression of Nanog and OCT4 almost doubled between day 18 and day 28 in the RH5 TrypLE sample. However, reproducibility of this data suggests this was not a significant increase ($p = 0.379$ and 0.213, Nanog and OCT4 respectively). A similar increase in average Nanog expression was detected in the HUES7 cell line but this was not significantly different to expression levels at day 18 ($p = 0.460$). Error bars represent 1SE. Shef3 - orange, HUES7 – red, RH5 cut - blue and RH5 TrypLE - green.

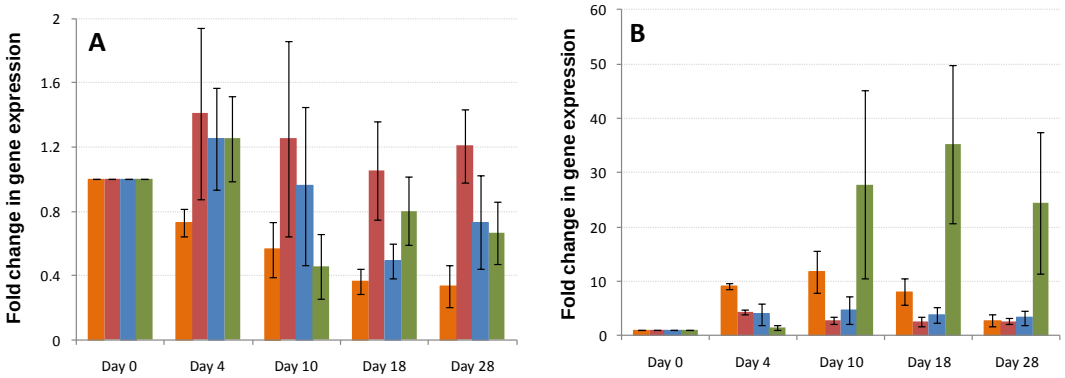

Figure 5.33. Gene expression analysis for SOX2 and Noggin.
SOX2 (A) expression remained consistent throughout differentiation in the HUES7, RH5 cut and RH5 TrypLE cell lines. However, expression of SOX2 was seen to consistently decreased throughout differentiation in the Shef3 cell line. Expression of Noggin (B) increased in the mechanically passaged cell lines to a peak at day10 (11.7 and 4.6-fold higher than day 0 in Shef3 and RH5 respectively). Noggin expression in HUES7 increased and to a plateau at approximately 2.5-fold higher expression than day 0. Considerably higher Noggin expression was detected in the RH5 TrypLE cell line when compared to the additional lines up regulated to between 24.5 and 35.5-fold higher expression than day 0, between day 4 and day 10. Error bars represent 1SE. Shef3 - orange, HUES7 – red, RH5 cut - blue and RH5 TrypLE - green.

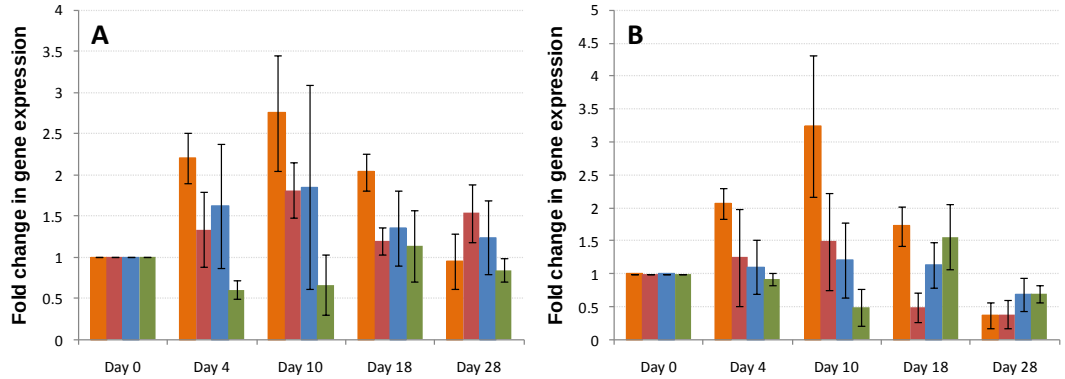

Figure 5.34. Analysis of PTEN and REST expression.
The average expression of PTEN (A) in RH5 TrypLE were consistently lower than in Shef3, HUES7 and RH5 cut. In Shef3, HUES7 and RH5 cut PTEN expression peaked as day 10 followed by down regulation. In Shef3 and HUES7 REST (B) peaked at day 10 followed by down regulation. At day 10 average REST was higher in RH5 cut than RH5 TrypLE, there was no real change in REST across the remaining sample period. Error bars represent 1SE. Shef3 - orange, HUES7 – red, RH5 cut - blue and RH5 TrypLE - green.

Average expression of the neural stem cell self-renewal regulator, phosphatase and tensin homolog (PTEN) was consistently lower in RH5 TrypLE than in RH5 cut, HUES7 and Shef3 (Figure 5.34A). RE1-silencing transcription factor (REST) expression peaked at day 10 in the Shef3 cell line (3.25-fold increase from day 0) followed by down regulation. Expression of REST, an additional regulator of neural stem cell self-renewal, did not vary significantly in HUES7 or RH5 cut throughout differentiation ($p = 0.465$ and 0.866 respectively). Average REST expression decreased by half in the RH5 TrypLE on day 10 (Figure 5.34B).

High levels of both Teratocarcinoma derived growth factor 1 (TDGF1) and undifferentiated embryonic cell transcription factor 1 (UTF1), markers of pluripotent hESCs (Okuda et al., 1998; Babaie et al., 2007), were detected in pluripotent populations of all four hESC lines, as determine by comparatively low Ct values from the raw Q-PCR data. Results from this study revealed a rapid decrease in TDGF1 expression (0.1-fold change) in the Shef3 cell line by day 4, to almost undetectable levels throughout the remainder of differentiation. Expression of TDGF1 in the remaining three hESC lines, also decreased to basal levels following differentiation, but large error bars in the day 4 samples highlight a greater variability in the rate of down regulation (Figure 5.35A). Expression of the UTF1 gene decreased from day 0 throughout differentiation in all four hESC lines. However, in RH5 TrypLE the average expression levels increased in the latter stages of differentiation from the minimal expression levels at day 10 (0.02-fold change from day 0) to a 0.12-fold change in expression at day 28, relative to day 0 (Figure 5.35B).

5.2.11.5 Expression of ectodermal genes

Nestin expression increased in Shef3 and HUES7 from day 0 to a peak at day 10, followed by a slow decline (Figure 5.36A). This would correspond to an increase in the number of neural progenitors, followed their commitment into a mature neuronal cell fate. For the HUES7 cell line, decreased Nestin expression correlates with an increased expression of the matured neuronal markers synaptophysin (SYP) and tyrosine hydroxylase (TH). Expression of these genes was highest in the HUES7 cell line, reaching 126-fold increased expression from day 0 (Figure 5.37). This suggests that the largest proportion of mature dopaminergic neurons was derived from the HUES7 cell line. Tyrosine hydroxylase was not detected at day 0, therefore analysis of gene expression for this marker was standardised to day 4. Interestingly, Nestin expression peaked in both the RH5 cut and RH5 TrypLE cell lines at day 28, suggesting a continued expansion of neural progenitors within the cell pool. This

was confirmed by the increased numbers of neurons visible under bright field microscopy in the two RH5 cell lines, when compared to Shef3 and HUES7. Both SYP and TH also increased throughout differentiation (Figure 5.37) in the RH5 cell lines confirming that there were mature neurons amongst the neural precursors on day 28.

The cellular retinoic acid binding protein 2 (CRABP2) was expressed in high amounts throughout differentiation but increased to a peak at day 10 in the Shef3, HUES7 and RH5 cut cell lines, followed by a gradual decrease in expression by day 28. In the RH5 TrypLE cell line CRAPB2 continued to increase in expression throughout differentiation, with down regulation only seen in one of the three replicates of this cell line on day 28 (Figure 5.36B).

The oligodendrocyte lineage transcription factor 2 (OLIG2) is a marker of oligodendrocyte precursors (Lu et al., 2000); however, it is also expressed in motor neuron precursors (Novitch et al., 2001). In Shef3 and HUES7 the average levels of OLIG2 expression increased to a peak at day 10. In the RH5 cut and RH5 TrypLE cell lines, OLIG2 continued to increase throughout differentiation. There was no change in GFAP expression throughout differentiation, confirming the negative staining for GFAP antibody (*data not included*).

PAX6 gene expression was not detected at day 0 in the RH5 TrypLE sample, therefore changes in expression of PAX6 were standardised to levels at day 4. In RH5 TrypLE, PAX6 expression increased by 134-fold on day 28 from levels at day 4. In contrast, RH5 cut PAX6 expression was considerably lower with just a 5.34-fold increased from day 4 to day 28. PAX6 expression in the Shef3 cell line was up regulated by 155-fold from day 0 to its peak on day 10, followed by subsequent down regulation (Figure 5.38A). PAX6 expression also increased in HUES7 to a 142-fold increase from day 0 at the peak on day 28 (Figure 5.38). Expression of PAX6 in HUES7 and RH5 TrypLE were not significantly different ($p = 0.925$) but were significantly different between RH5 cut and RH5 TrypLE (0.025 at day 4 and $p = 0.002$ ad day 18), despite originating from the same starting cell pool.

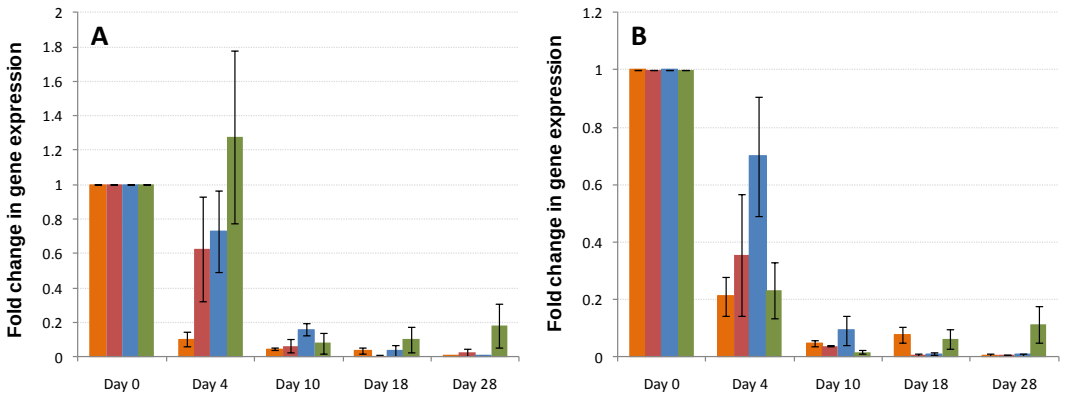

Figure 5.35. Analysis of gene expression for TDGF1 and UTF1.

Expression of both TDGF1 (A) and UTF1 (B) was detected in the pluripotent populations from all four cell lines. Expression of TDGF1(A) was down regulated through differentiation, most extensively in Shef3 between day 0 and day 4. Expression of UTF1 (B) was also down-regulated in all lines throughout differentiation. Error bars represent 1SE. Shef3 - orange, HUES7 – red, RH5 cut - blue and RH5 TrypLE - green.

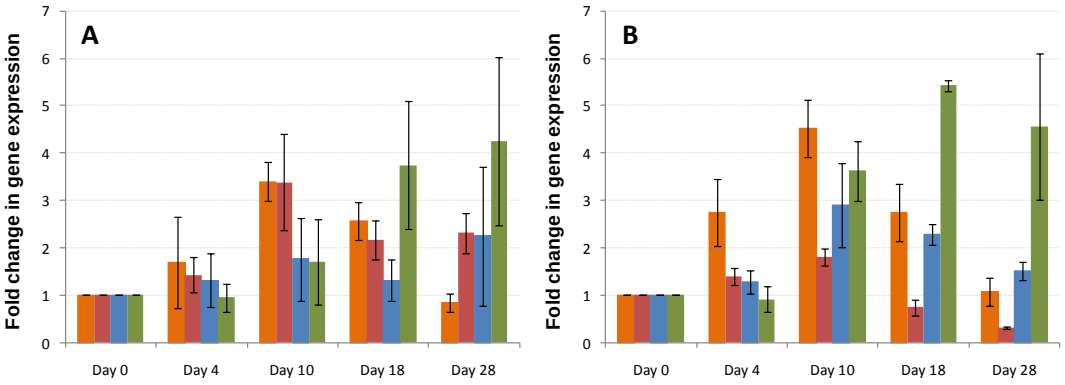

Figure 5.36. Analysis of changes in Nestin and CRABP2 expression.

Average expression of the Nestin (A) and CRABP2 (B) increased to a peak on day 10 in the Shef3 and HUES7 cell lines. Both Nestin and CRABP2 expression continued to increase the RH5 TrypLE line until day 28. The levels of Nestin and CRABP3 detected in RH5 cut at day 28 was considerably lower than levels seen in RH5 TrypLE. Error bars represent 1SE. Shef3 - orange, HUES7 – red, RH5 cut - blue and RH5 TrypLE - green.

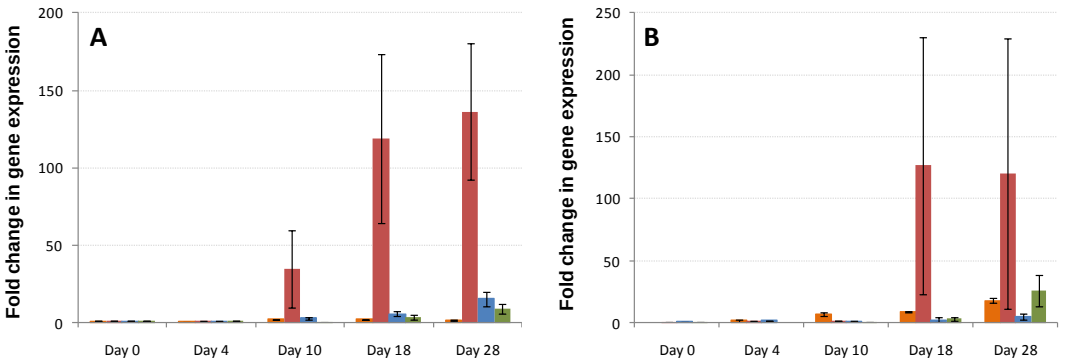

Figure 5.37. Analysis of gene expression for SYP and TH

The expression levels of both synaptophysin (A) and TH (B) were significantly higher in the HUES7 cell line than in either of the additional cell lines screened. TH and SYP expression increased steadily in the remaining cell lines throughout differentiation, peaking at day 28. Error bars represent 1SE. Shef3 - orange, HUES7 – red, RH5 cut - blue and RH5 TrypLE - green.

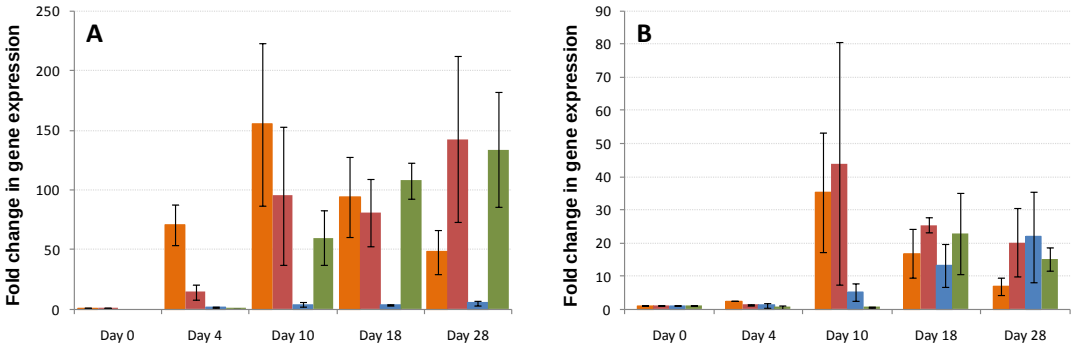

Figure 5.38. Analysis of changes in PAX6 and OLIG2 expression.

Expression of PAX6 (A) in the RH5 TrypLE cell line was consistently up regulated throughout differentiation to a peak on day 28, 134-fold higher than day 0 levels. This was considerably higher than day 28 expression in RH5 increasing in expression by just 5.34-fold from day 0. PAX6 expression in HUES7 peaked on day 28 (142-fold increase from day 0). Expression of PAX6 and OLIG2 (B) increased to a peak on day 10 in Shef3 followed by down regulation. A peak in OLGI2 expression was also detected in HUES7 at day 10. OLIG2 was up regulated in all four hESC lines between day 4 and day 10. OLIG2 expression continued to increase in the RH5 cell lines throughout differentiation. Shef3 - orange, HUES7 – red, RH5 cut - blue and RH5 TrypLE - green.

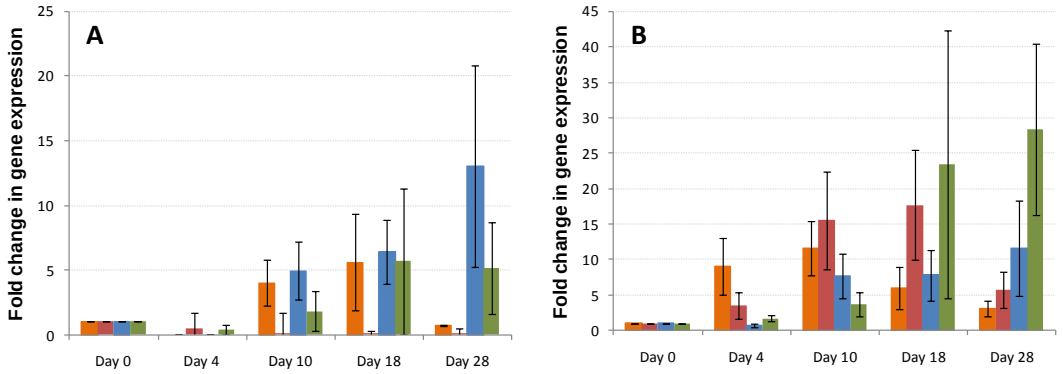

Figure 5.39. Analysis of changes in expression of HLXB9 and ISL1.

HLXB9 gene expression (A) increased from day 0 to day 28 in RH5 cut and RH5 TrypLE. No change was detected in HUES7. Expression of HLXB9 peaked in the Shef3 cell line at day 18, followed by a decline. ISL1 (B) expression peaked in Shef3 on day 10, followed by down regulation. The average ISL1 expression in HUES7 peaked at day 18 but was not significantly different to the levels detected at day 10 ($p = 0.844$). ISL1 expression increased throughout differentiation in the RH5 TrypLE and cut cell lines, peaking on day 28. Error bars represent 1SE. Shef3 - orange, HUES7 – red, RH5 cut - blue and RH5 TrypLE - green.

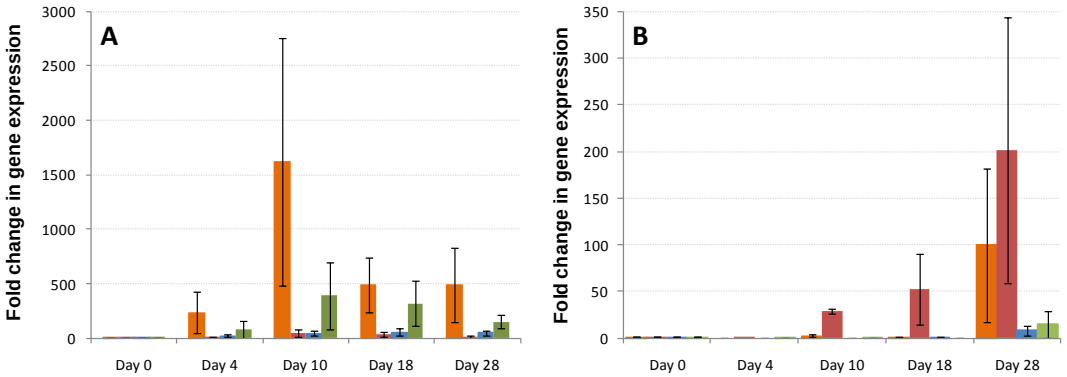

Figure 5.40. Changes in gene expression for AFP and PTF1A.

AFP (A) expression increased from day 0 to a peak at day 10. AFP expression was highest in Shef3 (1617-fold increase from day 0). AFP expression for HUES7, RH5 cut and TrypLE reached 46.3, 388.6 and 42.5 –fold increase from day 0 respectively. PTF1A (B) expression was consistently low in the Shef3, RH5 cut and RH5 TrypLE until day 28 where expression increased by 99.73, 8.17 and 14.65-fold respectively. In the HUES7 expression levels of PTF1A increased from day 10 onwards, peaking on day 28 at 201.9-fold increased from day 0. Shef3 - orange, HUES7 – red, RH5 cut - blue and RH5 TrypLE - green.

Expression of the motor neurons specific homeobox gene HB9 (HLXB9, also known as motor neuron and pancreas homeobox 1, MNX1) continued to increase from day 0 until day 28 in both RH5 cell lines (Figure 5.39A). No change in HLXB9 expression was detected in the HUES7 cell line. HLXB9 expression peaked in the Shef3 cell line at day 18 followed by a decline in expression.

Islet1 (ISL1) is best known for its activation of the insulin, glucagon and somatostatin gene in the pancreas (Karlsson et al., 1990; Leonard et al., 1992; Wang and Drucker, 1995). However it is also one of the earliest markers of motor neuron commitment (Ericson et al., 1992; Ando et al., 2003). ISL1 expression peaked in the Shef3 cell line at day 10, followed by a decrease in expression of these cells (Figure 5.39B). In the HUES7 cell line, the average ISL1 expression peaked at day 18 , although this was not significantly different to the levels at day 10 ($p = 0.844$). Levels of ISL1 continued to increase in the RH5 TrypLE and cut lines, confirming an increase in motor neuron progenitors in the later stages of differentiation.

5.2.11.6 Alternative germ lineages

Expression of the endodermal marker alpha feto protein (AFP), increased in the early stages of differentiation, with peak expression in all four lines on day 10 and decreasing thereafter (Figure 5.40). The highest AFP expression was seen in the Shef3 cell line; 1617-fold increased expression from day 0, considerably higher than for HUES7, RH5 cut and RH5 TrypLE: showing a 46.3, 388.6 and 42.5 -fold increased at day 10 respectively. Interestingly, after 18S and ACTB, AFP was the highest expressed gene across all samples, as determined by the raw gene expression Ct values.

Expression of NODAL decreased throughout differentiation of the HUES7 and RH5 TrypLE cell lines as would be expected due to its role in mesodermal and endodermal tissue specification. In both the RH5 cut and Shef3 cell line, an anomalous peak in expression was seen at day 10, amidst a gradual decline of expression throughout differentiation (*data available upon request*). Expression of Brachyury homolog (T) increased to a peak between 4-18 days in the four cell lines followed by a decline in expression to undetectable levels.

The pancreas specific transcription factor 1a (PTF1A) is involved in GABAergic neuronal differentiation (Glasgow et al., 2005; Dullin et al., 2007). Expression of PTF1A remained low in the Shef3, RH5 cut and RH5 TrypLE cell lines until day 28 where expression increased to a peak from day 0 by 99.73, 8.17 and 14.65-fold respectively (Figure 5.40B). Expression of

PTF1A started to increase considerably earlier in the HUES7 cell line, from day 10 onwards to a peak 201.9-fold increase by day 28. Up-regulation of PFT1A expression around 28 days of differentiation corresponded to the increases in immunostaining of the matured neurons for GABA.

The comparative gene expression study herein has confirmed inherent variability between pluripotent hESC lines in response to neuronal differentiation, highlighting distinct differences in the terminal neural cell fate of choice amongst cell lines which would seem to be identical by appearance.

5.2.12 Neural potential in part differentiated vs undifferentiated colonies.

Data presented within, demonstrates the ability of all four hESCs lines to differentiate into functional neurons; however, the reproducibility and efficiency of neuronal differentiation relied upon consistent pluripotent hESC starting populations. Pluripotent hESC expansion was shown in the previous chapter to rely upon consistent support from the iMEF layer and a balance in the growth factors controlling pluripotency. However, to date, no investigation has been carried out on the effect of differentiating hESCs within a colony, on the surrounding cells of that colony, and indeed on the surrounding colonies. A large amount of autocrine and paracrine cell-cell signalling takes place across a hESC colony and culture (Dvorak et al., 2005; Kunath et al., 2007; Stewart et al., 2008). To determine whether variability in differentiation was a result of partial differentiation within a culture or colony, an experiment was carried out to compare the differentiation capability of pluripotent hESCs (as determined by morphology) isolated from colonies presenting areas of spontaneous differentiation, with hESCs from wholly undifferentiated colonies.

This experiment was carried out using the two mechanically passaged hESC lines RH5 cut and Shef3 because the alternative hESC lines grew in a monolayer formation. Pluripotent hESCs were manually dissected from wholly undifferentiated and partly differentiated colonies (Figure 5.41) according to Section 2.10.4 (5-22 fragments were induced to differentiate per well). Embryoid bodies were monitored using bright field microscopy and scored for size, shape, attachment and the visible presence of outgrowing neurons. After five days in culture, EBs from partially differentiated colonies were larger and more uniform in shape than EBs from entirely undifferentiated cells (Figure 5.42).

In RH5 cut, the percentage of EBs which attached to the culture surface within five days of plating following neuronal differentiation was higher in the group of EBs derived from wholly undifferentiated hESC colonies (82.2 % ± 16.7), compared with EBs comprising hESCs from colonies displaying areas of partial differentiation (68.6 % ± 16.3); however, this difference was not significant as determined by ANOVA ($p = 0.333$). Images of EBs following plating were captured. Examples of attached fragments which displayed areas of neuronal outgrowth were scored as and presented in Figure 5.43. Examples of these EBs were seen in both cell lines. Analysis of the attached EBs for neuronal outgrowth (Figure 5.44) demonstrated that after 3 weeks differentiation, the wholly undifferentiated cells resulted in a higher proportion of neuronal differentiation (88.9 % ± 19.4) when compared to the hESC from spontaneously differentiating colonies (42.4 % ± 30.6); however, ANOVA demonstrated that these results were not significantly ($p = 0.07$). When repeated in the Shef3 cell line, the results suggested higher efficiency of neuronal differentiation from partly differentiating colonies (50.0 %) than from undifferentiated colonies (28.6 %), confirming the insignificance of spontaneously differentiating cells on the fate of remaining pluripotent cells in a colony.

5.2.13 The effect of EB size on neuronal yield.

Having demonstrated that differentiating cells did not appear to significantly control the fate of remaining pluripotent cells, the effect of the size of differentiating EB on the fate of cells within was investigated. Embryoid bodies were generated using mechanical dissection for both enzymatically and mechanically passaged cell lines; however, due to the large numbers of samples processed, it was not possible to precisely standardise the size of the fragments and consequently EBs varied in size (Figure 5.8D). In 2006, a UK stem cell group proposed a method for standardising number of cells within an EB using forced aggregation (Burridge et al., 2007). This method was applied to determining the optimal sized EB for neuronal differentiation.

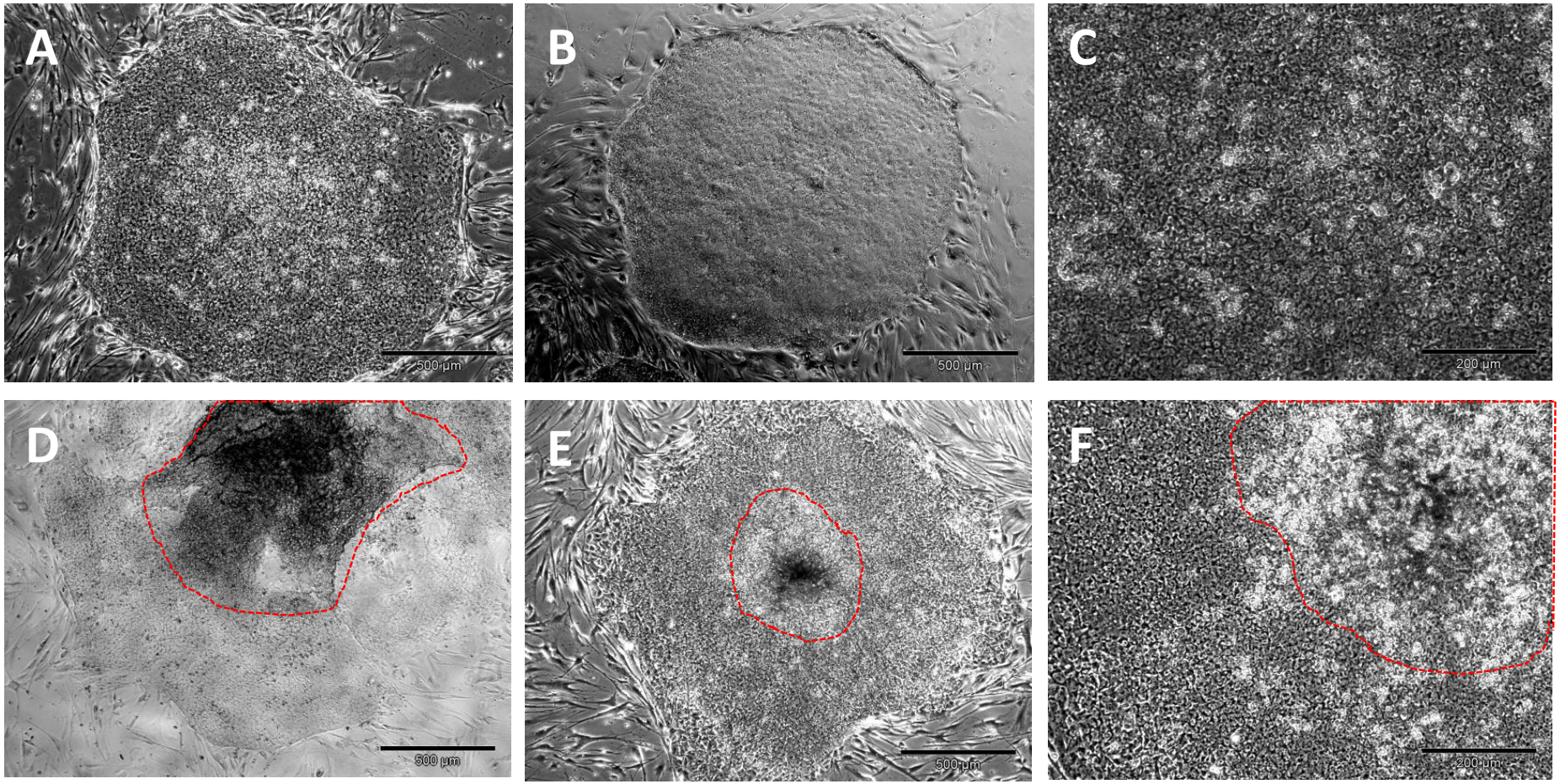

Figure 5.41. Undifferentiated vs part differentiated hESC colonies.

Wholly undifferentiated colonies (A-B x4 magnificaiton, C x10 magnificiation) were dissected into fragments (~ 200 µM) for comparision of neuronal differentiation efficieny with hESCs from colonies which displayed regions of spontaneously differentiated cells (highlighted in red; D-E x4 magnification, F x10 magnification).

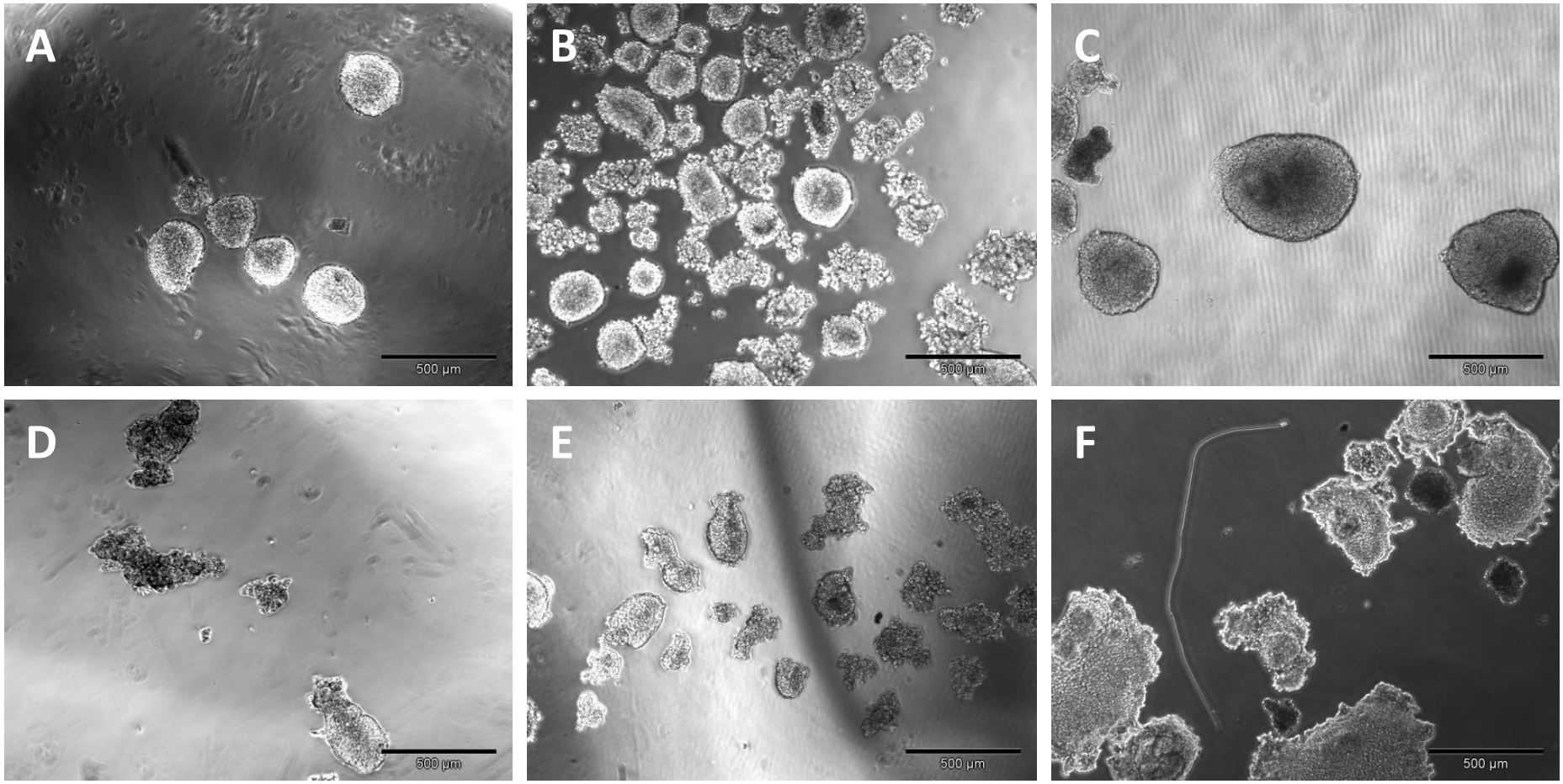

Figure 5.42. Embryoid body from undifferentiated and part differentiated hESCs.

EBs (five days post induction) from hESCs dissected from colonies which had undergone spontaneously differentiation were larger and more uniform in shape (A-B x4 magnification, C x10 magnification) than EBs from hESCs dissected from entirely undifferentiated colonies (D-E x4 magnification, F x10 magnification).

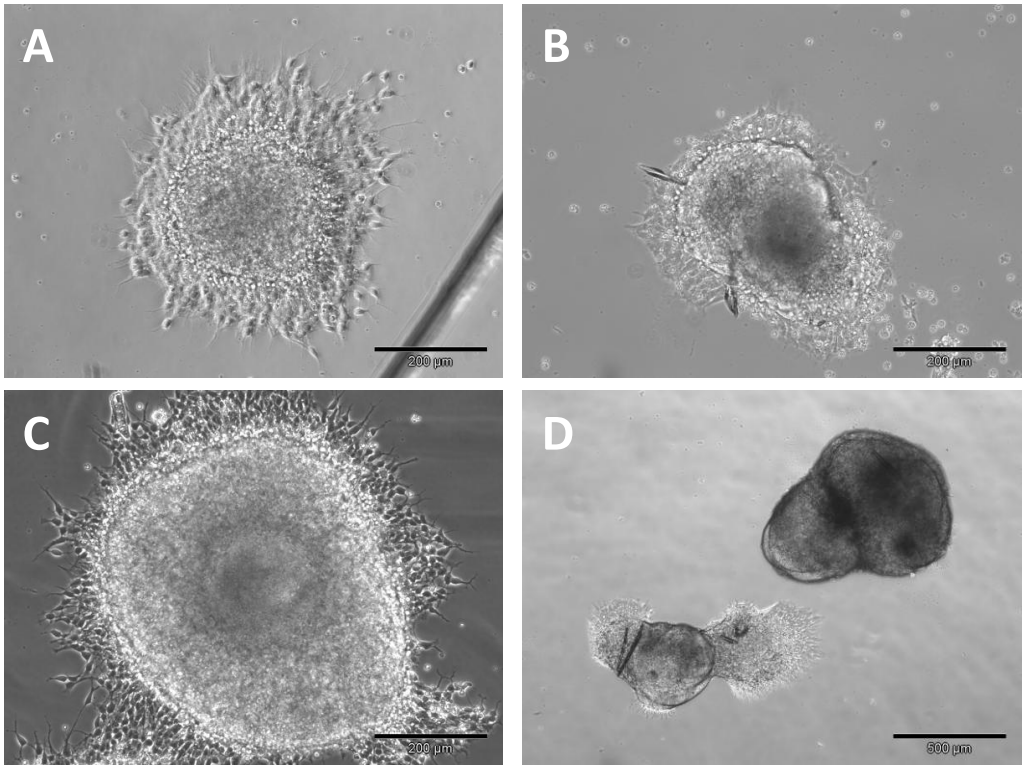

Figure 5.43. Embryoid body attachment from undifferentiated and part differentiated hESCs.

EBs with visible neurons spreading were identified from wholly undifferentiated (A) and partly differentiated hESC colonies (C). Additionally examples of EBs which did not display any signs of neuronal differentiation were also visible from undifferentiated (B) and partly differentiated hESC colonies (D).

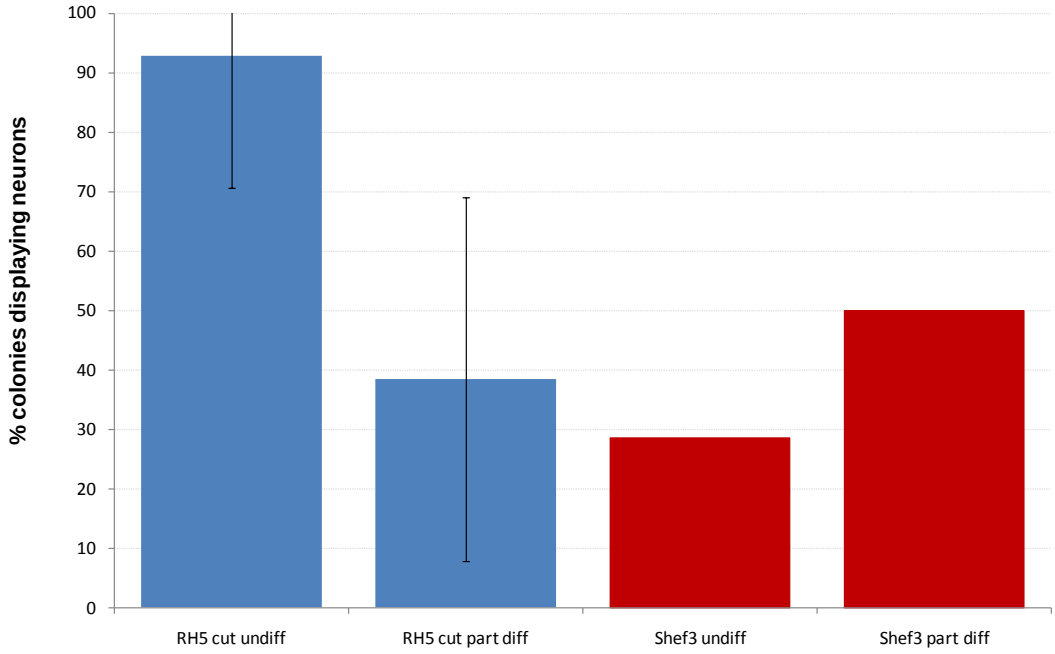

Figure 5.44. Neuronal yield from undifferentiated and part differentiated colonies.

The number of fragments which were directed into neuronal lineage was higher in RH5 (blue) wholly undifferentiated colonies (92.9 %) when compared to colonies with areas of partial spontaneous differentiation (38.5 %), despite all cells forming the EBs being of pluripotent hESC morphology as detailed in Section 4.2.1. The difference in neuronal differentiation between the two cell pools was not significant ($p = 0.07$). When repeated in Shef3 a higher proportion of neuronal differentiation was higher from EBs derived from spontaneously differentiating colonies (50.0 %) when compared to undifferentiated colonies (28.6 %).

5.2.14 Forced aggregation

The cell signalling within an EB varies depending on its size which is controlled by the number of cells within (Itskovitz-Eldor et al., 2000). In an attempt to standardise the size of the EB and identify an optimal size for neuronal differentiation, pluripotent hESCs were dissociated into single cells using TrypLE^{TM} Express, counted and seeded into v-bottomed 96-well plates (1,000 – 100,000 cells/well) in 200 µL NI media/well. The 96-well plate was centrifuged at 400 g for five minutes, forcing the cells into a pellet. Embryoid bodies with fewer than 5,000 cells did not aggregate and instead were smeared against the side of the wells (Figure 5.45). In samples with >10,000 cells, EBs formed rounded aggregates which were resuspended after 48 hours using the force from dispensing a multi-channel pipette. Embryoid bodies were differentiated for the remaining period as detailed in Section 2.10.4.

Images of EBs were captured through differentiation and variation in neuronal yield determined by visual inspection of attached and spreading EBs. After ten days in culture the number of attached and floating EBs were recorded (Figure 5.47). There was no significant difference ($p = 0.984$) in the rate of attachment between EBs comprising different cell numbers, as determined by ANOVA. The number of fragments from which neurons were spreading recorded no significant difference between EBs of different cell size ($p = 0.847$, Figure 5.48). However, the total yield and purity of neurons per aggregate was higher in EBs of 5,000 and 10,000 cells than 25,000 and 50,000 cells. This was observational using bright field microscopy; however, neurons from larger EBs were mixed amongst non-neuronal (epithelial-like) cells (Figure 5.49), where neurons from smaller EBs were almost pure in population, suggesting that smaller EBs would be better for neuronal differentiation. This observation was taken from two repeated experiments using RH5 TrypLE but would need to be repeated again with analysis and quantification of final neuronal yields for confirmation.

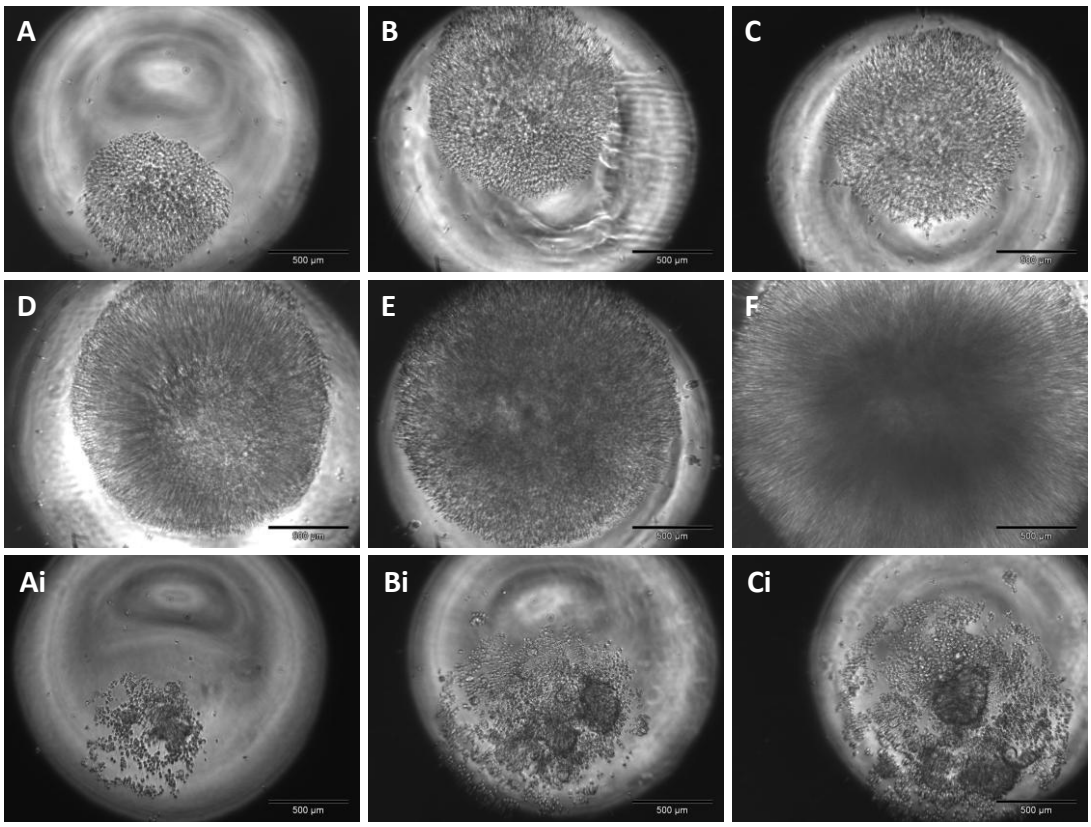

Figure 5.45. Forced aggregation of hESCs.

Human ESCs forced into aggregation using 400 g, 1,000 (A), 3,000 (B), 5,000 (C), 10,000 (D), 20,000 (E), 100,000 (F). After 24 hours EBs had formed in wells with ≥ 10,000 cells, in 1,000 (Ai), 3,000 (Bi) and 5,000 (Ci) cells multiple small EBs formed with unknown cell number.

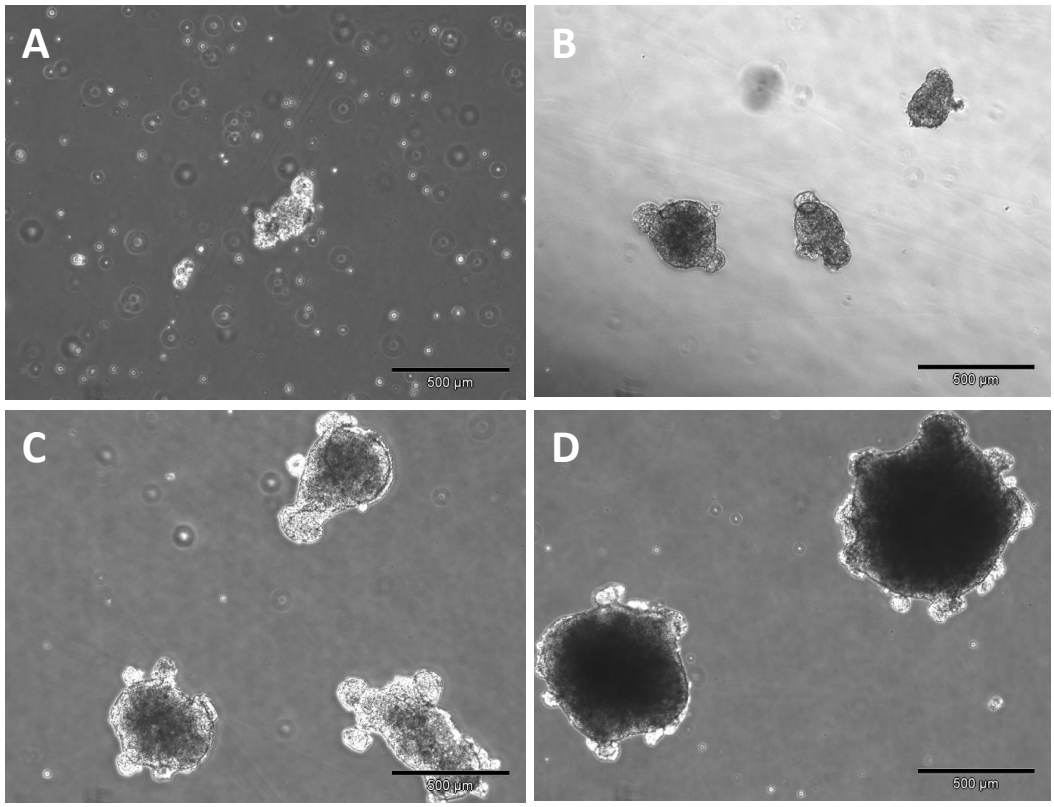

Figure 5.46. Floating aggregates 24 hours after resuspension

Embryoid bodies were uniform in size following forced aggregation, however, the shape of the EBs remained irregular: 5,000, (A) 10,000 (B), 20,000 cells (C) and 100,000 cells (D).

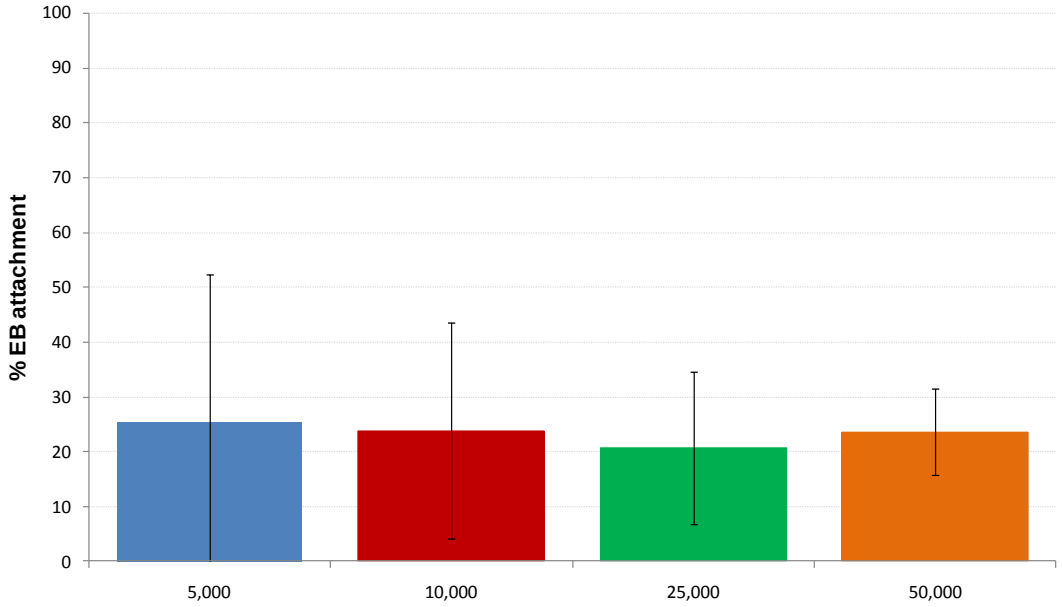

Figure 5.47. Attachment of forced EBs.

Embryoid bodies of 5,000 cells (blue), 10,000 cells (red), 25,000 cells (green) and 50,000 cells (orange), were generated following centrifugation. Embryoid bodies were differentiated neuronally according to the method outlined in Section 2.10.4. There was no significant difference in the attachment of EBs of varying cell numbers at determined by ANOVA ($p = 0.984$). Error bars represent 2SE.

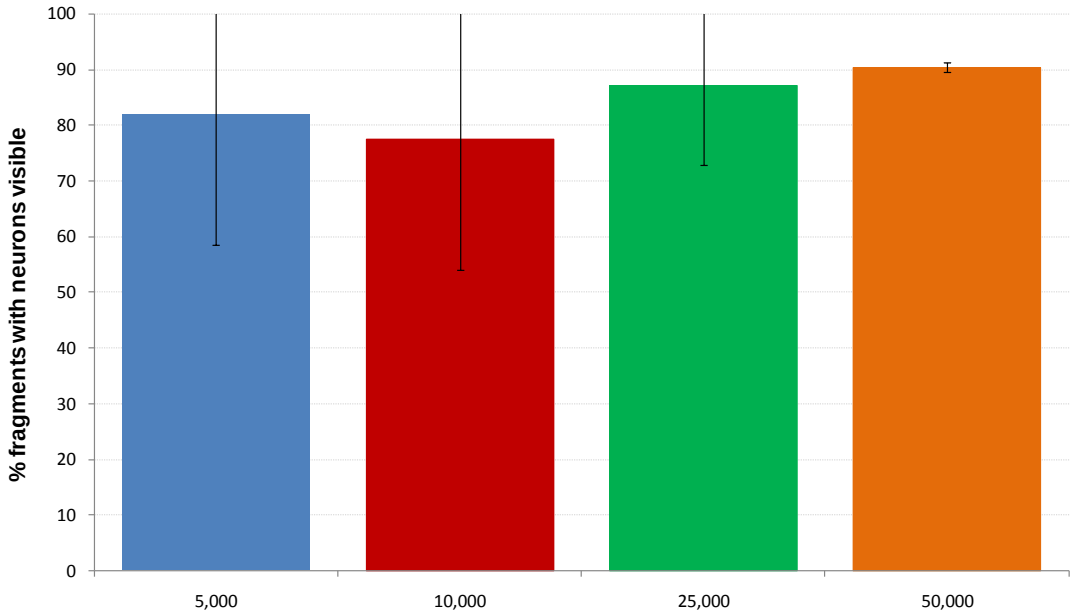

Figure 5.48. Efficiency of forced aggregation on neuronal differentiation.

After 28 days in culture the number of EBs from which neurons were spreading was recorded. No significant difference ($p = 0.847$) in the number of attached EBs containing 5,000 cells (blue), 10,000 cells (red), 25,000 cells (green) and 50,000 cells (orange) which generated neurons was identified. Despite this, the number of neurons from each EBs varied dramatically, indicating a larger and purer neuronal yield from EBs of 5-10,000 cells when compared to EBs of 25-50,000 cells.

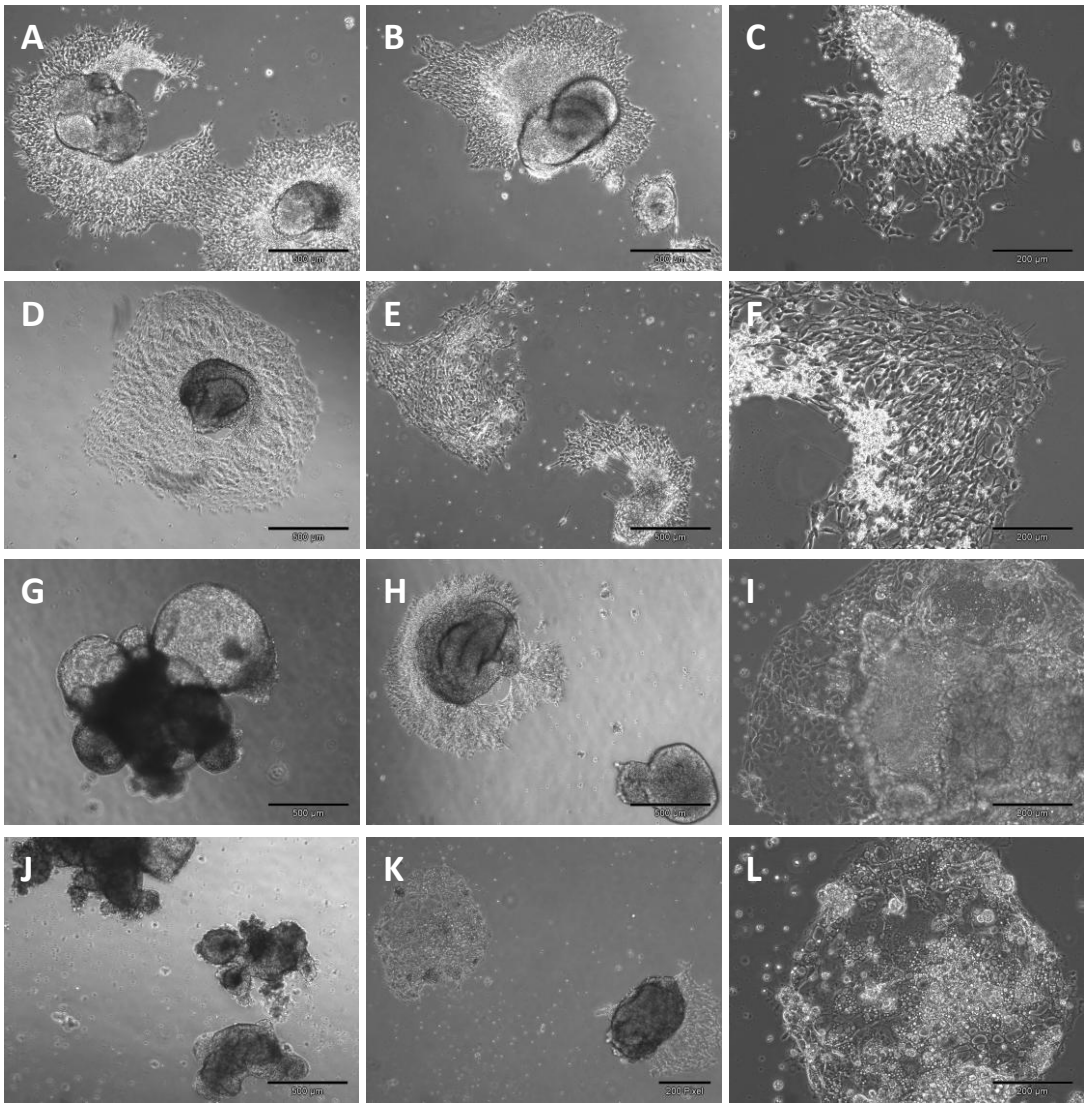

Figure 5.49. Cell morphology from attached EBs following forced aggregation.

Images of neuronal outgrowth from EBs of different cell number were captured nine days after plating: 5,000 (A-C), 10,000 (D-F), 25,000 (G-I), 50,000 (J-L). Neurons were visible spreading from all attached fragments. EBs from 25,000 and 50,000 cells, were highly irregular in shape yielding large numbers of non-neuronal cells in addition to neurons. Many of the larger EBs displayed signs of apoptosis and high levels of cell debris.

5.3 Discussion

Throughout this chapter, the responses of four hESCs lines (cultured using mechanical and enzymatic passaging techniques) were compared for their response to neuronal differentiation. Data from this study demonstrated inherent variability between the differentiation responses of these hESC lines. For the purpose of this comparative study, the phenotype of the end stage neurons was not directed allowing hESCs to respond to neuronal differentiation stimuli according to their endogenous programming.

5.3.1 Development of the enhanced EB neuronal differentiation protocol

During the early phases of this study, hESCs were established under routine culture and an enhanced protocol for neuronal differentiation developed. Due to limited access to hESC lines on commencing this project, the early experiment were carried out using Shef3; one of the only hESC lines accessible from the UKSCB. Shef3 was non-responsive to motor neuron and dopaminergic neuronal differentiation using ATRA and FGF8/SHH induced differentiation (Baharvand et al., 2007; Li et al., 2007); however, upon reflection the protocols used for these trials were not true replicates of the publications. Human ESCs used for differentiation in the adherent ATRA protocol were cultured in the presence of the BMP inhibitor Noggin thus restricting commitment into mesodermal and endodermal germ lineages and enhancing the neuronal outcome. Incorporation of Noggin has been used in this way to enhance neuronal yield in a range of differentiation studies (Bachiller et al., 2000; Pera et al., 2004; Iacovitti et al., 2007; Sonntag et al., 2007), thus explaining the improved response in the publication to that of Shef3 cells in this study.

Expression of CRABP2 gene expression by Shef3 would suggest that this line should have responded to ATRA induced differentiation using the adherent differentiation protocol (Baharvand et al., 2007); however, hECs expressing high levels of the CRABP2 protein were previously shown to be non-reponsive to ATRA induced neuronal differentiation, suggesting that CRABP2 is involved but does not control ATRA induced motor neuron differentiation (Matthaei et al., 1983). In addition, the adherent ATRA induced differentiation was carried out in hESCs adapted to feeder-free Matrigel^{TM} culture, but was repeated in this study in the presence of the iMEF layer. Although the metabolic activity of iMEFs is reduced over time (Villa-Diaz et al., 2009), the presence of iMEFs during differentiation would inevitably have altered molecular signalling in the dish, and hence might explain poor success of protocol in the Shef3 line when recapitulating the published protocol for differentiation. Despite this, the ability of Shef3 to commit into mature neurons was later demonstrated following a process of

semi-directed differentiation, whereby spontaneously differentiated neural rosettes, were mechanically dissected and directed into functional neurons by exposure to NBD media, thus confirming the ability of Shef3 to differentiate neuronally.

Following these early observations an enhanced neuronal protocol was generated which proved to be successful at generating neurons from each of the four hESC lines. Differentiation was induced following a suspension EB culture for the first nine days of differentiation in a neural induction medium. These medium contained neurotrophins which worked towards the immediate induction of ectodermal commitment (McKeehan et al., 1976; Chirgwin et al., 1979), reducing the loss of hESCs into non-neuronal germ lineages.

Removal of bFGF enhanced the neuronal differentiation and purity amongst neural stem cells by reducing the proliferation of non-neuronal cells in culture (Qian et al., 1997; Lee et al., 2000; Schwindt et al., 2009). The absence of bFGF was also found to improve neuronal maturation, generating neurons with functional K^+ ions channels, capable of firing reverberating APs following stimulation which were not generated by neurons derived in the presence of bFGF. However, the complete removal of bFGF from culture resulted in a decrease of neuronal health and the accumulation of cell debris over time (as determined by the formation of vacuoles and blebbing amongst neuronal populations). A similar effect was observed amongst neuronal populations from NTERA2 following removal of the supportive epithelial cell layer. Basic FGF has been shown to enhance neuronal survival both directly and indirectly via its affect on surrounding cells (Unsicker et al., 1992), confirming the requirement by neurons for additional support from surrounding cells. With this in mind, supplementation of cultures with survival promoting growth factors such as glial cell derived neurotrophic factor (GDNF) and brain derived neurotrophic factor (BDNF) in the end stages of differentiation, may have improved neuronal health and hence yield by reducing the detachment and death of neurons in culture (Sauer et al., 1993; Encinas et al., 2000; Tapia-Arancibia et al., 2004; Zeng et al., 2006; Bakshi et al., 2006).

5.3.2 Embryoid bodies

The poor attachment and cell spreading of EBs following plating made it difficult to isolate and process differentiating cells for characterisation. Comparative analysis of different culture surfaces revealed that poly-L-ornithine increased EB attachment and laminin improved neuronal outgrowth; thus supporting claims that laminin positively selects for neural precursors by enhancing their survival and proliferation in culture (Lathia et al., 2007; Hall et al., 2008; Ma et al., 2008). Fibronectin resulted in high rates of EB attachment but outgrowth

comprised mainly non-neuronal cells which were similar in appearance to pluripotent NTERA2 (Figure 5.1C). Fibronectin is incorporated into many of the feeder-free surface coatings for hESC expansion and has recently been proven to increase the survival and proliferation of hESCs (Amit et al., 2004; Baxter et al., 2009), explaining the outgrowth of pluripotent-like cells in these cultures. For this reason, selective attachment of EBs containing neural precursors was achieved with a combination of poly-L-ornithine and laminin.

5.3.3 Neuronal yield and functionality

Following development of a successful differentiation protocol, all hESC lines were shown to generate neurons with typical neuronal morphology. Neurons from all hESC lines fired Na^+ APs in response to stimulation, which were reversibly inhibited by TTX; however, there were clear differences in the neuronal yields and reproducibility of differentiation between each of the four cell lines.

Neuronal differentiation in Shef3 cell was highly variable, with a frequent failure to generate any cells of neuronal morphology. Instead Shef3 demonstrated a preference for mesodermal differentiation, spontaneously differentiating into beating cardiomyocyte tissue (*video available upon request*). Upon successful neuronal differentiation, the neuronal yield from Shef3 was consistently lower than was seen in the other hESC lines. Embryoid body formation was also more variable in Shef3, with cell fragments frequently dissociating in suspension (*Images available upon request*).

Differentiation amongst the RH5 cut cell line was more reproducible than in Shef3, yielding higher numbers of neurons; however, the neuronal yield was considerably lower than was seen in RH5 TrypLE. This was considered to be a result of the differences in karyotype of these two cell lines, resulted from 18 months of diversion and adaptation to passaging. Interestingly, the enzymatically passaged cell lines were more reliable in neuronal differentiation than mechanically passaged cell lines, yielding proportionally higher numbers of neurons. This was unexpected due to their karyotypic instability. However, this confirmed that the karyotypic stability of the cell line did not directly impact upon the ability a hESCs to differentiate neuronally. Although different hESC lines have inherent differences in cell behaviour, the improved neuronal yield from enzymatically passaged cell lines was not only attributable to cell line variation, confirmed by the higher neuronal yield of RH5 TrypLE compared to RH5 cut, despite arising from the same original cell line.

It was not possible to definitively quantify the differences in neuronal yield amongst these different hESC lines, due to damage caused to neurons during processing for flow cytometry. Instead, *in situ* immuno fluorescence images were used in combination with bright field microscopy to compares neuronal yields between populations. Quantification of differences between different hESC lines could have been achieved using a TissueFAX system (Tissue Gnostics, Vienna, Austria) to analyse fluorescent images *in situ.* Unfortunately, this facility was not available for use during this study but would be adopted for analysis in the event of its repetition.

Neurons derived from all four hESC lines positively expressed neuronal markers TUBB3, MAP2; but it was noticed that the staining for TUBB3 was considerably greater than that of MAP2. The tubulin family of proteins comprise three main isoforms (α, β γ-tubulin) which together form cytoskeletal microtubules across a range of cell types (Sullivan, 1988). Beta-III-tubulin (TUBB3) is specifically expressed amongst neurons (Sullivan, 1988; Lee et al., 1990). Cross reactivity with non-neuronal tubulins was ruled out by the co-expression of TUBB3 and the 70 kDa Neurofilament protein which is also neuron specific. According to early publications, TUBB3 is expressed throughout mature nerve cells in both dendrites and axons. In contrast, MAP2 is preferentially localized towards dendrites with little or no staining amongst mature axons; this would explain the higher proportion of immunostaining for TUBB3 than MAP2 (Bernhardt and Matus, 1984; Caceres et al., 1986; Chen et al., 1992).

5.3.4 Comparison of gene expression in response to neuronal differentiation

Early attempts at semi-quantitative RT-PCR were unsuccessful due to continuous detection of expression from pluripotency and neuronal genes throughout all stages of differentiation. This was considered to be a result of too many PCR cycles and poor primer specificity. Efforts were therefore transferred to Q-PCR analysis for relative quantification of gene expression throughout differentiation, using LDA gene expression cards (Adewumi et al., 2007). Gene expression across each of the four hESC lines were screened at days 0, 4, 10, 18 and 28 which were considered to be key time points for neuronal differentiation. The use of commercial LDA card meant that it was not possible to ensure gene specific amplification without pseudogene interference; however, pseudogenes were identified prior to designing the LDA cards providing reassurance of amplification for the true GOI (*Personal communication: Ms. K. Warrington, ABI*).

5.3.4.1 Determining the endogenous control gene

Prior to analysis of gene expression, it was necessary to identify a suitable endogenous control gene to which all expression was standardised. This gene was used to account for variation in loading or amplification efficiency between samples, enabling a comparison between cell lines. In an ideal system, the endogenous control gene would have a similar level of expression as the GOI (Bustin et al., 2005); however, the majority of Q-PCR studies, analysis of gene expression are carried out on continuous cell populations, within which the control genes are stability expressed. In this study the hESCs were actively changing from a homogeneous pluripotent starting pool to a heterogeneous neuronal final population, with entirely different cell behaviour and structure. Therefore identification of the endogenous control gene for this study was more complex. All 96 genes included on the LDA card were analysed for stability in expression, which identified three suitable candidate genes which were the most stably expressed throughout the differentiating populations: RAF1, ACTB and GAPDH.

RAF1 is an oncogenes which is involved in a range of cellular functions including proliferation, differentiation and apoptosis (Avruch et al., 1994; O'Shea et al., 1996; Sewing et al., 1997; Alberts et al., 2002a; Chen and Sytkowski, 2005). Within each hESC line, RAF1 was the most consistently expressed gene throughout neuronal differentiation; however, when compared across hESC lines, RAF1 expression was more variable. This was considered to be due to the differences in karyology of the different hESC lines. Mutations in the RAF1 can cause interruption of the cell cycle resulting in tumorigenesis (Wang et al., 2005b). The differences in RAF1 expression between cell lines might explain the difference in cell cycle duration of each of the cell lines. RAF1 was therefore considered to be an unsuitable endogenous control gene.

Beta-actin is a major cytoskeletal protein, expressed by all cells to control the structure, motility and integrity of the cell (Lambrechts et al., 2004), as such it is commonly assigned as an endogenous control for gene expression analysis. Alterations in β-actin expression through differentiation have been described in detail (Serazin-Leroy et al., 1998; Ruan and Lai, 2007). In this example, variable ACTB expression was expected due to the difference in cell shape and structure of a neuron when compared to a hESCs, explaining its higher variability in expression throughout differentiation than GAPDH.

Glyceraldehyde-3-phosphate dehydrogenase (GAPDH) has long been known for its involvement in glycolysis and more recently for its role in endocytosis, gene expression, DNA replication and repair and apoptosis (Mansur et al., 1993; Ishitani et al., 1996; Sirover, 1997; Suzuki et al., 2000b). As such, GAPDH iss constitutively expressed in all cells and is widely used as an endogenous control for gene expression analysis. GAPDH expression has been shown to

vary throughout the cell cycle and between different tissue types (Sirover, 1996; Radonic et al., 2004; Barber et al., 2005); however, in this study GAPDH gene expression was the least variable throughout differentiation than any of the alternative genes screened. For this reason, expression of all pluripotency and neural genes were standardised to GAPDH.

For the purpose of LDA data analysis, a single endogenous control gene was used. An alternative approach for analysis may have been to use a number of endogenous control genes for standardisation, or to pool RNA from triplicate samples for identification of an endogenous control. This would have removed potential variability from sample loading or preparation, enabling true analysis of the most stable gene expressed (Warrington et al., 2000; Vandesompele et al., 2002).

5.3.4.2 Comparative analysis of gene expression during differentiation

Prior to differentiation, all populations expressed common markers of pluripotency (Table 1.1). In addition to expression of a range of genes associated with pluripotent populations DNMT3B, EBAF, FGF4, GDF3, TDGF1, UTF1 and TERT (Adewumi et al., 2007). These markers were down regulated following neuronal differentiation in all populations. However, in the latter stages of differentiation in RH5 cut, RH5 TrypLE and HUES7, expression of the pluripotency marker OCT4 began to increase. An increase in expression of Nanog was also detected in the day 28 differentiating samples in several of the biological replicates, suggesting an outgrowth of pluripotent populations. Despite the increase in OCT4 expression, the pluripotency specific OCT4B1 was not detected by immunostaining in day 28 neuronal samples. Applied Biosystems^{TM} do not provide the primer sequence for amplification, therefore it was not possible to rule out amplification of alternative OCT4 isoforms which are expressed in somatic cells (Atlasi et al., 2008). This would explain the increase in expression in later populations; however, outgrowth of pluripotent populations from differentiating cells has been previously identified following directed differentiation (Ramírez et al., 2007). The reason for this is unclear, but it is possible that a trisomy for chromosome 12 which were detected amongst these cell lines may be partially responsible. Nanog is a master regulator of pluripotency and is located on chromosome 12 (Chambers et al., 2003; Hyslop et al., 2005). An addition copy of this gene may enhance the survival of pluripotent populations throughout differentiation (Draper et al., 2004a). This would need to be further investigated. If proven to be true, it's effect of reversion to pluripotency (or reluctance on cells to terminally commit into differentiation), would drastically limit the number of hESC lines and methods of culture which could be applied to cell therapy preparations.

The expression of SOX2 was variable between biological replicates but did not change significantly throughout differentiation in the RH5 cut, RH5 TrypLE or HUES7 cell lines. In contrast the average SOX2 expression in the Shef3 cell line consistently decreased throughout differentiation. SOX2 is a key player in pluripotency (Fong et al., 2008) but is also expressed in neural precursors of the developing CNS and has been shown to play an active role in retaining neural progenitor identity, inhibiting further differentiation (Graham et al., 2003; Avilion et al., 2003). The loss of SOX2 in Shef3 following differentiation is indicative of a loss of pluripotency and neural progenitors, and might explain why a reduced number of neurons were generated in this cell line, when compared to the other three hESC lines. Poor neuronal yields in Shef3 may also be explained by its comparatively high levels of AFP during differentiation. AFP is a marker for endodermal differentiation, indicating that a higher proportion of cells were lost into the endodermal lineage during Shef3 differentiation than in the other three hESC lines.

The higher neuronal yields from RH5 TrypLE could be attributed to the high levels of endogenous Noggin expression within these samples. Noggin is an inhibitor of BMP signalling which is required for mesodermal or endodermal commitment (Pera et al., 2004; Gerrard et al., 2005a; Sonntag et al., 2007). Recombinant Noggin is frequently added in to differentiating neuronal culture to increase ectodermal lineage commitment and thus increase neuronal yield (Iacovitti et al., 2007; Sonntag et al., 2007). It would therefore seem logical to assign some of the increased neuronal yield to the Noggin expression. Interestingly, the Noggin gene is located upon chromosome 17 (NCBI, Entrez Gene), which is commonly duplicated upon prolonged hESC culture. This might explain why the three hESC lines with trisomies for chromosome 17 were more efficient in response to neuronal differentiation than the karyotypically normal hESC line such as Shef3.

The expression patterns of PTEN and RE1-silencing transcription factor (REST) also explain the differences in neuronal yields amongst the four hESC lines. PTEN is a tumour suppressor gene which is involved in regulation of neural stem cell self renewal (Groszer et al., 2001). Down regulation of PTEN results in a shorter cell cycle and therefore increased rates of proliferation (Groszer et al., 2001; Qu and Shi, 2009). Average expression of PTEN was consistently lower in the RH5 TrypLE than in RH5 cut, HUES7 and Shef3 cell lines, which might explain the increased proliferation of neural progenitors in the RH5 TrypLE population. In addition, REST plays a regulatory role in neural stem cells renewal, preventing their differentiation and maturation (Sun et al., 2005; Johnson et al., 2008; Jørgensen et al., 2009; Buckley et al., 2009). A down regulation of REST has been correlated to increased neuronal maturation (Ballas et al., 2005; Sun et al., 2005). Interestingly, REST expression was considerably higher in the Shef3

population during the mid stages of differentiation than in the other hESC lines, thus contributing to its lower neuronal yield.

Nestin is an intermediate filament protein which is commonly used as a marker for neural progenitor cells, with lower expression levels in post-mitotic neurons (Lendahl et al., 1990). During this study, positive Nestin gene and protein expression was detected in pluripotent populations through to neuronal day 28 samples. Nestin expression was particularly evident amongst neurons in RH5 TrypLE, RH5 cut and HUES7 day 28 samples These neurons were visibly proliferating in culture as demonstrated using live cell imaging (*Video available upon request*) which was indicative of neural precursors. Prolonged retention and proliferation of neural precursors within these lines would explain their higher neuronal yield. Expression of mature neuronal markers SYP, TH and HLXB9, demonstrated the ability of RH5 TrypLE derived neurons to commit into terminal differentiation under the correct stimuli. If the maturity of the neurons derived from RH5 TrypLE could be enhanced to mimic the response of a primary neurons, RH5 TrypLE would make a good candidate cell line for the production of large numbers of neurons for pharmacological screening.

Amongst Shef3 and HUES7, Nestin gene expression increased to a peaked mid differentiation indicative of commitment into a neural lineage, followed by a decrease in expression during neuronal maturation. This suggests a faster maturation of neurons amongst these lines. Indeed, the decreased expression of Nestin in HUES7 correlated with an increase in expression of the matured neuronal marker SYP. SYP expression was higher in HUES7 than any other hESCs, suggesting that the largest proportion of synaptically mature neurons of were derived from this cell line. Comparatively low detection of SYP gene expression in RH5 cut, RH5 TrypLE and Shef3 lines would explain the absence of positive immuno staining for these lines. It would be interesting to determine whether SYP expression increased in the remaining hESC line if samples were analysed after six weeks of differentiation, which would confirm the ability of neurons within these population to form mature synaptic vesicles for communication.

The PAX6 gene encodes a transcription factor expressed by neuroectodermal and neural precursor to controls neural stem cell proliferation and differentiation during mammalian forebrain development (Perrier et al., ; Simpson and Price, 2002). The gene expression levels of PAX6 increased throughout differentiation in RH5 TrypLE and HUES7, indicative of an increased neural progenitor pool; however, PAX6 expression was significantly lower in RH5 cut when compared to the other hESC lines and in combination with Noggin was one of the main differences in gene expression between the two RH5 cell lines.

OLIG2, ISL1 and CRABP2 are all markers for motor neuron commitment (Ericson et al., 1992; Novitch et al., 2001; Ando et al., 2003; Chaerkady et al., 2009). The gene expression patterns of these genes in Shef3, RH5 cut and HUES7 were indicative of an increase in motor neuronal precursors within the EB, followed by their maturation following plating. In contrast, expression of these genes continued to increase throughout differentiation in RH5 TrypLE. In combination with the continued increased in Nestin and PAX6 expression, this data is conclusive of an expansion of neuronal precursors throughout RH5 TrypLE differentiation.

Despite the persistence of neural precursors amongst differentiating populations in RH5 TrypLE, gene expression for mature neuronal markers such as SYP, TH and HLXB9 were detected, in addition to the ability of neurons from this population to reproducibly fire genuine sodium action potentials. Therefore it was proven possible for RH5 TrypLE derived neurons to terminally differentiate. HLXB9 is a motor neuron specific marker (Lim et al., 2006); its expression increased throughout differentiation in both RH5 cell lines. Gene expression for HLXB9 was also detected in the Shef3 samples, peaking at day 18, followed by a rapid decline at day 28 which might be explained by the loss of Shef3 neurons in culture during feeding. Interestingly, in the HUES7 cell line, HLXB9 was continually down regulated throughout differentiation. Gene expression patterns amongst the HUES7 cell line were more indicative of midbrain dopaminergic and forebrain GABAergic neuronal differentiation, rather than the generation of hindbrain motor neurons. This was supported by the up regulation of TH and PTF1A during the later stages of HUES7 differentiation.

PTF1A is most commonly associated with endodermal differentiation (Afelik et al., 2006; Jarikji et al., 2009), however, it is also expressed amongst GABAergic neurons in the retina and cerebellum (Hoshino et al., 2005; Dullin et al., 2007). PTF1A expression was up regulated throughout differentiation in all hESC lines but most significantly amongst the HUES7 cell line, indicative of increased GABAergic neuronal populations amongst each of the hESC lines. Up regulation of PTF1A corresponded to positive immunostaining hESC derived neurons for GABA.

This study suggest than enzymatically passaged hESC lines were more responsive and reproducible in neuronal differentiation than the mechanically passaged lines. The difference in neuronal yields from RH5 cut and RH5 TrypLE ruled out the possibility of this being simply due to cell line variation. Although the reasons for this are not clear, it is possible that the lower yield in mechanically passaged hESC lines was a result of the iMEF feeder layer on which the pluripotent cells were cultures. Amongst enzymatically passaged cells, the iMEF density for retaining pluripotency was lower due to monolayer culture of these enzymatically passaged

hESCs. Amongst mechanically passaged line, the ratio of hESCs:iMEFs was lower, as such the pluripotency regulation of these lines may have been under more control by the iMEFs, making these cells less responsive to directed differentiation. Adaptation of both hESC lines onto feeder-free culture systems followed by a repeated comparison would confirm whether the differences between mechanically and enzymatically passaged hESC lines were due to the effects of a more concentrated iMEF layer, or due to the karyotypic instability of the hESCs which enhance neuronal differentiation.

Throughout the analysis of these four hESC lines, the reproducibility of gene expression was poor, as indicated by large error bars. This variation may have in part been due to variation in the expression of the endogenous control GAPDH which has been shown to vary in expression throughout different tissue types (Barber et al., 2005). In addition, although successful in generating functional neurons, the enhance differentiation protocol used the formation of EBs to initiate differentiation. The size of EB is difficult to control, introducing variation in gradients of signalling molecules across the EB. In an attempt to minimise the variation in differentiation using EBs an experiment was carried out to monitor the neuronal differentiation amongst EBs of a defined cell number.

5.3.5 Standardising EB size

The size and shape of EBs was difficult to standardise due to the large numbers of samples prepared and the tendency of EBs to aggregate together in culture forming irregular shapes. Aggregation of EBs was reduced by restricting the number of EBs per dish and gently triturating the samples every two days. In an attempt to standardise the size of EB, a defined cell number was forced into aggregation using v-bottomed well plates, following methods first described by Burridge et al., 2007. Preliminary data suggested that smaller EBs induced a purer neuronal yield than larger EB; however, the neuronal yield was not significantly different between EBs of 5,000 - 50,000 cells ($p = 0.847$). Differences in neuronal yield may not have been as affected by EB size as mesodermal cardiac differentiation, because neurons from the ectodermal germ lineage which sits on the outer surface of the EB (Alberts et al., 2002b). The outer EB surface was continuously exposed to neuronal stimuli, regardless of their internal dimensions. In this case, the size of EB should be enhanced to minimise commitment of cells into alternative germ lineages, rather than to enhance ectodermal differentiation. The results from this experiment were taken from just two repeated experiments and would therefore need to be repeated under controlled conditions for confirmation. Gene expression analysis of

these EBs of different sizes would also provide good insight into the communication of cells within larger aggregates.

The apparent null-effect of EB size on neuronal differentiation, suggested that alternative factors may be involved in the variability of neuronal differentiation between samples. Cells within a population are in constant communication with each other via gap-junctions and secreted signalling molecule (Harb et al., 2008; Fox et al., 2008). Therefore it would be fair to assume that the behaviour in one cell may impact upon the fate of its neighbour. In this case, spontaneous differentiation within a cell colony may have restricted the terminal cell fate of the remaining pluripotent cells surrounding it.

5.3.6 The effect of neighbouring hESCs on directability of differentiation

Spontaneous differentiation is a common occurrence within hESCs; to determine whether pluripotent hESCs from colonies containing differentiating cells, had the same differentiation potential as pluripotent hESCs from entirely undifferentiated colonies, a preliminary comparative study to compare these two groups was carried out. However, no significant difference in the neuronal differentiation of these two populations was identified by morphology. A recent study modelled on mouse embryonic stem cells suggested that cells separated by more than 400 µM were not affected by each other's signalling which might explain why pluripotent cells taken from undifferentiated areas of large hESC colonies were not significantly different in behaviour to those from wholly undifferentiated colonies (Peerani et al., 2009).

5.3.7 Summary

Results from this chapter have clearly demonstrated that all four hESC lines were capable of neuronal differentiation following the enhanced neuronal differentiation protocol. Each hESC line was shown to be capable of generating neurons which fired electrical impulses upon stimulation; however, this was the extent of the similarities in neuronal differentiation between the different hESC lines. The highest overall neuronal yield was achieved from the RH5 TrypLE hESC line, although the largest proportion of mature neurons after 28 days were generated by HUES7, confirming a difference in the rate of neuronal maturation between different hESC lines. The neuronal yield form RH5 cut and RH5 TrypLE were surprisingly different, considering these two cell lines originated from the same starting population. The differences in karyology of these lines, detected in Chapter 4 may in part explain the difference

in neuronal yield, due to the variable expression of genes known to be involved brain development. The Shef3 line was highly variable in its response to neuronal differentiation, demonstrating an apparent preference for mesodermal and endodermal differentiation with high AFP gene expression and formation of beating cardiomyocytes upon differentiation.

These results have clearly demonstrated that not all pluripotent hESCs are equally directable to neuronal cell fate. These data have demonstrated that pluripotent hESC line culture using both mechanically and enzymatic techniques are capable of neuronal differentiation when provided with the correct stimuli.

The difference in response of RH5 cut and RH5 TrypLE was indicative of an affect of passaging technique on the success of neuronal differentiation, thereby challenging *hypothesis 3*. This may have been indirectly caused by the karyotypic stability of these lines, or the interaction with the iMEF layer which are consequential of the passaging technique; however, this clearly demonstrates a difference in the affect of culture on neuronal differentiation. The incorporation of a wide range of techniques of passaging hESCs, may in part explain the different behaviours of hESCs which are observed amongst worldwide laboratories.

6 Product development of a live cell imaging facility – Linkam Scientific

The differentiation studies detailed in previous chapters was carried out under part sponsorship from Linkam Scientific, a UK based engineering company. Linkam Scientific are world experts in the field of temperature controlled microscopy and currently market a diverse range of products suited towards real-time imaging under cold temperatures. On commencing this project, facilities for live cell imaging studies worldwide were identified to be restricted to short term time courses (<3-4 days), due to limitations with poor environmental stability and reduced humidity resulting in evaporation of long term applications such as the differentiation studies. For this reason, Linkam undertook to develop, in collaboration with UCL and NIBSC, a novel live cell imaging system which would facilitate long term studies using neuronal differentiation as a model, the negating detrimental effects of evaporation and environmental stability. The research and development for this system was carried out throughout the four year duration of this thesis, the process of which has been detailed herein.

6.1 Importance of live cell imaging

Biological imaging systems provide a valuable insight into the structure and interaction of cells, both with each other and with the environment around them. Standard methods of imaging provide just snap shots of information of long term processes. In contrast, live cell imaging (LCI) generates an entire story of the behaviour within a culture, enabling tracking of individual cells/events over time.

There are a multitude of systems available for LCI; however, none of these systems truly facilitate long term studies (< week) under a stable culture environment. The major limitation for long term LCI is the inability to retain a humidified atmosphere within an arrangement which is suitable for imaging. Poor humidity control causes evaporation which increases the osmolarity of the culture media, resulting in cell shrinkage and death.

This project was carried out in collaboration with Linkam Scientific Ltd (Surrey, UK), world leaders in temperature controlled microscopy, and set out to design a novel LCI device with accurate environmental control, overcoming common issues of humidity and evaporation, to facilitate long term studies on hESC culture behaviour and differentiation.

6.2 Current live cell imaging systems

To develop a novel system which improved upon the quality and reliability of current LCI facilities, it was first necessary to compare and contrast the features that current systems incorporate. A range from the market share in LCI systems were evaluated and combined for their advantages and disadvantages (Table 6.1).

6.2.1 Micro-CO_2 microscope incubator

One of the first facilities for LCI with control over CO_2 atmosphere was described in 1983 (Ince et al., 1983). This early device incorporated temperature control accurate to ± 0.3 °C with CO_2 flow culturing cells in 35 mm petri-dishes (Figure 6.1). Evaporation and sterility were controlled using a fine layer of mineral oil over the culture media; however, temperature was controlled by a heating coil surrounding the sides of the culture dish, which resulted in temperature gradients through the media and culture surface.

6.2.2 Acrylic box

Today, the most commonly used systems for LCI are variations of an acrylic box (Figure 6.2A) which sits around an inverted microscope. The box is supplied with a CO_2 feed and is heated to the desired temperature by a flow of warm air around the chamber. These systems are easy to set up but are not easily removed, therefore requiring sole use of a microscope. Systems of this size typically suffer from large temperature gradients especially when located in air conditioned laboratories. In addition, the nature and size of the system with poor sealing around the microscope mean that accurate gas control is difficult to achieve. A humidified atmosphere is achieved with internal water reservoirs and gas pumped through a bubbler to humidify before entering the system. However, the incorporation of the microscope within the box means that the maximum humidity levels reach only ~40 %, atmospheres higher than this causes condensation on the microscope lenses and subsequent interference to imaging. These systems are practical for short term studies which require warming and CO_2 buffering but are not suitable for longer term studies due to media evaporation from the culture vessel. The large size of the vessels also mean that they require a number of hours to equilibrate at a stable humidified 37 °C atmosphere before an experiment can be run.

There are a multitude of suppliers of these environmentally controlled boxes but the main supplier in the UK is Solent Scientific, which design systems to fit around a range of commercial microscopes. Alternative systems designed specifically for Leica, Nikon, Olympus and Zeiss

microscopes are also available. In addition, In Vivo Scientific and Okolab supply similar systems using the same basic technology.

6.2.3 Wafergen - SmartSlide

The Wafergen (Fremont, Cailfornia, USA) SmartSlide use a proprietary 6-well plate format with integrated software for a temperature and gas (CO_2 and O_2) controlled system in addition to a facility for media exchange without interruption of the sample, thus extending the duration of imaging (Figure 6.2B). This system has independent control over the culture environment within each of the 6-chambers enabling simultaneous screening of multiple conditions when incorporated into a motorised microscope stage; however, the proprietary dishes add additional costs and require adaptation of the cells in culture. See http://www.wafergen.com/smartslide/index.htm for further information.

6.2.4 Okolab CO_2 incubator stage

Okolab (Napoli, Italy) have two systems available for LCI: an acrylic box incubator which is similar in style to those detailed above, with additional black-out panels, excluding background light during fluorescence imaging (Section 6.2.2). The alternative Okolab device uses a 6-well plate or six 35 mm culture dish format. This system supplies humidity and gas control and a facility for cooling to extend the experimental temperature range between 10 – 50 °C (Figure 6.2C). This device uses pre-warmed water to maintain a stable temperature, therefore the dynamic response time is slow; however, this is one of the only LCI systems which enable hypothermic studies. Humidity and gas is controlled by a large external control box, reducing the portability of the system. For further information: http://www.oko-lab.com/39.page

6.2.5 Chipman - Cell IQ

The Cell IQ (Chipman, Tampere, Finland) is an environmentally controlled incubator, similar in size to a standard laboratory incubator, with an integrated microscope and intelligent image analysis software (Figure 6.2D). The Cell IQ accommodates tissue culture flasks and well plates, and can culture and image two vessels simultaneously. Gas atmosphere is supplied via a continual flow of pre-mixed gas through a patented perfusion lid. Humidity is controlled via water reservoirs between the culture wells. However, CO_2 retention is poor and continual air flow over the culture vessel causes large levels of evaporation. For further information: http://www.chipmantech.com/Cell_IQ.asp?ID=17&Level1ID=13

6.2.6 In Vivo Scientific

In Vivo Scientific have two systems for LCI. The first is a large environmentally controlled acrylic box set up around an inverted microscope as described in Section 6.2.2. The alternative system is a small CO_2 only controlled device which uses autoclavable cover slips within a small chamber perfused with gas (Figure 6.2E). This system does not incorporate temperature control but it can be combined with the larger acrylic box system to maintain a warmed environment. This system is portable and so does not require a dedicated microscope; however, the lack of temperature control means this system alone is only not ideal for mammalian cell studies.

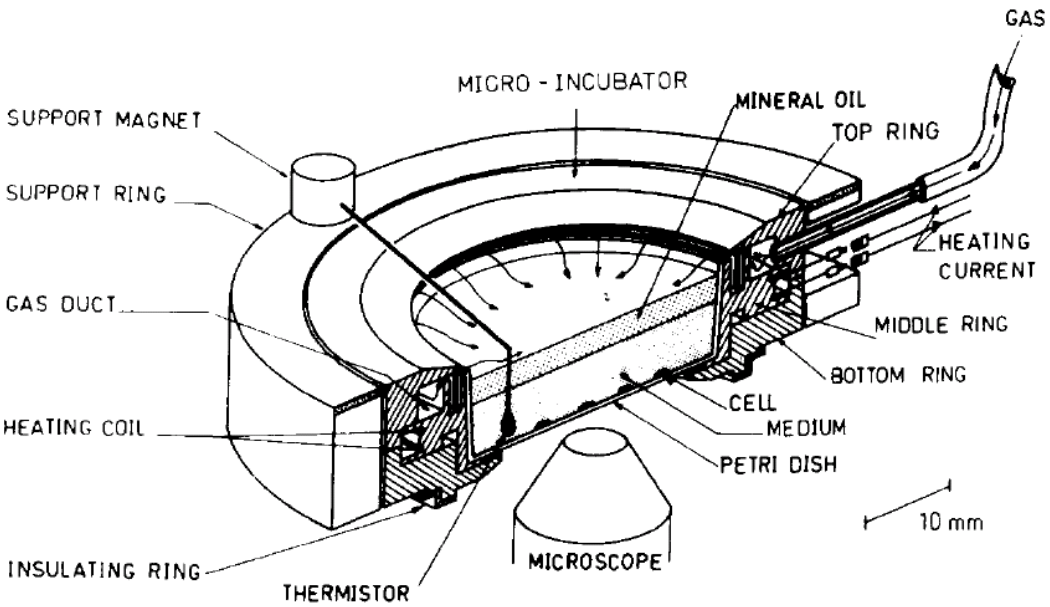

Figure 6.1. Micro-CO_2 microscope incubator

Sealed miniature temperature and CO_2 controlled environment with imaging live cells. Cell culture media covered with mineral oil to minimise evaporation and aid uniform temperature (Ince et al., 1983).

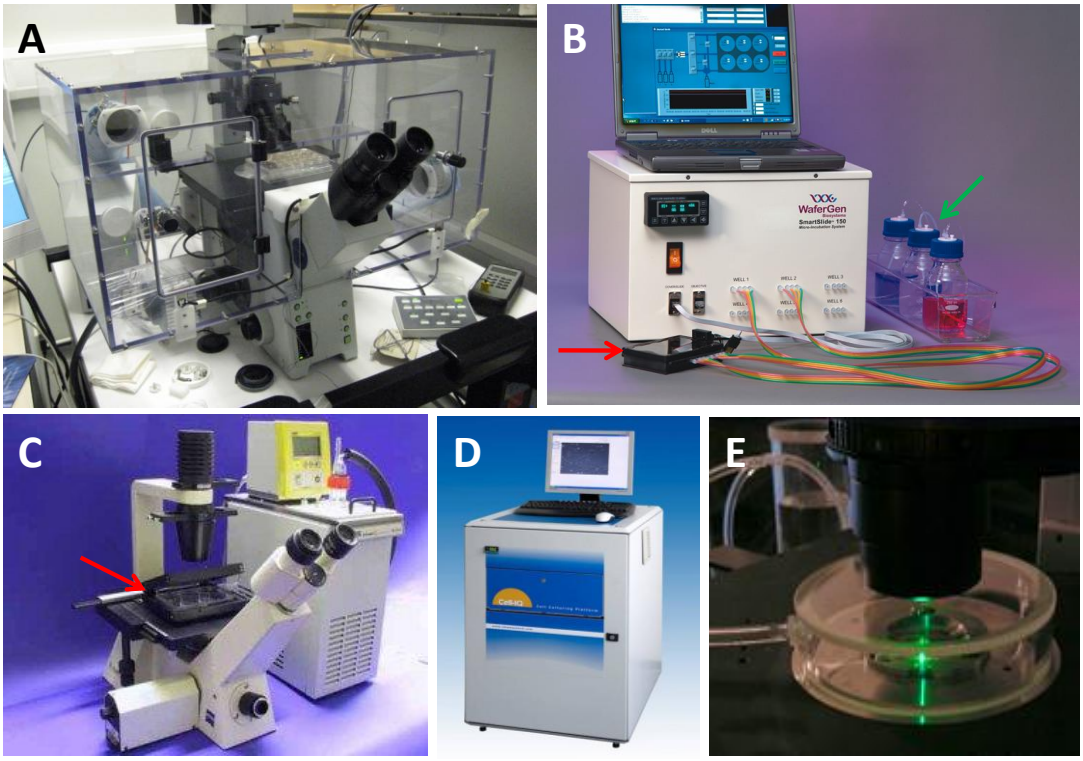

Figure 6.2. Live cell imaging systems.

The typical acrylic box style incubator pictured here - Solent Scientific on an Olympus inverted microscope, systems by alternate manufacturers are similar in appearance (A). Wafergen 6-well plate format proprietary incubator (B - red arrow) with integrated control software and set-up for media exchange (B - green arrow). Okolab 6-well plate format humidified chamber with heating and cooling facility (C – red arrow). Chipman - Cell IQ, combined incubator and microscope with integrated analysis software (D). In Vivo Scientific CO_2 controlled chamber (E).

6.3 Key design considerations

Use of and exposure to the acrylic box style incubator, Cell IQ, and Wafergen LCI facilities made clear the strengths and weaknesses of each system. With this it was possible to identify a range of key parameters which were critical for improvement in the Linkam LCI facility for optimised culture and imaging of hESCs.

- Sample size: cover glass, micro-wells or tissue culture flasks.
- Duration: How long is the study: minutes, hours, days, weeks.
- Sterility: it is necessary to run in a sterile environment?
- Temperature control: How accurately does temperature control need to be? Does the system need to run at a range of temperatures? If so, does the system need a heating and cooling facility?

Research and development rarely requires imaging of large numbers of cells at once, thus it was considered acceptable to use small culture vessels (35 mm dish) in the Linkam system. This reduced the size of the culture chamber and consequently improved the accuracy of control over environmental parameters.

Studies using mammalian cells, especially hESCs frequently last days/weeks, and therefore require a CO_2 supply to buffer the pH of the culture media. For long term studies without disruption to imaging, a media exchange facility would be an advantage. The system must also be easily cleaned (autoclavability would be an advantage), to avoid contamination in long term studies.

Contamination risk could be reduced by ergonomic design. Ease of loading to avoid spillage and sample disruption was an important consideration. In addition the system should be sealed to contain the sample in any event of spillages, preventing contamination of the laboratory space or leakage onto the microscope optics.

The sole occupancy of a piece of equipment on a laboratory microscope is not ideal for small laboratories and requires availability of an alternative microscope for any snap shot imaging. With this in mind a portable system would appeal to a larger range of customers. In addition, a portable system which was detachable from the microscope would create the opportunity for multiple systems to be run in parallel with varying environmental conditions. If the system could retain control over culture environment during transit, cells would not be exposed to changes in culture environment as is currently standard practice during imaging.

6.4 Development of the Linkam Live cell imaging facility

With these design requirements in mind, work was carried out to develop a suitable LCI system. Initial designs for the LCI system were provided by Arnold Kamp, Vince Kamp, Peter Grocutt and Rob Duncan at Linkam Scientific. Manufacturing was carried out in by Linkam Scientific (Holland). Modifications and design developments, creating a product for market were the result of this collaborative study.

6.4.1 Linkam LCI facility - Prototype 1

On commencement of this project, prototype 1 (Figure 6.3) was designed to offer fine control over temperature to ± 0.1 ˚C with easy access for sample loading using 35 mm round petri-dishes (Corning, 430165) into a glass plate located within a aluminium base and an easily machinable delrin lid. This system was heated to temperature with a low vibration fan circulating air around the sample and out through vents in the base. Temperature was controlled from a feedback sensor placed inside the cell culture media.

6.4.1.1 Limitations with prototype 1.

It was necessary to ensure that modifications and design features in the stage did not affect growth and stability of the cells in culture, mimicking the conditions within a standard laboratory incubator as best possible. Using an invasive temperature sensor for feedback control on culture environment introduced an obvious entry point for contamination and obstruction to imaging. It was therefore necessary to identify an alternative site within the system for locating the temperature sensor for control.

The use of this system for long term studies was limited by the absence of a CO_2 gas supply, for buffering the pH of the culture media. Any gas supply should be supplied into a humidified atmosphere in order to control media evaporation, the necessity for which was demonstrate by a three day study of hESC proliferation in the Olympus acrylic box LCI system. This study highlighted the adverse effects of low humidity (40 %) when running at 37 °C with a gas feed. Almost complete evaporation of the culture media occurred within three days resulting in the detachment and death of the cells in culture (*video available on request*).

	Ince	Acrylic box	Cell IQ	Okolab CO_2 incubator	Wafergen	In Vivo Scientific CO_2 chamber
Portable	✓	✗	✗	✓✗	✓✗	✓
Temperature range (˚C)	37	RT+10 - 42	20-40	RT+3 - 50	25 - 50	✗
Temperature accuracy (˚C)	± 0.3	± 0.1	± 0.2	± 0.2	± 0.2	✗
Gas control	pre-mix	✓	pre-mix	CO_2 0 - 100 %	pre-mix	pre-mix
Time to ready	min	hr	min/hr	min	min	sec
Humidity (%)	✗	≤ 40	5-50	✓ not controlled	✓ not controlled	✓ not controlled
Vessel size	35 mm dish	any	well plates flasks	petri-dish, glass slide, well plate	Wafergen vessel	coverglass
Specialist consumables	✓	✗	✗	✗	✓	✗
Media feed	✗	✗	✗	✗	✓	✗
Autoclavable	?	✗	✗	✗	✗	✓
Comments	mineral oil prevents evaporation	sole use of microscope	integrated analysis software	cooling circuit, Light blackout	6 simultaneous conditions	quick + easy to use

Table 6.1. Comparison commercially available of live cell imaging facilities.

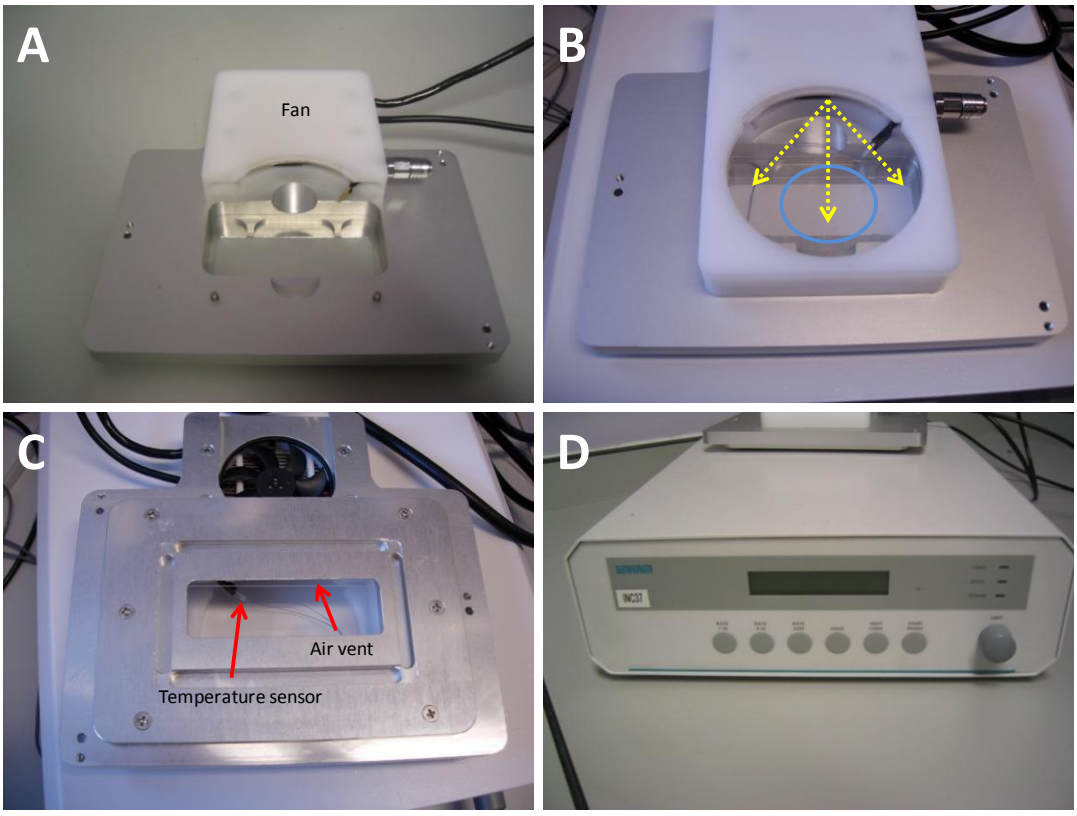

Figure 6.3. Linkam LCI facility - Prototype 1.

The removable lid in combination with the alimunium base improved ease of sample loading (A). A 35 mm petri-dish (blue circle; B) was placed on top of a glass slide base. When powered heated air flowed from the fan outlet around the dish (yellow arrows - B) and out of the chamber through vents under a glass base slide (C). The power and temperature was controlled by a feedback sensor (C) and control box (D) accurate to ± 0.1 °C.

6.4.2 Linkam LCI facility - Prototype 2

Prototype 2 was designed to incorporate a CO_2 gas feed around the culture vessel enabling longer term studies. Utilising the theory that it is easier to control a small environment than a larger one, the system was split into two chambers. The small inner chamber contained the sample under a gas controlled environment reducing the gas consumption. The outer chamber served as an insulator to retain uniform heating of the inner chamber.

6.4.2.1 Temperature control

During heating, air was drawn over the fan and pushed around the outer chamber of the device, heating the inner chamber by convection. The location of the fan to one side of the stage meant that it was necessary to ensure heating across the culture surface was uniform for consistent cell culture. Thermocouples calibrated to ± 0.5 °C were placed on the base of the culture dish close to the fan (Figure 6.4A -X) and on the opposite side away from the fan (Figure 6.4A –Y). The system was set to run at 37°C and temperature readings were recorded every minute for 1 hour.

No overall difference in temperature was noted within the media across the base of the petri-dish despite one side being closer to the fan (Figure 6.5). There was also no observed difference in the time taken for the media at each location to reach 37 °C (25 min). Reassured that the temperature was constant across the culture surface it was possible to remove the temperature sensor from the culture surface into an alternative non-invasive location thus reducing the likelihood of contamination.

The inner chamber contained the cell culture dish; therefore the conditions within this chamber must be controlled to the desired environment for culture. The temperature and humidity sensor was therefore relocated to the inside the wall of the inner chamber (Figure 6.4A). The system was set to run at 37 °C and the temperature variation in the inner chamber, recorded every second. Temperature control was extremely consistent varying by just -0.1 °C below the 37 °C set point (Figure 6.6). Interestingly the temperature never increased above 37 °C, so the cells were not exposed to even slight overheating.

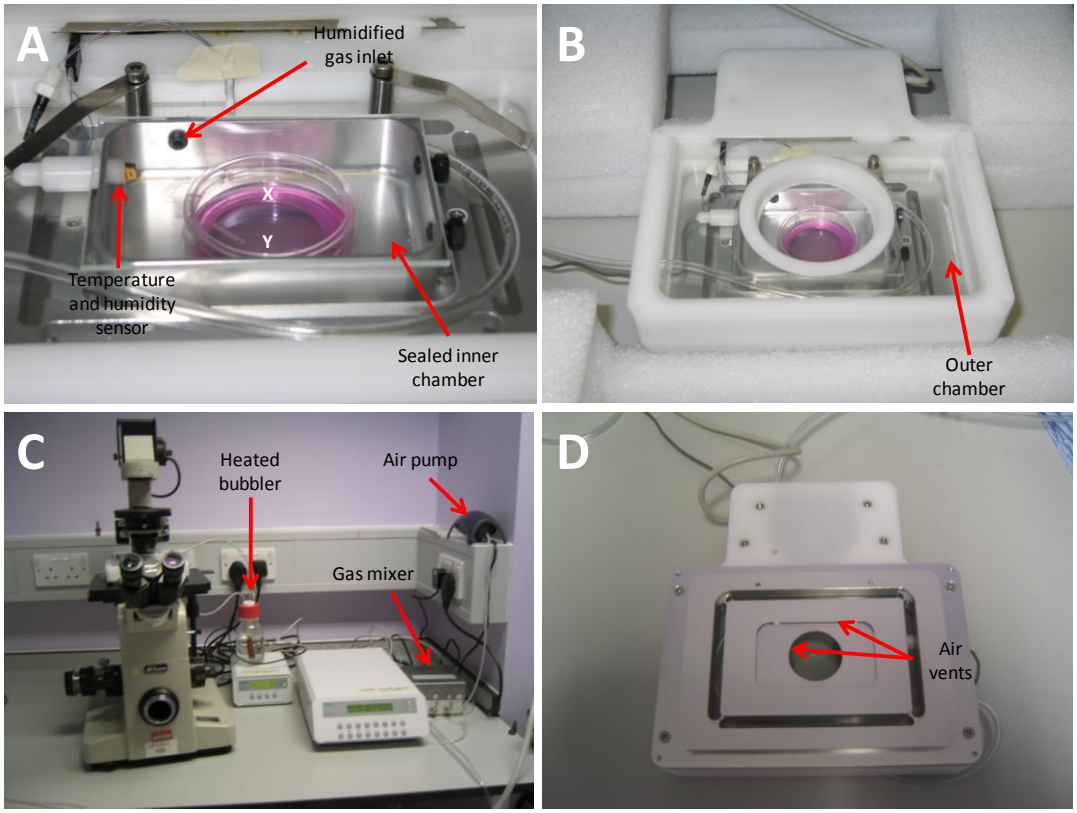

Figure 6.4. Temperature and gas controlled stage - Prototype 2.

The system was designed with two main chambers the inner chamber to hold the petri-dish, which was machined flat to seal with a glass slide (A). Heated air was blown into the outer chamber (B) to heat the inner chamber via convection avoiding a flow of heated air over the culture surface. Gas was mixed to the desired CO_2 composition in the gas mixer (C) and pumped through a heated bubbler to humidify before entering system. Air exited the system through vents under the petri-dish and inner chamber (D).

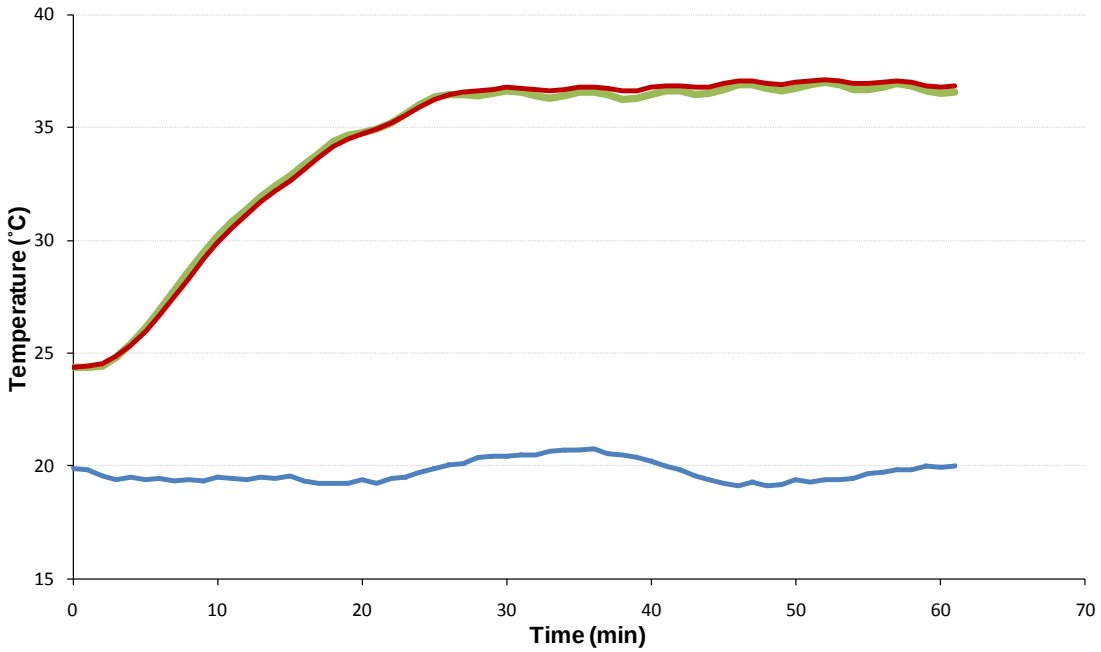

Figure 6.5. Comparison of the temperature across the base of the petri-dish.

Thermocouples were located on the base of the culture dish as shown in Figure 6.4A. close to the fan (X, green), away from the fan (Y, red) and on the laboratory bench (blue). No variation in temperature across the chamber was detected, despite the different distance from the heat source.

6.4.2.2 Evaporation

After running the Linkam system at 37 °C, it became obvious that media was evaporating from the culture dish, 42.57 % ± 6.32 after just 48 hours (Figure 6.7). Petri-dishes are subject to evaporation even in standard laboratory incubators because they are not sealed culture vessels. In an attempt to understand whether the high level of evaporation was due to the dish or the conditions within the stage, the evaporation from the 35 mm dish in the stage was compared to that in a humidified 37 °C laboratory incubator (Heraeus, Hera Cell 150). A comparison was run between the 35 mm dishes and three sizes of standard tissue culture flask T25, T75 and T150.

Sixty 35 mm petri-dishes were each filled with 2 ml cell culture media. Thirty dishes were randomly distributed throughout a 37 °C humidified incubator and the remaining thirty dishes at 4 °C as a control. Triplicate sample from tissue culture flasks (T25, T75 and T150) were filled with cell culture media (5 ml, 15 ml and 30 ml respectively), maintaining a constant surface area: volume ratio in all vessels. The weight of the empty vessel and vessel with media was recorded at the start of the experiment (Mettler-Toledo, AB240S). On each day of ten days, three samples were weighed. The percentage of evaporation was calculated from each vessel and the volume of remaining media presented (Figure 6.7). Error bars represent 2 standard errors (SE = standard deviation/$\sqrt{}$(n), where n = sample number).

Media loss from petri-dishes was significantly higher than that lost from all three sizes of T-flask as determined by ANOVA on day ten samples ($p < 0.001$) and was more variable as indicated by larger error bars. This is likely to be due to the small neck of the flask which is fitted with 0.2 micron filter in the lid, serving mainly to prevent contamination but also reducing surface area for evaporation.

Significantly more evaporation occurred from the Linkam stage compared to the laboratory incubator by day three; 42.6 % and 12.4 % evaporation respectively ($p = 0.003$). The extreme level of evaporation from the 35 mm dishes indicated a requirement for frequent media feed/replacements or much improved humidity to decrease the rate of evaporation within the stage. This was addressed in the next prototype.

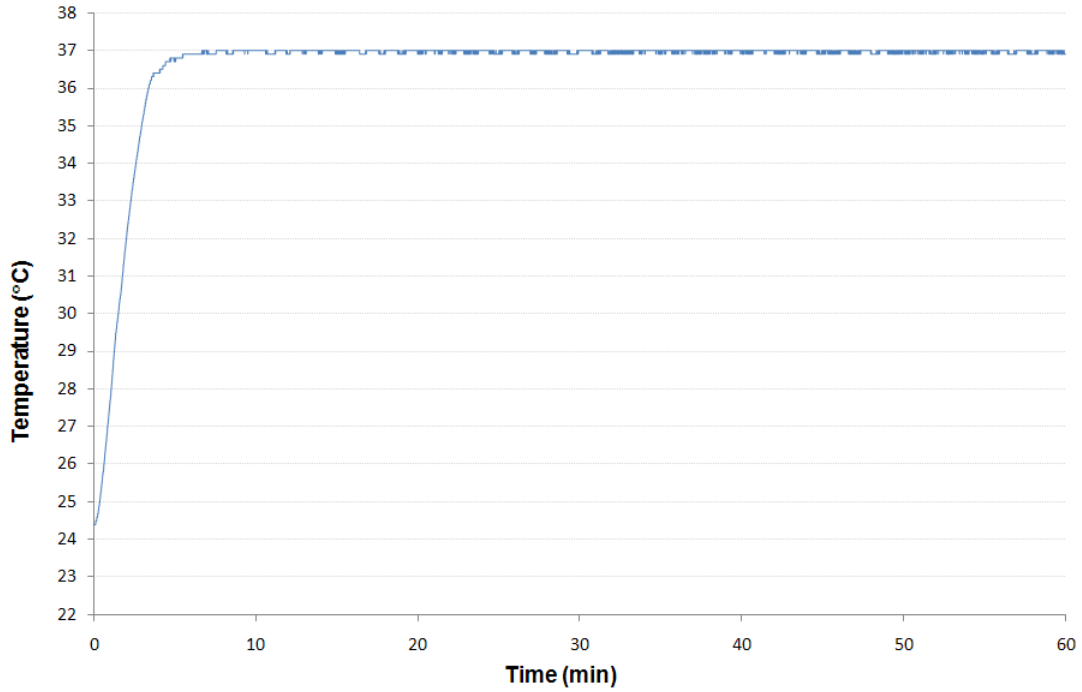

Figure 6.6. Temperature stability of inner chamber.

The temperature sensor was moved to the wall of the inner chamber and set to run at 37 °C. the temperature within the inner chamber remained stable at 37 °C (-0.1 °C) throughout the duration of the study.

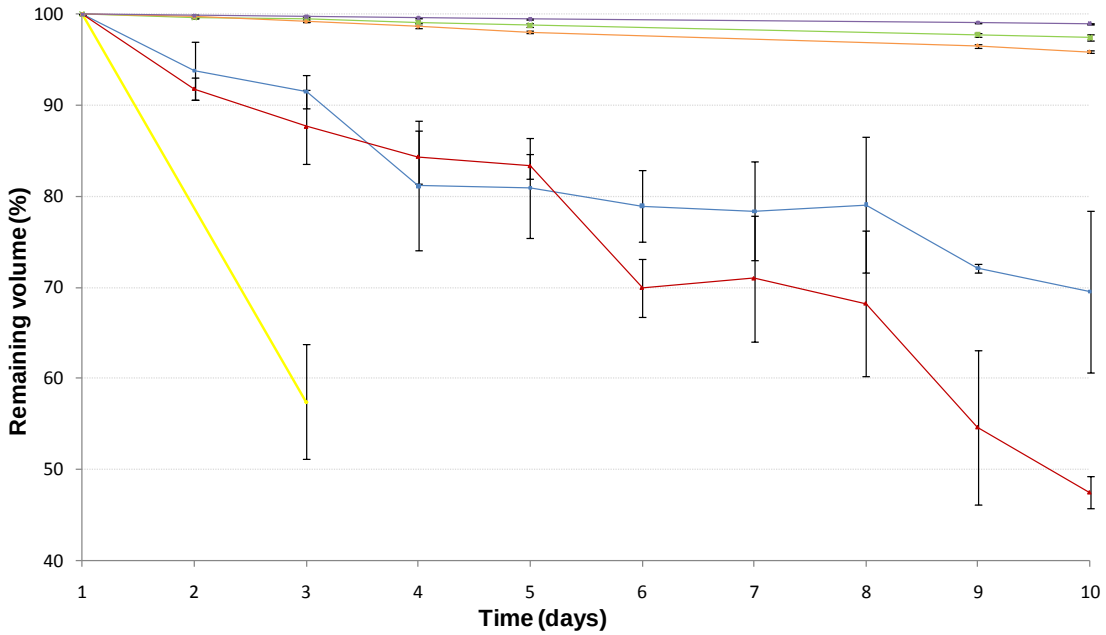

Figure 6.7. Media loss due to evaporation in petri-dishes and T-flasks.

Media was incubated under a 37 °C, humidified 5 % CO_2 atmosphere for ten days. Surface area:volume ratio was consistent in all vessels. The remaining media was plotted from T25 (orange, n=3), T75 (green, n=3), T150 (purple, n=3), 37 °C incubated petri-dishes (red, n=3), 4 °C refrigerated petri-dishes (blue, n=3) and a petri-dish within the Linkam stage (yellow, n=2). Media loss from petri-dishes was considerably larger and more variable than the lost from all three sizes of T-flask. By day three, 42.57 % of media had evaporated from the Linkam stage, which is comparable to evaporation levels in a standard incubator after nine days incubation at 37 °C (45.4 % loss) demonstrating a significantly higher rate of evaporation within the Linkam stage ($p = 0.003$ at day 3). Error bars indicate ± 2SE.

6.4.2.3 Ease of loading

The sample loading in prototype 2 was not ideal due to the narrow width of the culture dish compared with the inner chamber (Figure 6.8). The cell culture dish could not be lowered into place and so was dropped into the chamber disturbing the sample and risking contamination from aerosol formation. For this reason the method of loading was addressed in the overall design of the next prototype.

6.4.2.4 CO_2 control

In an attempt to provide a CO_2 atmosphere for prolonged cell culture, the desired CO_2 gas mix was created with a gas mixer and sensor (Figure 6.4C) and passed through a heated bubbler to humidify before entering the stage. Carbon dioxide is used in cell culture to balance the pH of the media (Freshney, 2005). Its presence can be identified by the colour of the phenol red within cell culture media. Accounting for subjectivity in colour, phenol red indicator is purple at pH 7.8, pink at pH 7.6, red at pH 7.4, orange at pH 7.0, yellow at pH 6.6 and lemon yellow below pH 6.5 (Freshney, 2005). A change in colour is therefore indicative of a change in pH. In the absence of cells, the colour of the media provides an idea of the CO_2 atmosphere within the chamber. The consistent purple colour of the media, confirmed that CO_2 was either not entering, or was being continually lost from the inner chamber of the stage. In order to reduce variables in the system, the gas mixer was removed for experimentation and premixed 5 % CO_2 bottles were purchased with certification from BOC for all further experiments. Finally, it was suspected that the CO_2 was dissolving in the water reservoir of the heated bubbler which would need to become saturated with CO_2 before the correct concentration of CO_2 would enter the stage which would be difficult to control. With introduction of a water reservoir in the inner chamber it was thought to be no longer necessary to humidify the gas input. The bubbler was therefore removed from further models.

6.4.3 Linkam LCI facility - Prototype 3

Ideally, an internal CO_2 sensor would have been incorporated into the inner chamber to control the CO_2 environment. Carbon dioxide sensors use adsorption of infra red to determine the concentration of CO_2, and as such require a minimum distance for detection, which exceeded the length of the inner chamber. As an alternative to a CO_2 sensor, a pH probe was inserted into the culture vessel through the lid of the inner chamber to monitor the pH for

correlation to CO_2. This was not designed as a feature for a final model, but rather as a method for monitoring CO_2 within the chamber for optimised design.

To aid sample loading, the inner chamber was altered to a base plate for the sample with a lid on springs forming all remaining walls of the inner chamber which sealed with a rubber seal when the system was closed. To increase humidity and therefore reduce evaporation, two water reservoirs were machined into the base plate. To improve heat circulation, the single horizontal fan was exchanged for two smaller vertical fans.

6.4.3.1 Limitations with Prototype 3

It rapidly became apparent that incorporation of a pH probe was unsuitable for monitoring the CO_2 atmosphere because the 35 mm dish was loaded with 2 ml media to a 2 mm depth as standard. To correctly measure pH, the probe must be submersed in media which was only just possible at a 2 mm depth. After several days with consistently high evaporation, the pH probe was no longer submerged sufficiently to function. The probe was removed for further studies and analysis reverted to the phenol red indicator used as a rough measure of CO_2 until a suitable alternative was identified. Using colour as an indicator, a CO_2 environment within the inner chamber was only possible with a continual flow of premixed 5 % CO_2 gas. However, with a continual gas flow, evaporation remained a significant issue and despite incorporation of two water reservoirs, culture media dried up within days, demonstrating the need for a sealed inner chamber, to retain the humidified atmosphere.

Figure 6.8. Sample loading in prototype 2.

The narrow dimensions of the inner of the chamber restricted the delicate loading of the culture dish which was dropped into place disturbing the sample, demonstrating a need alter the design of the system.

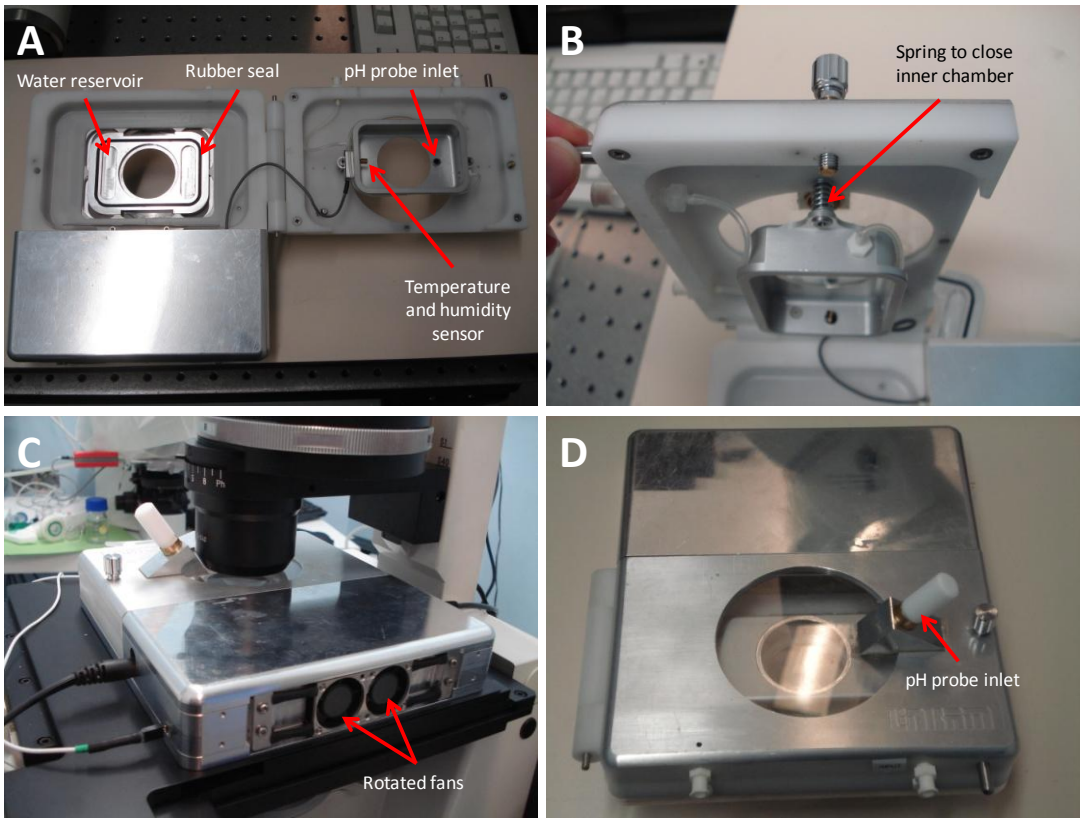

Figure 6.9. Linkam LCI facility - Prototype 3.

The layout of the inner chamber was reversed to load sample onto a base plate and seal into a closed chamber when the entire system was shut. Water reservoirs increased the humidity within inner chamber (A). A pH probe was inserted into the culture media through an opening in the lid (A). The inner chamber was sealed by tension and a rubber seal (A, B). The single horizontal fan in prototype 2 was exchanged for two smaller fans, rotated into a vertical position to aid even heat distribution (C).

6.4.4 Linkam LCI facility - Prototype 4

In prototype 4, the inner chamber was sealed from below with a glass slide in the base plate to prevent water loss and reduce evaporation. The outer chamber was also modified to divert the air flow around the inner chamber to aid even heating (Figure 6.10). Outlets for the warm air were place on either side of the inner chamber to encourage the air to flow below the base plate and warm the glass slide.

An external CO_2 sensor was incorporated into the stage design (Figure 6.11). With a pre-mixed 5 % CO_2 feed, purged into the inner chamber (frequency of purge was set by the user). The gas outlet from the inner chamber was connected to the external CO_2 sensor.

6.4.4.1 Limitations with prototype 4

The external CO_2 valve failed to measure CO_2 in the atmosphere of the gas outlet from the inner chamber, confirming an absence of CO_2 for cell culture. It was possible that the CO_2 was absorbed by the length of the PVC tubing, before reaching the sensor. All tubing was switched to silicone to prevent loss of CO_2. This tubing is used in hospitals because it is non-reactive, non-toxic and durable and was therefore considered suitable for use in this facility. Using this system it was possible to record a short video of the behaviour of hESC derived neurons in culture (*Video available on request*). However, all neurons detached from the culture surface over the 48 hours recording, indicating suboptimal culture conditions which were thought to be attributable to a lack of CO_2, resulting in too high pH for cell survival. Neurons remained attached and healthy in a control sample cultured within a standard laboratory incubator.

Further efforts were made to identify a CO_2 sensor which could be incorporated into the inner chamber for a feedback control system on gas purging when CO_2 atmosphere dropped below the set point, rather than on a defined purge rate set by the user, reducing fluctuations in atmosphere which were not comparable to standard cell culture.

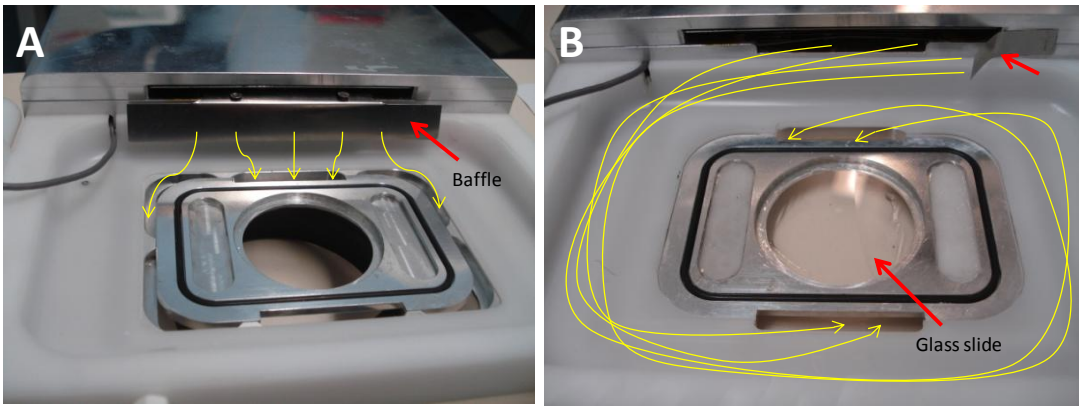

Figure 6.10. Linkam LCI facility - Prototype 4 altered air flow.

Warm air flow was diverted (yellow arrow) around the outside of the inner chamber in a circle (B) maintaining temperature of inner chamber rather than air flow above and below the inner chamber as in prototype 3 (A) using metal baffles (red arrows). A glass slide was added to base of inner chamber, creating a sealed environment to retain gas control and humidity for reduced evaporation.

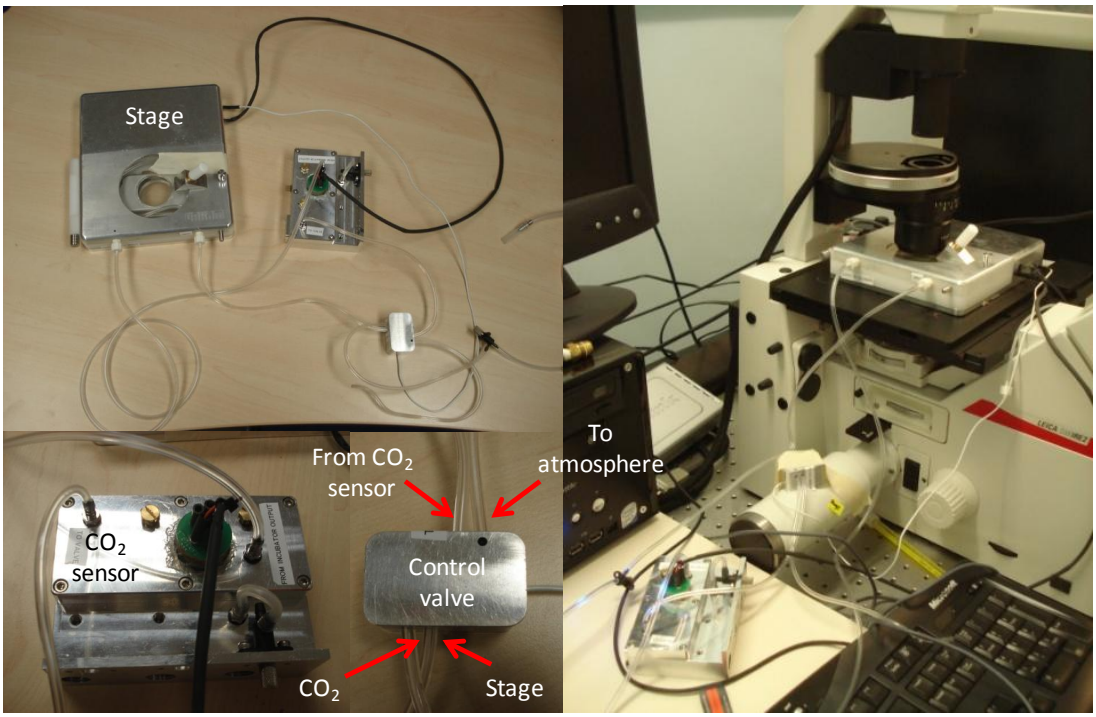

Figure 6.11. Linkam LCI facility - Prototype 4 - external CO_2 sensor.

The external CO_2 sensor was set to measure the CO_2 atmosphere from the gas outlet of the inner chamber. Gas flow was set to 50 cc/min and controlled with a valve. Frequency and duration of purging was controlled by the user using LinkSYS software.

6.4.5 Linkam LCI facility - Prototype 5

Two years after beginning this project, a small CO_2 sensor was identified which was small enough for use with the stage (Figure 6.12 A-B). The sensor was positioned on the outside of the inner chamber, measuring CO_2 within the chamber through glass panels. LinkSYS software was modified to incorporate feedback control on CO_2 for purging as necessary. The inner chamber remained sealed with water reservoirs. The shape of the outer chamber and baffles for heated air flow were altered to remove dead space which retained cooled air pockets and improved air flow and circulation.

6.4.5.1 Limitations with prototype 5

The new design and weight of the fans and electronics created and imbalance on the stage causing it to tip when not placed securely on the microscope (Figure 6.12E). While this was not a problem for imaging, for portability, the system must be stable when moved from the microscope to prevent spillage in transit.

Sealing the inner chamber with a glass slide contained the humidity within the chamber successfully resolved the problem with evaporation. However, when running at 37 °C at 90 % humidity, condensation began to build up between the base of the petri-dish and the glass slide. The glass slide was exposed to the warm inner chamber on one side, and the cold air-conditioned room and microscope on the other, creating a cooled surface on which the water from the humidified chamber condensed. It was possible to generate a 48 hour video of mouse embryonic fibroblasts in culture before loss of focus due to condensation (*video available on request*); however, condensation eventually interfered with imaging. The viability of the iMEFs from this run (96.0 %) were comparable to a control sample from a standard laboratory incubator (95.4 %); however, the overall cell number from the Linkam incubator sample was lower (1.2×10^5/ml) than a standard laboratory incubator (1.55×10^5/ml) suggesting a slower rate of proliferation in the stage, and thus suboptimal culture conditions. Modifications to the next model were aimed towards preventing condensation between the lens and the cell culture surface.

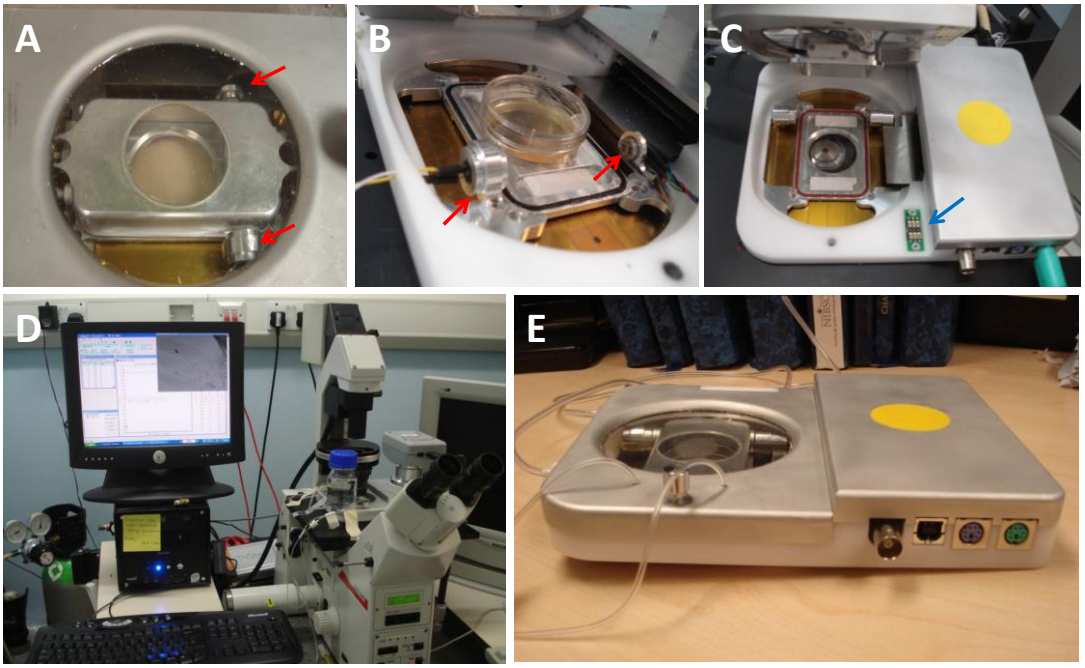

Figure 6.12. Linkam LCI facility - Prototype 5.

In built CO_2 sensor (A-B; red arrows). Lid shut sensor (C; blue arrow). Combined system with LinkSYS software (D). Imbalance on stage due to weight of fan (E). Modifications to the inner chamber to incorporate a media feed system were installed ready for the programming software to process this system. These pipes were sealed on the inlet and outlet to the chamber to prevent gas escaping through these tubes, until ready for use (Figure 6.13).

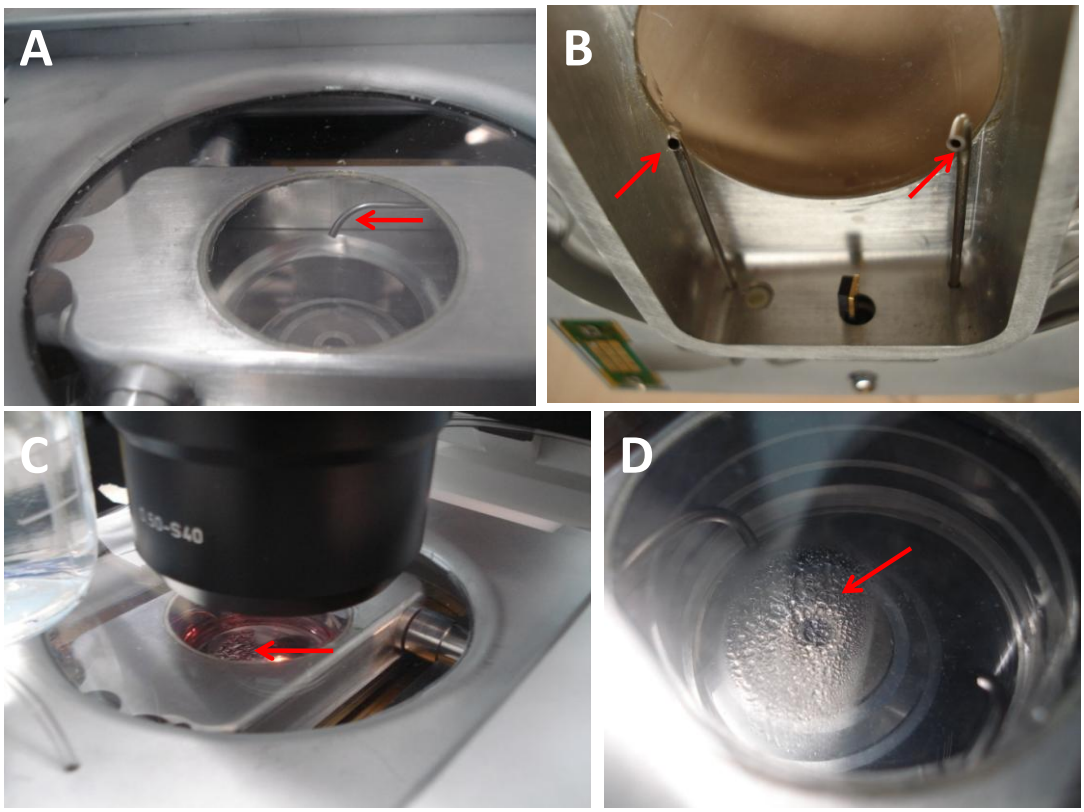

Figure 6.13. Media feed and condensation in prototype 5.

Media in and outlet pipes were incorporated into the design to enable feeding of long term cultures (A-B). Feed pipes are stainless steel to enable ethanol and/or autoclave sterilisation. The sealed inner chamber retained > 90 % humidity but the heat sink from the microscope and air conditioned room below the chamber caused condensation to build up between the culture dish and glass base plate (C, D).

6.4.6 Linkam LCI facility - Prototype 6

Final modifications to the imaging system removed the glass slide from the inner chamber base plate so there was no longer a surface on which condensation could build up. Instead the inner chamber was sealed around the petri-dish with a silicone ring to prevent loss of humidity and gas from the inner chamber (Figure 6.14). In addition, the inner chamber was rotated 90° with two outlets for heated air from the fan, improving the dispersal of warm air around the inner chamber. In this way, warm air exited the system underneath the culture dish from two directions, reducing the heat sink from below the culture surface in the cooled laboratory atmosphere.

Due to time restrictions on the duration of this project, it was not possible to fully trial Prototype 6 of the Linkam stage (Figure 6.15). However, initial studies showed promising results for retained humidity ≥ 90 %, with a tightly controlled 5 % CO_2 atmosphere and considerably reduced media loss over time (54.4 % evaporation after 7 days, when compared to the earlier 43.5 % evaporation after just 3 days in prototype 2), demonstrating that this system provides a facility which significantly improves upon the environmental conditions of current LCI systems.

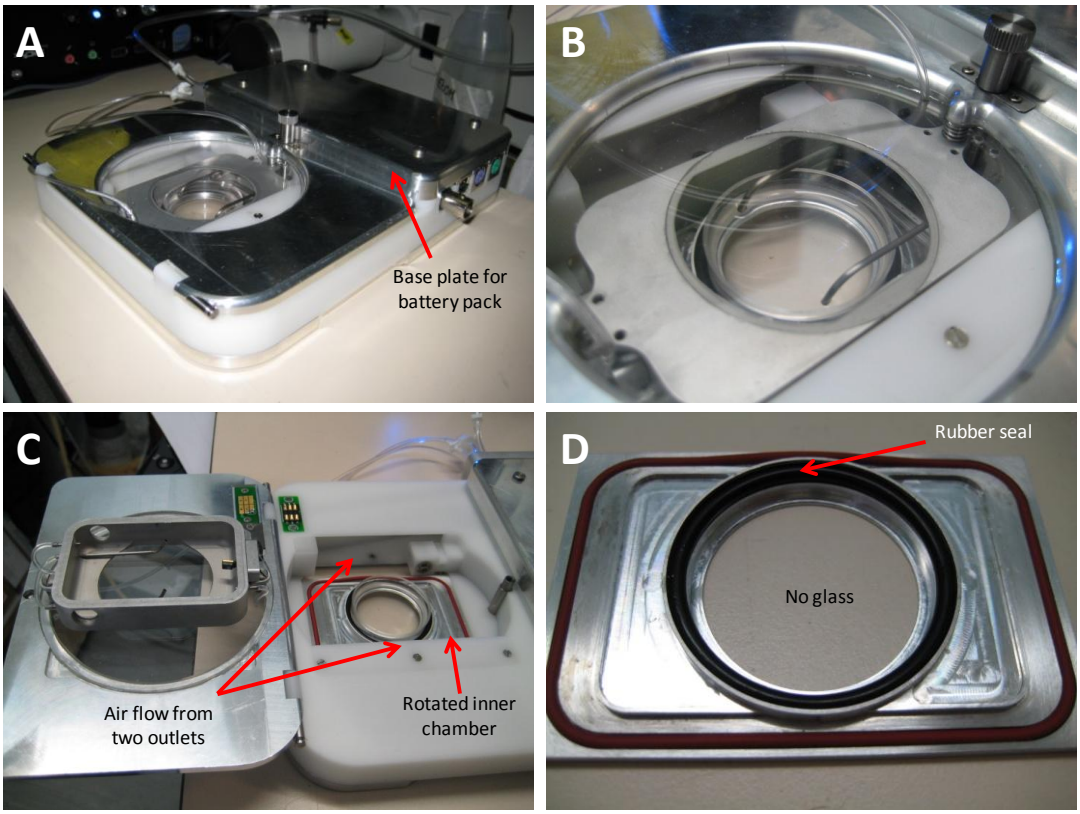

Figure 6.14. Linkam LCI facility - Prototype 6

Rotated inner chamber to allow heated air flow from two sides of the culture dish, preventing a exposure of a cooled surface for condensation to build up. The inner chamber was sealed with a silicone ring around the culture dish to retain a humidified atmosphere and controlled CO_2 environment.

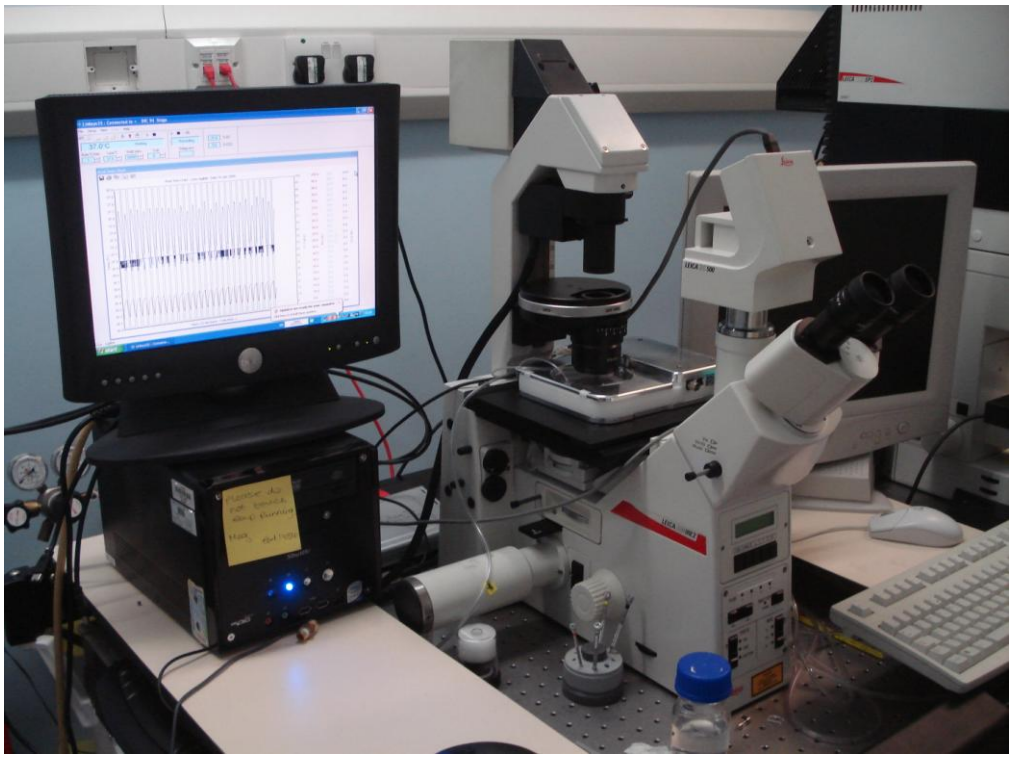

Figure 6.15. Linkam live cell imaging system.

A portable incubator which facilitates long term LCI studies, with automated control over culture environment. Suitable for use with any laboratory microscope.

6.5 Discussion

Although many of the environmentally controlled microscope incubator chambers on the market today provide fine control over temperature, humidity and gas flow, the portability and ease of use of the Linkam stage gives it an advantage over other products.

Linkam Scientific have tailored this product for use in laboratories worldwide, minimising cost, whilst maximising the potential applications. The use of readily available tissue culture dishes and the minimal gas consumption from a certified pre-mixed supply minimises running costs, whilst maximising confidence over culture environment. Limitations to the usability of the Linkam system remain in the user software which is currently undergoing modifications to incorporate changes introduced to by advances in CO_2 and temperature control. On completion of these modifications a baseline model for LCI will be ready for market launch.

Over the coming year, additional features will be developed and introduced as supplements to the basic model resulting from this study. These additional features will be aimed and increasing the market audience for this product and will include suggestions resulting from use of the system in this study. Modifications will include a gas mixing facility to enable hypoxic cells culture, a battery supply for improved portability between laboratories enabling concurrent systems to be run, a media feeding facility to enable long term uninterrupted imaging for differentiation studies and adaptations to suite culture vessels of different sizes (Section 8.5). With these modifications, the stability of culture environment within the Linkam live cell imaging system, suggest a real place in the scientific research and development market for this system, providing an affordable option for laboratories to benefit from the advantages of live cell imaging.

7 Final Discussion

Pluripotent cells are capable of both self-renewal and differentiation into any cell type of the body (Thomson et al., 1995). As such they are able to generate unlimited numbers of any desired cell type with huge potential for application to pharmacological screening and regenerative therapies where process is limited by cell supply. However, the differentiation capabilities of these cells are variable between cell lines and laboratories, and conflicting evidence with regards to their stability in culture, raises concerns over their suitability for therapy.

Throughout this project a comparative study into the stability and neuronal differentiation capability of a range of pluripotent cell lines (hEC and hESC) has been carried out. Comparative analysis of cell behaviour and morphology was achieved using a combination of bright field microscopy, epi-fluoresence microscopy and a live cell imaging facility, which was designed throughout the project for this purpose. Finally an in depth comparison of the changes in gene and protein expression of the different hESC lines following induction of neuronal differentiation was undertaken, which highlighted internal programming amongst different hESC lines, that confer a preferential cell fate for differentiation.

7.1 Expansion and stability of pluripotent cell lines in culture

Five pluripotent cell lines were combined for comparison in this study of both hEC and hESC origin (NTERA2, Shef3, HUES7, RH5 TrypLE and RH5 cut). The RH5 cut was a sub culture of the original enzymatically passaged RH5 cell line (referred to as RH5 TrypLE throughout this project), adapted into mechanical passaging, enabling a comparison of cell behaviour between two mechanically passaged (Shef3 and RH5 cut) and two enzymatically passaged cell lines (HUES7 and RH5 TrypLE).

No differences were observed in the expression of OCT4, SOX2, SSEA4 and Tra-1-60 amongst pluripotent populations of each of the five cell lines studied. However, there were significant differences in the behaviour of these lines in culture, and their susceptibility to spontaneous differentiation. Seeding at low densities induced differentiation in all cell lines but this was most noticeably in the NTERA2. Amongst mechanically passaged hESC lines, spontaneous differentiation was observed when cultured on low iMEF densities $< 2.6 \times 10^4$ cell/cm^2. In all cases, low cell density resulted in cells of an epithelial morphology. These cells were not fully characterised in culture but have been identified previously by multiple laboratories (Damjanov and Andrews, 1983; Pleasure et al., 1992; Amit et al., 2000).

In contrast, the effect of high seeding density induced differentiation was varied across the pluripotent lines (high iMEF density for mechanical passaged lines), generating a haphazard array of different cell types which were different between each of the hESCs studied. In Shef3, spontaneous differentiation frequently resulted in the formation of patches of beating cells, similar in appearance to those of cardiomyocytes (Burridge et al., 2007), which were rarely observed in the HUES7 cell line and never observed in the NTERA2 or RH5 cut/TrypLE lines. In itself, the cell types formed during spontaneous differentiation could be considered a good indicator of the preferred cell fate of a cell line.

Additional observed differences between the pluripotent cell lines included the speed of proliferation. Indeed reports of hESC doubling times range from 13-72 hours between different cell lines and laboratories (Cowan et al., 2004; Rosler et al., 2004; Thomson et al., 2008), demonstrating inherent variation in the behaviour of different hESC lines. In this study, mechanically passaged cell lines were considerably slower growing than the enzymatically passaged lines, which required passaging at approximately twice the frequency to retain pluripotent characteristics. The increased proliferation in enzymatically passaged cell lines would enable rapid expansion of cell numbers, facilitating scaled-up bioprocessing of these lines for therapy. However, rather than pluripotent cells, it is their differentiated progeny which would be used for therapy and in order to differentiate, a cell must exit the cell cycle (Walsh and Perlman, 1997; Maione and Amati, 1997; Brown et al., 2003). It was therefore hypothesised that the apparent preference to proliferate would reduce the capacity of a cell line to subsequently differentiate (Section 7.3).

Alterations in a cell's behaviour, such as the speed of the cell cycle, are brought about by changes to the internal programming of the cell. Indeed an increased rate of proliferation has been correlated to older hESC cultures, in which karyotypic abnormalities were more frequently detected (Cowan et al., 2004).

7.2 Karyotypic stability in pluripotent cell lines

The causes of karyotypic alterations in hESCs are the subject of huge debate in the field, with conflicting opinion over the influence of single cell dissociation by enzymatic passaging on hESC karyotypic stability (Cowan et al., 2004; Buzzard et al., 2004a; Draper et al., 2004a; Mitalipova et al., 2005; Suemori et al., 2006; Ellerström et al., 2007; Thomson et al., 2008). Data within this report largely supports concerns which suggest that enzymatic passaging of pluripotent cell lines induces the selection of chromosomal aberrations. The HUES7 cell line was originally derived with a normal 46 XY karyotype (Cowan et al., 2004); however,

preparation of the UKSCB MCB resulted in additional copies of chromosomes 12 and 17 and over 45 subsequent passages further trisomies for chromosomes 14 and X were detected. In contrast the mechanically passaged Shef3 retained its normal 46 XY karyotype throughout the project. This data suggests that enzymatic passaging contributes towards karyotypic instability; however, it does not account for the possibility that one cell line may be more susceptible to aberrations than another (Buzzard et al., 2004a). The adaptation of RH5 into mechanical passaging also resulted in small but significant alterations in the karyotype. These alterations may have occurred as a result of previous abnormalities from earlier enzymatic passaging; however, the original 101 XX karyotype of this line upon derivation would suggest an inherent susceptibility to karyotypic instability.

Chromosomal duplications, deletions and translocations can be detected using G-banding analysis, but this technique does not enable detection of smaller duplications/deletions in single loci, which were identified in RH5 cut and TrypLE using aCGH analysis. Array CGH was not carried out on the Shef3 cell line in this study. It is therefore possible that despite an apparently normal karyotype under G-banding analysis, the genomic content may indeed have undergone small alterations during culture which would require confirmation using aCGH analysis. It could therefore be speculated that the lack of karyotypic instabilities reported amongst hESC culture laboratories result from inadequate G-banding analysis, rather than true stability of hESCs in culture. Indeed recent publications which adopted aCGH technology for karyotypic analysis of hESC lines also detected smaller alterations which were missed under G-banding analysis, further supporting this theory (Thomson et al., 2008).

Array CGH comparison of the RH5 cut and TrypLE populations, detected four minor variations between the lines. Two of these were considered to be suitable candidates for the observed differences in neuronal yields of these cell lines. RH5 cut demonstrated a loss of chromosomal region 5q35.1 which encodes the BTRCP2 gene (FBXW11; NCBI, Entrez Gene). BTRCP2 is expressed at high levels in the foetal forebrain to regulate development (Koolen et al., 2006) and interacts with the BTRCP1 protein to form a dimer which is responsible for degradation of the REST protein (Suzuki et al., 2000a; Westbrook et al., 2008). Down regulation of REST is required for neuronal differentiation (Ballas et al., 2005; Sun et al., 2005; Johnson et al., 2008; Jørgensen et al., 2009; Buckley et al., 2009). Indeed gene expression analysis demonstrated a higher average REST expression in RH5 cut than in RH5 TrypLE. Therefore the loss of this chromosomal region may in part explain the lower neuronal yield from RH5 cut than RH5 TrypLE. In addition aCGH analysis detected a gain of chromosomal region 2p25.2 in RH5 TrypLE. A loss of this region has been previously associated with Autism (Lo-Castro et al., 2009), which has been linked to a reduction in the number of inhibitory neurons within the

cortical region of the brain (Vaccarino et al., 2009). With this in mind, an additional copy of the 2p25.2 chromosomal region may be implicated in the production of GABAergic inhibitory neurons, which were generated in higher numbers by the RH5 TrypLE cell line than any of the other three hESC lines investigated.

Since the two RH5 cell lines arose from the same starting cell pool and were cultured in parallel using the same media, the mode of passaging was the only variable to cause differences in cell behaviour. Therefore, the effect of passaging did not only impact upon length of the cell cycle and but also on the subsequent ability of the different lines to be directed into a neuronal cell fate. With this in mind, the five pluripotent cell lines were compared for their gene expression profiles in response to induction of neuronal differentiation.

7.3 Comparative neuronal differentiation in pluripotent cell lines

Early neuronal differentiation studies were modelled on the established ATRA induced motor neuronal differentiation in NTERA2 (Pleasure et al., 1992). The efficiency of differentiation using NTERA2 was highly variable, despite enhancements to the protocol. On occasion, no neuronal differentiation occurred, generating cells of epithelial-like morphology.

Upon successful differentiation, neurons were identifiable in culture just 10 days after ATRA induction, characterised by the expression of the neuronal markers TUBB3 and MAP2. The number of neurons continued to increase throughout the subsequent weeks in culture.

One of the key limitations for use of cell line derived neurons in pharmacological screening is their reduced response to neurotransmitter stimuli when compared to primary sourced neurons (Personal communication Dr. T. Sesardic, Bacteriology, NIBSC). For this reason, emphasis was placed on ensuring neuronal functionality amongst differentiated populations, with comparison to behaviour of primary neurons in response to stimulation. Patch clamp analysis of NTERA2-derived neurons throughout differentiation demonstrated the ability to fire genuine sodium action potentials in response to manual depolarisation after just two weeks. This was the first study to compare the functionality of NTERA2 derived neurons throughout differentiation, and demonstrated that prolonged culture resulted in an increase in the overall neuronal yield, in addition to improvements in neuronal functionality.

Calcium imaging enabled a visible comparison of the behaviour between NTERA2 derived neurons and primary neurons. Rat neural tissue is frequently used for pharmacological screening, and as such was considered to be a suitable control for the comparison of cell line

derived and primary neural tissue. Due to the detection of GABAergic neurons in NTERA2 derived neuronal populations, primary neurons were sourced from the ganglionic eminence of an e14 rat, which is the source of GABAergic interneurons in the brain (Ang et al., 2003). Primary neurons generated recurrent, electrical communication across the monolayer of cells in culture in the absence of external stimulation. Spontaneous activity was not seen in NTERA2 neuronal populations and required manual depolarisation to induce a response; however, this may simply have been a result of lower neuronal cell density in NTERA2 populations with subsequently reduced production of neurotransmitter for stimulation of surrounding cells, rather than in inability to respond to surrounding signals.

Maturation of NTERA2 neurons was demonstrated after prolonged culture by the generation of recurrent AP's following stimulation; however, the size of electrical impulse from 6-week differentiated NTERA2 was much reduced from that of the primary neurons. In addition, the calcium influx in response to glutamate was considerably less than was seen in primary neurons with an average cytosolic calcium levels reaching ~150 nM in comparison to ~800 nM in primary neurons. This suggests a reduction in the number of functional glutamate ion channels when compared to primary neurons, thus reducing the electrical impulse generated by the cell.

Transplantation of NTERA2 derived neurons into the brain of a 71-year old stroke victim, demonstrated the ability of cell line derived neurons to integrate into host tissue following transplantation (Nelson et al., 2002); however, minimal recovery of function was observed, which is a likely result of their immature neuronal phenotype. The survival of these cells following transplant, in the absence of tumour formation is a promising result for the use of pluripotent derived cell lines in therapy; however, the poor efficacy of these cell *in vivo* actively demonstrates the requirement for improvements to cell line-derived neuronal function, in addition to neuronal yield.

The NTERA2 cell line was originally derived from a germ cell tumour in 1975, and reported to have a hypertriploidy karyotype 63 XY t(12;13)(q13;qter) (Andrews et al., 1990; Andrews et al., 1994). Preparations for karyotypic analysis of this cell line during this study, failed to generate sufficient metaphase spreads for G-banding; however, given the propensity of pluripotent hESC lines to accumulate karyotypic alterations following extended culture (Section 7.2), it would be reasonable to assume that more than 30 years in culture under selection for pluripotent populations may have affected the ability of these cells to respond to differentiation stimuli, thus resulting in heterogeneity in differentiation. With this in mind, it

was hypothesised that the irreproducible response of NTERA2 to differentiation, was a result of its original tumour origin and abnormal karyotype resulting from culture adaptation.

To investigate this further, neuronal differentiation amongst a selection of hESCs was compared to that of NTERA2. Pluripotent hESC lines with varying degrees of chromosomal abnormalities (Section 4.1.1) were selected for investigation. In addition, the effect of passaging technique on the subsequent differentiation of the hESC lines was also investigated by comparison of the mechanically and enzymatically passaged cell lines. Pluripotent populations were differentiated following the enhanced neuronal differentiation protocol developed within this study.

Neuronal differentiation was initiated by standard EB formation but was selective for cells of ectodermal cell fate using a neural induction media. Induction of differentiation in this media reported a more rapid down regulation of pluripotency (according to OCT4) and enhanced commitment of cells into the ectodermal fate, as confirmed by increased expression of Nestin after four days in NI media when compared to alternative media for EB differentiation methods (Li et al., 2007). Additional improvements to neuronal purity were achieved by the removal of serum from differentiation media which reduced the overgrowth of non-neuronal cells in culture (Brewer et al., 1993; Brewer, 1995). In a similar way, removal of bFGF from differentiation media after the first four days in culture, also enhanced neuronal purity as determined by TUBB3 expression (Schwindt et al., 2009).

Neurons derived from all four hESC lines stained positively for neuronal markers TUBB3, MAP2 and 70 kDa Neurofilament. Data on the expansion of human neural precursor populations from a range of brain regions suggests that GABAergic neurons are the default neuronal phenotype of *in vitro* neuronal differentiation (Jain et al., 2003). Correspondingly, immunostaining of hESC derived neurons confirmed a proportion of inhibitory GABAergic neurons within all hESC lines. No positive staining for TH or SERT was detected in end stage populations; however, in the absence of a positive neuronal control for immunostaining studies, it was difficult to confirm negative staining. Damage to the neuronal networks during preparation for flow cytometry analysis meant that it was not possible to quantify the neuronal yields for comparison between these lines. However, visible inspection of colonies following differentiation, highlighted clear variations between the neuronal yield and purity from each hESC lines following differentiation; RH5 TrypLE was the most responsive cell line to neuronal differentiation, with the greatest reproducibility and highest neuronal yields. In contrast, Shef3 was highly variable. Neurons were visible following Shef3 differentiation but failed to spread in monolayer culture and were easily detached from the tissue culture surface

during feeding. These observations of neuronal yields were confirmed by Q-PCR analysis of differentiating populations.

Pluripotency prior to differentiation was confirmed by the expression OCT4, SOX2, Tra-1-60 and SSEA4, in addition to positive expression of genes associated with pluripotency (DNMT3B, FGF4, EBAF, GDF3, TDGF1, UTF1 and TERT). With the exception of SOX2, all of these genes were down regulated in the four hESC lines upon differentiation. In addition to regulating pluripotency, SOX2 is also expressed amongst neural progenitors, regulating proliferation and inhibiting terminal differentiation (Graham et al., 2003). Interestingly, SOX2 was significantly down regulated from day 0 in Shef3 ($p = 0.007$ to day 28), suggesting a reduced number of neural progenitors in this line, compared to the other hESC lines (HUES7, RH5 cut and RH5 TrypLE) which retained consistent SOX2 expression throughout differentiation ($p = 0.950$, 0.479, and 0.118 respectively).

The reduced neuronal differentiation of Shef3 can be explained by several reasons. Most significantly, a larger proportion of Shef3 cells were lost into the endodermal lineage during the EB stage of differentiation as determined by the highest expression of AFP of all hESC cell lines, 3-, 5.3- and 17.4-fold higher expression than RH5 cut, HUES7 and RH5 TrypLE respectively. In addition Shef3 expressed the highest levels of REST, of all three lines, which inhibits neuronal differentiation (Ballas et al., 2005; Sun et al., 2005). Despite this, some neuronal differentiation was identified in Shef3, suggesting that it was not completely blocked. Neuronal differentiation in Shef3 was mainly forebrain derived GABAergic neurons, as detected by higher up regulation of PAX6 and PTF1A than the motor neuronal markers: HXLB9, CRABP2 and ISL1. In addition, gene expression analysis detected the up regulation of TH, a marker for midbrain dopaminergic neurons amongst day 28 samples although this was considerably lower than levels detected in the HUES7 populations.

The HUES7 cell line was easily established in culture and responsive to neuronal differentiation. This cell line also presented minimal motor neuronal differentiation with a continual down regulation of the motor neuron specific marker HLXB9. Neurons derived from this line were of predominantly forebrain and midbrain phenotype, with high levels of PAX6 and PTF1A and TH, peaking at day 28 with 142.5, 201.9 and 127-fold increase from day 0 respectively. This was the highest expression levels of TH in all of the four hESC lines, suggesting that this line may be best applied for studies wishing to generate dopaminergic neurons. GABA was identified amongst HUES7 day 28 populations by immunostaining but TH positive neurons were not. In the absence of a positive control it was not possible to confirm whether this was true negative staining. However, the large error bars in TH gene expression

are suggestive of a variable dopaminergic neuronal yield in the HUES7 cell line. As such it is possible that the immunostained samples were from a preparation when dopaminergic yield was genuinely low. In light of this data, the immunostaining of final neuronal populations should be repeated in the presence of a positive control.

HUES7 showed the greatest propensity for neuronal maturation of the four hESC lines, indicating the highest proportion of mature neurons as detected by SYP 136-fold increase in expression form day 0, compared to 15.42, 9.25, and 1.78-fold increase in expression by day 28 in RH5 cut, RH5 TrypLE and Shef3 respectively.

The RH5 cut cell line responded differently to neuronal differentiation than was seen in RH5 TrypLE, despite arising from the same starting population of cells. From this it could be concluded that the culture techniques of these two lines, do impact upon their outcome of differentiation. However this cell line was passaged 36 times using enzymatic techniques prior to adaptation, suggesting that the hESC lines in culture are subject to continual adaptations.

The largest differences between the neuronal differentiation of RH5 cut and RH5 TrypLE were observed in the expression of Noggin, whereby RH5 TrypLE expression increased by 27.8-fold on day 10 compared to 4.6-fold increase in RH5 cut on the same day (relative to day 0). Noggin is a BMP inhibitor which blocks the commitment of pluripotent cells in a mesodermal or endodermal cell fate (Pera et al., 2004; Gerrard et al., 2005a; Sonntag et al., 2007). With this in mind, it was not surprising to see a higher overall neuronal yield in RH5 TrypLE than RH5 cut. Indeed, the RH5 TrypLE cell line presented the highest expression of Noggin in all four hESC lines, and might explain the high success of neuronal differentiation in this line. Perhaps more interestingly, the Noggin gene is located on chromosome 17q21-22 (NCBI, Entrez gene), a region which is frequently duplicated upon enzymatic adaptation to culture. This might explain why the HUES7 and RH5 TrypLE were apparently more reproducible in their neuronal differentiation than the mechanically passaged lines, and might suggest a benefit to enzymatic culture of hESC lines for use in pharmacological screening assays or neurodegenerative therapies.

RH5 TrypLE retained high expression of many neural precursors including Nestin, PAX6, OLIG2, ISL1 and PTF1A, in addition to up regulation of mature neuronal markers in the latter stages of differentiation (SYP, TH and HLXB9) which was indicative of neuronal generation from all three developmental regions of the CNS (forebrain, midbrain and spinal cord). However, expression of SYP and HLXB9 were lower in RH5 TrypLE than in RH5 cut, which in combination with the retention of precursor markers, was suggestive of a large proportion of immature neurons within the final day 28 population. In addition, expression of PTEN was lowest in RH5 TrypLE

than in the other three hESC lines. PTEN inhibits proliferation of neural stem cells, thus a reduction of PTEN would explain higher proliferation amongst the RH5 TrypLE population of neurons (Groszer et al., 2001; Qu and Shi, 2009).

The largely abnormal karyotype of the RH5 TrypLE cell line means that its incorporation into transplantation therapies is unlikely due to a risk of tumour formation following transplantation. The risk of this was further emphasised by the apparent up regulation of pluripotency genes OCT4 and Nanog in day 28 samples which was also observed in the alternative enzymatically passaged cell line HUES7, suggesting an outgrowth of pluripotent cells within the differentiated populations. However, the large reproducible neuronal yield from this cell line would be ideal for incorporation into pharmacological screening, reducing reliance upon primary tissue, and thus reducing animal sacrifice.

The incorporation of cell line derived neurons into cell based assays is currently limited by both supply and sensitivity. Neural precursors derived from pluripotent lines have a restricted capacity for proliferation prior to commitment into their terminal neuron cell fate (Maric and Barker, 2005; De Filippis et al., 2008). Yet, the RH5 TrypLE cell line has demonstrated an enhanced expansion of neural precursors when compared to alternative cell lines, and an ability to terminally differentiate into a defined neuronal phenotype. Thus, providing a near perfect solution to the shortage of cells for use in pharmacological screening, requiring only proof of sufficient sensitivity in the function of RH5 TrypLE derived neurons.

Human ESC derived neurons were screened for their ability to generate an electrical impulse using patch-clamp analysis. Neurons from all four hESC lines fired genuine rapid sodium action potentials which were reversibly inhibited following exposure to TTX. However, similarly to the responses seen in immature NTERA2 derived neurons, only single AP's were fired in response to stimulation, suggesting an immaturity in the behaviour of hESC derived neurons, and thus considered to be suboptimal when compared to the response of primary cells. The functional data from these cells emphasises the requirement for further modifications to differentiation, in order to generate a more responsive end product (Section 8.2)

7.4 Summary

Data from this study supports concerns that enzymatic passaging of pluripotent hESCs induces karyotypic instabilities, following identification of trisomies for chromosomes 12, 14, 17 and X in enzymatically passaged HUES7, and the retention of an outwardly normal karyotype in mechanical passaged Shef3. However, aCGH analysis would need to be carried out on the Shef3 cell line to confirm the absence of minor alterations, after the identification of minor alterations in the RH5 cut line, suggesting that on the contrary to *hypothesis 1*, the method of culture does have an affect the karyotypic stability of a pluripotent cell line in culture.

In disagreement with *hypothesis 2*, data from this study suggests that pluripotent cells are not equally directable into neuronal differentiation when cultured under optimal conditions. Spontaneous differentiation amongst each of the pluripotent cell lines demonstrated variation in the preferential cell fate of different cell lines, NTERA2 favoured epithelial differentiation, Shef3 appeared to favour mesodermal and endodermal differentiation with large variation in the response to neuronal differentiation. Both RH5 cell lines were responsive to neuronal differentiation; however, RH5 TrypLE was more reproducible and yielded high numbers of neurons than RH5 cut, thought to be a results of endogenous inhibition towards mesodermal and endodermal lineages. Finally, HUES7 was reproducibly induced into a neuronal cell fate but demonstrated restricted expansion of neural precursor populations.

Finally, data from this study provides evidence against *hypothesis 3: 'The method of culture does not affect the ability of a pluripotent cell line to be differentiated into a functional neuron'*. All five pluripotent cell lines investigated were responsive to neuronal differentiation; however, the parallel culture of RH5 under mechanical and enzymatic passaging demonstrated divergence in their genomic content, including alterations in two candidate genes which influence neurogenesis, and may in part explain the differences in neuronal yields between the two RH5 cell lines. These data suggest that the method of culture can indirectly affect the ability of a cell line to differentiate towards the target neuronal cell fate, by inducing karyotypic alterations within the population.

8 Future work

In the event of any in-detailed research, the results obtained generate further areas for investigation. As was the case with this project, the findings within highlighted a number of areas which required further attention, these have been outlined below. Indeed, work on a number of these topics has begun in response to the results from this study and as such, represent the ongoing works to enhance neuronal yields from pluripotent cell lines with a view to future applications in regenerative therapies.

8.1 Karyotypic analysis

Data within this report supports concerns, which suggest that enzymatic passaging of pluripotent cell lines induces the selection of chromosomal aberrations. However, the differences between enzymatic and mechanical passaging may not be considered truly representative in this study due to the comparison of a cell line which was abnormal from derivation, suggesting a propensity for karyotypic instability. The effects of culture on karyotypic stability would therefore be better demonstrated with the adaptation of a range of hESC both normal and abnormal in starting pools into enzymatic passaging from mechanical and *vice versa*. The populations would need to be cultured for a minimum of 20 passages under each condition (during which time most reports of abnormalities had been identified), followed by in depth analysis of gDNA content using both G-banding and aCGH technologies. Each sample would need to be compared to the genomic content of the original starting cell population. In this way, it would be possible to clearly identify the impact of different passaging techniques on the stability of hESC lines in culture over time. Subsequent comparison of the neuronal differentiation in mechanically or enzymatically passaged lines would then re-confirm the effects of passaging on the later directability into differentiation.

8.2 Enhancing neuronal yield, survival and functionality

8.2.1 Mesendodermal blockers

The enhanced EB differentiation protocol within this study utilised a nine day EB formation stage. Although selection for neural cells was induced from initiation of differentiation, studies into the development of EBs have clearly demonstrated the commitment of pluripotent cells into cell fates from all three germ lineages (Itskovitz-Eldor et al., 2000). Through the duration of differentiation, culture media continued to select for neuronal populations, thus improving the purity of neurons as differentiation progressed. However, neural precursors have a finite

expansion potential in culture (Jain et al., 2003; De Filippis et al., 2007; Elkabetz et al., 2008; Bajpai et al., 2009), and commitment of pluripotent cells into mesodermal or endodermal lineages in the early stages of differentiation, will have directly reduced the final neuronal yield. Alternative differentiation protocols, incorporate incubations with BMP blockers such as Noggin to prevent the commitment of pluripotent cells into mesodermal or endodermal cell fates (Pera et al., 2004; Iacovitti et al., 2007), thereby enhancing the final neuronal yield. Additional studies have shown that incubation with Nodal inhibitors (Lefty and Cerb-S) also enhance neuroectodermal commitment, thus increasing neuronal yields from pluripotent populations (Vallier et al., 2004). With this in mind, incorporation of Noggin and or Lefty/Cerb-S into the early stages of differentiation in NI media should therefore improve the commitment into ectodermal fate, thus enhancing subsequent neuronal yields. This would prove to be a valuable addition to the media.

8.2.2 Supplementation of Neurotrophins

Results from the gene expression analysis study all suggest that the RH5 TrypLE cell line retained a progenitor state for longer in culture, enabling expansion of the neural precursors for generation of a larger neuronal yield. Up regulation of mature neuronal marker SYP in addition to the demonstrable electrophysiological activity of this cell line confirmed the ability of this cell line to differentiate further into a more mature neuronal phenotype. For this reason, The RH5 TrypLE cell line would seem to be an ideal candidate cell line for the production for large numbers of neurons for pharmacological screening. However, it would first be necessary to demonstrate that RH5 TrypLE derived neurons could be matured into a neuronal phenotype with the sensitivity of a primary neuron to stimulation. Neuronal maturation might be achievable by the addition of GDNF and BDNF into the maturing neuronal populations. These neurotrophins have proven to be successful in aiding neuronal differentiation and maturation, in addition, to improved neuronal survival, thus reducing the high levels of cell death amongst differentiated neurons (Sauer et al., 1993; Encinas et al., 2000; Obrietan et al., 2002; Zeng et al., 2006; Bakshi et al., 2006; Xuan et al., 2008).

The effect of GDNF and BDNF on neuronal maturity would be easily investigated following supplementation into culture by the comparative behaviour under calcium imaging to neurotransmitter stimulation. Additional functionality of these neurons could be carried out using High Performance Liquid Chromatography (HPLC) analysis to detect manufacture and release of the neurotransmitters following stimulation. In the event of HPLC studies it would

be essential to supplement neuronal culture with all non-essential amino acids, from which the neurotransmitters could be synthesised (Wurtman, 1988).

8.2.3 Hypoxic culture

One of the main hurdles for using primary neurons, or neurons derived from progenitor lines in culture, is in overcoming their poor survival in culture, this should be enhanced following incorporation of GDNF and BDNF into culture; however, further alterations to differentiation may prove to be of additional benefit. The bulk of the CNS is formed during the first trimester of embryonic development, prior to full vascularisation of the placenta and foetus (Gellén, 1976; Hustin and Schaaps, 1987; O'rahilly and Müller, 1999a), as such, the nervous system develops mainly under a hypoxic environment, preventing damage by reactive oxygen species. Under laboratory differentiation, neurons are cultured in an ambient oxygen environment, with demonstrable susceptibility to damage by oxidative free radicals (Davis and Maher, 1994; Tan et al., 1998). With this in mind, differentiation and extended culture of neurons under hypoxic conditions (1-2 % O_2) should reduce the oxidative damage and thus enhance neuronal survival. Preliminary studies have shown that the neuronal differentiation of mESCs is enhanced under hypoxic culture (Mondragon-Teran et al., 2009); however, this is yet to be translated into hESCs.

In combination, the inhibition of mesodermal and endodermal commitment, supplementation of differentiation media with survival enhancing growth factors and hypoxic culture form the main focus of work continuing on from this project, with a view to enhancing neuronal yield for the treatment of neurodegenerative therapies.

8.2.4 Electrical stimulation

The neuronal phenotype generated during neurulation is largely dependent upon the developmental signalling from the cells and differentiation media around them. A large number of neurons are formed during prenatal neurogenesis (O'rahilly and Müller, 1999b), with further neurogenesis and neuronal maturation occurring postnatally. Therefore, it is likely that during neuronal maturation, early electrical impulses from pre-committed neurons are present. In the same way that bone, muscle and tendons develop and regenerate in response to mechanical forces and stimuli around them to enhance their function (Benjamin and Hillen, 2003) it is possible that electrical stimulation of neurons throughout differentiation would improve their sensitivity and response to stimuli. Indeed electrical stimulation of a

differentiating EB has demonstrably enhanced neuronal yields from mESCs but is yet to be demonstrated in hESCs (Yamada et al., 2007).

Exposure to electrical impulses in culture could be achieved by differentiation a micro-electrode array (MEA) system. Modern MEA's comprise culture surface integrated with a number of platinum electrodes which are intended for recording electrical impulses across slices of excitable tissue; however, differentiation upon these arrays would enable regular burst of electrical stimulation across the culture at regular defined intervals. In addition, these systems could record electrical activity and therefore enable continued monitoring of neuronal maturity throughout differentiation without disruption of the cells in culture. Research into this hypothesis would provide a new area of focus for improved neuronal differentiation from pluripotent cells.

8.3 Neuronal characterisation

Despite clear differences in the numbers of neurons generated from the four different cell lines, the behaviour, morphology and functionality of the neuronal generated did not appear different according to live cell imaging and patch-clamping analysis. Identification of the subclasses of neurons generated by each cell line would provide a better insight into the suitability of using these end stage cells for clinical or pharmaceutical applications.

Immunostaining of neuronal populations using antibodies for dopaminergic (TH), serotonergic (SERT) and GABAergic (GABA) neurons were purchased for this study, but additional staining was restrict by the time and budget available within this project. The presence of GABAergic neurons were identified amongst end stage neuronal populations; however, not all neurons in culture were GABAergic and without the incorporation of a positive control it was not possible to rule out the presence of TH and SERT neuronal populations. Determination of neuronal subtype would ideally be repeated with optimised working antibodies for the aforementioned neuronal classes, in addition to screening for additional neuronal subclasses: glutamatergic, cholinergic, noradrenergic, glycinergic neurons, some of which have been demonstrably derived following ESC neuronal differentiation (Reyes et al., 2008; Michibata et al., 2009).

8.4 Proteomics

Data from within this study has correlated changes in gene expression to the success of neuronal differentiation; however, it is the proteins which are encoded by these genes which regulate a cell's behaviour. Interaction of different proteins within a cell can alter its

behaviour, thus regulation of differentiation, is controlled at a post-transcriptional level in addition to the level of gene expression. The effect of differences between gene and protein expression were observed during his study by the up regulation of the OCT4 gene with no detection of the protein under immunofluorescence analysis, thus highlighting discrepancies in the assumed and true protein content of a cell.

Proteomics enables the direct analysis of the proteins which are present within a cell (James, 1997). An understanding of the changes in protein expression can provide a valuable insight into essential components which direct neuronal differentiation, resulting in the visible change in phenotype. In this way, proteomics analysis is able to identify the protein targets for recombinant substitution into differentiation media, for improvements to neuronal differentiation.

In response to development of a reproducible protocol for differentiation, collaboration was set up for a comparative proteomic analysis of hESCs throughout neuronal differentiation (Dr. Jun Wheeler, and Dr. Iolanda Vendrell, Laboratory for Molecular structure, NIBSC). This work aims to identify key target proteins which are up and down regulated upon successful neuronal differentiation to further enhance our understanding of the signalling required for successful neuronal differentiation.

This work in currently ongoing; however, to date, proteins from the five differentiation time points of RH5 TrypLE have been analysed using 2D Gel electrophoresis. A number of proteins which consistently showed up or down regulations between triplicate samples were identified by the intensity of staining. These proteins will be isolated and identified using mass spectrophotometery, generating a range of candidate proteins which could be used for further enhancement of neuronal differentiation *in vitro*.

8.5 Modifications to the Linkam live cell imaging facility

Throughout this study, the Linkam LCI system was transformed from a basic short term facility without environmental control, to a high end environmentally controlled chamber which facilitated LCI over several days in culture, limited only by the requirement for media exchange. Future modifications to the system are currently under development following feedback and data from within this study (as detailed below), generating a wide LCI product range, with a 'mix and match' style system to design a LCI imaging facility which covers the wide range of requirements for different research targets.

8.5.1 Media feed and flow rate

The main limiting factor for long term LCI of mammalian cells is the need for regular media exchange, removing toxic build up and supplying the cells in culture with the necessary nutrients for survival. The Wafergen system (Section 6.2.3) is currently the only LCI facility available which enables uninterrupted imaging during cell feeding. However, culture of cells in this system demonstrated that evaporation of culture media and cell death was still a real problem. In addition, the Wafergen system was not autoclavable and subsequent sterility of long term studies proved to be problematic (Personal communication Mr. P. Mondragon-Teran).

The Linkam system is autoclavable and issues of evaporation have been considered and resolved in the design. Using the stainless steel feed pipes in the current model, it would be possible to manually pump sterile media into and out of the dish. However, this would cause movement and interruption to imaging which is not ideal. Plans for modifications to the LinkSYS software for automated feeding are also in progress as an additional feature.

8.5.2 Portability

The ability to culture cells in a continuous environment and image will have huge advantages to understanding cell behaviour. The Linkam system offers and affordable option for LCI in laboratories where the microscope cannot be dedicated solely to a single imaging experiment. The system can be easily moved on and off the microscope as required. In addition, a battery power supply is currently under development to enable detachment from mains power and the gas supply, and transport under a controlled environment, providing an opportunity to move samples from building to building without exposure to suboptimal culture environment in transit. This additional feature might also appeal to non-imaging based projects where live cell transport is necessary for experimentation such as functionality studies.

8.5.3 Pressure control

Stem cells cultured for therapeutic applications need to be cultured under in GMP grade facilities, which run under positive pressure (Healy et al., 2005). It would be interesting to see what affect this pressure has on the growth and behaviour of cells and could be monitored in real time using the Linkam system with an incorporated pressure sensor. Using the sealed inner chamber and a gas feed on valve control; it would be possible to modify the system to incorporate a pressure sensor to run experiments under different atmospheric pressures. This

facility is not available on any marketed imaging system and would create an additional niche market for the Linkam imaging system. Designs for such a modification are in discussion.

8.5.4 Dynamic temperature control

There are a number of design features of the Linkam stage which limit its use for monitoring cellular activity. Expansion of the stages temperature range to 4 °C - 40 °C, would enable hypothermic and hyperthermic studies on cellular behaviour to be carried out. However, this would require the presence of an active cooling circuit, which would increase the size of the system, reducing portability and also increase cost.

8.5.5 Electrophysiology

Incorporation of an MEA system into the stage, (Alpha MED Sciences Co., Ltd, Osaka, Japan) would combine electrophysiological studies with environmental control under live cell observation, creating a system which is not provided by any other manufacturer. This would enable electrical stimulation throughout differentiation (Section 8.2.4) and would also facilitate electrophysiological recordings of developing neurons in culture. The inner chamber would need to be enlarged to incorporate an MEA (50 mm x 50 mm square in addition to surrounding space for the connection leads), which would still sit neatly inside the overall outer chamber of the device. However, is likely to alter the heating currents around the system which would need to be carefully mapped and may need further design modifications.

8.5.6 Gas mixing

The Linkam system was designed to run from pre-mixed gas supplies with an in built CO_2 sensor. Development of system for additional monitoring and control of O_2 is currently underway to enable hypoxic studies. The refinement of the gas mixing feature (in prototype 2) would enable dynamic studies of oxygen tension to be carried out over long periods and is currently under investigation for sale as an additional feature to the system. This additional feature will be incorporated into future investigations into the effect of hypoxic culture on neuronal differentiation in hESCs, and will be of particular interest when studying the effect of hypoxic culture on neuronal survival (Section 8.2.3).

9 Closing remarks

The data from this study have highlighted clear differences in the responses of all pluripotent hESC lines to neuronal differentiation stimuli. Inherent differences within the genetic programming of pluripotent populations have been identified demonstrating the requirement a detailed and informed cell line selection before undertaking lengthy differentiation studies at the risk of using cell lines with an alternative pre-determined cell fate.

10 References

1. Abbott,N.J., Ronnback,L., and Hansson,E. (2006). Astrocyte-endothelial interactions at the blood-brain barrier. Nat Rev Neurosci *7*, 41-53.

2. Adewumi,O., Aflatoonian,B., Ahrlund-Richter,L., Amit,M., Andrews,P.W., Beighton,G., Belo,J.A., Benvenisty,N., Berry,L.S., Bevan,S., Blum,B., Brooking,J., Chen,K.G., Choo,A.B., Churchill,G.A., Corbel,M., Damjanov,I., Draper,J.S., Dvorak,P., Emanuelsson,K., Fleck,R.A., Ford,A., Gertow,K., Gertsenstein,M., Gokhale,P.J., Hamilton,R.S., Hampl,A., Healy,L.E., Hovatta,O., Hyllner,J., Imreh,M.P., Itskovitz-Eldor,J., Jackson,J., Johnson,J.L., Jones,M., kee,K., King,B.L., Knowles,B.B., Lako,M., Leclerc,N., Mallon,B.S., Manning,D., Mayshar,Y., McKay,R.D., Michalska,A.E., Mikkola,M., Mileikovsky,M., Minger,S.L., Moore,H.D., Mummery,C.L., Nagy,A., Nakatsuji,N., O'Brien,C.M., Oh,S.K., Olsson,C., Otonkoski,T., Park,K.Y., Passier,R., Patel,H., Pedersen,R.A., Pera,M.F., Piekarczyk,M.S., Pera,R.A., Reubinoff,B., Robins,A.J., Rossant,J., Rugg-Gunn,P., Schulz,T.C., Semb,H., Shevinsky,L.H., Siemen,H., Stacey,G.N., Stojkovic,M., Suemori,H., Szatkiewicz,J., Turner,R.S., Tuuri,T., van den Brink,S., Vintersten,K., Vuoristo,S., Ward,D., Weaver,T.A., Young,L.A., and Zhang,W. (2007). Characterization of human embryonic stem cell lines by the International Stem Cell Initiative. Nature Biotechnology *25*, 803-816.

3. Afelik,S., Chen,Y., and Pieler,T. (2006). Combined ectopic expression of Pdx1 and Ptf1a/p48 results in the stable conversion of posterior endoderm into endocrine and exocrine pancreatic tissue. Genes Dev *20*, 1441-1446.

4. Alberts,B., Johnson,A., Lewis,J., Raff,M., Roberts,K., and Walter,P. (2002a). Cell Communication. In Molecular Biology of the Cell, (New York, USA: Garland Science.), pp. 831-906.

5. Alberts,B., Johnson,A., Lewis,J., Raff,M., Roberts,K., and Walter,P. (2002b). Development of Multicellular Organisms. In Molecular Biology of the Cell, (New York, USA: Garland Science.), pp. 1158-1258.

6. Alitalo,K., Kuismanen,E., Myllyla,R., Kiistala,U., sko-Seljavaara,S., and Vaheri,A. (1982). Extracellular matrix proteins of human epidermal keratinocytes and feeder 3T3 cells. J. Cell Biol. *94*, 497-505.

7. Alonso,L. and Fuchs,E. (2003). Stem cells of the skin epithelium. Proceedings of the National Academy of Sciences of the United States of America *100*, 11830-11835.

8. ALS Society of BC. ALS Society of BC. ALS Society of BC . 2009.
Ref Type: Internet Communication

9. Alzheimer's Society. Alzheimer's Society. Alzheimer's Society website - What causes Alzheimer's? 2009.
Ref Type: Internet Communication

10. Alzheimers Research Trust. Alzheimers Research Trust. Alzheimers Research Trust . 2009.
Ref Type: Internet Communication

11. Ambrosetti,D.C., Scholer,H.R., Dailey,L., and Basilico,C. (2000). Modulation of the Activity of Multiple Transcriptional Activation Domains by the DNA Binding Domains

Mediates the Synergistic Action of Sox2 and Oct-3 on the Fibroblast Growth Factor-4 Enhancer. J. Biol. Chem. *275*, 23387-23397.

12. Amit,M. (2006). Feeder Free Culture of Human Embryonic Stem Cells. In Methods in Enzymology. Stem Cell Tools and Other Experimental Protocols, Irina Klimanskaya and Robert Lanza, ed. Academic Press), pp. 37-49.

13. Amit,M., Carpenter,M.K., Inokuma,M.S., Chiu,C.P., Harris,C.P., Waknitz,M.A., Itskovitz-Eldor,J., and Thomson,J.A. (2000). Clonally Derived Human Embryonic Stem Cell Lines Maintain Pluripotency and Proliferative Potential for Prolonged Periods of Culture. Developmental Biology *227*, 271-278.

14. Amit,M., Margulets,V., Segev,H., Shariki,K., Laevsky,I., Coleman,R., and Itskovitz-Eldor,J. (2003). Human Feeder Layers for Human Embryonic Stem Cells. Biol Reprod *68*, 2150-2156.

15. Amit,M., Shariki,C., Margulets,V., and Itskovitz-Eldor,J. (2004). Feeder Layer- and Serum-Free Culture of Human Embryonic Stem Cells. Biol Reprod *70*, 837-845.

16. Anderson,L. and Caldwell,M.A. (2007). Human neural progenitor cell transplants into the subthalamic nucleus lead to functional recovery in a rat model of Parkinson's disease. Neurobiology of Disease *27*, 133-140.

17. Ando,K., Shioda,S., Handa,H., and Kataoka,K. (2003). Isolation and characterization of an alternatively spliced variant of transcription factor Islet-1. J Mol Endocrinol *31*, 419-425.

18. Andrews,P.W., Benvenisty,N., McKay,R., Pera,M.F., Rossant,J., Semb,H., and Stacey,G.N. (2005). The International Stem Cell Initiative: toward benchmarks for human embryonic stem cell research. Nature Biotechnology *23*, 795-797.

19. Andrews, P. W, Bronson, D. L, Benham, F, Struckland, S, and Knowles, B. B. A comparative study of eight cell lines derived from human testicular teratocarcinoma. International Journal of Cancer 26, 269-280. 1980. Ref Type: Generic

20. Andrews,P.W., Casper,J., Damjanov,I., Duggan-Kenn,M., Giwercman,A., Hata,J., von Keitz,A., Looijenga,L.H., Millán,J.L., Oosterhuis,J.W., Pera,M., Sawada,M., Schmoll,H.J., Skakkebaek,N.E., van Putten,W., and Stern,P. (1996). Comparative analysis of cell surface antigens expressed by cell lines derived from human germ cell tumours. International Journal of Cancer *66*, 806-816.

21. Andrews,P.W., Damjanov,I., Berends,J., Kumpf,S., Zappavigna,V., Mavilio,F., and Sampath,K. (1994). Inhibition of proliferation and induction of differentiation of pluripotent human embryonal carcinoma cells by osteogenic protein-1 (or bone morphogenetic protein-7). Laboratory investigation; a journal of technical methods and pathology *71*, 243-251.

22. Andrews,P.W., Damjanov,I., Banting,G., Carlin,C., Dracopoli,N.C., and Fogh,J. (1984). Pluripotent embryonal carcinoma clones derived from the human teratocarcinoma cell line Tera-2. Differentiation in vivo and in vitro. Laboratory investigation; a journal of technical methods and pathology *50*, 147-162.

23. Andrews,P.W., Gönczöl,E., Plotkin,S.A., Dignazio,M., and Oosterhuis,J.W. (1986). Differentiation of TERA-2 human embryonal carcinoma cells into neurons and HCMV permissive cells. Induction by agents other than retinoic acid. Differentiation *31*, 119-126.

24. Andrews,P.W., Goodfellow,P.N., Shevinsky,L.H., Bronson,D.L., and Knowles,B.B. (1982). Cell-surface antigens of a clonal human embryonal carcinoma cell line: morphological and antigenic differentiation in culture. International Journal of Cancer *29*, 523-531.

25. Andrews,P.W., Nudelman,E., Hakomori,S., and Fenderson,B.A. (1990). Different patterns of glycolipid antigens are expressd following differentiation of TERA-2 human embryonal carcinoma cells induced by retinoic acid, hexamethylene bisacetamide (HMBA) or bromodeoxyuridine (BUdR). Differentiation *43*, 132-138.

26. Andrews,P.W., Przyborski,S.A., and Thomson,J.A. (2001). Embryonal Carcinoma Cells and Embryonic Stem Cells. In Stem Cell Biology, Cold Spring Harbor Laboratoy Press), pp. 231-265.

27. Andrews,P.W. (1984). Retinoic acid induces neuronal differentiation of a cloned human embryonal carcinoma cell line in vitro. Dev Biol *103*, 285-293.

28. Ang,E.S.B.C., Haydar,T.F., Gluncic,V., and Rakic,P. (2003). Four-Dimensional Migratory Coordinates of GABAergic Interneurons in the Developing Mouse Cortex. J. Neurosci. *23*, 5805-5815.

29. Anisimov,S.V., Christophersen,N.S., Correia,A.S., Li,J.Y., and Brundin,P. (2007). "NeuroStem Chip": a novel highly specialized tool to study neural differentiation pathways in human stem cells. BMC Genomics *8*, 46.

30. Artinger,K.B., Chitnis,A.B., Mercola,M., and Driever,W. (1999). Zebrafish narrowminded suggests a genetic link between formation of neural crest and primary sensory neurons. Development *126*, 3969-3979.

31. Atala,A., Bauer,S.B., Soker,S., Yoo,J.J., and Retik,A.B. (2006). Tissue-engineered autologous bladders for patients needing cystoplasty. The Lancet *367*, 1241-1246.

32. Atlasi,Y., Mowla,S.J., Ziaee,S.A.M., Gokhale,P.J., and Andrews,P.W. (2008). OCT4 spliced variants are differentially expressed in human pluripotent and non-pluripotent cells. Stem Cells 2008-0530.

33. Avilion,A.A., Nicolis,S.K., Pevny,L.H., Perez,L., Vivian,N., and Lovell-Badge,R. (2003). Multipotent cell lineages in early mouse development depend on SOX2 function. Genes & Development *17*, 126-140.

34. Avruch,J., Zhang,X.F., and Kyriakis,J.M. (1994). Raf meets Ras: completing the framework of a signal transduction pathway. Trends in Biochemical Sciences *19*, 279-283.

35. Babaie,Y., Herwig,R., Greber,B., Brink,T.C., Wruck,W., Groth,D., Lehrach,H., Burdon,T., and Adjaye,J. (2007). Analysis of Oct4-Dependent Transcriptional Networks Regulating Self-Renewal and Pluripotency in Human Embryonic Stem Cells. Stem Cells *25*, 500-510.

36. Babich,H., Liebling,E., Burger,R., Zuckerbraun,H., and Schuck,A. (2009). Choice of DMEM, formulated with or without pyruvate, plays an important role in assessing the in vitro cytotoxicity of oxidants and prooxidant nutraceuticals. In Vitro Cellular & Developmental Biology - Animal *45*, 226-233.

37. Bachiller,D., Klingensmith,J., Kemp,C., Belo,J.A., Anderson,R.M., May,S.R., McMahon,J.A., McMahon,A.P., Harland,R.M., Rossant,J., and De Robertis,E.M. (2000). The organizer factors Chordin and Noggin are required for mouse forebrain development. Nature *403*, 658-661.

38. Baharvand,H., Mehrjardi,N.J., Hatami,M., Kiani,S., Rao,M., and Haghighi,M.M. (2007). Neural differentiation from human embryonic stem cells in a defined adherent culture condition. International Journal of Developmental Biology *51*, 371-378.

39. Baharvand,H., Ashtiani,S.K., Taee,A., Massumi,M., Valojerdi,M.R., Yazdi,P.E., Moradi,S.Z., and Farrokhi,A. (2006). Generation of new human embryonic stem cell lines with diploid and triploid karyotypes. Development, Growth & Differentiation *48*, 117-128.

40. Bajpai,R., Coppola,G., Kaul,M., Talantova,M., Cimadamore,F., Nilbratt,M., Geschwind,D.H., Lipton,S.A., and Terskikh,A.V. (2009). Molecular stages of rapid and uniform neuralization of human embryonic stem cells. Cell Death Differ.

41. Bakshi,A., Shimizu,S., keck,C.A., Cho,S., LeBold,D.G., Morales,D., Arenas,E., Snyder,E.Y., Watson,D.J., and McIntosh,T.K. (2006). Neural progenitor cells engineered to secrete GDNF show enhanced survival, neuronal differentiation and improve cognitive function following traumatic brain injury. European Journal of Neuroscience *23*, 219-2134.

42. Ballas,N., Grunseich,C., Lu,D.L., Spehand,J.C., and Mandel,G. (2005). REST and Its Corepressors Mediate Plasticity of Neuronal Gene Chromatin throughout Neurogenesis. Cell *121*, 645-657.

43. Bani-Yaghoub,M., Bechberger,J.F., Underhill,T.M., and Naus,C.C.G. (1999). The Effects of Gap Junction Blockage on Neuronal Differentiation of Human NTera2/Clone D1 Cells. Experimental Neurology *156*, 16-32.

44. Barber,R.D., Harmer,D.W., Coleman,R.A., and Clark,B.J. (2005). GAPDH as a housekeeping gene: analysis of GAPDH mRNA expression in a panel of 72 human tissues. Physiol. Genomics *21*, 389-395.

45. Barnes,D. and Sato,G. (1980). Methods for growth of cultured cells in serum-free medium. Analytical Biochemistry *102*, 255-270.

46. Baroffio,A., Dupin,E., and Le Douarin,N.M. (1988). Clone-forming ability and differentiation potential of migratory neural crest cells. Proceedings of the National Academy of Sciences USA *85*, 5325-5329.

47. Baxter,M.A., Camarasa,M.V., Bates,N., Small,F., Murray,P., Edgar,D., and Kimber,S.J. (2009). Analysis of the distinct functions of growth factors and tissue culture substrates necessary for the long-term self-renewal of human embryonic stem cell lines. Stem Cell Research *3*, 28-38.

48. Beck,S., Le Good,J.A., Guzman,M., Haim,N.B., Roy,K., Beermann,F., and Constam,D.B. (2002). Extraembryonic proteases regulate Nodal signalling during gastrulation. Nat Cell Biol *4*, 981-985.

49. Benjamin,M. and Hillen,B. (2003). Mechanical Influences on Cells, Tissues and Organs - 'Mechanical Morphogenesis'. European Journal of Morphology *41*, 3-7.

50. Berger,M., Gray,J.A., and Roth,B.L. (2009). The Expanded Biology of Serotonin. Annual Review of Medicine *60*, 355-366.

51. Bernhardt,R. and Matus,A. (1984). Light and electron microscopic studies of the distribution of microtubule-associated protein 2 in rat brain: a difference between dendritic and axonal cytoskeletons. The Journal of Comparative Neurology *226*, 203-221.

52. Bertelli,E., Regoli,M., Fonzi,L., Occhini,R., Mannucci,S., Ermini,L., and Toti,P. (2007). Nestin Expression in Adult and Developing Human Kidney. J. Histochem. Cytochem. *55*, 411-421.

53. Biedler,J.L., Helson,L., and Spengler,B.A. (1973). Morphology and Growth, Tumorigenicity, and Cytogenetics of Human Neuroblastoma Cells in Continuous Culture. Cancer Res *33*, 2643-2652.

54. Bilican,B., Fiore-Heriche,C., Compston,A., Allen,N.D., and Chandran,S. (2008). Induction of Olig2+ Precursors by FGF Involves BMP Signalling Blockade at the Smad Level. PLoS ONE *3*, e2863.

55. Björklund,A. and Dunnett,S.B. (2007). Dopamine neuron systems in the brain: an update. Trends in Neurosciences *30*, 194-202.

56. Bliss,T.V.P. and Collingridge,G.L. (1993). A synaptic model of memory: long-term potentiation in the hippocampus. Nature *361*, 31-39.

57. Booth,H.A. and Holland,P.W.H. (2004). Eleven daughters of NANOG. Genomics *84*, 229-238.

58. Bottenstein,J.E. (1985). Growth and differentiation of neural cells in defined media. In Cell Cultures in the Neurosciences, G.Sato, ed. (New York: Plenum Pub Corp).

59. Boullin,D.J., Adams,C.B., and Du Boulay,G.H. (1978). Human behavioural arousal induced by dopamine. British Journal of Clinical Pharmacology *6*, 369-370.

60. Boyer,L.A., Lee,T.I., Cole,M.F., Johnstone,S.E., Levine,S.S., Zucker,J.P., Guenther,M.G., Kumar,R.M., Murray,H.L., Jenner,R.G., Gifford,D.K., Melton,D.A., Jaenisch,R., and Young,R.A. (2005). Core Transcriptional Regulatory Circuitry in Human Embryonic Stem Cells. Cell *122*, 947-956.

61. Brennan,J., Lu,C.C., Norris,D.P., Rodriguez,T.A., Beddington,R.S.P., and Robertson,E.J. (2001). Nodal signalling in the epiblast patterns the early mouse embryo. Nature *411*, 965-969.

62. Brewer,G.J. (1995). Serum-free B27/neurobasal medium supports differentiated growth of neurons from the striatum, substantia nigra, septum, cerebral cortex, cerebellum, and dentate gyrus. Journal of Neuroscience Research *42*, 674-683.

63. Brewer,G.J., Torricelli,J.R., Evege,E.K., and Price,P.J. (1993). Optimized survival of hippocampal neurons in B27-supplemented neurobasal™, a new serum-free medium combination. Journal of Neuroscience Research *35*, 567-576.

64. Brown,A.S. and Gershon,S. (1993). Dopamine and depression. Journal of Neural Transmission *91*, 75-109.

65. Brown,G., Hughes,P.J., and Michell,R.H. (2003). Cell differentiation and proliferation--simultaneous but independent? Experimental Cell Research *291*, 282-288.

66. Buckley,N.J., Johnson,R., Sun,Y.M., and Stanton,L.W. (2009). Is REST a regulator of pluripotency? Nature *457*, E5-E6.

67. Buddhala,C., Hsu,C.C., and Wu,J.Y. (2009). A novel mechanism for GABA synthesis and packaging into synaptic vesicles. Neurochemistry International *55*, 9-12.

68. Burridge,P.W., Anderson,D., Priddle,H., Barbadillo Munoz,M.D., Chamberlain,S., Allegrucci,C., Young,L.E., and Denning,C. (2007). Improved Human Embryonic Stem Cell Embryoid Body Homogeneity and Cardiomyocyte Differentiation from a Novel V-96 Plate Aggregation System Highlights Interline Variability. Stem Cells *25*, 929-938.

69. Bustin,S.A., Benes,V., Nolan,T., and Pfaffl,M.W. (2005). Quantitative real-time RT-PCR - a perspective. J Mol Endocrinol *34*, 597-601.

70. Buzzard,J.J., Gough,N.M., Crook,J.M., and Colman,A. (2004a). Karyotype of human ES cells during extended culture. Nature Biotechnology *22*, 381-382.

71. Buzzard,J.J., Gough,N.M., Crook,J.M., and Colman,A. (2004b). Karyotype of human ES cells during extended culture. Nat Biotech *22*, 381-382.

72. Caceres,A., Banker,G.A., and Binder,L. (1986). Immunocytochemical localization of tubulin and microtubule-associated protein 2 during the development of hippocampal neurons in culture. J. Neurosci. *6*, 714-722.

73. Carmignoto,G. (2000). Reciprocal communication systems between astrocytes and neurones. Progress in Neurobiology *62*, 561-581.

74. Carpenter,M.K., Inokuma,M.S., Denham,J., Mujtaba,T., Chiu,C.P., and Rao,M.S. (2001). Enrichment of Neurons and Neural Precursors from Human Embryonic Stem Cells. Experimental Neurology *172*, 383-397.

75. Catalina,P., Montes,R., Ligero,G., Sanchez,L., de la Cueva,T., Bueno,C., Leone,P., and Menendez,P. (2008). Human ESCs predisposition to karyotypic instability: Is a matter of culture adaptation or differential vulnerability among hESC lines due to inherent properties? Molecular Cancer *7*, 76.

76. Cauffman,G., liebaers,I., van Steirteghem,A., and Van de Velde,H. (2006). POU5F1 Isoforms Show Different Expression Patterns in Human Embryonic Stem Cells and Preimplantation Embryos. Stem Cells *24*, 2685-2691.

77. Cha,R.S. and Thilly,W.G. (1993). Specificity, efficiency, and fidelity of PCR. PCR Methods Appl. *3*, S18-S29.

78. Chadalavada,R.S., Houldsworth,J., Olshen,A.B., Bosl,G.J., Studer,L., and Chaganti,R.S. (2005). Transcriptional program of bone morphogenetic protein-2-induced epithelial

and smooth muscle differentiation of pluripotent human embryonal carcinoma cells. Funct Integr Genomics *5*, 59-69.

79. Chaerkady,R., Kerr,C.L., Marimuthu,A., Kelkar,D.S., Kashyap,M.K., Gucek,M., Gearhart,J.D., and Pandey,A. (2009). Temporal Analysis of Neural Differentiation Using Quantitative Proteomics. Journal of proteome research *8*, 1315-1326.

80. Chambers,I., Colby,D., Robertson,M., Nichols,J., Lee,S., Tweedie,S., and Smith,A. (2003). Functional Expression Cloning of Nanog, a Pluripotency Sustaining Factor in Embryonic Stem Cells. Cell *113*, 643-655.

81. Chandran,S., Kato,H., Gerreli,D., Compston,A., Svendsen,C.N., and Allen,N.D. (2003). FGF-dependent generation of oligodendrocytes by a hedgehog-independent pathway. Development *130*, 6599-6609.

82. Chen,C. and Sytkowski,A.J. (2005). Apoptosis-linked gene-2 connects the Raf-1 and ASK1 signalings. Biochemical and Biophysical Research Communications *333*, 51-57.

83. Chen,J., Kanai,Y., Cowan,N.J., and Hirokawa,N. (1992). Projection domains of MAP2 and tau determine spacings between microtubules in dendrites and axons. Nature *360*, 674-677.

84. Chen,S., Choo,A., Chin,A., and Oh,S.K.W. (2006). TGF-[beta]2 allows pluripotent human embryonic stem cell proliferation on E6/E7 immortalized mouse embryonic fibroblasts. Journal of Biotechnology *122*, 341-361.

85. Chirgwin,J.M., Przybyla,A.E., MacDonald,R.J., and Rutter,W.J. (1979). Isolation of biologically active ribonucleic acid from sources enriched in ribonuclease. Biochemistry *18*, 5294-5299.

86. Choi,J., Zheng,L., Ha,E., Lim,Y., Kim,Y., Wang,Y.P., and Lim,Y. (2006). Comparative Genomic Hybridization Array Analysis and Real-Time PCR Reveals Genomic Copy Number Alteration for Lung Adenocarcinomas. Lung *184*, 355-362.

87. Chomczynski,P. and Sacchi,N. (1987). Single-step method of RNA isolation by acid guanidinium thiocyanate-phenol-chloroform extraction. Analytical Biochemistry *162*, 156-159.

88. Choo,A.B., Padamanabhan,J., Chin,A.C., and Oh,S.K. (2004). Expansion of pluripotent human embryonic stem cells on human feeders. Biotechnology and Bioengineering *88*, 321-331.

89. Christopher-Hennings,J., Dammen,M., Nelson,E., Rowland,R., and Oberst,R. (2006). Comparison of RNA extraction methods for the detection of porcine reproductive and respiratory syndrome virus from boar semen. Journal of Virological Methods *136*, 248-253.

90. Chung,S., Shin,B.S., Hedlund,E., Pruszak,J., Ferree,A., Kang,U.J., Isacson,O., and Kim,K.S. (2006). Genetic selection of sox1GFP-expressing neural precursors removes residual tumorigenic pluripotent stem cells and attenuates tumor formation after transplantation. Journal of Neurochemistry *97*, 1467-1480.

91. Cicero,S.A., Johnson,D., Reyntjens,S., Frase,S., Connell,S., Chow,L.M.L., Baker,S., Sorrentino,B.P., and Dyer,M.A. (2009). Cells previously identified as retinal stem cells are pigmented ciliary epithelial cells. PNAS *106*, 6685-6690.

92. Conner,D.A. (2001). Mouse embryo fibroblasts (MEF) feeder cell preparation. Current Protocols in Molecular Biology *Chapter 23*.

93. Cowan,C.A., Klimanskaya,I., McMahon,J., Atienza,J., Witmyer,J., Zucker,J.P., Wang,S., Morton,C.C., McMahon,A.P., Powers,D., and Melton,D.A. (2004). Derivation of Embryonic Stem-Cell Lines from Human Blastocysts. N Engl J Med *350*, 1353-1356.

94. Damjanov,I. and Andrews,P.W. (1983). Ultrastructural Differentiation of a Clonal Human Embryonal Carcinoma Cell Line in Vitro. Cancer Res *43*, 2190-2198.

95. Danesin,C., Agius,E., Escalas,N., Ai,X., Emerson,C., Cochard,P., and Soula,C. (2006). Ventral Neural Progenitors Switch toward an Oligodendroglial Fate in Response to Increased Sonic Hedgehog (Shh) Activity: Involvement of Sulfatase 1 in Modulating Shh Signaling in the Ventral Spinal Cord. J. Neurosci. *26*, 5037-5048.

96. Dang,S.M., Gerecht-Nir,S., Chen,J., Itskovitz-Eldor,J., and Zandstra,P.W. (2004). Controlled, Scalable Embryonic Stem Cell Differentiation Culture. Stem Cells *22*, 275-282.

97. Dang,S.M., Kyba,M., perlingeiro,R., Daley,G.Q., and Zandstra,P.W. (2002). Efficiency of embryoid body formation and hematopoietic development from embryonic stem cells in different culture systems. Biotechnology and Bioengineering *78*, 442-453.

98. Davis,J.B. and Maher,P. (1994). Protein kinase C activation inhibits glutamate-induced cytotoxicity in a neuronal cell line. Brain Research *652*, 169-173.

99. De Camilli,P. and Navone,P. (1987). Regulated secretory pathways of neurons and their relation to the regulated secretory pathway of endocrine cells. Annals of the New York Academy of Sciences *493*, 461-479.

100. De Filippis,L., Ferrari,D., Rota Nodari,L., Amati,B., Snyder,E., and Vescovi,A.L. (2008). Immortalization of human neural stem cells with the c-myc mutant T58A. PLoS ONE *3*, e3310.

101. De Filippis,L., Lamorte,G., Snyder,E.Y., Malgaroli,A., and Vescovi,A.L. (2007). A Novel, Immortal And Multipotent Human Neural Stem Cell Line Generating Functional Neurons And Oligodendrocytes. Stem Cells 2007-0040.

102. Denis-Donini,S. and Estenoz,M. (1988). Interneurons versus efferent neurons: Heterogeneity in their neurite outgrowth response to glia from several brain regions. Developmental Biology *130*, 237-249.

103. Diecke,S., Quiroga-negreira,A., Redmer,T., and Besser,D. (2008). FGF2 signaling in mouse embryonic fibroblasts is crucial for self-renewal of embryonic stem cells. Cells Tissues Organs *1-2*, 52-61.

104. Dilworth,D.D. and McCarrey,J.R. (1992). Single-step elimination of contaminating DNA prior to reverse transcriptase PCR. PCR Methods Appl. *1*, 279-282.

105. Draper,J.S., Smith,K., Gokhale,P., Moore,H.D., Maltby,E., Johnson,J., Meisner,L., Zwaka,T.P., Thomson,J.A., and Andrews,P.W. (2004a). Recurrent gain of chromosomes 17q and 12 in cultured human embryonic stem cells. Nature Biotechnology *22*, 53-54.

106. Draper,J.S., Moore,H.D., Ruban,L.N., Gokhale,P.J., and Andrews,P.W. (2004b). Culture and Characterization of Human Embryonic Stem Cells. Stem Cells and Development *13*, 325-336.

107. Dullin,J.P., Locker,M., Robach,M., Henningfeld,K., Parain,K., Afelik,S., Pieler,T., and Perron,M. (2007). Ptf1a triggers GABAergic neuronal cell fates in the retina. BMC Developmental Biology *7*, 110.

108. Dunant,Y. and Bloc,A. (2003). Low- and High-Affinity Reactions in Rapid Neurotransmission. Neurochemical Research *28*, 659-665.

109. Duran,C., Talley,P.J., Walsh,J., Piggot,C., Morton,I.E., and Andrews,P.W. (2001). Hybrids of pluripotent and nullipotent human embryonal carcinoma cells: partial retention of a pluripotent phenotype. International Journal of Cancer *93*, 324-332.

110. Dvorak,P., Dvorakova,D., Koskova,S., Vodinska,M., Najvirtova,M., Krekac,D., and Hampl,A. (2005). Expression and potential role of fibroblast growth factor 2 and its receptors in human embryonic stem cells. Stem Cells *23*, 1200-1211.

111. Eagle,H. (1955). The specific amino acid requirements of a mammalian cell (strain L) in tissue culture. J. Biol. Chem. *214*, 839-852.

112. Elkabetz,Y., Panagiotakos,G., Al Shamy,G., Socci,N.D., Tabar,V., and Studer,L. (2008). Human ES cell-derived neural rosettes reveal a functionally distinct early neural stem cell stage. Genes Dev. *22*, 152-165.

113. Ellerström,C., Strehl,R., Noaksson,K., Hyllner,J., and Semb,H. (2007). Facilitated expansion of human embryonic stem cells by single cell enzymatic dissociation. Stem Cells 2006-0607.

114. Encinas,M., Iglesias,M., Liu,Y., Wang,H., Muhausen,A., Cena,V., Gallego,C., and Comella,J.X. (2000). Sequential Treatment of SH-SY5Y Cells with Retinoic Acid and Brain-Derived Neurotrophic Factor Gives Rise to Fully Differentiated, Neurotrophic Factor-Dependent, Human Neuron-Like Cells. Journal of Neurochemistry *75*, 991-1003.

115. Episkopou,V. (2005). SOX2 functions in adult neural stem cells. Trends in Neurosciences *28*, 219-221.

116. Ericson,J., Rashbass,P., Schedl,A., Brenner-Morton,S., Kawakami,A., van Heyningen,V., Jessell,T.M., and Briscoe,J. (1997). Pax6 Controls Progenitor Cell Identity and Neuronal Fate in Response to Graded Shh Signaling. Cell *90*, 169-180.

117. Ericson,J., Thor,S., Edlund,T., Jessell,T.M., and Yamada,T. (1992). Early stages of motor neuron differentiation revealed by expression of homeobox gene Islet-1. Science *256*, 1555-1560.

118. Evans,M. and Kaufman,M. (1981). Establishment in culture of pluripotent cells from mouse embryos. Nature *292*, 154.

119. Fairbanks,D. and Maughan,P. (2006). Evolution of the NANOG pseudogene family in the human and chimpanzee genomes. BMC Evolutionary Biology *6*, 12.

120. Faulkner,J. and Keirstead,H.S. (2005). Human embryonic stem cell-derived oligodendrocyte progenitors for the treatment of spinal cord injury. Transplant Immunology *15*, 131-142.

121. Fertuzinhos,S., Krsnik,Z., Kawasawa,Y.I., Rasin,M.R., Kwan,K.Y., Chen,J.G., Judas,M., Hayashi,M., and Sestan,N. (2009). Selective Depletion of Molecularly Defined Cortical Interneurons in Human Holoprosencephaly with Severe Striatal Hypoplasia. Cereb. Cortex *19*, 2196-2207.

122. Fletcher,J.M., Ferrier,P.M., Gardner,J.O., Harkness,L., Dhanjal,S., Serhal,P., Harper,J., Delhanty,J., Brownstein,D.G., Prasad,Y.R., Lebkowski,J., Mandalam,R., Wilmut,I., and De Sousa,P.A. (2006). Variations in Humanized and Defined Culture Conditions Supporting Derivation of New Human Embryonic Stem Cell Lines. Cloning and Stem Cells *8*, 319-334.

123. Fogh,J. and Trempe,G. (1975). New human tumor cell lines. In Human tumor cell lines in vitro, J.Fogh, ed. (New York: Plenum Press), pp. 115-159.

124. Fong,H., Hohenstein,K.A., and Donovan,P.J. (2008). Regulation of Self-renewal and Pluripotency by Sox2 in Human Embryonic Stem Cells. Stem Cells 2007-1002.

125. Fox,V., Gokhale,P.J., Walsh,J.R., Matin,M., Jones,M., and Andrews,P.W. (2008). Cell-cell signaling through NOTCH regulates human embryonic stem cell proliferation. Stem Cells *26*, 715-723.

126. Franklin,R.J.M. and ffrench-Constant,C. (2008). Remyelination in the CNS: from biology to therapy. Nat Rev Neurosci *9*, 839-855.

127. Freshney,R.I. (2005). Culture of Animal Cells. (Hoboken, New Jersey, USA: Wiley).

128. Friesel,R.E. and Maciag,T. (1995). Molecular mechanisms of angiogenesis: fibroblast growth factor signal transduction. FASEB J. *9*, 919-925.

129. Frojdman,K., Pelliniemi,L.J., Lendahl,U., Virtanen,I., and Eriksson,J.E. (1997). The intermediate filament protein nestin occurs transiently in differentiating testis of rat and mouse. Differentiation *61*, 243-249.

130. Gardner,R.L., Papaioannou,V.E., and Barton,S.C. (1973). Origin of the ectoplacental cone and secondary giant cells in mouse blastocysts reconstituted from isolated trophoblast and inner cell mass. Journal of Embryology and Experimental Morphology *30*, 561-572.

131. Gasser,U.E. and Hatten,M.E. (1990). Neuron-glia interactions of rat hippocampal cells in vitro: glial- guided neuronal migration and neuronal regulation of glial differentiation. J. Neurosci. *10*, 1276-1285.

132. Gassmann,M., Fandrey,J., Bichet,S., Wartenberg,M., Marti,H.H., Bauer,C., Wenger,R.H., and Acker,H. (1996). Oxygen supply and oxygen-dependent gene expression in differentiating embryonic stem cells. PNAS *93*, 2867-2872.

133. Gellén,J. (1976). Cellular development of some embryonic organs and the chorion during the first trimester of human pregnancy. Brithish Journal of Obstetrics and Gynaecology *83*, 790-794.

134. Gerrard,L., Rodgers,L., and Cui,W. (2005a). Differentiation of Human Embryonic Stem Cells to Neural Lineages in Adherent Culture by Blocking Bone Morphogenetic Protein Signaling. Stem Cells *23*, 1234-1241.

135. Gerrard,L., Zhao,D., Clark,A.J., and Cui,W. (2005b). Stably Transfected Human Embryonic Stem Cell Clones Express OCT4-Specific Green Fluorescent Protein and Maintain Self-Renewal and Pluripotency. Stem Cells *23*, 124-133.

136. Glasgow,S.M., Henke,R.M., MacDonald,R.J., Wright,C.V.E., and Johnson,J.E. (2005). Ptf1a determines GABAergic over glutamatergic neuronal cell fate in the spinal cord dorsal horn. Development *132*, 5461-5469.

137. Glukhova,L., Goguek,A.F., Chudoba,I., Angevin,E., Pavon,C., Terrier-Lacombe,M.J., Meddeb,M., Escudier,B., and Bernheim,A. (1998). Overrepresentation of 7q31 and 17q in renal cell carcinomas. Genes, Chromosomes and Cancer *22*, 171-178.

138. Gonzalez,R., Wesselschmidt,R.L., Schwartz,P.H., and Loring,J.F. (2007). Human Embryonic Stem Cell Culture. In Human Stem Cell Manual: A Laboratory Guide, J.F.Loring, R.L.Wesselschmidt, and P.H.Schwartz, eds. Elsevier), pp. 4-15.

139. Goulding,M.D., Lumsden,A., and Gruss,P. (1993). Signals from the notochord and floor plate regulate the region-specific expression of two Pax genes in the developing spinal cord. Development *117*, 1001-1016.

140. Graham,V., Khudyakov,J., Ellis,P., and Pevny,L. (2003). SOX2 Functions to Maintain Neural Progenitor Identity. Neuron *39*, 749-765.

141. Gratsch,T.E. and O'Shea,K.S. (2002). Noggin and Chordin Have Distinct Activities in Promoting Lineage Commitment of Mouse Embryonic Stem (ES) Cells. Developmental Biology *245*, 83-94.

142. Groszer,M., Erickson,R., Scripture-Adams,D.D., Lesche,R., Trumpp,A., Zack,J.A., Kornblum,H.I., Liu,X., and Wu,H. (2001). Negative Regulation of Neural Stem/Progenitor Cell Proliferation by the Pten Tumor Suppressor Gene in Vivo. Science *294*, 2186-2189.

143. Guerri,C.B., Porta,S.E., Schlamilch,A.M., González,C.F., and Maldonado,V. (1989). Effects of glia-conditioned medium on primary cultures of central neurons. Histology and Histopathology *4*, 217-222.

144. Guillemain,I., Alonso,G., Patey,G., Privat,A., and Chaudieu,I. (2000). Human NT2 neurons express a large variety of neurotransmission phenotypes in vitro. Journal of Comparative Neurology *422*, 380-395.

145. Hall,P., Lathia,J., Caldwell,M., and ffrench-Constant,C. (2008). Laminin enhances the growth of human neural stem cells in defined culture media. BMC Neuroscience *9*, 71.

146. Ham,R.G. (1965). Clonal growth of mammalian cells in a chemically defined, synthetic medium. PNAS *53*, 288-293.

147. Hanaoka,T., Toyoda,H., Mizuno,T., Kikuyama,H., Morimoto,K., Takahata,R., Matsumura,H., and Yoneda,H. (2003). Alterations in NMDA Receptor Subunit Levels in the Brain Regions of Rats Chronically Administered Typical or Atypical Antipsychotic Drugs. Neurochemical Research *28*, 919-924.

148. Harb,N., Archer,T.K., and Sato,N. (2008). The Rho-Rock-Myosin signaling axis determines cell-cell integrity of self-renewing pluripotent stem cells. PLoS ONE *3*, e3001.

149. Hardarson,T., Caisander,G., Sjogren,A., Hanson,C., Hamberger,L., and Lundin,K. (2003). A morphological and chromosomal study of blastocysts developing from morphologically suboptimal human pre-embryos compared with control blastocysts. Hum. Reprod. *18*, 399-407.

150. Hardingham,G.E. and Bading,H. (2003). The Yin and Yang of NMDA receptor signalling. Trends in Neurosciences *26*, 81-89.

151. Hartley,R.S., Margulis,M., Fishman,P.S., Lee,V.M., and Tang,C.M. (1999). Functional synapses are formed between human NTera2 (NT2N, hNT) neurons grown on astrocytes. Journal of Comparative Neurology *407*, 1-10.

152. Hatten,M.E. (1999). Central Nervous Sysytem Neuronal Migration. Annual Review of Neuroscience *22*, 511-539.

153. Healy,L., Hunt,c., Young,L., and Stacey,G. (2005). The UK Stem Cell Bank: Its role as a public research resource centre providing access to well-characterised seed stocks of human stem cell lines. Advanced Drug Delivery Reviews *57*, 1981-1988.

154. Heeg-Truesdell,E. and LaBonne,C. (2006). Neural induction in Xenopus requires inhibition of Wnt-[beta]-catenin signaling. Developmental Biology *298*, 71-86.

155. Hemmati-Brivanlou,A., Kelly,O.G., and Melton,D.A. (1994). Follistatin, an antagonist of activin, is expressed in the Spemann organizer and displays direct neuralizing activity. Cell *77*, 283-295.

156. Hongo,I., Kengaku,M., and Okamoto,H. (1999). FGF Signaling and the Anterior Neural Induction in *Xenopus*. Developmental Biology *216*, 561-581.

157. Hoshino,M., Nakamura,S., Mori,K., Kawauchi,T., Terao,M., Nishimura,Y.V., Fukuda,A., Fuse,T., Matsuo,N., Sone,M., Watanabe,M., Bito,H., Terashima,T., Wright,C.V., Kawaguchi,Y., Nakao,K., and Nabeshima,Y. (2005). Ptf1a, a bHLH transcriptional gene, defines GABAergic neuronal fates in cerebellum. Neuron *47*, 201-213.

158. Hull,E.M., Lorrain,D.S., Du,J., Matuszewich,L., Lumley,L.A., Putnam,S.K., and Moses,J. (1999). Hormone-neurotransmitter interactions in the control of sexual behavior. Behavioural Brain Research *105*, 105-116.

159. Hustin,J. and Schaaps,J.P. (1987). Echographic and anatomic studies of the maternotrophoblastic border during the first trimester of pregnancy. Americal Jounal of Obstetrics and Gynecology *157*, 162-168.

160. Hyslop,L., Stojkovic,M., Armstrong,L., Walter,T., Stojkovic,P., Przyborski,S.A., Herbert,M., Murdoch,A., Strachan,T., and Lako,M. (2005). Downregulation of NANOG induces differentiation of human embryonic stem cells to extraembryonic lineages. Stem Cells *23*, 1035-1043.

161. Iacovitti,L., Donaldson,A.E., Marshall,C.E., Suon,S., and Yang,M. (2007). A protocol for the differentiation of human embryonic stem cells into dopaminergic neurons using

only chemically defined human additives: Studies in vitro and in vivo. Brain Research *1127*, 19-25.

162. Ince,C., Ypey,D.L., esselhoff-Den Dulk,M.M.C., Visser,J.A.M., De Vos,A., and Van Furth,R. (1983). Micro-CO2-incubator for use on a microscope. Journal of Immunological Methods *60*, 269-275.

163. Ishitani,R., Sunaga,K., hirano,A., Saunders,P., Katsube,N., and Chuang,D. (1996). Evidence that Glyceraldehyde-3-Phosphate Dehydrogenase Is Involved in Age-Induced Apoptosis in Mature Cerebellar Neurons in Culture. Journal of Neurochemistry *66*, 928-935.

164. Itskovitz-Eldor,J., Schuldiner,M., Karsenti,D., Eden,A., Yanuka,O., Amit,M., Soreq,H., and Benvenisty,N. (2000). Differentiation of human embryonic stem cells into embryoid bodies compromising the three embryonic germ layers. Molecular Medicine *6*, 88-95.

165. Itsykson,P., Ilouz,N., Turetsky,T., Goldstein,R.S., Pera,M.F., Fishbein,I., Segal,M., and Reubinoff,B.E. (2005). Derivation of neural precursors from human embryonic stem cells in the presence of noggin. Molecular and Cellular Neuroscience *30*, 24-36.

166. Jain,M., Armstrong,R.J.E., Tyers,P., Barker,R.A., and Rosser,A.E. (2003). GABAergic immunoreactivity is predominant in neurons derived from expanded human neural precursor cells in vitro. Experimental Neurology *182*, 113-123.

167. James,P. (1997). Protein identification in the post-genome era: the rapid rise of proteomics. Quarterly Reviews of Biophysics *30*, 279-331.

168. Jarikji,Z.H., Vanamala,S., Beck,C.W., Wright,C.V.E., Leach,S.D., and Horb,M.E. (2009). Differential ability of Ptf1a and Ptf1a-VP16 to convert stomach, duodenum and liver to pancreas. Developmental Biology *304*, 786-799.

169. Jessell,T.M. and Sanes,J.R. (2000). Development: The decade of the developing brain. Current Opinion in Neurobiology *10*, 599-611.

170. Johansson,B.M. and Wiles,M.V. (1995). Evidence for involvement of activin A and bone morphogenetic protein 4 in mammalian mesoderm and hematopoietic development. Mol. Cell. Biol. *15*, 141-151.

171. Johnson,J.W. and Ascher,P. (1987). Glycine potentiates the NMDA response in cultured mouse brain neurons. Nature *325*, 529-531.

172. Johnson,R., Teh,C.H., Kunarso,G., Wong,K.Y., Srinivasan,G., Cooper,M.L., Volta,M., Chan,S.S., Lipovich,L., Pollard,S.M., Karuturi,R.K.M., Wei,C., Buckley,N.J., and Stanton,L.W. (2008). REST Regulates Distinct Transcriptional Networks in Embryonic and Neural Stem Cells. PLoS Biol *6*, 2205-2219.

173. Jones-Villeneuve,E.M., McBurney,M.W., Rogers,K.A., and Kalnins,V.I. (1982). Retinoic acid induces embryonal carcinoma cells to differentiate into neurons and glial cells. J. Cell Biol. *94*, 253-262.

174. Jørgensen,H.F., Chen,Z.F., Merkenschlager,M., and Fisher,A.G. (2009). Is REST required for ESC pluripotency? Nature *457*, E4-E5.

175. Káradóttir,R. and Attwell,D. (2007). Neurotransmitter receptors in the life and death of oligodendrocytes. Neuroscience *145*, 1426-1438.

176. Karlsson,O., Thor,S., Norberg,T., Ohlsson,H., and Edlund,T. (1990). Insulin gene enhancer binding protein Isl-1 is a member of a novel class of proteins containing both a homeo-and a Cys-ûHis domain. Nature *344*, 879-882.

177. Kasamatsu,A., Endo,Y., Uzawa,K., Nakashima,D., Koike,H., Hashitani,S., Numata,T., Urade,M., and Tanzawa,H. (2005). Identification of candidate genes associated with salivary adenoid cystic carcinomas using combined comparative genomic hybridization and oligonucleotide microarray analyses. The International Journal of Biochemistry & Cell Biology *37*, 1869-1880.

178. Katoh,H., Shibata,T., Kokubu,A., Ojima,H., Loukopoulos,P., Kanai,Y., Kosuge,T., Fukayama,M., Kondo,T., Sakamoto,M., Hosoda,F., Ohki,M., Imoto,I., Inazawa,J., and Hirohashi,S. (2005). Genetic profile of hepatocellular carcinoma revealed by array-based comparative genomic hybridization: Identification of genetic indicators to predict patient outcome. Journal of Hepatology *43*, 863-874.

179. Keirstead,H.S., Nistor,G., Bernal,G., Totoiu,M., Cloutier,F., Sharp,K., and Steward,O. (2005). Human Embryonic Stem Cell-Derived Oligodendrocyte Progenitor Cell Transplants Remyelinate and Restore Locomotion after Spinal Cord Injury. J. Neurosci. *25*, 4694-4705.

180. Keller,G.M. (1995). In vitro differentiation of embryonic stem cells. Current Opinion in Cell Biology *7*, 862-869.

181. Kemp,J.A. and Leeson,P.D. (1993). The glycine site of the NMDA receptor -- five years on. Trends in Pharmacological Sciences *14*, 20-25.

182. Kessaris,N., Pringle,N., and Richardson,W.D. (2001). Ventral Neurogenesis and the Neuron-Glial Switch. Neuron *31*, 677-680.

183. Kleckner,N.W. and Dingledine,R. (1988). Requirement for Glycine in Activation of NMDA-Receptors Expressed in Xenopus Oocytes. Science *241*, 835-837.

184. Kleinman,H.K. and Martin,G.R. (2005). Matrigel: Basement membrane matrix with biological activity. Seminars in Cancer Biology *15*, 378-386.

185. Kleinman,H.K., McGarvey,M.L., Liotta,L.A., Robey,P.G., Tryggvason,K., and Martin,G.R. (1982). Isolation and characterization of type IV procollagen, laminin, and heparan sulfate proteoglycan from the EHS sarcoma. Biochemistry *21*, 6188-6193.

186. Kleinsmith,L.J. and Pierce,G.B. (1964). Multipotentiality of Single Embryonal Carcinoma Cells. Cancer Res *24*, 1544-1551.

187. Klimanskaya,I., Chung,Y., Becker,S., Lu,S.J., and Lanza,R. (2006). Human embryonic stem cell lines derived from single blastomeres. Nature *444*, 481-485.

188. Knudtzon,S. (1974). In Vitro Growth of Granulocytic Colonies From Circulating Cells in Human Cord Blood. Blood *43*, 357-361.

189. Koolen,D.A., Herbergs,J., Veltman,J.A., Pfundt,R., van Bokhoven,H., Stroink,H., Sistermans,E.A., Brunner,H.G., Geurts van Kessel,A., and de Vries,B.B.A. (2006).

Holoprosencephaly and preaxial polydactyly associated with a 1.24 Mb duplication encompassing FBXW11 at 5q35.1. Journal of Human Genetics *51*, 721-726.

190. Koul, N and Seth, P. Astrocyte, the star avatar: redefined. Journal of Biotechnology 33[3], 405-421. 2008.
Ref Type: Generic

191. Krnjevic,K. and Schwartz,S. (1967). The action of Gamma Aminobutyric acid on cortical neurones. Experimental Brain Research *3*, 320-336.

192. Kumar,M., Kaushalya,S.K., Gressens,P., Maiti,S., and Mani,S. (2008). Optimized derivation and functional characterization of 5-HT neurons from human embryonic stem cells. Stem Cells and Development.

193. Kunath,T., Saba-El-Leil,M.K., lmousailleakh,M., Wray,J., Meloche,S., and Smith,A. (2007). FGF stimulation of the Erk1/2 signalling cascade triggers transition of pluripotent embryonic stem cells from self-renewal to lineage commitment. Development *134*, 2895-2902.

194. Lamb,T.M., Knecht,A.K., Smith,W.C., Stachel,S.E., Economides,A.N., Stahl,N., Yancopolous,G.D., and Harland,R.M. (1993). Neural induction by the secreted polypeptide noggin. Science *262*, 713-718.

195. Lambrechts,A., Van Troys,M., and Ampe,C. (2004). The actin cytoskeleton in normal and pathological cell motility. The International Journal of Biochemistry & Cell Biology *36*, 1890-1909.

196. Langer,R. and Vacanti,J.P. (1993). Tissue engineering. Science *260*, 920-926.

197. Lardon,J., Rooman,I., and Bouwens,L. (2002). Nestin expression in pancreatic stellate cells and angiogenic endothelial cells. Histochemistry and Cell Biology *117*, 535-540.

198. Lathia,J.D., Patton,B., Eckley,D.M., Magnus,T., Mughal,M.R., Sasaki,T., Caldwell,M.A., Rao,M.S., Mattson,M.P., and ffrench-Constant,C. (2007). Patterns of laminins and integrins in the embryonic ventricular zone of the CNS. J Comp Neurol *505*, 630-643.

199. Le Douarin,N.M. and Dupin,E. (2003). Multipotentiality of the neural crest. Current Opinion in Genetics & Development *13*, 529-536.

200. Lee,H., Al Shamy,G., Elkabetz,Y., Schoefield,C.M., Harrsion,N.L., Panagiotakos,G., Socci,N.D., Tabar,V., and Studer,L. (2007). Directed Differentiation And Transplantation of Human Embryonic Stem Cell Derived Motoneurons. Stem Cells 2007-0097.

201. Lee,M.K., Tuttle,J.B., Rebhun,L.I., Cleveland,D.W., and Frankfurter,A. (1990). The expression and posttranslational modification of a neuron-specific beta-tubulin isotype during chick embryogenesis. Cell Motility and the Cytoskeleton *17*, 118-132.

202. Lee,S.H., Lumelsky,N., Studer,L., Auerbach,J.M., and McKay,R.D. (2000). Efficient generation of midbrain and hindbrain neurons from mouse embryonic stem cells. Nature Biotechnology *18*, 675-679.

203. Lendahl,U., Zimmerman,L.B., and McKay,R.D.G. (1990). CNS stem cells express a new class of intermediate filament protein. Cell *60*, 585-595.

204. Leonard,J., Serup,P., Gonzalez,R., Edlund,T., and Montminy,M. (1992). The LIM family transcription factor Isl-1 requires cAMP response element binding protein to promote somatostatin expression in pancreatic islet cells. J. Biol. Chem. *270*, 12646-12652.

205. Levenstein,M.E., Ludwig,T.E., Xu,R.H., Llanas,R.A., VanDenHeuvel-Kramer,K., Manning,D., and Thomson,J.A. (2006). Basic Fibroblast Growth Factor Support of Human Embryonic Stem Cell Self-Renewal. Stem Cells *24*, 568-574.

206. Levine,A.J. and Brivanlou,A.H. (2006). GDF3, a BMP inhibitor, regulates cell fate in stem cells and early embryos. Development *133*, 209-216.

207. Li,X.J., Du,Z.W., Zarnowska,E.D., Pankratz,M., Hansen,L.O., Pearce,R., and Zhang,S.C. (2005). Specification of motoneurons from human embryonic stem cells. Nature Biotechnology *23*, 215-221.

208. Li,X.J., Yang,D., and Zhang,S.C. (2007). Motor Neuron and Dopamine Neuron Differentiation. In Human Stem Cell Manual: A Laboratory Guide, J.F.Loring, R.L.Wesselschmidt, and P.H.Schwartz, eds. Elsevier), pp. 185-209.

209. Li,X.J., Hu,B.Y., Jones,S.A., Zhang,Y.S., LaVaute,T., Du,Z.W., and Zhang,S.C. (2008). Directed Differentiation of Ventral Spinal Progenitors and Motor Neurons from Human Embryonic Stem Cells by Small Molecules. Stem Cells 2007-0620.

210. Liedtke,S., Enczmann,J., Waclawczyk,S., Wernet,P., and Kögler,G. (2007). Oct4 and Its Pseudogenes Confuse Stem Cell Research. Cell Stem Cell *1*, 364-366.

211. Liedtke,S., Stephan,M., and Kögler,G. (2008). Oct4 expression revisited: potential pitfalls for data misinterpretation in stem cell research. Biological Chemistry *389*, 845.

212. Lim,D.A., Tramontin,A.D., Trevejo,J.M., Herrera,D.G., Garc∅a-Verdugo,J.M., and varez-Buylla,A. (2000). Noggin Antagonizes BMP Signaling to Create a Niche for Adult Neurogenesis. Neuron *28*, 713-726.

213. Lim,U.M., Sidhu,K.S., and Tuch,B.E. (2006). Derivation of Motor Neurons from three Clonal Human Embryonic Stem Cell Lines. Current Neurovascular Research *3*, 281-288.

214. Limb,G.A., Daniels,J.T., Cambrey,A.D., Secker,G.A., Shortt,A.J., Lawrence,J.M., and Khaw,P.T. (2006). Current Prospects for Adult Stem CellΓÇôBased Therapies in Ocular Repair and Regeneration. Current Eye Research *31*, 381-390.

215. Lindvall,O. and Kokaia,Z. (2009). Prospects of stem cell therapy for replacing dopamine neurons in Parkinson's disease. Trends in Pharmacological Sciences *30*, 260-267.

216. Lindvall,O., Rehncrona,S., Brundin,P., Gustavii,B., Åstedt,B., Widner,H., Lindholm,T., Björklund,A., Leenders,K.L., Rothwell,J.C., Frackowiak,R., Marsden,C.D., Johnels,B., Steg,G., Freedman,R., Hoffer,B., Seiger,Å., Bygdeman,M., Strömberg,M.A., and Olson,L. (1989). Human fetal dopamine neurons grafted into the striatum in two patients with severe Parkinson's Disease. Archives of Neurology *46*, 615-631.

217. Lindvall,O., Gustavii,B., +stedt,B., Lindholm,T., Rehncrona,S., Brundin,P., Widner,H., Bj÷rklund,A., Leenders,K.L., Frackowiak,R., Rothwell,J.C., Marsden,C.D., Johnels,B., Steg,G., Freedman,R., Hopper,B.J., Seiger,+., Str÷mberg,I., and Olson,M.B. (1988). Fetal Dopamine-rich mesencehpalic grafts in Parkinson's Disease. The Lancet *332*, 1483-1484.

218. Livak,K.J. and Schmittgen,T.D. (2001). Analysis of Relative Gene Expression Data Using Real-Time Quantitative PCR and the 2-[Delta][Delta]CT Method. Methods *25*, 402-408.

219. Lloyd,K. and Hornykiewicz,O. (1970). Parkinson's Disease: Activity of L-Dopa Decarboxylase in Discrete Brain Regions. Science *170*, 1212-1213.

220. Lo-Castro,A., Giana,G., Fichera,M., Castiglia,L., Grillo,L., Musumeci,S.A., Galasso,C., and Curatolo,P. (2009). Deletion 2p25.2: A cryptic chromosome abnormality in a patient with autism and mental retardation detected using aCGH. European Journal of Medical Genetics *52*, 67-70.

221. Lovelock,J.E. and Bishop,M.W.H. (1959). Prevention of Freezing Damage to Living Cells by Dimethyl Sulphoxide. Nature *183*, 1394-1395.

222. lu,P., Blesch,A., and Tuszynaski,m.H. (2004). Induction of bone marrow stromal cells into neruons: differentiation, transdifferentiation or artifact? Journal of Neuroscience Research *77*, 174-191.

223. Lu,Q.R., Yuk,D., Alberta,J.A., Zhu,Z., Pawlitzky,I., Chan,J., McMahon,A.P., Stiles,C.D., and Rowitch,D.H. (2000). Sonic Hedgehog-Regulated Oligodendrocyte Lineage Genes Encoding bHLH Proteins in the Mammalian Central Nervous System. Neuron *25*, 317-329.

224. Ludwig,T.E., Levenstein,M.E., Jones,J.M., Berggren,W.T., Mitchen,E.R., Frane,J.L., Crandall,L.J., Daigh,C.A., Conard,K.R., Piekarczyk,M.S., Llanas,R.A., and Thomson,J.A. (2006a). Derivation of human embryonic stem cells in defined conditions. Nature Biotechnology *24*, 185-187.

225. Ludwig,T.E., Bergendahl,V., Levenstein,M.E., Yu,J., Probasco,M.D., and Thomson,J.A. (2006b). Feeder-independent culture of human embryonic stem cells. Nature Methods *3*, 637-646.

226. Ma,W., Tavakoli,T., Derby,E., Serebryakova,Y., Rao,M.S., and Mattson,M.P. (2008). Cell-Extracellular Matrix Interactions Regulate Neural Differentiation of Human Embryonic Stem Cells. BMC Dev Biol. *8*, 90.

227. Macchiarini,P., Jungebluth,P., Go,T., Asnaghi,M.A., Rees,L.E., Cogan,T.A., Dodson,A., Martorell,J., Bellini,S., Parnigotto,P.P., Dickinson,S.C., Hollander,A.P., Mantero,S., Conconi,M.T., and Birchall,M.A. (2008). Clinical transplantation of a tissue-engineered airway. The Lancet *372*, 2023-2030.

228. Mack,E., Neubauer,A., and Brendel,C. (2007). Comparison of RNA yield from small cell populations sorted by flow cytometry applying different isolation procedures. Cytometry. Part A *71*, 404-409.

229. Maione,R. and Amati,P. (1997). Interdependence between muscle differentiation and cell-cycle control. Biochimica et Biophysica Acta (BBA) - Reviews on Cancer *1332*, M19-M30.

230. Mansur,N.R., Meyer-Siegler,K., Wurzer,J.C., and Sirover,M.A. (1993). Cell cycle regulation of the glyceraldehyde-3-phosphate dehydrogenase/uracil DNA glycosylase gene in normal human cells. Nucl. Acids Res. *21*, 993-998.

231. Marchal-Victorion,S., Deleyrolle,L., De Weille,J., Saunier,M., Dromard,C., Sandillon,F., Privat,A., and Hugnot,J.P. (2003). The human NTERA2 neural cell line generates neurons on growth under neural stem cell conditions and exhibits characteristics of radial glial cells. Molecular and Cellular Neuroscience *24*, 198-213.

232. Maric,D. and Barker,J.L. (2005). Fluorescence-based sorting of neural stem cells and progenitors. Current Protocols in Neuroscience *Chapter 3*, Unit 3.18.

233. Marom,K., Fainsod,A., and Steinbeisser,H. (1999). Patterning of the mesoderm involves several threshold responses to *BMP-4* and *Xwnt-8*. Mechanisms of Development *87*, 33-44.

234. Martin,M.J., Muotri,A., Gage,F., and Varki,A. (2005). Human embryonic stem cells express an immunogenic nonhuman sialic acid. Nat Med *11*, 228-232.

235. Martinez,H.R., Gonzalez-Garza,M.T., Moreno-Cuevas,J.E., Caro,E., Gutierrez-Jimenez,E., and Segura,J.J. (2009). Stem-cell transplantation into the frontal motor cortex in amyotrophic lateral sclerosis patients. Cytotherapy *11*, 26-34.

236. Matthaei,K.I., Andrews,P.W., and Bronson,D.L. (1983). Retinoic acid fails to induce differentiation in human teratocarcinoma cell lines that express high levels of a cellular receptor. Experimental Cell Research *143*, 471-474.

237. Mayshar,Y., Rom,E., Chumakov,I., Kronman,A., Yayon,A., and Benvenisty,N. (2008). Fibroblast growth factor 4 and its novel splice isoform have opposing effects on the maintenance of human embryonic stem cell self-renewal. Stem Cells *26*, 767-774.

238. McKeehan,W.L., Hamilton,W.G., and Ham,R.G. (1976). Selenium is an essential trace nutrient for growth of WI-38 diploid human fibroblasts. PNAS *73*, 2023-2027.

239. Michibata,H., Okuno,T., Konishi,N., Kyono,K., Wakimoto,K., Aoki,K., Kondo,Y., Takata,K., Kitamura,Y., and Taniguchi,T. (2009). Human GPM6A Is Associated With Differentiation and Neuronal Migration of Neurons Derived from Human Embryonic Stem Cells. Stem Cells and Development *18*, 629-640.

240. Mitalipova,M.M., Rao,R.R., Hoyer,D.M., Johnson,J.A., Meisner,L.F., Jones,K.L., Dalton,S., and Stice,S.L. (2005). Preserving the genetic integrity of human embryonic stem cells. Nature Biotechnology *23*, 19-20.

241. Mitsui,K., Tokuzawa,Y., Itoh,H., Segawa,K., Murakami,M., Takahashi,K., Maruyama,M., Maeda,M., and Yamanaka,S. (2003). The homeoprotein Nanog is required for maintenance of pluripotency in mouse epiblast and ES cells. Cell *113*, 631-642.

242. Mokry,J., Cizkova,D., Filip,S., Ehrmann,J., Osterreicher,J., Kolar,Z., and English,D. (2004). Nestin Expression by Newly Formed Human Blood Vessels. Stem Cells and Development *13*, 658-664.

243. Mondragon-Teran,P., Lye,G.J., and Veraitch,F.S. (2009). Lowering oxygen tension enhances the differentiation of mouse embryonic stem cells into neuronal cells. Biotechnol. Prog. *Epub ahead of print*.

244. Moore,H. (2006). The medium is the message. Nature Biotechnology *24*, 160-161.

245. Moore,S. and Stein,W.H. (1973). Chemical Structures of Pancreatic Ribonuclease and Deoxyribonuclease. Science *180*, 458-464.

246. Moscatelli,D., Presta,M., Joseph-Silverstein,J., and Rifkin,D.B. (1986). Both normal and tumor cells produce basic fibroblast growth factor. Journal of Cellular Physiology *129*, 273-276.

247. Moulton,D.G. (1970). Dynamics of cell populations in the Olfactory epithelium. Annals of the New York Academy of Sciences *237*, 52-61.

248. Multiple Sclerosis Society. Multiple Sclerosis Society. Multiple Sclerosis Society . 2009. Ref Type: Internet Communication

249. Munoz-Sanjuan,I. and Brivanlou,A.H. (2002). Neural induction, the default model and embryonic stem cells. Nat Rev Neurosci *3*, 271-280.

250. Neher,E., Sakmann,B., and Steinbach,J.H. (1978). The extracellular patch clamp: A method for resolving currents through individual open channels in biological membranes. European Journal of Physiology *375*, 219-228.

251. Nelson,P.T., Kondziolka,D., Wechsler,L., Goldstein,S., Gebel,J., DeCesare,S., Elder,E.M., Zhang,P.J., Jacobs,A., McGrogan,M., Lee,V.M.Y., and Trojanowski,J.Q. (2002). Clonal Human (hNT) Neuron Grafts for Stroke Therapy : Neuropathology in a Patient 27 Months after Implantation. Am J Pathol *160*, 1201-1206.

252. Newman,E.A. (2003). New roles for astrocytes: Regulation of synaptic transmission. Trends in Neurosciences *26*, 536-542.

253. Ng,E.S., Davis,R.P., Azzola,L., Stanley,E.G., and Elefanty,A.G. (2005). Forced aggregation of defined numbers of human embryonic stem cells into embryoid bodies fosters robust, reproducible hematopoietic differentiation. Blood *106*, 1601-1603.

254. Nichols,J., Zevnik,B., Anastassiadis,K., Niwa,H., Klewe-Nebenius,D., Chambers,I., Schöler,H., and Smith,A. (1998). Formation of Pluripotent Stem Cells in the Mammalian Embryo Depends on the POU Transcription Factor Oct4. Cell *95*, 379-391.

255. Nistor,G.I., Totoiu,M.O., Haque,N., Carpenter,M.K., and Keirstead,H.S. (2005). Human embryonic stem cells differentiate into oligodendrocytes in high purity and myelinate after spinal cord transplantation. Glia *49*, 385-396.

256. Niwa,H., Miyazaki,J., and Smith,A.G. (2000). Quantitative expression of Oct-3/4 defines differentiation, dedifferentiation or self-renewal of ES cells. Nature Genetics *24*, 372-376.

257. Novitch,B.G., Chen,A.I., and Jessell,T.M. (2001). Coordinate Regulation of Motor Neuron Subtype Identity and Pan-Neuronal Properties by the bHLH Repressor Olig2. Neuron *31*, 773-789.

258. O'rahilly,R. and Müller,F. (1999b). Minireview: summary of the initial development of the human nervous system. Teratology *60*, 39-41.

259. O'rahilly,R. and Müller,F. (1999a). Minireview: summary of the initial development of the human nervous system. Teratology *60*, 39-41.

260. O'Shea,C.C., Crompton,T., Rosewell,I.R., Hayday,A.C., and Owen,M.J. (1996). Raf regulates positive selection. European Journal of Immunology *26*, 2350-2355.

261. Obeso,J.A., Rodriguez-Oroz,M., Marin,C., Alonso,F., Zamarbide,I., Lanciego,J.L., and Rodriguez-Diaz,M. (2004). The origin of motor fluctuations in Parkinson's disease: Importance of dopaminergic innervation and basal ganglia circuits. Neurology *62*, 17S-30.

262. Obrietan,K., Gao,X.B., and van den Pol,A.N. (2002). Excitatory Actions of GABA Increase BDNF Expression via a MAPK-CREB-Dependent Mechanism---A Positive Feedback Circuit in Developing Neurons. J Neurophysiol *88*, 1005-1015.

263. Okita,K., Ichisaka,T., and Yamanaka,S. (2007). Generation of germline-competent induced pluripotent stem cells. Nature *448*, 313-317.

264. Okuda,A., Fukushima,A., Nishimoto,M., Drimo,A., Yamagishi,T., Nabeshima,Y., Kuro-o,M., Nabeshima,Y.I., Boon,K., Keaveney,M., Stunnenberg,H.G., and Muramatsu,M. (1998). UTF1, a novel transcriptional coactivator expressed in pluripotent embryonic stem cells and extra-embryonic cells. The EMBO Journal *17*, 2019-2032.

265. Orentas,D.M., Hayes,J.E., Dyer,K.L., and Miller,R.H. (1999). Sonic hedgehog signaling is required during the appearance of spinal cord oligodendrocyte precursors. Development *126*, 2419-2429.

266. Ozdener,H. (2007). Inducible functional expression of Bcl-2 in human astrocytes derived from NTera-2 cells. Journal of Neuroscience Methods *159*, 8-18.

267. Pain,D., Chirn,G.W., Strassel,C., and Kemp,D.M. (2005). Multiple Retropseudogenes from Pluripotent Cell-specific Gene Expression Indicates a Potential Signature for Novel Gene Identification. J. Biol. Chem. *280*, 6265-6268.

268. Pakalnis,A., Splaingard,M., Splaingard,D., Kring,D., and Colvin,A. (2009). Serotonin Effects on Sleep and Emotional Disorders in Adolescent Migraine. Headache: The Journal of Head and Face pain *epub ahead of print*.

269. Park,E., Velumian,A.A., and Fehlings,M.G. (2004). The Role of Excitotoxicity in Secondary Mechanisms of Spinal Cord Injury: A Review with an Emphasis on the Implications for White Matter Degeneration. Journal of Neurotrauma *21*, 754-774.

270. Park,H., Varadi,A., Seok,H., Jo,J., Gilpin,H., Liew,C.G., Jung,S., Andrews,P.W., Molnar,E., and Cho,K. (2007). mGluR5 is involved in dendrite differentiation and excitatory synaptic transmission in NTERA2 human embryonic carcinoma cell-derived neurons. Neuropharmacology *52*, 1403-1414.

271. Parkinson's Disease Society. Parkinson's Disease Society. Parkinson's Disease Society . 2009.
Ref Type: Internet Communication

272. Patani,R., Compston,A., Puddifoot,C.A., Wyllie,D.J.A., Hardingham,G.E., Allen,N.D., and Chandran,S. (2009). Activin/Nodal Inhibition Alone Accelerates Highly Efficient Neural Conversion from Human Embryonic Stem Cells and Imposes a Caudal Positional Identity. PLoS ONE *4*, e7327.

273. Patel,Y., Collaco Moraes,Y., Latchman,D., Coffin,R., and de Belleroche,J. (2002). Neuroprotective effects of copper/zinc-dependent superoxide dismutase against a wide variety of death-inducing stimuli and proapoptotic effect of familial amyotrophic lateral sclerosis mutations. Molecular Brain Research *109*, 189-197.

274. Peerani,R., Onishi,K., Mahdavi,A., Kumacheva,E., and Zandstra,P.W. (2009). Manipulation of Signaling Thresholds in ΓÇ£Engineered Stem Cell NichesΓÇØ Identifies Design Criteria for Pluripotent Stem Cell Screens. PLoS ONE *4*, e6438.

275. Pera,E.M., Ikeda,A., Eivers,E., and De Robertis,E.M. (2003). Integration of IGF, FGF, and anti-BMP signals via Smad1 phosphorylation in neural induction. Genes Dev. *17*, 3023-3028.

276. Pera,M.F., Andrade,J., Houssami,S., Reubinoff,B., Trounson,A., Stanley,E.G., Ward-van Oostwaard,D., and Mummery,C. (2004). Regulation of human embryonic stem cell differentiation by BMP-2 and its antagonist noggin. J Cell Sci *117*, 1269-1280.

277. Perea-Gomez,A., Vella,F.D.J., Shawlot,W., Oulad-Abdelghani,M., Chazaud,C., Meno,C., Pfister,V., Chen,L., Robertson,E., Hamada,H., Behringer,R.R., and Ang,S.L. (2002). Nodal Antagonists in the Anterior Visceral Endoderm Prevent the Formation of Multiple Primitive Streaks. Developmental Cell *3*, 745-756.

278. Perrier,A.L., Tabar,V., Barberi,T., Rubio,M.E., Bruses,J., and Topf,N. Derivation of midbrain dopamine neurons from human embryonic stem cells.

279. Petit-Zeman,S. (2001). Regenerative medicine. Nature Biotechnology *19*, 201-206.

280. Petty,E.M., Miller,D.E., Grant,A.L., Collines,E.E., Glover,T.W., and Law,D.J. (1996). FISH localization of the soluble thymidine kinase gene (TK1) to human 17q25, a region of chromosomal loss in sporadic breast tumors. Cytogenetics and Cell Genetics *72*, 319-321.

281. Pevny,L.H., Sockanathan,S., Placzek,M., and Lovell-Badge,R. (1998). A role for SOX1 in neural determination. Development *125*, 1967-1978.

282. Pfendler,K.C., Catuar,C.S., Meneses,J.J., and Pedersen,R.A. (2005). Overexpression of Nodal Promotes Differentiation of Mouse Embryonic Stem Cells into Mesoderm and Endoderm at the Expense of Neuroectoderm Formation. Stem Cells and Development *14*, 162-172.

283. Pfrieger,F.W. and Barres,B.A. (1997). Synaptic Efficacy Enhanced by Glial Cells in Vitro. Science *277*, 1684-1687.

284. Piccini,P., Brooks,D.J., Bjorklund,A., Gunn,R.N., Grasby,P.M., Rimoldi,O., Brundin,P., Hagell,P., Rehncrona,S., Widner,H., and Lindvall,O. (1999). Dopamine release from nigral transplants visualized in vivo in a Parkinson's patient. 1137-1140.

285. Piccini,P., Lindvall,O., Björklund,A., Brundin,P., Hagell,P., Ceravolo,R., Oertel,W., Quinn,N., Samuel,M., Rehncrona,S., Widner,H., and Brooks,D.J. (2000). Delayed recovery of movement-related cortical function in Parkinson's disease after striatal dopaminergic grafts. Annals of Neurology *48*, 689-695.

286. Piccolo,S., Sasai,Y., Lu,B., and De Robertis,E.M. (1996). Dorsoventral patterning in Xenopus: Inhibition of ventral signals by direct binding of Chordin to BMP-4. Cell *86*, 589-598.

287. Pittenger,M.F., Mackay,A.M., Beck,S.C., Jaiswal,R.K., Douglas,R., Mosca,J.D., Moorman,M.A., Simonetti,D.W., Craig,S., and Marshak,D.R. (1999). Multilineage Potential of Adult Human Mesenchymal Stem Cells. Science *284*, 143-147.

288. Plantaz,D., Mohapatra,G., Matthay,K.K., Pellarin,M., Seeger,R.C., and Feuerstein,B.G. (1997). Gain of chromosome 17 is the most frequent abnormality detected in neuroblastoma by comparative genomic hybridization. Am J Pathol *150*, 81-89.

289. Pleasure,S.J., Page,C., and Lee,V.M. (1992). Pure, postmitotic, polarized human neurons derived from NTera 2 cells provide a system for expressing exogenous proteins in terminally differentiated neurons. J. Neurosci. *12*, 1802-1815.

290. Podrygajlo,G., Tegenge,M., Gierse,A., Paquet-Durand,F., Tan,S., Bicker,G., and Stern,M. (2009). Cellular phenotypes of human model neurons (NT2) after differentiation in aggregate culture. Cell and Tissue Research *336*, 439-452.

291. Potten,C.S. and Loeffler,M. (1990). Stem cells: attributes, cycles, spirals, pitfalls and uncertainties. Lessons for and from the crypt. Development *110*, 1001-1020.

292. Prowse,A.B., McQuade,L.R., Bryant,K.J., Marcal,H., and Gray,P.P. (2007). Identification of Potential Pluripotency Determinants for Human Embryonic Stem Cells Following Proteomic Analysis of Human and Mouse Fibroblast Conditioned Media. Journal of proteome research *6*, 3796-3807.

293. Pyle,A.D., Lock,L.F., and Donovan,P.J. (2006). Neurotrophins mediate human embryonic stem cell survival. Nature Biotechnology *24*, 344-350.

294. Qian,X., Davis,A.A., Goderie,S.K., and Temple,S. (1997). FGF2 Concentration Regulates the Generation of Neurons and Glia from Multipotent Cortical Stem Cells. Neuron *18*, 81-93.

295. Qu,Q. and Shi,Y. (2009). Neural stem cells in the developing and adult brains. Journal of Cellular Physiology *21*, 5-9.

296. Radonic,A., Thulke,S., Mackay,I.M., Landt,O., Siegert,W., and Nitsche,A. (2004). Guideline to reference gene selection for quantitative real-time PCR. Biochemical and Biophysical Research Communications *313*, 856-862.

297. Ramírez,M.A., Pericuesta,E., Fernández-González,R., Pintado,B., and Gutiérrez-Adán,A. (2007). Inadvertent presence of pluripotent cells in monolayers derived from differentiated embryoid bodies. The International Journal of Developmental Biology *51*, 397-407.

298. Reis,H.J., Guatimosim,C., Paquet,M., Santos,M., Ribeiro,F.M., Kummer,A., Schenatto,G., Salgado,J.V., Vieira,L.B., Teixeira,A.L., and Palotas,A. (2009). Neuro-Transmitters in the Central Nervous System their Implication in Learning and Memory Processes. Current Medicinal Chemistry *16*, 796-840.

299. Rendt,J., Erulkar,S., and Andrews,P.W. (1989). Presumptive neurons derived by differentiation of a human embryonal carcinoma cell line exhibit tetrodotoxin-sensitive sodium currents and the capacity for regenerative responses. Experimental Cell Research *180*, 580-584.

300. Ressler,K.J. and Nemerodd,C.B. (2000). Role of serotonergic and noradrenergic systems in the pathophysiology of depression and anxiety disorders. Depression and Anxiety *12*, 2-19.

301. Reyes,J.H., O'Shea,K., Wys,N.L., Velkey,J.M., Prieskorn,D.M., Wesolowski,K., Miller,J.M., and Altschuler,R.A. (2008). Glutamatergic Neuronal Differentiation of Mouse Embryonic Stem Cells after Transient Expression of Neurogenin 1 and Treatment with BDNF and GDNF: In Vitro and In Vivo Studies. J. Neurosci. *28*, 12622-12631.

302. Reynolds,B.A. and Weiss,S. (1992). Generation of neurons and astrocytes from isolated cells of the adult mammalian central nervous system. Science *255*, 1707-1710.

303. Ribes,V., Wang,Z., Dolle,P., and Niederreither,K. (2006). Retinaldehyde dehydrogenase 2 (RALDH2)-mediated retinoic acid synthesis regulates early mouse embryonic forebrain development by controlling FGF and sonic hedgehog signaling. Development *133*, 351-361.

304. Richards,M., Fong,C.Y., Chan,W.K., Wong,P.C., and Bongso,A. (2002). Human feeders support prolonged undifferentiated growth of human inner cell masses and embryonic stem cells. Nat Biotech *20*, 933-936.

305. Roelink,H., Porter,J.A., Chiang,C., Tanabe,Y., Chang,D.T., Beachy,P.A., and Jessell,T.M. (1995). Floor plate and motor neuron induction by different concentrations of the amino-terminal cleavage product of sonic hedgehog autoproteolysis. Cell *81*, 445-455.

306. Rosler,E.S., Fisk,G.J., Ares,X., Irving,J., Miura,T., Rao,M.S., and Carpenter,M.K. (2004). Long-term culture of human embryonic stem cells in feeder-free conditions. Developmental Dynamics *229*, 259-274.

307. Rossant,J. and Ofer,L. (1977). Properties of extra-embryonic ectoderm isolated from postimplantation mouse embryos. Journal of Embryology and Experimental Morphology *39*, 183-194.

308. Rothstein,J.D., Dykes-Hoberg,M., Pardo,C.A., Bristol,L.A., Jin,L., Kuncl,R.W., Kanai,Y., Hediger,M.A., Wang,Y., Schielke,J.P., and Welty,D.F. (1996). Knockout of Glutamate Transporters Reveals a Major Role for Astroglial Transport in Excitotoxicity and Clearance of Glutamate. Neuron *16*, 675-686.

309. Roy,A., Krzykwa,E., Lemieux,R., and Néron,S. (2001). Increased Efficiency of gamma-Irradiated versus Mitomycin C-Treated Feeder Cells for the Expansion of Normal Human Cells in Long-Term Cultures. Journal of Hematotherapy & Stem Cell Research *10*, 873-880.

310. Ruan,W. and Lai,M. (2007). Actin, a reliable marker of internal control? Clinica Chimica Acta *385*, 1-5.

311. Saha,S., Ji,L., de Pablo,J.J., and Palecek,S.P. (2008). TGF[beta]/Activin/Nodal Pathway in Inhibition of Human Embryonic Stem Cell Differentiation by Mechanical Strain. Biophysical Journal *94*, 4123-4133.

312. Saiki,R.K., Gelfand,D.H., Stoffel,S., Scharf,S.J., Higuchi,R., Horn,G.T., Mullis,K.B., and Erlich,H.A. (1988). Primer-directed enzymatic amplification of DNA with a thermostable DNA polymerase. Science *239*, 487-491.

313. Sanchez,M.C., Benitez,A., Ortloff,L., and Green,L.M. (2009). Alterations in Glutamate Uptake in NT2-Derived Neurons and Astrocytes after Exposure to Gamma Radiation. Radiation Research *171*, 41-52.

314. Sauer,H., Fischer,W., Nikkhah,G., Wiegand,S.J., Brundin,P., Lindsay,R.M., and Björklund,A. (1993). Brain-derived neurotrophic factor enhances function rather than survival of intrastriatal dopamine cell-rich grafts. Brain Research *626*, 37-44.

315. Schell-Apacik,C., Rivero,M., Knepper,J.L., Roessler,E., Muenke,M., and Ming,J.E. (2003). Sonic hedgehog mutations causing human holoprosencephaly impair neural patterning activity. Human Genetics *113*, 170-177.

316. Schier,A.F. (2003). Nodal signaling in vertebrate development. Annual Review of Cell and Developmental Biology *19*, 589-621.

317. Schneider,R.A., Hu,D., Rubenstein,J.L.R., Maden,M., and Helms,J.A. (2001). Local retinoid signaling coordinates forebrain and facial morphogenesis by maintaining FGF8 and SHH. Development *128*, 2755-2767.

318. Schuldiner,M., Eiges,R., Eden,A., Yanuka,O., Itskovitz-Eldor,J., Goldstein,R.S., and Benvenisty,N. (2001). Induced neuronal differentiation of human embryonic stem cells. Brain Research *913*, 201-205.

319. Schwartz,C.M., Spivak,C.E., Baker,S.C., McDaniel,T.K., Loring,J.F., Nguyen,C., Chrest,F.J., Wersto,R., Arenas,E., Zeng,X., Freed,W.J., and Rao,M.S. (2005). NTera2: A Model System to Study Dopaminergic Differentiation of Human Embryonic Stem Cells. Stem Cells and Development *14*, 517-534.

320. Schwindt,T.T., Motta,F.L., Barnabé,G.F., Massant,C.G., Guimarães,A.O., Calcagnotto,M.E., Conceição,F.S., Pesquero,J.B., Rehen,S., and Mello,L.E. (2009). Short-Term Withdrawal of Mitogens Prior to Plating Increases Neuronal Differentiation of Human Neural Precursor Cells. PLoS ONE *4*, e4642.

321. Sebald,W. (2002). Growth Factors in Tissue Engineering and Regenerative Medicine. Chemie Ingenieur Technik *74*, 715.

322. Serazin-Leroy,V., Denis-Henriot,D., Morot,M., de Mazancourt,P., and Giudicelli,Y. (1998). Semi-quantitative RT-PCR for comparison of mRNAs in cells with different amounts of housekeeping gene transcripts. Molecular and Cellular Probes *12*, 283-291.

323. Sewing,A., Wiseman,B., Lloyd,A.C., and Land,H. (1997). High-intensity Raf signal causes cell cycle arrest mediated by p21Cip1. Mol. Cell. Biol. *17*, 5588-5597.

324. Shim,J., Kim,S., Woo,D., Kim,S., Oh,C., McKay,R., and Kim,J. (2007). Directed differentiation of human embryonic stem cells towards a pancreatic cell fate. Diabetologia *50*, 1228-1238.

325. Shin,S., Dalton,S., and Stice,S.L. (2005). Human Motor Neuron Differentiation from Human Embryonic Stem Cells. Stem Cells and Development *14*, 266-269.

326. Shinawi,M. and Cheung,S.W. (2008). The array CGH and its clinical applications. Drug Discovery Today *13*, 760-770.

327. Simpson,T.I. and Price,D.J. (2002). Pax6; a pleiotropic player in development. Bioessays *24*, 1041-1051.

328. Singh Roy,N., Nakano,T., Xuing,L., Kang,J., Nedergaard,M., and Goldman,S.A. (2005). Enhancer-specified GFP-based FACS purification of human spinal motor neurons from embryonic stem cells. Experimental Neurology *196*, 224-234.

329. Sirover,M.A. (1997). Role of the glycolytic protein, glyceraldehyde-3-phosphate dehydrogenase, in normal cell function and in cell pathology. Journal of Cellular Biochemistry *66*, 133-140.

330. Sirover,M.A. (1996). Emerging new functions of the glycolytic protein, glyceraldehyde-3-phosphate dehydrogenase, in mammalian cells. Life Sciences *58*, 2271-2277.

331. Skotheim,R.I., Monni,O., Mousses,S., Fossa,S.D., Kallioniemi,O.P., Lothe,R.A., and Kallioniemi,A. (2002). New Insights into Testicular Germ Cell Tumorigenesis from Gene Expression Profiling. Cancer Res *62*, 2359-2364.

332. Sonntag,K.C., Pruszak,J., Yoshizaki,T., van Arensbergen,J., Sanchez-Pernaute,R., and Isacson,O. (2007). Enhanced Yield of Neuroepithelial Precursors and Midbrain-Like Dopaminergic Neurons from Human Embryonic Stem Cells Using the Bone Morphogenic Protein Antagonist Noggin. Stem Cells *25*, 411-418.

333. Squires,P.E., Wakeman,J.A., Chapman,H., Kumpf,S., Fidock,M.D., Andrews,P.W., and Dunne,M.J. (1996). Regulation of intracellular Ca2+ in response to muscarinic and glutamate receptor agonists during the differentiation of NTERA2 human embryonal carcinoma cells into neurons. European Journal of Neuroscience *8*, 783-793.

334. Stewart,M., Bendall,S., and Bhatia,M. (2008). Deconstructing human embryonic stem cell cultures: niche regulation of self-renewal and pluripotency. Journal of Molecular Medicine *86*, 875-886.

335. Stottman,R.W., Berrong,M., Matta,K., Choi,M., and Klingensmith,J. (2006). The BMP antagonist Noggin promotes cranial and spinal neurulation by distinct mechanisms. Developmental Biology *295*, 647-663.

336. Stubban,C. and Wesselschmidt,R.L. (2007). Mouse Embryonic Fibroblast Feeder Cells. In Human Stem Cell Manual: A Laboratory Guide, J.F.Loring, R.L.Wesselschmidt, and P.H.Schwartz, eds. Elsevier).

337. Suemori,H., Yasuchika,K., Hasegawa,K., Fujioka,T., Tsuneyoshi,N., and Nakatsuji,N. (2006). Efficient establishment of human embryonic stem cell lines and long-term maintenance with stable karyotype by enzymatic bulk passage. Biochemical and Biophysical Research Communications *345*, 926-932.

338. Sullivan,K.F. (1988). Structure and Utilization of Tubulin Isotypes. Annual Review of Cell Biology *4*, 687-716.

339. Sun,Y.M., Greenway,D.J., Johnson,R., Street,M., Belyaev,N.D., Deuchars,J., Bee,T., Wilde,S., and Buckley,N.J. (2005). Distinct Profiles of REST Interactions with Its Target Genes at Different Stages of Neuronal Development. Mol. Biol. Cell *16*, 5630-5638.

340. Suzuki,H., Chila,T., Suzuki,T., Fujita,T., Ikenoue,T., omata,M., Furuichi,K., Shikama,H., and Tanaka,K. (2000a). Homodimer of two F-box proteins betaTrCP1 or betaTrCP2 binds to IkappaBalpha for signal-dependent ubiquitination. The Journal of Biological Chemistry *275*, 2877-2884.

341. Suzuki,T., Higgins,P.J., and Crawford,D.R. (2000b). Control selection for RNA quantitation. BioTechniques *29*, 332-337.

342. Takahashi,H., Tanabe,Y., Ohnuji,M., Narita,M., Ichisaka,T., Tomoda,K., and Yamanaka,S. (2007). Induction of pluripotent stem cells from adult human fibroblasts by defined factors. Cell *131*, 861-872.

343. Takahashi,K. and Yamanaka,S. (2006). Induction of Pluripotent Stem Cells from Mouse Embryonic and Adult Fibroblast Cultures by Defined Factors. Cell *126*, 663-676.

344. Tan,S., Wood,M., and Maher,P. (1998). Oxidative stress induces a form of programmed cell death with characteristics of both apoptosis and necrosis in neuronal cells. Journal of Neurochemistry *71*, 95-105.

345. Tapia-Arancibia,L., Rage,F., Givalois,L., and Arancibia,S. (2004). Physiology of BDNF: focus on hypothalamic function. Frontiers in Neuroendocrinology *25*, 77-107.

346. ten Berge,D., Koole,W., Fuerer,C., Fish,M., Eroglu,E., and Nusse,R. (2008). Wnt signaling mediates self-organization and axis formation in embryoid bodies. Cell Stem Cell *3*, 508-518.

347. Teramura,T., Takehara,T., Kishi,N., Mihara,T., Kawata,N., Takeuchi,H., Takenoshita,M., Matsumoto,K., Saeki,K., Iritani,A., Sagawa,N., and Hosoi,Y. (2007). A Mouse and Embryonic Stem Cell Derived from a Single Embryo. Cloning and Stem Cells *9*, 485-494.

348. Thampy,K.G. and Barnes,E.M.J. (1984). gamma-Aminobutyric acid-gated chloride channels in cultured cerebral neurons. J. Biol. Chem. *259*, 1753-1757.

349. Thomas,E.D., Lochte,H.L.J., Lu,W.C., and Ferrebee,J.W. (1957). Intravenous infusion of bone marrow in patients receiving radiation and chemotherapy. N Engl J Med *257*, 491-496.

350. Thomas,R.J., Anderson,D.J., Chandra,A., Amith,N.M., Young,L.E., Williams,D., and Denning,C. (2008). Automated, scalable culture of human embryonic stem cells in feeder-free conditions. Biotechnology and Bioengineering *102*, 1636-1644.

351. Thomson,A., Wojtacha,D., Hewitt,Z., Priddle,H., Sottile,V., Di Domenico,A., Fletcher,J., Waterfall,M., Corrales,N.L., Ansell,R., and McWhir,J. (2008). Human Embryonic Stem Cells Passaged Using Enzymatic Methods Retain a Normal Karyotype and Express CD30. Cloning and Stem Cells *10*, 89-106.

352. Thomson,J.A., Kalishman,J., Golos,T.G., Durning,M., Harris,C.P., Becker,R.A., and Hearn,J.P. (1995). Isolation of a primate embryonic stem cell line. Proceedings of the National Academy of Sciences USA *92*, 7844-7848.

353. Thomson,J.A., Itskovitz-Eldor,J., Shapiro,S.S., Waknitz,M.A., Swiergiel,J.J., Marshall,V.S., and Jones,J.M. (1998). Embryonic Stem Cell Lines Derived from Human Blastocysts. Science *282*, 1145-1147.

354. Tienari,J., Alanko,T., Saksela,O., Vesterinen,M., and Lehtonen,E. (1995). Fibroblast growth factor-mediated stimulation of differentiating teratocarcinoma cells: evidence for paracrine growth regulation. Differentiation *59*, 193-199.

355. Tucek,S. (1985). Regulation of acetylcholine synthesis in the brain. Journal of Neurochemistry *44*, 11-24.

356. Unsicker,K., Reichert-Preibsch,H., and Wewetzer,K. (1992). Stimulation of neuron survival by basic FGF and CNTF is a direct effect and not mediated by non-neuronal

cells: evidence from single cell cultures. Brain Research. Developmental Brain Research *65*, 285-288.

357. Urbanc,B., Cruz,L., Buldyrev,S.V., Havlin,S., Irizarry,M.C., Stanley,H.E., and Hyman,B.T. (1999). Dynamics of Plaque Formation in Alzheimer's Disease. Biophysical Journal *76*, 1330-1334.

358. Vaccarino,F., Grigorenko,E., Smith,K., and Stevens,H. (2009). Regulation of Cerebral Cortical Size and Neuron Number by Fibroblast Growth Factors: Implications for Autism. Journal of Autism and Developmental Disorders *39*, 511-520.

359. Vallier,L., Alexander,M., and Pedersen,R.A. (2005). Activin/Nodal and FGF pathways cooperate to maintain pluripotency of human embryonic stem cells. J Cell Sci *118*, 4495-4509.

360. Vallier,L., Reynolds,D., and Pedersen,R.A. (2004). Nodal inhibits differentiation of human embryonic stem cells along the neuroectodermal default pathway. Developmental Biology *275*, 403-421.

361. Vandesompele,J., De Preter,K., Pattyn,F., Poppe,B., Van Roy,N., De Paepe,A., and Speleman,F. (2002). Accurate normalization of real-time quantitative RT-PCR data by geometric averaging of multiple internal control genes. Genome Biology *3*, research0034.

362. Vanin,E.F. (1985). Processed pseudogenes: characteristics and evolution. Annual Review of Gentics *19*, 272.

363. Vargas,A.P., Carod-Artal,F., Bomfim,D., Vazquez-Cabrera,C., and Dantas-Barbosa,C. (2003). Unusual Early-Onset Huntington's Disease. J Child Neurol *18*, 429-432.

364. Varlet,I., Collignon,J., and Robertson,E.J. (1997). nodal expression in the primitive endoderm is required for specification of the anterior axis during mouse gastrulation. Development *124*, 1033-1044.

365. Veal,E., Groisman,R., Eisenstein,M., and Gill,G. (2000). The secreted glycoprotein CREG enhances differentiation of NTERA-2 human embryonal carcinoma cells. Oncogene *19*, 2120-2128.

366. Villa-Diaz,L.G., Pacut,C., Slawny,N.A., Ding,J., O'Shea,K.S., and Smith,G.D. (2009). Analysis of the Factors that Limit the Ability of Feeder Cells to Maintain the Undifferentiated State of Human Embryonic Stem Cells. Stem Cells and Development *18*, 641-652.

367. Wai,M.S.M., Zhang,L., and Yew,D.T. (2008). Ganglionic Eminence Revisited: A Review Embracing Observations from Our Laboratory. Neuroembryology and aging *5*, 121-126.

368. Waldrip,W.R., Bikoff,E.K., Hoodless,P.A., Wrana,J.L., and Robertson,E.J. (1998). Smad2 Signaling in Extraembryonic Tissues Determines Anterior-Posterior Polarity of the Early Mouse Embryo. Cell *92*, 797-808.

369. Walker,F.O. (2007). Huntington's disease. The Lancet *369*, 218-228.

370. Walker,N.J. (2002). A Technique Whose Time Has Come. Science *296*, 557-559.

371. Wallace,T.L. and Johnson,E.M. (1989). Cytosine arabinoside kills postmitotic neurons: evidence that deoxycytidine may have a role in neuronal survival that is independent of DNA synthesis. J. Neurosci. *9*, 115-124.

372. Walsh,K. and Perlman,H. (1997). Cell cycle exit upon myogenic differentiation. Current Opinion in Genetics & Development *7*, 597-602.

373. Wang,G., Zhang,H., Zhao,Y., Li,J., Cai,J., Wang,P., Meng,S., Feng,J., Miao,C., Ding,M., Li,D., and Deng,H. (2005a). Noggin and bFGF cooperate to maintain the pluripotency of human embryonic stem cells in the absence of feeder layers. Biochemical and Biophysical Research Communications *330*, 934-942.

374. Wang,M. and Drucker,D.J. (1995). The LIM Domain Homeobox Gene isl-1 Is a Positive Regulator of Islet Cell-specific Proglucagon Gene Transcription. J. Biol. Chem. *270*, 12646-12652.

375. Wang,Z., Mandell,K.J., Parkos,C.A., Mrsny,R.J., and Nusrat,A. (2005b). The second loop of occludin is required for suppression of Raf1-induced tumor growth. Oncogene *24*, 4412-4420.

376. Warrington,J.A., NAIR,A.R.C.H., MAHADEVAPPA,M.A.M.A., and TSYGANSKAYA,M.A.Y.A. (2000). Comparison of human adult and fetal expression and identification of 535 housekeeping/maintenance genes. Physiol. Genomics *2*, 143-147.

377. Watanabe,D., Suetake,I., Tada,T., and Tajima,S. (2002). Stage- and cell-specific expression of Dnmt3a and Dnmt3b during embryogenesis. Mechanisms of Development *118*, 187-190.

378. Watson,J.D., Baker,T.A., Bell,S.P., Gann,A., Levine,M., Losick,R., and CSHLP,I. (2008). Molecular Biology of the Gene. Pearson Education).

379. Weiss,S., Reynolds,B.A., Vescovi,A.L., Morshead,C., Craig,C.G., and van der Kooy,D. (1996). Is there a neural stem cell in the mammalian forebrain? Trends in Neurosciences *19*, 387-393.

380. Wernig,M., Tucker,K.L., Gornik,V., Schneiders,A., Buschwald,R., Wiestler,O.D., Barde,Y., and Brüstle,O. (2007). Tau EGFP embryonic stem cells: An efficient tool for neuronal lineage selection and transplantation. Journal of Neuroscience Research *69*, 918-924.

381. Westbrook,T.F., Hu,G., Ang,X.L., Mulligan,P., Pavlova,N.N., Liang,A., Leng,Y., Maehr,R., Shi,Y., Harper,J.W., and Elledge,S.J. (2008). SCF[bgr]-TRCP controls oncogenic transformation and neural differentiation through REST degradation. Nature *452*, 370-374.

382. Westermann,F. and Schwab,M. (2002). Genetic parameters of neuroblastomas. Cancer Letters *184*, 127-147.

383. Williams,P.W. (1894). Notes on diabetes treated with extract and by grafts of sheep's pancreas. Bristish Medical Journal *2*, 1303-1304.

384. Wilson,S.I., Graziano,E., harland,R., Jessell,T.M., and Edlund,T. (2000). An early requirement for FGF signalling in the acquisition of neural cell fate in the chick embryo. Current Biology *10*, 421-429.

385. Wilson,S.I. and Edlund,T. (2001). Neural induction: toward a unifying mechanism. Nat Neurosci.

386. Winnier,G., Blessing,M., Labosky,P.A., and Hogan,B.L. (1995). Bone morphogenetic protein-4 is required for mesoderm formation and patterning in the mouse. Genes Dev. *9*, 2105-2116.

387. Wolpert,L., Beddington,R., Jessel,T., Lawrence,P., Meyerowitz,E., and Smith,J. (2002). Patterning the vertebrate body plan II: The mesoderm and early nervous system. In Principles of Development, (New York: Oxford University Press), pp. 109-142.

388. Wurtman,R.J. (1988). Effects of dietary amino acids, carbohydrates, and choline on neurotransmitter synthesis. The Mount Sinai journal of medicine, New York *55*, 75-86.

389. Xu,C., Inokuma,M.S., Denham,J., Golds,K., Kundu,P., Gold,J.D., and Carpenter,M.K. (2001). Feeder-free growth of undifferentiated human embryonic stem cells. Nature Biotechnology *19*, 971-974.

390. Xu,R.H., Peck,R.M., Li,D.S., Feng,X., Ludwig,T., and Thomson,J.A. (2005). Basic FGF and suppression of BMP signaling sustain undifferentiated proliferation of human ES cells. Nature Methods *2*, 185-190.

391. Xuan,A.G., Long,D.H., Gu,H.G., Yang,D.D., Hong,L.P., and Leng,S.L. (2008). BDNF improves the effects of neural stem cells on the rat model of Alzheimer's disease with unilateral lesion of fimbria-fornix. Neuroscience Letters *440*, 331-335.

392. Yamada,M., Tanemura,K., Okada,S., Iwanami,A., Nakamura,M., Mizuno,H., Ozawa,M., Ohyama-Goto,R., Kitamura,N., Kawano,M., Tan-Takeuchi,K., Ohtsuka,C., Miyawaki,A., Takashima,A., Ogawa,M., Toyama,Y., Okano,H., and Kondo,T. (2007). Electrical Stimulation Modulates Fate Determination of Differentiating Embryonic Stem Cells. Stem Cells *25*, 562-570.

393. Yan,Y., Yang,D., Zarnowska,E.D., Du,Z., Werbel,B., Valliere,C., Pearce,R.A., Thomson,J.A., and Zhang,S.C. (2005). Directed Differentiation of Dopaminergic Neuronal Subtypes from Human Embryonic Stem Cells. Stem Cells *23*, 781-790.

394. Yang,C., Przedborski,S., Cooke,M.J., Zhang,X., Stewart,R., Anyfantis,G., Atkinson,S.P., Saretzki,G., Armstrong,L., and Lako,M. (2008). A key role for telomerase reverse transcriptase unit in modulating human embryonic stem cell proliferation, cell cycle dynamics, and in vitro differentiation. Stem Cells *26*, 850-863.

395. Yuan,H., Corbi,N., Basilico,C., and Dailey,L. (1995). Developmental-specific activity of the FGF-4 enhancer requires the synergistic action of Sox2 and Oct-3. Genes Dev. *9*, 2635-2645.

396. Zeng,X., Chen,J., Deng,X., Liu,Y., Rao,M.S., Cadet,J.L., and Freed,W.J. (2006). An In Vitro Model of Human Dopaminergic Neurons Derived from Embryonic Stem Cells: MPP+ Toxicity and GDNF Neuroprotection. Neuropsychopharmacology *31*, 2708-2715.

397. Zhang,S.C., Wernig,M., Duncan,I.D., Brustle,O., and Thomson,J.A. (2001). In vitro differentiation of transplantable neural precursors from human embryonic stem cells. Nature Biotechnology *19*, 1129-1133.

398. Zhang,Z. and Gerstein,M. (2003). The human genome has 49 cytochrome c pseudogenes, including a relic of a primordial gene that still functions in mouse. Gene *312*, 61-72.

Appendix 1: ESACT UK 18th annual scientific meeting - poster.
1st prize winner of poster competition. January 2008.

Neuronal differentiation, as a precursor to the provision of functional neuronal cell substrates for use in a bioassay.

Gillett M.L[1,2]., Bolsover S[3]., Ranasinghe S[3]., Healy L[2]., Stacey G[2]., Fleck R.A[2]., Mason C[1].

[1] Regenerative Medicine, Department of Biochemical Engineering, University College London.

[2] Cell Biology and Imaging, National Institute for Biological Standards and Control. [3] Depart ment of Physiology, University College London.

Introduction

The ability to produce various neural cell types from pluripotent (stem) cells has been discussed in depth over recent years. The application of these neural cells into cell based therapies and in bioassays for drug screening carries huge potential for the advancement of disease treatment. One of the best established method of neuronal production uses retinoic acid induction of the human embryonal carcinoma (EC) cell line (NTERA2). However, this method typically results in a heterogenous population of neural and non-neural cells with varying levels of functionality. Here we aim to highlight some of these issues using immunostaining, patch clamping and calcium imaging techniques.

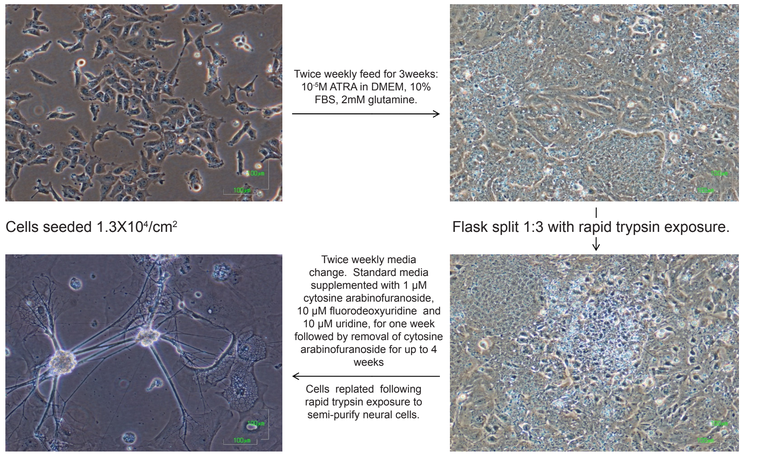

Figure 1. Materials and methods of NTERA2 neural differentiation

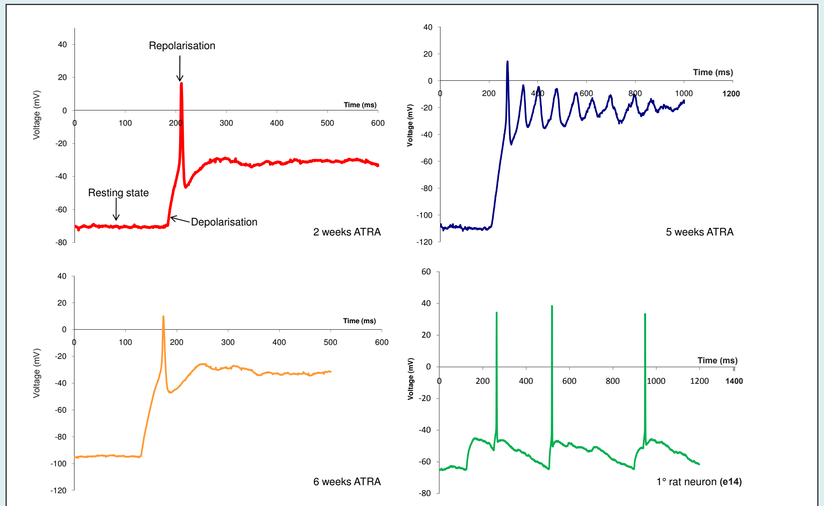

Figure 3. Action potentials (AP) generated 2 weeks (top left), 5 weeks (top right), 6 weeks (bottom left) of ATRA treatment. Action potential from 1° neuron (bottom right). Some cells generated a series of APs following manual depolarisation (seen here at 5 weeks and 1° neurons).

Figure 4. Calcium imaging of NTERA2 neurons after 6 weeks ATRA. Cells (left), Calcium reading (right). Both cells responded of glutamate and to K^+ depolarisation with an influx of calcium in the same pattern, but different levels of influx was observed. Neither cell responded to ATP.

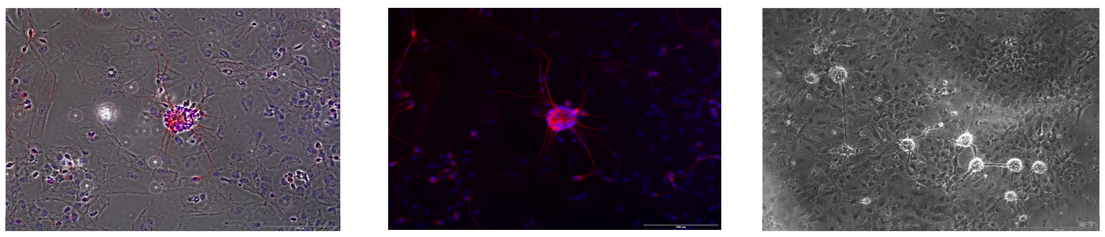

Figure 2. Beta-III-tubulin staining (red) of NTERA2 neurons following 6 weeks ATRA exposure (left and middle). Demonstrate proportion of neuronal cells in a given population (right).

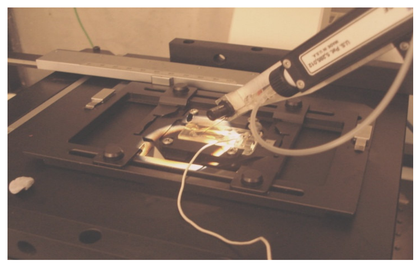

Figure 5. Patch clamping rig

Results

- Physical constraints meant it was not possible to patch non-neuronal, or cells before 2 weeks of differentiation.
- Voltage-gated channels were detected in < 50% cells beyond 2 weeks
- The proportion of cells with functional voltage gated channels increased from 50 % at 2 weeks to 100 % at 6 weeks ATRA exposure.
- Not all cells with voltage gated channels were able to generate APs.
- 100% primary neurons successfully patched demonstrated functional voltage gated channels and the ability to fire APs.
- A maximum of 19 cells could be patched on a single day. Low sample number → difficulties in accurate determination cell function across the population.

Cell type	ATRA exposure (weeks)	Tested	Lost	No response	Inward current	% cells with inward current	Action potential	% cells generating AP
NTERA2 (Undifferentiated)	0	3	3	0	0	0	0	0
NTERA2	1	9	6	3	0	0	0	0
NTERA2	2	8	0	3	4	50	1	13
NTERA2	3	8	4	2	2	50	1	25
NTERA2	4	9	1	2	6	75	3	38
NTERA2	5	13	6	3	4	57	3	43
NTERA2	6	4	1	0	3	100	2	67
e14 Sprague-Dawley rat (primary neurons)	N/A	4	1	0	3	100	3	100

Figure 6. Cumulative data from patched cells

Discussion

Cells with neuronal morphology and electrophysiological activity can be generated from the pluripotent cell line; NTERA2. Techniques used here highlight the variability in the number of functional neurons from any given culture of pluripotent cells. Patch-clamping is a highly skilled and low throughput technique, making it difficult to screen of large numbers of cells. Calcium imaging can be used as an alternative to monitor the flux of calcium ions across large numbers of cells, in response to various typical neurotransmitters, in a just a single run.

Conclusion: Functional neurons can be generated from pluripotent (EC) cells. However, numbers and function of the cells generated can vary enormously. This work is currently being translated in human embryonic stem cell lines with an aim to increase overall yield of function end stage neurons.

Acknowledgements: We would like to thank the EPSRC, Linkam Scientific and NIBSC, for their contributions to this work, without which it would not have taken place.

Appendix 2: NIBSC SPAC review poster.
Department of Cell Biology and Imaging. June 2008.

Neuronal differentiation in human embryonic stem cells

Gillett, M.L[1]., Bolsover, S[3]., Healy, L[4]., Stacey, G[1,4]., Mason, C[2]., Fleck, R.A[1].

1 Cell Biology and Imaging. The National Institute for Biological Standards and Control

2 Regenerative medicine, Department of Biochemical engineering, University College London.

3 Department of Physiology, University College London.

4 UK Stem cell Bank. The National Institute for Biological Standards and Control.

INTRODUCTION

As our knowledge of human embryonic stem cells increases, so do the applications of these cells for the treatment and screening of drugs for neurodegenerative disease such as Alzheimer's and Parkinson's disease. Current methods for neurological drug screening utilise either primary neuronal cells, often from animal sources with associated supply and ethical considerations, or neural cell lines such as SHSY-5-Y cell lines which have proven to yield low and variable numbers of functional cells. An effective cell based assay requires a reliable and reproducible supply of functional cells. We set out to develop and optimise a reliable method for neuronal differentiation of the human embryonic stem cell lines HUES7 and Shef3, for incorporation into a cell based drug screening assay.

MATERIALS AND METHODS

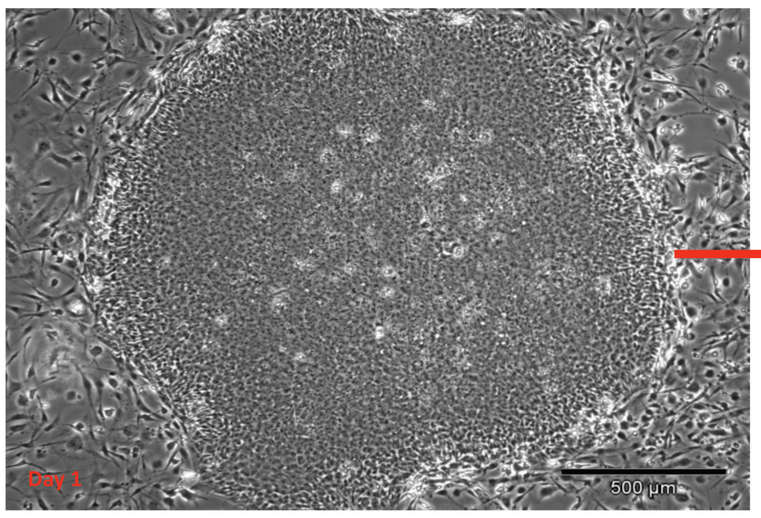

Undifferentiated human embryonic stem cell colony cultured in knock-out DMEM, KO-serum replacement, beta-mercaptoethanol, non-essential amino acids, glutamine on a high density feeder layer ($5X10^4/cm^2$.).

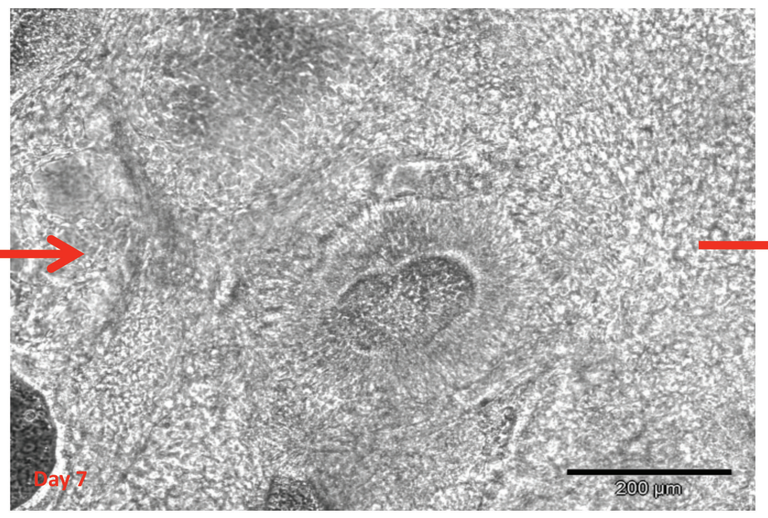

Cells fed daily with standard hES media results in formation of rosettes up to 7 days following passaging. These rosettes take on similar morphology to the neural tube formation and can be manually dissected out and purified.

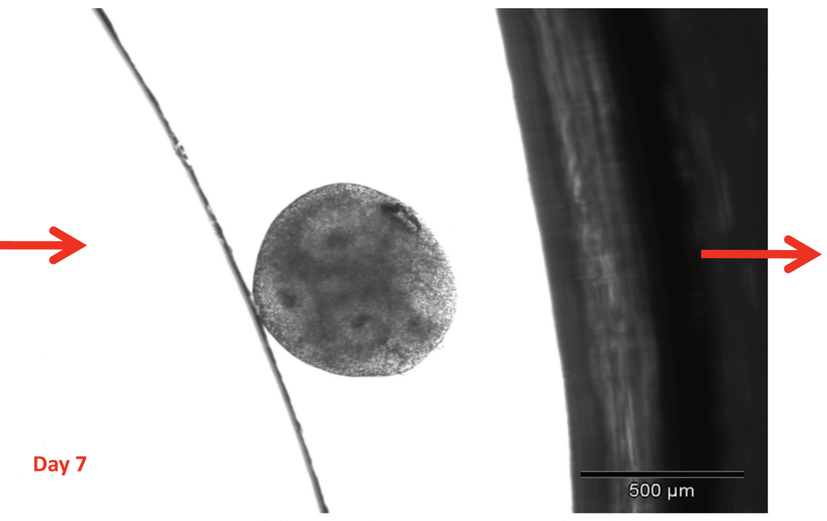

Rosettes in suspension following dissection are transferred onto a poly-ornithine and laminin coated surface and cultured in Neurobasal media, supplemented with neurotrophins (N2 and B27).

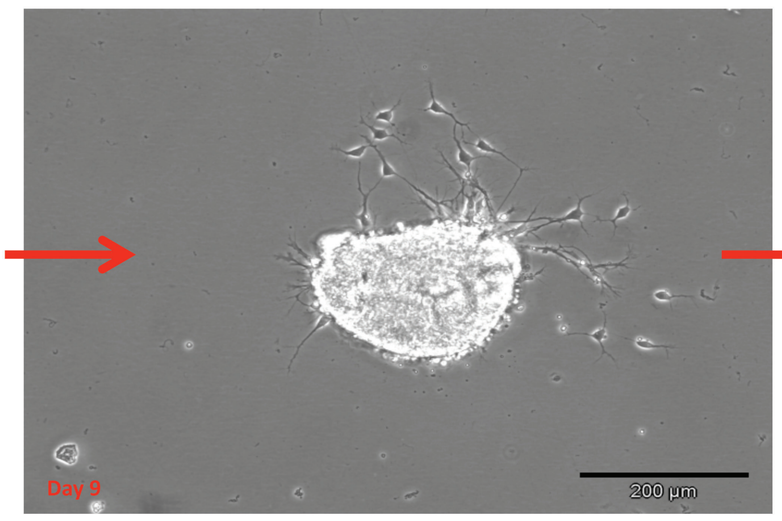

Following attachment to the poly-ornithine and laminin surface, neurons being to grow out and spread from the rosette fragment.

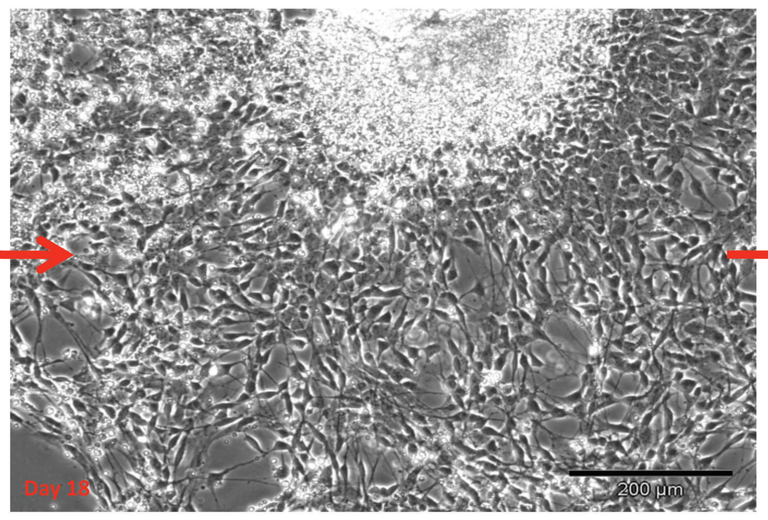

Neurons continue to grow out and can be treated with Trypsin and replated onto a fresh slide to form a neuronal monolayer for functionality studies.

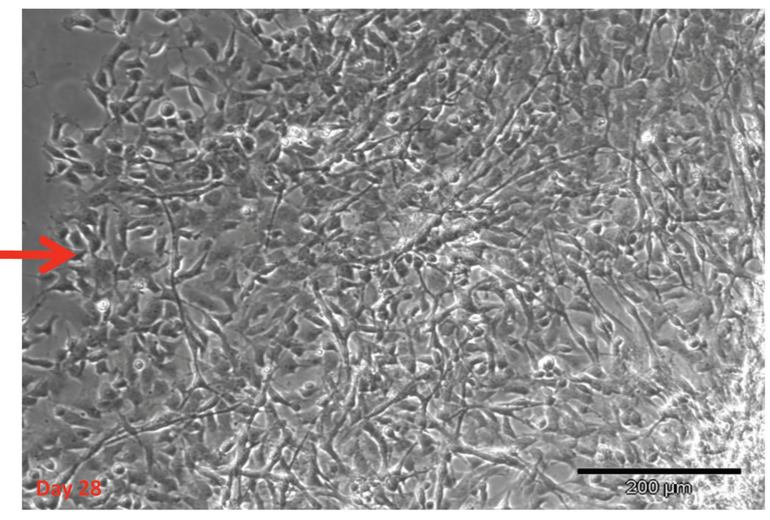

Matured neurons can be maintained in culture for many weeks, in neurobasal media.

Neuronal differentiation of human embryonic stem cells.

RESULTS

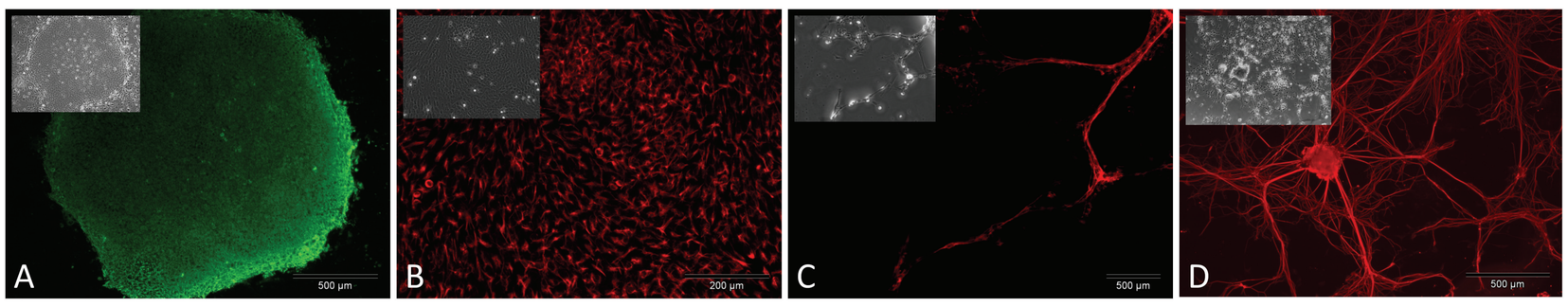

Cells were stained for pluripotent stem cell markers, including SSEA4 (A). Nestin was shown to be expressed in neural precursor cells (B). End stage neuronal cells were stained for neuronal markers: neurofilament (C) and beta-III-tubulin (D) to confirm neuronal morphology.

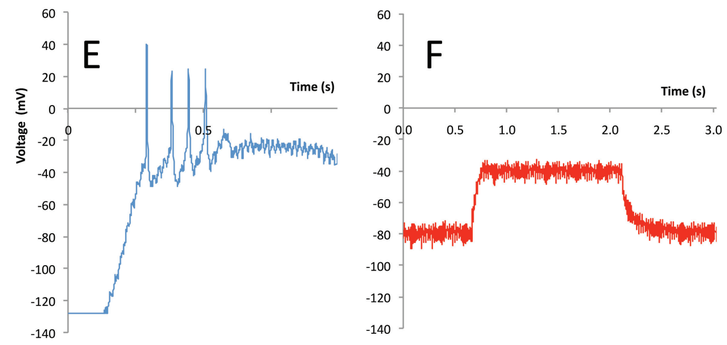

Patch clamping data demonstrated the cells ability to fire action potentials in response to depolarisation (E), Action potentials were inhibited by exposure to TTX which blocks membrane sodium channels (F). Recovery of action potentials was seen following a 5minute wash step, demonstrating that the neuronal morphology corresponds to neuronal functionality in these cells.

DISCUSSION

Over recent years, many research groups have published methods for neuronal differentiation of hES cells with varying levels of success. We set out to develop a method for obtaining such cells from the hES cell lines; HUES7 and Shef3. Both lines were successfully differentiated using the method detailed above, into cells of neuronal morphology which were shown to express neuronal markers; beta-III-tubulin and 70kD neurofilament. In addition, electrophysiology studies of these cells using patch clamping demonstrated that the derived neurons were able to generate action potentials, upon manual depolarisation, which were inhibited by TTX. Further characterisation of the resulting neurons will be necessary for use in specific applications, however, initial results suggest that this method of neuronal differentiation from hES cells may provide a suitable alternative cell source to primary cells/ less optimal cell lines for use as functional neuronal cells in drug screening bioassays.

Appendix 3: NIBSC PhD poster competition

Joint first prize winner - November 2008. Poster also submitted to UCL stem cell open day Spring 2009.

Neuronal differentiation of human embryonic stem cells

Gillett, M.L[1]., Bolsover, S[3]., Stacey, G[2,4]., Fleck, R.A[2]., Mason, C[1].

[1] Regenerative medicine, Advanced Centre for Biochemical engineering, University College London.
[2] Cell Biology and Imaging. The National Institute for Biological Standards and Control
[3] Department of Physiology, University College London.
[4] UK Stem cell Bank. The National Institute for Biological Standards and Control

INTRODUCTION

Human embryonic stem cells (hESCs) are capable of developing into any cell type within the human body and as such carry huge potential for the understanding and treatment of human disease. Neurodegenerative diseases such as Parkinson's and Alzheimer's are just two of the potential targets for hESCs therapy. In order to develop a successful therapy, either cell-or drug-based, it is necessary to produce large numbers of the desired cell type which match both the physical and behavioural properties of the damaged neurons. Many of the current studies into hESC – derived neuronal differentiation focus on the morphology and physical properties of the cells, rather than their functionality i.e. whether the cells are able to generate the electrical impulse of a primary neuron. This project has focused on the development of a robust protocol for the differentiation of hESC lines HUES7, Shef3 and RH5 to produce neurons which display both the morphological and electrophysiological characteristics of a neuron. Studies into changes in gene and protein expression throughout this differentiation process were carried out in addition to neuronal functionality studies using calcium imaging and patch clamping techniques, thus demonstrating successful *in vitro* differentiation of functional neurons from hESCs.

METHOD

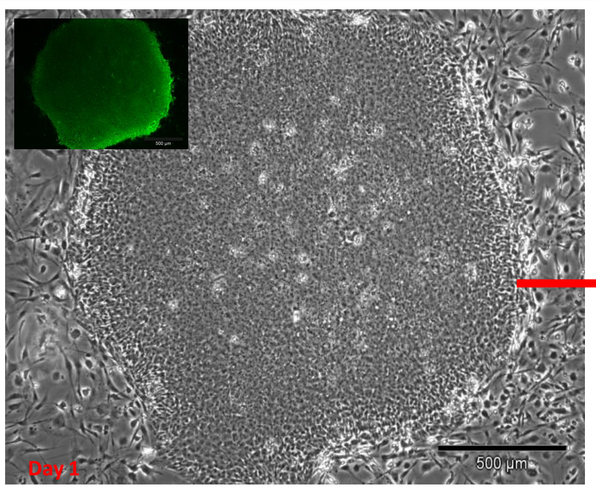

Figure 1. Undifferentiated human embryonic stem cell colony cultured in knock-out hES medium (express markers of pluripotency (SSEA4 – green). Fragments are cut from the undifferentiated colony and cultured in suspension in a neural induction media supplemented with bFGF for 5 days.

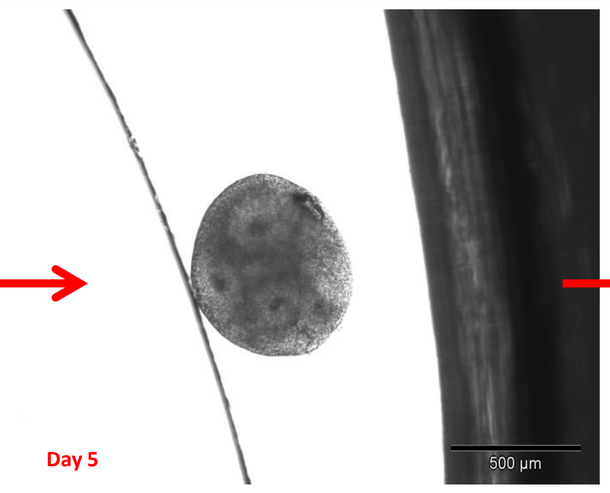

Rosette formation occurs within the floating fragments which are transferred into a Neurobasal media supplemented with neurotrophins but removing bFGF from culture for a further 5 days.

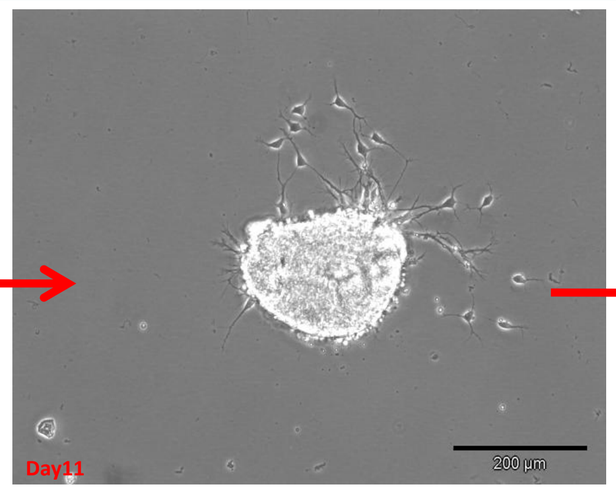

Floating fragments are transferred to a poly-ornithine/laminin coated substrate after 10 days in suspension culture. Outgrowth of neurons can be seen by day 11. Cells are cultured on for a further 18 days in Neurobasal media.

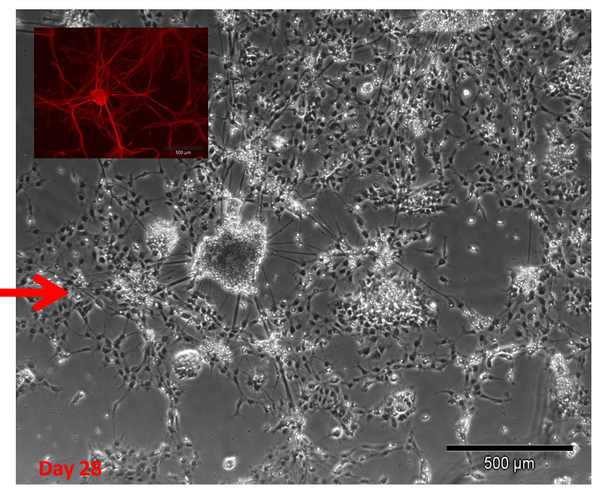

Outgrowth of neurons Cells treated with Trypsin and replated in the presence of neurotrophins for functionality studies. Matured neurons express Beta-III-tubulin (red) and can be maintained in culture for many weeks.

RESULTS

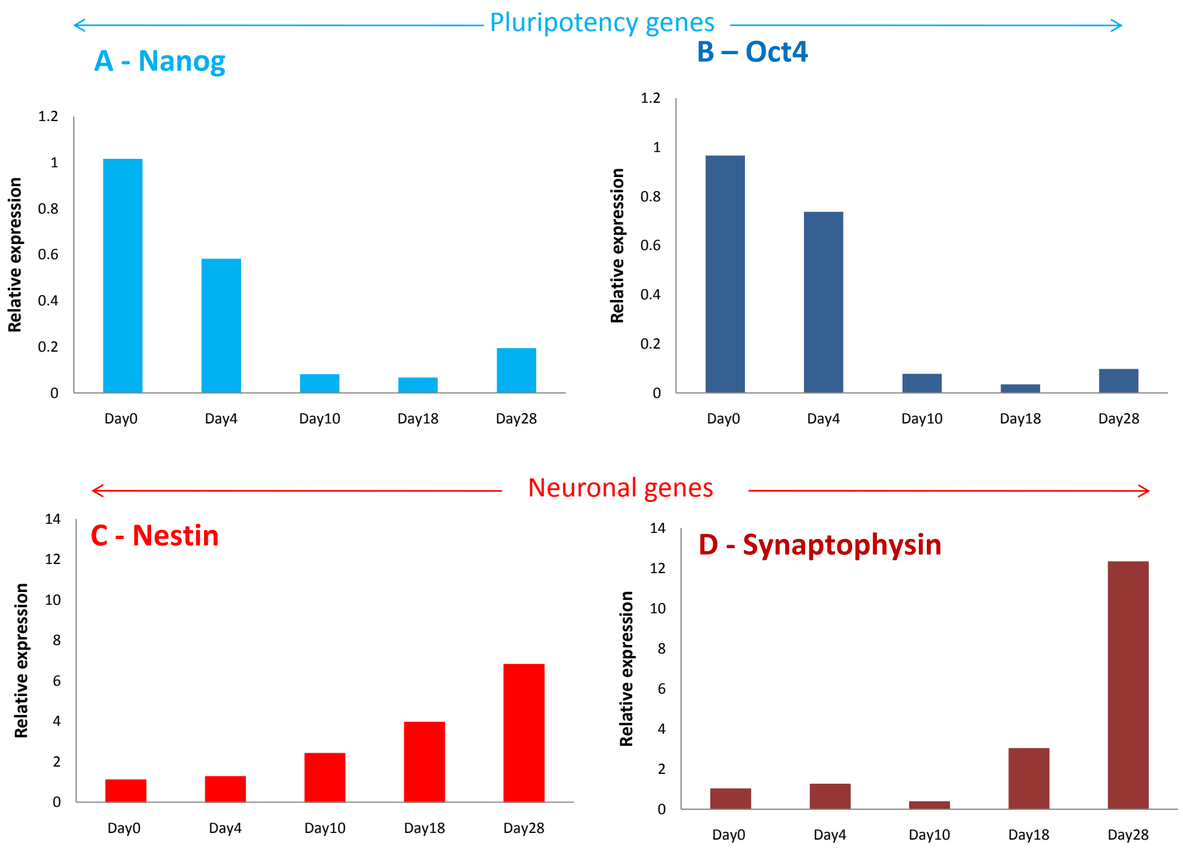

Figure 2. Gene expression patterns throughout differentiation. RH5 Cell samples were taken on day 0, 4, 10, 18 and 28 of differentiation. RNA was extracted following the Ambion Rnaqueous protocol, DNase treated and cDNA synthesised before running on an ABI human pluripotency gene expression low density array card to analyse changes in gene expression throughout differentiation. All samples are presented relative to the Day0 expression levels, standardised to Raf1 housekeeping gene which remained constant throughout the process. Expression of pluripotency genes: Nanog (A) and Oct4 (B) reduce over the 28day protocol. Expression of Nestin (C), found in neural stem cells and synaptophysin, found in mature neurons (D) were shown to increase 6.8-fold and 12.2-fold respectively with time.

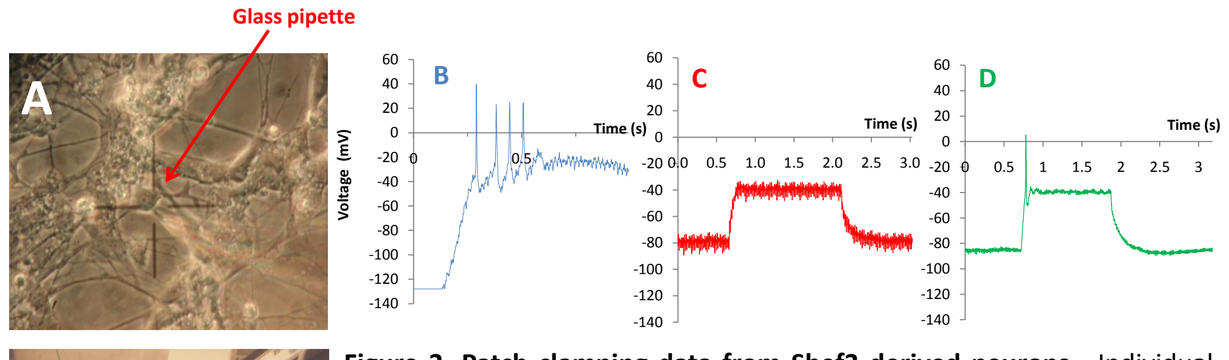

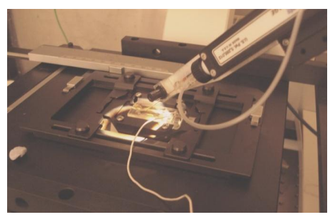

Figure 3. Patch clamping data from Shef3 derived neurons. Individual cells were patch clamped with a glass pipette (A). Cells were manually depolarised resulting in a series of action potentials fired (B). Following 2 minutes incubation with TTX action potentials were inhibited (C). Cells washed in buffer for 5 minutes following TTX showed recovery in action potential generation (D).

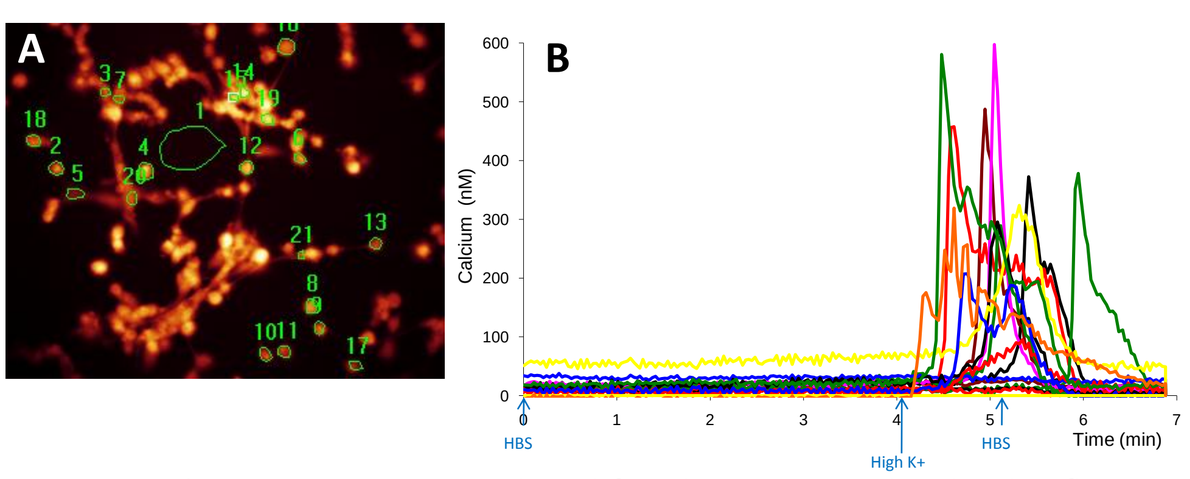

Figure 4. Calcium imaging. Neurons derived from hESCs were incubated with a fluorescent calcium indicator Fura2 (A). Exposure to 60mM Potassium stimulated opening of membrane calcium channels. Calcium waves continued to be seen following washing with Hanks buffered saline solution suggesting cells are continuing to respond to signals from each other. Each of the coloured spikes (B) is the calcium response from a different cell shown in image A.

DISCUSSION AND CONCLUSION

Throughout this project, an optimised protocol for neuronal differentiation of hESCs has been developed. This method has shown it is possible to produce cells with neuronal morphology from pluripotent human embryonic stem cells. Under immuno-fluorescence the derived neurons can be seen to express 70kDa neurofilament (not shown) and beta-III-tubulin both key neuronal markers. Prior to differentiation high levels of pluripotency markers Oct4 and Nanog were expressed which dramatically reduce during differentiation. Genes associated with neural stem cells; Nestin, and matured neurons; Synaptophysin where shown to increase by 7-fold and 12-fold respectively over 28 days of differentiation. Most importantly, the end stage neurons were shown to express functional calcium channels which open in response to Potassium depolarisation. Patch-clamping studies into these cells after 4 weeks of differentiation showed the ability to fire true sodium action potentials in response to manual depolarisation. These were reversibly inhibited by the sodium channel blocker TTX. Whilst optimisation of differentiation is still necessary to increase the cellular yield, the outlook for production of reliably functional neurons from hESCs for use in drug screening and successful transplantation therapies is increasingly positive.

ACKNOWLEDGEMENTS

We would like to thank the EPSRC and Linkam Scientific for funding this project.

Appendix 4: ISSCR 7th Annual Meeting - poster
July 2009.

Comparison of three human embryonic stem cell lines for neuronal differentiation efficiency with confirmed functionality using electrophysiology.

Gillett M.L*[,1,2,4]., Bolsover, S[3]., Healy, L[4]., Stacey, G [2,4]., Fleck, R.A[2]., Mason, C[1].

1 Regenerative Medicine, Advanced Centre for Biochemical Engineering, University College London.
2 Cell Biology and Imaging. The National Institute for Biological Standards and Control.
3 Department of Physiology, University College London.
4 The UK Stem Cell Bank. The National Institute for Biological Standards and Control.

INTRODUCTION

Human embryonic stem cells (hESCs) are pluripotent cell lines which have the potential to differentiate into neurons following exposure to chemical stimuli. This project compared the relative ability of three hESC lines; Shef3, RH5 and HUES7 to differentiate into a neuronal cell fate. A robust 28 day differentiation protocol was established. Screening to compare changes in gene expression of each line, at days 0, 4, 10, 18 and 28 of differentiation was carried out using Low Density Array Cards (Applied Biosystems). Neuronal status was confirmed by the generation of action potentials using patch-clamping techniques and immuno staining for common neuronal markers.

METHODS

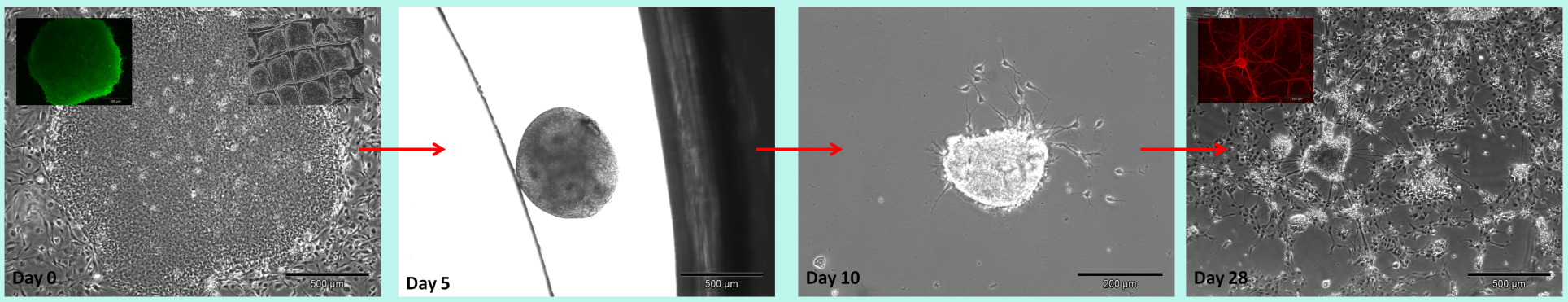

hESC colony. SSEA4 positive (green). Cut into fragments and transferred to suspension culture in neural induction (NI) media, 20ng/ml bFGF.

Colony fragments cultured as embryoid bodies (EB) in NI media for 4 days before transferral into Neurobasal media with N2 and B27 (NB media).

EBs plated onto poly-ornithine/laminin coated surface on day 9 in NB media. Neurons begin to spread out and can be visibly identified by day 10.

Extended outgrowth of neurons from attached cluster after 4 weeks in culture. Neurons stain positive for TUBB3 (red).

RESULTS

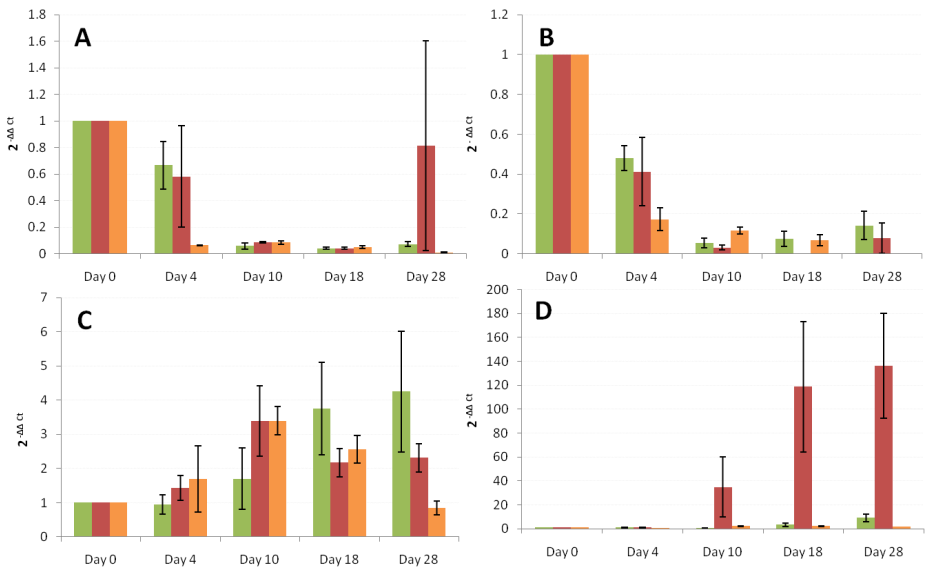

Figure 1. Gene Expression Analysis. RH5 (green), HUES7 (red), Shef3 (orange). Markers of pluripotency Oct4 (A) and Nanog (B) were detected in high levels at day 0. Oct4 expression reduced by 95 % and 80 % respectively by differentiation day 28 in all samples with the exception of HUES7, where expression increased in the later stages of differentiation to 81% of levels at day 0. Expression of the neural stem cell marker Nestin (C) peaked on day 10 in Shef3 and HUES7 but continued to increase until day 28 in RH5 to a 4.25-fold increase from day 0. Expression of the mature neuronal marker Synaptophysin (D) varied significantly between lines with 1.78 (±0.71), 9.25 (±3.18) , 136 (±44)-fold increase by day 28 in Shef3, RH5, HUES7 respectively.

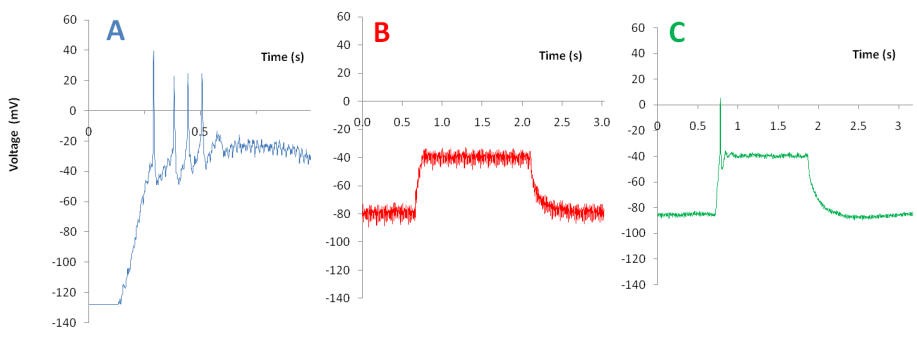

Figure 2. Patch clamping. All 3 hESC lines fired sodium action potentials in response to manual depolarisation (A; shef3 results presented). Multiple and single action potentials were fired by different neurons but no pattern within cell lines was identified. Action potentials were reversibly inhibited by 2 minute exposure to the sodium channel blocker TTX (B) followed by a 5 minute saline wash (C).

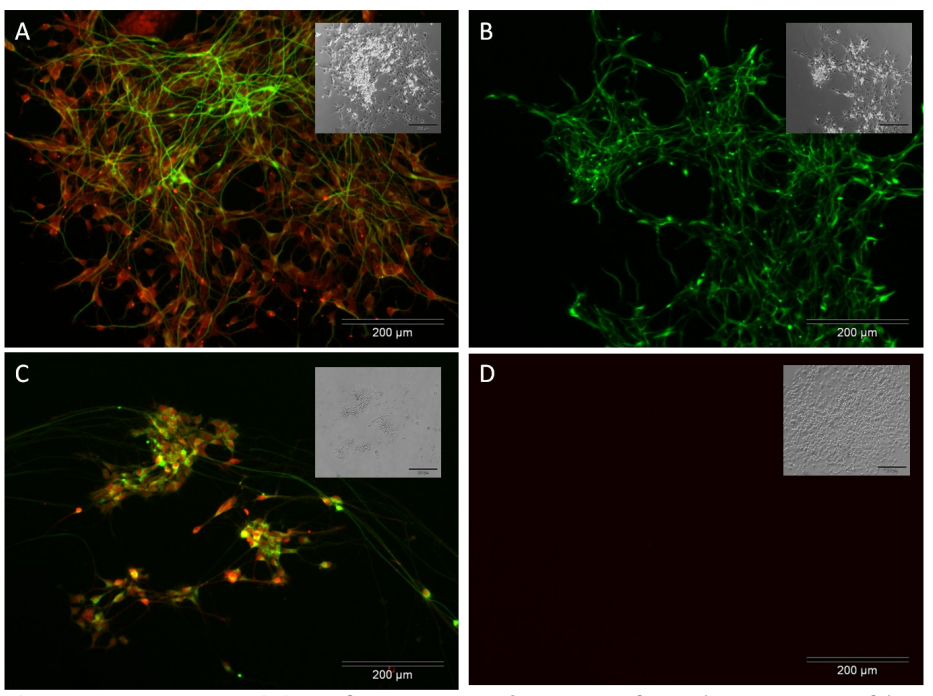

Figure 3. Immuno-staining of neurons at day 28 confirmed expression of key neuronal markers TUBB3 (A – green), Nestin (B – green), and the 70 kDa Neurofilament (C – green). The presence of glial cells within the population was also confirmed with GFAP staining (A – red). Neuronal population was predominantly of GABAergic phenotype as defined by the detection of GABA (D – red). Oct4 was not detected by immuno fluorescence in day 28 cells (D – red).

DISCUSSION AND CONLUSIONS

This project has shown that it is possible to generate functional neurons from multiple different hESC lines. Immuno-fluorescence demonstrated that hESC derived neurons expressed key markers of neuronal maturity including, but not limited to the 70 kDa neurofilament, TUBB3 and MAP2. Gene expression analysis throughout the differentiation period highlights the inherent variability between different hESC lines. Although the Oct4 protein was not detected in HUES7 day 28 samples, the rise in gene expression in latter stages of differentiation is of concern when considering this line for therapeutic application. This emphasises the importance of thorough screening of hESC lines selected for their differentiation potential. Whilst optimisation of differentiation is necessary to improve neuronal yield and purity, studies such as this bring us closer to understanding the comparative differentiation behaviour of hESCs lines and their ultimate potential for use in drug screening assays or cellular transplantation therapies. Work on these cells was performed as part of the development of QC methods for the UKSCB under its permission granted by the steering committee to perform banking development.

ACKNOWLEDGEMENTS

We would like to thank the EPSRC and Linkam Scientific for funding this project. We would also like to thank ESACT-UK and the UCL Graduate School for funding attendance to ISSCR 2009.